WOODHEAD PUBLISHING
IN MECHANICAL ENGINEERING

Industrial gas turbines

Performance and operability

A. M. Y. Razak

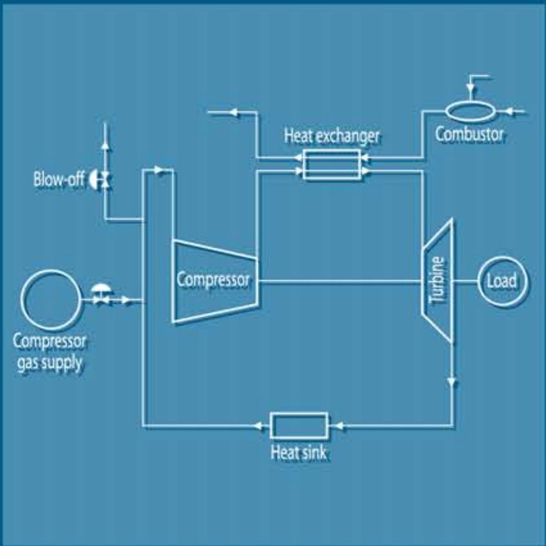

CRC
WP

Industrial gas turbines

Industrial gas turbines

Performance and operability

A. M. Y. Razak

CRC Press
Boca Raton Boston New York Washington, DC

WOODHEAD PUBLISHING LIMITED
Cambridge England

Published by Woodhead Publishing Limited, Abington Hall, Abington,
Cambridge CB21 6AH, England
www.woodheadpublishing.com

Published in North America by CRC Press LLC, 6000 Broken Sound Parkway, NW,
Boca Raton, FL 33487, USA

First published 2007, Woodhead Publishing Limited and CRC Press LLC

British Library Cataloguing in Publication Data
A catalogue record for this book is available from the British Library.

Library of Congress Cataloging in Publication Data
A catalog record for this book is available from the Library of Congress.

Woodhead Publishing ISBN 978-1-84569-205-6 (book)
Woodhead Publishing ISBN 978-1-84569-340-4 (e-book)
CRC Press ISBN 978-1-4200-4455-3
CRC Press order number WP4455

The publishers' policy is to use permanent paper from mills that operate a sustainable forestry policy, and which has been manufactured from pulp which is processed using acid-free and elementary chlorine-free practices. Furthermore, the publishers ensure that the text paper and cover board used have met acceptable environmental accreditation standards.

Typeset by Replika Press Pvt Ltd, India
Printed by TJ International Limited, Padstow, Cornwall, England

Contents

Foreword *xiii*

Preface *xv*

Acknowledgements *xvii*

Note about the CD-ROM accompanying this book *xviii*

CD-ROM: copyright information and terms of use *xix*

Abbreviations and notation *xxi*

1 Introduction 1

1.1 The gas turbine 2
1.2 Gas turbine layouts 3
1.3 Closed cycle gas turbine 6
1.4 Environmental impact 7
1.5 Engine controls 9
1.6 Performance deterioration 9
1.7 Gas turbine simulators 10
1.8 References 10

Part I Principles of gas turbine performance

2 Thermodynamics of gas turbine cycles 13

2.1 The first law of thermodynamics 13
2.2 The second law of thermodynamics 13
2.3 Entropy 14
2.4 Steady flow energy equation 15
2.5 Pressure–volume and temperature–entropy diagram 16
2.6 Ideal simple cycle gas turbine 16

2.7 Ideal regenerative gas turbine cycle 21
2.8 Reversibility and efficiency 25
2.9 Effect of irreversibility on the performance of the ideal simple cycle gas turbine 31
2.10 Effect of pressure losses on gas turbine performance 32
2.11 Variation of specific heats 32
2.12 Enthalpy and entropy 37
2.13 Combustion charts 39
2.14 Heat exchanger performance 40
2.15 Performance of an actual (practical) simple cycle gas turbine 42
2.16 Performance of an actual (practical) regenerative gas turbine cycle 45
2.17 Turbine entry temperature and stator outlet temperature 50
2.18 Worked examples 51
2.19 References 59

3 Complex gas turbine cycle 60

3.1 Intercooled gas turbine cycles 60
3.2 Reheat gas turbine cycle 72
3.3 Intercooled, reheat and regenerative cycles 85
3.4 Ericsson cycle 89
3.5 Combined cycle gas turbines 94
3.6 Co-generation systems 95
3.7 Hybrid fuel cell–gas turbine system 96
3.8 References 97

4 Compressors 98

4.1 Axial compressors 98
4.2 Compressor blading 99
4.3 Work done factor 102
4.4 Stage load coefficient 103
4.5 Stage pressure ratio 106
4.6 Overall compressor characteristics 109
4.7 Rotating stall 110
4.8 Compressor surge 110
4.9 Compressor annulus geometry 113
4.10 Compressor off-design operation 115
4.11 References 118

5 Axial turbines 120

5.1 Turbine blading 120

5.2 Stage load and flow coefficient 122
5.3 Deviation and profile loss 125
5.4 Stage pressure ratio 125
5.5 Overall turbine characteristics 127
5.6 Turbine creep life 129
5.7 Turbine blade cooling 130
5.8 Turbine metal temperature assessment 133
5.9 Effect of cooling technology on thermal efficiency 134
5.10 References 136

6 Gas turbine combustion 137

6.1 Combustion of hydrocarbon fuels 137
6.2 Gas turbine combustion system 140
6.3 Combustor cooling 146
6.4 Types of gas turbine combustor 147
6.5 Fuel injection and atomisation 149
6.6 Combustion stability and heat release rate 152
6.7 Combustion pressure loss and efficiency 154
6.8 Formation of pollutants 156
6.9 NO_x suppression using water and steam injection 157
6.10 Selective catalytic reduction (SCR) 158
6.11 Dry low emission combustion systems (DLE) 158
6.12 Variable geometry combustor 160
6.13 Staged combustion 160
6.14 Rich-burn, quick-quench, lean-burn (RQL) combustor 162
6.15 Lean premixed (LPM) combustion 164
6.16 Catalytic combustion 165
6.17 Impact of engine configuration on DLE combustion systems 166
6.18 Correlations for prediction of NO_x, CO and UHC and the calculation of CO_2 emissions 168
6.19 References 173

7 Off-design performance prediction 174

7.1 Component matching and component characteristics 174
7.2 Off-design performance prediction of a single-shaft gas turbine 177
7.3 Off-design performance prediction of a two-shaft gas turbine with a free power turbine 181
7.4 Matrix method of solution 185
7.5 Off-design performance prediction of a three-shaft gas turbine with a free power turbine 187

7.6 Off-design performance prediction of a two-shaft gas turbine 188
7.7 Off-design performance prediction of a three-shaft gas turbine 190
7.8 Off-design performance prediction of complex gas turbine cycles 191
7.9 Off-design prediction of a two-shaft gas turbine using a free power turbine and employing intercooling, regeneration and reheat 196
7.10 Off-design prediction of a three-shaft gas turbine using a power turbine and employing intercooling, regeneration and reheat 198
7.11 Variable geometry compressors 200
7.12 Variable geometry turbines 201
7.13 References 201

8 Behaviour of gas turbines during off-design operation 202

8.1 Steady-state running line 202
8.2 Displacement of running line (single- and two-shaft free power turbine gas turbine) 208
8.3 Three-shaft gas turbine operating with a free power turbine 217
8.4 Displacement of running line (three-shaft gas turbine) 221
8.5 Running line for a two-shaft gas turbine 223
8.6 Running lines of gas turbine complex cycles 226
8.7 Running line, non-dimensional parameters and correcting data to standard conditions 236
8.8 Power turbine curves 237
8.9 Gas power and gas thermal efficiency 239
8.10 Heat rate and specific fuel consumption 240
8.11 References 240

9 Gas turbine performance deterioration 241

9.1 Compressor fouling 242
9.2 Variable inlet guide vane (VIGV) and variable stator vane (VSV) problems 246
9.3 Hot end damage 248
9.4 Tip rubs and seal damage 250
9.5 Quantifying performance deterioration and diagnosing faults 250
9.6 References 261

10 Principles of engine control systems and transient performance 262

10.1 PID loop 263
10.2 Signal selection 266
10.3 Acceleration–deceleration lines 267
10.4 Control of variable geometry gas turbines 270
10.5 Starting and shutdown 275
10.6 Transient performance 277
10.7 References 288

Part II Simulating the performance of a two-shaft gas turbine

11 Simulating the effects of ambient temperature on engine performance, emissions and turbine life usage 293

11.1 Compressor running line 293
11.2 Representation of other non-dimensional parameters 294
11.3 Effects of ambient temperature on engine performance (high-power operating case) 296
11.4 Effect of reduced power output during a change in ambient temperature 313
11.5 Effect of humidity on gas turbine performance and emissions 320

12 Simulating the effect of change in ambient pressure on engine performance 323

12.1 Effect of ambient pressure on engine performance (high-power case) 324
12.2 Effect of ambient pressure changes on engine performance at lower power outputs 329

13 Simulating the effects of engine component deterioration on engine performance 337

13.1 Compressor fouling (high operating power) 337
13.2 Compressor fouling (low operating power) 349
13.3 Turbine damage 357
13.4 References 375

14 Power augmentation 376

14.1 Peak rating 377

14.2 Maximum continuous rating 380
14.3 Power augmentation at very low ambient temperatures 383
14.4 Power augmentation by water injection 388
14.5 Turbine inlet cooling 393
14.6 Power turbine performance 402
14.7 The effect of change in fuel composition on gas turbine performance and emissions 404
14.8 References 408

15 Simulation of engine control system performance 409

15.1 Proportional action 409
15.2 Proportional and integral action 410
15.3 Signal selection 414
15.4 Acceleration and deceleration lines 417
15.5 Integral wind-up 421
15.6 Engine trips 425
15.7 References 428

Part III Simulating the performance of a single-shaft gas turbine

16 Simulating the effects of ambient temperature on engine performance, emissions and turbine life usage 431

16.1 Configuration of the single-shaft simulator 431
16.2 Effect of ambient temperature on engine performance at high power 432
16.3 Effect of ambient temperature on engine performance at low power 444
16.4 Effect of ambient temperature on engine performance at high power (single-shaft gas turbine operating with an active variable inlet guide vane) 454
16.5 Effect of humidity on gas turbine performance and emissions 463

17 Simulating the effect of change in ambient pressure on engine performance 466

17.1 Effect of ambient pressure on engine performance at high power 467
17.2 Effect of ambient pressure on engine performance at low power 472

17.3 Effect of ambient pressure on engine performance at low power (single-shaft gas turbine operating with an active variable inlet guide vane) 479

18 Simulating the effects of engine component deterioration on engine performance 489

18.1 Compressor fouling (high-power operation) 489
18.2 Compressor fouling (low-power operation) 497
18.3 Compressor fouling at low-power operation (single-shaft gas turbine operating with an active variable inlet guide vane) 504
18.4 Turbine damage (hot end damage) at high-power outputs 508
18.5 Hot end damage at low power with active VIGV operation 515

19 Power augmentation 524

19.1 Peak rating 525
19.2 Power augmentation by increasing VIGV angle 528
19.3 Power augmentation using water injection 533
19.4 Power augmentation at low ambient temperatures 537
19.5 Turbine inlet cooling 543

20 Simulation of engine control system performance 545

20.1 VIGV control system simulation 545
20.2 VIGV control when the VIGV is active during the normal operating power range 549
20.3 Optimisation of the EGT limit for a single-shaft gas turbine with ambient temperature 563

21 Simulation exercises 566

Exercises using the single-shaft gas turbine simulator
21.1 Effects of ambient temperature and pressure on engine performance 566
21.2 Effects of component performance deterioration 568
21.3 Power augmentation 568
21.4 Combined cycle and co-generation 570
21.5 Engine control systems 571
21.6 Gas turbine emissions 571

Exercises using the two-shaft gas turbine simulator
21.7 Effects of ambient temperature, pressure and humidity on engine performance 573

21.8 Effects of component performance deterioration 575
21.9 Power augmentation 576
21.10 Combined cycle and co-generation 578
21.11 Engine control systems 579
21.12 Gas turbine emissions 579
21.13 Answers to exercises 582

Appendix: Steady flow energy equation and stagnation properties 589

A1.1 Steady flow energy equation 589
A1.2 Stagnation temperatures and pressures 590
A1.3 References 591

Index *593*

Foreword

Improving gas turbine performance involves the bringing together and optimisation of the disciplines and skills required to achieve an operationally competitive gas turbine engine. Certainly, the design and performance of individual engine components, such as the compressors, combustors and turbine, could alone present an engineer with a worthwhile career. It is, however, the overall performance of the gas turbine that the customer actually purchases. The optimisation process involves many uncertainties and a proper understanding of these, together with the established facts and the method of handling this information, is required to permit manufacturers to develop their engines successfully and allow operators to operate the machines to their best advantage. This is particularly true in the de-regulated market in which many operate today and which others will be joining in the near future.

Although there are many very remarkable books on industrial gas turbine performance and engineering, this book offers something different through a combined approach to the theory of gas turbines, their performance, and the use of gas turbine simulators. Simulators form an analysis method which can be used to bring together the many disciplines involved and which provides a way of assessing the impact of uncertainties. The combination of the book with the example simulators provides an added dimension to the product and this seems to conform to what many educational and training experts in this field have been demanding for some time. The book/simulator combination provides a useful reference text for students and practising engineers in both gas turbine manufacturing and operations.

The book initially covers the theory of gas turbine performance from a design and off-design point of view, including transient analysis, and gives much detail on these two very important aspects of engine performance. The latter part of the book revisits the earlier chapters, using the simulators to highlight in detail the issues facing industrial gas turbines in the real world. The simulators are effectively virtual engines with respect to performance, deterioration, emissions, control, and life usage. There is also a useful life cycle calculation module. This provides a clear view of the operability of the gas turbine under different conditions.

The book includes numerous simulation exercises. These exercises are not restrictively academic but include much of the author's experience, gained from an operator's viewpoint. Unlike numerical exercises, which give a somewhat narrow understanding of the problem, simulation exercises provide a holistic view of performance, which students, manufacturers and operators will find invaluable.

Robin Elder, BSc, PhD, C Eng, FIMechE
Director, PCA Engineers Limited

Preface

The use of industrial gas turbines is widespread in many industries that require power. The power is used to generate electricity or drive equipment such as pumps and process compressors. Gas turbines are also used extensively in naval propulsion and in this case are often referred to as naval gas turbines. In any of these applications, the performance of the gas turbines is the end product that strongly influences the profitability of the business that employs them. Industrial gas turbines often have to operate for prolonged periods at conditions that do not correspond to their design conditions. Therefore, understanding the performance of gas turbines at such operating conditions is particularly important, especially in a deregulated market.

Other factors in addition to the performance of gas turbines affect their operability. These factors include emissions, deterioration, life usage and controls. For example, legislation may result in emissions being too high and the means to control them could affect the engine performance and thus revenue. Gas turbine performance deterioration is inevitable. This could be due to compressor fouling, which can be easily rectified by compressor washing, or to more serious damage to compressors or turbines. Therefore, an understanding of performance deterioration is now paramount. Various engine operating limits are imposed by manufacturers and correspond to the exhaust gas turbine limit, speed and power. These are necessary to achieve suitable engine life, namely turbine creep life. It is the responsibility of the engine control system to ensure that such operating limits are not exceeded. Furthermore, it is also the job of the control system to ensure that any engine load changes occur safely.

Improving the understanding of the above issues has provided the impetus to write this book. The book begins with a brief revision of engineering thermodynamics before considering the design point performance of gas turbines, including both simple and complex cycles. The performance of gas turbine components (compressors, combustors and turbines) is also discussed. Means to improve dry low-emission combustion systems are included. The prediction and modelling of the off-design performance of gas turbines is discussed, including the modelling of complex cycles which employ intercooling, reheat and regeneration. The impact and detection of performance deterioration and the importance of such detection and rectification are also discussed. Control system performance, including the prediction of the transient performance of gas turbines, is considered. Furthermore, the application of control systems to improve the performance of dry low-emission combustion systems by the use of variable geometry components is discussed.

The CD accompanying the book contains two gas turbine simulators, which correspond to single-shaft and two-shaft engines. These two engine configurations cover the vast majority of industrial gas turbines operating in the field. Much of the text describing the performance and operability of industrial gas turbines can be illustrated and enlivened by the use of these gas turbine simulators. The simulators are used extensively in Parts II and III to:

(1) simulate the effects of ambient temperature, pressure and humidity on performance, turbine creep life and emissions, including the impact of inlet and exhaust losses;
(2) simulate the effects of engine deterioration on performance, creep life and emissions;
(3) simulate the impact of power augmentation and enhancement using turbine inlet cooling, peak rating, water injection and optimisation on performance, creep life and emissions;
(4) simulate control system performance on engine operability including proportional off-set, integral wind-up and engine trips;
(5) simulate the effect of a change in fuel type (e.g. natural gas or diesel) on performance and emissions.

There are nearly 50 simulation exercises included using each simulator. Exercises using simulators give a holistic view of engine performance and operability which numerical exercises fail to achieve. Nevertheless, numerical exercises are essential to augment the understanding of engine performance and some worked examples are given.

The simulators include other useful features and can show:

(1) impact on life cycle costs, revenue and profitability (including the impact of emissions taxes such as CO_2 and NO_x on life cycle costs and, thus, profitability);
(2) output from the turbine inlet cooling simulation which can be used to evaluate the suitability of turbine inlet cooling for any gas turbine for a particular site;
(3) trends for many engine parameters, including key parameters such as EGT and speeds that protect the engine from damage;
(4) compressor characteristics and the operating point during engine transients;
(5) bar charts;
(6) simulated data that can be exported to other computer packages (e.g. Microsoft Excel spreadsheets).

Acknowledgements

Much of this work would have been impossible without the support, help and suggestions from friends and colleagues. In particular, I wish to thank Dr John Greenbank and John Layton for their expert proofreading, which has improved the quality of the text and presentation of the book. Also, my friend and mentor Professor Robin Elder, who is wholly responsible for first introducing me to serious engineering computing, for his encouragement and support throughout the writing and preparation of this book. Also, I thank Woodhead Publishing for its patience during the preparation of the manuscript, particularly Sheril Leich for her thorough checking of the manuscript and suggestions.

I also wish to remember J. R. (Jimmy) Palmer of Cranfield Institute of Technology (now Cranfield University) who, in his day, was considered one of the authorities on gas turbine performance. I am privileged to have known him.

Note about the CD-ROM accompanying this book

As stated in the Preface, this CD-ROM includes software simulating the operation of a single-shaft gas turbine and a two-shaft gas turbine. The simulators are built on the engine modelling concepts discussed in the book and should be used to repeat the simulation discussion in Parts II and III and to perform the exercises in Chapter 21.

- **Minimum system requirements**

This CD-ROM is intended for use with Windows-compatible computers. You will require an internet connection for registration (see below).

Please note that, as part of the registration process, you will need to make a note of the **Disk ID Number**. This can be found **on the front of the plastic wallet containing the CD-ROM**. We suggest you make a **note of this number now**. You need take no further steps in the registration process until you install the CD-ROM.

- **Software requirements**

Adobe® Reader®

- **Installation instructions**

Insert the CD-ROM into the CD-ROM drive. The CD-ROM should auto-run. If the CD-ROM does not auto-run, open Microsoft Internet Explorer® on your computer and open the file *index.html*. If you continue to experience difficulties, please contact Gas Path Analysis Ltd for help (e-mail: support@gpal.co.uk)

- **Registration process**

Once you have inserted the CD-ROM and want to install the simulator software, you will need to go through a registration process to ensure uninterrupted use of the software. The registration process is designed to prevent unauthorised copying and distribution of the software. The CD-ROM contains an installation guide which will take you through the relevant steps.

CD-ROM: copyright information and terms of use

 Use of the CD-ROM is governed by the terms of the software licence agreement which follows. The licence grants licensees a non-exclusive, non-transferable, single-user licence. The licensed software may be installed on only one computer at a time. Installation of the software on two or more computers requires the purchase of additional licences from Gas Path Analysis Ltd. Loading the CD-ROM implies you agree to the terms of the software licence agreement. You will be asked to confirm your agreement to the terms of the licence as part of the installation process for the CD-ROM.

Gas Path Analysis Ltd (GPAL) gas turbine simulator software licence agreement

This licence is issued by:

Gas Path Analysis Ltd
Email: support@gpal.co.uk
Website: www.gpal.co.uk

Read this agreement carefully as it constitutes the terms of the software licence agreement.

1. Software product

This agreement is for a single-user licence of the GPAL Gas Turbine Simulator Software CD-ROM ('the Software') supplied with your purchase of *Industrial gas turbines: performance and operability* from Woodhead Publishing Limited.

2. Software licence

Gas Path Analysis Limited (GPAL) 'the Licensor' grants to the Licensee a non-exclusive, non-transferable, single-user licence. The registered version of the Software may only be installed on one computer at a time and requires a registration code to function properly. The registration code can be obtained from the Licensor. Installation of the Software on a second or more computers requires the purchase of additional licences which can be obtained from Gas Path Analysis Limited.

3. Liability

The CD-ROM contains information from authentic and highly-regarded sources. Reprinted material is quoted with permission, and sources are indicated. Reasonable efforts have been made to publish reliable data and information, but neither Gas Path Analysis Limited and Woodhead Publishing Limited, nor anyone else associated with this CD-ROM, are engaged in rendering professional services and shall not be liable for any loss, damage or liability directly or indirectly caused or alleged to be caused by any material contained in this CD-ROM or the accompanying book.

4. Proprietary rights

The Licensee agrees that the Software is the property of the Licensor. Any rights under patents, copyrights, trademarks, and trade secrets related to the Software are and shall remain vested in the Licensor. The Licensee agrees to preserve any copyright notices contained within the Software. The Licensee acknowledges that he or she is specifically prohibited from reverse engineering or disassembling the Software in whole or in part.

Unless otherwise stated in the installation guide and user guides contained in this CD-ROM, neither this CD-ROM nor the accompanying book or any part may be reproduced or transmitted in any form or by any means, electronic or mechanical, including photocopying, microfilming and recording, or by any information storage or retrieval system, without permission in writing from Gas Path Analysis Limited. The consent of Gas Path Analysis Limited does not extend to copying for general distribution, for promotion, for creating new works, or for resale. Specific permission must be obtained in writing from Gas Path Analysis Limited for such copying.

5. General

The laws of England shall govern in all respects as to the validity, interpretation, construction and enforcement of this licence.

6. Copyright

All rights are reserved and all copyrights in the Software belong to Gas Path Analysis Limited (UK company registration number: 3447319).

Abbreviations and notation

C	thermal capacity ratio
CO	carbon monoxide
CO_2	carbon dioxide
c_p	specific heat at constant pressure
c_v	specific heat at constant volume
DLE	dry low emission
EGT	exhaust gas temperature
GG	gas generator
H	enthalpy
HP	high pressure
ICRHR	intercooled, reheat and regenerative cycle
IP	intermediate pressure
ISO	International Standards Organisation
J	Joules
K	Kelvin
kg	kilogram
LP	low pressure
LPM	lean premixed
m	mass flow rate
MCFC	molten carbonate fuel cell
MEA	methanol amine
MW	MegaWatt or molecular weight
NGV	nozzle guide vane
NO_x	oxides of nitrogen
NTU	number of transfer units
P	pressure
PID	Proportional, Integral and Derivative
pr	pressure ratio
Q	heat input
R	gas constant
RQL	Rich-burn, Quick-quench, Lean-burn
s	second

S	entropy
SCR	selective catalytic reduction
SOFC	solid oxide fuel cells
SOT	stator outlet temperature
T	temperature
TET	turbine entry temperature
UHC	unburnt hydrocarbons
VIGV	variable inlet guide vane
VSV	variable stator vane
W	work output
x	number of carbon atoms
y	number of hydrogen atoms
Z	compressibility factor
γ	ratio of specific heats
ε	effectiveness of heat exchanger
η	efficiency
ϕ	relative humidity
ω	specific or absolute humidity

1
Introduction

The history of the gas turbine goes back to 1791, when John Barber took out a patent for 'A Method for Rising Inflammable Air for the Purposes of Producing Motion and Facilitating Metallurgical Operations'. Many endeavours have been made since then particularly in the early 1900s to build an operational gas turbine. In 1903, a Norwegian, Aegidius Elling, built the first successful gas turbine using a rotary/dynamic compressor and turbines, and is credited with building the first gas turbine that produced excess power of about 8 kW (11 hp). By 1904 Elling had improved his design, achieving exhaust gas temperatures of 773 K (500 degrees Celsius), up from 673 K (400 degrees Celsius), producing about 33 kW (44 hp). The engine operated at about 20 000 rpm. Much of his later work was carried out (from 1924 to 1927) at Kongsberg, in Norway.

Elling's gas turbine was very similar to Frank Whittle's jet engine, which was patented in 1930 in England. Whittle's design also consisted of a centrifugal compressor and an axial turbine and the engine was subsequently tested in April 1937. Meanwhile, in 1936, Hans von Ohain and Max Hahn, in Germany, developed and patented their own design. Unlike Frank Whittle's design, von Ohain's engine employed a centrifugal compressor and turbine placed very close together, back to back. The work by both Whittle and Ohain effectively started the gas turbine industry.[1]

Today, gas turbines are used widely in various industries to produce mechanical power and are employed to drive various loads such as generators, pumps, process compressors, or a propeller. The gas turbine began as a relatively simple engine and evolved into a complex but reliable and high efficiency prime mover. The performance and satisfactory operation of gas turbines are of paramount importance to the profitability of industries, varying from civil and military aviation to power generation, and also oil and gas exploration and production.

In the quest to perfect the gas turbine, compressor pressure ratios have increased from about 4:1 to over 40:1 together with high operating temperatures (about 1800 K), resulting in thermal efficiencies exceeding 40%. These features make the gas turbine a formidable competitor to other types of prime movers. In increasing the performance of the gas turbine, various engine configurations have evolved and such engine component arrangements and their applications will be discussed. However, the principles of the gas turbine and the main components that are required for these engines will be discussed first.

1.1 The gas turbine

For a turbine to produce power, it must have a higher inlet pressure than that at the exit. A compressor is normally used to provide this increase in pressure into the turbine. If the compressor discharge flow through the turbine is expanded, the turbine power output will be less than the power absorbed by the compressor because of losses in the compressor and turbine. Under these conditions, the whole engine will cease to rotate.

If energy is added into the compressor discharge air, corresponding to the losses in the compressor and turbine, then the system will run but will not produce any net power output. To produce net power from the gas turbine, additional energy needs to be supplied into the compressor discharge air. The energy supplied to the compressor discharge air is normally achieved by burning fuel in the compressor discharge air and this is accomplished in a combustion chamber or combustor, which is located or positioned between the compressor and turbine as shown in Fig. 1.1.

Clearly, the power output from a gas turbine depends on the efficiency of the compressor, turbine and the combustor. The higher the efficiency of these components, the better will be the performance of the gas turbine, resulting in increased power output and thermal efficiency.

The gas turbine has developed over 50 years into a high efficiency prime mover, and compressor and turbine efficiencies (polytropic) above 90% can be achieved today.

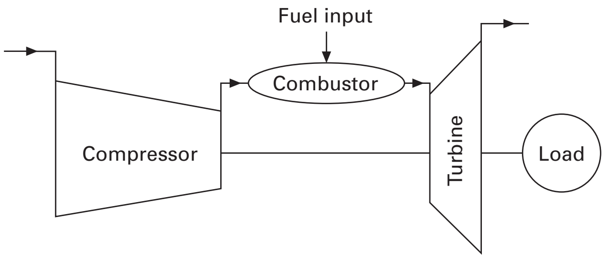

1.1 Schematic layout of a single-shaft gas turbine.

From the above discussion, a gas turbine must therefore have at least the following components:

(1) compressor
(2) combustor
(3) turbine.

A gas turbine comprising these components is often referred to as a simple cycle gas turbine. Gas turbines can include other components, such as intercoolers to reduce the compression power absorbed, re-heaters to increase the turbine power output and heat exchangers to reduce the heat input. These types of gas turbines are referred to as complex cycles. Although such complex cycles were developed in the early days of the gas turbine, today, simple cycle gas turbines dominate, and this is due to the high levels of performance achieved by engine components such the compressor, turbine and combustor. However, there is a renewed interest in complex cycle designs as a means of improving the performance of the gas turbine further.

1.2 Gas turbine layouts

Various arrangements of the gas turbine components have evolved over the years. Some are better suited for certain applications such as power generation (constant speed operation of the load, i.e. the generator) and other layouts are more suited to mechanical drive applications where the gas turbine is used to drive a process compressor or a pump (where the speed of the driven equipment can vary with load). In this section, we shall discuss these various arrangements, highlighting their advantages and disadvantages.

1.2.1 Single-shaft gas turbine

A single-shaft gas turbine consists of a compressor, combustor and a turbine as shown in Fig. 1.1. The compressor draws in air and increases its pressure. This compressed air is then introduced into the combustor, where heat is added by burning fuel. The hot, high-pressure gases are then expanded in a turbine to extract useful power. Part of the turbine power output is absorbed by the compressor, thus providing power for the compression process via the shaft connecting the compressor and turbine. The remaining power output from the turbine is used to drive a load such as a generator.

Single-shaft gas turbines are most suited for fixed speed operation such as base-load power generation. Single-shaft gas turbines have the advantage of preventing over-speed conditions due to the high power required by the compressor and can act as an effective brake should the loss of electrical load occur.

1.2.2 Two-shaft gas turbine with a power turbine

The expansion process in the turbine shown in Fig. 1.1 above may be split into two separate turbines. The first is used to drive the compressor and the second is used to drive the load. The mechanically independent (free) turbine driving the load is called the power turbine. The remaining turbine or high-pressure turbine, compressor and the combustor are called the gas generator. Figure 1.2 shows a schematic layout of a two-shaft gas turbine with a power turbine and is probably the most common engine configuration that is employed for gas turbines in general.

The function of the gas generator is to produce high pressure and high temperature gases for the power turbine. Two-shaft gas turbines operating with a power turbine are often used to drive loads where there is a significant variation in the speed with power demand (mechanical drive applications such as gas compression). Examples are pipeline compressors and pumps. The process conditions may be such that the load runs at low speed but absorbs or demands a large amount of power. In such a situation, the power turbine can run at the speed of the load and the gas generator can run at its maximum speed. If a single shaft gas turbine were employed to provide the power requirements for such applications, the whole engine would be constrained to run at the speed of the load thus resulting in poor engine performance due to the low operating speed condition.

Two-shaft gas turbines are also employed in industrial power generation with the power turbine designed to operate at a fixed speed determined by the generator. Unlike a single-shaft engine, the gas generator speed will vary with electrical load. The main advantage is smaller starting power requirements, as the gas generator only needs to be turned during starting, and better off-design performance. The disadvantage is that the shedding of the electrical load can result in over-speeding of the power turbine.

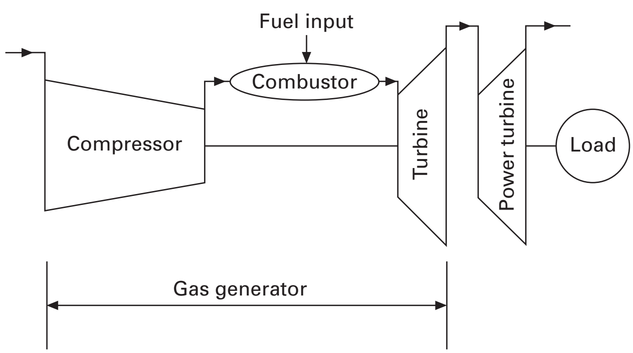

1.2 Schematic layout of a two-shaft gas turbine with a power turbine.

1.2.3 Three-shaft gas turbine with a power turbine

The gas generator (GG), as discussed in Section 1.2.2, can be divided further to produce a two-shaft or a twin spool gas generator. When this is done, the high-pressure GG turbine drives the high-pressure GG compressor, and the low pressure GG turbine drives the low pressure GG compressor. However, there is no mechanical linkage between the high pressure and low pressure shafts in the gas generator. Figure 1.3 shows a schematic layout of a three-shaft gas turbine with a power turbine. The power turbine is still mechanically independent from the gas generator as described in Section 1.2.2.

Such three-shaft arrangements, as with a two-shaft gas turbine with its own power turbine, are widely used in mechanical drive applications. Much higher-pressure ratios and thermal efficiencies may be achieved with such a layout without having to resort to variable geometry compressors as would be required by two-shaft gas engines when designed to operate at high compressor pressure ratios.

Three-shaft gas turbines also have the added advantage of lower starting powers because only the high-pressure compressor and turbine in the gas generator need to be turned during starting. Engines that use such a configuration are often derived from aircraft gas turbines and are referred to as aero-derivatives.

1.2.4 Two-shaft gas turbine

As seen in the power turbine configurations described in Sections 1.2.2 and 1.2.3, the power turbine can over-speed if the electrical load is shed when driving a generator. The two-shaft gas turbine overcomes this problem and still requires smaller starting powers than the single shaft gas turbine. The configuration is very similar to that of a three-shaft gas turbine but the power turbine is now an integral part of the LP turbine and drives both the LP

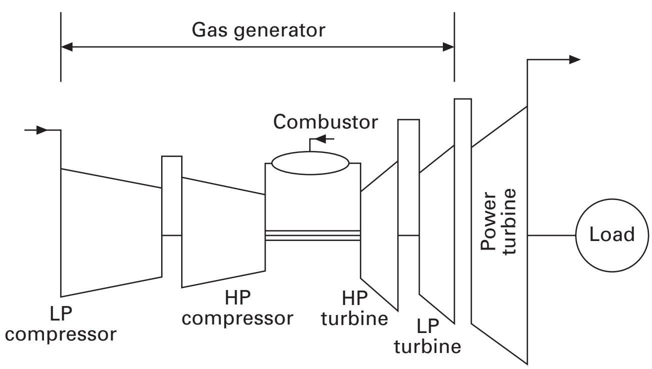

1.3 Schematic layout of a three-shaft gas turbine with a power turbine.

compressor and load. Should electrical load shedding occur, the LP compressor would now act as a brake, thus providing a useful means of over-speed protection as with a single shaft engine. However, starting power requirements are low because we only need to turn the HP spool during the starting of the gas turbine. Figure 1.4 shows a schematic layout of a two-shaft gas turbine.

1.3 Closed cycle gas turbine

One of the weaknesses of a gas turbine is its poor performance when operating at low powers. This is due to the reduction in the turbine entry temperature and compressor pressure ratios when operating at low power outputs, resulting in poor thermal efficiencies. The effect of turbine entry temperature and pressure ratio on engine performance is discussed in more detail in Chapter 2.

Unlike the open cycle gas turbine discussed previously, the closed cycle gas turbine is a self-contained system in which the system pressure is varied to alter the power output from the gas turbine. Thus, it is possible to operate a closed cycle gas turbine at constant turbine entry temperature and compressor pressure ratio, thereby maintaining good thermal efficiency at low powers. Essentially, the mass flow rate through the engine is reduced by reducing the working pressure due to the opening of the blow-off valve as shown in Fig. 1.5, which is a schematic representation of a closed cycle gas turbine. This results in lower power outputs. The heat supplied to the gas turbine is absorbed by the heat exchanger, which is supplied by hot gases from the combustor as shown in Fig. 1.5.

Although the off-design performance of the engine is improved using a closed cycle gas turbine, the design point thermal efficiency of the closed cycle gas turbine is lower than that of an open cycle gas turbine. The reasons for the efficiency drop are the imperfections of the heat exchanger. The heat exchanger cannot transfer all the heat generated by the combustor to the

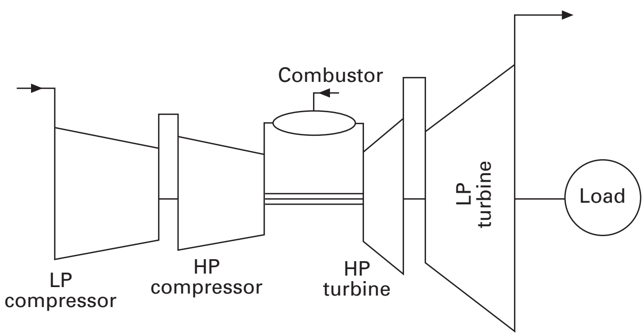

1.4 Schematic layout of a two-shaft gas turbine.

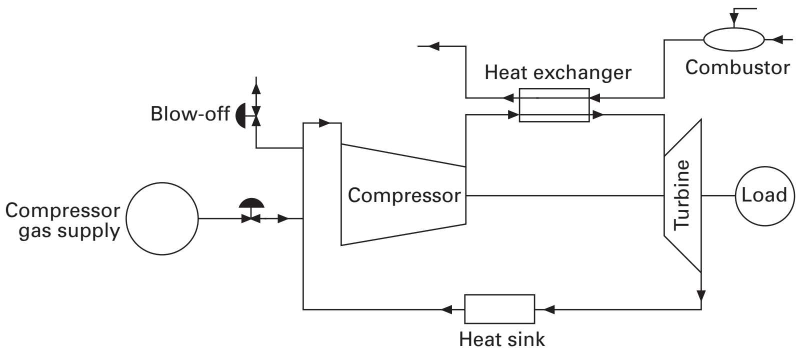

1.5 Schematic representation of a closed cycle gas turbine.

closed cycle gas turbine, because some of this heat is lost at the exit of the heat exchanger, resulting in a lower thermal efficiency at design point conditions.

On the positive side, the working pressure of a closed cycle gas turbine can be higher than atmospheric pressure, thus reducing the size of the turbo machinery and compensating for the increased bulk of a closed cycle gas turbine. The increase in working pressure also improves the heat transfer characteristics of the heat exchanger. Furthermore, the working fluid in a closed cycle gas turbine need not be air, and other gases such as helium can be used. This has better thermal properties than air, resulting in a smaller engine size and higher heat transfer coefficients, which help improve the design point thermal efficiency. Because of the self-containment of the working fluid of a closed cycle gas turbine, this type has been actively considered for nuclear power generation applications.[2]

1.4 Environmental impact

All combustion systems including those in gas turbines produce pollutants such as oxides of nitrogen (NO_x), carbon monoxide (CO) and unburned hydrocarbons (UHC). NO_x formation occurs due to the high combustion pressure and temperatures that prevail, resulting in the oxidation of atmospheric nitrogen. The formation of CO and UHC is generally due to poor combustion efficiencies. NO_x has been associated with the formation of acid rain and smog, and it has also been associated with the depletion of the ozone layer. CO is a poisonous gas whereas UHC is not only toxic but UHCs also combine with NO_x to produce smog. Combustion systems that use hydrocarbon fuels produce carbon dioxide (CO_2) and water vapour (H_2O) due to the oxidation of carbon and hydrogen. Although CO_2 and H_2O are considered non-toxic, they are greenhouse gases and have been associated with global warming.

The need to reduce emissions is now of paramount importance in protecting health and the environment. The last decade has seen a rapid change in regulations for controlling gas turbine emissions. Such regulations have resulted in the development of dry low emission (DLE) combustion systems and, today, many gas turbines operate using such combustors.

Although DLE combustion systems have reduced emissions of NO_x, CO and UHC appreciably, for a given fuel, the reduction of CO_2 and H_2O can only be achieved by improving the thermal efficiency of the gas turbines without resorting to carbon capture and storage. To achieve this improvement, combined cycle and co-generation systems, where the exhaust heat from the gas turbine is utilised to improve the overall thermal efficiency of the power plant, are now in operation. These systems can achieve overall thermal efficiencies of about 60% and 80%, respectively. Other technologies, where fuel cells are used in conjunction with gas turbines, are capable of producing power at thermal efficiencies approaching 70%. The use of low carbon content fuel or carbon-free fuels, such as hydrogen, will also help reduce or eliminate CO_2 emissions.

Other systems considered include CO_2 capture using solvents such as methanol amine (MEA) and storage, therefore preventing these gases from entering the atmosphere. This is often referred to as post-combustion carbon capture and storage and is being actively considered for current gas turbine power plants. Another method involves the removal and capture of CO_2 before combustion and is therefore referred to as pre-combustion carbon capture and storage. Here, the fuel, normally natural gas, is converted to CO and H_2. Steam (H_2O) is added in the presence of a catalyst where the steam is reduced to hydrogen (H_2) and oxygen (O_2). The CO is now oxidised to CO_2, which is then captured and stored. The reduction of H_2O and oxidation of CO is often referred to as the water gas shift reaction and was discovered by the Italian physicist, Felice Fontana, in 1780. The hydrogen (from the fuel and steam) is burnt in the gas turbine to produce power. A third method of carbon capture and storage, known as oxyfuel, involves the burning of fuel in oxygen. Thus the only gaseous emission is CO_2, which is captured and stored. The oxygen required for combustion is captured or separated from the air. The above methods of carbon capture and storage are discussed in Andersen *et al.*[3] and in Griffiths *et al.*[4]

The use of fuel cells, such as solid oxide fuel cells, in combination with gas turbines, can also be used to capture CO_2 by keeping the CO_2 stream and the water vapour streams separate. This is achieved by avoiding mixing the cathode and anode exit streams as the anode stream in principle is a mixture of CO_2, water vapour and some unused fuel. As stated above, the high thermal efficiencies reduce the amount of required CO_2 emissions for removal and storage.

In oil and gas exploration and production, oil and gas wells deplete over time and affect production. The storage of CO_2 in these depleted wells not only provides a means of storage but also increases the pressures in these wells, therefore enhancing production. The additional cost of carbon capture and storage can therefore be offset partly by the increased production of oil and gas.

1.5 Engine controls

The power output from the gas turbine is controlled primarily by the amount of fuel that is burnt in the combustion system. Excess or uncontrolled fuel addition results in overheating of the turbine and over-speeding, which can seriously damage the engine. It is the responsibility of the engine control system to prevent any engine operating limits from being exceeded. However, in the process it should not compromise the performance of the gas turbine. Control systems are quite complex, particularly in controlling DLE gas turbines, where the added requirements of maintaining air–fuel ratios within acceptable limits to maintain low emissions of NO_x, CO and UHC now exist. These issues are discussed in some detail later in this book.

1.6 Performance deterioration

One area that has been of increased interest is gas turbine performance monitoring. This approach has received significant amounts of attention in the last three decades. All gas turbines deteriorate in performance during operation, leading to reduced capacity and thermal efficiency. Loss of capacity results in lost production, affecting revenue. Loss in thermal efficiency increases fuel consumption and therefore leads to higher fuel costs. Both these factors reduce profits. Performance deterioration generally results in increased emissions of NO_x and CO_2. If emissions are taxed, then a further increase in operating costs occurs due to performance deterioration, and is reflected in still higher life cycle costs.

The most common form of performance deterioration is compressor fouling and this manifests itself by the ingestion of dirt and dust from the environment. Compressor fouling results in reduced compressor capacity and efficiency, but regular washing of the engine should remedy this problem. Other causes of performance deterioration include increased clearance between rotor tips but the casings enclosing components such as compressors and turbines. Seals are also provided to prevent leakage from the high-pressure sections to the low-pressure sections. During usage, these clearances increase due to tip rubs, resulting in reduced performance of the gas turbine. Unlike compressor fouling, which can be mitigated by washing, an engine overhaul is required to return these increased clearances to their design condition.

1.7 Gas turbine simulators

Much of what is said and discussed in this book can be elegantly illustrated by the use of a gas turbine simulator. The concept of component matching (the interaction of gas turbine components), which determines engine performance, and modelling of engine control systems as discussed in this book, has been used to build two industrial gas turbine simulators. These correspond to a two-shaft gas turbine operating with a free power turbine and a single-shaft gas turbine, respectively. Thus, these simulators now cover a majority of applications of industrial gas turbines.

The simulators are used extensively in the course of this book to illustrate the factors that affect engine performance, gas turbine emissions and engine life.

It is worth pointing out that such simulators are of paramount importance in the management of assets such as gas turbines. For example, these simulators may be used to understand changes in performance, emissions and life usage of the gas turbine due to changes in ambient conditions, deterioration and methods of power augmentation (e.g. peak rating, water injection and turbine inlet cooling where the inlet air is cooled by the evaporation of water or the use of chillers). Such information enables the user to obtain a deeper insight into gas turbine performance and operation, and information obtained by such means is sometimes referred to as knowledge management.

1.8 References

1. Fifty years of civil aero gas turbines, 9th Young Engineers Forum Lecture, Singh, R., *ASME TURBO EXPO* (1996).
2. *Closed-cycle Gas Turbines: Operating Experience and Future Potential*, 1st Edition, Frutschi, H. U., ASME Press (2005).
3. Gas turbine combined cycle with CO_2 capture using auto thermal reforming of natural gas, Andersen, T., Bolland, O. and Kvamsdal, H., *ASME 2000-GT-126*, (2000).
4. *Carbon Capture and Storage: An Arrow in the Quiver or a Silver Bullet to Combat Climate Change? A Canadian Primer*, Griffiths, M., Cobb, P. and Marr-Laing, T., The Pembina Institute, (November 2005).

Part I

Principles of gas turbine performance

The book has three parts. Part I deals with the theory of gas turbine performance applied to industrial gas turbines and discusses the principle of gas turbine combustion and control. The principles of compressors and turbines are also included in order to introduce the concept of component characteristics, which is of paramount importance in the prediction of off-design performance of gas turbines.

In Parts II and III, we revisit Part I to further explain the concepts behind gas turbine performance and operability using gas turbine simulators in a series of simulations. We first consider the two-shaft gas turbine operating with a free power turbine. This is the most common configuration based on the number of gas turbines operating in the field although, on an installed power basis, the single-shaft gas turbine is more common. Furthermore, the concept of (approximate) unique running lines prevalent within a two-shaft gas turbine facilitates easier understanding of gas turbine performance, and therefore makes it worth considering before the single-shaft gas turbine simulator.

2
Thermodynamics of gas turbine cycles

It was stated in Chapter 1 that gas turbines produce power by converting heat into work and that the heat input is achieved by burning fuel in the combustion system. Thus the performance analysis of a gas turbine is best achieved by applying the principles of thermodynamics. Two of the laws of thermodynamics concern us regarding gas turbine cycles: the first and the second laws of thermodynamics. There are many definitions of these laws, particularly the second law of thermodynamics. The following definitions will be used.

2.1 The first law of thermodynamics

The first law of thermodynamics states simply that energy cannot be created or destroyed but can only be converted from one type or form to another. For example, if we supply 10 MJ of heat into a thermodynamic system operating in a cycle to produce work, then only up to 10 MJ of work can be produced.

2.2 The second law of thermodynamics

The second law of thermodynamics is normally associated with a heat engine. A heat engine is a device operating in a cycle, producing work from a heat source and rejecting heat to a heat sink as shown in Fig. 2.1. It should be noted that when thermodynamic systems such as a heat engine operate in a cycle, this results in the initial and final states being identical. One definition of the second law limits the amount of work that can be produced. In other words, if we supply 10 MJ (Q_1) of heat to produce work (W), we can only develop less than 10 MJ of work, because the heat rejected to the sink, Q_2, cannot be zero. Therefore, the efficiency of a heat engine, which is the ratio of the work output, W, and the heat input, Q_1, can never be unity, because some heat must always be rejected by the system (i.e. Q_2 cannot be zero). The immediate question that arises is 'what is the maximum efficiency a heat engine can produce'? This is best answered by using the Carnot efficiency.

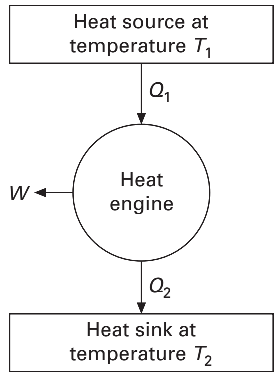

2.1 Representation of a heat engine.

Carnot showed that the maximum thermal efficiency '$\eta_{th,max}$' a heat engine can develop is given by Equation 2.1.

$$\eta_{th,max} = 1 - \frac{T_2}{T_1} \quad [2.1]$$

where T_1 and T_2 are the temperatures of the heat source and heat sink, respectively and the efficiency $\eta_{th,max}$ is called the Carnot efficiency. Clearly, the Carnot efficiency will increase as the ratio T_2/T_1 decreases, as expressed in Equation 2.1. To satisfy the Carnot efficiency condition, all the heat supplied from the heat source must occur at a constant temperature, T_1, and all the heat rejected to the heat sink must also occur at a constant temperature, T_2.

2.3 Entropy

The availability and accessibility of energy is important in producing work from a heat engine. The more accessible the energy is, the lower is its entropy. Consequently, the less available the energy, the higher is its entropy. Entropy is a thermodynamic property given the symbol S, and the change in entropy during a thermodynamic process is defined as:

$$\Delta S = \int \frac{dQ}{T} \quad [2.2]$$

If it is assumed that the work done, W, by the heat engine is zero, then $Q_1 = Q_2 = Q$ as would be required by the first law of thermodynamics. The decrease in entropy of the heat source is given by $\Delta S_{source} = -Q/T_1$ and the increase in entropy of the heat sink is $\Delta S_{sink} = Q/T_2$, as convention states that the heat lost from a thermodynamic system is negative and the work done by a thermodynamic system is positive. The net change in the entropy of the system ΔS_{system} is:

$$\Delta S_{\text{system}} = \Delta S_{\text{source}} + \Delta S_{\text{sink}} \tag{2.3}$$

$$\Delta S_{\text{system}} = \frac{Q}{T_2} - \frac{Q}{T_1} = Q\left(\frac{1}{T_2} - \frac{1}{T_1}\right) \tag{2.4}$$

Since T_1 must be higher than T_2 for heat to flow from the heat source to the heat sink, from Equation 2.4 the change in the entropy of the system will be positive. Although the entropy of the heat source decreases, the increase in the entropy of the heat sink is greater than the decrease in the entropy of the heat source. Thus the entropy of a system cannot decrease, but will increase whenever possible, and this is another statement of the second law of thermodynamics.

What prevents the heat engine above from achieving 100% thermal efficiency is this increase in entropy or degradation of energy, thus preventing the heat rejected to the heat sink (Q_2) from reaching zero. Therefore, some heat must be rejected from a heat engine (i.e. Q_2 cannot be zero). This condition is effectively the statement of the second law of thermodynamics. Further information on entropy and the second law of thermodynamics may be found in Rogers and Mayhew[1] and in Eastop and McConkey.[2]

2.4 Steady flow energy equation

Unlike a piston engine, where the compression and expansion processes are intermittent, the gas turbine cycle is a continuous flow process. Therefore, the governing equation that satisfies the first law of thermodynamics is the steady flow energy equation. The steady flow energy equation may be simply described as:

$$Q - W = \Delta H \tag{2.5}$$

where

Q represents the heat input into a steady flow thermodynamic system
W represents the work done by the thermodynamic system
ΔH represents the change in the energy of the gas in the system.

ΔH has capacity to hold heat (specific heat) and is called the change in the stagnation or total enthalpy in the thermodynamic system. (See the Appendix for details on the steady flow energy equation and stagnation properties.)

For an ideal gas, the change in enthalpy can be represented by:

$$\Delta H = m \times c_p \times \Delta T \tag{2.6}$$

where

m is the mass flow rate
c_p is the specific heat of the gas at constant pressure

ΔT is the total temperature change in the thermodynamic system. We can therefore rewrite the steady flow energy Equation 2.5 as:

$$Q - W = m \times c_p \times \Delta T \qquad [2.7]$$

2.5 Pressure–volume and temperature–entropy diagram

Thermodynamic processes may be represented on a pressure–volume diagram and on a temperature–entropy diagram. Figure 2.2 shows an example of an isothermal expansion process in these respective diagrams, where the temperature of the gas remains constant during the thermodynamic process. The areas shown in the pressure–volume and temperature–entropy diagrams correspond to the work and heat transfers, respectively.

The work and heat transfers shown in Fig. 2.2 can be determined by solving the integrals $\int p\mathrm{d}v$ and $\int t\mathrm{d}S$, respectively. Note the increase in entropy during the expansion process on the temperature–entropy diagram. Of the many thermodynamic processes that exist in the gas turbine, we are particularly interested in reversible and adiabatic processes, which are also known as isentropic processes. In such an ideal process both the heat transfer and the entropy changes are zero. Such a process is represented as a vertical straight line on a temperature–entropy diagram as shown in Fig. 2.4.

2.6 Ideal simple cycle gas turbine

The ideal gas turbine can be considered as a heat engine because it works in a cycle exchanging heat from a heat source and exhausting heat to a heat sink

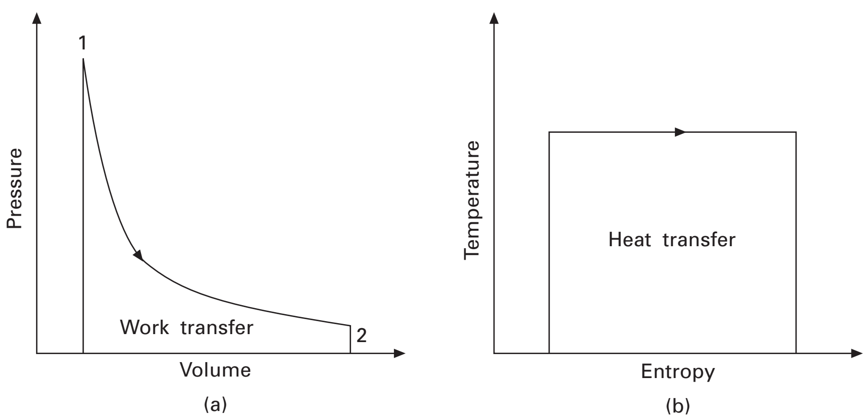

2.2 Work and heat transfers on (a) pressure – volume and (b) temperature – entropy diagrams.

and producing work. The processes involved in the ideal gas turbine cycle, are shown on Fig. 2.3:

1 compression (isentropic)
2 heat addition (constant pressure)
3 expansion (isentropic)
4 heat rejection (constant pressure).

The gas turbine cycle is best represented on a temperature–entropy diagram as shown in Fig. 2.4, which illustrates the thermodynamic processes involved. From the steady flow energy equation, the adiabatic compression work required will be given by:

$$W_{12} = c_p(T_2 - T_1) \tag{2.8}$$

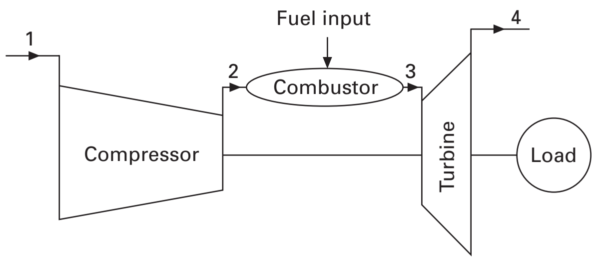

2.3 Representation of a simple cycle gas turbine.

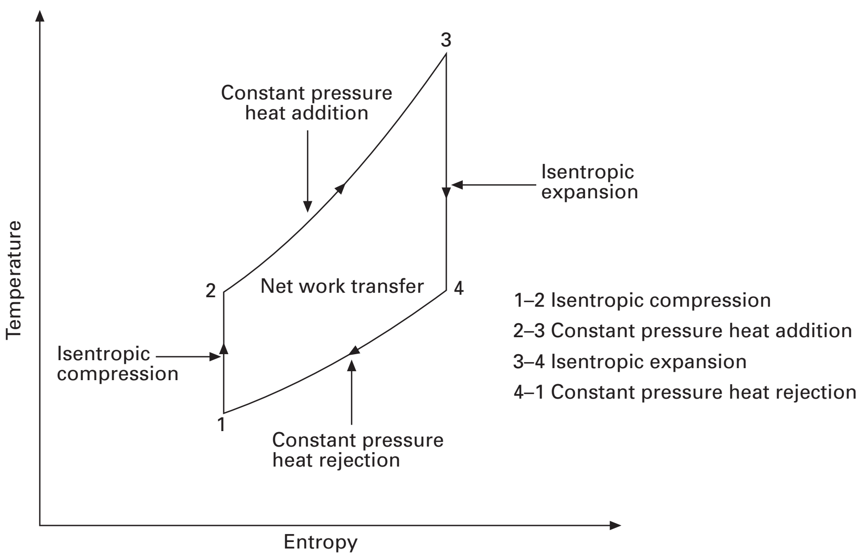

2.4 Representation of gas turbine cycle on temperature–entropy diagram.

and the compressor discharge temperature, T_2, for an isentropic compression is given by:

$$T_2 = T_1\left(\frac{P_2}{P_1}\right)^{\frac{\gamma-1}{\gamma}} \qquad [2.9]$$

where

γ is the ratio of specific heats of the gas (c_p/c_v) and is known as the isentropic index, and c_v is the specific heat at constant volume.

Similarly, the adiabatic expansion work and expander exit temperature, T_4, is given by:

$$W_{34} = c_p(T_3 - T_4) \qquad [2.10]$$

and

$$T_4 = T_3\left(\frac{P_4}{P_3}\right)^{\frac{\gamma-1}{\gamma}} \qquad [2.11]$$

The heat input is given by Equation 2.12. Since the work done in the combustion system is zero, the heat input, Q_{23}, is:

$$Q_{23} = c_p(T_3 - T_2) \qquad [2.12]$$

The net work done by the cycle per unit mass flow rate (specific work, W_{net}) is the difference between the expansion and compression work. Hence W_{net} is given by:

$$W_{net} = c_p(T_3 - T_4) - c_p(T_2 - T_1) \qquad [2.13]$$

The cycle thermal efficiency, η_{th}, is defined as the ratio of the net work done and the heat input. Hence the thermal efficiency is given by:

$$\eta_{th} = \frac{W_{net}}{Q_{23}} \qquad [2.14]$$

which can be rewritten as

$$\eta_{th} = \frac{c_p(T_3 - T_4) - c_p(T_2 - T_1)}{c_p(T_3 - T_2)} \qquad [2.15]$$

$$\eta_{th} = \frac{(T_3 - T_2) - (T_4 - T_1)}{T_3 - T_2} \qquad [2.16]$$

$$\eta_{th} = 1 - \frac{T_4 - T_1}{T_3 - T_2} \qquad [2.17]$$

Substituting for T_2 and T_4 using Equations 2.9 and 2.11, respectively, into Equation 2.17 reduces Equation 2.17 to:

$$\eta_{th} = 1 - \frac{T_1}{T_2} \tag{2.18}$$

Hence the ideal gas turbine cycle thermal efficiency is dependent only on the compressor temperature ratio. Comparing the ideal gas turbine cycle efficiency with the corresponding Carnot efficiency ($\eta_{th} = 1 - T_1/T_3$), the ideal gas turbine efficiency is less than the Carnot efficiency, since T_2 is less than T_3.

We can represent Equation 2.18 in terms of compressor pressure ratio using Equation 2.9 giving:

$$\eta_{th} = 1 - \frac{1}{c} \tag{2.19}$$

where

$$c = \left(\frac{P_2}{P_1}\right)^{\frac{\gamma-1}{\gamma}}$$

The thermal efficiency will therefore increase with the pressure ratio, and maximum possible thermal efficiency is achieved when T_2 tends to T_3, as this corresponds to the Carnot efficiency. The thermal efficiency will be zero as the pressure ratio tends to 1, which now results in T_3 tending to T_4. The temperature–entropy diagram for these limiting cases is shown in Fig. 2.5.

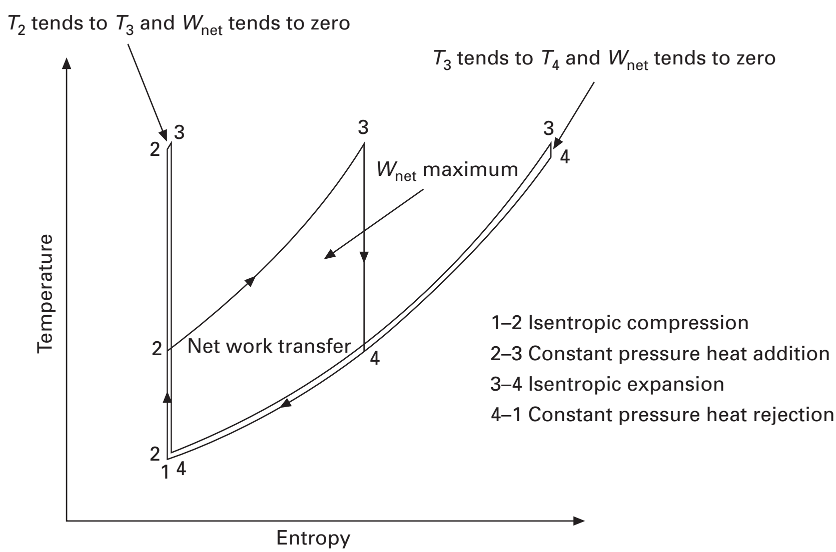

2.5 Effect of pressure ratio on the temperature–entropy diagram for an ideal gas turbine cycle when T_3 is constant.

The specific work W_{net} given in Equation 2.13 can be rewritten as:

$$W_{net} = c_p T_1 \left(\frac{c-1}{c}\right)\left(\frac{T_3}{T_1} - c\right) \quad [2.20]$$

Thus, for a given gas the specific work of the ideal gas turbine cycle depends on the compressor pressure ratio, P_2/P_1, the maximum to minimum temperature ratio, T_3/T_1, and compressor inlet temperature, T_1. Increasing the temperature ratio, T_3/T_1, for a given T_1 will increase the specific work, whereas increasing the pressure ratio will increase the specific work initially, but this will decrease at high pressure ratios. When the compressor pressure ratio equals unity, the specific work, W_{net}, will be zero. When the compressor pressure ratio is increased such that $c = (P_2/P_1)^{(\gamma-1)/\gamma}$, which is equal to T_3/T_1 from Equation 2.19, the specific work will again reduce to zero. Thus, the maximum specific work occurs at some pressure ratio between these values, and this optimum pressure ratio will depend on γ, T_1 and T_3/T_1.

Differentiating Equation 2.20 with respect to c enables us to find an expression for the compressor pressure ratio, which will correspond to the case when the specific work is a maximum. Thus, it can be shown that:

$$C_{opt} = \sqrt{\frac{T_3}{T_1}} \quad [2.21]$$

where

$$C_{opt} = (pr_{opt})^{\frac{\gamma-1}{\gamma}}$$

and

pr_{opt} is the optimum pressure ratio.

At the optimum pressure ratio, when the specific work is a maximum, the expander or turbine exit temperature, T_4, is equal to the compressor discharge temperature, T_2.

Figure 2.5 shows the temperature–entropy diagram for the limit cases and the optimum case when the specific work is a maximum.

Advanced gas turbines operate at very high maximum cycle temperatures up to about 1800 K and achieve very high simple cycle thermal efficiencies in the order of 40%. However, for discussion and illustrative purposes, low values for maximum cycle temperature will be assumed as these yield low and realistic pressure ratio ranges when explaining the features discussed up to now. The performance of gas turbines using higher values for maximum cycle temperatures will be considered later in this chapter and will illustrate how efficient gas turbines are. For a given gas, it has been shown that the thermal efficiency of an ideal simple cycle gas turbine is dependent only on the pressure ratio, whereas the specific work is dependent on the pressure ratio and the maximum to minimum cycle temperature. This is illustrated in

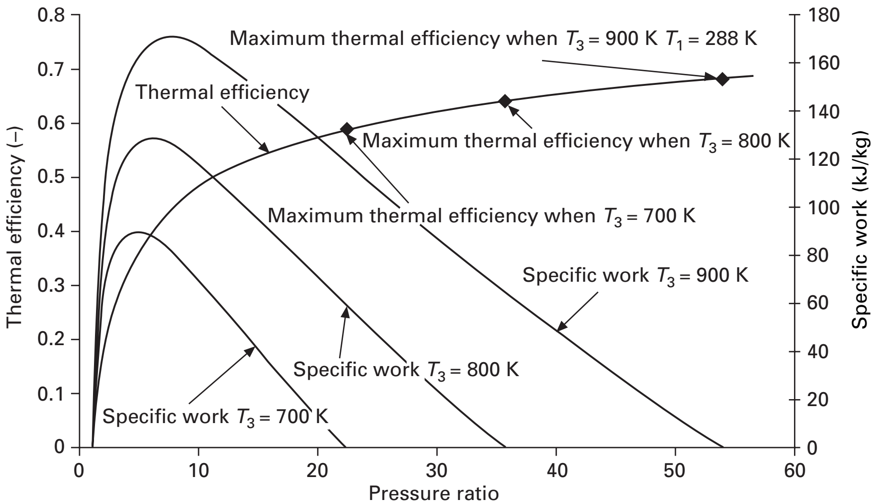

2.6 Variation of thermal efficiency and specific work with compressor pressure ratio.

Fig. 2.6, which also shows the effect of maximum cycle temperature, T_3. The specific work curve has been displayed for three values of T_3, which correspond to 700 K, 800 K and 900 K. The limiting thermal efficiencies for each value of T_3 are also shown and they correspond to the points where the specific work is zero. Note also that the optimum compressor pressure ratio increases with T_3 when the specific work is a maximum, as described by Equation 2.21.

It is worth pointing out that the maximum thermal efficiency points shown in Fig. 2.6 correspond to the Carnot thermal efficiency for each T_3 value. Although the Carnot efficiency can be achieved by the ideal simple cycle gas turbine, at these compressor pressure ratios, the turbine work done equals the compressor work absorbed, hence resulting in zero net specific work. Thus the thermal efficiency cannot continue to be increased simply by increasing the pressure ratio as implied by Equation 2.19. The maximum thermal efficiency that can be achieved by the ideal simple cycle gas turbine is indeed the Carnot efficiency, therefore complying with the second law of thermodynamics.

2.7 Ideal regenerative gas turbine cycle

It has been seen from the analysis of an ideal simple cycle gas turbine that the maximum specific work occurs when the turbine exit temperature, T_4, is equal to the compressor discharge temperature, T_2, and the optimum pressure ratio is determined by Equation 2.21. At pressure ratios below this optimum value the turbine exit temperature, T_4, will be higher than the compressor discharge temperature, T_2. Clearly, there is potential to transfer some of the heat rejected by the simple cycle to the compressor discharge air, thereby reducing the heat input. Although the specific work is reducing, the resultant reduction in heat input more than compensates for the loss in specific work and therefore improves the thermal efficiency. This is the concept of the regenerative gas turbine cycle. In effect some of the degraded energy is being utilised to produce useful work. A schematic representation of the regenerative gas turbine cycle is shown in Fig. 2.7. The only additional component is the heat exchanger, needed to transfer heat from the turbine exit to the compressor discharge.

The temperature at the exit of the turbine is cooled ideally from T_5 to T_2, while the compressor discharge gas is heated from T_2 to T_5 at point 3 by the heat exchanger. The heat source increases the gas temperature further from T_3 to T_4, which is now the maximum cycle temperature and the temperature at point 6 is reduced by the heat sink from T_2 to T_1. The temperature–entropy diagram in Fig. 2.8 shows the potential of heat transfer to the compressor discharge gas.

The heat input for the regenerative cycle is therefore given by:

$$Q_{34} = c_p(T_4 - T_3) \qquad [2.22]$$

The equation defining the net specific work output is the same and is given by Equation 2.13:

$$W_{net} = c_p(T_4 - T_5) - c_p(T_2 - T_1) \qquad [2.23]$$

Therefore, the thermal efficiency of the regenerative cycle is given by:

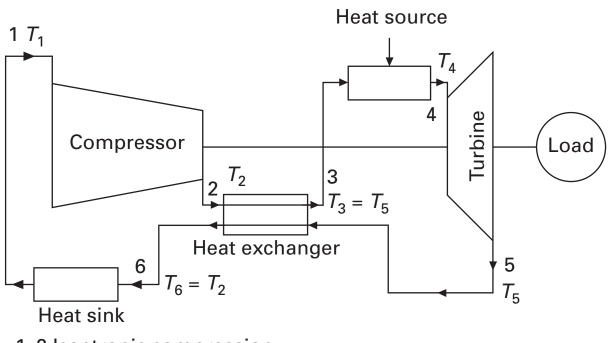

1–2 Isentropic compression
2–3 Constant pressure heat addition via heat exchanger
3–4 Constant pressure heat addition via external heat source
4–5 Isentropic expansion
5–6 Constant pressure heat transfer for heating process 2–3
6–1 Constant pressure heat rejecton

2.7 Schematic representation of a regenerative cycle.

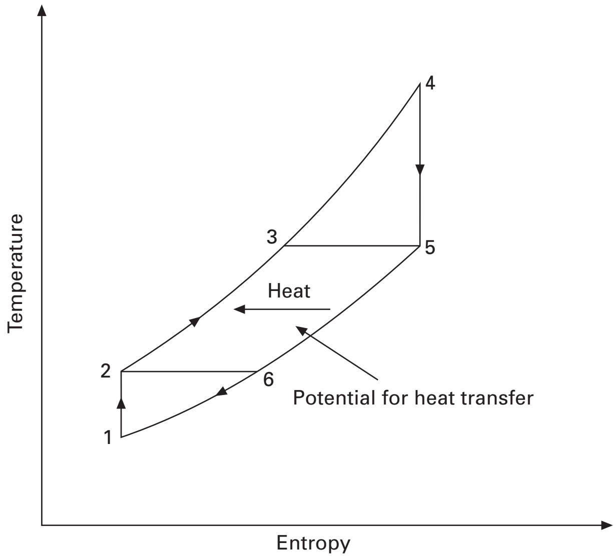

1–2 Isentropic compression
2–3 Constant pressure heat addition via heat exchanger
3–4 Constant pressure heat addition via external heat source
4–5 Isentropic expansion
5–6 Constant pressure heat transfer for heating process 2–3
6–1 Constant pressure heat rejecton

2.8 Heat transfer for a regenerative gas turbine cycle.

$$\eta_{\text{th}} = \frac{c_p\,(T_4 - T_3) - c_p\,(T_2 - T_1)}{c_p\,(T_4 - T_3)} \qquad [2.24]$$

which reduces to

$$\eta_{\text{th}} = 1 - \frac{T_1}{T_4}\,c \qquad [2.25]$$

where

$c = \left(\dfrac{P_2}{P_1}\right)^{\frac{\gamma-1}{\gamma}}$ and T_4 is now the maximum cycle temperature.

Unlike the simple cycle, the thermal efficiency of the regenerative cycle is dependent on the cycle temperatures, particularly the ratio of the maximum to minimum temperature ratio, T_4/T_1. The effect of the pressure ratio on the thermal efficiency is opposite to that for a simple cycle gas turbine. The thermal efficiency of the regenerative cycle increases as the pressure ratio decreases and, when the pressure ratio tends to unity, the thermal efficiency tends to that of the Carnot cycle efficiency, $1 - T_1/T_4$. This result is not entirely surprising because, when the pressure ratio tends to unity, all the heat is supplied at the maximum temperature and all the heat rejected occurs at the minimum temperature. This is the Carnot requirement as discussed in Section 2.2. Although the work output tends to zero as the pressure ratio tends to unity and is of little practical importance, it is important to realise that the maximum thermal efficiency cannot exceed the Carnot efficiency, as required by the second law of thermodynamics.

The variation of thermal efficiency with pressure ratio for a regenerative gas turbine cycle is shown in Fig. 2.9. The thermal efficiency is shown for three different values of T_4. The Figure also shows the simple cycle gas turbine thermal efficiency for comparison. The limiting pressure ratio for the regenerative cycle occurs when the turbine exit temperature T_5 equals the compressor discharge temperature, T_2. The variation of the specific work for the ideal regenerative cycle is no different from that of the ideal simple cycle and will correspond to the curves shown in Fig. 2.6.

Further improvement in performance of the ideal simple cycle is possible by intercooling the compression process and reheating the working fluid as it passes through the compressor and turbine, respectively. Such modifications will improve the specific work output but will generally have a detrimental effect on the ideal cycle thermal efficiency unless a heat exchanger is added. This approach is discussed in detail in Chapter 3.

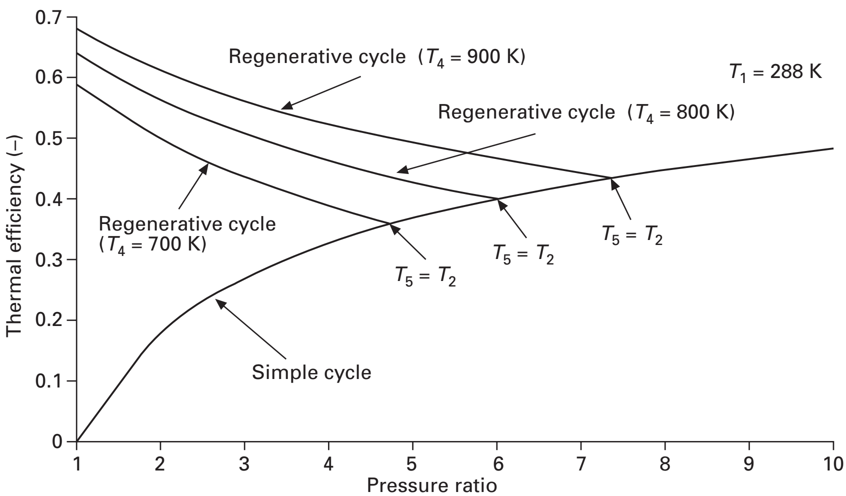

2.9 Effect of T_4 and pressure ratio on the thermal efficiency of a regenerative cycle. The limiting pressure ratios when $T_5 = T_2$ are shown.

2.8 Reversibility and efficiency

Until now we have discussed the thermodynamic cycles of the gas turbine assuming that there are no thermodynamic losses in any of the components. In practice, however, this is not the case and the individual processes of compression, expansion and heat addition will each have losses. It has been stated that, in any thermodynamic process, the energy is degraded thus making the energy unavailable when increasing the entropy. This feature gives rise to the concept of efficiency in a thermodynamic process such as compression and expansion.

2.8.1 Reversibility

Using the temperature–entropy diagram shown in Figure 2.10, consider an ideal compression process where the pressure is increased from P_1 to P_2 along the process 1 to 2′ and is then followed by an ideal expansion from P_2 to P_1 along the process 2′ to 1.

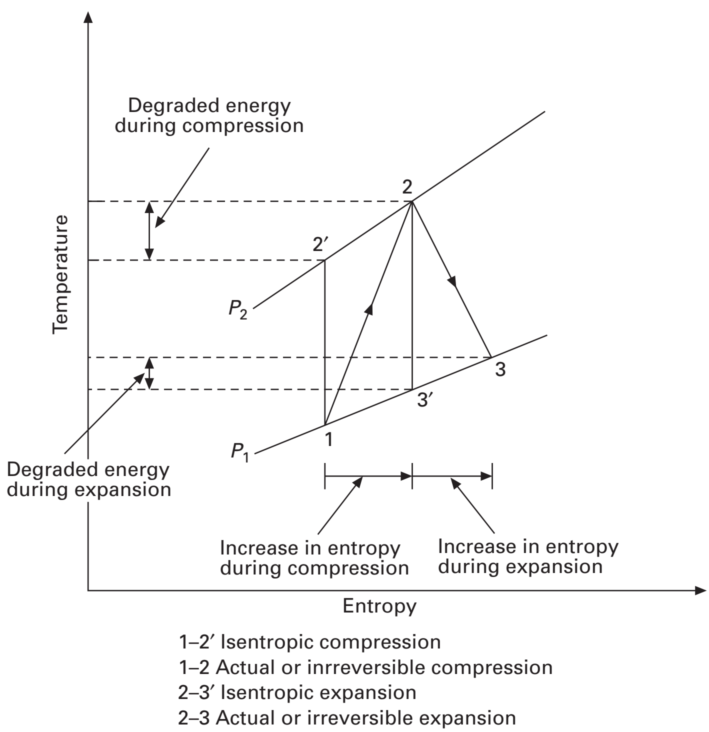

2.10 Ideal and actual compression and expansion processes on the temperature–entropy diagram.

The compression work per unit flow rate will be:

$$W_{\text{comp}} = c_p\,(T_{2'} - T_1) \qquad [2.26]$$

And the expansion work will be identical and therefore equal to:

$$W_{\text{expansion}} = c_p\,(T_{2'} - T_1) \qquad [2.27]$$

These compression and expansion processes are then said to be reversible. In practice, however, the actual compression and expansion processes, including losses, will be along the process line 1 to 2 and from 2 to 3, respectively, as is also shown in Fig. 2.10. The Figure also shows the amount of energy that has been degraded during compression and has to be supplied in addition to the theoretical amount of work needed to increase the pressure from P_1 to P_2. This additional work corresponds to $c_p(T_2 - T_{2'})$. Similarly, the energy unavailable during the expansion due to energy degradation is given by $c_p(T_3 - T_{3'})$. The resultant increases in entropy during the actual compression and expansion processes are also shown in Fig. 2.10.

The efficiency of the compression process may be defined as the ratio of the ideal compression work to the actual compression work. For an expansion process, the efficiency is the ratio of the actual expansion work to the ideal expansion work. The efficiency will be less than unity because of the presence of irreversibilities.

2.8.2 Isentropic efficiency

The definition for efficiency given in Section 2.8.1 is indeed the isentropic efficiency and, referring to Fig. 2.10, the compressor efficiency is therefore given by:

$$\eta_c = \frac{c_p\,(T_{2'} - T_1)}{c_p\,(T_2 - T_1)} = \frac{T_{2'} - T_1}{T_2 - T_1} \qquad [2.28]$$

For an isentropic process $\dfrac{T_{2'}}{T_1} = c$

where

$c = \left(\dfrac{P_2}{P_1}\right)^{\frac{\gamma-1}{\gamma}}$. Therefore

$$\eta_c = \frac{T_1(c-1)}{T_2 - T_1} \qquad [2.29]$$

Similarly, the isentropic efficiency for an expansion process is given by:

$$\eta_c = \frac{c_p\,(T_2 - T_3)}{c_p\,(T_2 - T_{3'})} = \frac{T_2 - T_3}{T_2 - T_{3'}} \qquad [2.30]$$

For an isentropic process,

$$T_{3'}/T_2 = 1/c,$$

then

$$\eta_t = \frac{T_2 - T_3}{T_2\left(1 - \frac{1}{c}\right)} \qquad [2.31]$$

where η_t is the expander/turbine isentropic efficiency

2.8.3 Polytropic efficiency

The isentropic efficiency considers only the start and end states of the compression and expansion processes and pays no attention to the actual paths the compression and expansion processes take. Since the work is not a thermodynamic property and depends on the actual path, the polytropic analysis endeavours to account for the path taken during the compression and expansion processes in determining the actual work.

In a polytropic process, the compression or expansion process takes place in small steps (infinitesimally small steps). Calculating the work for the polytropic process involves the summation of the work for each step. To calculate the work for each infinitesimal step, we use the isentropic analysis discussed in Section 2.8.2.

For a compression process:

$$\eta_p = \frac{\mathrm{d}T'}{\mathrm{d}T} \qquad [2.32]$$

where

$\mathrm{d}T'$ is the ideal temperature rise, $\mathrm{d}T$ is the actual temperature rise for each step

η_p is now the polytropic efficiency.

For an isentropic process:

$$\frac{T'}{P^{\frac{\gamma-1}{\gamma}}} = \text{constant} \qquad [2.33]$$

where P is the pressure, and

$$\gamma = \frac{c_p}{c_v}$$

This equation in differential form is given by

$$\frac{\mathrm{d}T'}{T} = \frac{\gamma - 1}{\gamma} \times \frac{\mathrm{d}P}{P} \qquad [2.34]$$

Substituting $\mathrm{d}T'$ from Equation 2.34 into Equation 2.32:

$$\eta_p \times \frac{dT}{T} = \frac{\gamma - 1}{\gamma} \times \frac{dP}{P} \qquad [2.35]$$

Integrating Equation 2.35:

$$\eta_p = \frac{\left(\ln\left(\frac{P_2}{P_1}\right)\right)^{\frac{\gamma-1}{\gamma}}}{\ln\left(\frac{T_2}{T_1}\right)} \qquad [2.36]$$

Given the polytropic efficiency and pressure ratio, the compressor discharge temperature can be calculated from:

$$T_2 = T_1\left(\frac{P_2}{P_1}\right)^{\frac{\gamma-1}{\gamma\eta p}} \qquad [2.37]$$

Similarly, for an expansion process expanding from state 3 to 4 (expander inlet to expander exit), the polytropic efficiency is given by:

$$\eta_p = \frac{\ln\left(\frac{T_4}{T_3}\right)}{\left(\ln\left(\frac{P_4}{P_3}\right)\right)^{\frac{\gamma-1}{\gamma}}} \qquad [2.38]$$

The expander exit temperature is calculated from:

$$T_4 = T_3\left(\frac{P_4}{P_3}\right)^{\frac{\eta_p(\gamma-1)}{\gamma}} \qquad [2.39]$$

We can derive an expression relating the polytropic efficiency to the isentropic efficiency via the pressure ratio.

For a compressor, the isentropic efficiency is

$$\eta_c = \frac{T_{2'} - T_1}{T_2 - T_1} = \frac{\frac{T_{2'}}{T_1} - 1}{\frac{T_2}{T_1} - 1} \qquad [2.40]$$

Hence,

$$\eta_c = \frac{\left(\frac{P_2}{P_1}\right)^{\frac{\gamma-1}{\gamma}} - 1}{\left(\frac{P_2}{P_1}\right)^{\frac{\gamma-1}{\gamma\eta_p}} - 1} \qquad [2.41]$$

And for an expander, the isentropic efficiency is

$$\eta_t = \frac{1 - \dfrac{T_4}{T_3}}{1 - \dfrac{T_{4'}}{T_3}} \qquad [2.42]$$

Hence,

$$\eta_t = \frac{1 - \left(\dfrac{P_4}{P_3}\right)^{\frac{\eta_p(\gamma-1)}{\gamma}}}{1 - \left(\dfrac{P_4}{P_3}\right)^{\frac{\gamma-1}{\gamma}}} \qquad [2.43]$$

It can be seen from Equations 2.41 and 2.43 that, for a given polytropic efficiency, the compressor isentropic efficiency decreases, whereas the turbine isentropic efficiency increases with increase in pressure ratio. This is illustrated in Fig. 2.11, where the polytropic efficiency of the compressor and turbine is assumed to be 0.87. During the compression process, as defined by a polytropic path, there is an increase in the inlet temperature to each compression stage due to irreversibility (degradation) in the previous stage, thus resulting in increased compressor work demand. However, in a turbine this increase in temperature will be recovered partly by the expansion in the next turbine stage and this explains the different trends in the isentropic efficiencies for the compressor and turbine, as shown in Fig. 2.11. Note that the isentropic

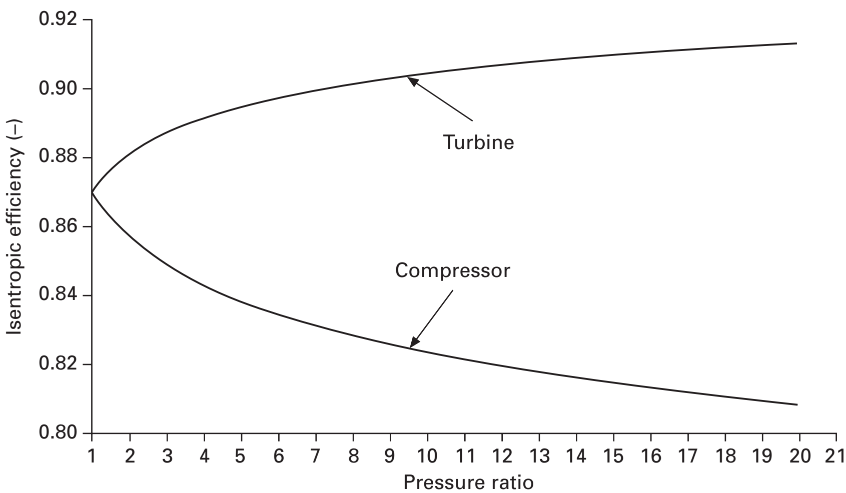

2.11 Variation of the isentropic efficiency with pressure ratio for a polytropic efficiency of 0.87.

efficiency tends to the polytropic efficiency as the pressure ratio tends to unity.

To analyse the polytropic efficiency further, let us consider an axial compressor comprising three stages increasing the pressure from P_1 to P_4, as shown in Fig. 2.12. It will be assumed that the pressure ratio in each state is small enough, such that the path described by each stage is polytropic. Furthermore, it will also be assumed that the isentropic efficiency of each stage is equal and would now be the polytropic efficiency η_p due to the small stage pressure ratio.

The stage temperature rise is given by $\Delta T_s = \Delta T_{s'}/\eta_p$ where $\Delta T_{s'}$ is the ideal stage temperature rise. The total temperature rise across the compressor would therefore be $\Delta T = 1/\eta_p \times \Sigma\Delta T_{s'}$. However, $\Delta T = \Delta T'/\eta_c$, where η_c is the isentropic efficiency of the compressor. Thus $\eta_p/\eta_c = \Sigma\Delta T_{s'}/\Delta T'$. Since lines of constant pressure diverge on the temperature–entropy diagram, $\Sigma\Delta T_{s'}$ will be greater than $\Delta T'$. Hence η_p will be greater than η_c for the compression process as discussed in Saravanamuttoo *et al.*[3]

If more stages are added to the compressor, then the difference between these two efficiencies will also increase. However, the increase in the number of stages will also increase the pressure ratio of the compressor. Thus the decrease in compressor isentropic efficiency with pressure ratio is observed as shown in Fig. 2.11.

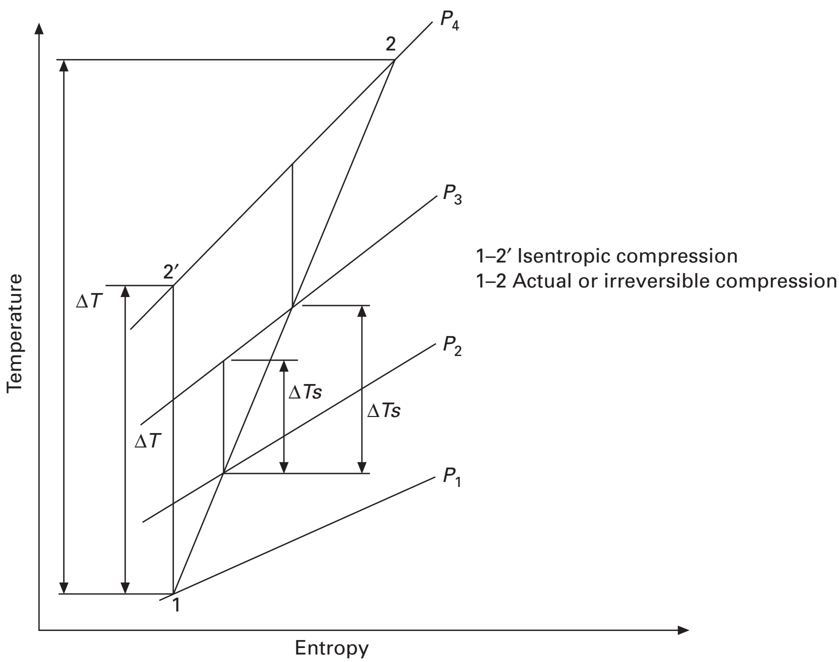

2.12 Polytropic process of a multi-stage compressor.

Similarly, it can be shown that, for a turbine, the isentropic efficiency will increase with pressure ratio and this is due to the reheating of the gas entering the next turbine stage due to the losses in the previous stage.

2.9 Effect of irreversibility on the performance of the ideal simple cycle gas turbine

It has been shown that, for an ideal simple cycle gas turbine, the thermal efficiency is dependent only on the pressure ratio and the working fluid. When irreversibilities are present, the thermal efficiency is also dependent on the cycle temperatures, namely the ratio of the maximum to minimum temperature, T_3/T_1.

Figure 2.13(a) shows a gas turbine cycle on a temperature–entropy diagram, when irreversibilities are present and no heat addition is assumed (1,2,3,4). The turbine work output will be less than the compressor work absorbed, resulting in a negative net work output from the cycle. This implies that energy has to be provided to sustain the cycle and the amount of energy needed corresponds to $c_p(T_4 - T_1)$ to make the cycle self-sustaining.

If enough heat is supplied such that the turbine work is just sufficient to drive the compressor ($c_p(T_3 - T_4) = c_p(T_2 - T_1)$), the net work output and the thermal efficiency will be zero because a finite amount of heat has to be supplied (Fig. 2.13(b)). Any further increase in heat input (i.e. T_3 increases to $T_{3'}$), then the thermal efficiency and the specific work output will also increase. Thus, when irreversibilities are present, as we would find in practice,

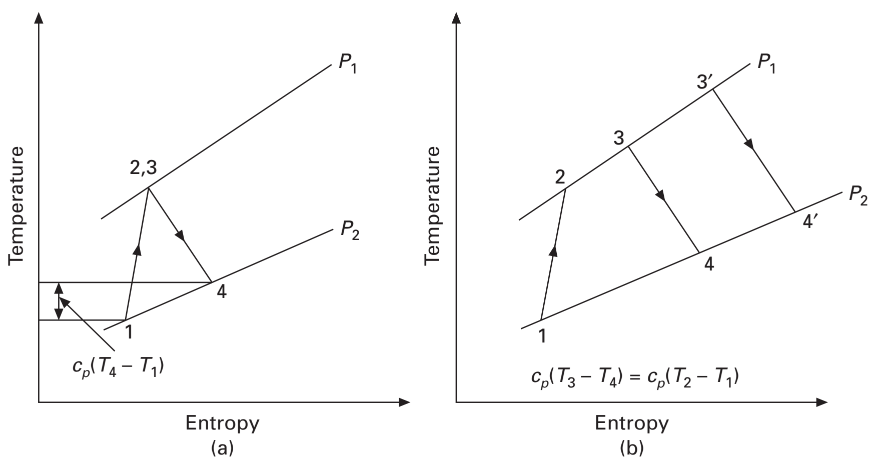

1–2 Actual or irreversible compression
2–3 and 2–3′ Constant pressure heat addition
3–4 and 3′–4′ Actual or irreversible expansion

2.13 (a) and (b) Effect of irreversibilities on temperature–entropy.

the simple cycle gas turbine performance also depends on T_3 and improves as T_3 increases. Similarly, it can be shown that the thermal efficiency of the actual or practical gas turbine increases with decrease in the minimum cycle temperature T_1. In fact, the practical gas turbine thermal efficiency is dependent on the pressure ratio and the maximum to minimum cycle temperature ratio, T_3/T_1.

2.10 Effect of pressure losses on gas turbine performance

The heat addition and the heat rejection in an ideal gas turbine cycle occur at constant pressure. In a practical gas turbine the heat is supplied by burning fuel in a combustor. The combustor and the heat addition process incur pressure losses and therefore the heat addition is not a constant pressure process in a practical gas turbine cycle. Similarly, the heat sink in a practical gas turbine cycle is the atmosphere, and the ductwork to remove the exhaust gases from the gas turbine will also incur a pressure loss. Furthermore, practical gas turbines normally operate on open cycles and air is drawn in continuously to provide fresh working fluid for the gas turbine. As a result, there is also a pressure loss in the inlet system.

The combustion pressure loss varies from about 1% of the compressor discharge pressure for an industrial gas turbine to about 5% for an aero-derived gas turbine. Inlet and exhaust losses are much smaller and a typical pressure loss is about 10 mBar. Pressure losses that occur in the combustion, inlet and exhaust systems reduce the turbine work output and increase the compressor work absorbed, therefore increasing the sensitivity of the cycle performance to cycle temperatures, namely T_3/T_1. Figure 2.14 shows the temperature–entropy diagram of a practical gas turbine cycle including combustor inlet and exhaust system losses.

2.11 Variation of specific heats

In the ideal gas turbine cycle we have assumed that the specific heat, c_p, and the isentropic index, γ, which is the ratio of specific heats (c_p/c_v), are constant during the various thermodynamic processes. In practice, however, the specific heats vary during compression, heat addition and expansion. In open cycle gas turbines, air is the working fluid and, at the normal operating pressures and temperatures that occur in a gas turbine cycle, the specific heat is only a function of temperature (i.e. air acts as a perfect gas).

Furthermore, the burning of fuel changes the composition of the air to products of combustion, hence this change is another factor affecting the specific heat and the isentropic index. The specific heats for air and products of combustion may be expressed as a polynomial in temperature or as an

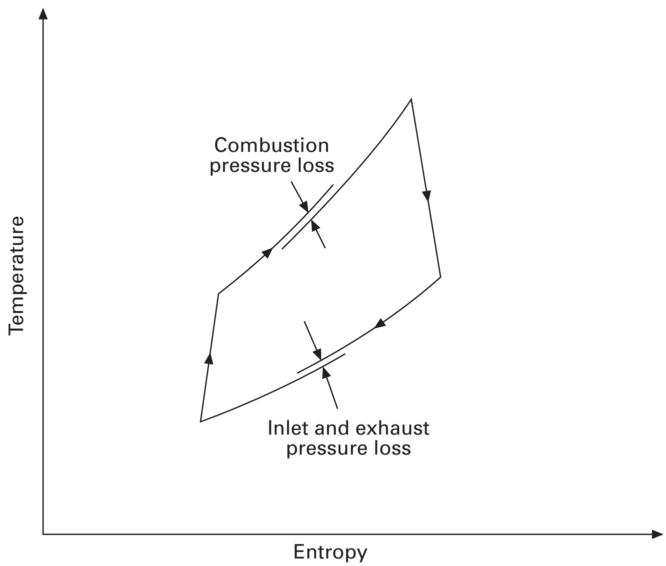

2.14 Temperature–entropy diagram for a practical gas turbine cycle.

equation as a function of temperature, as shown by Equation 2.44. The ratios of specific heats, γ, may then be calculated from Equation 2.45. Further discussion on thermo-physical properties of air and products of combustion applicable to gas turbines are discussed in Walsh and Fletcher.[4]

$$c_p = a + b\,\frac{T}{100} + c\left(\frac{T}{100}\right)^{-2} \qquad [2.44]$$

where

T is temperature in K

a, b and c are constants for a given gas; their values are given in Table 2.1. They have been taken from Harman.[5]

c_p is the specific heat at constant pressure whose units are J/kg K.

Another excellent source for thermophysical properties of air and its components is Rogers and Mayhew.[6]

$$\gamma = \frac{c_p}{c_p - R} \qquad [2.45]$$

where R is the gas constant, which is given by Equation 2.46

$$R = \frac{R_0}{MW} \qquad [2.46]$$

where

MW is the molecular weight of the air or products of combustion and R_0 is the universal gas constant.

The composition of dry air on a gravimetric or mass analysis basis is shown in Table 2.2. To determine the specific heat, c_p, of air for a given

Table 2.1 Coefficients for calculating the specific heat of air and products of combustion

Coefficients →	*a*	*b*	*c*	Molecular weight
O_2	936	13.1	–523	31.999
N_2	1020	13.4	–179	28.013
H_2O	1695	57.1	0.0	18.030
CO_2	1005	20.0	–1959	44.010
Ar	521	0.0	0.0	39.948

Table 2.2 Composition of dry air on a gravimetric basis

Component	Gravimetric or mass fraction
N_2	0.7553
O_2	0.2314
Ar	0.0128
CO_2	0.0005

temperature, we calculate the specific heat c_p for each component of air from Equation 2.44 using the corresponding constants *a*, *b* and *c* given above. The specific heat, c_p, of air for a given temperature is then computed by:

$$c_p \text{ air} = 0.7553 \times c_p\text{N}_2 + 0.2314 \times c_p\text{O}_2 + 0.0128 \times c_p\text{Ar} + 0.0005 \times cp\text{CO}_2 \quad [2.47]$$

where $c_p\text{N}_2$, $c_p\text{O}_2$, $c_p\text{Ar}$ and $c_p\text{CO}_2$ in Equation 2.47 are the specific heats for N_2, O_2, Ar and CO_2 at the given temperature, respectively, and are calculated by Equation 2.44 using the data given in Table 2.1.

When the changes in specific heat are considered in the calculation of compressor and turbine exit temperatures, the process is implicit or iterative. The iterative process begins with computation of the exit temperatures for the compression and expansion process by assuming the exit values for c_p and γ for air or products of combustions are equal to the inlet values. New c_p and γ values at exit are computed as described above and the process repeated. However, at the start of the subsequent iteration, the values for c_p and γ are based on the average temperature change in the compression or expansion process. After each iterative step, the current values of c_p and γ at the exit of the compressor or turbine are compared with the values of the previous iteration. The iterative process is repeated until there is sufficient agreement between the current and previous values of c_p and γ.

The flow chart described in Fig. 2.15 summarises the above iterative process in calculating the compressor or turbine exit temperatures for a given inlet pressure, temperature and fuel–air ratio, taking into account the variation of c_p and γ.

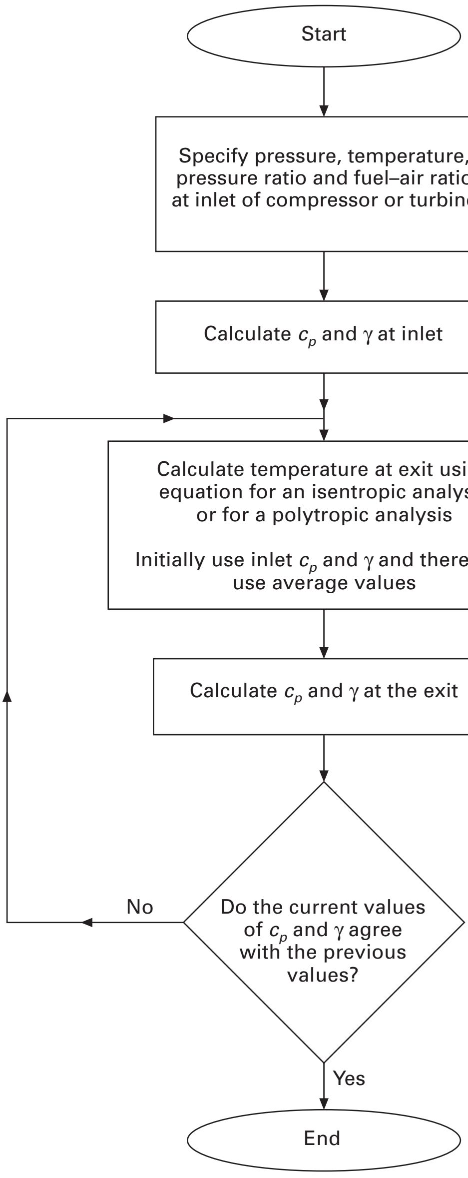

2.15 Flowchart describing the process to compute the exit temperature from a turbine or compressor when c_p and γ vary.

2.11.1 Effect of humidity

The above analysis considers the calculation of gas properties such as c_p and γ for dry air. However, air contains water vapour and, at high ambient temperatures, the effect of humidity can be significant and has to be accounted for in the calculation of the gas properties. The humidity of air is presented normally as the amount of water vapour needed to saturate the air and is referred to as the relative humidity. It is defined as the ratio of the water vapour pressure to the saturated water pressure and is given in Equation 2.48.

$$\phi = \frac{p}{p_s} \times 100 \qquad [2.48]$$

where p is vapour pressure of water, p_s is the saturated water vapour pressure and ϕ is the relative humidity as a percentage. The units for p and p_s are normally in millibars.

The saturated vapour pressure, p_s, can be determined from:

$$p_s = 6.112 \times e^{\frac{17.67 \times T}{T+243.5}} \qquad [2.49]$$

where T is the ambient temperature in Celsius.

Thus, given the ambient temperature and relative humidity, the vapour pressure of water vapour can be determined from Equation 2.48.

For gas turbine performance calculations, we need to know the amount of water vapour on a mass basis. This can now be determined using the definition of specific humidity, which is the mass of water vapour present in a unit mass of dry air and is given by Equation 2.50.

$$\omega = \frac{\text{mass}_w}{\text{mass}_a} \qquad [2.50]$$

Using Dalton's laws of partial pressures, Equation 2.50 can be represented as:

$$\omega = 0.622 \frac{p}{P - p} \qquad [2.51]$$

where P is the ambient pressure in millibars (mb).

Given the relative humidity, ambient pressure and temperature, the mass of water vapour can be determined using the equations discussed in this section. This can be incorporated in the specific heat calculations, where the c_p humid is now given by:

$$c_p \text{ humid} = c_p \text{ air} \times mf \text{ air} + c_p \text{ water} \times mf \text{ water} \qquad [2.52]$$

where

c_p humid = specific heat at constant pressure for humid air
c_p air = specific heat at constant pressure of dry air
c_p water = specific heat at constant pressure of water vapour
mf air = mass of dry air in 1 kg of humid air
mf water = mass of water vapour in 1 kg of humid air.

Clearly, specific humidity and relative humidity are related. This can be illustrated on the psychrometric chart shown in Fig. 2.16. For a given increase in relative humidity, there is also an increase in specific humidity. However, the increase in specific humidity and therefore the change in the mass of vapour in the air, are small at low ambient temperature, and are shown as the dry bulb temperature. It is at high ambient temperatures that the effects of humidity are noticeable in performance calculations. It should be pointed out that Fig. 2.16 is valid only for a given ambient pressure that corresponds to 1 bar. The impact of humidity on engine performance is discussed in Mathioudakis *et al*.[7]

2.12 Enthalpy and entropy

Although the use of mean specific heats in performance calculations gives good accuracy to within 1%, for rigorous calculations, enthalpy and entropy should be used. The specific enthalpy of a gas may be given by:

$$H = H_0 + \int c_p \, \mathrm{d}T + H^R \qquad [2.53]$$

where

H^R is the residual property and is given by:

$$H^R = -RT^2 \int \left(\frac{\partial Z}{\partial T}\right)_p \frac{\mathrm{d}P}{P} \text{ const } T \qquad [2.54]$$

For a perfect gas, the compressibility factor, Z, is very close to unity and is

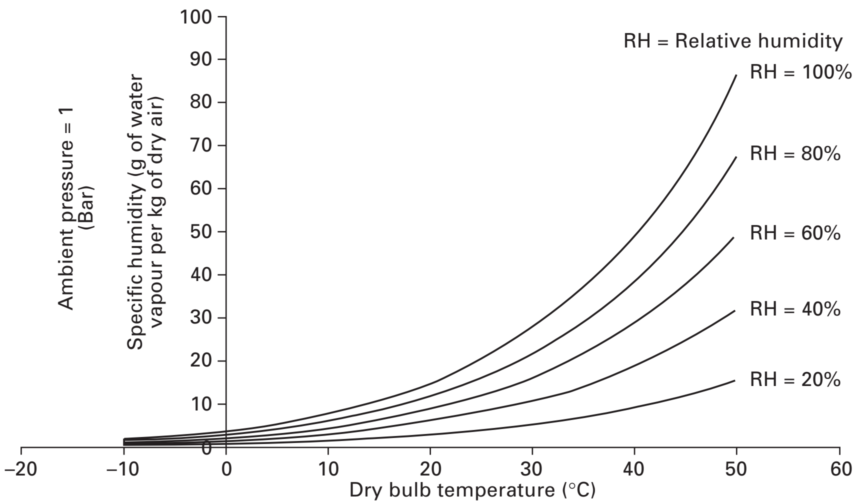

2.16 Typical psychrometric chart at a pressure of 1 Bar.

independent of pressures and temperatures that occur in gas turbines. Thus H^R can be considered to be zero. Therefore Equation 2.53 reduces to:

$$H = H_0 + \int c_p \, \mathrm{d}T \tag{2.55}$$

The specific heat, c_p, is a polynomial in temperature T or a suitable equation such as that defined by Equation 2.44. The units for specific enthalpy are kJ/kg. Since the first and second law of thermodynamics do not permit the calculation of the absolute value enthalpy, we need a reference temperature where the enthalpy is zero (usually 273 K). However, in gas turbine performance calculations, the reference specific enthalpy is unimportant as our interest is in the change in specific enthalpy in such calculations. A similar argument holds for entropy, which will be discussed next.

The specific entropy of a gas may be given as:

$$S = S_0 + \int c_p \frac{\mathrm{d}T}{T} - R \ln \frac{P}{P_0} + S^R \tag{2.56}$$

where S^R is the residual property and given by:

$$S^R = -RT \int \left(\frac{\partial Z}{\partial T}\right)_p \frac{\mathrm{d}P}{P} - \int (Z-1)\frac{\mathrm{d}P}{P} \text{ const } T \tag{2.57}$$

Again, for a perfect gas, we can neglect the residual term and Equation 2.56 reduces to:

$$S = S_0 + \int c_p \frac{\mathrm{d}T}{T} - R \ln \frac{P}{P_0} \tag{2.58}$$

The reference temperature and pressure, when the entropy is zero, is usually 273 K and 1.013 Bar-A, respectively. The units for entropy are kJ/kg K.

The evaluation of the residual terms for enthalpy and entropy requires an equation of state and these issues are discussed in detail in Smith *et al.*[8] As stated above, the temperature and pressure ranges that occur in gas turbines are such that these residual terms are very small and can be neglected (i.e. air and products of combustion behave as a perfect gas for this temperature and pressure range).

Given a pressure ratio, inlet temperature T_1 and pressure P_1, the calculation of discharge temperatures for a compression or expansion process is as follows. The inlet specific entropy, S_1, is evaluated using Equation 2.58. Using the discharge pressure for the compression or expansion process, the temperature discharge temperature $T_{2'}$ from Equation 2.58 will be calculated such that the specific entropy at the end of the compression or expansion process is equal to S_1 (i.e. isentropic compression or expansion). Using Equation 2.55, the ideal specific enthalpy, $H_{2'}$, is calculated at the compressor or turbine discharge. From Equation 2.55 the specific enthalpy at the inlet, H_1, is also calculated The isentropic efficiency equation using specific enthalpies is:

$$\eta_{\text{isen}} = \frac{H_{2'} - H_1}{H_2 - H_1} \text{ for compression} \quad [2.59]$$

or

$$\eta_{\text{isen}} = \frac{H_2 - H_1}{H_{2'} - H_1} \text{ for expansion} \quad [2.60]$$

Given an isentropic efficiency, the actual discharge specific enthalpy, H_2, is calculated for a compression or expansion process. Knowing H_2 from Equation 2.55, the discharge temperature, T_2, is calculated. The specific work, which is the work done per unit mass flow rate of air/gas, for the expansion or compression process, is simply the difference between these enthalpies (i.e. $H_2 - H_1$). A worked example using entropies and enthalpies is given in Section 2.18.3.

2.13 Combustion charts

The process described above may also be used to compute the heat input in a practical gas turbine cycle, taking into account the variation of specific heats or enthalpies during combustion. In practice, however, the heat input is computed from the combustion chart for a given fuel.

The following describes the computation of the combustion temperature rise using combustion charts. Combustion charts are normally plotted describing the combustion temperature rise with fuel–air ratio for a series of combustion inlet temperatures, as shown in Fig. 2.17, which, in this case, is applicable to kerosene. These charts are plotted for the theoretical fuel–air ratio (i.e.

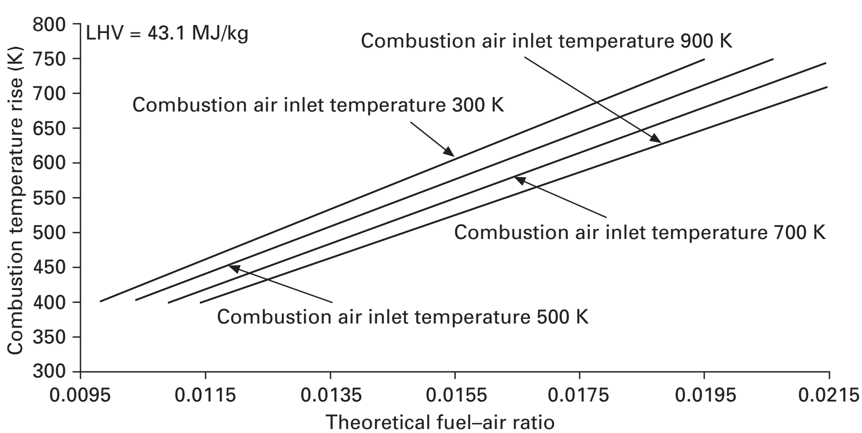

2.17 Combustion temperature rise versus fuel–air ratio.

combustion efficiency is 100%). For a given theoretical fuel–air ratio and combustion inlet temperature, the combustion temperature rise can be readily determined. If the combustion airflow is known, the theoretical heat input is calculated by $mc \times f/a \times$ LHV, where mc is the combustion air mass flow, f/a is the theoretical fuel–air ratio and LHV is the lower heating value of the fuel. For kerosene, the LHV corresponds to about 43 MJ/kg. Similarly, if the combustion temperature rise and inlet temperature are given, the theoretical fuel–air ratio can be determined.

The actual fuel–air ratios and hence the actual heat input is determined using the equation:

$$\eta b = \frac{\text{theoretical}\, f/a \text{ for a given } \Delta T}{\text{actual}\, f/a \text{ for a given } \Delta T} \qquad [2.61]$$

where ΔT is the combustion temperature rise and ηb is the combustion efficiency.

2.14 Heat exchanger performance

In Section 2.7 the design point performance of an ideal regenerative gas turbine cycle was discussed. A perfect heat exchanger results in the air exit temperature from the heat exchanger being equal to the turbine exit temperature. In addition, the exit temperature of the gas from the heat exchanger is equal to the compressor discharge temperature. In practice, these limiting temperatures are never reached due to the imperfections of the heat exchanger. An effectiveness parameter is used to determine the actual temperatures at exit from the heat exchanger and it is defined as:

$$\varepsilon = \frac{T_{a\text{out}} - T_{a\text{in}}}{T_{g\text{in}} - T_{a\text{in}}} \qquad [2.62]$$

where

ε is the heat exchanger effectiveness
$T_{a\text{out}}$ is the air temperature at exit from the heat exchanger (and will become the combustor inlet temperature) (K or Celsius)
$T_{a\text{in}}$ is the heat exchanger inlet temperature (which is also the compressor discharge temperature) (K or Celsius)
$T_{g\text{in}}$ is the heat exchanger gas inlet temperature (which is also the turbine exit temperature) (K or Celsius).

The gas temperature at exit from the heat exchanger is calculated from the energy balance according to the first law of thermodynamics and is given by:

$$T_{g\text{out}} = T_{g\text{in}} - \frac{ma \times c_p am}{c_p gm \times mg}\,(T_{a\text{out}} - T_{a\text{in}}) \qquad [2.63]$$

where

ma is the air flow rate (into the heat exchanger)
$c_p am$ is the mean specific heat at constant pressure of the air being heated in the heat exchanger (kJ/kg K)
mg is the gas flow rate into the heat exchanger from the turbine exit (kg/s)
$c_p gm$ is the mean specific heat at constant pressure of the turbine exit gases being cooled in the heat exchanger (kJ/kg K)
T_{gout} is the gas temperature at exit from the heat exchanger (K or Celsius).

Furthermore, $C = \dfrac{c_p\, am \times ma}{c_p\, gm \times mg}$ is known as the ratio of thermal capacities of air and combustion gases. This ratio must be always less than, or equal to, unity to satisfy the second law of thermodynamics.

The evaluation of the heat exchanger effectiveness depends on the type of heat exchanger. The types of heat exchangers that have been employed by gas turbines are counter- and cross-flow recuperators, where the heat exchange takes place through a separating (conducting) wall, and regenerators. With regenerators, the hot exhaust gases heats a matrix, after which the cold air is passed through the matrix to absorb the heat given up by the hot gases. Thus, with regenerators the matrix requires a large thermal capacity whereas with recuperators, the separating wall requires a small thermal capacity and good conduction.

The effectiveness of the heat exchanger may be determined from its performance curves, which depend on the type of the heat exchanger, as discussed above. The performance curves for a heat exchanger are shown in Fig. 2.18, where the effectiveness of the heat exchanger is plotted against the

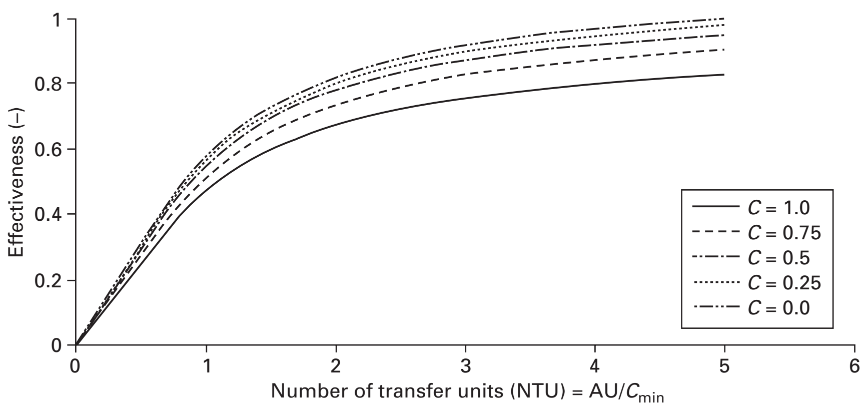

2.18 Performance curves of a typical counter flow heat exchanger.

number of transfer units (NTU), for a series of thermal capacity ratios (C) of the cold and hot fluids. NTU is defined as:

$$\mathrm{NTU} = \frac{UA}{C_{\mathrm{min}}} \qquad [2.64]$$

where

U is the overall heat transfer coefficient (kW/m^2 K)
A is the heat transfer area of the heat exchanger (m^2), and
C_{min} is the smallest thermal capacity of the two fluids (kW/kg K).

The calculation of the overall heat transfer coefficient is given in detail in Kays and London[9] and in Simonson.[10] It is observed that the effectiveness of the heat exchanger depends on C, which is the ratio of the thermal capacities of the air and combustion gases. In gas turbines, the exhaust flow normally has a higher thermal capacity due to the higher temperatures, and different gas composition due to combustion. Typically, the values of thermal capacity ratio, C, for gas turbines are in the range of 0.97 to 1.0 and this restricts the effectiveness of the heat exchanger to about 0.9. Currently, regenerative gas turbines are not very common due to the improved performance of the simple cycle gas turbine. However, they will appear in the future, particularly when intercooling and reheat gas turbines are considered as the means to increase the thermal efficiency of the gas turbine to over 50%. These features will be discussed in Chapter 3. Regenerative gas turbines are also capable of achieving better off-design thermal efficiency when compared with the simple cycle gas turbine. They are likely to appear in mechanical drive and naval applications, where a substantial amount of operation may occur at reduced power conditions.

2.15 Performance of an actual (practical) simple cycle gas turbine

The above analysis discussed the performance of an ideal simple cycle gas turbine where the compression and expansion were assumed to be reversible. The effects of irreversibility were also discussed and it was shown that the thermal efficiency for an actual cycle is dependent on the maximum to minimum cycle temperature ratio (T_3/T_1) and on the pressure ratio. This is illustrated in Fig. 2.19, where the thermal efficiency is plotted for a series of maximum cycle temperatures (T_3). Note T_1 is set to 288 K. These curves have been drawn for a compressor and turbine polytropic efficiency of 87%, respectively.

Three values of T_3 varying from 700 K to 900 K, enable comparison of the performance with the ideal simple cycle as discussed in Section 2.6. The variation of thermal efficiency with pressure ratio for a maximum cycle

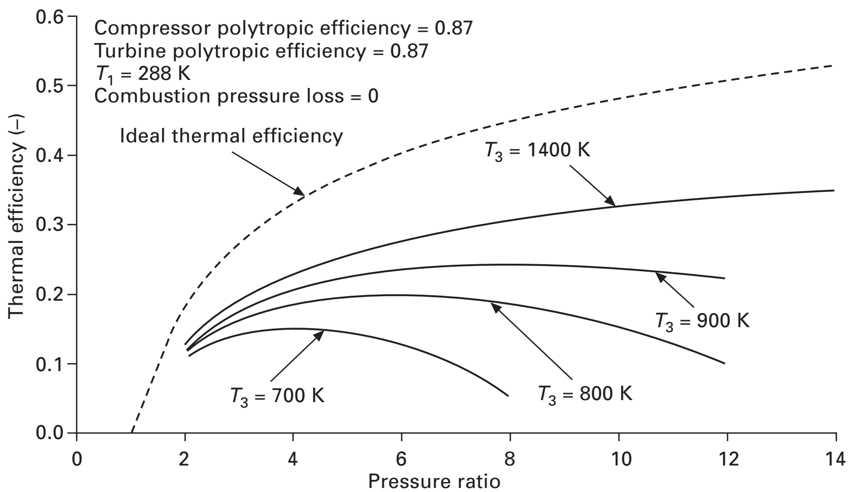

2.19 Simple gas turbine thermal efficiency varying with pressure ratio.

temperature of 1400 K is also shown and is likely to be found in existing gas turbines. The ideal cycle thermal efficiency is also shown for comparison. Unlike the ideal cycle case, the thermal efficiency initially increases with pressure ratio and then decreases as the pressure ratio is further increased. The thermal efficiency therefore peaks and the peak thermal efficiency, and the pressure ratio at which it occurs, also increase with T_3. For example, when T_3 equals 700 K, the peak efficiency occurs at a pressure ratio of about 4 and corresponds to about 15%. At a T_3 value of 900 K, the peak thermal efficiency occurs at a pressure ratio of about 8 and the peak thermal efficiency is about 24%.

Although the specific work of an ideal cycle is dependent on the maximum to minimum cycle temperature ratio, the effect of irreversibility is to reduce the specific work, as illustrated in Fig. 2.20. The ideal specific work is also shown in dotted lines for comparison. The peak specific work occurs at a pressure ratio lower than that where the maximum thermal efficiency occurs. For example, at a T_3 value of 700 K, the maximum specific work occurs at a pressure ratio of about 3, whereas the maximum thermal efficiency occurs at a pressure ratio of 4 (see Fig. 2.19). The maximum specific work corresponds to about 44 kJ/kg. When T_3 equals 900 K, the maximum specific work corresponds to about 98 kJ/kg and the pressure ratio is about 5. The maximum thermal efficiency, when T_3 equals 900 K, occurs at a pressure ratio of about 8. At a maximum cycle temperature of 1400 K, the maximum thermal efficiency occurs at a pressure ratio greater than 14, whereas the maximum specific work occurs at about 12. The thermal efficiency and specific work are significantly greater for this case, which corresponds to about 35% and 315kJ/kg, respectively.

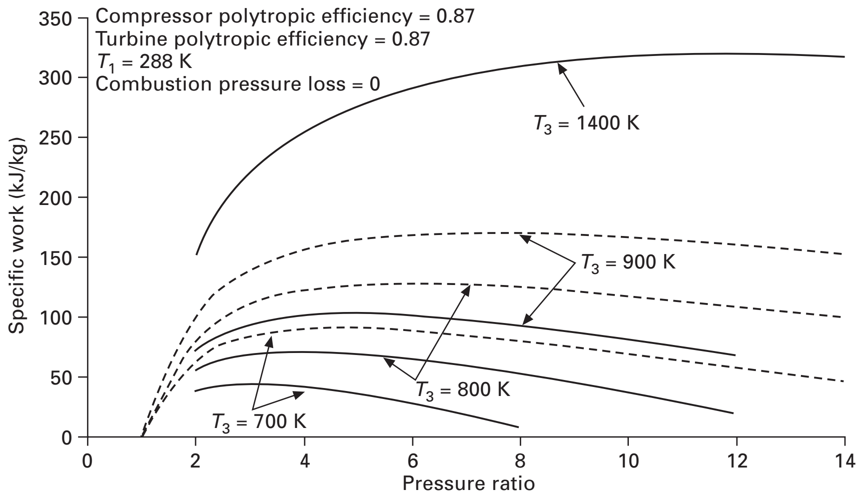

2.20 Variation of specific work with pressure ratio.

Increasing the maximum cycle temperature and pressure ratio generally increases the thermal efficiency and specific work. The increase in thermal efficiency results in reduced fuel consumption and the increase in specific work reduces the size of the gas turbine. As stated, the values for T_3 and pressure ratios are rather low for a practical gas turbine because of low thermal efficiency, and the gas turbine will be large due to a low specific work output. Currently, gas turbine designs can utilise a maximum cycle temperature up to about 1800 K and pressure ratios up to about 45. This range is illustrated in Fig. 2.21, where the performance of a practical gas turbine is displayed when operating at current values for pressure ratios and maximum cycle temperatures.

Maximum cycle temperatures are unlikely to exceed 1800 K because at higher temperatures NO_x emissions become prohibitive, as discussed in Chapter 6. At higher maximum cycle temperatures, there are claims that the thermal efficiency may actually decrease, as reported by Wilcock *et al.*[11] The changes in gas properties (increase in *cp* and decrease in γ) of the actual combustion gases at such high temperatures introduce irreversibilities into the cycle and could explain this unexpected performance behaviour.

At a pressure ratio of 20 and a maximum cycle temperature of 1400 K, the thermal efficiency and specific work correspond to about 36% and 300 kJ/kg, respectively. These values are more typical for existing gas turbines. As stated above, gas turbines operating at a maximum cycle temperature of 1800 K and pressure ratio of 40 have been developed with increased compressor and turbine efficiencies, thus improving the thermal efficiency of the gas turbine further. With such developments, the thermal efficiency of simple cycle gas turbines has increased to about 42%.

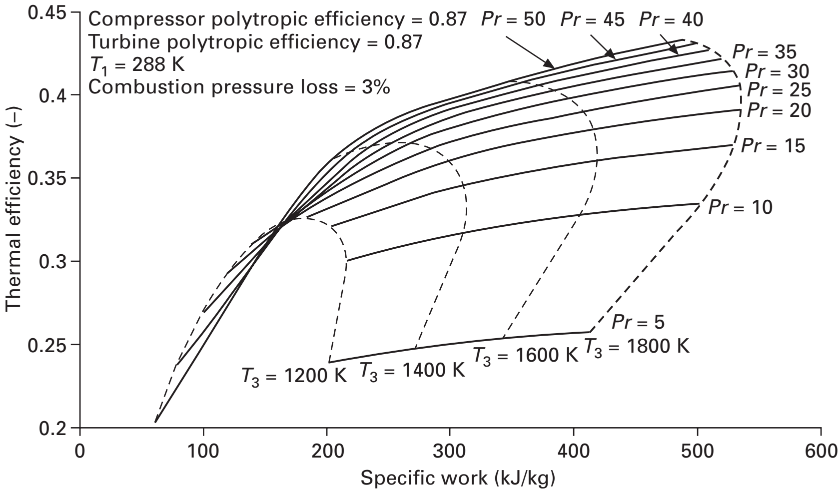

2.21 Performance of a practical simple gas turbine cycle as a carpet plot for a series of maximum cycle temperatures and pressure ratios.

2.16 Performance of an actual (practical) regenerative gas turbine cycle

From the analysis of an ideal regenerative gas turbine cycle in Section 2.7, it was shown that the efficiency increases with decrease in pressure ratio, and the limiting value for the thermal efficiency occurs when the pressure ratio tends to unity. The thermal efficiency under this limiting case corresponds to the Carnot efficiency. However, when the pressure ratio tends to unity, the specific work tends to zero and this limiting case is only of academic interest.

In the forementioned description of the ideal case, it was assumed that the heat exchanger was perfect and therefore had an effectiveness of unity. In a practical cycle, however, the effectiveness is less than unity. When the pressure ratio tends to unity, the imperfection in the heat exchanger will require a finite amount of heat to be supplied to maintain the required value of the maximum cycle temperature, T_4. Since the work output, W, is zero and a finite amount of heat is supplied ($Q \neq 0$), the thermal efficiency, W/Q, will be zero.

This is illustrated in Fig. 2.22, where the thermal efficiency of a practical regenerative cycle is plotted against pressure ratio. Three cases of effectiveness are shown varying from 0.7 to 0.9. The practical simple cycle thermal efficiency is also shown for comparative purposes. The value of the maximum cycle temperature T_4 for both the regenerative and simple cycle cases is assumed to be 900 K.

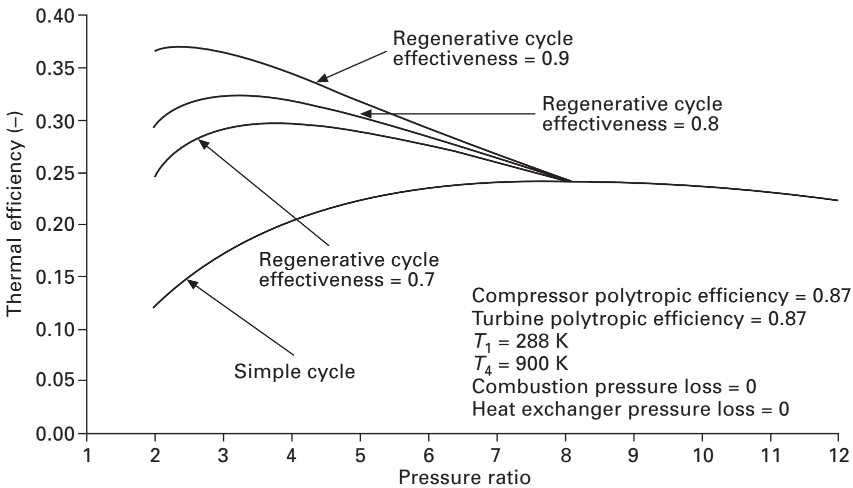

2.22 Effect of heat exchanger effectiveness on thermal efficiency.

The pressure ratio where the maximum thermal efficiency occurs is significantly less than that of a simple cycle. Furthermore, the optimum pressure ratio decreases as the heat exchanger effectiveness increases and this is expected, since the actual regenerative cycle tends towards the ideal cycle. Increasing the heat exchanger effectiveness increases the thermal efficiency as more of the waste heat can be recovered.

For a heat exchanger effectiveness of 0.7, the maximum thermal efficiency occurs at a pressure ratio of about 3.5 and the corresponding thermal efficiency is about 28%. When the effectiveness is increased to 0.9, the optimum pressure ratio is about 2.5 and the thermal efficiency is increased to about 36%. The maximum thermal efficiency of the simple cycle is about 23%, requiring a pressure ratio of about 8.

Increasing the maximum cycle temperature has a larger beneficial effect on the performance of the regenerative cycle compared with the simple cycle. This result is because the ideal regenerative cycle thermal efficiency is dependent on the ratio of the maximum to minimum cycle temperature, whereas the ideal simple cycle efficiency is independent of maximum to minimum temperature ratio. This is illustrated in Fig. 2.23, where the variation of thermal efficiency with pressure ratio is shown for a series of maximum cycle temperatures. The heat exchanger effectiveness is kept constant at a value of 0.8. The maximum cycle temperature is increased from 700 K to 900 K in steps of 100 K.

The pressure ratio corresponding to the maximum thermal efficiency increases with the maximum cycle temperature T_4. However, the increase in this pressure ratio is greater for the simple cycle compared with the regenerative cycle. The above analysis shows that regenerative cycle gas turbines are

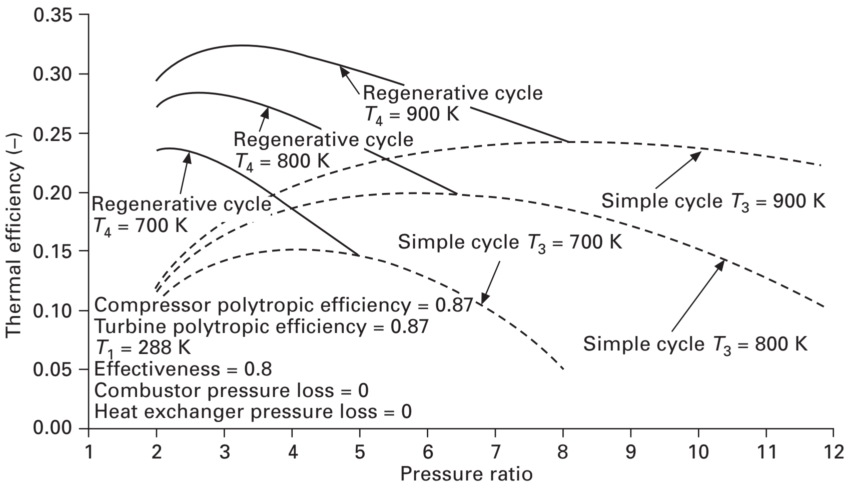

2.23 Effect of maximum cycle temperature on the thermal efficiency of a regenerative cycle.

more efficient than simple cycle gas turbines and their thermal efficiency increases significantly with increase in maximum cycle temperature and heat exchanger effectiveness. Furthermore, the pressure ratios required are smaller than that required by a simple cycle gas turbine to achieve the maximum thermal efficiency.

The specific work output curves for a regenerative cycle will be similar to those of a simple cycle, as shown in Fig. 2.20. However, the specific work of the regenerative cycle will be less than that of a simple cycle engine, resulting in a bigger gas turbine due to lower pressure ratios employed by the regenerative gas turbine. The addition of the heat exchanger will also add to the bulk and weight of the engine. Furthermore, the heat exchanger introduces an additional pressure loss in the heat addition and heat rejection processes – as discussed later. These are the main drawbacks to the regenerative cycle design. However, the lower pressure ratios required may result in a smaller compressor, compensating for part of the increased weight and bulk. The low compressor pressure ratios also result in colder cooling air temperatures that may be needed for turbine blade cooling and this will reduce the amount of cooling air requirements, as discussed in Chapter 5.

Figure 2.24 shows a carpet plot illustrating the variation of the thermal efficiency with specific work for a series of pressure ratios and maximum cycle temperatures T_4. A heat exchanger effectiveness of 0.9 is assumed and a heat exchanger pressure loss of 5% is also assumed for both the hot and cold side, respectively. The values for the maximum cycle temperatures used are more practical and therefore give an indication of what a practical regenerative cycle can achieve in terms of performance. In spite of the high

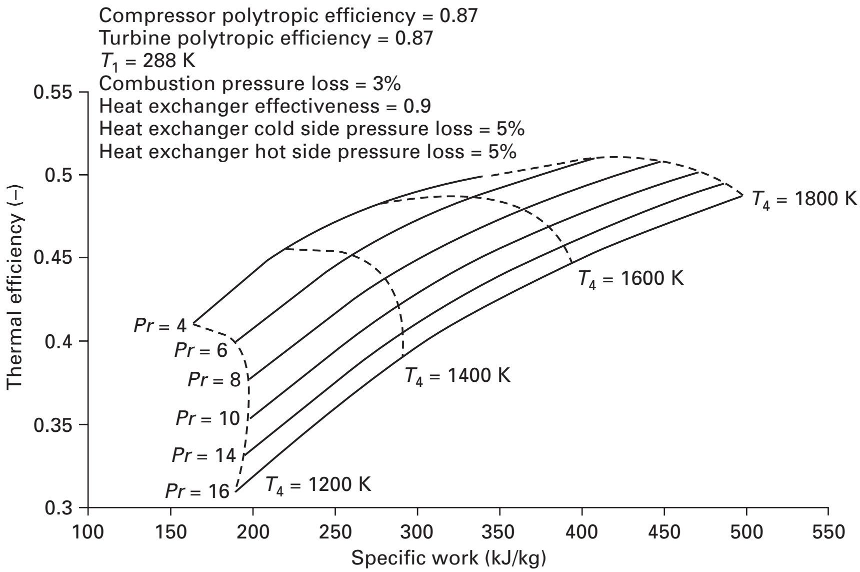

2.24 Carpet plot for a regenerative gas turbine cycle.

pressure losses in the heat exchanger, thermal efficiencies of over 50% are possible with a regenerative cycle, which compares with about 42% for a simple cycle gas turbine.

2.16.1 Effect of heat exchanger pressure losses on thermal efficiency for a regenerative cycle

The discussion in Section 2.10 described the effect of pressure losses during the heat addition and heat rejection processes on gas turbine performance. When a heat exchanger is added to the simple gas turbine cycle, the decrease in thermal efficiency of the gas turbine is generally less sensitive to these losses. The reason for the reduced sensitivity of the regenerative cycle thermal efficiency to pressure losses is primarily due to the reduction in heat input as the pressure losses increase. This is illustrated on the temperature–entropy diagram in Fig. 2.25. As the pressure losses increase, there is also an increase in the turbine (expander) exit temperature. Thus the heat available for recovery by the heat exchanger increases. This results in a reduction in the heat addition to the regenerative cycle, hence partly compensating for the reduced specific work due to the increased pressure loss. In a simple-cycle gas turbine the heat input is unaffected by increased pressure losses and consequently the thermal efficiency loss is greater and decreases proportionally with the decrease in specific work. This is illustrated in Fig. 2.26, which shows the loss in thermal efficiency due to the pressure

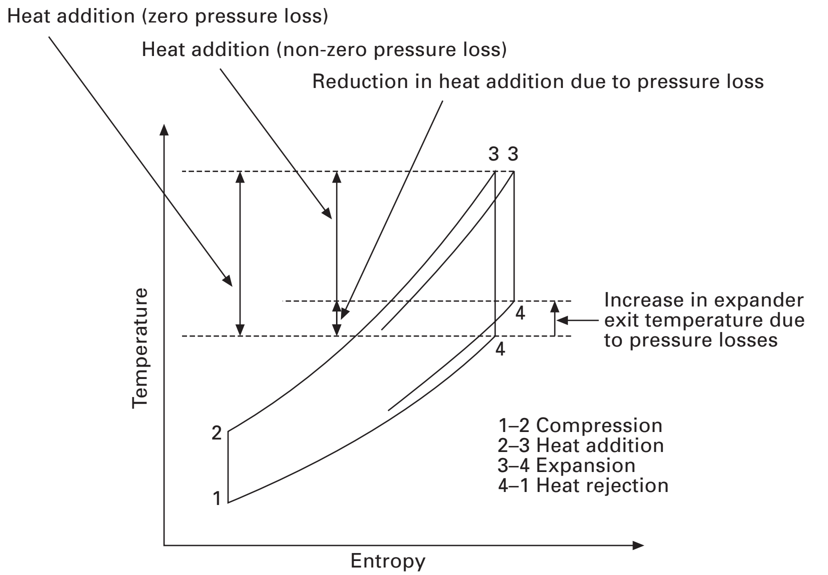

2.25 Effect of reduction in heat addition for a regenerative cycle due to pressure losses in the heat addition and rejection processes.

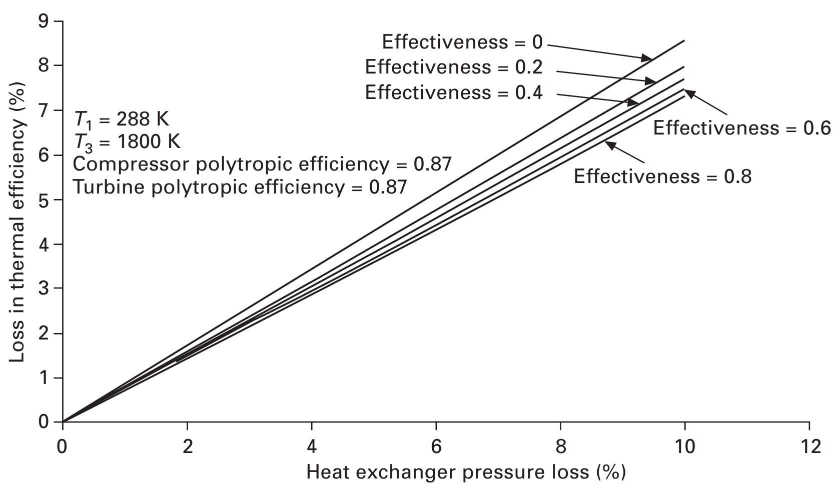

2.26 Loss in thermal efficiency due to heat exchanger pressure loss and effectiveness.

losses in the heat exchanger and for a series of heat exchanger effectiveness. It has been assumed that the losses on both the hot and cold side of the heat exchanger are equal.

2.17 Turbine entry temperature and stator outlet temperature

The maximum cycle temperatures discussed previously have varied from 1200 K to 1800 K. It has also been shown that the higher the maximum cycle temperature, the better the performance of the gas turbine cycles. It is the turbine that is subjected to high gas temperatures and the materials used in the manufacture of the turbine must be capable of withstanding such temperatures. This issue is illustrated in Fig. 2.27, which shows the trends in material temperature capability and the significant increase in turbine blade temperature that has occurred over the years. Further significant increase in gas temperature, known as the turbine entry temperature (TET), is also possible by employing cooling of the turbine, also shown in Fig. 2.27.

Turbine cooling reduces the blade temperature such that the turbine creep life remains satisfactory during operation. This technology is discussed further in Chapter 5 (Section 5.7). The cooling air is generally divided into three parts and is used to cool the stator or nozzle guide vane, the rotor and the disc, as shown in Fig. 2.28. After carrying out the cooling function, the cooling air enters the gas stream at the stator and rotor trailing edge. The mixing of the stator cooling air with the gas stream reduces the rotor inlet temperature and therefore requires a higher TET to obtain the required power from the turbine as all the work in a turbine stage is done by the rotor. Thus the rotor inlet temperature is an important parameter and many manufacturers refer to this temperature as the stator outlet temperature (SOT) or the first rotor temperature. The SOT may be as much as 150 degrees lower than the TET. The rotor cooling air is unavailable for producing power and would be

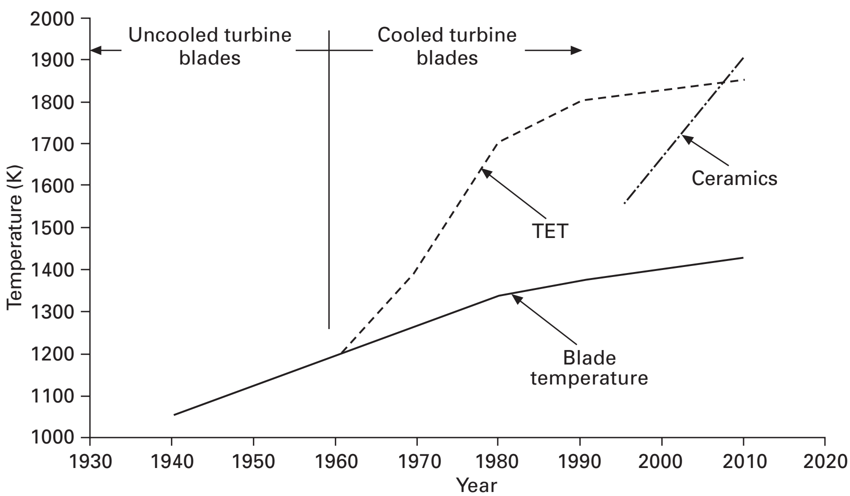

2.27 Trends in high-temperature material technology for turbines.

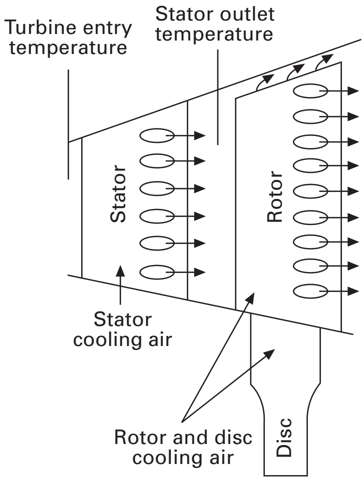

2.28 Schematic representation of a cooled turbine stage.

lost unless there is a further turbine stage downstream. The disc cooling air may enter the gas stream and contribute to turbine power production. The amount of turbine cooling air required depends on the material used for the manufacture of the turbine blades, the TET and the cooling air temperature. For high performance gas turbines, the amount of cooling bled from the high pressure stages of the compressor can amount to 15% of the total compressor flow. The turbine cooling air, of course, bypasses the combustion system of the gas turbine. Turbine cooling also compromises the performance of the turbine and thus the performance of the gas turbine engine and these matters are discussed further in Section 5.9.

Recently, steam cooling has been considered and applied to turbine cooling.[12] Here, the steam cooling system is external to the gas turbine, the drop in gas temperature across the nozzle guide vane is significantly smaller, and the SOT is typically only about 50 degrees lower than the TET with steam cooling systems. Furthermore, the penalties of loss in flow through the turbine due to air cooling systems do not apply to steam-cooled blades. A water cooling system, similar to that of steam cooling, can also be considered but such systems have proved less reliable and may present corrosion problems and produce scale deposits, thereby reducing cooling effectiveness.

2.18 Worked examples

The design point calculation of a simple cycle gas turbine will be considered using three methods. The first method, described by Rogers and Mayhew,[1] is where the gas properties, c_p and γ, are considered equal for the compression, heat addition and expansion processes. The second method corresponds to that discussed by Saravanamutto *et al.*[3] where fixed but different values for c_p and γ are used. The heat addition is determined from combustion charts as shown in Fig. 2.17. In the third method the enthalpy–entropy approach is used, as discussed in Section 2.12. The heat input is determined by using the combustion charts shown in Figure 2.17. The effect of increased turbine flow rate due to the addition of fuel in the combustor is ignored as this increased flow rate can approximately be assumed to be lost due to leakages and cooling effects.

Design point data correspond to the following:

- working media is air
- compressor inlet temperature, $T_1 = 288\,\text{K}$
- compressor inlet pressure, $P_1 = 1.013$ Bar
- compressor pressure ratio, $Rpc = 20$
- compressor isentropic efficiency, $\eta_c = 0.87$
- combustor pressure loss, $\Delta P = 5\%$ of compressor delivery pressure
- combustion efficiency, $\eta_b = 0.99$
- turbine entry temperature, $T_3 = 1400\,\text{K}$
- turbine isentropic efficiency, $\eta_t = 0.9$
- inlet and exhaust losses = 0
- fuel is kerosene

2.18.1 First method

For the first method, the values for c_p and γ are set as 1.005 and 1.4, respectively, for the compression heat addition and expansion process present in the gas turbine cycle.

From Equation 2.29 the compressor discharge temperature, T_2, is calculated by:

$$T_2 = T_1 + \frac{T_1}{\eta_c}\left((Rpc)^{\frac{\gamma-1}{\gamma}} - 1\right)$$

$$T_2 = 288 + \frac{288}{0.87}\left((20)^{\frac{1}{3.5}} - 1\right) = 736.07\,\text{K}$$

The compressor specific work input, W_c

$$W_c = 1.005 \times (736.07 - 288) = 450.31\,\text{kJ/kg}$$

and the compressor discharge pressure, P_2 equals

$$P_2 = P_1 \times Rpc = 1.013 \times 20 = 20.26 \text{ Bar-A}$$

The turbine inlet pressure, P_3 is equal to:

$$P_3 = P_2 \times (1 - \Delta P/100) = 20.26 \times (1 - 5/100) = 19.247 \text{ Bar-A}$$

Therefore the turbine pressure ratio is given by:

$$Rpt = 19.247/1.013 = 19$$

From Equation 2.31 the turbine exit temperature is given by:

$$T_4 = T_3 - T_3 \times \eta t \times \left(1 - \frac{1}{Rpt}\right)^{\frac{1}{3.5}}$$

$$T_4 = 1400 - 1400 \times 0.9 \times \left(1 - \left(\frac{1}{19}\right)^{\frac{1}{3.5}}\right) = 683.266\,\text{K}$$

and the turbine specific work output, W_t is:

$$W_t = 1.005 \times (1400 - 683.266) = 720.318\,\text{kJ/kg}$$

The specific heat input, Q_{in} is given by Equation 2.12:

$$Q_{\text{in}} = 1.005 \times (1400 - 736.07)/0.99 = 673.99\,\text{kJ/kg}$$

The net turbine specific work, $W_{\text{net}} = W_t - W_c$

$$W_{\text{net}} = 720.318 - 450.31 = 270.01\,\text{kJ/kg}$$

The thermal efficiency is the ratio of the net turbine specific work to the heat input. The thermal efficiency, η_{th}, is therefore:

$$\eta_{\text{th}} = \frac{270.01}{673.99} = 0.401$$

2.18.2 Second method

The second method also considers fixed values for c_p and γ but uses different values for the compression and expansion processes. These values for the compression process are the same as those used in the first method. Therefore, the compressor discharge temperature and the compressor specific work are the same as that calculated in Section 2.18.1. Thus:

$$T_2 = 736.07\,\text{K}$$

$$Wc = 450.31\,\text{kJ/kg}$$

Since the compressor pressure ratio and the combustor pressure loss are the same as above, the compressor discharge pressure and turbine inlet pressure would also be the same as that determined in Section 2.18.1. Therefore:

$$P_2 = 20.26 \text{ Bar-A}$$

The turbine inlet pressure is equal to:

$$P_3 = 19.247 \text{ Bar-A}$$

The combustion temperature rise $T_{32} = T_3 - T_2$.

$$T_{32} = 1400 - 736.07 = 663.93\,\text{K}$$

For the combustor inlet temperature of 736.07 K, which is equal to the compressor discharge temperature, and combustor temperature rise of 663.93 K, from Fig. 2.17 the theoretical fuel–air f is 0.0195. The actual fuel–air ratio $f_a = f/\eta b$. Thus the actual fuel–air ratio is $f_a = 0.0197$. We have assumed the fuel is kerosene, which has a lower heating value (LHV): Q_{net} is 43 100 kJ/kg. Therefore, the specific heat input is equal to:

$$Q_{\text{in}} = f_a \times Q_{\text{net}} = 0.0197 \times 43\,100 = 849.07\,\text{kJ/kg}$$

For the expansion process we shall assume that c_p and γ are 1.148 and 1.333, respectively. The turbine exit temperature equals:

$$T_4 = 1400 - 1400 \times 0.9 \times \left(1 - \left(\frac{1}{19}\right)^{\frac{0.333}{1.333}}\right) = 743.84\,\text{K}$$

The turbine specific work is:

$$Wt = 1.148 \times (1400 - 743.84) = 753.318\,\text{kJ/kg}$$

The net specific work is

$$W_{\text{net}} = 753.318 - 450.31 = 303.008\,\text{kJ/kg}$$

The thermal efficiency for this case is:

$$\eta_{\text{th}} = \frac{303.008}{849.07} = 0.35687$$

2.18.3 Third method

The third method determines the performance of the gas turbine using the enthalpies and entropies at the various salient points in the cycle. It is considered the most accurate method for calculating the design point performance of a gas turbine. The method is much more detailed and is usually carried out using a computer program developed for this purpose. However, the processes involved will be outlined.

Integrating Equation 2.44, which describes the variation of specific heat with temperature for air and products of combustion, equations for enthalpy and entropy can be developed. Therefore:

$$H = a(T - T_0) + b\frac{T^2 - T_0^2}{2} - c\left(\frac{1}{T} - \frac{1}{T_0}\right) \qquad [2.65]$$

$$S = a \ln \frac{T}{T_0} + b(T - T_0) - \frac{c}{2}\left(\frac{1}{T^2} - \frac{1}{T_0^2}\right) - R \ln \frac{P}{P_0} \qquad [2.66]$$

where T and P are the temperature and pressure of air or gas, respectively, and T_0 and P_0 are the reference temperature and pressure when the enthalpy and entropy, respectively, are assumed to be zero, when the temperature and pressure are 273 K and 1.013 Bar-A, respectively.

The constants a, b and c are determined as follows:

$$a = \sum_{i=1}^{\text{noc}} a_i \times mf_i$$

$$b = \sum_{i=1}^{\text{noc}} b_i \times mf_i$$

$$c = \sum_{i=1}^{\text{noc}} c_i \times mf_i$$

a_i, b_i and c_i are the constants defined in Table 2.1 for each component and *noc* are the number of components in air or products of combustion.

In the example, the compressor inlet pressure and temperature is 1.013 Bar and 288 K. From Equations 2.65 and 2.66 we calculate the enthalpy and entropy at the compressor inlet as:

$$H_1 = 14.876 \text{ kJ/kg}$$

$$S_1 = 0.053 \text{ kJ/kg K.}$$

For a compressor pressure ratio of 20, the compressor discharge pressure, P_2 = 20.26 Bar-A. From Equation 2.66 the isentropic compressor discharge temperature can be determined. This is achieved by using P_2 for the pressure term in Equation 2.66 and varying the temperature until the entropy equals 0.053 kJ/kg K. The isentropic compressor discharge temperature, $T_{2'}$, works out to:

$$T_{2'} = 659.452 \text{ K.}$$

Using this value in Equation 2.65, the enthalpy at compressor discharge, $H_{2'}$ due to isentropic compression is obtained:

$$H_{2'} = 402.286 \text{ kJ/kg}$$

The isentropic efficiency Equation 2.28 for a compression process can be written in terms of enthalpies as:

$\eta_c = \dfrac{H_{2'} - H_1}{H_2 - H_1}$ where H_2 is the actual enthalpy at the discharge of the compressor which corresponds to:

$$H_2 = 460.175 \text{ kJ/kg}$$

Using the value for H_2 in Equation 2.65, the actual compressor discharge temperature, T_2, can be determined implicitly:

$$T_2 = 713.102\,\text{K}$$

The compressor-specific work: $Wc = H_2 - H_1$. Therefore:

$$Wc = 445.3 \text{ kJ/kg}$$

The fuel–air ratio may now be computed similarly to that discussed in Method 2. The combustor inlet temperature and combustor temperature rise for this case are 702.86 K and 697.14 K, respectively. A theoretical fuel–air ratio, f, of 0.0195 is obtained. The actual fuel–air ratio, $f_a = 0.0195/0.99 = 0.0197$. The heat input Q_{in} is:

$$Q_{\text{in}} = 0.0197 \times 43100 = 849.388 \text{ kJ/kg}$$

The fuel used is kerosene and can be modelled as $C_{12}H_{24}$. Knowing the fuel–air ratio and the air composition, the composition of the products of combustion can be calculated, as described by Goodger.[13]

$$\mathrm{C}_x\mathrm{H}_y + m\left(\mathrm{O}_2 + \frac{0.7809}{0.2095}\mathrm{N}_2 + \frac{0.0093}{0.2095}\mathrm{Ar} + \frac{0.0003}{0.2095}\mathrm{CO}_2\right)$$

$$= n_1\mathrm{CO}_2 + n_2\mathrm{H}_2\mathrm{O} + n_3\mathrm{N}_2 + n_4\,\mathrm{Ar} + n_5\mathrm{O}_2 \qquad [2.67]$$

The quantities 0.7809, 0.0093, 0.003 and 0.2095 are the volume-fractions or molar-fractions (mole-fraction) of N_2, Ar, CO_2 and O_2 in air, respectively, and n_1, n_2, n_3, n_4 and n_5 are the mole-fraction of CO_2, H_2O, N_2, Ar and O_2 in the products of combustion, respectively. The terms x and y are the mole-fractions of carbon and hydrogen in the fuel. For kerosene, $x = 12$ and $y = 24$ and the term m is the excess air which is determined using the fuel–air ratio (f_a) as follows:

$$f_a = \frac{12.01x + 1.008y}{\left(1 + \frac{0.7809}{0.2095} + \frac{0.0093}{0.2095} + \frac{0.0003}{0.2095}\right)MW}$$

where MW is the mole-weight of air and the factors 12.01 and 1.008 are the atomic weights of carbon and hydrogen, respectively.

By performing a molar balance using Equation 2.67, the mole-fraction of the products of combustion (n_1, n_2, n_3, n_4 and n_5) can be determined in a manner similar to that discussed in Chapter 6 (Section 6.18.4).

Since the turbine entry temperature, T_3, pressure, P_3, and the combustion gas composition are now known, Equations 2.65 and 2.66 can be used to determine the enthalpy, H_3 and entropy, S_3 at turbine entry. The enthalpy at the exit due to isentropic expansion must be determined. This is achieved by using Equation 2.66 and varying the turbine exit temperature, T_4, until the entropy equals the value determined at the inlet of the turbine, S_3. From

Equation 2.65 the enthalpy, $H_{4'}$ at turbine exit due to isentropic expansion can be determined. The turbine isentropic efficiency in Equation 2.30 can be represented as:

$$\eta_t = \frac{H_3 - H_4}{H_3 - H_{4'}}$$

where H_4 is the actual enthalpy at turbine exit.

The values for H_3, S_3 and $H_{4'}$ are 1272.995 kJ/kg, 0.958 kJ/kg K and 428.005 kJ/kg, respectively. For a turbine isentropic efficiency of 0.9, the actual enthalpy at exit from the turbine is 512.504 kJ/kg and the entropy at turbine exit is 1.0768 kJ/kg K. Thus the turbine specific work, Wt, is:

$$Wt = H_3 - H_4 = 1272.995 - 512.504 = 760.491 \text{ kJ/kg}$$

The net specific work (W_{net}) from the gas turbine is:

$$W_{\text{net}} = Wc - Wt = 760.491 - 445.3 = 315.191 \text{kJ/kg}$$

The thermal efficiency (η_{th}) is:

$$\eta_{\text{th}} = \frac{W_{\text{net}}}{Q_{\text{in}}} = \frac{315.191}{849.388} = 0.3711.$$

The specific heats at the salient points 1, 2, 3 and 4, as shown in Fig. 2.29, correspond to 1.0011, 1.083, 1.2193 and 1.1198, respectively. The corresponding values for the ratios of specific heats, $\gamma = c_p/c_v$, at the salient points 1, 2, 3 and 4 are 1.402, 1.3607, 1.3082 and 1.345, respectively. The increase in c_p due to compression is due to the increase in temperature as described by Equation 2.44. Similarly, there is an increase in c_p at salient point 3 and a decrease at point 4. However, the increase in c_p at point 3 is

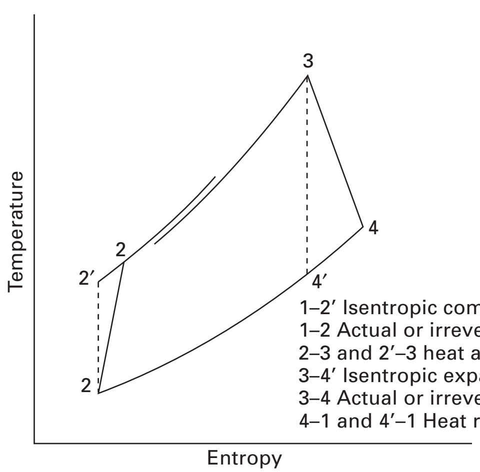

2.29 Turbine cycle on the temperature–entropy diagram.

also due to the increase in water vapour in the products of combustion, which is significant, as can be seen in Table 2.3. Also, note there is an increase in CO_2 content in the products of combustion, a greenhouse gas and thought to be responsible for global warming. Therefore, gas turbines operating with fuels such as natural gas or methane, which have a higher hydrogen content, will result in increased specific work due the high content of water vapour in the products of combustion. With methane as fuel, this increase in power output may be as high as 2% compared with that when using kerosene. Note that the increases in specific heats have resulted in a decrease in γ.

The above example considered dry air. The effects of humidity can also be included in the analysis. For example, given the relative humidity of the air, the specific humidity can be calculated, as discussed in Section 2.11.1, which is the mass of water vapour per unit of dry air. Therefore, the specific humidity can be added to the composition of air as shown in Table 2.2 and air/gas composition normalised to determine the gravimetric composition of moist/humid air and then repeat the above procedure. The additional heat input required to heat the water vapour from the compressor discharge temperature, T_2, to the turbine entry temperature, T_3, needs to be calculated. This can be determined using Equation 2.68:

$$H_s = 2.232T_s + 2352.623 \tag{2.68}$$

where H_s is the water/steam enthalpy (kJ/kg) and T_s is the water vapour/steam temperature in Celsius.

2.18.4 Summary of calculations

Table 2.4 summarises the error due to the different methods of calculating the design point performance of gas turbines. Error 1 in Table 2.4 is the percentage error between Method 1 and 3 and Error 2 is the percentage error between Method 2 and 3. Note that the first method gives the greatest error, particularly in the heat input. This is because the method of calculating the heat input pays no attention to the change in gas composition during combustion. The error using Method 2 is quite small and this is because we are calculating the heat input using combustion curves and endeavouring to adjust for the

Table 2.3 Composition of products of combustion

Component	Gravimetric or mass fraction
N_2	0.744
O_2	0.162
Ar	0.009
CO_2	0.061
H_2O	0.025

Table 2.4 Error in methods of calculating the design point performance of gas turbines relative to Method 3

Method→	1	2	3	Error 1 (%)	Error 2 (%)
T_2 (K)	736.07	736.07	713.102	3.221	3.221
Wc (kJ/kg)	450.631	450.631	445.3	1.197	1.197
Q_{in} (kJ/kg)	673.99	836.14	849.388	20.65	−1.597
T_4 (K)	683.266	743.84	750.103	−8.91	−0.835
Wt (kJ/kg)	720.318	753.27	760.491	−5.283	−0.95
W_{net} (kJ/kg)	270.01	303.008	315.191	−14.334	−3.865
η_{th}(−)	0.401	0.35687	0.3711	8.057	−3.835

change in gas composition by using different values for c_p and γ during expansion. Since these values are closer to the true average values for c_p and γ, the errors in the calculation of the design point performance are small. It must be pointed out that Method 2 is unsuitable for designing gas turbines and Method 3 should be adopted. However, Method 2 gives a quick way of estimating the design point performance of gas turbines.

2.19 References

1. *Engineering Thermodynamics, Work and Heat Transfer*, 4th Edition. Rogers, G.F.C. and Mayhew, Y.R., Longman (1992).
2. *Applied Thermodynamics for Engineers and Technologists*, 5th Edition, Eastop, T.D. and McConkey, A., Longman (1993).
3. *Gas Turbine Theory*, 5th Edition, Saravanamuttoo H.I.H., Rogers, G.F.C. and Cohen, H, Longman (2001).
4. *Gas Turbine Performance*, 2nd Edition, Walsh, P.P. and Fletcher, P., Blackwell Publishing (2004).
5. *Gas Turbine Engineering,* Harman*,* R.T.C.*,* Macmillan Press (1981).
6. *Thermodynamic and Transport Properties of Fluids*, Rogers, G.F.C. and Mayhew, Y.R., Blackwell (1994).
7. Increasing diagnostics effectiveness by inclusion of fuel composition and water injection effects, Mathioudakis, K., Aretakis, N. and Tsalavoutas, A., *ASME Turbo Expo 2002*, Paper GT-2002-30032, (2002).
8. *Introduction to Chemical Engineering Thermodynamics*, 5th Edition, Smith, J.M., Van Ness, H.C. and Abbot, M.M., McGraw-Hill (1996).
9. *Compact Heat Exchangers*, Kays, W.M and London, A.L., MacGraw-Hill (1964).
10. *Engineering Heat Transfer*, Simonson, J.R., Macmillan Press (1975).
11. Gas properties as a limit to gas turbine performance, Wilcock, R.C., Young, J.B. and Horlock, J.H., *ASME Paper GT-2002-30517*, (2002).
12. H system steams on, *Modern Power Systems*, February 2004.
13. *Hydrocarbon Fuels*, Goodger, E.M., Macmillan Press (1975).

3
Complex gas turbine cycle

In Chapter 2 the design point performance of the simple cycle gas turbine, which consists of a compressor, combustor and turbine, was considered. Although the inclusion of a heat exchanger (referred to as the regenerative cycle) was also considered, it is the addition of intercooling to reduce the compressor work, and reheat to augment the turbine work, that are usually referred to as complex cycles. In this chapter the design point performance of such cycles, including the addition of a heat exchanger, will be considered.

3.1 Intercooled gas turbine cycles

When the performance of the simple and regenerative cycle gas turbine was considered, it was assumed that the compression process was isentropic. The compression work required by these cycles may be reduced by dividing the compression process into two stages. These comprise the LP and the HP stages as shown in Fig. 3.1, and also cooling to reduce the LP compressor discharge air temperature, T_2, back to its inlet temperature (i.e. reducing T_3 to T_1). It was shown in Chapter 2 that the compressor-specific work requirement to achieve a given pressure ratio is given by:

$$W_{\mathrm{comp}} = c_p(T_2 - T_1)$$

which, for an isentropic process, can be expressed as

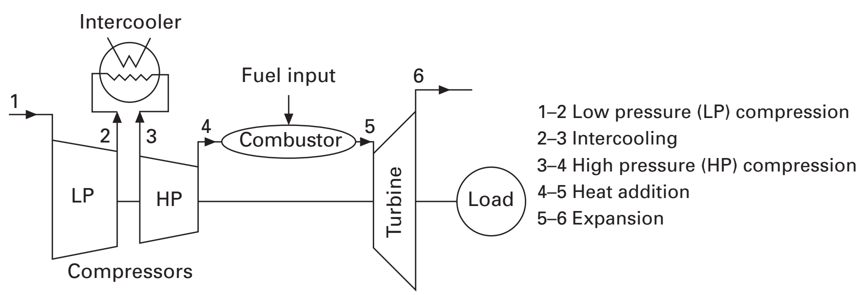

3.1 Schematic representation of an intercooled gas turbine.

$$W_{comp} = c_p\, T_1\,((Pr)^{\frac{\gamma-1}{\gamma}} - 1)$$

Therefore, reducing T_1 will reduce the compressor work required to achieve a given compressor pressure ratio, Pr. Thus, intercooling results in a reduction in the compressor work requirement of the HP compressor and hence reduces the overall compression work required to achieve a given overall compressor pressure ratio, P_4/P_1.

3.1.1 Optimisation of intercooled compressors

The optimisation of an intercooled compressor involves the determination of the LP and HP compressor pressure ratios such that the compression power required is a minimum. If the LP compressor pressure ratio is unity or equal to the overall pressure ratio, P_4/P_1, then no reduction in compressor work absorbed will occur. The question that arises is 'what LP compressor pressure ratio will result in the minimum compressor work absorbed'. The compression process for intercooled compressors is shown on the temperature–entropy diagram in Fig. 3.2 for an arbitrary value for the LP compressor ratio, Pr_{lp}. The HP pressure ratio, Pr_{hp}, will then be given by Pr_o/Pr_{lp}, where Pr_o is the overall pressure ratio, P_4/P_1. The compression work, W_{comp}, is therefore:

$$W_{comp} = c_p(T_2 - T_1) + c_p(T_4 - T_3)$$

Since $T_3 = T_1$ due to intercooling

$$W_{comp} = c_p[(T_2 - T_1) + c_p(T_4 - T_1)] \qquad [3.1]$$

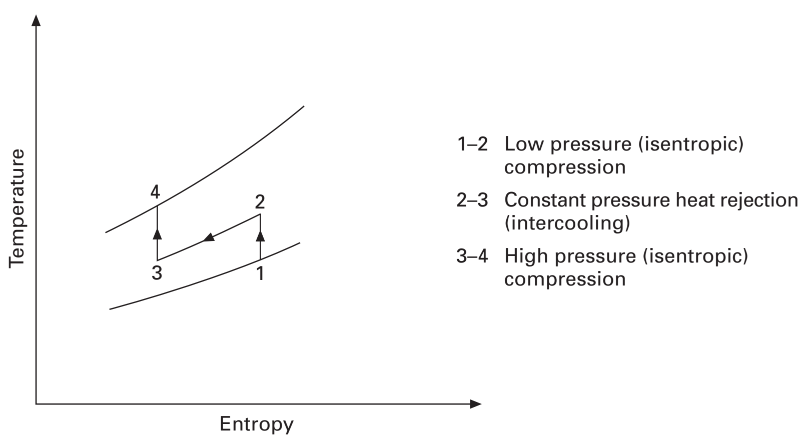

3.2 Two-stage intercooled compression process on the temperature–entropy diagram.

Equation 3.1 can be represented in terms of the LP and overall pressure ratio as:

$$W_{\text{comp}} = c_p\, T_1 \left[(Pr_{lp})^{\frac{\gamma-1}{\gamma}} + \left(\frac{Pr_o}{Pr_{lp}} \right)^{\frac{\gamma-1}{\gamma}} - 2 \right] \qquad [3.2]$$

Differentiating Equation 3.2 with respect to Pr_{lp} and equating to zero gives:

$$Pr_{lp} = \sqrt{Pr_o} \qquad [3.3]$$

By considering the second derivative of Equation 3.2, it can be shown that the condition expressed in Equation 3.3 is a minimum. Therefore, the minimum work absorbed by an intercooled compression system occurs when the LP and HP compressor pressure ratios are equal.

3.1.2 Thermal efficiency and specific work of an ideal intercooled gas turbine

The intercooled gas turbine shown in Fig. 3.1 may be represented on the temperature–entropy diagram as shown in Fig. 3.3. Since we are considering the ideal performance of the cycle, the thermodynamic processes involved are:

- 1–2 isentropic compression
- 2–3 constant pressure heat rejection
- 3–4 isentropic compression
- 4–5 constant pressure heat addition
- 5–6 isentropic expansion.

In fact, it may be considered that an ideal intercooled gas turbine cycle consists of two ideal simple cycle gas turbines (2–3–4–4′ and 1–4′–5–6), as shown in Fig. 3.3. The increased specific work of the intercooled gas turbine is due to the specific work of the smaller simple cycle gas turbine 2–3–4–4′. The smaller gas turbine cycle requires an additional heat input which corresponds to the heat input from 4–4′. However, the pressure ratio of the smaller simple cycle gas turbine, P_4/P_3, is less than the pressure ratio of the larger simple cycle gas turbine 1–4′–5–6. Therefore, the ideal thermal efficiency of the smaller ideal gas turbine cycle is less than that of the larger gas turbine cycle. In effect, a less efficient gas turbine cycle has been added to a more efficient cycle. Thus the ideal thermal efficiency of an intercooled gas turbine cycle is less than that of the simple cycle gas turbine whose overall pressure ratios are the same as illustrated in Fig. 3.4.

Furthermore, for a given minimum cycle temperature, T_1, increasing the maximum cycle temperature, T_5, increases the specific work of the larger

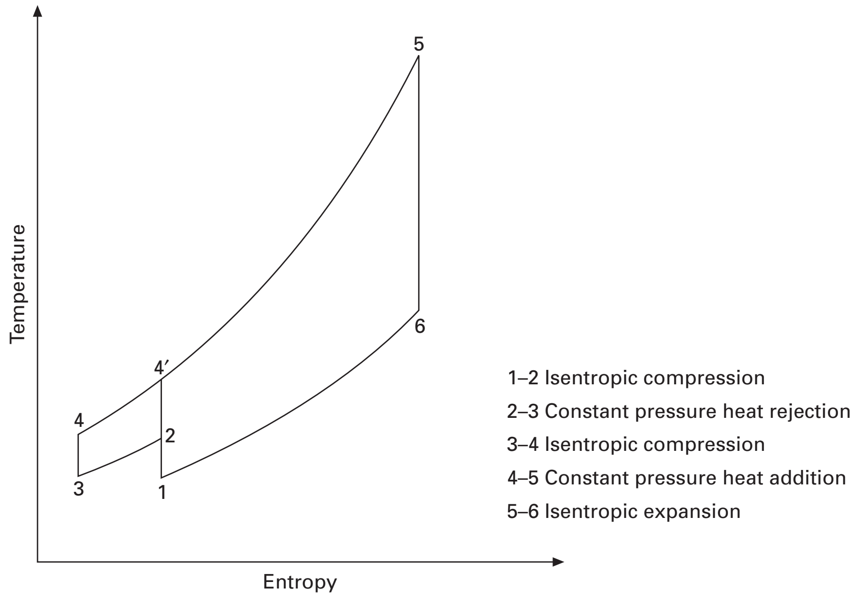

3.3 Temperature–entropy diagram of an ideal, intercooled gas turbine.

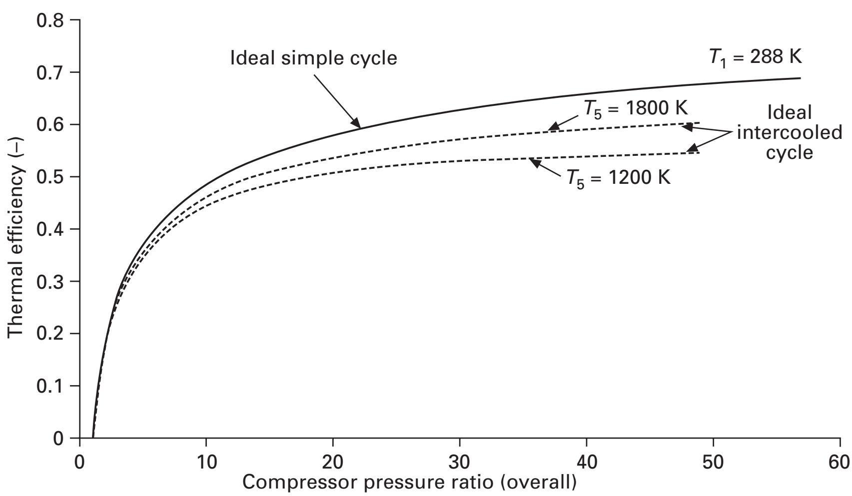

3.4 Variation of thermal efficiency with pressure ratio and maximum cycle temperature for an ideal, intercooled gas turbine.

gas turbine cycle and requires additional heat input to this cycle. Since the ideal thermal efficiency of the larger gas turbine is greater than the smaller gas turbine, the ideal thermal efficiency of the intercooled gas turbine cycle will increase with increase in the maximum cycle temperature, as illustrated in Fig. 3.4.

Therefore, the ideal thermal efficiency of an intercooled gas turbine cycle increases with an increase in maximum to minimum cycle temperature ratio, and this differs from the case of the simple gas turbine cycle, where the ideal thermal efficiency is independent of this temperature ratio. Of course, the specific work of the intercooled gas turbine is higher than that of the ideal simple cycle gas turbine, as shown in Fig. 3.5. As was found with the ideal simple cycle gas turbine, the specific work of the ideal intercooled gas turbine is dependent on the maximum to minimum cycle temperature ratio, as shown in Fig. 3.5. It is additionally observed that the maximum specific work occurs at a higher pressure ratio compared with the simple cycle gas turbine.

3.1.3 Practical intercooled cycle

The ideal intercooled cycle considers only isentropic compression and expansion processes and ignores any pressure losses during the heat addition and heat rejection processes. In a practical cycle, such assumptions are never achieved and the effect of irreversibilities discussed in Chapter 2 results in a significant loss in thermal efficiency and specific work. Furthermore, the conclusion that an ideal intercooled cycle always results in a lower thermal efficiency compared with the simple cycle gas turbine may not hold.

This is illustrated by considering the case discussed in Section 2.9 where the impact of irreversibilities on the performance of the simple cycle gas turbine was investigated. In particular, the case where the maximum cycle temperature was increased sufficiently so that the turbine expansion work

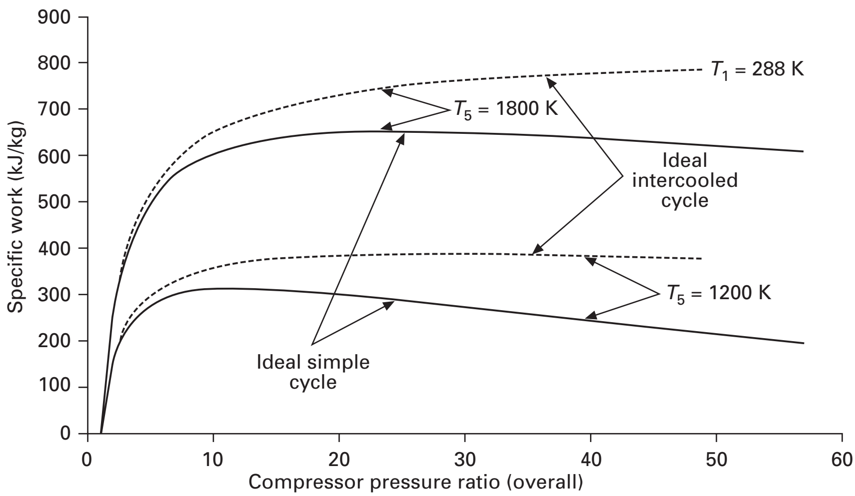

3.5 Variation of specific work with pressure ratio for an ideal, intercooled cycle.

was equal to the compressor absorbed work will be considered. Since a finite amount of heat was supplied, the thermal efficiency was zero. If the compression process is intercooled, the reduction in compressor specific work will now result in a finite specific work from the intercooled gas turbine cycle, i.e. the turbine work remains the same, while the compression work decreases.

Although the heat input has now increased to maintain the same maximum cycle temperature, as illustrated in Fig. 3.6, the positive specific work from the intercooled gas turbine cycle will result in a positive thermal efficiency. Thus, when irreversibilities are considered, intercooling can increase the thermal efficiency compared with the simple cycle gas turbine. The optimisation of a practical intercooled gas turbine for maximum thermal efficiency may not result in the LP and HP compressor pressure ratios being equal and generally the LP compressor pressure ratio will be much less than the optimum value for minimum compression work.

Optimisation of the split in the LP and HP compressor pressure ratios can therefore achieve a worthwhile increase in the thermal efficiency compared with the simple cycle gas turbine. This point is illustrated in Fig. 3.7 where the optimised intercooled gas turbine thermal efficiency is plotted against specific work for a series of overall pressure ratios, *Pr*, and maximum cycle temperatures, T_5. Thermal efficiencies of the order of 45% are possible with intercooling and one major manufacturer is seriously considering the manufacture of such gas turbines.[1] A discussion of the benefits is given in *Modern Power Systems*.[2] The optimised LP compressor pressure ratios are shown in Fig. 3.8. It is observed that the optimised LP compressor pressure increases with overall pressure ratio and decreases with increase in maximum

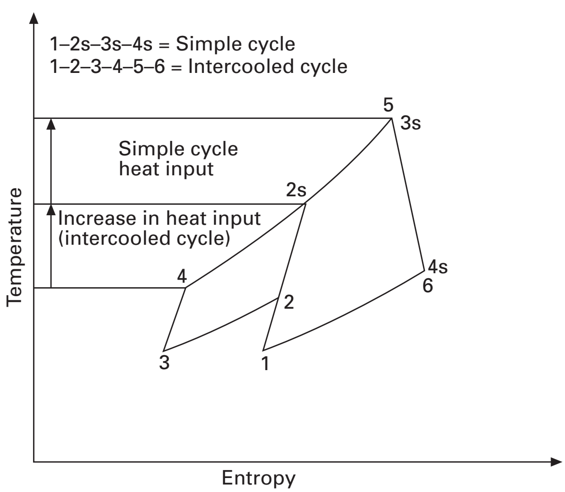

3.6 Change in the temperature–entropy diagram due to intercooling a practical simple cycle gas turbine.

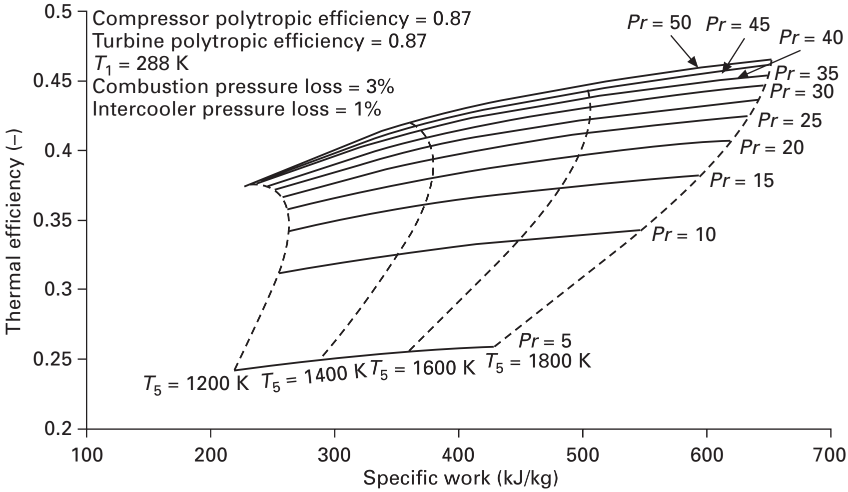

3.7 Variation of thermal efficiency with specific work for a practical intercooled gas turbine when optimised for maximum thermal efficiency.

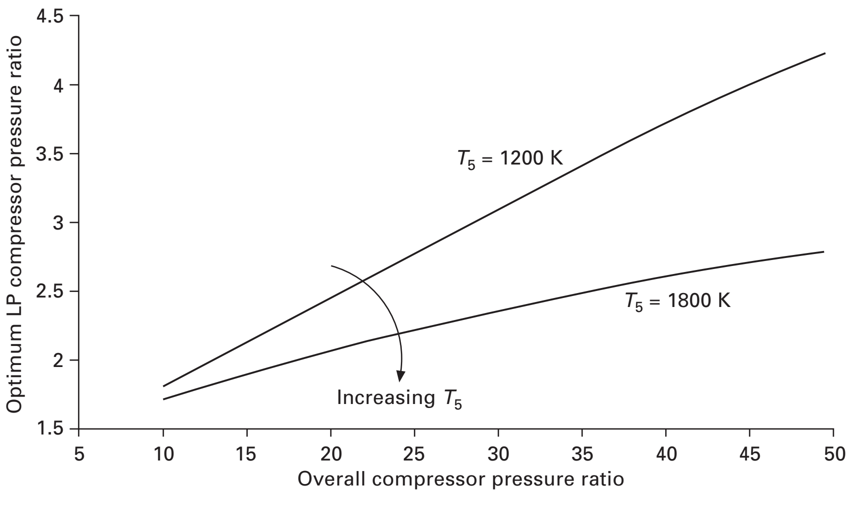

3.8 Optimised low-pressure (LP) compressor pressure ratio to achieve maximum thermal efficiency in a practical intercooled gas turbine.

cycle temperature. The optimised LP compressor pressure ratio is well below the case when the specific work is maximum, which corresponds to the square root of the overall compressor pressure ratio.

Optimising the LP compressor pressure ratio to maximise the specific work results in a lower thermal efficiency as is illustrated in Fig. 3.9. In this case the LP pressure ratio is approximately equal to the square root of the overall compressor pressure ratio. It has been assumed that the LP and HP compressor polytropic efficiencies are equal. It is when different values of polytropic efficiencies for respective compressors are considered that the optimised pressure ratio for maximum specific work departs from the square root relationship. The compressor pressure ratio split will be biased towards the higher efficiency compressor.

3.1.4 Ideal intercooled and regenerative gas turbine cycle

The thermal efficiency of the ideal intercooled cycle may be increased by the addition of a heat exchanger to recover the exhaust heat and transfer it to the compressor discharge air before combustion. A schematic representation of such a cycle, known as the intercooled regenerative cycle, is shown in Fig. 3.10. It is very similar to the regenerative cycle discussed in Section 2.7 but differs due to the addition of an intercooled compressor.

In the case of the ideal cycle, the compressor discharge air at station 4 is heated by the exhaust gas such that the temperature of the compressor discharge air rises to the turbine exhaust temperature, T_7, at station 5. The temperature of the heated air leaving the heat exchanger is then increased to the maximum cycle temperature by burning fuel in the combustor. The work done by the turbine, which drops the turbine exhaust temperature to T_7, drives both the

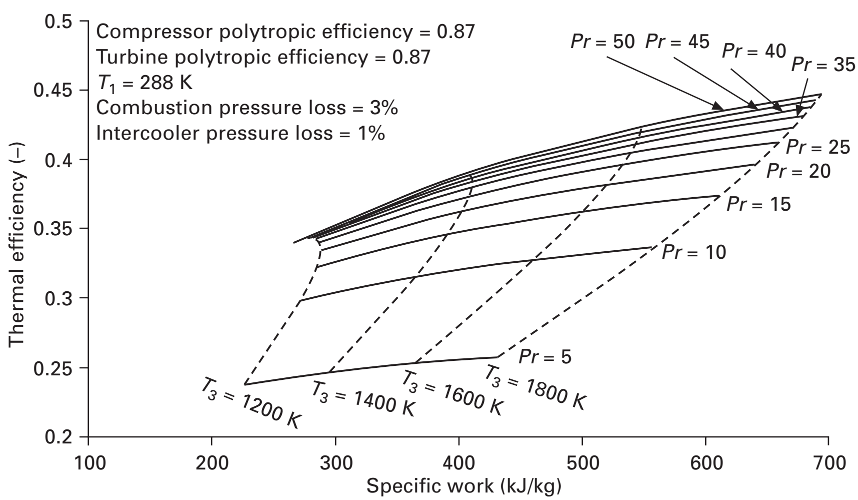

3.9 Variation of thermal efficiency with specific work for a practical intercooled gas turbine, where low-pressure (LP) compressor pressure ratio is optimised for maximum specific work.

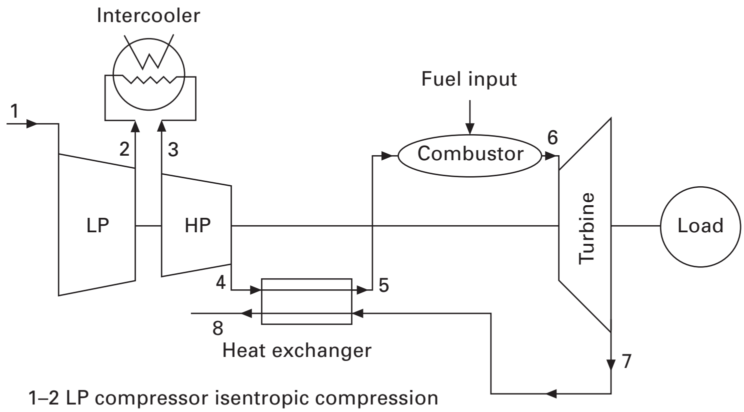

1–2 LP compressor isentropic compression
2–3 Constant pressure heat rejection (intercooling)
3–4 HP compressor isentropic compression
4–5 Constant pressure heat addition via heat exchanger
5–6 Constant heat addition via external heat source
6–7 Isentropic expansion
7–8 Constant pressure heat transfer for heating process 4–5

3.10 Schematic representation of an intercooled, regenerative gas turbine cycle.

load and the intercooled compressors. The heating of the compressor discharge air by the exhaust heat from the turbine results in the turbine exhaust temperature decreasing to T_4 at station 8.

These thermodynamic processes are displayed on the temperature–entropy diagram in Fig. 3.11. The case for the non-intercooled regenerative cycle is also shown for comparative purposes. In the ideal case the heat input, $Q_{56} = c_p(T_6 - T_5)$, for the intercooled regenerative cycle (1–2–3–4–5–6–7–8) is no different to that of the non-intercooled regenerative cycle (1–4′–5–6–7–7′). However, the specific work output from the intercooled cycle is greater, as discussed in Section 3.1. Thus the thermal efficiency of the intercooled regenerative cycle will be greater. For a given heat input, the thermal efficiency will be a maximum when the specific work is a maximum and will correspond to the case when the compressor work absorbed is a minimum. It was shown in Section 3.1 that the work absorbed by the intercooled compressors will be a minimum when the pressure ratios of the LP and HP compressors are equal. Thus, in the ideal case, the temperatures T_4, T_2 and T_8 shown in Fig. 3.11 will be equal. A relatively simple expression may be derived for the optimised ideal thermal efficiency, η_{th}, for an intercooled regenerative cycle as follows:

It was shown for the maximum thermal efficiency case that the compressor work is a minimum and equals $2c_p(T_2 - T_1)$. This occurs at equal LP and HP

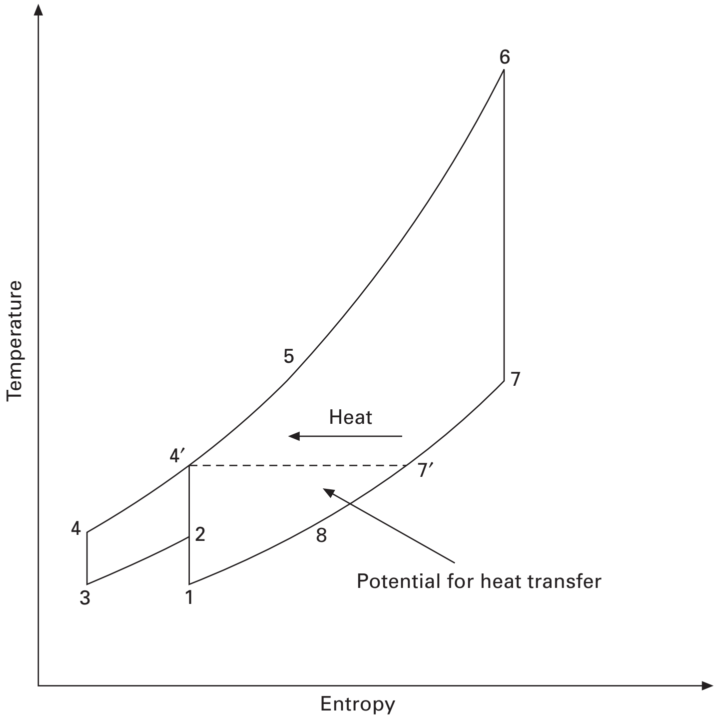

1–2 LP compressor isentropic compression
2–3 Constant pressure heat rejection (intercooling)
3–4 HP compressor isentropic compression
4–5 Constant pressure heat addition via heat exchanger
5–6 Constant heat addition via external heat source
6–7 Isentropic expansion
7–8 Constant pressure heat transfer for heating process 4–5
8–1 Constant pressure heat rejection

3.11 Temperature–entropy diagram for the intercooled and non-intercooled, regenerative gas turbine cycles.

compressor pressure ratios. Therefore, the thermal efficiency of the intercooled regenerative cycle is:

$$\eta_{\text{th}} = \frac{c_p\,(T_5 - T_6) - 2c_p\,(T_2 - T_1)}{c_p\,(T_5 - T_6)} \qquad [3.4]$$

$$\eta_{\text{th}} = 1 - \frac{2(T_2 - T_1)}{(T_5 - T_6)} \qquad [3.5]$$

The LP compressor discharge temperature is expressed as

$$T_2 = T_1 \times (Pr_{lp})^{\frac{\gamma-1}{\gamma}}$$

where

$$Pr_{lp} = P_2/P_1.$$

Similarly,

$$T_6 = T_5 \times \left(\frac{1}{Pr_o}\right)^{\frac{\gamma-1}{\gamma}}$$

where

$$Pr_o = P_5/P_6$$

is the overall pressure ratio. If

$$c_1 = (Pr_{lp})^{\frac{\gamma-1}{\gamma}}$$

and

$$c = (Pr_o)^{\frac{\gamma-1}{\gamma}}$$

and substituting T_2 and T_6 into Equation 3.5,

$$\eta_{\text{th}} = 1 - \frac{2T_1(c_1 - 1)}{T_5\left(1 - \dfrac{1}{c}\right)} \qquad [3.6]$$

Since $c = c_1^2$ for minimum compressor work requirement, $c_1 = \sqrt{c}$. Therefore,

$$\eta_{\text{th}} = 1 - \frac{2T_1}{T_5}\left(\frac{\sqrt{c} - 1}{c - 1}\right)c \qquad [3.7]$$

Factorising $(c - 1)$ gives $(\sqrt{c} - 1)(\sqrt{c} + 1)$. Therefore, the thermal efficiency becomes

$$\eta_{\text{th}} = 1 - \frac{T_1}{T_5}\, c\left(\frac{2}{(\sqrt{c} + 1)}\right) \qquad [3.8]$$

Equation 3.8 is identical to Equation 2.25, which describes the thermal efficiency for a simple cycle employing regeneration, except for the factor $\left(\dfrac{2}{(\sqrt{c} + 1)}\right)$. Since $\sqrt{c} + 1 > 2$ for $c > 1$, the thermal efficiency of the intercooled regenerative cycle is greater than that of the simple regenerative cycle. When $c = 1$, the thermal efficiencies of both regenerative cycles are the same and equal to the Carnot efficiency. By differentiating $c\left(\frac{2}{(\sqrt{c}+1)}\right)$ with respect to c, it can be shown that the thermal efficiency of an intercooled regenerative cycle decreases with increase in pressure ratio P_4/P_1 or P_6/P_7. From Equation 3.8, the thermal efficiency increases as T_1/T_5 decreases. These conclusions are similar to that of the regenerative cycle discussed in Section 2.7.

Figure 3.12 illustrates the variation of the thermal efficiency with pressure ratio for the regenerative cycles. For comparison, the figure also shows the variation of thermal efficiency with pressure ratio for the simple and intercooled cycles. The point where the curves for the regenerative cycles meet the simple and intercooled cycles corresponds to the condition that the turbine exit temperature equals the compressor discharge temperature. The pressure ratio for this condition is greater for the intercooled cycle.

3.1.5 Practical intercooled regenerative cycle

When irreversibilities in the various thermodynamic processes are considered, there is a decrease in the ideal thermal efficiency of the intercooled regenerative cycle. Nonetheless, very high thermal efficiencies may be achieved using such a cycle. This is illustrated in Figure 3.13, where the variation of thermal efficiency with specific work is shown for a series of maximum cycle temperatures and pressure ratios.

Thermal efficiencies in the order of 55% are possible with such cycles

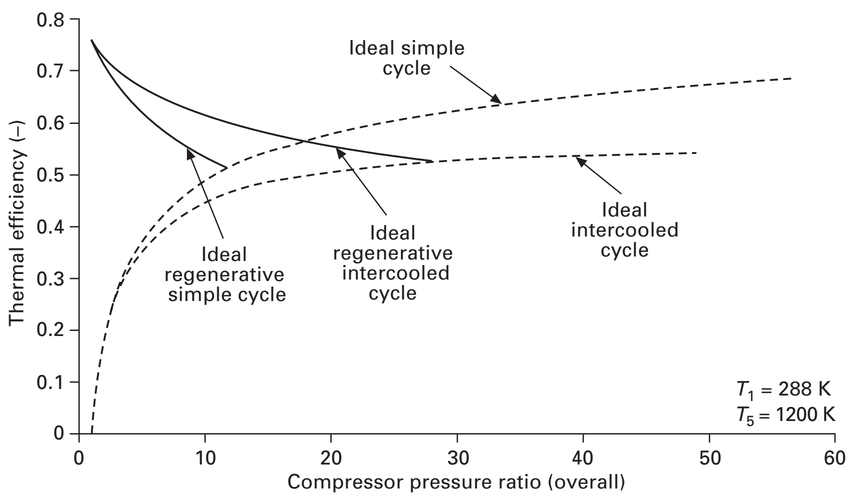

3.12 Variation of thermal efficiency with pressure ratio for ideal, regenerated cycles (intercooled and simple).

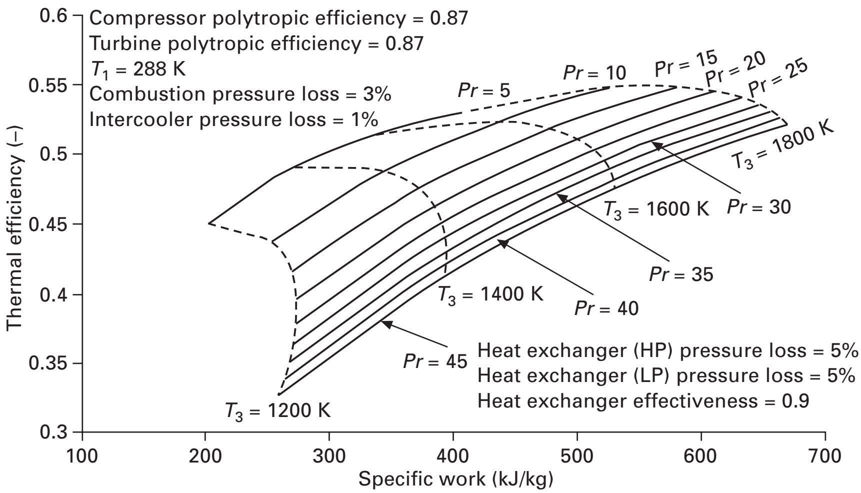

3.13 Variation of thermal efficiency with specific work for a practical intercooled, regenerative gas turbine cycle

and represent a step increase in the thermal efficiency when compared with the practical intercooled cycle. Furthermore, the optimum overall pressure ratio is significantly smaller compared with the practical intercooled cycle, resulting in a simpler compression system for the gas turbine. The turbine cooling air temperature will also be lower, thus reducing cooling air flow requirements. The optimum compressor pressure ratio split is close to the case of maximum specific work for a given overall compressor pressure ratio (i.e. the LP and HP compressor pressure ratios are equal) but at high heat exchanger effectiveness. As the heat exchanger effectiveness decreases, the optimum LP pressure ratio will be lower than that required for maximum specific work, as illustrated in Fig. 3.14.

3.2 Reheat gas turbine cycle

The turbine work of the ideal simple cycle gas turbine may be augmented by reheating the gases back to the maximum cycle temperature at some intermediate point. This is illustrated in Fig. 3.15, which shows a schematic representation of a reheat gas turbine cycle. The gases leaving the HP turbine are reheated by burning additional fuel in the reheat combustor to increase the gas temperature to the maximum cycle temperature, T_3, at station 5, before it is expanded in the LP turbine. It was shown in Chapter 2 that the specific work output for a turbine is given by $W_{turb} = c_p(T_3 - T_4)$, where T_3 is the turbine entry temperature and T_4 is the turbine exit temperature. For an isentropic process, the specific work can be expressed as:

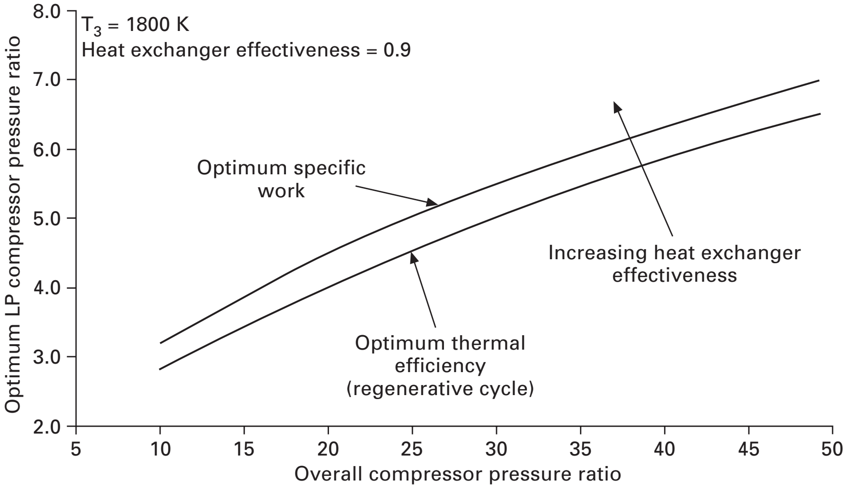

3.14 Variation of the optimum low-pressure (LP) compressor pressure ratio to achieve maximum thermal efficiency in a practical intercooled, regenerative gas turbine cycle.

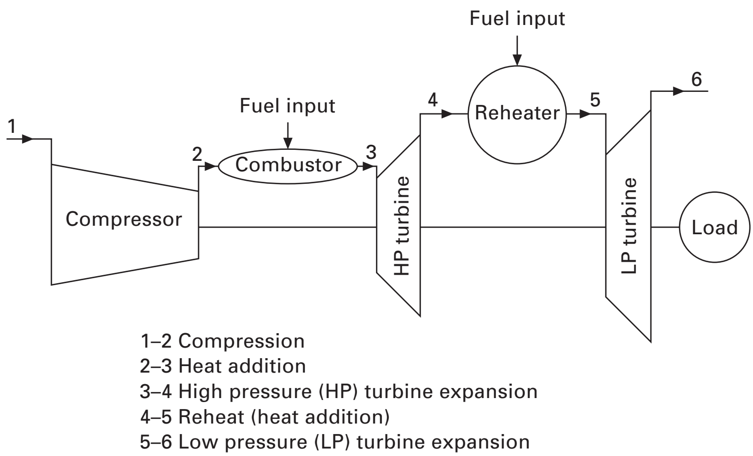

3.15 Schematic representation of a reheat gas turbine.

$$W_{\text{turb}} = c_p T_3 \left(1 - \left(\frac{1}{Pr} \right)^{\frac{(\gamma - 1)}{\gamma}} \right)$$

where Pr is the pressure ratio.

Thus, for a given turbine pressure ratio, Pr, the turbine specific work, W_{turb}, will increase with T_3. Hence, reheating the turbine, as shown in Figure 3.15, increases the total turbine work output.

3.2.1 Optimisation of reheated turbines

The analysis carried out for intercooled compressors in Section 3.1.1 may also be used to determine the optimum pressure ratio split, which will maximise the turbine work output. Referring to Fig. 3.16, for two stages of reheat the turbine-specific work output is given by:

$$W_{\text{turb}} = c_p(T_3 - T_4) + c_p(T_5 - T_6) \tag{3.9}$$

Since $T_5 = T_3$ due to reheating, and substituting the HP and overall pressure ratios, Pr_{hp} and Pr_o, respectively, into Equation 3.9, for an isentropic process:

$$W_{\text{turb}} = c_p T_3 \left[2 - \left(\frac{1}{Pr_{hp}} \right)^{\frac{\gamma-1}{\gamma}} - \left(\frac{Pr_{hp}}{Pr_o} \right)^{\frac{\gamma-1}{\gamma}} \right] \tag{3.10}$$

By differentiating Equation 3.10 with respect to Pr_{hp}, it can be shown that the maximum turbine work occurs when the HP turbine pressure equals the LP turbine pressure. Thus, the HP turbine pressure ratio Pr_{hp}, is given by:

$$Pr_{hp} = \sqrt{Pr_o} \tag{3.11}$$

where Pr_o is the overall pressure ratio, which in this case equals the compressor pressure ratio, P_2/P_1.

3.2.2 Thermal efficiency and specific work of an ideal reheat gas turbine

From the discussion in Section 3.2, the specific work of an ideal simple cycle gas turbine may be augmented by the application of reheat. The

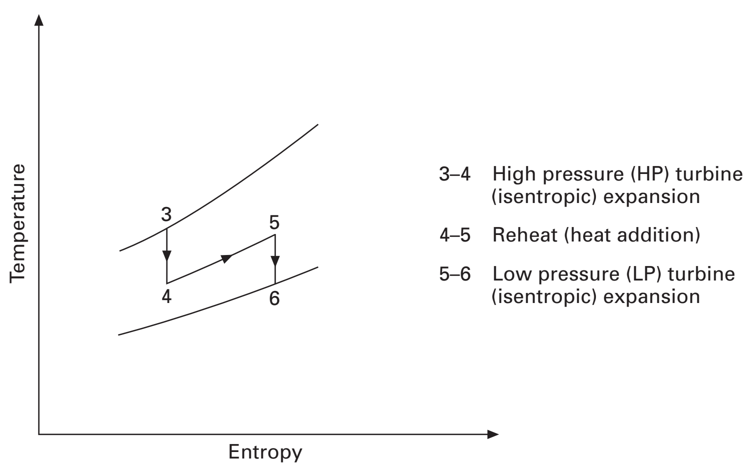

3.16 Two-stage reheat expansion process.

temperature–entropy diagram for such a cycle is shown in Fig. 3.17. Since the ideal cycle is being considered, the thermodynamic processes involved in an ideal reheat gas turbine cycle are:

- 1–2 isentropic compression
- 2–3 constant pressure heat addition
- 3–4 isentropic expansion
- 4–5 constant pressure heat addition
- 5–6 isentropic expansion.

As with the intercooled cycle discussed in Section 3.1.2 above, we can consider the ideal reheat gas turbine cycle consisting of two ideal simple cycles (1–2–3–4′ and 4′–4–5–6) as shown in Fig. 3.17.

Note that the pressure ratio of the ideal simple cycle representing the reheating part of the cycle (4′–4–5–6) has a low pressure ratio and therefore a lower thermal efficiency compared with the base ideal cycle 1–2–3–4′. Thus, by the argument made in Section 3.1.2 when the ideal intercooled cycle was considered, the thermal efficiency of the reheat cycle will be less than that of the ideal simple cycle gas turbine. Furthermore, the thermal efficiency of the reheat cycle will also depend on the maximum to minimum cycle temperature for the same reason discussed in Section 3.1.2. The more efficient base cycle (1–2–3–4′) produces more of the specific work developed by the reheat cycle as the maximum cycle temperature, T_3, is increased and therefore there is an increase in thermal efficiency. This is illustrated in Figs 3.18 and 3.19, which show the variation of thermal efficiency and specific work with pressure ratio for the reheat cycle.

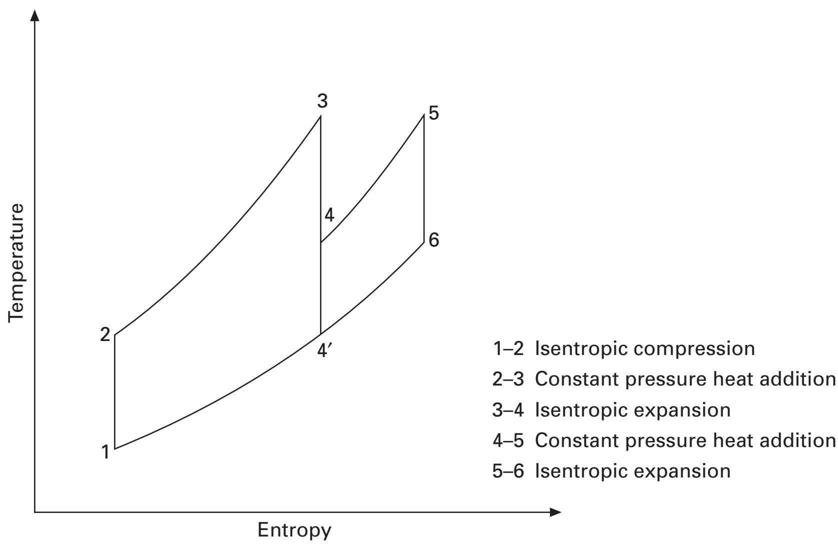

3.17 Temperature–entropy diagram for an ideal, reheat gas turbine cycle.

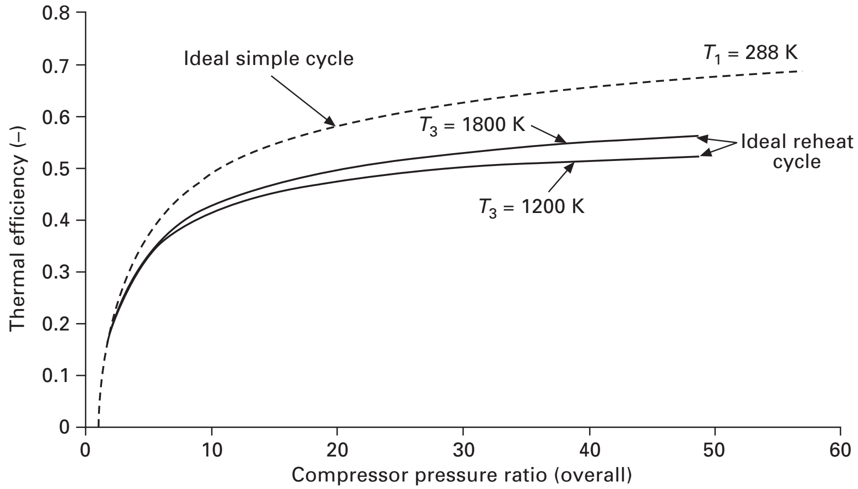

3.18 Variation of thermal efficiency with pressure ratio and maximum cycle temperature for an ideal, reheat gas turbine cycle.

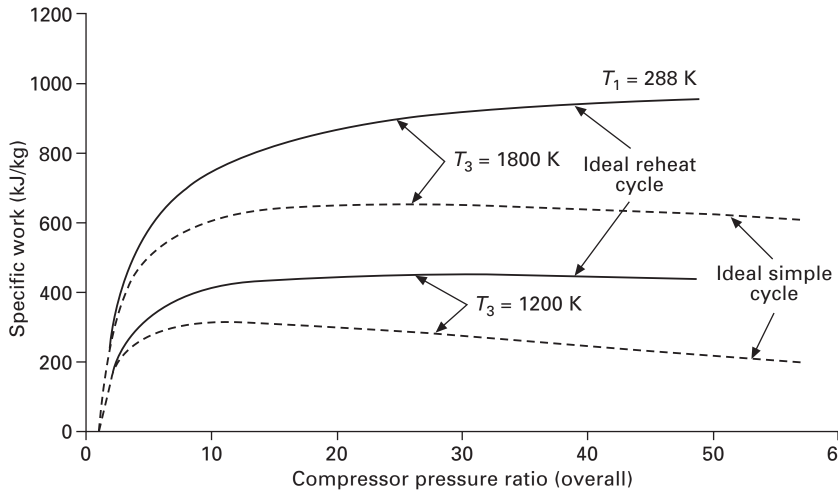

3.19 Variation of specific work with pressure ratio and maximum cycle temperature for an ideal reheat gas turbine cycle.

3.2.3 Comparison of performance of the ideal intercooled and reheat cycle

To compare the performance of the ideal intercooled and reheat cycle, it is necessary to consider the performance of the added simple gas turbine cycles to the base cycle when intercooling and reheat is applied. These cycles correspond to (2–3–4–4′) in Fig. 3.11 and to (4′–4–5–6) in Fig. 3.17 for the intercooled and reheat cycles, respectively.

Since only the optimised case for these added cycles has been considered, the LP compressor and HP turbine pressure ratios as shown (Sections 3.1.1 and 3.2.1) are equal for the respective cases. Furthermore, this condition results in the exhaust temperatures for these added cycles being equal to the compressor discharge temperatures (i.e. $T_2 = T_4$ in Fig. 3.11 and $T_6 = T_4$ in Fig. 3.17). This is indeed the condition for maximum specific work for these gas turbine cycles as discussed in Chapter 2 (Section 2.6).

If the overall compressor pressure ratios for the intercooled and reheat cycles (P_4/P_1 and P_2/P_1, respectively) are the same, then the compressor pressure ratios for each of the added cycles will also be the same (i.e. P_4/P_3 in Fig. 3.11 and $P_4/P_{4'}$ in Fig. 3.17). This also results in the maximum to minimum temperature ratios for the added cycle being the same. Thus the thermal efficiencies of these added cycles are indeed the same due to the same compressor pressure ratio but they are less than those for the base cycle due to the higher compressor pressure ratio of the base cycle as explained above. The specific work of the added cycles are, however, different and the reheat cycle will produce a larger specific work which is due to the higher minimum temperature of this cycle compared with the corresponding case for the intercooled cycle (i.e. $T_{4'} > T_1$). Also, see Equation 2.20, which describes the specific work in terms of cycle pressure ratio, temperature ratio and minimum temperature. Thus the reheat cycle will have a higher specific work but lower thermal efficiency compared with the intercooled cycle as shown in Fig. 3.4 and 3.18, which show the thermal efficiencies of the intercooled and reheat cycles respectively. However, a comparison of Fig. 3.5 and 3.19 shows that the reheat cycle has a higher specific work output.

3.2.4 Practical reheat cycle

It was shown in Section 3.1.3 that, when irreversibilities are considered in the compression, expansion and heat transfer processes, intercooling can increase the thermal efficiency of a practical simple cycle gas turbine. Referring to Fig. 3.20 a similar argument can be made when the effects of irreversibilities are considered for a practical reheat gas turbine cycle. Thus the thermal efficiency of the reheat gas turbine can exceed the thermal efficiency of a practical simple cycle gas turbine, particularly at lower maximum cycle temperatures.

This can be seen by comparing Fig. 3.21 with Fig. 2.21 in Chapter 2, which shows the variation of thermal efficiency with specific work for a series of overall pressure ratios and maximum cycle temperatures for practical reheat and simple cycles respectively. The curves in Fig. 3.21 are optimised for maximum thermal efficiency. When the practical reheat cycle is optimised for maximum specific work, there is a significant loss in thermal efficiency, as shown in Fig. 3.22.

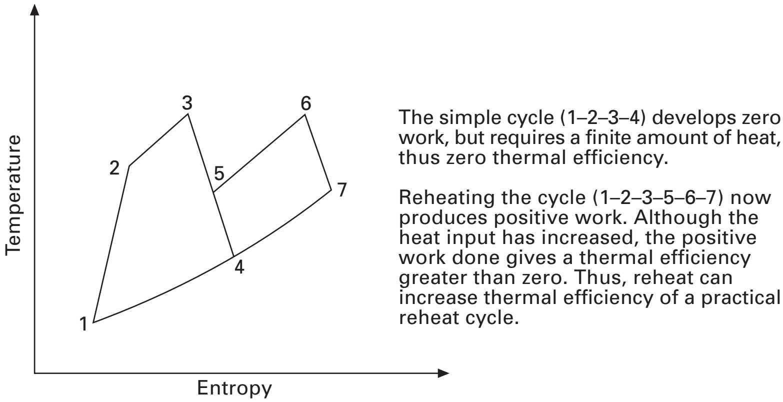

3.20 Change in temperature–entropy diagram due to reheating a practical simple cycle gas turbine.

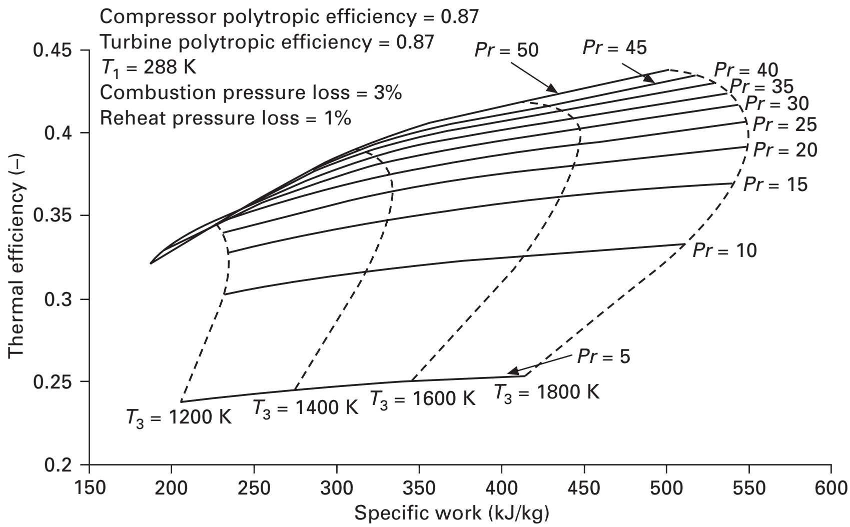

3.21 Variation of thermal efficiency with specific work when optimised for maximum thermal efficiency.

The variation of optimised HP turbine pressure ratio with overall pressure ratio to achieve maximum thermal efficiency is illustrated in Fig. 3.23. The figure shows the variation of HP turbine pressure ratios for two maximum cycle temperatures. Particularly at low maximum cycle temperatures, the increase in compressor pressure ratio increases the effects of irreversibility, thus the optimum HP turbine pressure ratio increases with the increase in overall pressure ratio.

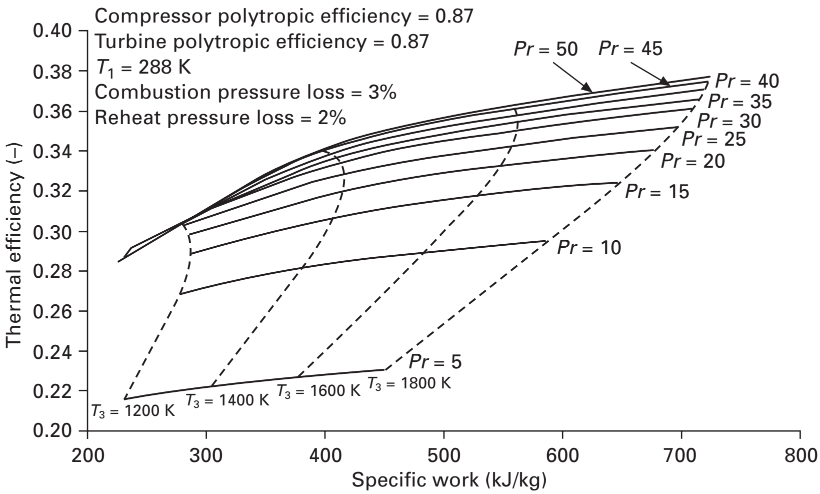

3.22 Variation of thermal efficiency with specific work when optimised for maximum specific work.

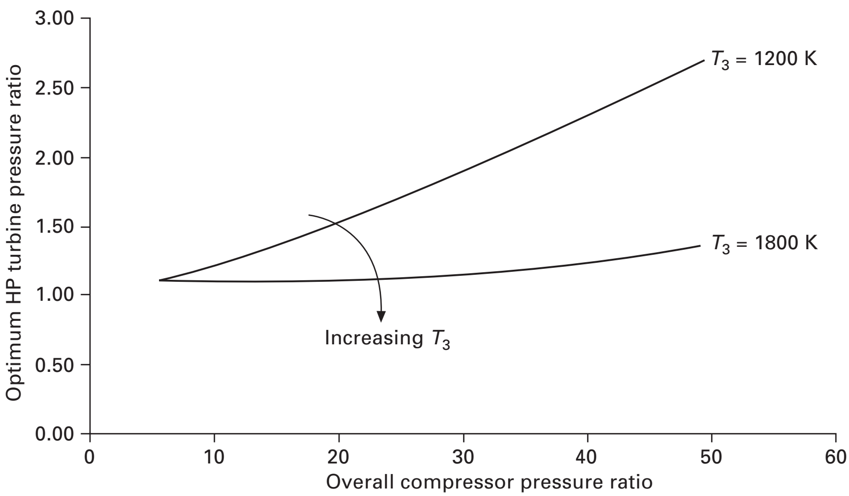

3.23 Variation of optimum high-pressure (HP) turbine pressure ratio with overall pressure ratio to maintain maximum thermal efficiency.

3.2.5 Ideal reheat and regenerative cycle

The thermal efficiency of the ideal reheat gas turbine cycle can be increased by the addition of a heat exchanger. A schematic representation of such a reheat–regenerative cycle is shown in Fig. 3.24. The reheat–regenerative gas turbine recovers some of the exhaust heat from the LP turbine via the heat exchanger. The compressor discharge air is heated ideally from T_2 to T_7, i.e.

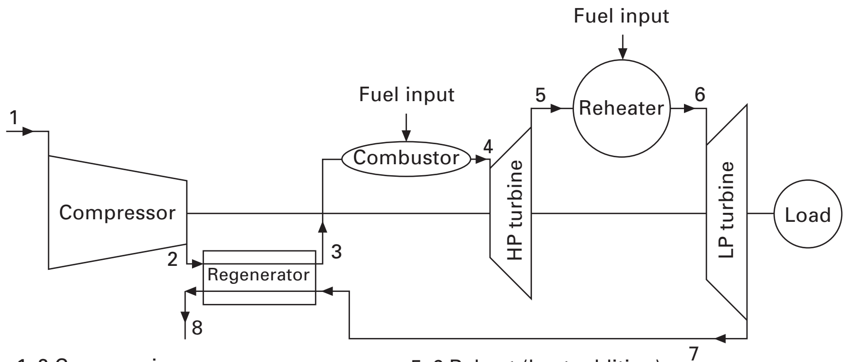

1–2 Compression
2–3 Heat addition via heat exchanger
3–4 Heat addition
4–5 HP turbine expansion
5–6 Reheat (heat addition)
6–7 LP turbine expansion
7–8 Heat transfer for heating process 2–3

3.24 Schematic representation of a reheat–regenerative gas turbine.

the temperature at station 3 is equal to the LP turbine exhaust temperature, T_7. The air leaving the regenerator at station 3 is heated further, normally by burning fuel in the combustor until it reaches the maximum cycle temperature at station 4. The gases at station 7 are cooled in the heat exchanger by heating the compressor discharge air. Such preheating of the compressor discharge air decreases the heat input in the combustor and thereby increases the thermal efficiency.

The thermodynamic processes for a reheated regenerative cycle may be displayed on the temperature–entropy diagram as shown in Fig. 3.25. The potential for heat recovery is also shown. The combustor heat input decreases from:

$$Qs = c_p(T_4 - T_2)$$

to

$$Qs = c_p(T_4 - T_3)$$

where Qs is the combustor heat input and c_p is the specific heat at constant pressure.

Although there is a decrease in the combustor heat input, the additional heat input in the reheat chamber, $Qr = c_p(T_6 - T_5)$ needs to be accounted for. In spite of increased heat input due to reheat, the increased specific work results in an increase in thermal efficiency compared with the ideal simple cycle. The total heat input (Q_{net}) is therefore:

$$Q_{\text{net}} = c_p(T_4 - T_3) + c_p(T_6 - T_5)$$

For a perfect heat exchanger $T_3 = T_7$

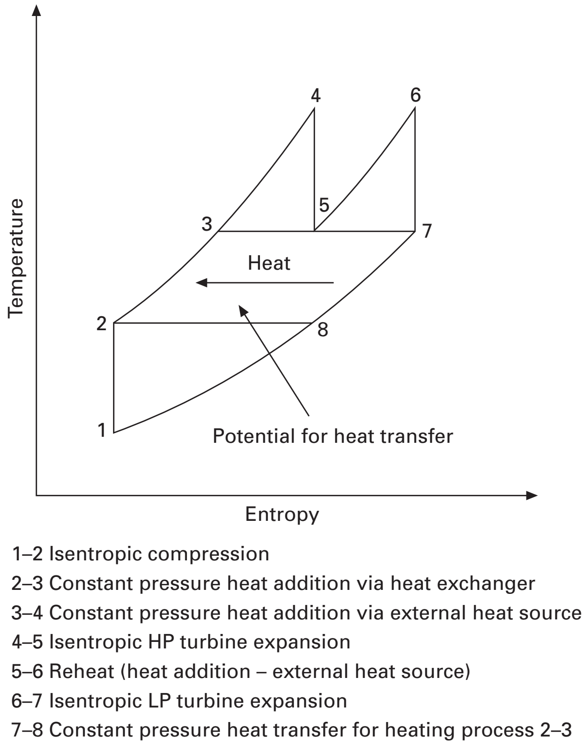

3.25 The reheat–regenerative cycle on the temperature–entropy diagram.

Therefore,

$$Q_{net} = c_p(T_4 - T_7) + c_p(T_6 - T_5)$$

Rearranging gives

$$Q_{net} = c_p(T_4 - T_5) + c_p(T_6 - T_7) \qquad [3.12]$$

Equation 3.12 is the same as the total turbine work, irrespective of the HP and LP turbine pressure ratio split. As discussed in Section 3.2.1, the maximum turbine work occurs when the HP and LP turbine pressure ratios are equal. Therefore, when the turbine pressure ratio split is optimised for maximum work, the total heat input is also a maximum.

By considering the net work and heat transfers, we may derive an expression relating the thermal efficiency, η_{th}, with overall pressure ratio and temperature as follows:

$$\eta_{th} = \frac{W_{net}}{Q_{net}} = \frac{W_t}{Q_{net}} - \frac{W_c}{Q_{net}}$$

where W_{net} is the net specific work, W_t is the total turbine work, W_c is the compressor work and Q_{net} is the total heat input. As discussed, in an ideal regenerative reheat cycle $Q_{\text{net}} = W_t$
then:

$$\eta_{\text{th}} = 1 - \frac{W_c}{Q_{\text{net}}} \qquad [3.13]$$

Therefore, from Equation 3.13, the thermal efficiency will be a maximum when W_c/Q_{net} is a minimum. For a given compressor pressure ratio, W_c/Q_{net} is a minimum when Q_{net} is a maximum, which occurs when the HP and LP turbine pressure ratios are equal (i.e. when turbine pressure ratios are optimised for maximum specific work). Optimised (equal) turbine pressure ratios also result in $T_3 = T_5 = T_7$ (see Fig. 3.25). Thus Q_{net} becomes:

$$Q_{\text{net}} = 2c_p(T_4 - T_5)$$

and the compressor work, W_c is given by:

$$W_c = c_p(T_2 - T_1)$$

Hence, from Equation 3.13, the thermal efficiency of the ideal reheated–regenerative cycle is:

$$\eta_{\text{th}} = 1 - \frac{(T_2 - T_1)}{2(T_4 - T_5)} \qquad [3.14]$$

where $T_2 = T_1 \times c$ and $T_5 = T_4 \dfrac{1}{\sqrt{c}}$

and when $c = (Pr_o)^{\frac{\gamma-1}{\gamma}}$ and $Pr_o = \dfrac{P_2}{P_1}$

Therefore, Equation 3.14 becomes:

$$\eta_{\text{th}} = 1 - \frac{T_1(c-1)}{2T_4\left(1 - \dfrac{1}{\sqrt{c}}\right)} = 1 - \frac{T_1}{T_4}\frac{\sqrt{c}}{2}\frac{(c-1)}{(\sqrt{c}-1)} \qquad [3.15]$$

Factorising $(c - 1) = (\sqrt{c} - 1)(\sqrt{c} + 1)$ and substituting into Equation 3.15 gives:

$$\eta_{\text{th}} = 1 - \frac{T_1}{T_4}\frac{\sqrt{c}}{2}(\sqrt{c} + 1)$$

Multiplying and dividing by $\sqrt{c}$ gives:

$$\eta_{\text{th}} = 1 - \frac{T_1}{T_4} c \frac{\sqrt{c} + 1}{2\sqrt{c}} \qquad [3.16]$$

Since $\frac{1}{\sqrt{c}} \le 1$ for $c \ge 1$, it can be shown that $\frac{\sqrt{c}+1}{2\sqrt{c}} \le 1$. Therefore, the thermal efficiency of the reheat–regenerative cycle is greater than the thermal efficiency of the conventional regenerative cycle whose thermal efficiency is given in Chapter 2 by Equation 2.25. When $c = 1$, the thermal efficiencies of the conventional and reheat–regenerative cycles give the same thermal efficiency and this equals the Carnot efficiency.

The thermal efficiency of the reheat regenerative cycle can also be determined as less than the thermal efficiency of the intercooled regenerative cycle. This can be proved by considering the inequality:

$$(\sqrt{c} - 1)^2 \ge 0 \text{ for } c \ge 1 \tag{3.17}$$

Expanding:

$$c - 2\sqrt{c} + 1 \ge 0$$

Adding $4\sqrt{c}$ gives:

$$c + 2\sqrt{c} + 1 \ge 4\sqrt{c}$$

Factorising gives:

$$(\sqrt{c} + 1)^2 \ge 4\sqrt{c} \tag{3.18}$$

Dividing by $2(\sqrt{c} + 1)$ then multiplying by $-\frac{T_1}{T_4}c$ and adding 1 we get

$$1 - \frac{T_1}{T_4} c \frac{\sqrt{c}+1}{2\sqrt{c}} \le 1 - \frac{T_1}{T_4} c \frac{2}{\sqrt{c}+1} \tag{3.19}$$

The left-hand side of inequality 3.19 is the thermal efficiency of the reheat–regenerative cycle while the right-hand side is the thermal efficiency of the intercooled regenerative cycle. T_4 is the maximum cycle temperature for both the intercooled and reheat regenerative cycles. Thus, the thermal efficiency of the ideal intercooled regenerative cycle is greater than the thermal efficiency of the ideal reheat–regenerative cycle.

The variation of the thermal efficiency of the ideal reheated regenerative cycle with compressor pressure ratio is shown in Fig. 3.26. The figure also shows the variation of thermal efficiency of the simple cycle, conventional regeneration cycle and the reheat cycle for comparison. The variation of specific work with pressure ratio is the same as that shown in Fig. 3.19.

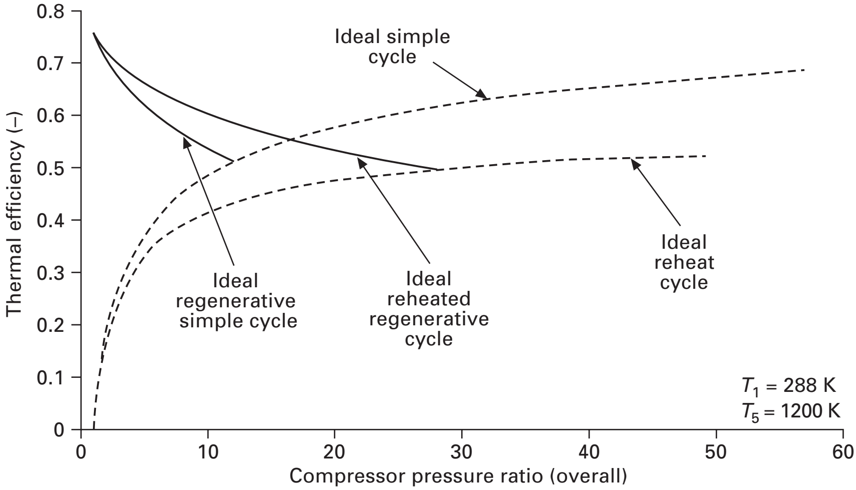

3.26 Variation of thermal efficiency with pressure ratio.

3.2.6 Practical reheat–regenerative gas turbine cycle

Allowing for losses, the reheat regenerative cycle is quite capable of achieving respectable thermal efficiencies as is shown in Fig. 3.27. The optimum compressor ratios for maximum thermal efficiency are lower than for the simple cycle and similar to that for the intercooled regenerative cycle. The pressure ratio range where regeneration is possible is smaller than that for an intercooled regenerative cycle and this is due to the lower compressor discharge temperature due to intercooling. The turbine exhaust temperatures, on the other hand, are much higher for the reheated regenerative cycle. For example, at a compressor pressure ratio of 10 and maximum cycle temperature of 1800 K, the turbine exhaust temperature is in the order of 1450 K (1177 Celsius). The corresponding case for the intercooled regenerative cycle is about 1200 K (927 Celsius). Thus ceramic-based materials such as silicon carbide and nitride must be employed for the heat exchanger when operating at the higher exhaust gas temperatures. Such materials have been used in the process industry for many years and can operate at temperatures in the order of 2000 K. Thus the reheated regenerative cycle should not be ruled out because of the higher turbine exhaust temperatures. Thermal efficiencies of about 50% are possible with such cycles but they are lower than those of the intercooled cycle. This is primarily due to the lower ideal thermal efficiency compared with the intercooled regenerative cycle. On the other hand, bulky intercoolers and cooling systems are unnecessary and the self-contained nature of the gas turbine is preserved with the reheat–regenerative gas turbine cycle.

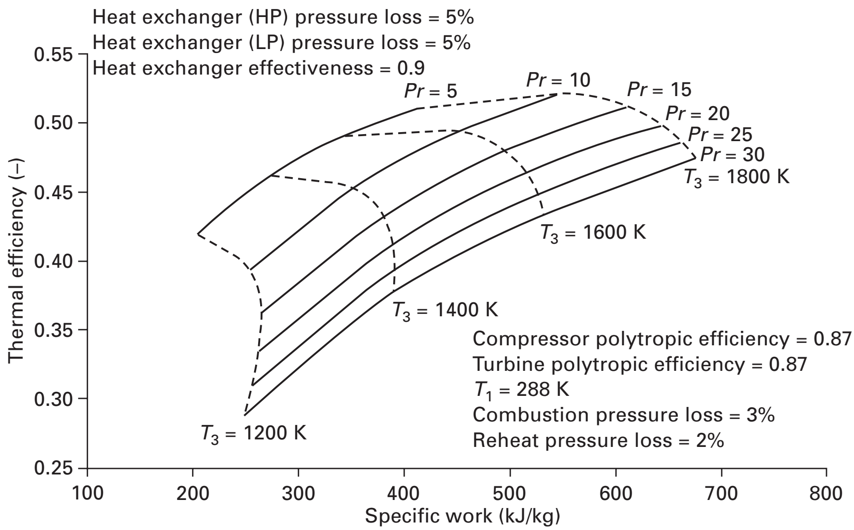

3.27 Variation of thermal efficiency with specific work for practical reheated–regenerative cycle.

At high heat exchanger effectiveness, the optimum HP turbine pressure ratio for maximum thermal efficiency also approaches the case when optimised for maximum specific work. This is shown in Fig. 3.28, which shows the variation of optimum HP turbine pressure ratio with the overall pressure ratio.

3.3 Intercooled, reheat and regenerative cycles

The inclusion of intercoolers and reheaters will no doubt increase the specific work of the ideal simple cycle gas turbine. A combined intercooled and reheat cycle will give a very similar performance to that discussed in Section 3.1.3. But it is the addition of a heat exchanger to such a cycle that will further increase the thermal efficiency of the gas turbine. The design point performance of gas turbine cycles that incorporate both intercooling, reheating and the addition of regeneration will now be discussed. A schematic representation of the ICRHR cycle is shown in Fig. 3.29.

3.3.1 Ideal ICRHR cycle

We have shown that the minimum compression specific work due to intercooling occurs when the LP and HP compressor pressure ratios are equal. We have also shown that the maximum turbine specific work due to reheating occurs when the HP and LP turbine pressure ratios are equal and corresponds to the condition when the heat input is a maximum. Thus, from the argument in Section 3.2.5, the maximum ideal cycle thermal efficiency

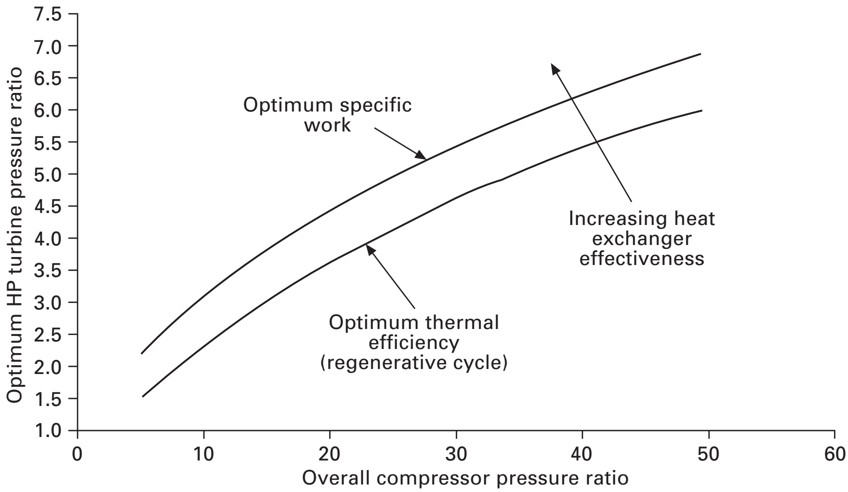

3.28 Optimum pressure ratio of the high-pressure (HP) turbine to achieve maximum specific work and thermal efficiency.

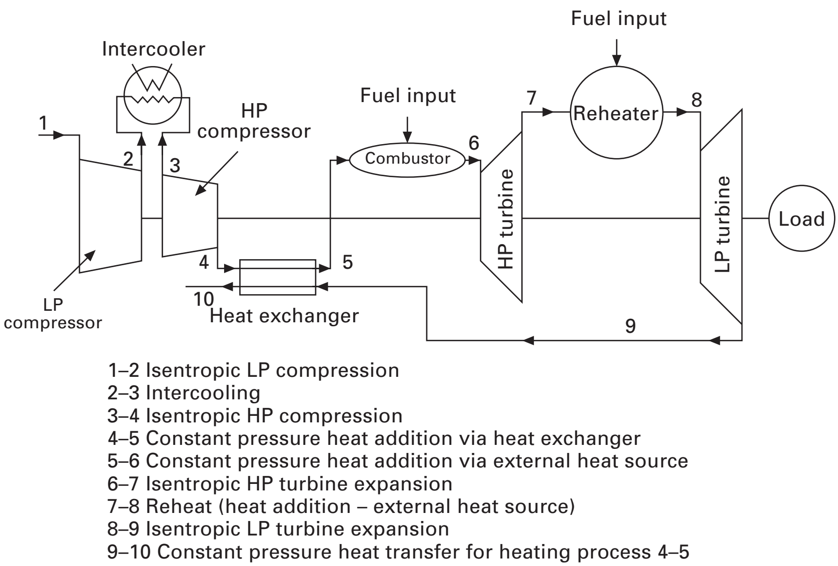

3.29 Schematic representation of an intercooled, reheat and regenerative cycle.

of the ICRHR cycle occurs when these optimum conditions apply. The temperature–entropy diagram for the ICRHR cycle is shown in Fig. 3.30. The potential for transfer of exhaust heat to the compressor discharge air is also shown. In fact, it can be argued that the ICRHR cycle consist of two

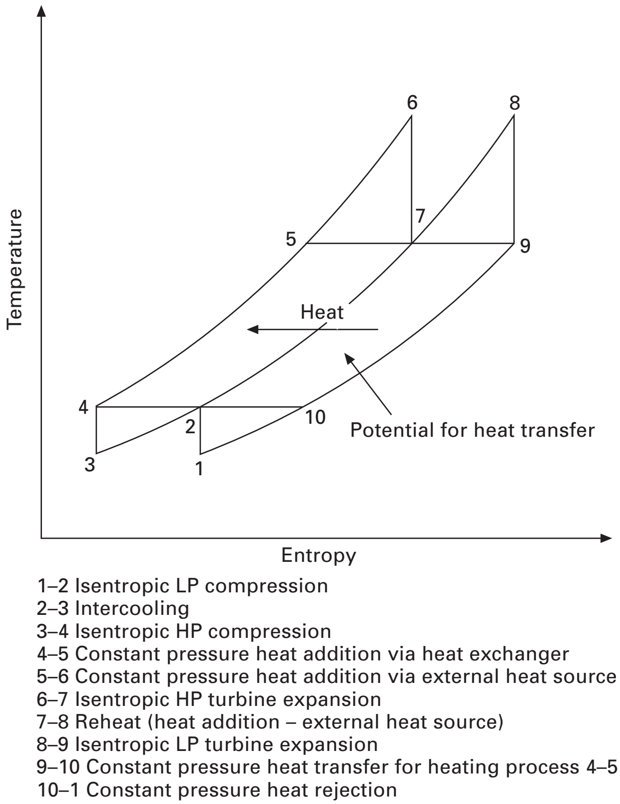

3.30 Temperature–entropy diagram for the intercooled, reheat and regenerative (ICRHR) cycle.

identical conventional regenerative cycles 1–2–8–9 and 3–4–6–7, as shown in Fig. 2.8 in Chapter 2 and therefore the thermal efficiency of the ICRHR cycle equals that of each cycle. Hence the thermal efficiency of the ICRHR cycle is given by:

$$\eta_{\text{th}} = 1 - \frac{T_1}{T_6}\sqrt{c} \qquad [3.20]$$

where T_6 is the maximum cycle temperature and

$$c = \left(\frac{P_4}{P_1}\right)^{\frac{\gamma-1}{\gamma}}.$$

Since $\sqrt{c} \le c$ for $c \ge 1$, the ICRHR cycle has a greater thermal efficiency than the conventional regenerative cycle and equals the conventional regenerative cycle when $c = 1$, which corresponds to the Carnot efficiency. It may also be concluded that the ideal thermal efficiency of the ICRHR is greater than that of the intercooled regenerative cycle and is therefore better than that of the reheated regenerative cycle by considering the inequality:

$$2 \geq 1 + \frac{1}{\sqrt{c}} \text{ for } c \geq 1$$

Therefore:

$$c\frac{2}{\sqrt{c}+1} \geq \frac{c}{\sqrt{c}} \qquad [3.21]$$

Multiplying inequality 3.21 by $-\frac{T_1}{T_6}c$ and adding 1 gives:

$$1 - \frac{T_1}{T_6}c\frac{2}{\sqrt{c}+1} \leq 1 - \frac{T_1}{T_6}\frac{c}{\sqrt{c}}c \qquad [3.22]$$

$$1 - \frac{T_1}{T_6}c\frac{2}{\sqrt{c}+1} \leq 1 - \frac{T_1}{T_6}\sqrt{c} \qquad [3.23]$$

The left-hand side of the inequality 3.23 is the ideal thermal efficiency of the intercooled–regenerative cycle and the right-hand side of the inequality is the thermal efficiency of ICRHR cycle. Thus the ICRHR has the highest thermal efficiency of all the gas turbine regenerative cycles discussed so far.

The variation of the ideal thermal efficiencies with overall compressor pressure ratios for the different regenerative cycles for a maximum cycle temperature of 1200 K is summarised in Fig. 3.31. Clearly, the Figure shows that the ICRHR cycle achieves the greatest thermal efficiency for pressure ratios greater than unity.

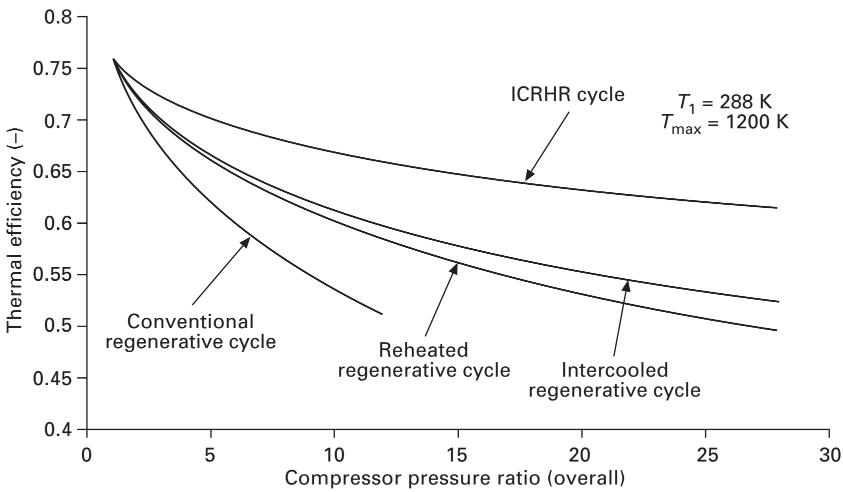

3.31 Variation of the ideal thermal efficiency with compressor pressure ratio.

3.3.2 Practical ICRHR cycle

When irreversibilities in the thermodynamic processes occur in the ICRHR cycle, there is a decrease in the thermal efficiency and specific work from the ideal case. In spite of the high pressure losses in the heating and cooling processes, thermal efficiencies approaching 60% are possible with such complexes as shown in Fig. 3.32.

3.4 Ericsson cycle

The intercooling and reheating processes in the compression and expansion in the ICRHR cycle may be increased from one to many stages. In the limiting case we may increase the number of intercooled and reheat stages to infinity. When this is done, the compression and expansion processes become isothermal. An expression for the specific work for an ideal isothermal compression and expansion can be derived from the equations:

$$W = \int p\mathrm{d}v \qquad [3.24]$$

and

$$pv = c \qquad [3.25]$$

where p is pressure, v is specific volume, and c is constant to give

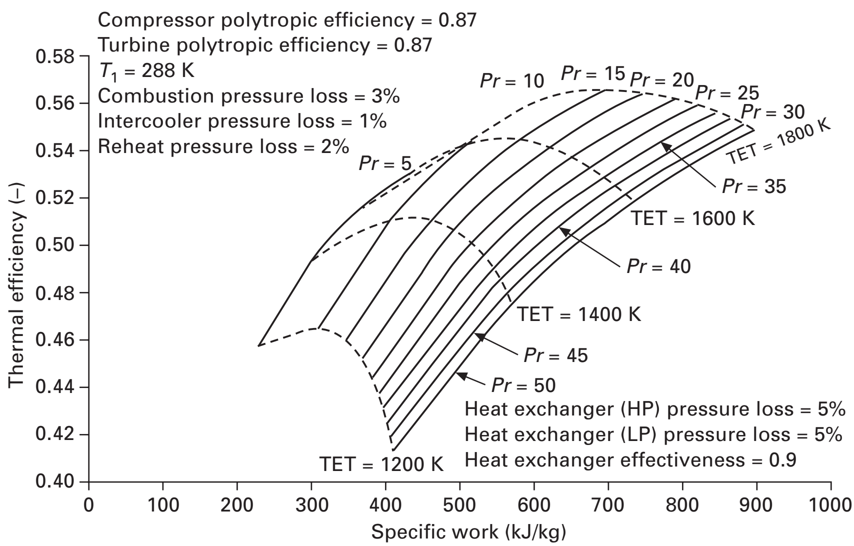

3.32 Variation of thermal efficiency with specific work for practical intercooled, reheat and regenerative (ICRHR) cycle.

$$W = RT_1 \ln (Pr_o) \qquad [3.26]$$

where T_1 is the temperature at the start of compression and expansion, Pr_o is the pressure ratio of the compression and expansion processes and R is the gas constant of the fluid being compressed or expanded, which is usually air. From the steady flow energy equation:

$$Q - W = c_p(T_2 - T_1)$$

For an ideal isothermal process, $T_2 = T_1$. Thus:

$$Q - W = 0$$

Hence, for an ideal isothermal process, the heat transfer equals the work transfer as described by Equation 3.26 above.

The ideal Ericsson cycle may be described on a temperature–entropy diagram as shown in Fig. 3.33. The thermodynamic processes involved in the cycle are:

- 1–2 isothermal compression
- 2–3 constant pressure heat addition
- 3–4 isothermal expansion
- 4–1 constant pressure heat rejection.

The heat rejected (4–1) by the Ericsson cycle may be transferred via a heat exchanger to supply all the constant pressure heat addition (2–3). Thus the net heat supplied in the Ericsson cycle is the heat transfer during isothermal expansion (3–4) and equals $W = RT_3 \ln (Pr_o)$.

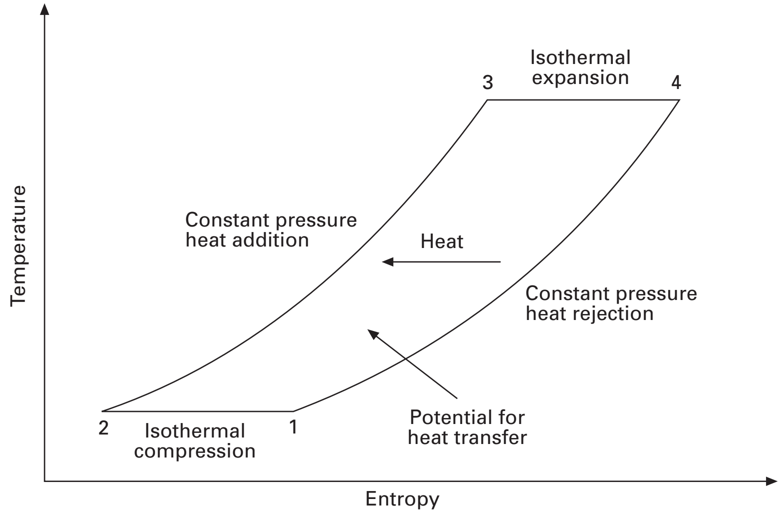

3.33 Ericsson cycle on the temperature–entropy diagram.

The ideal net work done by the Ericsson cycle is:

$$W_{\text{net}} = RT_3 \ln(Pr_o) - RT_1 \ln(Pr_o)$$

Thus, the ideal thermal efficiency of the Ericsson cycle is:

$$\eta_{\text{th}} = \frac{RT_3 \ln(Pr_o) - RT_1 \ln(Pr_o)}{RT_3 \ln(Pr_o)}$$

This reduces to:

$$\eta_{\text{th}} = 1 - \frac{T_1}{T_3} \tag{3.27}$$

Thus the ideal thermal efficiency of the Ericsson cycle is independent of pressure ratio and only depends on the maximum and minimum cycle temperatures, T_3 and T_1, respectively, and is equal to the Carnot efficiency. This is not entirely surprising as all the heat is supplied at the highest cycle temperature and all the heat is rejected at the lowest cycle temperature. This is indeed the Carnot requirement for maximum thermal efficiency and hence the Carnot efficiency is achieved. It should be pointed out that this is in contrast with the ideal simple cycle gas turbine, whose thermal efficiency is dependent only on the pressure ratio and is independent of the maximum to minimum cycle temperature ratio.

Other cycles have been previously encountered that can achieve the Carnot efficiency but these were at some limit condition when the work done by the cycle is zero. The Ericsson cycle, however, produces positive net work and therefore is of practical importance. It is possible to replace the constant pressure heat addition and heat rejection processes by constant volume heat addition and heat rejection. When this is done, the cycle is known as the Stirling cycle and it, too, is capable of achieving the Carnot efficiency. The Ericsson cycle may be implemented using gas turbine engines and the Stirling cycle finds applications in reciprocating engines.

There are two other gas powered cycles that are capable of attaining the Carnot cycle and they are both modified forms of the Ericsson and Stirling cycle. The modified Ericsson cycle consists of an isothermal compression process followed by an isentropic compression process. Heat is added at constant pressure followed by an isothermal expansion. The isothermal expansion is then followed by a constant pressure heat rejection process, which is then followed by an isentropic expansion, as illustrated in Fig. 3.34. It is necessary that the isothermal compression and expansion processes are of equal pressure ratio and therefore require that the isentropic compression and expansion pressure ratios are also equal. A heat exchanger is employed to transfer the constant pressure heat rejection process (5–6) to the constant pressure heat addition process (3–4). In the case of the modified Stirling

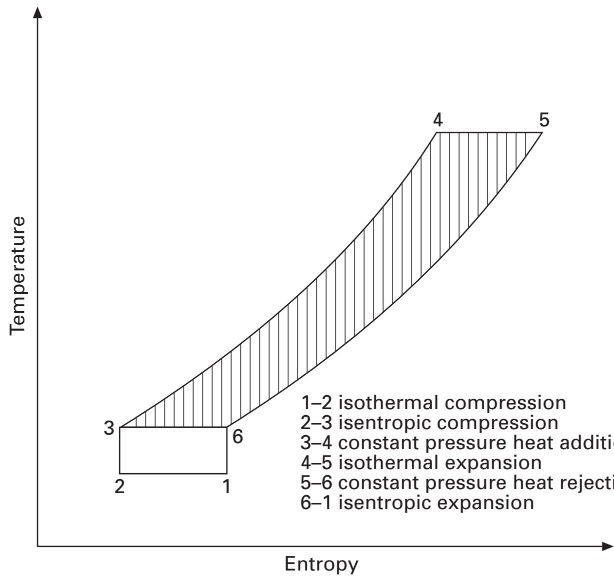

3.34 Temperature–entropy diagram for modified Ericsson cycle.

cycle, the constant pressure processes are replaced by constant volume processes.

The following list summarises the thermodynamic processes present in the modified Ericsson cycle:

- 1–2 isothermal compression
- 2–3 isentropic compression
- 3–4 constant pressure heat addition
- 4–5 isothermal expansion
- 5–6 constant pressure heat rejection
- 6–1 isentropic expansion.

Since a heat exchanger transfers all the constant pressure heat rejection 5–6 to supply all the constant pressure heat addition 3–4, all the heat is supplied at the maximum cycle temperature T_4 and all the heat rejection occurs at the minimum cycle temperature T_1. Hence the thermal efficiency of the modified Ericsson cycle corresponds to the Carnot efficiency

$$\eta_{th} = 1 - \frac{T_1}{T_4}$$

It can be argued that these modified cycles are a general case of the Ericsson and Stirling cycles since only when the isentropic compression and expansion pressure ratios tend to unity do these modified cycles approach the Ericsson and Stirling cycles. When the isothermal compression and expansion pressures ratio tend to unity, the modified Ericsson cycles approach the conventional regenerative cycle. Such regenerative cycles have been considered as a means to improve the part-load or off-design thermal efficiency of gas turbines.[3]

3.4.1 Practical Ericsson cycle

In practice, approximate isothermal compression involves many stages of intercooling and such compressors have been developed for application in the process industry. Typically, they consist of three or four stages of intercooling and are often referred to as *isotherm* compressors. Isothermal expanders for gas turbines are rare and, when developed, may consist of three or four stages of reheat. Furthermore, the thermodynamic processes in a practical cycle are not reversible. When such imperfections are taken into account, there is a significant departure in the thermal efficiency from the ideal case.

Nonetheless, thermal efficiencies exceeding 60% are possible, as illustrated in Fig. 3.35. However, it should be noted that the thermal efficiency is more dependent on the maximum cycle temperature than on pressure ratio, particularly at high cycle pressure ratios and this is due to the ideal Ericsson cycle thermal efficiency being dependent on temperatures rather than on pressure ratios.

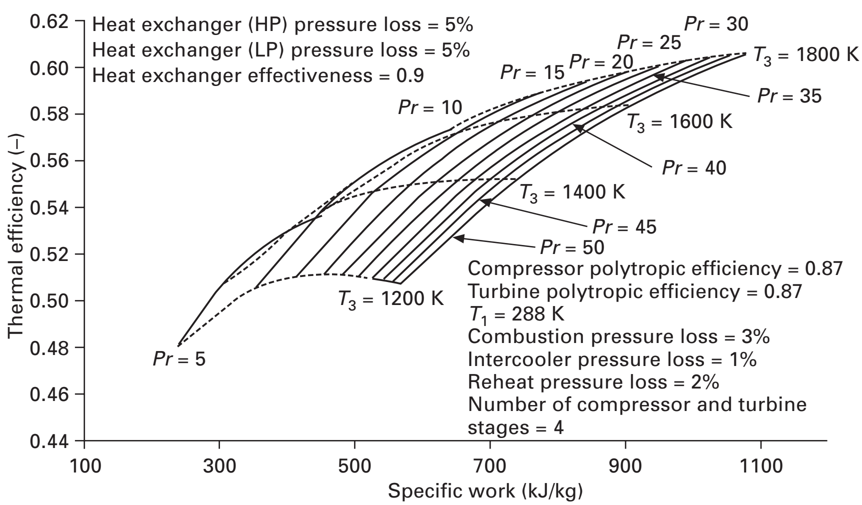

3.35 Variation of thermal efficiency with specific work for a practical Ericsson cycle.

3.5 Combined cycle gas turbines

With ideal regenerative gas turbine cycles, the increase in thermal efficiency is achieved by transferring some of the heat rejected into the compressor discharge air via a heat exchanger, resulting in a reduction in the heat input. The power output remains essentially the same. In combined cycle gas turbines, we utilise the rejected heat to produce more power thus increasing the thermal efficiency of the whole power-producing system. The waste heat or exhaust heat from the gas turbine is passed through a waste heat recovery boiler (WHB) to raise high-pressure steam, which is used by a steam turbine to produce power. Since the increase in power output occurs without the input of additional heat, the overall thermal efficiency is increased.

A schematic presentation of a combined cycle gas turbine plant using a dual pressure boiler system is shown in Fig. 3.36. A dual pressure systems increase the average temperature of the steam, as shown in Fig. 3.37, which describes the temperature–enthalpy diagram of a combined cycle gas turbine. This approach increases the thermal efficiency of the steam cycle, thus converting more of the exhaust heat from the gas turbine into useful power. However, dual pressure systems reduce the amount of superheat and would

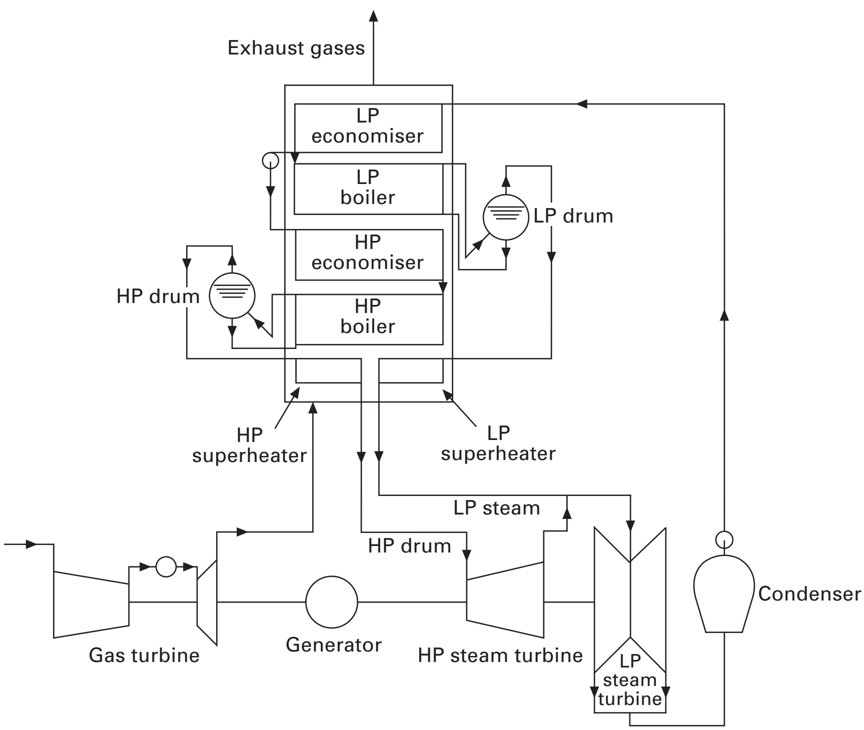

3.36 Schematic representation of a combined cycle gas turbine.

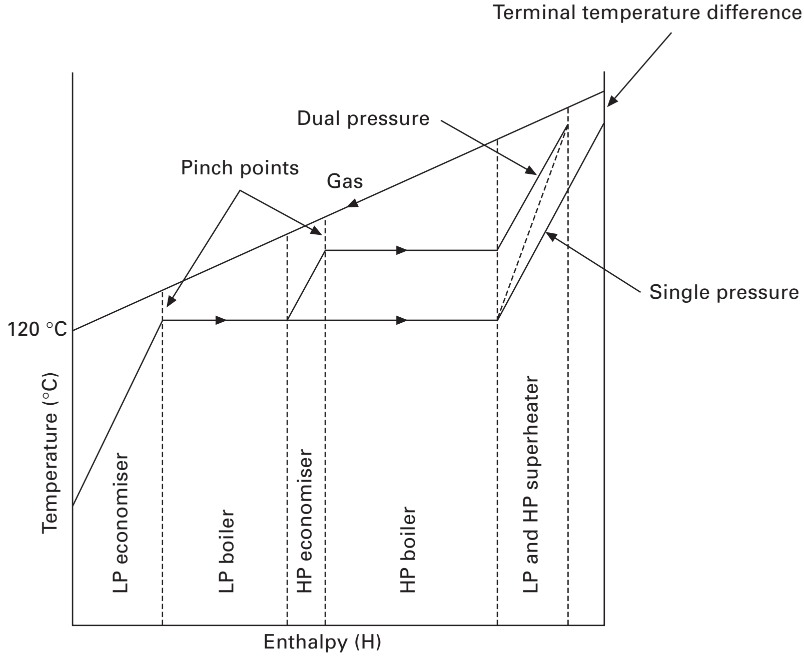

3.37 Temperature–enthalpy diagram for the waste heat recovery boiler (WHB).

reduce the dryness fraction of the steam leaving the steam turbine resulting in erosion problems in the LP stages of the steam turbine. Rogers and Mayhew[4] give further details on the performance of steam turbines and boilers.

Combined cycle gas turbines using a dual pressure system can achieve thermal efficiencies exceeding 55%. Triple pressure combined cycle gas turbines using a reheat gas turbine to increase the gas turbine exhaust gas temperature are being actively proposed. It is claimed that such systems are capable of achieving a thermal efficiency in the order of 60%. The pinch points and the terminal temperature difference should be about 20 °C for a boiler of economic size. The gas exit temperature should be above 120 °C to prevent corrosion.

3.6 Co-generation systems

Industries often require both power and heating loads. In these instances, the exhaust heat from the gas turbine may be used to provide the necessary heating load. Such systems are referred to as co-generation or combined heat and power. The steam generated by the boiler is now used for heating purposes rather than producing power. An overall efficiency of 90% is possible with co-generation systems, but the major problem is low efficiencies when heating demands are low. Such problems may be overcome by employing intercooled regenerative gas turbine cycles to improve the thermal efficiency when heat demand is low and bypassing the gas turbine heat exchanger when the heat demand is high.

Cooling load, as required by air conditioning and chilled water systems, may also be served by co-generation systems. Here, the exhaust heat from the gas turbine is used to drive absorption refrigeration systems to produce the necessary cooling loads. Although such refrigeration systems are less efficient than vapour compression systems, the lower efficiency is of little consequence as the heat source for such refrigeration systems would normally be wasted.

3.7 Hybrid fuel cell–gas turbine system

The employment of heat engines such as gas turbines in the production of electricity involves the gas turbine producing mechanical power, which is then converted to electrical energy by a generator. A fuel cell, on the other hand, directly converts chemical energy such as hydrogen in the presence of oxygen into electrical energy by an electrochemical reaction. As a result, the efficiency of conversion of chemical energy into electrical energy is not constrained by the Carnot efficiency. Thus, in theory, all the chemical energy can be converted into electrical energy, so achieving an equivalent thermal efficiency of 100%. In practice, however, about 80% of the energy can be converted directly into electricity. The electricity produced by fuel cells is direct current (DC) which is converted to alternating current by the use of an inverter.

Although fuel cells can use oxygen from the air, the lack of abundant hydrogen requires this element to be produced from hydrocarbons such as natural gas. This process is referred to as 'reforming' where steam reacts with the hydrocarbon to produce hydrogen, and carbon monoxide, which is oxidised to carbon dioxide. Thus a significant amount of energy from the fuel is lost and the overall efficiency of the fuel cells decreases to about 40%. Currently, fuel cells manufactured using solid-state material are being considered, which also carry out the reforming process but need to operate at high temperatures, typically at about 1000 degrees Celsius. The energy conversion efficiency of these fuel cells, known as solid oxide fuel cells (SOFC), is only about 50%. Nonetheless, this represents an impressive thermal efficiency. Another type of fuel cell that has been considered for use with hydrocarbon fuels and air is the molten carbonate fuel cell (MCFC).

The exhaust heat from such fuel cells, still at a high temperature, may be used to generate electricity via a heat engine. By combining such fuel cells with a gas turbine, practical thermal efficiencies approaching 70% can be achieved.[5] A schematic representation of a hybrid fuel cell–gas turbine system is shown in Fig. 3.38. The high pressure compressor discharge air is

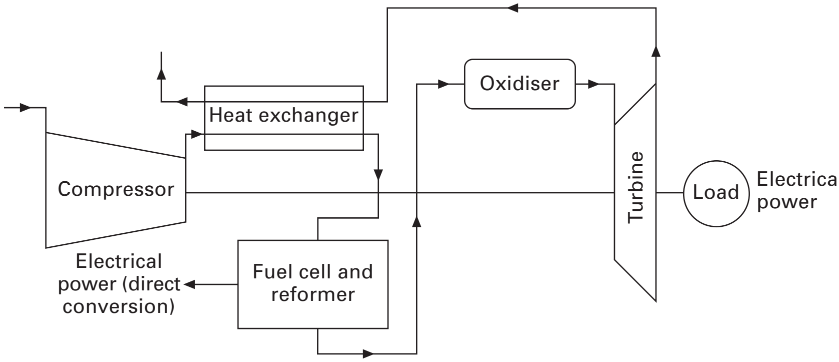

3.38 Schematic representation of a hybrid fuel cell–gas turbine system.

heated in the heat exchanger using the turbine exhaust gases. The heated compressor discharge air enters the fuel cell, where fuel is added and electricity is produced. The high temperature gases leaving the fuel cell enter the turbine, which produces power to drive the compressor and the electrical generator. An oxidiser is provided to ensure combustion is complete. Such a hybrid system is referred to as a 'direct fired turbine' system.

Hybrid fuel cell–gas turbine systems are currently under development and no doubt they will appear in the future. They may first find application in distributed power generation, where power is generated close to the user's site as opposed to centralised power generation, where power is transmitted to users over long distances. Fuel cells may also be used in co-generation systems, where both power and heat/cooling loads are needed by the user.

It must be pointed out that complex gas turbine cycles may also compete for distributed power generation, but will probably include a fuel cell when fully developed. Such complex cycles used in conjunction with fuel cells may be capable of practical thermal efficiencies in excess of 70%.

3.8 References

1. GE's LMS100, a game changer, *Diesel and Gas Turbine Worldwide*, January–February 2004.
2. Intercooled LMS100 pushes simple-cycle efficiency to new heights, *Modern Power Systems*, December 2003.
3. *Unconventional gas turbine cycles for transport application*, Razak, A.M.Y. MSc. dissertation, Cranfield Institute of Technology, 1983.
4. *Engineering Thermodynamics, Work and Heat Transfer*, 4th Edition, Rogers, G.F.C. and Mayhew, Y.R., Longman (1992).
5. *Fuel cell/gas turbine hybrid system*, Samuelsen, S., National Fuel Cell Research Centre, University of California, Irvine, CA 926997-3550, *ASME/International Gas Turbine Institute Conference*, 2004. http:/igti.asme.org/resources/articles/turbo-fuel-cell_report_feb04.pdf

4
Compressors

It has been stated earlier that a simple cycle gas turbine consists of a compression process, a heat addition process and an expansion process. Various devices are required to achieve these processes. Dynamic compressors normally carry out the compression processes in gas turbines and examples of these are centrifugal and axial compressors. Dynamic compressors are compact and quite efficient compared with other types of compressors such as the positive displacement compressor. In this book, the primary concern is with axial compressors, as their use is widespread in gas turbines. The design of axial compressors is a specialist area and only the elementary aspects of axial compressor design will be discussed. Further details on compressor design may be found in Saravanamuttoo *et al.*[1], Cumpsty[2] and McKenzie.[3] Early work on axial compressors may be found in Horlock[4] and Dunham.[5]

4.1 Axial compressors

An axial compressor consists of a series of stages where each stage comprises a rotor and a stator as shown in Fig. 4.1. The kinetic energy of the working fluid, which is usually air, is increased by the rotor and then diffused (the air velocity is reduced) in the stage to increase the static pressure at the outlet of the stage. The amount of diffusion in the rotor and stator is controlled by

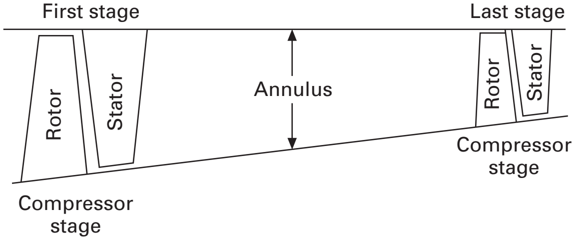

4.1 Axial compressor showing the first and last stages.

the design of the compressor and is often called the reaction of the stage. When all the diffusion takes place in the rotor, the reaction is said to be 100%, and when all the diffusion takes place in the stator, the reaction is 0% (also known as impulse stage). High diffusion in the rotor or stator reduces the efficiency of the compressor and it is normal practice to design for 50% reaction, in which case the diffusion is equal in the stator and the rotor. This is the case at blade mid-height. The reaction will vary from the root to the tip and is dependent on the design of the blade. Further details may be found in Saravanamuttoo *et al.*[1]

4.2 Compressor blading

The stage pressure ratio and efficiency is primarily dependent on blade profile. Figure 4.2 shows the blade profile of a compressor stage. The air enters the rotor and is deflected by the rotor through an angle suitable for the stator, which would prevent it from stalling. The air may diffuse as it passes through the rotor and stator depending on the reaction of the stage. Figure 4.2 also shows the velocity triangles at blade mid-height, where U is the rotor velocity. The air enters the rotor at a relative velocity of V_1. The absolute velocity is C_1 and the angles of V_1 and C_1 relative to the vertical are β_1 and α_1, respectively. The relative and absolute velocities of air leaving the rotor are V_2 and C_2 and their respective angles to the vertical are β_2 and α_2. The design assumes a constant axial velocity Ca and this can be allowed for

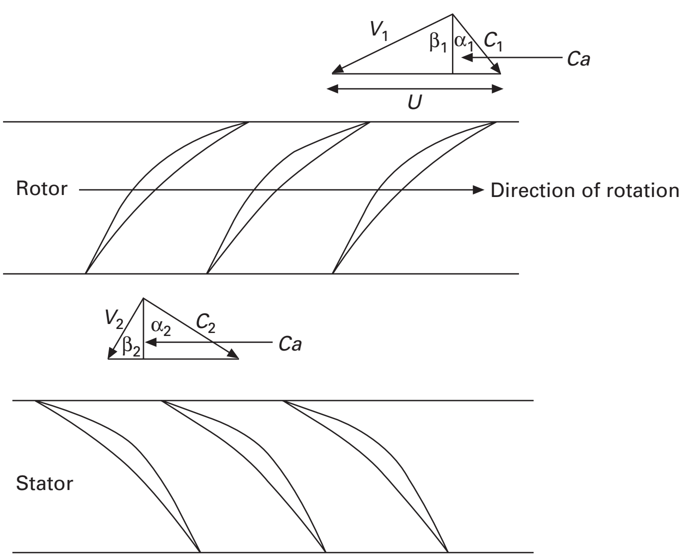

4.2 Blade profile of compressor stage.

by adjusting the convergence of the annulus due to the increase in density as the pressure rises in the compressor.

All the work input into the compressor stage can be entered only via the rotor due to its rotation. Since there is no change in the axial velocity, all the work absorbed by the compressor stage is due to the change in the tangential or whirl velocity (Cw_1 and Cw_2)

where $Cw_1 = Ca \tan(\alpha_1)$

and $Cw_2 = Ca \tan(\alpha_2)$.

For a unit mass flow rate through the stage, the change in whirl velocity is the rate of change in momentum. Newton tells us that the rate of change in momentum is the force acting on the rotor blade. Therefore, the power absorbed by the compressor stage is the force multiplied by the velocity, which in this case is the blade velocity, U. Therefore, the work done per unit mass flow rate, W, is given by:

$$W = U\Delta Vw = U(Cw_2 - Cw_1) = UCa(\tan(\alpha_2) - \tan(\alpha_1)) \qquad [4.1]$$

and the power absorbed will be:

Power = $W \times m$ where m is mass flow rate.

Equation 4.1 will be more useful if we represent the stage work using rotor air angles β_1 and β_2. When this is done, Equation 4.1 can be written as

$$W = UCa(\tan(\beta_1) - \tan(\beta_2)) \qquad [4.2]$$

where $\beta_2 - \beta_1$ is the deflection of the air by the rotor.

Since the two velocity triangles in Fig. 4.2 have the same height Ca and base U, they can be superimposed to produce the combined velocity triangle and this is shown in Fig. 4.3.

Figure 4.3 also shows the rotor and stator deflection and the change in whirl or tangential velocity ΔVw. The diffusion in the rotor and stator results in velocity vector V_2 being less than the velocity vector V_1, and the velocity vector C_1 being less than the velocity vector C_2. The greater is the rotor and stator deflection, the greater the diffusion in the rotor and stator. Since we

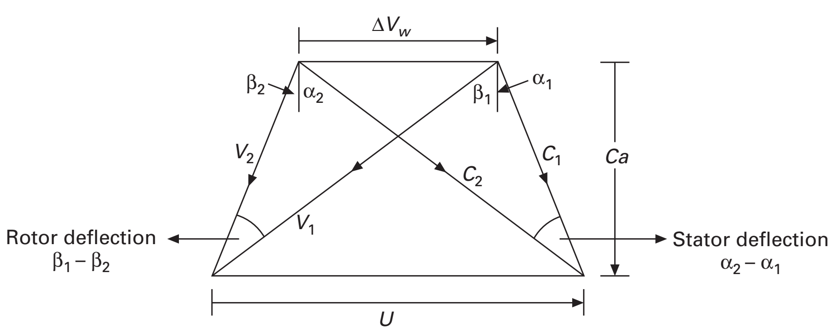

4.3 Combined velocity triangles for rotor and stator.

have constructed the velocity triangles such that the rotor and stator deflections are equal, therefore the amount of diffusion in the rotor and the stator is equal. Thus the reaction for this compressor stage is 50%.

It is evident from Equation 4.2 that the stage work absorbed will increase with the deflection, axial velocity and blade velocity. Increasing the stage work input will result in a smaller number of compressor stages to achieve a given overall pressure ratio.

4.2.1 Increased rotor deflection

Although increasing the deflection will increase the work input, an increase in deflection will also increase the amount of diffusion because it results in a reduction in velocity vector V_2. The change in the velocity triangles due to increased deflection is shown in Fig. 4.4 by the dotted lines. The diffusion may be defined as the ratio of V_2 and V_1. From Fig. 4.4, it is evident that V_2'/V_1 is less than V_2/V_1 and therefore an increase in diffusion will occur due to an increase in deflection. The amount of diffusion must be controlled, as high diffusion will result in increased losses in the stage resulting in lower stage efficiency. A design parameter employed to limit the amount of diffusion is the *de Haller* number, which is simply the ratio of V_2/V_1. Experience has shown that, for acceptable losses, the de Haller number must not be less than 0.72. Also note an increase in tangential or 'whirl' velocity and therefore an increase in stage work input will occur with increased deflection. The increase in diffusion in the rotor increases the reaction of the compressor stage.

4.2.2 Increased axial velocity

From Equation 4.2 it is evident that the stage work input will increase with the axial velocity, *Ca*. Increasing *Ca* also reduces the air flow area required

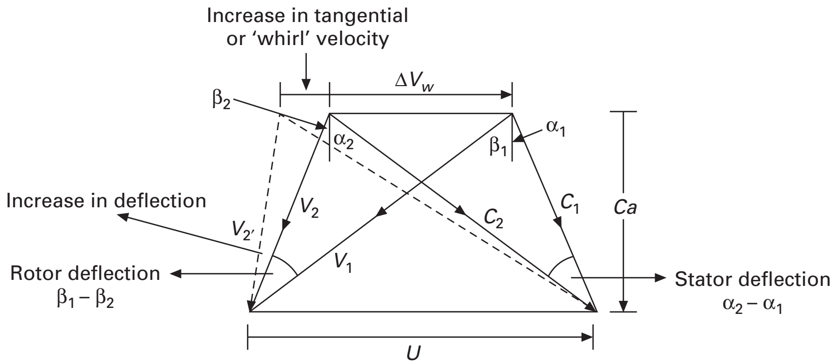

4.4 Change in velocity triangles due to increased deflection.

and the frontal area of the compressor will be smaller. Although of little importance in industrial gas turbines, this effect is of paramount importance in aero-engines to reduce drag. However, the increase in the axial velocity must be limited because the Mach number may be too high and will give rise to compressibility effects. The change in the velocity triangles due to the increase in axial velocity is shown in Fig. 4.5. Note the increase in tangential or whirl velocity. The increase in axial velocity and whirl velocity results in an increase in stage work input. There is also an increase in the stator deflection and therefore increased stator diffusion. This has to be controlled if high losses are to be avoided. The increase in stator diffusion reduces the reaction of the compressor stage.

4.2.3 Increased blade velocity

From Equation 4.2, the effect of increasing the blade velocity U results in increasing work demand by the compressor stage. The upper limit on increasing U is usually the centrifugal stress on the blade. Increasing the blade velocity is quite desirable because there is generally a reduction in deflection and hence in diffusion, as illustrated by Fig. 4.6. This has the effect of improving the stage efficiency. We observe that the stator diffusion has decreased, and therefore increasing the blade speed increases the reaction of the stage. It is quite possible to increase the blade speed such that the reaction is 50%. This will result in a reduction in both rotor and stator deflection.

4.3 Work done factor

The above discusses the aerodynamics of a single compressor stage at blade mid-height. However, the compressor will have many such stages along the

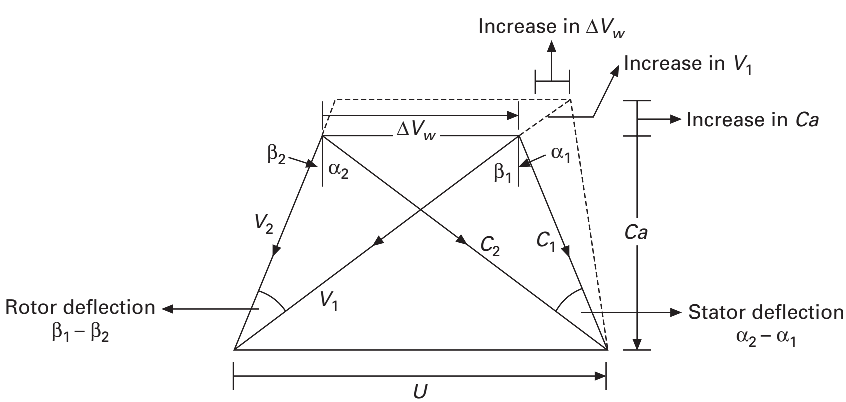

4.5 Effect on increasing *Ca* on velocity triangles.

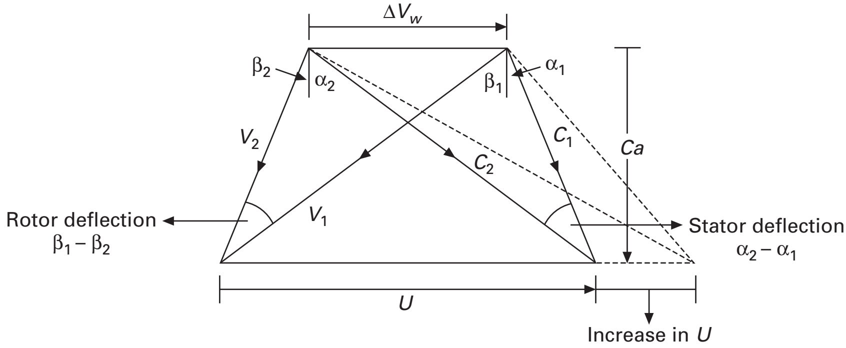

4.6 Effect of increasing *U* on velocity triangles.

annulus of the compressor. The nature of compression is to increase the pressure as the flow progresses along the annulus. This adverse pressure gradient, combined with the flow along an annulus, results in an increase in the thickness of the boundary layer along the annulus. The effect of the boundary layer growth is to reduce the flow area along the annulus and this reduces the work input into the stage due to the reduction in the axial velocity in the boundary layer.

The effect of the boundary layer is more profound at the latter stages (high-pressure stages) than at the front or low-pressure stages, due to the boundary layer thickness being the greatest at the high-pressure stages. This blockage effectively reduces the mean axial velocity *Ca*, thus reducing the stage work as illustrated in Fig. 4.7.

The effect of boundary layer build-up can be allowed for by including a factor λ, known as the work done factor, into Equation 4.2, which gives:

$$W = \lambda UCa(\tan(\beta_1) - \tan(\beta_2)) \qquad [4.3]$$

λ is less 1.

The variation of the work done factor from stage to stage for a typical compressor is shown in Fig. 4.8.

4.4 Stage load coefficient

Since the compression process is adiabatic, the work input, *W*, is equal to the change in stagnation enthalpy, and this is easily derived from the steady flow energy equation $Q - W = \Delta H$. Since $Q = 0$:

$$\Delta H = \lambda UCa(\tan(\beta_1) - \tan(\beta_2)) \qquad [4.4]$$

Dividing Equation 4.4 by U^2 and assuming an ideal compressor ($\lambda = 1$):

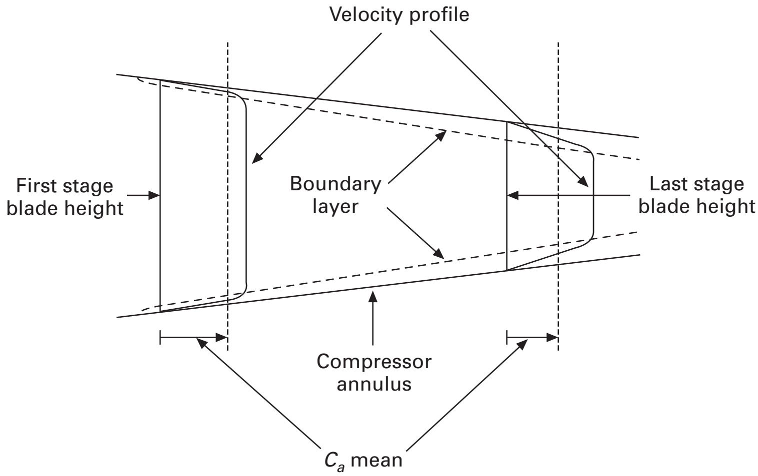

4.7 Growth of boundary layer along the compressor annulus, resulting in a decrease in mean axial velocity.

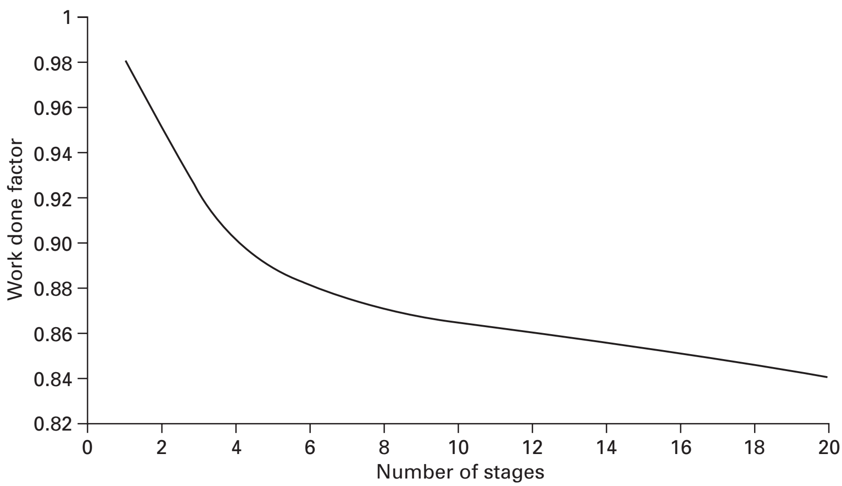

4.8 Typical variation of λ with the number of compressor stages.

$$\frac{\Delta H}{U^2} = \frac{Ca}{U}(\tan(\beta_1) - \tan(\beta_2)) \qquad [4.5]$$

$\Delta H/U^2$ is known as the stage-loading coefficient, ψ, and Ca/U is known as the flow coefficient, Φ. We can rearrange Equation 4.5 in terms of the air outlet angle of the previous stator α_1 and rotor air outlet angle β_2. These angles are determined largely by the blade geometry of the rotor and stator and, in the ideal case, may be assumed independent of the air incidence angles to the rotor, β_1 and the stator, α_2.

Since

$$\Delta Vw = U - Cw_1 - Cw_2 = U - Ca(\tan(\alpha_1) - \tan(\beta_2))$$

we can rewrite Equation 4.5 as

$$\frac{\Delta H}{U^2} = 1 - \frac{Ca}{U}(\tan(\alpha_1) - \tan(\beta_2)) \qquad [4.6]$$

Since we have assumed α_1 and β_2 to be constant, $(\tan(\alpha_1) - \tan(\beta_2))$ is also constant, and Equation 4.6 can be plotted as a straight line, as shown in Figure 4.9.

From Equation 4.6 we see that the stage-loading coefficient tends to 1 when the flow coefficient tends to zero. This implies that the blade speed, U, equals the change in tangential or whirl velocity, ΔVw. The velocity triangles described previously will be rectangular and the diffusion will be excessive, resulting in very low stage efficiency. For satisfactory operation, the stage-loading coefficient should not exceed about 0.5 (subsonic airfoils) if we are to achieve good stage efficiency.

Figure 4.9 also shows the actual characteristic. The deviation from the ideal characteristic is due to losses in the compression stage. The losses in a stage result from the stagnation pressure loss or profile loss across the blade. In an ideal stage the blade outlet angle and air exit angle will be the same (i.e. the deviation, δ, which is the difference between the air exit angle, α_2 and the exit blade angle will be zero) as shown in Fig. 4.10. Air is viscous and results in the growth of a boundary layer along the blade. The growth of the boundary

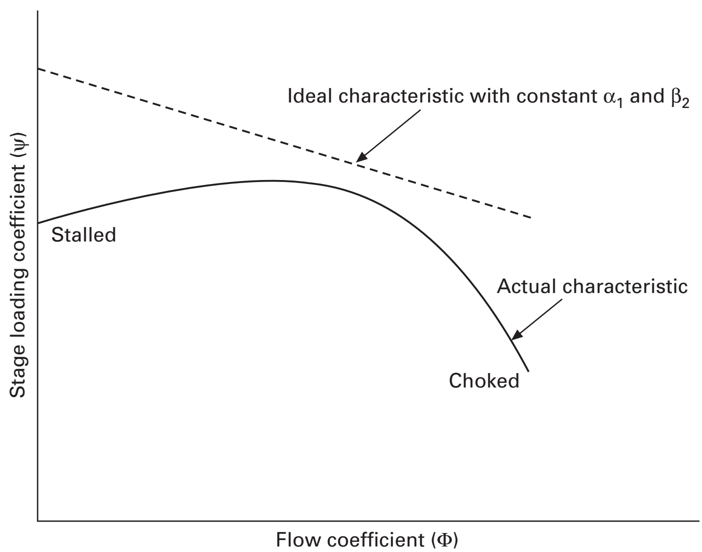

4.9 Ideal and actual stage characteristic.

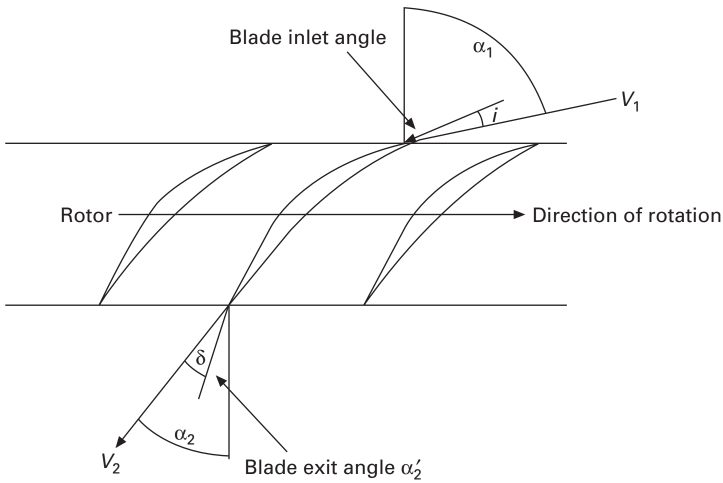

4.10 Deviation due to viscous effects.

layer prevents the air exit angle from reaching the blade exit angle, thus the deviation δ will not be zero. The growth of the boundary layer depends on the blade incidence, i. The larger the incidence, the greater is the boundary layer growth and this results in an increased amount of diffusion and loss, as illustrated by Fig. 4.11, which shows the profile loss varying with incidence. The profile loss manifests itself as a loss in compressor stage efficiency.

As the incidence continues to increase, the blade will eventually stall (i.e. the boundary layer will separate) and this results in a rapid increase in profile loss and deviation as illustrated in Figs 4.11 and 4.12, respectively. At negative incidence, flow increases through the stage resulting in increased profile loss. At very high flows, the inlet Mach number increases (above the critical Mach number) and the losses increase appreciably due to shock loss and are often referred to as negative shock stall. In addition, at high Mach numbers the compressor inlet will choke, restricting the flow in this part of the characteristic (see Fig. 4.9). Both negative and positive stall should be avoided in order to achieve good stage efficiency.

The effect of incidence on deflection is shown in Fig. 4.13. As the incidence, increases, the deflection, and thus the stage pressure ratio, increases. However, when stall starts, the deflection falls as the deviation increases rapidly because the flow cannot follow the blade profile. The start of stall also results in a rapid increase in profile loss, as shown in Fig. 4.11.

4.5 Stage pressure ratio

The temperature rise in the stage is determined by the stage stagnation enthalpy rise, ΔH. Assuming air as a perfect gas, the stage temperature rise, ΔT =

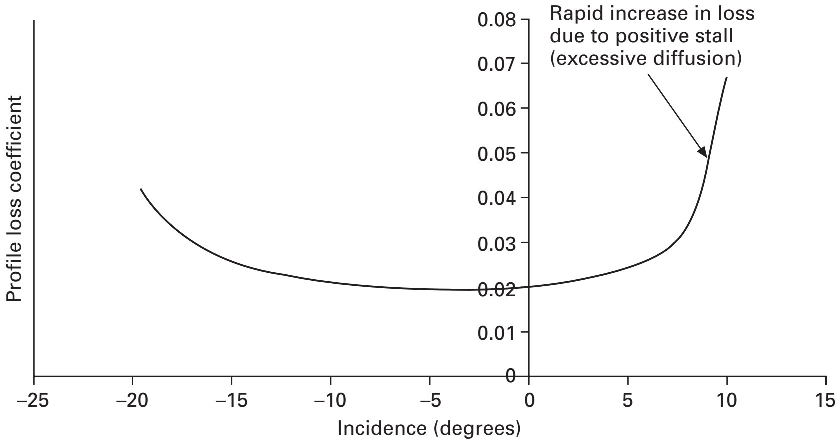

4.11 Variation of profile loss with blade incidence.

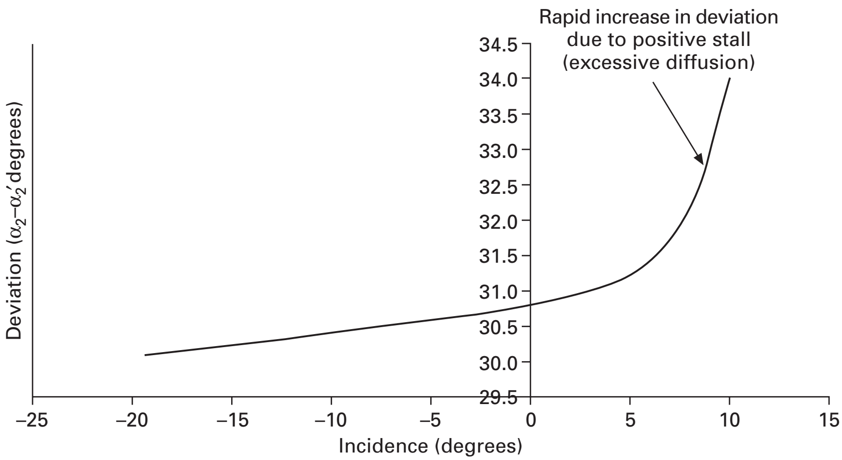

4.12 Variation of deviation with blade incidence.

$\Delta H/c_p$, where c_p is the specific heat of air at constant pressure. The stage pressure ratio Rs can be calculated from the expression:

$$Rs = \left[1 + \eta_s \frac{\Delta T}{T}\right]^{\frac{\gamma - 1}{\gamma}} \qquad [4.7]$$

where

η_s is the stage isentropic efficiency

$\gamma = c_p/c_v$ (ratio of specific heats)

and T is the stage stagnation inlet temperature.

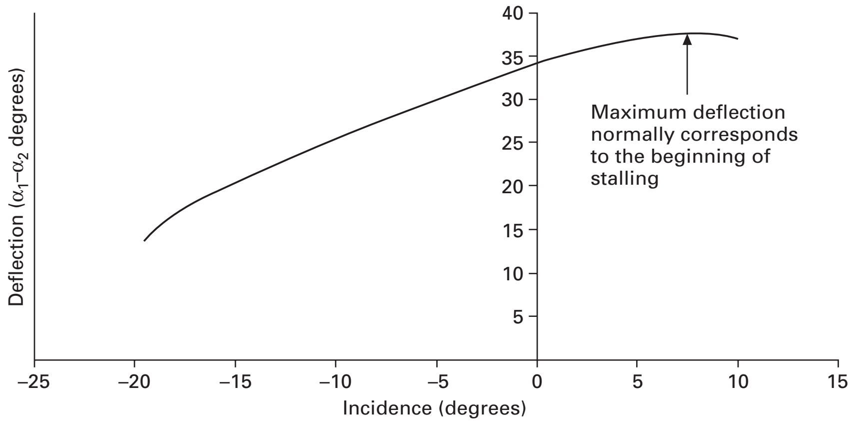

4.13 Effect of incidence on deflection.

4.5.1 Worked example

Stage-loading coefficient = 0.5
Blade velocity U = 250 m/s
Stage inlet temperature T_1 = 288 K
Stage isentropic efficiency η_s = 0.9

$$c_p = 1.005 \text{ kJ/kg K}$$

$$\gamma = 1.4$$

$$\Delta H = 0.5(250)^2/1000 = 31.25 \text{ kJ/kg}$$

$$\Delta T/T_1 = 31.25/288 = 0.1085$$

From Equation 4.7:

$$Rs = [1 + 0.87 \times 0.1085]^{1.4/(1.4-1)} = 1.37125$$

The stage outlet temperature will be:

$$T_2 = \Delta T + T_1 = 31.25 + 288 = 319.25 \text{ K}$$

If the compressor consists of 16 such stages, all having the same stage-loading coefficient and blade velocity at blade mid-height, the temperature rise per stage will be 31.25 K. However, the stage inlet temperature will increase progressively as we move along the compressor towards the higher-pressure stages. Therefore, stage pressure ratio will decrease at the high-pressure stages due to the increase in the stage inlet temperature. By an analysis similar to that discussed in Chapter 2 (Section 2.8.3), we can calculate the overall pressure ratio for all the 16 stages by repeating the above calculation but using the stage inlet temperature as the outlet temperature of the previous stage. When this is done, we get an overall pressure ratio for our compressor of about 21.

4.6 Overall compressor characteristics

Evaluating the engine performance using the compressor stage characteristics is rather cumbersome. A more useful means is to generate the overall compressor characteristic representing the effects of all the stages. This can be achieved by using the stage characteristics in conjunction with techniques such as stage stacking to generate the overall compressor characteristic.[6]

The overall characteristic is normally represented using non-dimensional groups. The groups used are non-dimensional flow, non-dimensional speed, pressure ratio and the isentropic efficiency. The definitions of these groups are as follows:

- non-dimensional flow $W_1\sqrt{T_1}/P_1$
- non-dimensional speed $N_1/\sqrt{T_1}$
- pressure ratio P_2/P_1
- isentropic efficiency η_{12}.

The station numbers 1 and 2 refer to the inlet and discharge of the compressor respectively. The non-dimensional flow and speed are in fact Mach numbers, based on the inlet flow rate and rotational speed, respectively. A typical overall compressor characteristic is shown in Fig. 4.14.

A feature of a compressor characteristic is that constant speed lines become vertical and bunch together as the speed increases. This is due to the compressor inlet stages choking. The figure also shows the contours of constant isentropic efficiency and the surge line on the compressor characteristic. Any operation

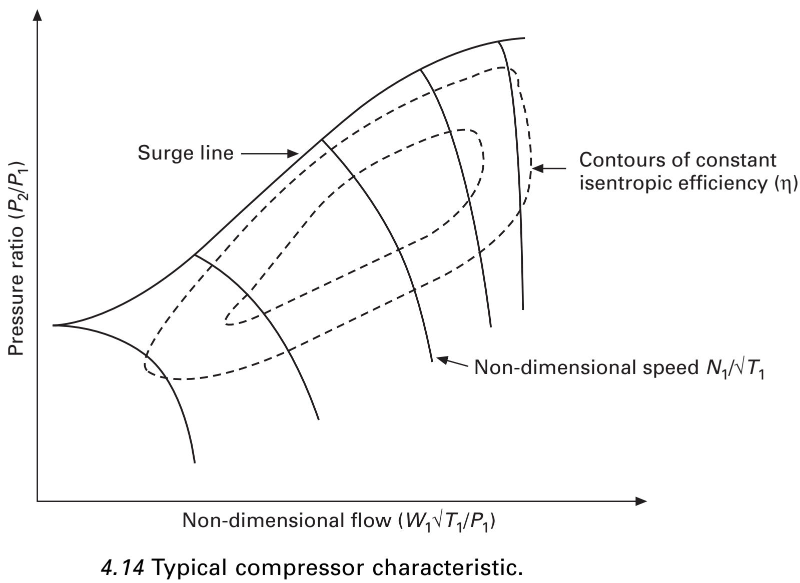

4.14 Typical compressor characteristic.

to the left of the surge line is not possible because of an unstable phenomenon known as surge, which is a violent aerodynamic-induced vibration and must be avoided.

4.7 Rotating stall

Another form of instability that gives rise to a loss in compressor efficiency and can lead into surge is termed rotating stall. As the incidence of the flow entering the blade increases, the flow passing over the blade will separate and stall, resulting in increased losses as shown in Fig. 4.11. Stalling results in increased boundary layer growth and reduces the effective flow area, similar to the discussion on blockage and work done factor.

The increase in boundary layer thickness results in the flow spilling into the adjacent blades, as shown in Fig. 4.15, where the flow into channel B has stalled. This reduces the incidence into channel C and increases the incidence into channel A, forcing channel A to stall. This process continues causing the stalled channel, or cell as it is commonly known, to rotate in a direction opposite to that of the blade. The efficiency loss during rotating stall is not sufficient for flow reversal but is often a precursor to surge. Axial compressors can operate with many of their stages stalled, particularly at low operating speeds.

4.8 Compressor surge

Compressor surge is a rather complex phenomenon but is associated with the stalling of the compressor blades due to high positive incidence. The following is a simplified explanation of surge.

The amount of diffusion has to be controlled and an excessive amount of diffusion will cause the flow to separate from the blade contours, resulting in stalling. Stalling gives rise to a significant loss in efficiency due to high profile losses, as shown in Fig. 4.11.

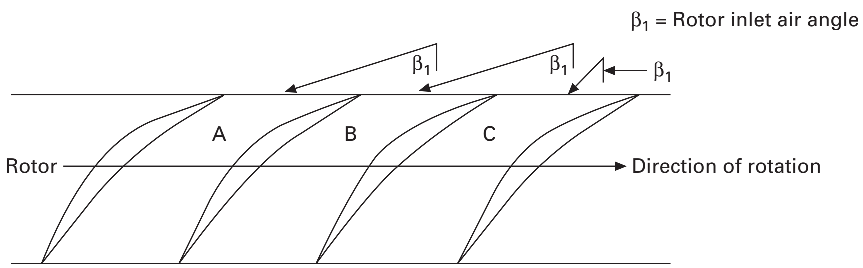

4.15 Rotating stall.

Closing the throttle valve shown in Fig. 4.16, which represents a schematic of a compressor test rig, can produce such conditions. For a given temperature rise across the compressor, the pressure ratio will fall as the efficiency decreases, due to stalling, and this is illustrated in Fig. 4.17, which represents the compression process on a temperature–entropy diagram. If the efficiency loss due to stalling is sufficiently large and rapid, the required discharge pressure cannot be delivered by the compressor and the flow will reverse. This flow reversal results in a reduction in pressure in the discharge volume downstream of the compressor.

When the pressure in the discharge volume has decayed sufficiently, the flow will progress in the normal direction and the discharge pressure will build up (normal compression). Since the conditions that gave rise to the flow reversal in the first instance still prevail, the flow can again break down (separate) and reverse.

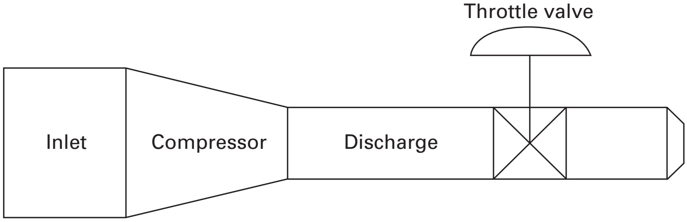

4.16 Schematic of a compressor test rig.

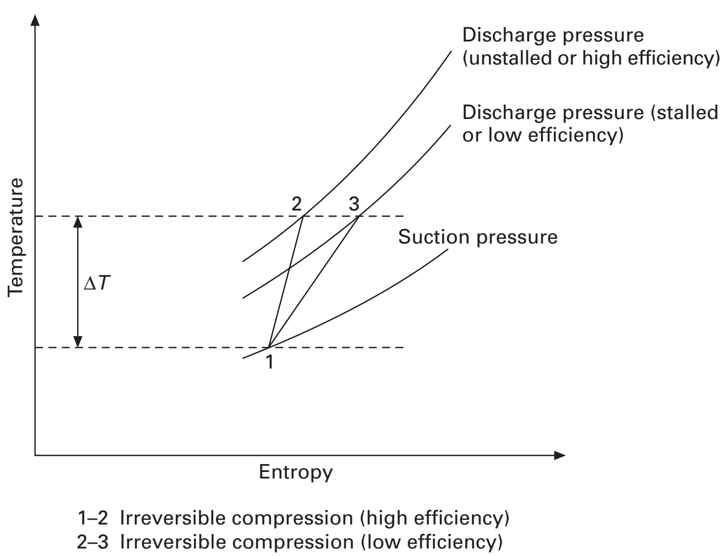

4.17 Effect of efficiency of the compressor discharge pressure on a temperature–entropy diagram.

Such a reversal can occur at quite a high frequency, referred to as surge, and can be very destructive to a compressor. This recompression of what is effectively the compressor discharge air, already at a high temperature, results in very high compressor discharge temperatures during surge. Figure 4.18 shows the stable and unstable, or surge, part of the characteristic for a given compressor speed.

Referring to Fig. 4.18, a small reduction in compressor inlet flow when operating on the stable part of the compressor characteristic (point A) would increase the compressor pressure ratio to point B and thus increase the discharge pressure. This increase in discharge pressure would increase the flow through the throttle valve (shown in Figure 4.16). The increase in flow through the valve will work its way upstream of the compressor during the transient and increase the compressor inlet flow, thus forcing the operating point to return to A. Thus, the compressor is stable when operating in the region where the gradient of the pressure ratio–flow curve is negative.

While operating at point C in Fig. 4.18, a small reduction in flow would decrease the compressor pressure ratio and hence discharge pressure (point D), which will decrease the flow through the valve. The decrease in the valve flow would make its way upstream of the compressor during the transient and further reduce the compressor inlet flow, thus forcing the operating point further to the left of the characteristic. Hence, this part of the compressor characteristic is unstable and would lead to compressor surge. The fall in compressor pressure ratio with flow in the unstable part of the characteristic, and degree of the instability, depend on the loss in compressor efficiency due

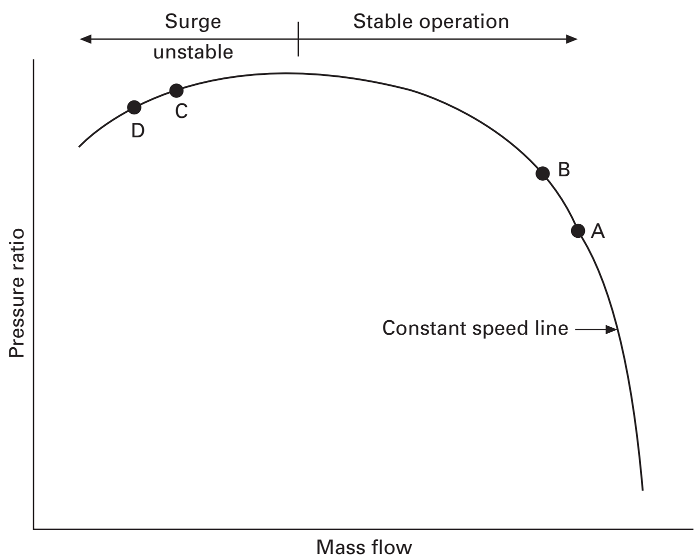

4.18 Theoretical characteristic showing regions and surge operation.

to stalling as discussed, the volumes associated with the compressor, and the discharge or downstream ducting. The flow reversal due to surge can be cyclic, as implied above, or settling or even stable. Greitzer[7] showed that a single parameter can determine the nature of surge. What is often referred to as the Greitzer B parameter is given by:

$$B = \frac{U}{2c}\sqrt{\frac{vp}{Ac \times Lc}}$$

where
U = blade velocity
c = velocity of sound
vp = downstream volume
Ac = compressor mean flow area
Lc = compressor length.

When the values for B are in the range of 0.8 to 5, the surge cycles are cyclic and a deep surge cycle occurs at the higher values of B. When values for B are in the range of 0.45 to 0.6, the surge cycles are settling and give rise to stable (non-oscillatory) conditions at the lower value.

4.9 Compressor annulus geometry

The above discussion describes a single compressor stage and the only reference that has been made to the annulus geometry is the work done factor, which primarily accounts for the boundary layer growth along the compressor annulus. The computation of the stage aerodynamic performance was carried out at the blade mid-height. Figures 4.19, 4.20 and 4.21 show possible annulus designs where the blade mid-height is rising, staying constant or falling.

The effect of increasing deflection, axial velocity and blade velocity can also be considered on the velocity triangles. It is observed that increase in deflection and axial velocity always increases the change in whirl or tangential velocity, resulting in an increase in stage loading coefficient, whereas increase in blade velocity results in a decrease in stage loading coefficient. It has also

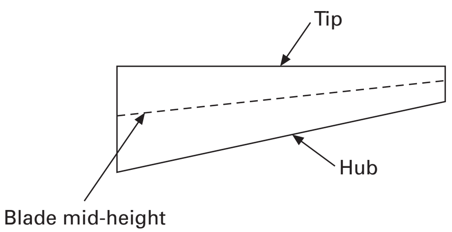

4.19 Rising blade mid-height annulus design.

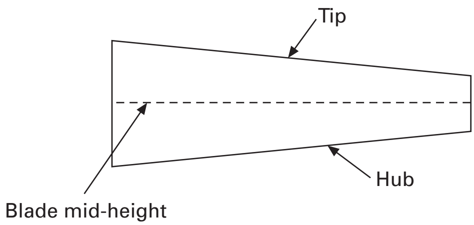

4.20 Constant blade mid-height annulus design.

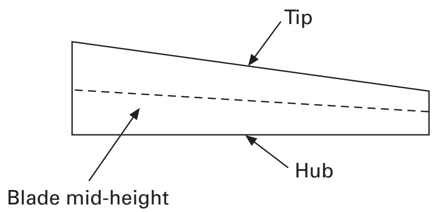

4.21 Falling blade mid-height annulus design.

been stated that the stage-loading coefficient should be about 0.5 or less, if good stage efficiency is to be achieved.

A rising line design as shown in Fig. 4.19 will increase the blade velocity at blade mid-height as we progress along the compressor annulus. Therefore, the stage loading will decrease, continuously improving the stage efficiency. Alternatively, for a given stage-loading coefficient, a higher stage pressure ratio can be obtained as we progress along the annulus with the rising line annulus design. This reduces the number of stages required to achieve a given overall pressure ratio. It may be thought that one always designs for a rising line for the annulus (Fig. 4.19). However, at the high pressure stages, the blade height will reduce and the boundary layer will increase, covering most of the blade height (i.e. the work done factor will decrease), particularly for high pressure ratio compressors.

A parameter that is used to ensure that the boundary layer does not affect the performance of a compressor stage is the hub-to-tip ratio. This ratio should not be allowed to exceed 0.9. For a given overall pressure ratio, the hub-to-tip ratio of the last stage is influenced by the hub-to-tip ratio of the first stage. Due to mechanical stress considerations of the first stage, its hub-to-tip ratio is not allowed to fall below 0.5. For a given compressor stage, the axial velocity, Va, and discharge density, ρ, which is determined by the discharge pressure and temperature, are largely fixed by the compressor blading (velocity triangles). For an air mass flow rate, m, the continuity equation $m = \rho \times Va \times A$ tells us the flow area; A must be fixed and corresponds to the annulus (flow) area as shown by Fig. 4.22.

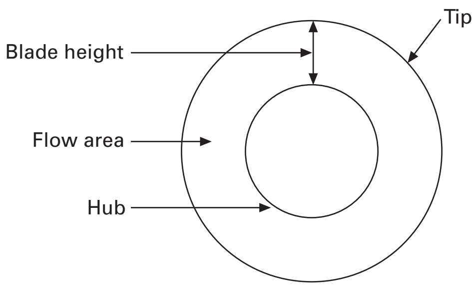

4.22 Typical compressor annulus and flow area.

The flow area is given by:

$$A = \pi h R_t \left(\frac{R_t}{R_h} + 1 \right) \qquad [4.8]$$

where

h is the blade height and equals $R_t - R_h$
R_h = hub radius
R_t = tip radius.

For a falling blade mid-height design, the hub radius is fixed (Fig. 4.21 above). For a given flow area, a reduction in the tip radius will result in a larger blade height, h, compared with a rising line design (Equation 4.8). Therefore, using a falling line design for the annulus, as shown in Fig. 4.21 above, for the HP stages, will result in less of the blade height being covered by the boundary layer. Hence, a higher work done factor is achieved. In other words, the hub-to-tip ratio will decrease. However, the velocity at blade mid-height is falling and a trade-off between lower blade velocity and hub-to-tip ratio should be made in order to optimise the compressor design. A general strategy is to design LP stages using a rising blade mid-height design followed by the IP stages using a constant blade mid-height design. Then the HP stage uses a falling blade mid-height design, particularly for very high pressure ratio compressors.

4.10 Compressor off-design operation

As discussed, an axial compressor comprises many stages. The satisfactory operation of the compressor at off-design conditions is of paramount importance because these conditions are often encountered during start-up and low power operation. Compressor stall and surge may be encountered under such conditions and may make starting the engine or low power operation impossible without some remedial action being taken.

As the compressor speed decreases, the airflow rate falls off more rapidly than the speed. The effect of this is to choke the HP or back stages of the compressor due to the increase in the axial velocity needed in these stages to maintain the flow through the compressor. This forces the LP or front stages to stall and may eventually lead to surge. Conversely, at high operating speeds, the LP or front stages will choke forcing the HP or back compressor stages to stall. The running line on the compressor characteristic, as shown in Fig. 4.23, may intersect the surge line at low compressor speeds, making starting or low power operation impossible. This running line is also dependent on the swallowing capacity of the turbines and will be discussed later. Means to remedy this problem involve incorporating blow-off valves, multi-spooled compressor and variable geometry stators. A detailed discussion on off-design performance of compressors may be found in Saravanamuttoo, *et al.*[1] Harman,[8] and Walsh and Fletcher.[9]

4.10.1 Blow-off valves

Blow-off valves are positioned at some intermediate stages and may be opened during starting. Blow-off reduces the flow to the HP or back stages, thereby reducing the velocity, hence preventing these stages from choking. Therefore, blow-off prevents the front stages from stalling and prevents compressor surge during start-up or low power operation. Blow-off also moves the running line away from the surge line, further improving the surge margin. However, blow-off is a waste of energy and should normally be used as little as possible.

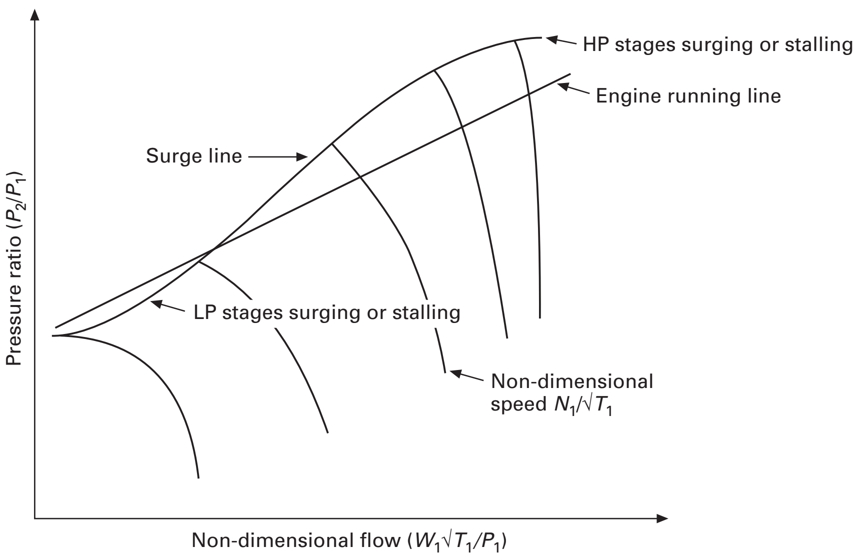

4.23 Compressor surge at different operating conditions.

4.10.2 Multi-spool compressors

As the compressor design pressure ratios increase, the difference in density at the HP stages at design and off-design conditions will increase. This increases the probability of the LP stages stalling and surging during start-up and at low speed operation. The use of blow-off has been discussed as a means of alleviating such surge conditions.

The compressor may also be divided into two or more spools, where there is no mechanical linkage between the two compressor spools, although an aerodynamic link exists between them. Such a division of the compressor results in the HP spool running at a higher speed than the LP spool. Therefore, at low LP compressor speed operation, the HP spool can run at a higher speed and pass more flow through the HP spool. This prevents the choke conditions in the HP stages that give rise to the surge problems at start-up and low speed operations. Clearly, blow-off can be eliminated or reduced during start-up and low speed operation, so improving the performance of the gas turbine under these conditions. Schematic representations of gas turbines using such compressor configurations are shown in Figs. 1.3 and 1.4 in Chapter 1.

4.10.3 Variable geometry compressors

An alternative to using multi-spooled compressors to improve the off-design performance of axial compressors operating at high pressure ratios is to use several variable stators at the front of the compressor. Closing these variable stators at low compressor speeds reduces the stage loading on these stages.

Figure 4.24 shows the effect of the closure of the stator on the velocity triangles (dotted lines). We observe how the rotor deflection ($\beta_1 - \beta_2$) and the

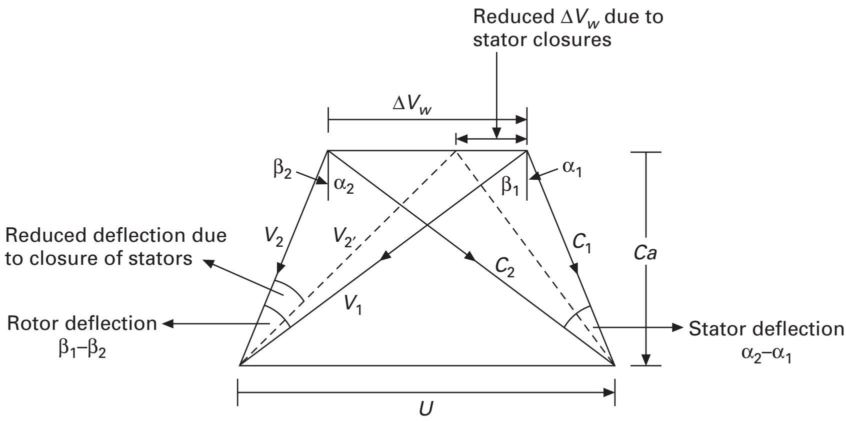

4.24 Effect of closure of the stator on the velocity triangles.

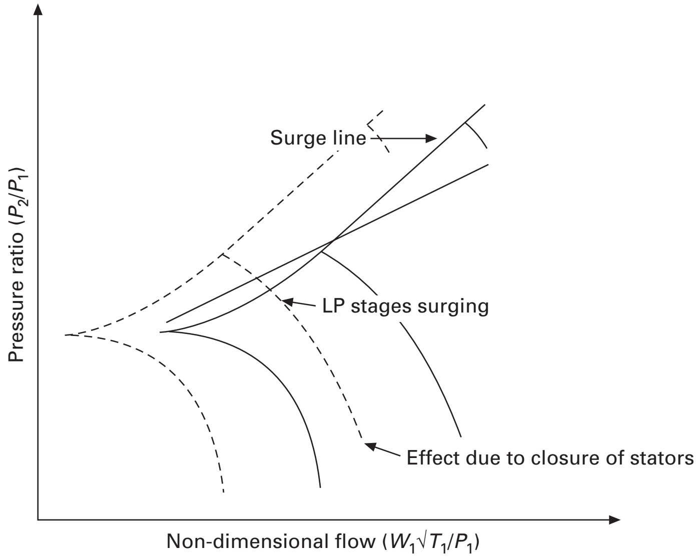

4.25 Effect of stator closure on the compressor characteristic.

amount of diffusion ($V_{2'}/V_1 > V_2/V_1$) decrease and prevent stalling of the front stages of the compressor. A similar effect is also seen on the stator deflection ($\alpha_2 - \alpha_1$). Note the reduction in whirl or tangential velocity ΔVw, resulting in a lower stage-loading coefficient.

The change in the compressor characteristic due to stator closure is shown in dotted lines in Fig. 4.25. With the stators closed, the running line does not intersect the surge line at low compressor speeds and the engine can now be started. At high compressor speeds, the front stages start to choke, forcing the back stages to stall. It would be possible to open the stators of the front stages to allow more flow in an attempt to prevent the back stages from stalling. However, there is a limit to opening the stators and as a result it is thought that the maximum pressure ratio that can be achieved in a single spool is limited to about 20.[10,11]

4.11 References

1. *Gas Turbine Theory*, 5th Edition, Saravanamuttoo, H.I.H., Rogers, C.F.G. and Cohen, H., Longman (2001).
2. *Compressor Aerodynamics*, Cumpsty, N.A., Longman (1989).
3. *Axial Flow Fans and Compressors*, McKenzie A.B., Ashgate (1997).
4. *Axial Compressors*, Horlock, A.J., Butterworth (1958).
5. A.R. Howell: Father of the British axial compressor, Dunham, J., *ASME paper 2000-GT-8*, 2000.
6. Effects of stage characteristics and matching on axial-flow compressor performance, Stone, A., *Transactions of the ASME*, 1958.

7. Surge, and rotating stall in axial flow compressors, *Journal of Engineering and Power*, Greitzer, E.M. 98 (April 1976) 190–217.
8. *Gas Turbine Engineering*, Harman, R.T.C., Macmillan Press (1981).
9. *Gas Turbine Performance*, 2nd Edition, Walsh, P.P. and Fletcher, P., Blackwell Publishing (2004).
10. Design and development of a 12:1 pressure ratio compressor for the Ruston 6 MW gas turbine, Carchedi, F. and Wood, G.R, *ASME Journal of Engineering for Power*, 1982.
11. Aerodynamic design and testing of an axial-flow compressor with a pressure ratio of 23.3 for the LM2500+ gas turbine, Wadia, A.R., Wolf, D.P. and Haaser, F.G., *ASME paper 99-GT-210*.

5
Axial turbines

An axial turbine, as with axial compressors, consists of a series of stages, with each stage composed of a stator and a rotor, as shown in Fig. 5.1. The gases are expanded through the turbine, which extracts work in the process. The amount of expansion in the stator and rotor is controlled by the design of the turbine and is called the reaction of the stage. When all the expansion takes place in the rotor, the reaction is said to be 100% and when all the expansion takes place in the stator, the reaction is 0% (impulse stage). More details on axial turbines may be found in Saravanamuttoo, *et al.*[1] Early notable work on axial turbines is given in Horlock.[2]

The pressure decreases through the stages and this condition is referred to as a favourable pressure gradient. As a result, there is no question of turbines surging, and the amount of work extracted from a turbine stage can be considerably larger than that absorbed by a stage of a compressor. Consequently, a single turbine stage can drive many compressor stages as is often observed in practice.

5.1 Turbine blading

As with compressors, the stage pressure ratio and efficiency is dependent mostly on the stator and rotor blade profile. Figure 5.2 shows the blade

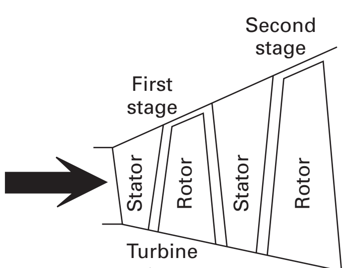

5.1 Axial turbine with two stages.

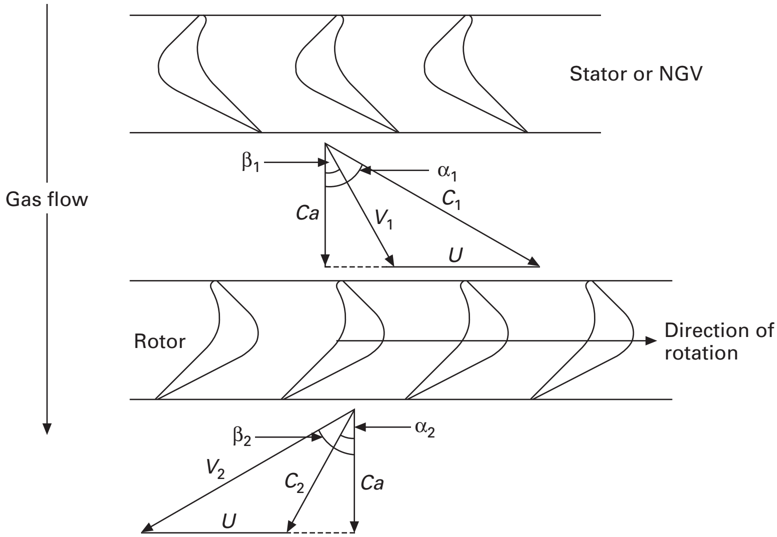

5.2 Turbine stage.

profile for a single turbine stage. The gas enters the stator, also known as the nozzle or nozzle guide vane (NGV), and is deflected through a suitable angle to the rotor to minimise losses (Denton, 1993). The gas may expand as it passes through the stator and the rotor, and the amount of expansion is determined by the reaction of the stage.

Figure 5.2 also shows the velocity triangles at inlet and exit from the rotor. The rotor produces all the work done from the turbine stage. Therefore, the power output by a turbine stage is the torque multiplied by the blade velocity. The torque is produced by a change in the swirl or tangential velocity.

The swirl or tangential velocity into the rotor, Cw_1, is given by:

$$Cw_1 = Ca \tan(\alpha_1) \tag{5.1}$$

and the swirl or tangential velocity at exit from the rotor, Cw_2, is given by:

$$Cw_2 = Ca \tan(\alpha_2) \tag{5.2}$$

Thus, the change in swirl velocity ΔVw is given by:

$$\Delta Vw = Cw_1 - (-Cw_2) = Cw_1 + Cw_2 \tag{5.3}$$

because Cw_2 acts in the opposite direction to Cw_1.

The work done per unit mass flow rate, W, is given by:

$$W = \Delta VwU \tag{5.4}$$

where U is the blade velocity.

$$\Delta Vw = Ca(\tan(\alpha_1) + \tan(\alpha_2)) \qquad [5.5]$$

Therefore:

$$W = UCa(\tan(\alpha_1) + \tan(\alpha_2)) \qquad [5.6]$$

where Ca is the axial velocity.

It is more useful to represent Equation 5.6 in terms of rotor angles. Using the relationship:

$$U = Ca(\tan(\alpha_1) - \tan(\beta_1)) = Ca(\tan(\beta_2) - \tan(\alpha_2)) \qquad [5.7]$$

$$W = UCa(\tan(\beta_1) + \tan(\beta_2)) \qquad [5.8]$$

where $\beta_1 + \beta_2$ is the rotor deflection.

Unlike compressors, with turbines the pressure decreases and, as a result, the boundary layer growth is much smaller in turbines compared with compressors. Consequently, the work done factor to account for the boundary layer growth is unnecessary and therefore the work done factor λ can be set to unity.

The flow area can be increased along the turbine to account for the reducing density in such a manner that the axial velocity, Ca, is constant. The inlet and exit velocity triangles can therefore be superimposed on a common base, U, which corresponds to the velocity diagram shown in Fig. 5.3.

5.2 Stage load and flow coefficient

From the steady flow energy equation ($Q - W = \Delta H$), where ΔH is the enthalpy change, for an adiabatic process we can rewrite Equation 5.8 as:

$$\Delta H = UCa(\tan(\beta_1 + \tan(\beta_2)) \qquad [5.9]$$

And dividing by U^2:

$$\frac{\Delta H}{U^2} = \frac{Ca}{U}(\tan(\beta_1) + \tan(\beta_2)) \qquad [5.10]$$

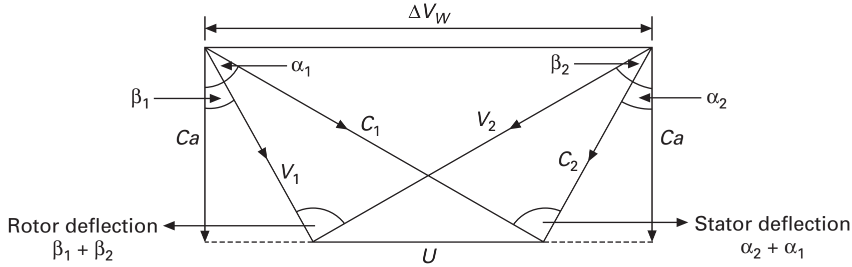

5.3 Combined velocity triangles for turbine stage.

$\Delta H/U^2$ and Ca/U are called the stage loading and flow coefficients, respectively. It is worth noting that the stage loading coefficient is also given by $\Delta Vw/U$.

Smith[4] generated a correlation relating turbine efficiency with the stage loading and flow coefficients and this is often referred to as the Smith plot. This is shown in Fig. 5.4. It is a useful source of data when designing a turbine.

Having selected a stage loading and flow coefficient, the designer can easily estimate the stage efficiency. For instance, with a flow coefficient of 0.8 and a stage loading coefficient of 2.5, the stage efficiency can be estimated to be between 88% and 89%. There is no equivalent diagram for compressors and the stage-loading coefficient for compressors as stated in Chapter 4 should be kept below 0.5 (subsonic compressors). Industrial engines may use low stage loading and flow coefficients in order to achieve high stage efficiency. Aero-derived gas turbines may use higher values in order to keep the weight and frontal area down.

From Equation 5.9 it is observed that the stage work done will increase as the rotor deflection ($\beta_1 + \beta_2$), axial velocity, Ca, and blade velocity, U, increase. Increasing one or more of these parameters will result in a smaller number of stages to achieve a given overall turbine pressure ratio and thus power output.

5.2.1 Rotor deflection

Increasing the deflection in the rotor will alter the velocity triangles as shown by the dotted lines in Fig. 5.5. There is an increase in the change in

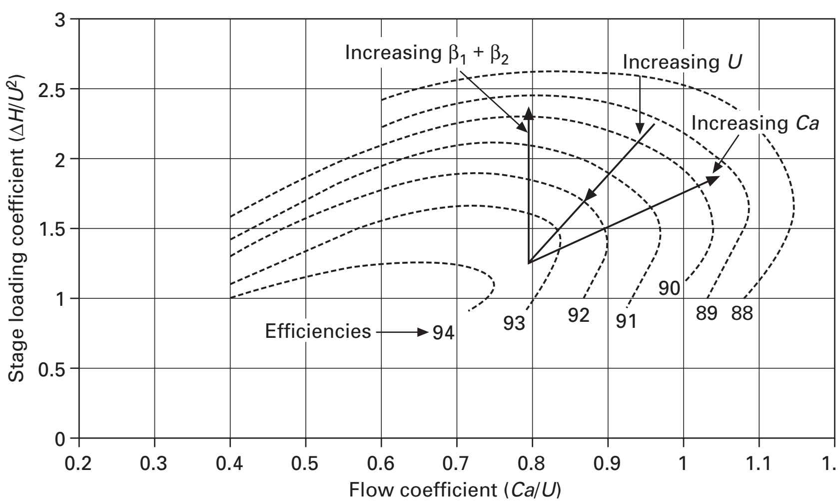

5.4 Variations of stage efficiency with stage loading and flow coefficient for axial turbines.

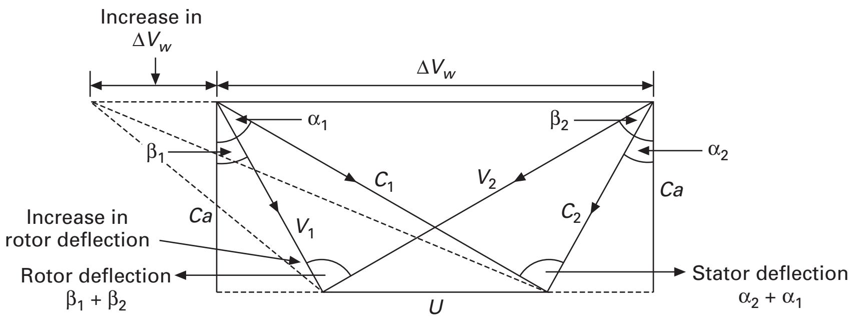

5.5 Effect of increased rotor deflection on velocity triangles.

swirl velocity ΔVw, which will result in an increase in the stage-loading coefficient $\Delta Vw/U$. The flow coefficient remains unaltered since U and Ca do not change. The increase in stage-loading coefficient will result in a decrease in stage efficiency, as shown on the Smith plot in Fig. 5.4. Increasing the rotor deflection increases the velocity of V_1 and C_1, thus resulting in increased losses.

5.2.2 Axial velocity

The effect on the velocity triangles of increasing the axial velocity is shown by the dotted lines in Fig. 5.6. Increasing the axial velocity, Ca, increases both the stage loading and flow coefficients.

Increases in stage loading and flow coefficients result in a reduction in the stage efficiency as shown in the Smith plot in Fig. 5.4. An increase in all velocity vectors with the exception of blade velocity is observed. There is also an increase in the stator deflection. The net effect results in a lower stage efficiency.

5.2.3 Blade velocity

Increasing blade velocity also increases the stage work done but achieves this at lower stage loading and flow coefficients. The effect of increasing blade velocity on the velocity triangles is shown by the dotted lines in Fig. 5.7.

Referring to Fig. 5.7, we observe a reduction in stage loading, $\Delta Vw/U$, and a low flow coefficient, Ca/U. This results in an increase in stage efficiency and therefore it is very desirable to maintain high blade velocity. The improved efficiency due to the increase in blade velocity is also shown in Fig. 5.4 (Smith plot).

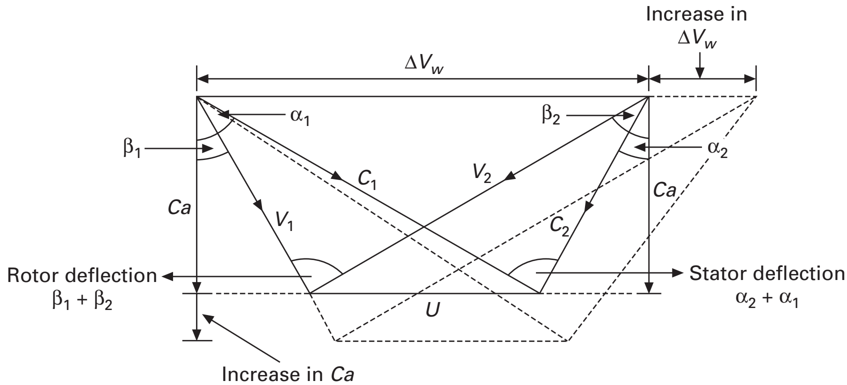

5.6 Effect of increased axial velocity on velocity triangles.

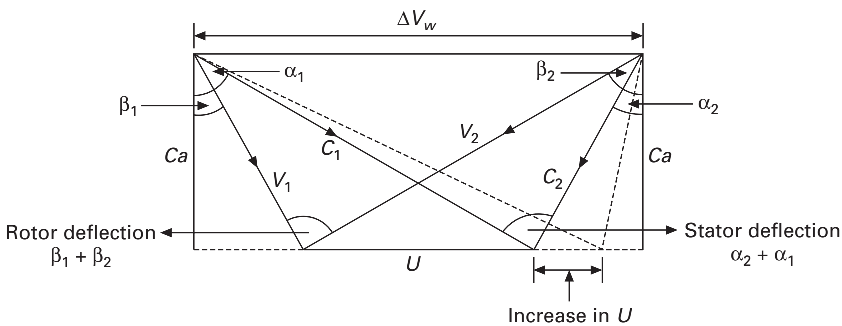

5.7 Effect of increased blade velocity on velocity triangles.

5.3 Deviation and profile loss

Unlike a compressor stage the favourable pressure gradient present in a turbine stage means that the gas outlet angle β_2 does not change very much with incidence and closely follows the blade outlet angle. This is primarily due to the small boundary layer growth, as stated earlier, enabling a work done factor of unity to be assumed. The profile loss will increase with incidence and this is due to the high stage velocities (particularly at positive incidence) caused by increasing friction loss. See Saravanamuttoo *et al.*[1] for further details regarding these issues.

5.4 Stage pressure ratio

The temperature change in the stage is determined by the stage stagnation enthalpy change ΔH. Assuming the products of combustion act as a perfect gas, the stage temperature change is given by $\Delta T = \Delta H/c_p$, where c_p is the specific heat of the gas at constant pressure. The stage pressure ratio, *Rs*, can be calculated from the expression:

$$Rs = \frac{1}{\left[1 - \dfrac{\Delta T}{T\eta_s}\right]^{\frac{\gamma}{\gamma-1}}} \qquad [5.11]$$

where
η_s is the stage isentropic efficiency
$\gamma = c_p/c_v$ (ratio of specific heats)
and T is the stage inlet temperature (total or stagnation).

5.4.1 Worked example

The turbine (Fig. 5.1) consists of two stages whose stage-loading coefficients are identical and the turbine uses a constant mean diameter design.

First stage

Stage-loading coefficient = 2.5
Blade velocity, U = 250 m/s
Stage inlet temperature, T_1 = 1400 K
Stage isentropic efficiency η_s = 0.9

$$c_p = 1.147 \text{ kJ/kg K}$$

$$\gamma = 1.333$$

$$\Delta H = 2.5(250)^2/1000 = 156.25 \text{ kJ/kg}$$

$$\Delta T = \Delta H/c_p = 156.25/1.147 = 136.22 \text{ K}$$

From Equation 5.11:

$$Rs = 1/[1 - 136.22/(1400 \times 0.9)]^{1.333/(1.333-1)} = 1.58036$$

The stage outlet temperature will be:

$$T_2 = T_1 - \Delta T = 1400 - 136.22 = 1263.78 \text{ K}$$

Second stage

$$\Delta H = 2.5(250)^2/1000 = 156.25 \text{ kJ/kg}$$

$$\Delta T = \Delta H/c_p = 156.25/1.147 = 136.22 \text{ K}$$

$$Rs = 1/[1 - 136.22/(1263.78 \times 0.9)]^{1.333/(1.333-1)} = 1.6657$$

$$T_2 = T_1 - \Delta T = 1263.78 - 136.22 = 1127.56 \text{ K}$$

The overall pressure ratio will be the product of the two stage pressure ratios. Hence the turbine overall pressure ratio $Pr_o = 1.58036 \times 1.6657 = 2.5045$.

If the two-stage turbine were to drive the compressor, as discussed in Chapter 4 (Section 4.5), there would be a shortage on power. The enthalpy rise per compressor stage is 31.25 kJ/kg. For 16 stages, the total enthalpy per unit mass flow rate would be 500 kJ/kg. The turbine produces only an enthalpy drop of $156.25 \times 2 = 312.5$ kJ/kg. If the blade velocity, U, is increased from 250 m/s to 325 m/s and the same enthalpy rise in the compressor is maintained, then the turbine will produce an enthalpy drop of 528.125 kJ/kg, which is in excess of that needed by the compressor.

A turbine entry temperature of 1400 K will require cooled turbine blades and the efficiency will be reduced to about 90%. A constant enthalpy rise has been maintained across the compressor stage and the speed has been increased. This will result in a reduced stage-loading coefficient and will benefit the compressor by improving the efficiency of the compressor.

It may be concluded that a two-stage turbine could drive the compressor discussed above, thus illustrating that the higher stage-loading coefficients present in turbines require fewer turbine stages to drive many stages of compressors.

5.5 Overall turbine characteristics

As with compressors, it is convenient to represent turbine performance in terms of non-dimensional parameters such as flows and speeds, which are based on all the stages in the turbine. This is very useful when we wish to carry out off-design performance calculations of the gas turbine. Typical turbine characteristics are shown in Figs 5.8, 5.9 and 5.10, where the inlet

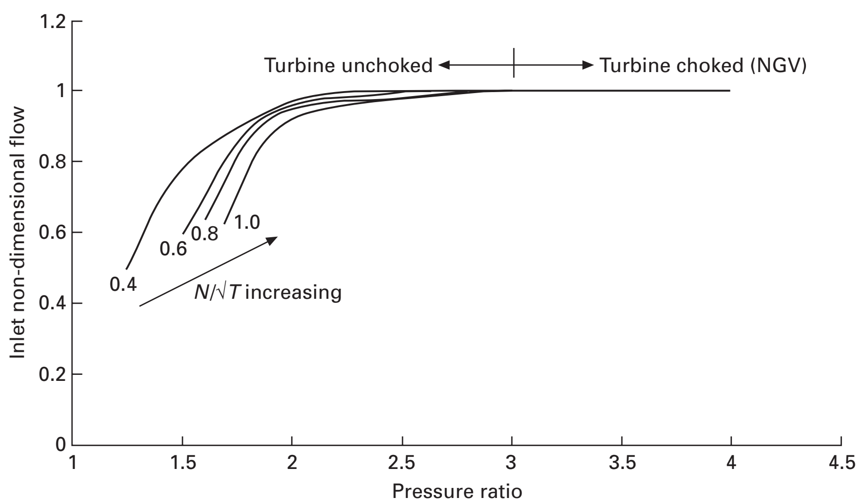

5.8 Turbine flow characteristic (NGV choked).

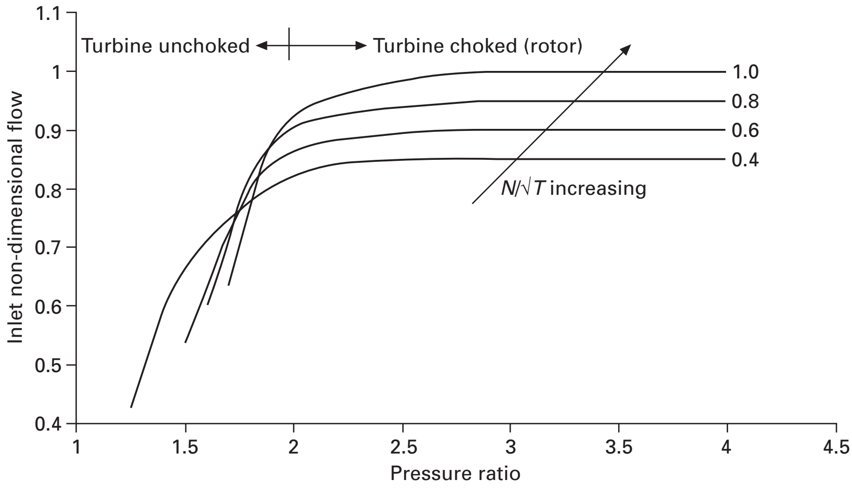

5.9 Turbine flow characteristic (rotor choked).

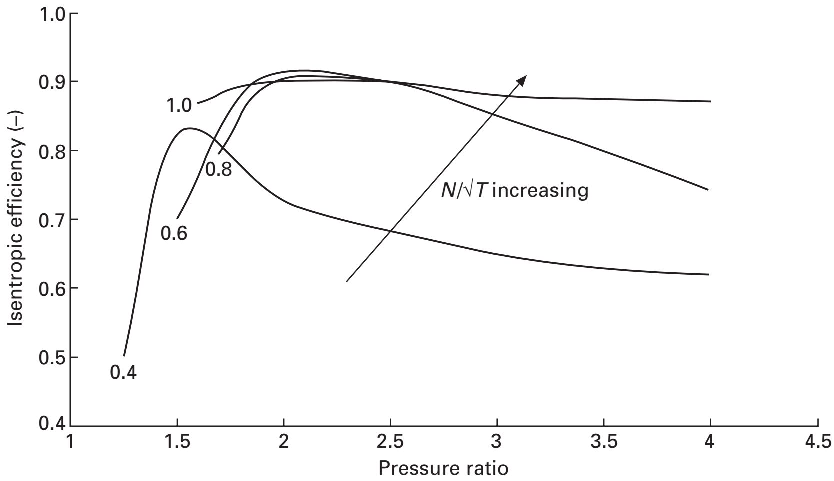

5.10 Turbine efficiency characteristic.

non-dimensional flow and turbine isentropic efficiency are plotted against the pressure ratio for a series of non-dimensional speeds. The non-dimensional mass flow and speeds are relative to the design. The non-dimensional mass flow increases with pressure ratio and beyond a certain pressure ratio the Mach number inside the aerofoil reaches unity and this restricts the amount of non-dimensional flow that can pass through the turbine. Under these operating conditions the turbine is said to be choked. The non-dimensional mass flow remains constant due to choking only if the stator (NGV) is choked, as shown in Fig. 5.8. If the rotor is choked, there is some variation of non-dimensional flow with turbine speed but this is usually small, particularly in the normal operating speed range (90% and above) of the turbine. The turbine characteristic for a choked rotor is shown in Fig. 5.9.

A typical turbine efficiency characteristic is shown in Fig. 5.10. There is some decrease in the efficiency with pressure ratio at lower speeds but in the normal operating speed range, at 80% and higher the efficiency is essentially constant.

5.6 Turbine creep life

Metals operating above a certain temperature under tensile stress will elongate with time. This phenomenon is commonly known as creep and is measured by the rate of strain per hour for a given stress and temperature. The higher the stress and temperature, the greater is the amount of creep strain. Creep deformation will eventually result in fracture of the turbine blade material.

As discussed previously, the importance of high turbine entry temperature on engine performance has been established. As a result, modern gas turbines operate at very high temperatures where creep is a serious problem. Special nickel-based alloys have been developed to resist creep. Currently, industrial gas turbines can operate continuously at blade metal temperatures at about 1000 K. Nonetheless, creep is a major factor that limits the allowable turbine entry temperature.

One parameter that has found widespread use in assessing creep life is the *Larson–Miller (LM) parameter*. This parameter combines temperature and creep life data and is a useful analytical technique for evaluating the effects of stress on creep life over a range of temperatures. The parameter, LM, is quoted as:

$$\mathrm{LM} = 1.8T(20 + \ln(t)) \qquad [5.12]$$

where T is the metal temperature in K and t is the creep life in hours. Figure 5.11 shows a typical Larson–Miller curve relating stress to the LM parameter.

If, for a given stress level, a creep life of say 25 000 hours is required at a blade temperature of 900 K, from Equation 5.12 a Larson–Miller parameter is obtained of 48 805. If the same blade now operates at a slightly lower temperature of 880 K but at a constant stress level, the creep life will be increased to 49 575 hours. The creep life has nearly doubled for a 20 K reduction in blade temperature at a constant stress level. A similar effect on creep life is also found with a change in tensile stress. However, the change in creep life is not as dramatic as is found with a change in blade temperature. Further details of turbine creep life and turbine materials may be found in Boyce.[5]

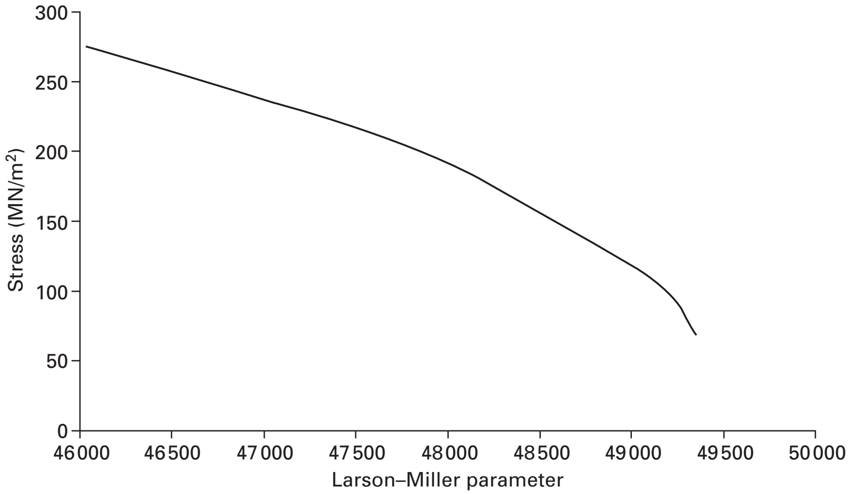

5.11 Example of a Larson–Miller curve.

5.7 Turbine blade cooling

Gas turbine performance is dependent on the gas temperature at entry to the turbine. In the absence of turbine blade cooling, the gas temperature and the turbine blade temperature will be the same. Significant increases in gas temperature can be achieved by cooling the turbine blade so as to maintain the blade metal temperature at an acceptable value, thus achieving the required creep life. The benefit in increased engine performance due to the higher gas temperature is still substantial, even after accounting for any additional losses in the turbine due to the effects of employing cooling techniques.

Turbine blade cooling can use either liquid or air as the cooling medium. Liquid cooling systems using water have been tried but have proved to be unreliable; currently, air as a cooling medium is used almost exclusively. However, steam, and mist (wet steam) cooling have been investigated and are currently applied to gas turbines used in combined cycle plants.

Air is normally bled from the compressor discharge and channelled into the turbine nozzle and rotor internal passages. The bleeding of air for cooling purposes has an impact on engine performance, and the cooling air is normally re-introduced into the gas stream after carrying out the cooling function, to minimise the loss due to these bleeds.

The four following techniques are used for turbine (air) cooling, based on convection, impingement, film and transpiration cooling processes.

5.7.1 Convection cooling

Convection cooling involves the cooling air being directed to flow inside the nozzles and rotor blades, thereby removing heat from the blade material. The flow is usually radial, making multiple passes through the nozzle or rotor blade. The cooling air normally re-enters the gas stream at the blade tip and trailing edge. Figure 5.12 shows a schematic of convection cooling.

5.7.2 Impingement cooling

Impingement cooling is similar to convection cooling but with a much higher intensity. The cooling air is forced to impinge on the blade internal surfaces, usually at the leading edge of the blade. The increased level of turbulence that is generated increases the heat transfer and is used to cool the leading edge of the blade where the maximum blade temperature usually occurs (stagnation point). The cooling air may also enter the gas stream at the trailing edge of the blade. An example of impingement cooling of the blade leading edge is shown in Fig. 5.13.

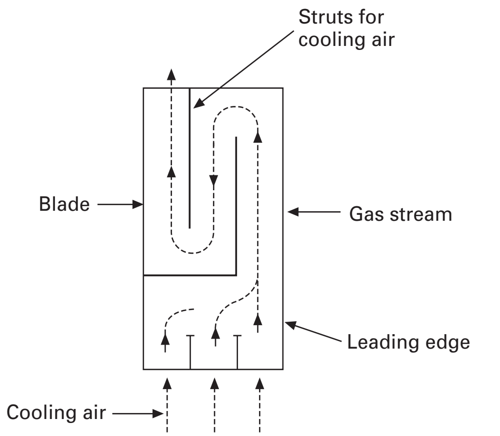

5.12 Schematic of a convection-cooled blade.

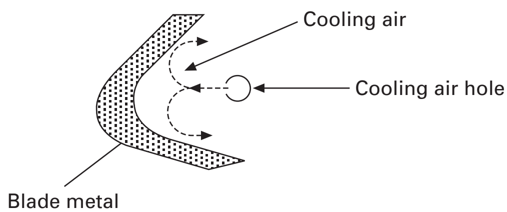

5.13 Impingement cooling.

5.7.3 Film cooling

Film cooling is achieved by allowing the cooling air to flow over the blade exterior, thus forming an insulating layer to protect the blade material from the hot gases. The cooling air leaves the blade internals through cooling slots on the blade surface as shown in Fig. 5.14.

5.7.4 Transpiration cooling

The method of cooling in transpiration cooling is similar to that of film cooling, but the cooling air leaves the internals of the blade through a porous section of the blade wall. The cooling air can cover the whole blade and therefore is very effective for very high temperature applications. However, it has a negative effect on stage efficiency.

5.7.5 Steam and mist cooling

As stated earlier, steam and mist cooling is a new development in turbine cooling and uses steam as the cooling medium. As explained in Chapter 2, there are advantages in employing steam cooling, particularly in reducing the temperature drop across the nozzle guide vane. As a result, steam cooling increases the stator outlet temperature (SOT) relative to an air-cooled turbine where the cooling air returns to the gas stream and reduces the gas temperature due to mixing. Therefore, air-cooled turbines require increased firing temperatures (TET) to maintain the required SOT, thus increasing NO_x emissions. However, a large amount of steam is needed and current developments are looking at the application of mist cooling where water vapour is injected into the steam for blade cooling. The high latent heat of water helps reduce the steam cooling requirements. Some issues of steam and mist cooling are discussed in Wang *et al.*[6]

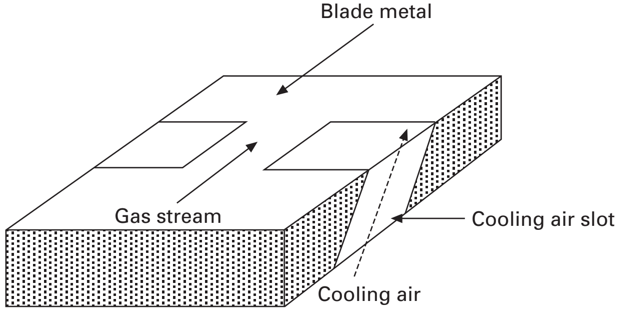

5.14 Blade surface being cooled by application of film cooling.

The scheme for steam cooling is similar to convection cooling as shown in Fig. 5.12; however, the steam does not enter the gas stream but returns to the external cooling system. In a combined cycle plant the turbine cooling steam is provided from the steam cycle, and the heat removed from the turbine blades is returned to the steam cycle, where it is utilised in power production, thus improving the performance of the combined cycle.[7] A schematic representation of a gas turbine combined cycle plant employing steam for turbine cooling is shown in Fig. 5.15. Steam for turbine cooling is taken at the exit of the high pressure (HP) steam turbine and returned to the inlet of the low pressure (LP) steam turbine after cooling the gas turbine blades.

5.8 Turbine metal temperature assessment

The previous section discussed the blade cooling technology that can be employed to lower the turbine blade metal temperature below that of the gas stream. For air-cooled turbines, the turbine metal temperature can be calculated by using the cooling effectiveness parameter which is defined by:

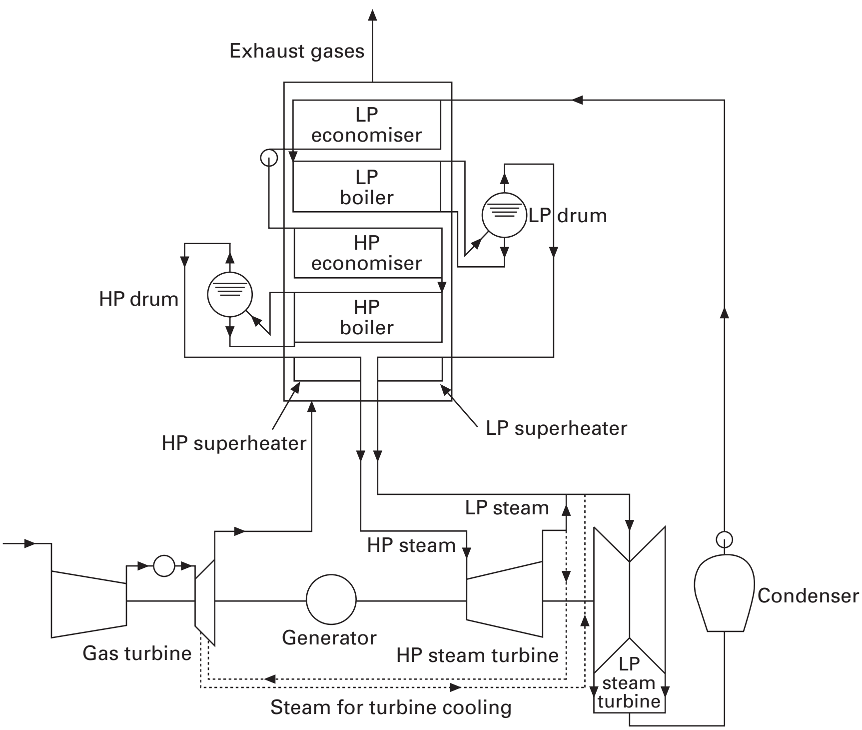

5.15 Gas turbine combined cycle plant employing steam for the turbine cooling system.

$$\varepsilon = \frac{T_g - T_m}{T_g - T_c} \qquad [5.13]$$

where
ε is the cooling effectiveness parameter
T_g is the gas temperature
T_m is the turbine blade metal temperature
T_c is the cooling air temperature.

The value of ε will vary depending on the cooling technology employed and, this value could be about 0.65 for film cooling, or higher for advanced cooling concepts.

The cooling air for the high-pressure turbine stages will be bled off at the compressor discharge and the cooling air temperature will be about 630 K. For a turbine entry temperature of 1400 K and a cooling effectiveness parameter of 0.65, the turbine metal temperature will then be about 900 K. From our analysis of turbine life using the Larson–Miller parameter above, these conditions will give a creep life of about 25 000 hours. The importance of the cooling air temperature on the metal temperature, hence on creep life, must be emphasised. A reduction in compressor efficiency will increase the compressor discharge temperature and therefore the cooling air temperature. If the cooling air temperature is raised by 20 K, due to poor compressor efficiency, the metal temperature will increase to 912.5 K. We have seen that a 20 K increase in metal temperature can reduce the creep life by about half. In this instance the creep life will reduce to about 16 500 hours, representing a significant loss in creep and therefore blade life. Thus, reducing the cooling air temperature by external cooling or employing intercooled cycles as discussed in Chapter 3 will be beneficial in significantly increasing the turbine creep life.

5.9 Effect of cooling technology on thermal efficiency

The cooling air requirements for two different cooling technologies are illustrated in Fig. 5.16 for a metal temperature of about 1000 K. The cooling air mass flow requirement for convection cooling is always higher than for film cooling. In fact, the cooling air requirement for convection cooling increases exponentially with increase in turbine entry temperature, and as the turbine entry temperature increases, the cooling air requirement becomes prohibitively high. This is also illustrated in Fig. 5.17, which shows the impact of these cooling technologies on the thermal efficiency of the gas turbine. Figure 5.17 shows the thermal efficiency actually decreasing with convection cooling at turbine temperatures above 1250 K.

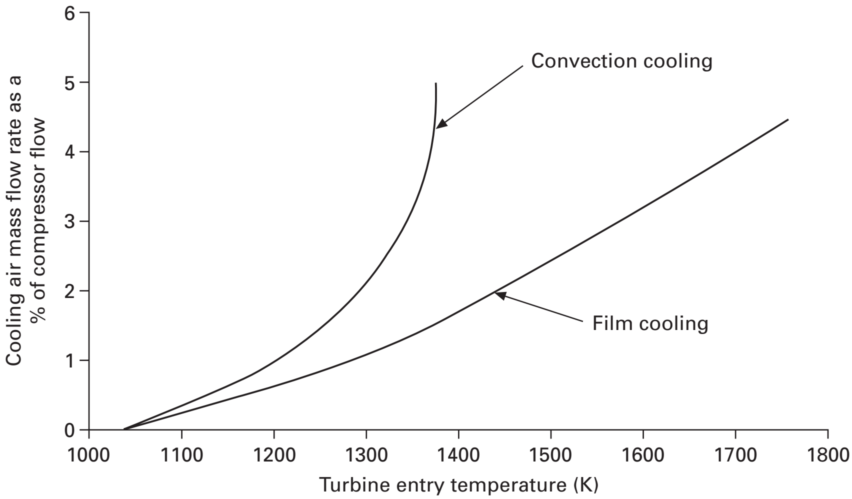

5.16 Cooling air requirements for two different cooling technologies for a given turbine metal temperature.

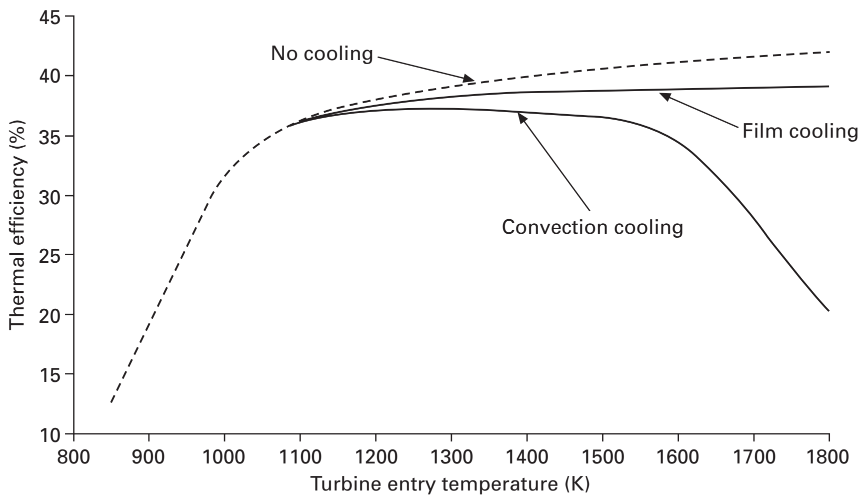

5.17 Impact of different cooling technologies on gas turbine thermal efficiency.

Although convection cooling is not as efficient compared with film cooling, it is more reliable as dirt and dust do not impact upon the cooling performance compared with film cooling, where the cooling holes are rather small and can easily become clogged. In practice, both these technologies are used in an attempt to obtain the best compromise.

5.10 References

1. *Gas Turbine Theory*, 5th Edition. Saravanamuttoo, H.I.H., Rogers, C.F.G, and Cohen, H., Longman (2001).
2. *Axial Flow Turbines*, Horlock, J.H., Butterworth (1966).
3. Loss mechanisms in turbomachines, Denton, J., *ASME – IGTI Scholar Lecture*, 93-GT-435, 1993.
4. Smith, F.A., A simple correlation of turbine efficiency. *Journal of Royal Aeronautical Society*, Vol 69, 1965.
5. *Gas Turbine Engineering Handbook*. Boyce, M.P., Gulf Publishing (1992).
6. Closed loop steam/mist cooling for advanced turbine systems. Wang, T., Gaddis, J.L., Guo, T., Li, X., Department of Mechanical Engineering, Clemson University, Box 5400921, Clemson, SC 29634-0921, USA.
7. H system steams on, *Modern Power Systems*, February 2004.

6
Gas turbine combustion

The power output of a gas turbine is controlled by the heat input, which is generated by burning fuel in the combustion chamber, using air from the discharge of the compressor. The use of hydrocarbon fuels is widespread in gas turbines. Liquid fuels such as kerosene, or gaseous fuels such as natural gas, are examples and the use of natural gas is becoming increasingly common in industrial gas turbines. The amount of heat input is often referred to as the net thermal input.

The combustion chamber exit temperature must be controlled to that required by the turbine in order that the creep life of the turbine component is not compromised. This is achieved by dividing the combustion process into two or three distinct parts. These are: the primary zone where the fuel is burnt and the heat from the fuel is released; an intermediate zone where additional air is introduced to complete the combustion; and the dilution zone where the remaining air is introduced to reduce the combustion chamber exit temperature to that required for the turbine.

As with compressors and turbines, combustion is a specialist area and only the fundamentals of gas turbine combustion are discussed in this chapter. The reader should consult references given at the end of this chapter for detailed information on aspects of gas turbine combustion.

6.1 Combustion of hydrocarbon fuels

Hydrocarbon fuels at atmospheric conditions do not burn in air spontaneously. In order to burn such fuels, they have to be heated to a high enough temperature where the fuel molecules are broken down into elementary parts called radicals. The energy input to produce these radicals is often called the activation energy. These radicals are generally unstable at normal atmospheric conditions and will revert back to their original hydrocarbon state in the absence of oxygen. However, such radicals have a strong affinity for oxygen and will readily react to form carbon dioxide and water and release heat in the process. Figure 6.1 summarises the combustion process.

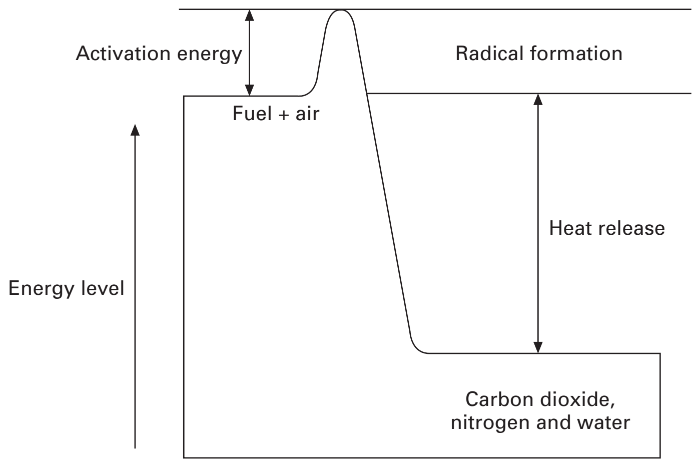

6.1 Main process in the combustion of hydrocarbon fuels.

The oxidation of carbon to carbon monoxide (CO) is fairly rapid but the oxidation of carbon monoxide to carbon dioxide is rather slow. The reaction between the hydroxyl radical and carbon monoxide is also fairly rapid and it is thought that the formation of CO_2 from burning hydrocarbon fuels is due to the reaction between CO and OH. In this reducing reaction, the OH radical is reduced to hydrogen H and the released oxygen combines with the CO to produce CO_2.

Fuels that have a high carbon–hydrogen ratio, such as heavy fuel oils, may thus require a longer burning time to convert the CO into CO_2. The burning time is an important factor in combustor design. It is referred to as the *residence time* and represents the time the fuel spends in the burning or primary zone. If large residence times are required, as with heavy fuel oils, the volume of the combustion chamber will have to increase.

An example of the chemical equation governing the combustion of methane (CH_4) in O_2 is given by Equation 6.1:

$$CH_4 + 2O_2 \xrightarrow[\text{Heat release}]{} (CO + OH + CH_3) \xrightarrow[\text{Heat release}]{} CO_2 + 2H_2O \qquad [6.1]$$

Thus one molecule of CH_4 will combine with two molecules of O_2 to produce one molecule of CO_2 and two molecule of H_2O.

The carbon and hydrogen content of the fuel determine the amount of fuel needed for complete combustion in air. For hydrocarbon fuels this can be represented by the carbon–hydrogen ratio. Any hydrocarbon may be represented as C_xH_y where x and y are the numbers of carbon and hydrogen atoms in the fuel, respectively.

The ratio of fuel to air on a mass basis for complete combustion is called the stoichiometric fuel–air ratio. Fuel–air mixtures that have excess air are called lean mixtures and when excess fuel is present are referred to as rich mixtures.

6.1.1 Stoichiometric fuel–air ratio

Air contains 1 molecule (mole) of O_2 and 3.76 molecules (moles) nitrogen (N_2). We have ignored the amount of carbon dioxide and argon as these are very small compared with the amount of oxygen and nitrogen in air. It has been stated that a molecule of a hydrocarbon fuel can be represented by its carbon–hydrogen ratio. The stoichiometric combustion equation can now be represented as:

$$\begin{aligned} &C_xH_y + ms(O_2 + 3.76N_2) \\ &= xCO_2 + (y/2)\,H_2O + 3.76\,ms\,N_2 \end{aligned} \tag{6.2}$$

and

$$C_xH_y + msO_2 = xCO_2 + (y/2)H_2O \tag{6.2a}$$

where ms are the moles of air required for complete combustion. For complete combustion, the number of moles of O_2 per mole of fuel is $ms = x + y/4$ (Equation 6.2a).

The stoichiometric fuel–air mass ratio $(FAR)_s$ is given by:

$$(FAR)_s = \frac{12.01x + 1.008y}{ms(32 + 3.76 \times 28.013)} \tag{6.3}$$

where 12.01 is the atomic weight of carbon, 1.008 is the atomic weight of H_2, 32 is the mole weight of O_2 and 28.013 is the mole weight of N_2.

Therefore, the stoichiometric fuel–air mass ratio is:

$$(FAR)_s = \frac{12.01x + 1.008y}{137.33\left(x + \dfrac{y}{4}\right)} \tag{6.4}$$

If we burn methane (CH_4, $x = 1$ and $y = 4$) in air, the stoichiometric fuel–air ratio is 0.0584. So we require, for complete combustion, 17.12 kg of air to burn 1 kg of methane. If we burn kerosene, which can be represented as $C_{12}H_{24}$, where $x = 12$ and $y = 24$, the stoichiometric fuel–air ratio is 0.068 and we require 14.71 kg of air to burn 1 kg of kerosene.

6.1.2 Combustion in excess air

Combustion in excess air will result in the presence of oxygen in the products of combustion and is the normal case in gas turbines. Equation 6.5 gives the molar balance for this case:

$$C_xH_y + m(O_2 + 3.76N_2) = xCO_2 + (y/2)H_2O + (m - x - y/4)O_2 + 3.76N_2 \quad [6.5]$$

where 'm' is now in excess of 'ms' and results in unreacted oxygen being present in the combustion gas stream. The fuel–air ratio (*FAR*) is:

$$FAR = \frac{12.01x + 1.008y}{137.33m} \quad [6.6]$$

6.1.3 Adiabatic flame temperature

The purpose of burning fuel in a combustion chamber is to increase the temperature of the gas stream, and the flame temperature is one of the factors because it influences the reaction rate of combustion. Another parameter that influences the reaction rate is the combustion pressure. In the absence of any external heat transfer, the temperature achieved is called the adiabatic flame temperature. In practice, there is always some heat transfer and the temperature achieved during combustion is always less than the true adiabatic flame temperature.

At flame temperatures above 1800 K, products of combustion may dissociate to form radicals and species. These reactions absorb energy (endothermic) and will further suppress the flame temperature. When comparing the flame temperature of different fuels, it is convenient to work with equivalence ratios. The equivalence ratio, ϕ, is defined as:

$$\phi = \frac{FAR}{(FAR)_s} = \frac{m}{ms} \quad [6.7]$$

For lean mixtures, the equivalence ratio will be less than one and for rich mixtures the equivalence ratio will be greater than one. Fuel–air ratios corresponding to the stoichiometric ratio have an equivalence ratio of one.

Figure 6.2 shows the adiabatic flame temperature for CH_4 varying with equivalence ratio. The figure also shows the deviation of the actual adiabatic flame temperature from the theoretical value due to the effects of dissociation. Note the maximum actual adiabatic flame temperature occurs at slightly rich mixtures (e.g. $\phi = 1.05$). The adiabatic temperature for higher carbon content fuels will be higher and the equivalence ratio where the maximum adiabatic flame temperature occurs also increases. Goodger[1] gives more details on the combustion of hydrocarbon fuels.

6.2 Gas turbine combustion system

The chemical kinetics of combustion have been discussed briefly above. The aspects of achieving combustion in a gas turbine will now be discussed. A

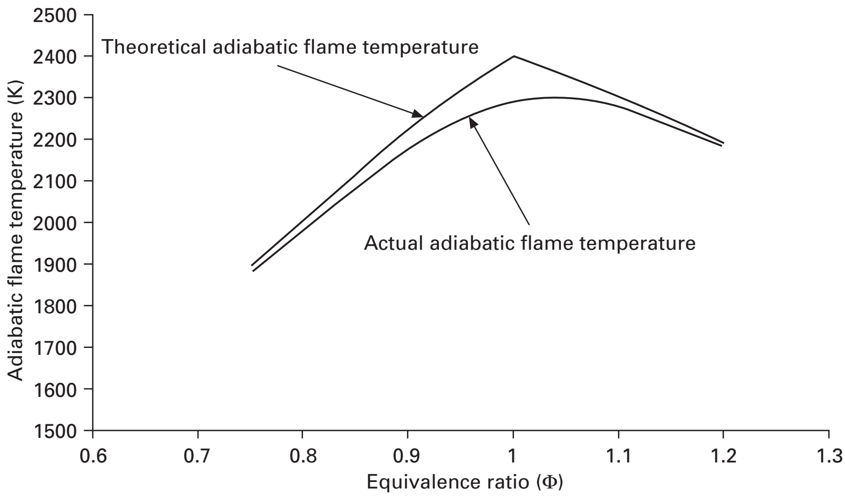

6.2 Effect of equivalence ratio on adiabatic flame temperature for CH_4.

gas turbine combustion system consists of the following regions and components:

(1) diffuser
(2) fuel nozzle
(3) primary zone
(4) intermediate zone
(5) dilution zone.

These regions are shown in Fig. 6.3, which is a schematic representation of a gas turbine combustion system.

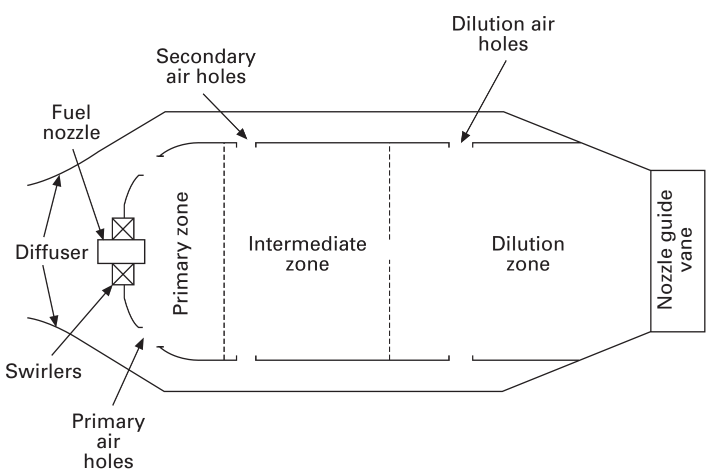

6.3 Schematic representation of a typical combustion chamber.

6.2.1 Diffuser

The function of the diffuser is to reduce the flow velocity sufficiently to help start the combustion process. Fuel is burnt in the compressor discharge air, which has a velocity of about 200 m/s. Apart from the significant combustion problems of burning fuel in such a high velocity air stream, the pressure loss in the combustor will be excessive, resulting in poor gas turbine performance. The velocity of the compressor exit air velocity must be reduced and this is achieved by the use of a diffuser.

A simple diffuser is essentially a straight-walled, divergent duct as shown in Fig. 6.4 where the air velocity is reduced resulting in an increase in static pressure. The function of the diffuser is to reduce the compressor exit air velocity to about a fifth of its initial value. For a given area ratio, the length of the diffuser has a big impact on the diffuser performance. If a diffuser is too long, the pressure loss increases due to frictional effects. If too short, the decelerating flow (adverse pressure gradient) will separate and stall, causing higher pressure losses. The effect of length on diffuser performance is illustrated in Fig. 6.5 and there is a specific length which corresponds to the minimum loss. The objective of the diffuser is to achieve the diffusion in the shortest possible length, incurring the lowest pressure loss. One diffuser design that has found favour particularly in aero-engine application is the vortex-controlled diffuser (VCD) which is shown in Fig. 6.6.[2]

A VCD achieves good diffusion in a short length by bleeding controlled amounts of air from the compressor discharge so that a vortex is generated and the resultant streamlines essentially act as the diffuser surface. About 80% of the theoretical static pressure rise is possible, thus reducing the velocity of the combustion air, but a significant bleed is required, which amounts to about 4% of the total flow. This bleed can be used for engine cooling purposes and therefore may not present a significant penalty. A VCD

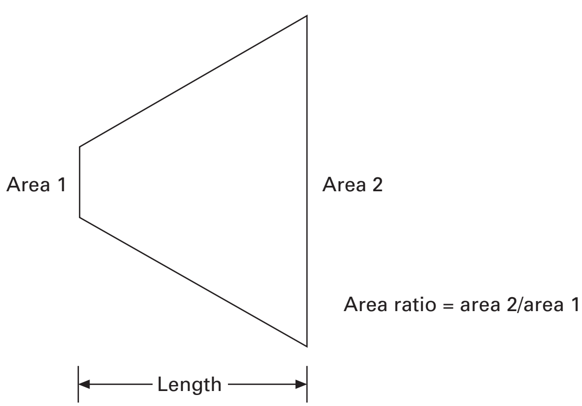

6.4 Schematic representation of a straight walled diffuser.

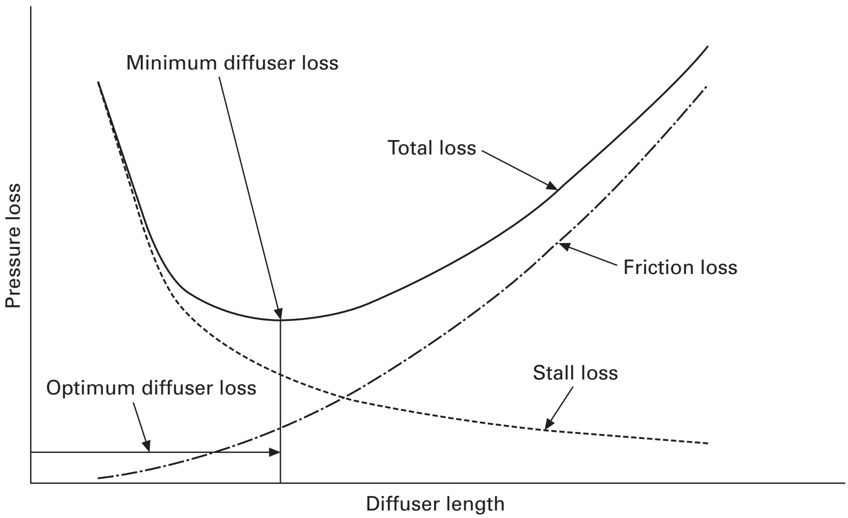

6.5 Influence of a diffuser length on pressure loss for a given area ratio.

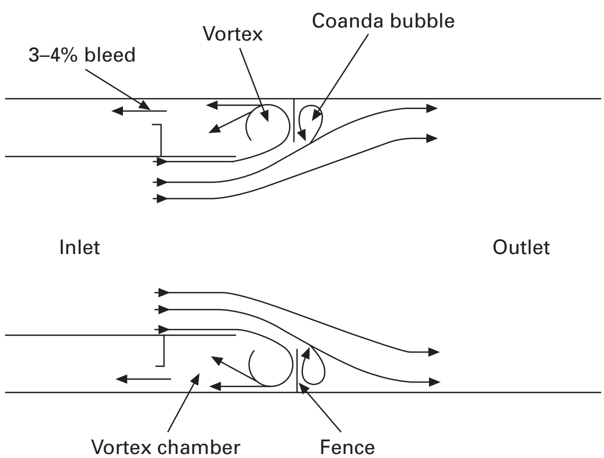

6.6 Vortex controlled diffuser.

can reduce the flow velocity to about 25 m/s, considerably better than a simple diffuser.

6.2.2 Primary zone

The velocity of the air leaving the diffuser is about 25 m/s and the flame velocity of hydrocarbon fuels is in the order of a few m/s (5 to 7 m/s). Any attempt to burn fuel in the air stream leaving the diffuser will result in the flame being extinguished. This is because the time available for combustion (chemical reaction) is less than the time needed to heat the fresh mixture to its ignition temperature (formation of radicals and species in the fuel). The velocity of the combustion air has to be reduced sufficiently to increase the time available to achieve stable combustion.

Bluff bodies

Bluff bodies are objects such as a flat plate or a Vee gutter placed in the air stream. The flows past these bluff bodies separate and form vortices just downstream of the bluff body as shown in Fig. 6.7 for a flat plate. The velocity at the eye of each vortex is zero and increases towards the tip of the vortex. This type of vortex is called a forced vortex.

Combustion can be initiated by injecting fuel into the eye of the vortex, where the air velocity will be below the flame velocity, resulting in sufficient time for the heat released to sustain combustion. The vortices formed by the bluff bodies will eventually break down into turbulence represented by smaller vortices. This increase in the level of turbulence will increase the rate of fuel being burnt, hence increasing the heat release rate, and will therefore enable smaller combustion volumes to be used for a given heat release rate.

In gas turbine combustion systems, air is introduced through the primary and secondary holes. These flows form a forced vortex and can increase the level of turbulence in the primary zone, resulting in better flame stabilisation and heat release rate. It must be pointed out that the primary zone is the major heat release zone in a gas turbine combustion system. The vortex pattern generated by the primary and secondary airflow is shown in Fig. 6.8.

Fuel is injected through the nozzle directed towards the eye of the vortex. The fuel mixes with the swirl air shown in Fig. 6.8, which helps break up the

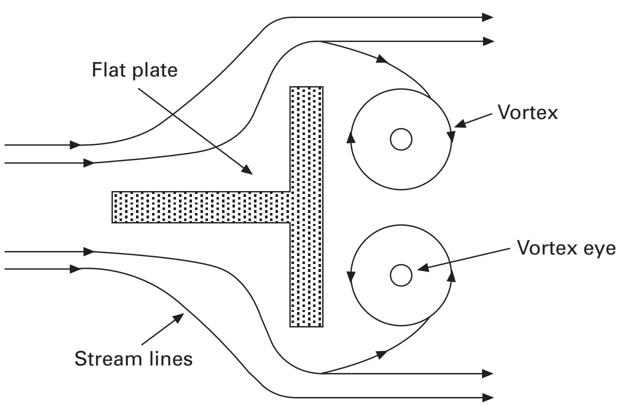

6.7 Flow passing over a bluff body.

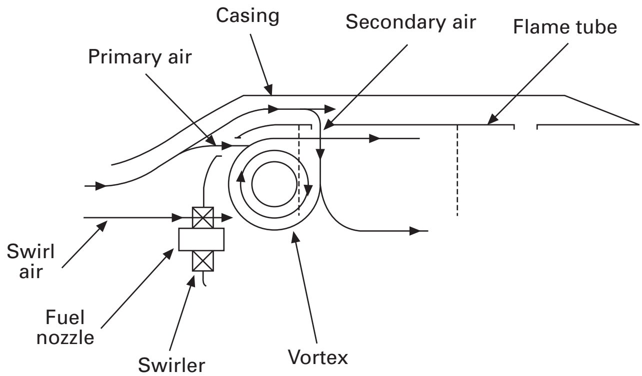

6.8 Section through a typical gas turbine combustor.

fuel into fine droplets. Combustion begins at a region near the eye of the vortex and the fuel resides in the vortex for a sufficient length of time (residence time), until the fuel is oxidised, liberating heat.

6.2.3 Intermediate zone

The equivalence ratio, ϕ, in the primary zone will be close to unity and the temperature of the gases and products of combustion leaving the primary zone is in the order of 2000 K. At these temperatures, the products will contain radicals and fuel species in the form of unburned hydrocarbons (UHC) and CO, due to dissociation of carbon dioxide and water.

Should the combustion gases pass directly to the dilution zone, they will be quenched, due to the large amount of air being added in the dilution zone. They will appear as pollutants and give an indication of poor combustion inefficiency. The intermediate zone reduces these species or radicals by introducing small amounts of air, which lower the temperature and encourage the formation of carbon dioxide and water vapour.

6.2.4 Dilution zone

The combustion gases leaving the intermediate zone will be at about 1800 K and may still be too hot for the turbine downstream. The dilution zone must ensure that the gas temperature entering the turbine is satisfactory and it achieves this by admitting the remaining air to mix with the products of combustion.

The pattern factor is a parameter that is used to determine how well the mixing has been performed by the dilution zone and is defined as:

$$PF = \frac{T_{max} - T_2}{T_2 - T_1} \qquad [6.8]$$

where

PF is the pattern factor

T_{max} is the maximum or peak temperature

T_2 is the average exit temperature

T_1 is the combustion inlet temperature and usually corresponds to the compressor discharge temperature.

A satisfactory value for the pattern factor is about 0.2. A typical temperature distribution at the exit of the combustion chamber is shown in Fig. 6.9.

6.3 Combustor cooling

The high temperatures that prevail within the combustion chamber during combustion subject the flame tube to a very high temperature. Although the air that bypasses the combustion process (dilution air) provides some cooling of the flame tube, additional cooling is normally required. Additional flame tube cooling is provided by including a number of slots along the flame tube to generate a film of cooling air over the flame tube material in a manner similar to that discussed in turbine film cooling. This film of cooling air acts as a thermal barrier and protects the flame tube, as is shown in Fig. 6.10.

Techniques such as transpiration cooling, as discussed in Section 5.7.4, can be applied to flame tube cooling. Such cooling techniques result in a significant reduction in cooling air requirements and it is claimed that about a 50% reduction in flame tube-cooling air occurs with such techniques.

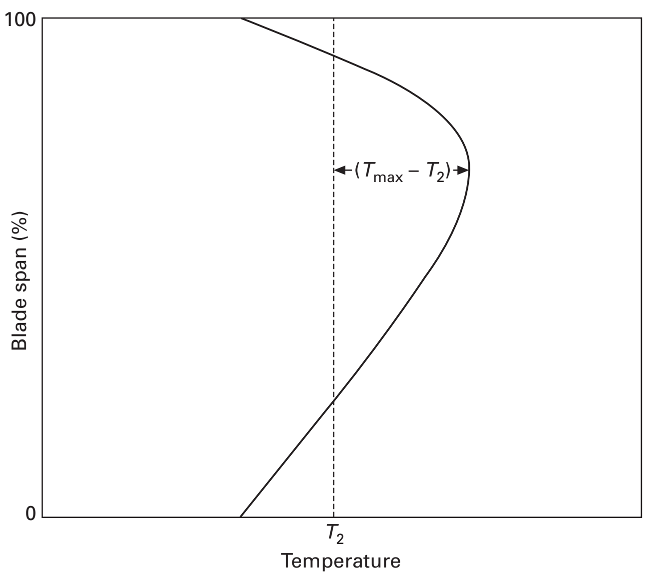

6.9 Typical combustor temperature exit profile.

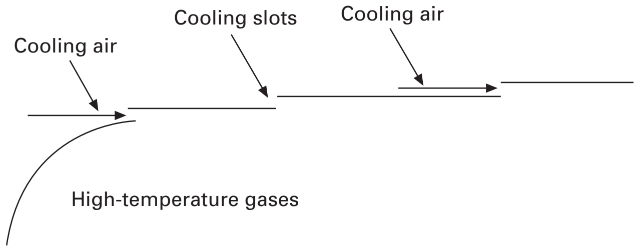

6.10 Example of film cooling applied to a combustor flame tube.

6.4 Types of gas turbine combustor

There are two categories of engines having different requirements regarding combustor size and weight. These are the aero-derivatives and the industrial gas turbines. As the name implies, the aero-derivatives are derived from aircraft engines where size and weight are of paramount importance. Industrial gas turbines are less concerned with size and weight issues but may be required to burn a wide range of fuel types.

6.4.1 Aero-derivative combustors

There are generally three types of combustors used in aero-derivatives, known as the tubular, tuboannular and the annular types.

Tubular combustor

The tubular combustor, also known as the 'can' combustor, consists of a flame tube enclosed within a cylindrical liner positioned concentrically, as shown in Fig. 6.11. The interconnector or crossover tubes are required to ensure light-up of all the cans during start-up by the flame spreading via the interconnector tubes. The cylindrical liner ensures that each flame tube has its own combustion air supply. These combustors were heavy and incurred a high pressure loss, eventually giving rise to the tuboannular combustor. Tubular combustors were used in the very early gas turbines such as the Whittle W2B and the Jumo 004.

Tuboannular combustor

The main difference between the tubular and tuboannular (can-annular) combustor is the common air supply to all the flame tubes. This is achieved by placing the flame tubes within a single cylindrical casing as shown in Fig. 6.12.

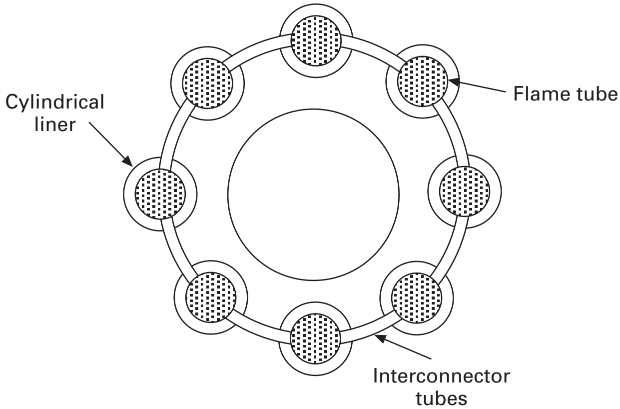

6.11 Cross-section of a tubular combustor.

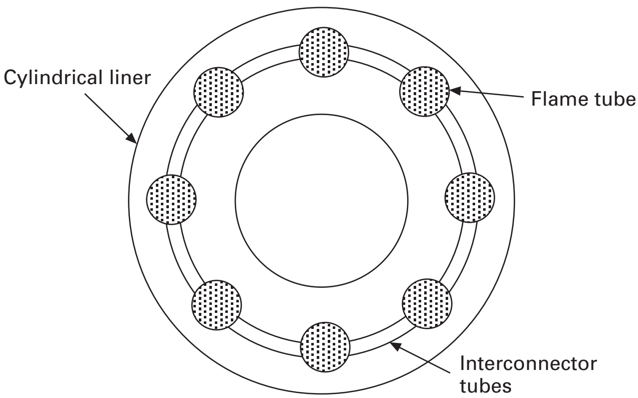

6.12 Cross-section of a tuboannular combustor.

Such an arrangement results in a more compact and lighter combustor. However, it is more difficult to achieve a satisfactory distribution of combustion air between the flame tubes when compared with the tubular combustor. Nonetheless, tuboannular combustors have been used extensively.

Annular combustor

In the annular combustor an annular flame tube is placed within the cylindrical liner or casing. The annular combustor has a lower pressure loss and is more compact, compared with the tuboannular design. Its use is now widespread in aero-engines and as a result it is also found in aero-derived gas turbines. Figure 6.13 shows a cross-sectional view of an annular combustor.

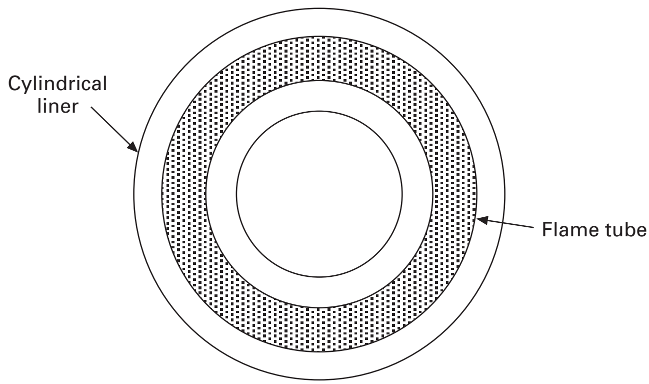

6.13 Cross-section of an annular combustor.

6.4.2 Industrial combustors

Industrial gas turbines are not normally constrained by size and weight and may need to burn a wider range of fuels varying from natural gas to treated crude oil. As a result, industrial combustors tend to be much larger than aero-derived gas turbine combustors.

The increase in combustor size results in an increase in the residence time, enabling lower quality fuels to be burnt. Also, the gas velocities are lower and this results in lower pressure losses in the combustor. Their appearance is similar to a large single tubular combustor as shown in Fig. 6.14.

6.5 Fuel injection and atomisation

For satisfactory combustion of liquid fuel, such as kerosene, sufficient quantities of fuel vapour must be produced to sustain the combustion process in gas turbines. The production of fuel vapour in necessary quantities starts with the atomisation of the fuel, where a large number of fine droplets are produced. However, the droplets are still liquid and have to be evaporated and heated to the ignition temperature. The droplet temperature increases until it reaches the fuel boiling point and then remains constant due to the absorption of latent heat required by the evaporation process. Clearly, the rate of evaporation depends on many factors such as the droplet size, combustion air pressure and temperature, and the specific heat of the fuel. Poor atomisation can lead to reduced combustion efficiency and the formation of pollutants such as CO and UHC.

6.5.1 Pressure swirl atomisers

Liquid fuels, as stated, require atomisation before combustion. Fuel under pressure is forced through an orifice to form a thin conical sheet of fuel. This

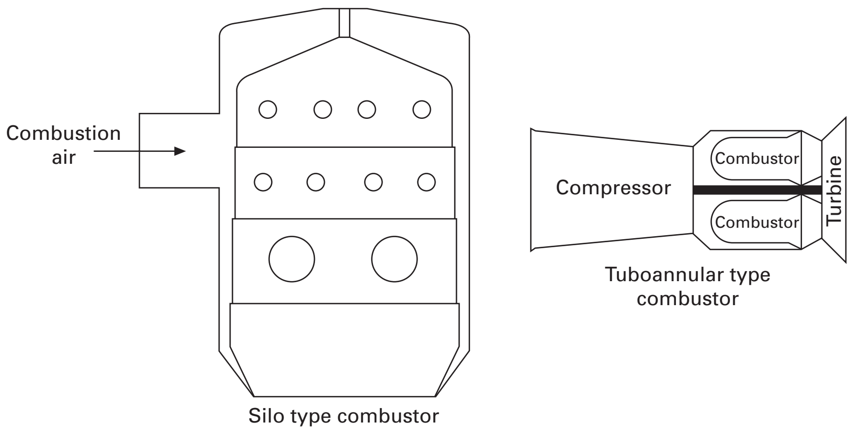

6.14 Industrial combustor.

sheet of fuel will become unstable when the external forces overcome the surface tension forces maintaining the sheet of fuel and divide the sheet of fuel into droplets. The mixing of the swirl air, as discussed, with the conical sheet of fuel will augment the atomisation process.

Figures 6.15(a) and (b) show a simplex pressure swirl atomiser. The fuel enters the vortex chamber tangentially (Fig. 6.15(b)) and leaves through the orifice producing a conical sheet of fuel as shown in Fig. 6.15(a). The major problem with a simplex atomiser is obtaining good atomisation over a wide fuel flow range. Typically, a gas turbine will require a fuel turndown of about 40:1 to cover its operating power range (i.e. idle power fuel flow requirements will be about 1/40th of the full power fuel flow requirements).

When the orifice is optimised (made small enough) to give good atomisation at low fuel flow rates, then the required pressures for high fuel flows becomes excessive. The problem may be resolved by providing a dual-orifice atomiser as shown in Fig. 6.16. The orifice for the pilot fuel is of a smaller size and operates during low power settings. At higher power settings, the main fuel flow is also active and passes fuel through its own swirl chamber and orifice.

6.5.2 Air blast atomiser

The atomisation process in an air blast atomiser is achieved by allowing high-speed air to flow over a surface where the air mingles with the fuel at the lip or at the end of this surface. Good atomisation is achieved with lower fuel pressures compared with the pressure swirl atomiser. Very little or no soot formation occurs, resulting in lower radiant heat, hence smaller flame tube cooling air requirements. The heat release rate is higher, resulting in a smaller combustor. Figure 6.17 shows a schematic of an air blast atomiser.

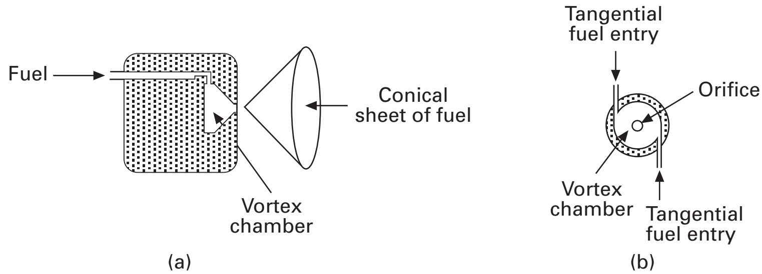

6.15 (a) and (b): Simplex pressure swirl atomiser.

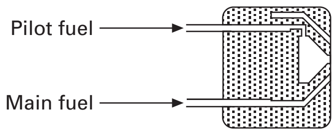

6.16 Duplex pressure swirl atomiser.

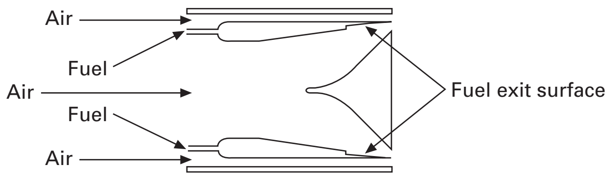

6.17 Air blast atomiser.

The disadvantages of this type of atomiser are a smaller stability limit and poor atomisation at lower airflow rates and start-up conditions. These problems are overcome by combining the air blast atomiser with a pressure swirl atomiser. This design is more complex because the fuel flow for the idle and low power operating conditions is supplied by the pressure swirl atomiser, whereas at higher power settings, the fuel supply is provided by the air blast atomiser.

6.5.3 Fuel vaporisers

As an alternative to atomisation, liquid fuels can be heated above their boiling point so that all the liquid is converted into vapour. Such methods of preparing fuel for combustion are applicable only to high-grade fuels which leave no solid residue. The fuel enters the vaporising system, as shown in Fig. 6.18, and is heated in the vaporising tube using the heat in the primary zone. The vaporised fuel now enters the primary zone and mixes with the combustion air where it is burnt.

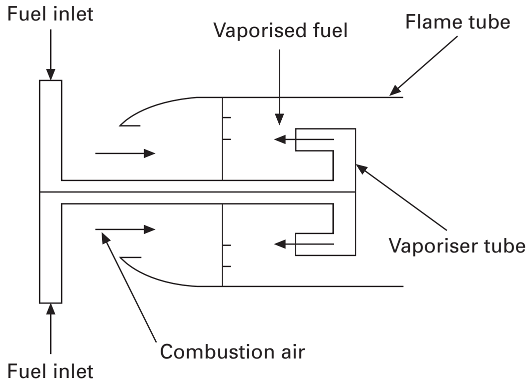

6.18 Fuel vaporising system.

Advantages of using a vaporising system are low fuel pressure requirements and low soot formation. Disadvantages are the likelihood of thermal damage to the vaporiser tube and poor vaporisation during starting, when the vaporiser tube is cold. Also, during rapid acceleration, the fuel schedule has to be controlled to prevent the increase in fuel flow from overcooling the tube and resulting in poor vaporisation and combustion.

6.5.4 Gaseous fuels and injection

Unlike liquid fuels, gaseous fuels do not require atomisation and vaporisation. The fuel–air mixture needs only to be heated to high enough temperatures to produce radicals and species to initiate combustion. They therefore present few problems, provided that the fuel has a high calorific value such as natural gas. Lower calorific value fuels result in a considerable increase in fuel flow and can represent a significant portion of the combustor mass flow. Fuels with a low calorific value can result in lower burning or heat release rates requiring longer residence times and hence combustion volumes. Even with natural gas, the content of non-combustibles, particularly of CO_2, has to be carefully monitored and controlled as a significant swing in calorific value can result due to a modest change in the CO_2 content because of its high molecular weight. With gaseous fuels, fuel injection is normally achieved by the use of swirlers or nozzles.

6.6 Combustion stability and heat release rate

There is only a narrow range of fuel–air ratios or equivalence ratios when combustion is possible. Figure 6.19 shows a typical combustion stability loop, where the equivalence ratio is plotted against the combustion airflow rate.

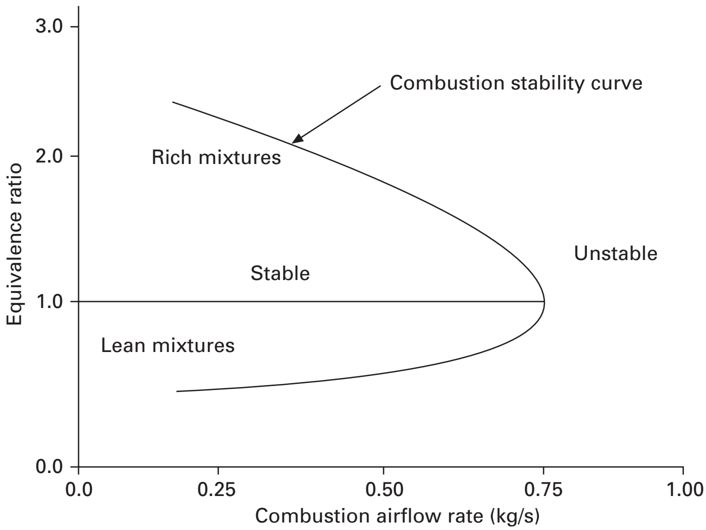

6.19 Typical combustion stability curve.

For a given combustion airflow rate, there is a lean and rich equivalence ratio range within which combustion is possible. Increasing the flow rate reduces the range of equivalence ratio when combustion is possible due to the increase in velocity, reaching a unique flow rate when these two stability ranges meet and this corresponds to an equivalence ratio of about 1.0 (stoichiometric fuel–air ratio).

The effect of combustion pressure on the stability loop is illustrated in Fig. 6.20. Decreasing the combustion pressure reduces the size of the stability loop and can be associated with a reduced reaction rate as the pressure reduces.

For a given equivalence ratio and airflow rate, the fuel flow can be determined by:

$$mf = ma\ \Phi\ (FAR)_s \qquad [6.9]$$

where

mf = fuel flow rate
ma = combustion airflow rate
Φ = equivalence ratio
$(FAR)_s$ = stoichiometric fuel–air ratio.

And the heat release rate, HRR, is given by

$$HRR = mf \times Q_{\text{net}}$$

then,

$$HRR = ma \times \Phi \times (\text{FAR})_s \times Q_{\text{net}} \qquad [6.10]$$

where Q_{net} is the lower heating value (LHV) of the fuel.

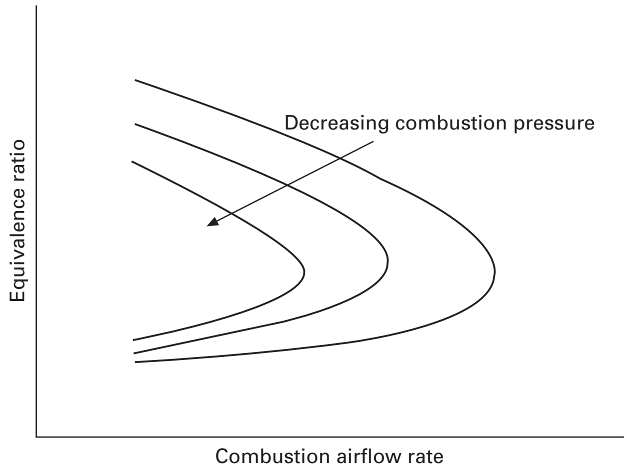

6.20 Effect of combustion pressure on stability.

Clearly, the heat release rate is proportional to the combustion airflow rate and the airflow rate represented on the x-axis in Fig. 6.20 could be replaced with the heat release rate when comparing fuel atomisation techniques. The higher the heat release rate, the smaller will be the combustion volume required. The method employed to atomise the fuel also has an impact on the combustion stability curve. Figure 6.21 shows the stability curves for an air blast atomiser and a pressure swirl atomiser, respectively. The atomisation of the fuel using an air blast atomiser is much greater than that achieved by the pressure swirl atomiser. Consequently, the heat release rate using an air blast atomiser is greater but the stability loop is much narrower compared with the pressure swirl atomiser. This is due to a more homogeneous mixture with air blast atomisers compared with the pressure swirl atomisers, which produce a larger variation of fuel–air ratios, thus resulting in a wider stability loop. More details on all aspects of turbine combustion may be found in Lefebvre.[3]

6.7 Combustion pressure loss and efficiency

Components of the combustor resist the flow of air, resulting in a pressure loss. The high level of turbulence necessary for combustion also extracts energy from the air entering the combustor. Both these factors result in a loss in (stagnation) pressure in the combustor. This pressure loss is called the cold loss and is proportional to the combustor inlet dynamic pressure $1/2\ \rho u^2$. There is another source of pressure loss and that is associated with the addition of heat. The addition of heat results in a reduction of density, which in turn increases the velocity and this is known as Rayleigh flow. A

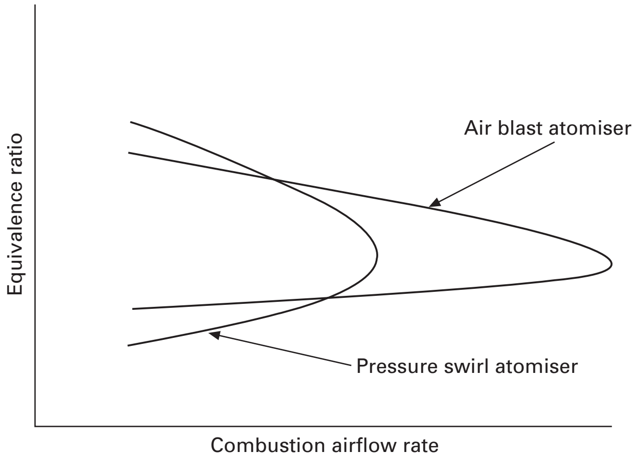

6.21 Effect of fuel preparation method on combustion stability.

pressure loss is necessary to increase the velocity (momentum) and is called the hot or fundamental loss.

The non-dimensional pressure loss can be expressed as:

$$\frac{\Delta P_{12}}{P_1} = \text{PLF}\left(\frac{W_1\sqrt{R_1 T_1/\gamma_1}}{P_1}\right)^2 \times \gamma \qquad [6.11]$$

where

ΔP_{12} is the combustor stagnation pressure drop
P_1 is the combustor inlet pressure
T_1 is the combustor inlet temperature
PLF is the combustor pressure loss factor
R_1 is the gas constant
γ is the isentropic index (c_p/c_v), where c_p and c_v are the specific heats at constant pressure and constant volume, respectively.

The pressure loss factor is given by:

$$\text{PLF} = K_1 + K_2\,(T_2/T_1 - 1) \qquad [6.12]$$

where K_1 and K_2 are constants for a given combustor, T_2 is the combustor exit temperature and T_2/T_1 is the ratio of the stagnation temperature rise across the combustor. The variation of the pressure loss factor with T_2/T_1 is shown in Fig. 6.22. Combustion pressure loss varies from about 2% for an industrial combustor to about 6% for an aero-derivative combustor.

The combustion efficiency is defined as the ratio of the actual heat released to that of maximum heat released due to the combustion. This translates to the theoretical fuel–air ratio for a given combustion temperature rise to that

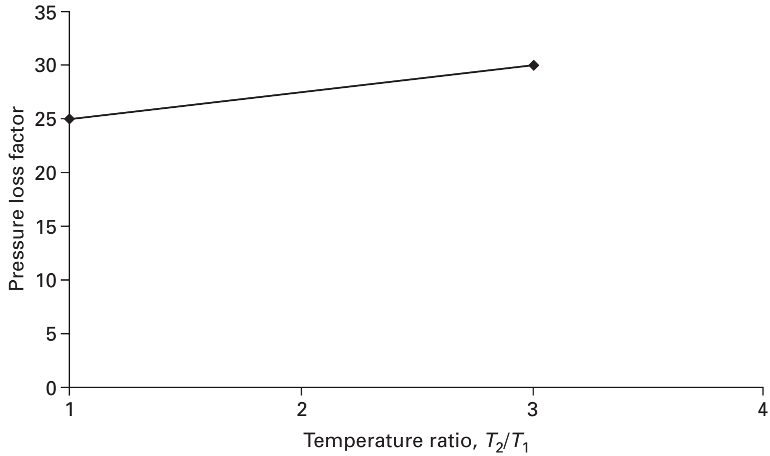

6.22 Variation of the pressure loss factor with temperature ratio.

of the actual fuel–air ratio for the same temperature rise. The values for the theoretical fuel–air ratio can be obtained from Fig. 2.17, Chapter 2. Therefore, the combustion efficiency η_b is given by:

$$\eta_b = (\text{theoretical } (F/A) \text{ for a given } \Delta T)/(\text{actual } (F/A) \text{ for a given } \Delta T) \quad [6.13]$$

where F/A is the fuel–air ratio and ΔT is the overall combustor temperature rise required.

6.8 Formation of pollutants

The combustion process described previously occurs because of the formation of radicals and species such as CO and hydrocarbon radicals (H–C). The intermediate zone of the combustor normally reduces these radicals by addition of more air and by forcing the chemical reaction towards the production of carbon dioxide and water.

The combustion efficiency is very high, typically 98.5% to 99.5%, but the 0.5% to 1.5% loss in combustion efficiency results in the presence of CO and H–C in the exhaust gases, usually referred to as unburned hydrocarbons (UHC). Conditions that promote the formation of UHCs also promote CO and both these compounds are toxic. Unlike CO, which is a colourless, odourless gas, UHCs have the characteristic smell usually found in airport environments.

Another pollutant formed during combustion is due to the oxidation of nitrogen found in the combustion air. Nitrogen does not take part in the combustion; however, the pressures and temperatures that prevail in the primary zone result in a small amount of nitrogen being oxidised. The impact of pressure and temperature is significant in the formation of NO_x and it increases exponentially with these parameters. The oxides that are formed, NO and NO_2, of which NO is dominant, are usually referred to as thermal NO_x. NO_x is toxic and also takes part in the formation of chemical smog, and enhances the depletion of ozone in the stratosphere. Another source of nitrogen for the formation of NO_x is from certain fuels and is often referred to as fuel-bound NO_x.

Clearly, the formation of pollutants is dependent on the combustion pressure, temperature and mixing of the fuel and combustion air. The higher the temperature and pressure, the higher is the reaction rate resulting in lower CO and UHC, but also in an increase in NO_x formation. The combustion pressure and temperature vary with engine load, decreasing when the load is reduced. Therefore, we observe increasing levels of CO and UHC and a decrease in the level of NO_x with the reduction in engine load, as illustrated in Fig. 6.23.

6.9 NO_x suppression using water and steam injection

We have stated that the formation of NO_x is very sensitive to combustion temperature. Introducing a heat sink to reduce the combustion temperature can dramatically reduce the amount of NO_x produced during combustion. Water is a good heat sink because of its high specific heat. Injection of water into the primary zone can significantly reduce the amount of NO_x. For example, if we inject equal amounts of water and fuel (i.e. water to fuel ratio of 1.0) we can reduce NO_x by some 80%.[4]

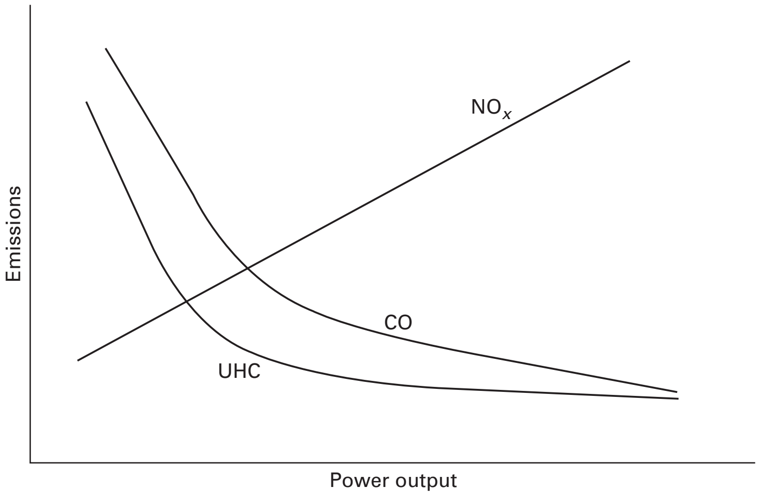

6.23 Variation of emissions with engine load.

Although water injection can dramatically reduce NO_x it has many disadvantages. The suppression of the combustion temperature results in increased production of CO and UHC. The cost of water treatment to improve the purity of water results in increased operating costs. Also, the potential exists for corrosion of hot sections and therefore increased maintenance costs. The heat absorbed by the water also results in increased fuel consumption. Although there is an increase in power output, the net effect is a reduction in thermal efficiency.

In spite of these drawbacks, water injection is used for NO_x suppression because, for many years, water injection was the most effective means to suppress NO_x emissions substantially. In fact, about 35% of industrial gas turbines currently employ water injection for NO_x suppression. When such engines use liquid fuels, water injection is probably the most effective means of NO_x control. Operators also use water injection for power augmentation. Although there is a loss in thermal efficiency, the increased power output is worthwhile in terms of increased production and revenue.

Steam injection has a similar impact in reducing NO_x but the impact on thermal efficiency is more favourable because the latent heat of evaporation is normally supplied from the turbine exhaust heat. However, NO_x suppression using water injection is greater.

6.10 Selective catalytic reduction (SCR)

Another means of reducing gas turbine emissions is to employ selective catalytic reduction. SCR converts NO_x into nitrogen by injecting ammonia into the exhaust stream in the presence of a catalyst. The CO and UHC are also removed by using an oxidation catalyst to convert these emissions into CO_2 and water vapour.

The NO_x levels may be first reduced by using water or steam injection to reduce the NO_x levels to about 30 ppmv, and SCR then reduces them further to about 10 ppmv. SCR systems are quite complex and work when the exhaust gas temperature is within a fairly narrow band ranging from 550 K to about 700 K. Therefore, SCR is normally restricted to applications where exhaust heat recovery is applicable, such as combined heat and power or combined cycle power plants. However, in simple-cycle power plants where no heat recovery is accomplished, high temperature catalysts (e.g. Zeolite), which can operate at temperatures up to 870 K, are an option.

6.11 Dry low emission combustion systems (DLE)

Methods of reducing emissions using water/steam injection and SCR methods have been discussed and their drawbacks highlighted. What is desirable is to achieve low emissions by controlling the combustion temperature. The effect of primary zone fuel–air ratio on NO_x is shown Fig. 6.24. The figure also shows the regions of fuel–air ratio where conventional (diffusion) combustion occurs giving high NO_x emissions and regions of low fuel–air ratio where NO_x formation is low, which is close to the lean extinction limit. The variation of NO_x with primary zone temperature, which is influenced by the primary zone fuel–air ratio, is illustrated in Fig. 6.25. The figure also shows the required operating range for low emissions.

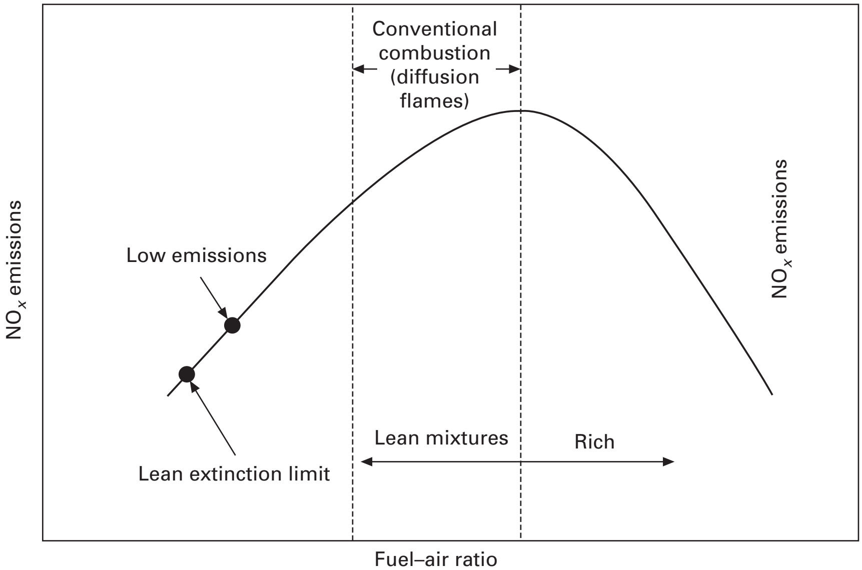

6.24 Influence of the fuel–air ratio on emissions.

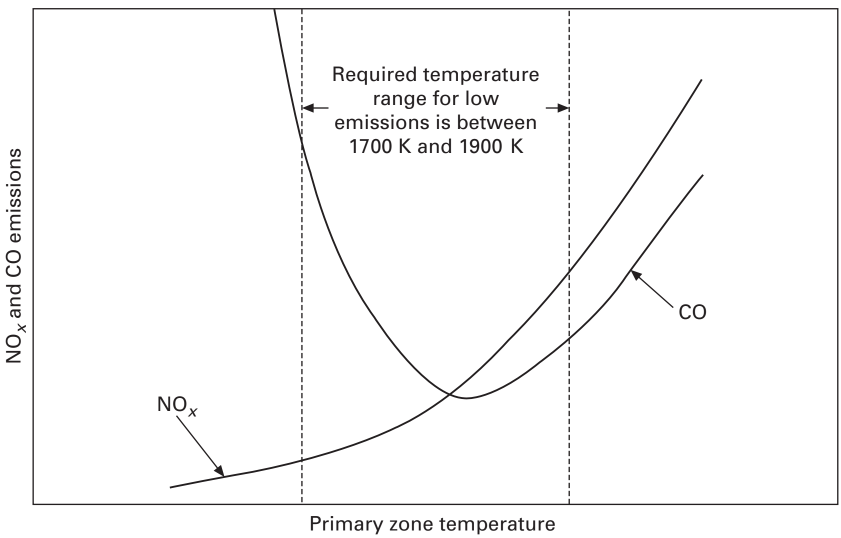

6.25 Influence of the primary zone temperature on emissions.

For a small range of primary zone temperatures, approximately between 1700 K and 1900 K, the NO_x and CO emissions are less than 25 ppmv. The principle behind combustors designed for low emissions is to maintain the primary zone temperature within these limits. This can be achieved if the primary zone fuel–air ratio is kept reasonably constant as the engine load varies.

6.12 Variable geometry combustor

A constant primary zone fuel–air ratio can be achieved as the load is reduced by diverting part of the primary zone air to the dilution zone by means of some variable geometry. This action maintains a constant primary zone temperature and low emissions. Figure 6.26 shows a schematic representation of a variable geometry combustor. The primary zone airflow is controlled by the variable geometry flow controller as the fuel flow changes, so maintaining a constant primary zone fuel–air ratio and thereby maintaining low emissions. Variable geometry has been used in large industrial gas turbines, but its reliability has proved to be a problem with smaller gas turbines.

6.13 Staged combustion

The problems presented by the variable geometry combustors have led to the development of the staged combustor. The variable geometry combustor controls the combustion temperature within the limits where low emissions occur by controlling or maintaining the fuel–air ratio as the engine load changes. This is achieved by switching combustion air from one zone (primary zone) to another (dilution zone) as the load changes. In staged combustion, the airflow distribution between zones is unaltered but the fuel flow is switched from one zone to another.

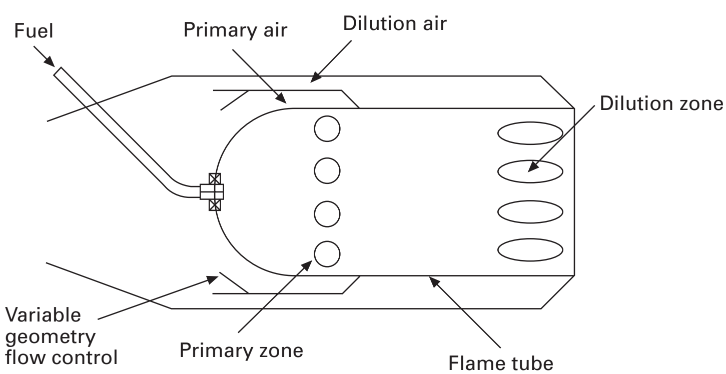

6.26 Schematic representation of a variable geometry combustor.

To obtain the same flexibility as variable geometry combustion systems, staged combustors will require many stages, which is impractical. In practice, however, staged combustors seldom exceed three stages. Two arrangements of staged combustion are possible and are referred to as parallel and series staging. Figure 6.27 shows a schematic representation of these two staged combustion systems.

The first stage is active at low power operation and both stages are active at high power settings. The main advantage of the parallel staging system is that the combustion system length is shorter compared with the series staging system. The series staging system often uses a radial inward arrangement to overcome the increased length but the combustion flow path can be tortuous, as shown in Fig. 6.28.

The main disadvantage of the parallel staging system is that the combustion air temperature for all the stages corresponds to the compressor discharge temperature, resulting in a poor lean extinction limit. Also, at low power settings, the lower temperature of the second stage may 'chill' the combustion in the first stage resulting in increased amounts of CO and UHC. Parallel

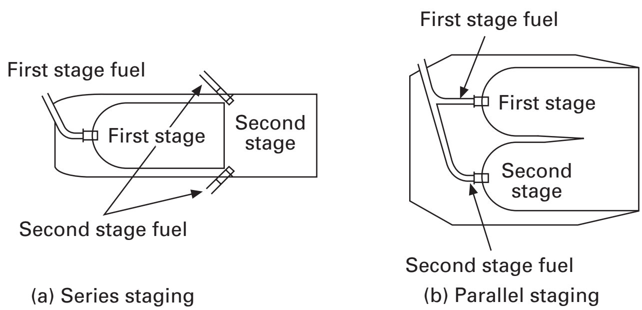

6.27 Schematic representation of (a) series and (b) parallel stage combustors.

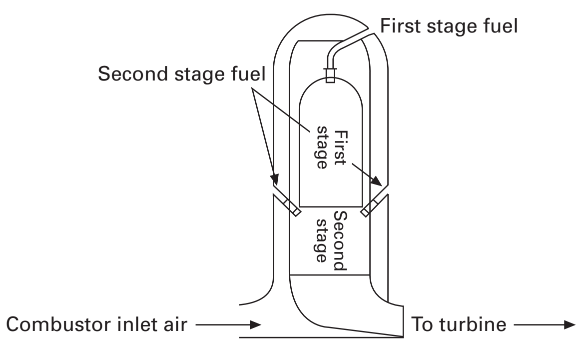

6.28 Radial inward arrangement in a series staging combustion system.

staging systems often employ combustion air bleeds to control the fuel–air ratio, thus preventing the increase in CO and UHC. These bleeds are normally dumped overboard and result in a loss in gas turbine performance.

Series staging has a lower lean extinction limit because the first stage act as a pilot for the second (main) stage and the hot gases from the first stage act as a reliable ignition source for the second stage. Also, the flow of hot gases from the pilot stage into the main stage ensures good combustion efficiency even at very low equivalence ratios. However, as the second stage combustion temperature starts to fall with engine load, CO will start to rise and bleeds as discussed for parallel staging may be required. By increasing the first stage temperature (higher equivalence ratio) at low loads, the CO may be reduced without having to use combustion bleeds.

6.13.1 DLE combustors for industrial gas turbines

The above description of staged combustion has found application in aero-derived gas turbines. There are a significant number of industrial designs, which have adapted a different approach and achieve low emission combustion effectively in a single stage. These engines are of the single shaft type and often employ a variable inlet guide vane to maintain approximately constant fuel–air ratio, as discussed in Section 6.17. A notable design developed by ABB/Alstom is the EV burner,[5] which uses two half cones, shifted to form two air slots of constant width[6] as shown in Fig. 6.29. Gaseous fuels are injected into the combustion air by means of fuel distribution tubes consisting of two rows of small holes perpendicular to the inlet ports of the swirler. The fuel and air is completely mixed shortly after injection. The swirl mixture of fuel and air then flows into the flame zone. The breakdown of the swirling flow at the outlet of the burner results in flame stabilisation in free space just downstream of the burner. During start-up, the EV burner is piloted by fuel supplied to a central fuel nozzle in the tip of the cone through a lance leading to a diffusion type flame. Other manufacturers such as General Electric have also designed DLE for their industrial gas turbines and these are described by Davis and Washam.[7]

6.14 Rich-burn, quick-quench, lean-burn (RQL) combustor

Series staging lends itself well to RQL combustion. The first stage operates at a high equivalence ratio of about 1.5. The incomplete combustion results in a low combustion temperature, thus producing low levels of NO_x. However, there will be substantial amounts of CO and UHC. These reactants and products of combustion are admitted into the second stage, where large amounts of air are introduced and mixed rapidly so that the equivalence ratio

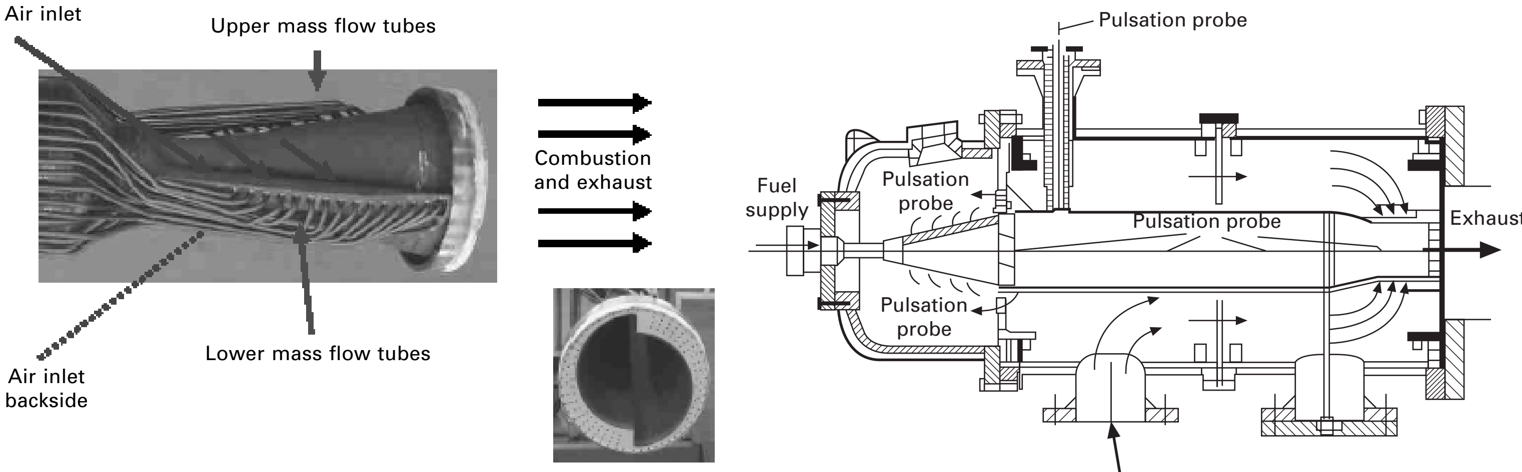

Taken from ASME 2003–GT–38393

6.29 Operating principle of the ABB/Alstom burner.

in any part of the second stage is never above 0.6. Combustion will continue in the second stage, but the low equivalence ratio will prevent high combustion temperatures in the second zone, hence preventing the formation of NO_x but will burn out the UHC and CO.

If the mixing is not thorough, then regions of high enough equivalence ratio will occur in the second stage, resulting in high temperatures giving rise to high levels of NO_x, particularly if the equivalence ratios approach unity. Figure 6.30 illustrates the principle of RQL combustion showing the high NO_x path due to poor mixing of the reactants and air in the second zone and the low NO_x path resulting from good mixing of air and reactants. The concept of RQL combustion has proved difficult to implement in a practical gas turbine.

6.15 Lean premixed (LPM) combustion

We have stated that good mixing of the fuel and air results in a high heat release rate, as was found with air blast atomisers in Section 6.6. The high heat release rate also increases the combustion temperature and will result in high NO_x emissions. However, when operating at low or lean fuel–air ratios, good mixing will result in homogeneous fuel and air mixtures, thus reducing the probability of regions in the mixture where the fuel–air ratio would be high enough to produce high NO_x levels. This will result in significant reductions in NO_x emissions and is illustrated in Fig. 6.31.

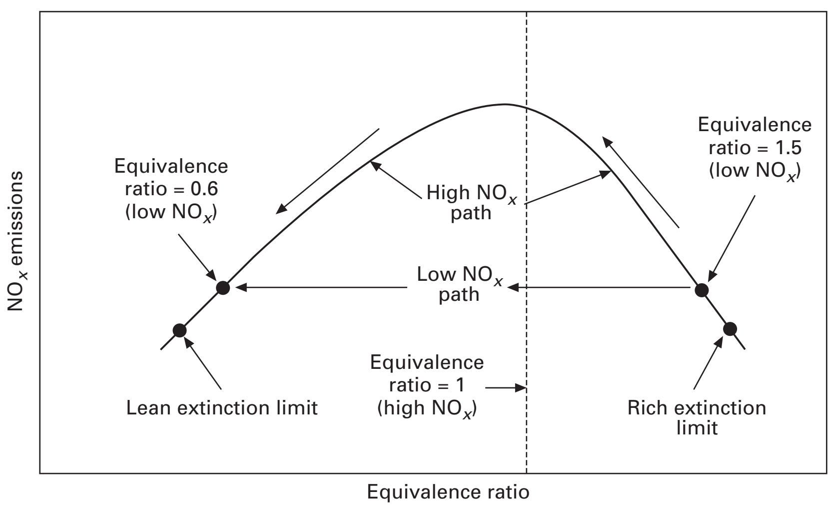

6.30 Principle of rich-burn, quick-quench combustion.

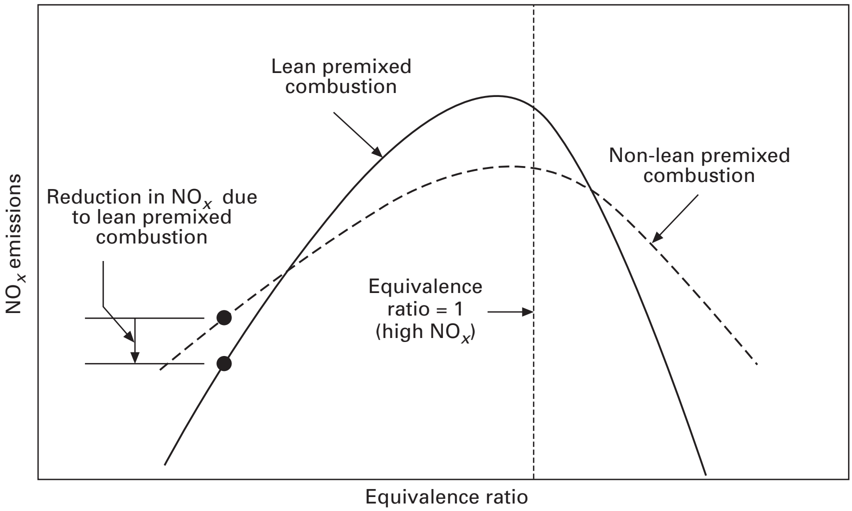

6.31 Impact of lean premixed (LPM) combustion on NO$_x$ reduction.

Fuel and air are thoroughly mixed upstream of the combustion zone, whereas the staged combustion discussed above assumed that the fuel and air mixes during the combustion process and the low overall equivalence ratios are primarily responsible for NO_x reduction. LPM combustion is used extensively in gas-fired engines and the concept can be extended to liquid fuels. However, the fuel must first be completely vaporised before mixing and then burnt in the combustion zone. Such systems are known as lean, premixed, pre-vaporised combustion or LPP combustion. LPP combustion has a tendency to auto-ignite, which is due to the long time periods needed to vaporise and mix the fuel and air. At the high combustor inlet temperatures that occur, high power conditions can result in the mixture igniting before reaching the combustion zone.

6.16 Catalytic combustion

Catalytic combustion is receiving a great deal of attention because it has the ability to reduce pollutants to levels far below that which can be achieved by the systems described previously. Fuel and air are mixed thoroughly before entering the catalyst, which promotes chemical reactions and therefore releases the heat of combustion. Catalytic combustion can take place at equivalence ratios that are well below the lean extinction limit encountered in conventional combustion systems. At such low temperatures, the NO_x levels are reduced dramatically. Figure 6.32 shows a possible schematic representation of a catalytic combustor. An intermediate zone is provided to convert any CO and UHC into products such as CO_2 and H_2O and is followed

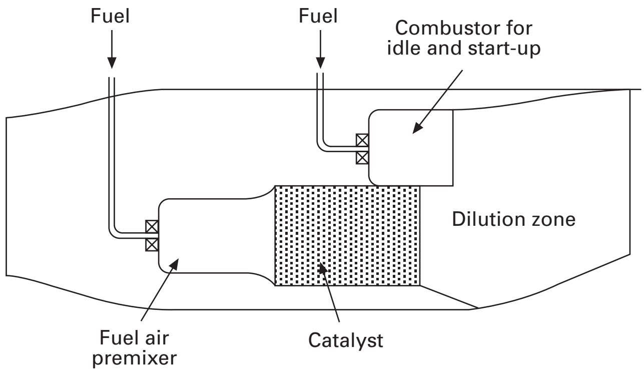

6.32 Schematic representation of a catalyst combustion system.

by a dilution zone to prepare the combustor exhaust gases for entry into the turbine section.

At start-up and idle, the compressor delivery temperature may be too low for the catalyst to be effective and a separate combustion chamber may be needed for start-up and during idle operating conditions. Catalytic combustion is still under development. The significant problems to overcome are satisfactory catalyst life and reliability in the harsh and varied operating conditions that prevail in a gas turbine combustor.

It must be pointed out that the turbine entry temperatures (TET) have increased progressively and gas turbines today operate at firing temperatures of 1800 K. At such high temperatures, the potential for emission reduction using catalytic combustion is limited, as stable combustion is possible with other forms of the low emission combustion systems discussed earlier. Since these combustion systems are quite well developed, catalytic combustion is most likely to find application in small units where the TET is below the weak extinction limit. However, if the control system for catalytic combustion is significantly simpler than the DLE combustion system (particularly if overboard bleeds are dispensed with), then there may be a strong case for widespread use of the catalytic combustion in gas turbines, provided the cost of such combustion systems are competitive. It is also worth pointing out that the turbine entry temperature is unlikely to exceed 1800 K because, at higher turbine entry temperatures, NO_x emissions increase significantly.

6.17 Impact of engine configuration on DLE combustion systems

It was stated in Section 6.12 that a variable geometry combustor can be used to maintain the primary zone temperature at a constant level where emissions are low. Gas turbines have also used variable geometry devices such as variable inlet guide vanes and stators in compressors and variable nozzle guide vanes in turbines for controlling the flow through compressors and turbines. Such devices may also be employed in maintaining the flow through combustors so that the combustor fuel–air ratio is constant, thus attaining low emissions at various engine loads.

6.17.1 Single-shaft gas turbines

The use of single-shaft gas turbines is widespread in power generation, particularly in combined cycle mode where they operate at constant speeds as required by the electrical power generation system. The use of variable inlet guide vanes is common in such engine configurations as they reduce starting power requirements and have the ability to maintain the exhaust gas temperature at low operating power output condition; this can improve gas turbine thermal efficiency under such conditions.

Maintaining constant exhaust gas temperature also results in the combustion temperature remaining approximately constant, thus having the potential of maintaining a constant primary zone temperature at low engine load. Thus, the incorporation of variable inlet guide vanes in the compressor can achieve all the requirements of variable geometry combustion. It is also possible to increase the combustion temperature at lower load above the design value, helping to maintain CO emissions, which tend to increase due to lower combustion pressure. As a result, variable inlet guide vanes are now a major part of DLE combustion gas turbines as described in Maghon *et al.*[8]

6.17.2 Free power turbines

Gas turbines incorporating free power turbines are widespread in applications such as mechanical drives, where the speed of the load varies significantly with power demand. The (single spool) gas generator, which consists of a compressor, combustor and a turbine, produces high pressure–high temperature gas necessary for the power turbine to generate the required power demanded by the load.

Although compressor variable geometry inlet guide vanes and stators are used widely in such engine configurations, they are there mainly to provide adequate surge margins for satisfactory operation rather than to control the flow through the engine. Thus, parallel staged DLE combustors or combustion systems that attempt to achieve the goals of low emissions in a single stage may use overboard bleeds to maintain the fuel–air ratios at low operating loads to prevent high emissions of CO and UHC and flame out at these operating conditions. This is due to combustor operation at conditions far removed from its design point. In effect, an overboard bleed is being used to maintain the combustion temperature and thus emissions, but at the expense of the inevitable loss in engine performance due to the overboard bleeds.

The loss in engine performance due to overboard bleeds is particularly profound at low ambient temperatures when the maximum engine power available may be constrained by gas generator speed rather than by exhaust gas temperature. During such an operation at constant gas generator speed, there is an inevitable reduction in fuel–air ratio as the ambient temperature decreases, hence increasing the emissions of CO and UHC. The reduction in the fuel–air ratio at these operating conditions also increases the risk of flame out due to the weak extinction limit being exceeded. Thus it may be necessary to bleed combustion air when maximum power demand is called for at such low ambient temperatures. This not only increases the fuel consumption but also reduces the maximum power available. Hence, the performance penalty due to combustion overboard bleeds is more severe at low ambient temperatures.

Variable geometry power turbines were developed and applied widely to regenerative gas turbines for automotive applications in the 1960s. They were needed to improve the off-design fuel efficiency. This was achieved by closing the power turbine nozzle guide vane at low loads, thus maintaining the maximum cycle temperature at these off-design conditions. Thus, the combustion temperature is also maintained at low loads, in effect maintaining the fuel–air ratio without the need of overboard bleeds.

At low ambient temperatures, when constant gas generator speed operation may occur, the use of variable nozzle guide vanes in the power turbine not only maintains low gas turbine emissions without the need for overboard bleeds, but also improves the gas turbine thermal efficiency at these ambient conditions. This is due to the higher compressor pressure ratios, which occur when the power turbine nozzle guide vanes are closed to maintain the exhaust gas temperature.

Variable geometry power turbines are employed currently by a few gas turbines which incorporate heat exchangers as a means of improving fuel efficiency at off-design conditions. Their application could be extended to cover all DLE gas turbines operating with power turbines, as this would result in better gas turbine performance while maintaining low emissions such as CO, UHC and NO_x, without increasing CO_2 emissions due to the application of overboard bleeds.

6.18 Correlations for prediction of NO_x, CO and UHC and the calculation of CO_2 emissions

Some of the factors that affect the formation of pollutants such as NO_x, CO and UHC have been discussed. The chemical reactions governing the formation of these pollutants are quite complex. Three predominant factors are combustion temperature, pressure and humidity. There are other parameters that also affect the formation of these pollutants, such as fuel–air ratio, fuel and air mixing, combustor geometry and residence times. Various correlations have been proposed and validated and serve as a very useful means of predicting emissions from gas turbines. CO_2 is also produced during combustion. Although it is not normally considered as a toxic pollutant, it is a greenhouse gas and thought to be responsible for global warming. The prediction of CO_2 is relatively straightforward. If the carbon–hydrogen ratio of the fuel is known, the CO_2 emissions can be readily calculated.

6.18.1 NO_x correlations

Many correlations have been developed and validated by various research programmes and some of these parametric models for predicting NO_x will now be discussed. The first correlation is due to Lefebvre,[9] who suggests that NO_x is given by:

$$NO_x = 9 \times 10^{-8}\, P^{1.25}\, Vc \exp(0.01Tst)Tpz/ma \qquad [6.14]$$

where
Vc is the combustion volume (m^3)
P is the combustion pressure, kPa
Tst is the stoichiometric temperature, K
ma is the combustion airflow, kg/s
Tpz is the average primary zone temperature, K
NO_x is calculated as an emissions index in g/kg of fuel.

The correlation has been developed for conventional spray combustors only. It is also claimed to work for lean pre-mixed vaporiser combustors provided that the primary zone temperature, *Tpz*, which will be the maximum temperature attained during combustion, is substituted for *Tst*.

Odgers and Kretschmer[10] also developed a correlation for predicting NO_x, based on aero-engines, and this is given by:

$$NO_x = 28\exp - (21670/Tc)P^{0.66}\, [1 - \exp - (250\tau)] \qquad [6.15]$$

where
Tc is the combustion temperature, K
P is combustion pressure in atmospheres
τ is the residence time in seconds.

They recommend that the time constant for air blast atomisers is set to 0.8 ms and for pressure swirl atomisers τ is set to 1.0 ms.
NO_x is calculated as an emissions index in g/kg of fuel.

Rokke *et al.*[11] also proposed a correlation for predicting the NO_x from natural gas fired gas turbines and it has been tested on various gas turbines whose power output varied from 1.5 MW to 35 MW. The correlation is:

$$NO_x = 18.1P^{1.42}ma^{0.3}f^{0.72} \qquad [6.16]$$

where
P is the combustion pressure in atmospheres
ma is the combustion airflow, kg/s
f is the fuel–air ratio
NO_x is given in ppmv at 15% O_2 dry.

Although the combustion temperature term is absent in this correlation, it is represented by the fuel–air ratio term.

The following correlation is due to Rizk and Mongia[12] and is given by:

$$NO_x = 0.15 \times 10^{16}(t - te)^{0.5}\exp - (71\,000/Tst)/P^{0.05}(\Delta P/P)^{0.5} \qquad [6.17]$$

where
t is the residence time in seconds and *te* is the evaporation time in seconds
P is the combustion pressure, kPa
Tst is the stoichiometric temperature, K
NO_x is calculated as an emissions index in g/kg of fuel.

This correlation is similar to that proposed by Lefebvre.

A correlation proposed and validated by Sullivan[13] is given by Equation 6.18:

$$NO_x = A_{nox} \times P^{0.5}f^{1.4}ma^{-0.22}\exp(Tc/250) \qquad [6.18]$$

where
A_{nox} is a reference parameter reflecting the combustor geometry
P is the combustion pressure, Pa
Tc is the combustion temperature, K
f is the fuel–air ratio
ma is the combustion airflow, kg/s
NO_x is given in ppmv at 15% O_2 dry.

Bakken and Skogly[14] proposed a similar correlation developed for natural gas fired gas turbines, as given by Equation 6.19.

$$NO_x = 62P^{0.5}f^{1.4}\exp - (635/Tc) \qquad [6.19]$$

where
P is the combustion pressure, Pa
Tc is the combustion temperature, C
f is the fuel–air ratio
NO_x is given in ppmv at 15% O_2 dry.

According to Bakken, the parameters should be corrected to standard condition (15 °C and 1.013 Bar). This implies that NO_x is dependent on Tc/T_1 and P/P_1, where T_1 and P_1 are the compressor inlet temperature and pressure, respectively, rather than the combustion temperature, Tc and pressure, P.

6.18.2 CO correlations

A correlation proposed by Lefebvre[9] for the prediction of CO is given in Equation 6.20:

$$CO = 86ma \times Tpz \times \exp - (0.00345Tpz)/(Vc - Ve)(\Delta P/P)^{0.5}P^{1.5} \quad [6.20]$$

where
Vc is the combustion volume, m^3
Ve is the volume occupied by the evaporated fuel, m^3
P is the combustion pressure, kPa
ΔP is the combustion non-dimensional pressure drop
ma is the combustion airflow, kg/s
Tpz is the average primary zone temperature, K
CO is calculated as an emissions index in g/kg of fuel.

The following correlation similar to that proposed by Lefebvre is given by Rizk and Mongia:[12]

$$CO = 0.179 \times 10^9 \exp(7800/Tpz)/P^2(t - 0.4te)(\Delta P/P)^{0.5} \quad [6.21]$$

where
t is the residence time in seconds and te is the evaporation time in seconds
P is the combustion pressure, kPa
Tpz is the primary zone temperature, K
CO is calculated as an emissions index in g/kg of fuel.

6.18.3 UHC correlation

Correlations for predicting UHC have been developed, but they tend to be less reliable than those developed for NO_x and CO. However, Rizk and Mongia[12] offer the following correlation for predicting UHC as an emissions index:

$$UHC = 0.755 \times 10^{11} \exp(9756/Tpz)/P^{2.5}(t - 0.35te)^{0.1} (\Delta P/P)^{0.6} \quad [6.22]$$

where
t is the residence time in seconds and te is the evaporation time in seconds
P is the combustion pressure, kPa
Tpz is the primary zone temperature, K.

6.18.4 Calculation of CO_2

The equation governing the formation of CO_2 during the burning of hydrocarbon fuels is given by:

$$C_xH_y + nO_2 = n_1CO_2 + n_2H_2O \qquad [6.23]$$

where

x/y is the carbon–hydrogen atomic ratio of the fuel.

The equation states that 1 molecule (mole) of the fuel will react with n moles of O_2 to produce n_1 moles of CO_2 and n_2 moles of H_2O. Performing a molar balance:

$$n_1 = x$$

$$n_2 = 0.5y$$

$$n = n_1 + 0.5n_2 = x + 0.25y$$

Substituting n, n_1 and n_2 into Equation 6.23:

$$C_xH_y + (x + 0.25y)O_2 = xCO_2 + 0.5yH_2O \qquad [6.24]$$

Therefore, 1 mole of fuel will produce x moles of CO_2. But 1 mole of fuel will weigh $x \times 12 + y \times 1$ kg and 1 mole of CO_2 will weigh 44 kg. Therefore:

$$1 \text{ kg of fuel} = 44x/(12x + y) \text{ kg of } CO_2 \qquad [6.25]$$

or

$$1 \text{ kg of fuel} = 44/(12 + y/x) \text{ kg of } CO_2 \qquad [6.26]$$

Values of 44 and 12 in Equations 6.25 and 6.26 represent the molecular weight and atomic weight of CO_2 and carbon, respectively. The atomic weight of hydrogen is, of course, unity.

If 1 kg of methane (CH_4) whose x/y ratio is 0.25 is burnt, from Equation 6.26, 2.75 kg of CO_2. If will be obtained 1 kg of kerosene ($C_{12}H_{24}$) whose x/y is 0.5 is burnt, 3.14 kg of CO_2 will be obtained, which represents about a 14% increase in CO_2.

In practice, the CO_2 emissions are greater. For example, if a gas turbine produces 20 MW of power at a thermal efficiency of 35%, the thermal input required is (20/0.35) = 57.14 MW. If methane is burnt, whose LHV is about 50 MJ/kg, a fuel flow rate of (57.14/50) 1.143 kg/s will be required and the CO_2 emissions will be 3.14 kg/s. If kerosene with a LHV of about 43 MJ/kg is used, the fuel flow required is (57.14/43) = 1.329 kg/s and the CO_2 emissions will be 4.17 kg/s of CO_2. This represents about a 16% increase in fuel flow and a 32% increase in CO_2. (It is assumed that there is no change in gas turbine performance due to the change in fuel from methane to kerosene. However, there is a slight loss in performance when burning kerosene.)

6.19 References

1. *Hydrocarbon Fuels*, Goodger, E.M., Macmillan Press (1975).
2. A short diffuser with low pressure loss, Adkins, R.C., *Journal of Fluid Engineering* (1975), p. 297–302.
3. *Gas Turbine Combustion*, Lefebvre, A.H., Taylor and Francis (1998).
4. Hung W.S.Y., Accurate method of predicting the effect of humidity or injected water on NO_x emissions from industrial gas turbines, *ASME Paper 74-WA/GT-6*, 1974.
5. Sattelmeyer, T., Felchlin, M.P., Haumann, J. and Styner, D., Second generation low emission combustors for ABB gas turbines – burner development test at atmospheric pressure, *Transactions of ASME*, 114, 1992.
6. Doebbeling, K., Eroglu, A., Joos, F. and Hellat, J. Novel technologies for natural gas combustion in turbine systems. *Eurogas 99*, Ruhr University Bochum, Germany, May 25–27, 1999.
7. Davis, L.B. and Washam, R.M., Development of a low NO_x combustor, *ASME paper 89-GT-255*, 1989.
8. Maghon, H., Berenbrink, P., Termuehlen, H. and Gartner, G., Progress in NO_x and CO emission reduction of gas turbines, *ASME paper 90-JPGC/GT-4*, 1990.
9. Lefebvre A.H., Fuel effects on gas turbine combustion – liner temperature, pattern factor, and pollutant emissions, *Journal of Aircraft*, 21, (11), 887–898, 1984.
10. Odgers, J. and Kretschmer, D., The prediction of thermal NO_x in gas turbines. *ASME Paper 85-1GT-126*, 1985.
11. Rokke, N.A., Husted, J.E. and Berg, S., Pollutant emissions from gas fired turbine engines in offshore practices – measurement and scaling. *ASME Paper 93-GT-170*, 1993.
12. Rizk, N.K and Mongia, H.C., Emissions predictions of different gas turbine combustors, *AIAA Paper 94-0118*, 1994.
13. Sullivan, D.A., A simple gas turbine combustor NO_x correlation including the effect of vitiated air. *Journal of Engineering for Power*, 1977.
14. Bakkan, L.E. and Skogly, L., *ASME Paper 95-GT-399*, 1995.

7
Off-design performance prediction

Chapters 2 and 3 discussed the evaluation of the design point performance of a gas turbine. The designer selects a pressure ratio, component efficiencies and a maximum cycle temperature T_3 (also known as the turbine entry temperature or TET) to achieve a required engine performance. The design point calculation determines the thermal efficiency and airflow rate for a given power demand. This information is used in the design of the turbomachinery and combustion system as described in Chapters 4, 5 and 6. The design of the turbomachinery and combustion system is a specialist area and the designer's experience is used to achieve the desired performance of these engine components.

An engine designed on this principle will usually achieve the design performance. However, gas turbines have to operate for prolonged periods at conditions outside their design conditions and this state is referred to as the off-design performance. An off-design condition manifests itself due to a change in engine load and ambient conditions. For example, the ambient temperature may change significantly from winter to summer and will have a significant impact on the engine performance. Hence, the engine will not only have to perform satisfactorily at the design conditions, but the off-design performance is also of paramount importance.

This chapter discusses the prediction of the off-design performance of gas turbines. An interesting alternative method for the prediction of the off-design performance of gas turbines is described in Saravanamuttoo *et al.*[1] Also, much information on gas turbine performance can be found in Walsh and Fletcher.[2]

7.1 Component matching and component characteristics

The off-design performance of a gas turbine is determined by the interaction of the engine components, namely the compressors, combustors and turbines.

The interaction of these gas turbine components is often referred to as component matching. Typical characteristics for a compressor and a turbine are shown in Figs 7.1, 7.2 and 7.3. Although a wide operating range is shown, the component interaction or the matching of the gas turbine components will restrict the operating range severely. Therefore, the performance of the component must be satisfactory in this restricted region to achieve satisfactory performance at off-design conditions.

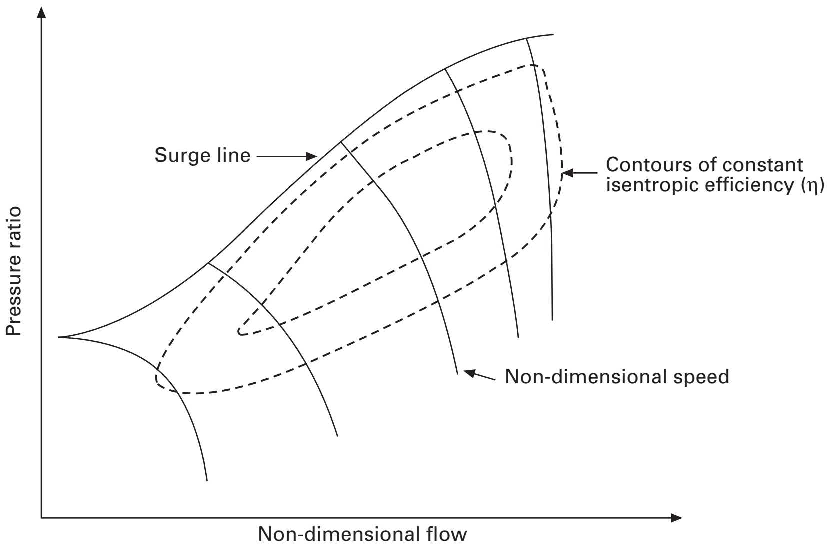

7.1 Typical axial compressor characteristics.

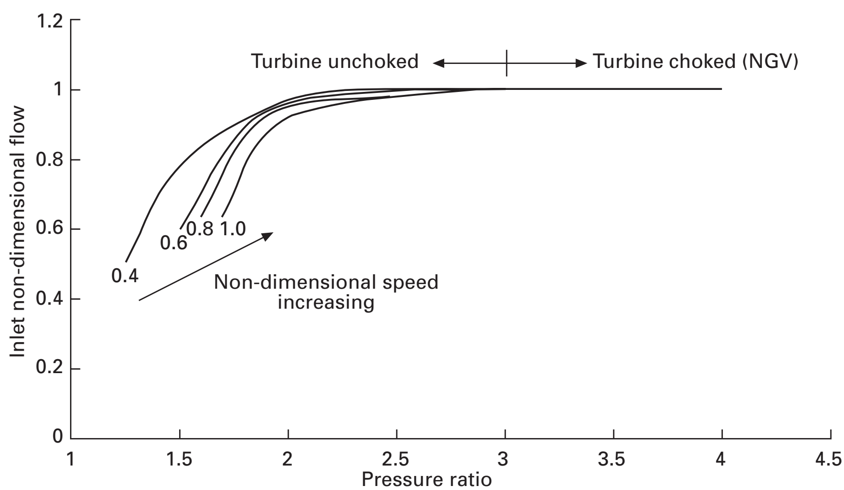

7.2 Turbine flow characteristics.

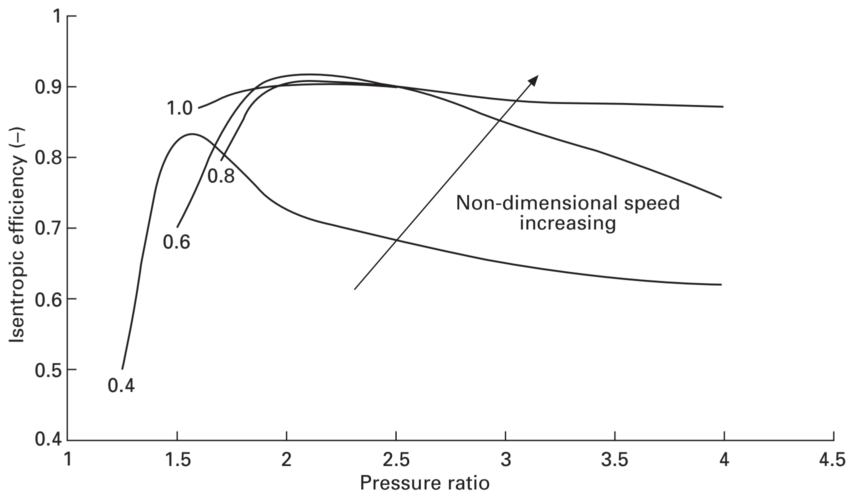

7.3 Typical turbine efficiency characteristics.

These characteristics are normally plotted on a non-dimensional basis so as to allow for the variation of pressure, temperature, speed and flow in a manageable manner. These groups, as discussed in Section 4.6, are the component non-dimensional mass flow, non-dimensional speed, pressure ratio and efficiency. Temperature ratios are often omitted because they can be derived from pressure ratio and efficiency. The representation of component efficiency in gas turbine practice is often the isentropic efficiency. The correct definitions of these non-dimensional groups are:

$$\text{Non-dimensional flow} = \frac{W_1\sqrt{R_1 T_1/\gamma_1}}{D^2 P_1}$$

$$\text{Non-dimensional speed} = \frac{N_1}{\sqrt{\gamma_1 R_1 T_1}}$$

$$\text{Pressure ratio} = \frac{P_2}{P_1}$$

where W_1, T_1, P_1 and D are the inlet mass flow rate, temperature, pressure and reference diameter of the compressor or turbine, respectively, and N_1 is the rotational speed of the compressor or turbine. P_2 is the discharge pressure of the compressor or turbine and R_1 and γ_1 are the gas constant and isentropic index (c_p/c_v), where c_p and c_v are the specific heats at constant pressure and volume, respectively. (Note the gas constant γ_1 and R_1 will be different for air and products of combustion.)

In fact, the non-dimensional mass flow and speed are Mach numbers. The flow rate W_1 is given by the continuity equation $W_1 = \rho_1 \times U_1 \times A_1$, where A_1 is the flow area and U_1 and ρ_1 are the inlet velocity and inlet density respectively. From the equation of state, pressure P_1 is given by $P_1 = \rho_1 \times R \times T_1$. The Mach number is defined as:

$$M = \frac{U_1}{\sqrt{\gamma R T_1}}$$

It can thus be shown that $\dfrac{W_1 \sqrt{RT_1/\gamma}}{D^2 P_1} \propto M_F$

where M_F is the Mach number based on inlet flow.

Similarly, the non-dimensional speed:

$$\frac{U_1}{\sqrt{\gamma R T_1}} \propto \frac{ND}{\sqrt{\gamma R T_1}} \propto M_R$$

where M_R is the Mach number based on rotational speed.

For a given compressor, the flow area is constant. It is usual to omit the geometry term D from the non-dimensional flow and speed parameters in representing compressor and turbine characteristics as these values do not change for a given compressor or turbine.

7.2 Off-design performance prediction of a single-shaft gas turbine

Single-shaft gas turbines are used widely in power generation. In this application the gas turbine is maintained at a constant speed, which corresponds to the synchronous speed of the electrical generator. Due to design considerations, if the gas turbine speed is different from that of the generator synchronous speed, a gearbox is used to step up/down the gas turbine speed to match the required generator speed. Nonetheless, the gas turbine speed is constant with varying generation load. A schematic representation of a single-shaft gas turbine is shown in Fig. 7.4.

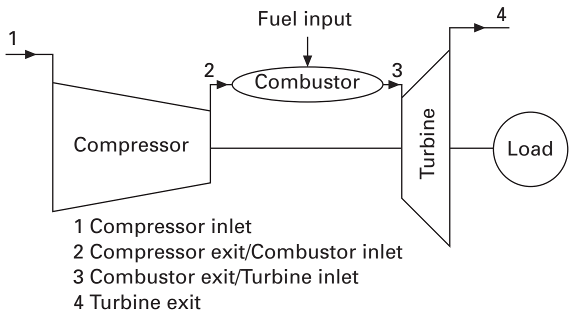

7.4 Schematic representation of a single shaft gas turbine (simple cycle).

The air enters the compressor at station 1 and exits the compressor at station 2 after compression. The high-pressure air enters the combustion chamber, where fuel is burnt and the air–gas temperature is increased. The high-pressure, high-temperature gases are expanded through the turbine and exit the gas turbine at station 4. Part of the turbine power, typically about 50%, is used to drive the compressor and the remaining turbine power drives the load, which is normally a generator.

Referring to Fig. 7.4, the matching process is as follows. The required power output, gas turbine speed, N_1, compressor inlet pressure, P_1, temperature, T_1, and humidity are specified. The temperature and humidity are used to determine gas constant R and the isentropic index γ, as discussed in Chapter 2. We shall ignore inlet and exhaust losses and therefore $P_4 = P_1$. For simplicity we shall also ignore any turbine blade cooling air requirements on engine performance.

Step 1 – Estimates

Step 1.1 Estimate the compressor inlet flow W_1, pressure ratio $\frac{P_2}{P_1}$ and combustion exit temperature or turbine entry temperature, (T_3).

Step 2 – Compressor

Step 2.1 Calculate the compressor inlet non-dimensional flow $\frac{W_1\sqrt{R_1T_1/\gamma_1}}{P_1}$.

Step 2.2 Using the compressor non-dimensional flow and pressure ratio $\frac{P_2}{P_1}$ determine the compressor non-dimensional speed $\frac{N_1}{\sqrt{\gamma_1 R_1 T_1}}$ and compressor isentropic efficiency η_{12} by interpolation using the compressor characteristic (Fig. 7.1).

Step 2.3 Calculate the compressor exit mass flow pressure, temperature and speed using the following, ignoring bleeds

$$W_2 = W_1 \tag{7.1}$$

$$P_2 = P_1 \times \frac{P_2}{P_1} \tag{7.2}$$

$$T_2 = T_1 + T_1/\eta_{12}\left[\left(\frac{P_2}{P_1}\right)^{\frac{\gamma a-1}{\gamma a}} - 1\right] \tag{7.3}$$

$$N_1 = \sqrt{\gamma_1 \times R_1 \times T_1}\ \sqrt{\frac{N_1}{\gamma_1 R_1 T_1}} \qquad [7.4]$$

where γa is the mean isentropic index between T_1 and T_2. γ_1 and R_1 are the isentropic index and gas constant at inlet to the compressor.

Step 2.4 Calculate the compressor power absorbed (*cpow*) using:

$$cpow = W_1 \times cpa(T_2 - T_1) \qquad [7.5]$$

Where *cpa* is the specific heat at constant pressure between T_1 and T_2

Step 3 – Combustor

Step 3.1 Using the estimated combustor exit temperature or turbine entry, temperature, T_3, calculate the fuel flow, *mf*, using the temperature rise, T_3–T_2, combustor inlet temperature T_2 and the combustion charts (Fig. 2.17 in Chapter 2).

Step 3.2 Calculate the combustor exit pressure, P_3 using Equations 7.6 and 7.7.

$$\frac{\Delta P_{23}}{P_2} = \text{PLF} \times \left(\frac{W_2\sqrt{R_2 T_2/\gamma_2}}{P_2}\right)^2 \gamma_2 + \left[K_1 + K_2\left(\frac{T_3}{T_2} - 1\right)\right] \qquad [7.6]$$

where PLF is the power loss factor, K_1 and K_2 are the cold loss (which corresponds to the combustion pressure loss due to friction), and hot loss or fundamental loss (which corresponds to the combustion pressure loss due to heat addition) of the combustor (See Section 6.7 in Chapter 6):

$$P_3 = P_2 \times \left(1 - \frac{\Delta P_{23}}{P_2}\right) \qquad [7.7]$$

Step 3.3 Calculate the exit mass flow. In the absence of bleeds:

$$W_3 = W_2 + mf \qquad [7.8]$$

Step 4 – Turbine

Step 4.1 Calculate the turbine inlet non-dimensional flow, pressure ratio and non-dimensional speed $\frac{W_3\sqrt{R_3 T_3/\gamma_3}}{P_3}$, $\frac{P_3}{P_4}$ and $\frac{N_3}{\sqrt{\gamma_3 R_3 T_3}}$, respectively.

Step 4.2 Using the turbine pressure ratio $\frac{P_3}{P_4}$ and the calculated non-dimensional speed $\frac{N_3}{\sqrt{\gamma_3 R_3 T_3}}$ in step 4.1, determine the turbine inlet non-dimensional flow $\left(\frac{W_3\sqrt{R_3T_3/\gamma_3}}{P_2}\right)_c$ and isentropic efficiency η_{34} by interpolation using the turbine characteristic (Figs. 7.2 and 7.3).

Step 4.3 Calculate the turbine exit temperature and power output using:

$$T_4 = T_3 - T_3 \times \eta_{34}\left[1 - \left(\frac{P_4}{P_3}\right)^{\frac{\gamma g-1}{\gamma g}}\right] \quad [7.9]$$

$$tpow = W_3 \times cpg(T_3 - T_4) \quad [7.10]$$

where γg and cpg are the mean isentropic index and specific heat at constant pressure between T_3 and T_4.

Step 5 – Check 1

Step 5.1 Compare the calculated turbine inlet non-dimensional flows

$$\left(\frac{W_3\sqrt{R_3T_3/\gamma_3}}{P_3}\right)$$

in step 4.1 and the turbine inlet non-dimensional flow determined from the turbine characteristic, in step 4.2. If they do not agree, return to step 3, estimate a different T_3 and repeat to step 5.1 until the two values for turbine inlet non-dimensional flows agree.

Step 6 – Check 2

Step 6.1 Calculate the net turbine power output, *pnet* using

$$pnet = tpow - cpow \quad [7.11]$$

Step 6.2 Compare the calculated turbine power output with the required power output from the gas turbine. If they do not agree, return to step 2, estimate a different compressor pressure ratio $\left(\frac{P_2}{P_1}\right)$ and repeat to step 6.2 until the powers agree.

Step 7 – Check 3

Step 7.1 Compare the compressor speed, N_1 calculated in step 2 with the speed required by the load. If they do not agree, estimate a different compressor inlet mass flow, W_1, return to step 2 and repeat to step 7.1 until the speeds agree.

7.3 Off-design performance prediction of a two-shaft gas turbine with a free power turbine

Gas turbines employing free power turbines are widely used where the speed of the load changes significantly. Applications where the load speed changes are pumps, gas compressors and fixed pitch propellers used in marine propulsion. They are generally designed for smaller power ranges (up to about 50 MW) compared with single shaft gas turbines and are also employed in power generation when no single shaft gas turbine is available in this power range. A schematic representation of a two-shaft gas turbine using a free power turbine is shown in Fig. 7.5. There is no mechanical coupling between the gas generator turbine and the power turbine but there exists a strong fluid or aerodynamic coupling between the gas generator turbine and the power turbine.

Air enters the compressor at station 1 as shown in Fig. 7.5. The compressor discharge air enters the combustor at station 2 and fuel is burnt to raise the air–gas temperature at station 3. The hot gases are expanded in the gas generator turbine to develop enough power to drive the compressor. The gases leaving the gas generator turbine are then expanded in the power turbine and leave the power turbine at station 5. The power output from the power turbine drives a load such as a gas compressor, pump or a propeller.

The matching process for a two-shaft gas turbine is as follows. The required power, compressor inlet temperature, pressure, humidity and the power turbine speed are specified. Making the same assumptions as in Section 7.2 regarding inlet and exhaust losses and turbine cooling, the matching procedure for a two-shaft gas turbine operating with a free power turbine involves:

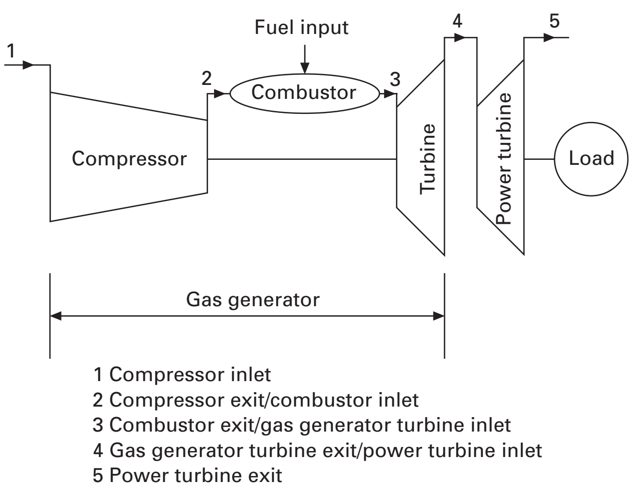

7.5 Schematic representation of a two-shaft gas turbine with a free power turbine.

Step 1 – Estimates

Step 1.1 Estimate the compressor inlet flow, W_1, pressure ratio, $\frac{P_2}{P_1}$ combustion exit temperature or turbine entry temperature, T_3, and the gas generator pressure ratio, $\frac{P_3}{P_4}$.

Step 2 – Compressor

Step 2.1 Calculate the compressor inlet non-dimensional flow $\frac{W_1\sqrt{R_1T_1/\gamma}}{P_1}$.

Step 2.2 Using the compressor non-dimensional flow and pressure ratio, determine the compressor non-dimensional speed $\frac{N_1}{\sqrt{\gamma_1 R_1 T_1}}$ and compressor isentropic efficiency η_{12} by interpolation using the compressor characteristic.

Step 2.3 Calculate the compressor discharge mass flow, pressure, temperature and gas generator speed, N_1 using the following:

In the absence of bleeds:

$$W_2 = W_1 \tag{7.12}$$

$$P_2 = P_1 \times \frac{P_2}{P_1} \tag{7.13}$$

$$T_2 = T_1 + T_1/\eta_{12}\left[\left(\frac{P_2}{P_1}\right)^{\frac{\gamma a-1}{\gamma a}} - 1\right] \tag{7.14}$$

$$N_1 = \sqrt{\gamma_1 \times R_1 \times T_1}\sqrt{\frac{N_1}{\gamma_1 R_1 T_1}} \tag{7.15}$$

where γ_a is the mean isentropic index between T_1 and T_2

Step 2.4 Calculate the compressor power absorbed using:

$$cpow = W_1 \times cpa(T_2 - T_1) \tag{7.16}$$

where *cpa* is the mean specific heat at constant pressure between T_1 and T_2.

Step 3 – Combustor

Step 3.1 Using the estimated combustor exit temperature or turbine entry temperature, T_3 calculate the fuel flow, *mf*, using the temperature rise, T_3–T_2, combustor inlet temperature T_2 and the combustion charts (Figure 2.17 in Chapter 2)

Step 3.2 Calculate the combustor exit pressure, P_3 using Equations 7.17 and 7.18.

$$\frac{\Delta P_{23}}{P_2} = \text{PLF} \times \left(\frac{W_2 \sqrt{R_2 T_2 / \gamma_2}}{P_2} \right)^2 \gamma_2 + \left[K_1 + K_2 \left(\frac{T_3}{T_2} - 1 \right) \right] \tag{7.17}$$

$$P_3 = P_2 \times \left(1 - \frac{\Delta P_{23}}{P_2} \right) \tag{7.18}$$

Step 3.3 Calculate the exit mass flow. In the absence of bleeds:

$$W_3 = W_2 + mf \tag{7.19}$$

Step 4 – Gas generator turbine

Step 4.1 Calculate the turbine inlet non-dimensional flow, pressure ratio and non-dimensional speed $\frac{W_3 \sqrt{R_3 T_3 / \gamma}}{P_3}$ and $\frac{N_3}{\sqrt{\gamma_3 R_3 T_3}}$, respectively, (note $N_3 = N_1$).

Step 4.2 Using the estimated turbine pressure ratio $\frac{P_3}{P_4}$ and the calculated non-dimensional speed $\frac{N_3}{\sqrt{\gamma_3 R_3 T_3}}$, determine the turbine inlet non-dimensional flow:

$$\left(\frac{W_3 \sqrt{R_3 T_3 / \gamma_3}}{P_3} \right)_c$$

and isentropic efficiency η_{34} by interpolation using the turbine characteristic.

Step 4.3 Calculate the turbine exit temperature and power output using:

$$T_4 = T_3 - T_3 \times \eta_{34} \left[1 - \left(\frac{P_4}{P_3} \right)^{\frac{\gamma g - 1}{\gamma g}} \right] \tag{7.20}$$

$$tpow = W_1 \times cpg(T_2 - T_1) \tag{7.21}$$

where γg and cpg are the mean isentropic index and specific heat at constant pressure between T_3 and T_4, respectively.

Step 4.4 Calculate the gas generator turbine exit pressure, P_4, using:

$$P_4 = P_3 \times \frac{P_4}{P_3} \tag{7.22}$$

Set the gas generator turbine exit mass flow, W_4 to W_3; that is $W_4 = W_3$ (no bleeds).

Step 5 – Power turbine

Step 5.1 Calculate the power turbine inlet non-dimensional flow, pressure ratio and non-dimensional speed, $\dfrac{W_4\sqrt{R_4T_4/\gamma_4}}{P_4}, \dfrac{P_4}{P_5}$ and $\dfrac{Npt}{\gamma_4 R_4 T_4}$, respectively. where *Npt* is the specified power turbine speed.

Step 5.2 Using the power turbine pressure ratio $\dfrac{P_4}{P_5}$ and the calculated non-dimensional speed $\dfrac{Npt}{\sqrt{T_4}}$, determine the power turbine inlet non-dimensional flow $\left(\dfrac{W_4\sqrt{R_4T_4/\gamma_4}}{P_4}\right)_c$ isentropic efficiency η_{pt} by interpolation using the power turbine characteristic.

Step 5.3 Calculate the turbine exit temperature and power output using:

$$T_5 = T_4 - T_4 \times \eta_{\text{pt}}\left[1 - \left(\frac{P_5}{P_4}\right)^{\frac{\gamma g-1}{\gamma g}}\right] \qquad [7.23]$$

$$ptpow = W_4 \times cpg(T_4 - T_5) \qquad [7.24]$$

where γ_g and *cpg* are the mean isentropic index and specific heat at constant pressure, respectively, between T_4 and T_5. *ptpow* is the power turbine power output.

Step 6 – Check 1

Step 6.1 Compare the calculated gas generator turbine inlet non-dimensional flow

$$\frac{W_3\sqrt{R_3T_3/\gamma_3}}{P_3}$$

and the corresponding non-dimensional flow determined from the gas generator turbine characteristic

$$\left(\frac{W_3\sqrt{R_3T_3/\gamma_3}}{P_3}\right)_c$$

in steps 4.1 and 4.2. If they do not agree, return to step 3, estimate a different T_3 and repeat to step 6.1 until the two values for the turbine inlet non-dimensional flows agree.

Step 7 – Check 2

Step 7.1 Compare the compressor absorbed power, *cpow*, and the gas generator turbine power output, *tpow*, (steps 2.4 and 4.3). If they do not agree, estimate a different gas generator turbine pressure ratio $\frac{P_3}{P_4}$ and repeat from step 4 to step 7.1 until these powers agree.

Step 8 – Check 3

Step 8.1 Compare the calculated power turbine inlet non-dimensional flow

$$\frac{W_4\sqrt{R_4 T_4/\gamma_4}}{P_4}$$

and the corresponding non-dimensional flow determined from the power turbine characteristic

$$\left(\frac{W_4\sqrt{R_4 T_4/\gamma_4}}{P_4}\right)_c$$

in steps 5.1 and 5.2. If they do not agree, return to step 2 and estimate a different compressor pressure ratio and repeat to step 8.1 until the two values for turbine inlet non-dimensional flows agree.

Step 9 – Check 4

Step 9.1 Compare the power turbine power output, *gtpow* calculated in step 5.3 with the required power output from the gas turbine. If they do not agree, return to step 2 and estimate a different compressor inlet mass flow, W_1 and repeat to step 9.1 until these powers agree.

7.4 Matrix method of solution

Clearly, the off-design analysis is tedious and a computer program is usually developed to determine the off-design performance of a gas turbine. Methods employed by computer programs often use matrix manipulations using the estimates and checks described above to solve a set of non-linear equations. In matrix notation, the solution of a set of equations is given by:

$$\mathbf{J}.\boldsymbol{\delta}\mathbf{x} = -\mathbf{F} \tag{7.25}$$

where **J** is a matrix that represents the rates of change of the variables used in the calculation of the checks above, such as non-dimensional flows and power balance with respect to the estimated variables such as compressor pressure ratio and turbine entry temperature, as discussed in Sections 7.2 and 7.3.

δx is a column matrix or a vector containing step changes in the estimated values used to calculate the rates of change in the matrix **J**.

F is a vector containing the function values (check values described in Section 7.2 and 7.3) and will represent the errors since we are solving these equations for the case **F** = **0**.

Solving Equation 7.25 will determine the vector **δx**. Thus a new set of values of **x** can be determined via **xnew = xold + δx**. These values are now used in Equation 7.25 and the process repeated until **F** = **0** or the value of **F** is within an acceptable error tolerance, usually within 10^{-6}.

The solution is started by providing Equation 7.25 with a set of initial estimates. For our single shaft simple cycle gas turbine, the estimated vectors will be:

(1) compressor inlet flow, W_1
(2) compressor pressure ratio, P_2/P_1
(3) turbine entry temperature, T_3.

Using these estimates, every engine parameter can be calculated (pressures, temperatures, speeds, flows and powers for each engine component). The calculated powers, flows and speeds may not necessarily satisfy the flow, power and speed compatibility but these errors or differences can be used to determine the check vectors **F** employed by Equation 7.25. This is achieved by considering:

(1) turbine flow compatibility $\left(\dfrac{W_3\sqrt{R_3T_3/\gamma_3}}{P_3}\right)$
(2) power compatibility (i.e. difference between gas turbine calculated power and required power)
(3) speed compatibility (i.e. difference between gas turbine speed and speed required by the load).

It is important that the number of estimates is at least equal to the number of checks. For the single shaft gas turbine, three estimates and checks have been described. A required fuel flow or compressor pressure ratio can be specified instead of a required power output in which case the power output will be calculated. The solution will result in the evaluation of all relevant thermodynamic parameters (e.g. pressures, temperature and flows).

For a two-shaft gas turbine operating with a free power turbine the vector data are as follows.
The estimated vectors are:

(1) compressor inlet flow, W_1
(2) compressor pressure ratio, P_2/P_1
(3) turbine entry temperature, T_3
(4) gas generator pressure ratio, P_3/P_4

And the check vectors are:

(1) gas generator flow compatibility $\left(\dfrac{W_3\sqrt{R_3T_3/\gamma_3}}{P_3}\right)$

(2) power balance between the compressor and gas generator turbine $W_1 \times cpa \times (T_2 - T_1)$ and $W_3 \times cpg \times (T_3 - T_4)$, respectively

(3) power turbine flow compatibility $\dfrac{W_5\sqrt{R_5T_5/\gamma_5}}{P_5}$

(4) the difference between the power output from the power turbine and the required power output.

There are four estimates and checks for a two-shaft gas turbine operating with a power turbine. Fuel flow, gas generator speed, compressor non-dimensional speed or compressor pressure ratio can be specified as check vectors instead of the required power output.

The matrix method effectively applies Newton's method (also known as the Newton-Raphson method) to solve a set of non-linear simultaneous equations. Teukolsky *et al.*[3] and Gerald and Wheatly[4] give further details.

7.5 Off-design performance prediction of a three-shaft gas turbine with a free power turbine

At high compressor pressure ratios, gas turbines may employ more than one spool in the gas generator to overcome the compressor instabilities, as discussed in Section 4.10.2. A schematic representation of a three-shaft gas turbine employing a free power turbine to drive the load is shown in Fig. 7.6. There is no mechanical coupling between the LP and the HP spool but there exists a strong fluid or aerodynamic coupling between these spools. The vector data needed for the prediction of the off-design performance of a three-shaft engine operating with a power turbine are as follows.

Referring to Fig. 7.6 the estimated vectors are:

(1) LP compressor inlet flow, W_1
(2) LP compressor pressure ratio, P_2/P_1
(3) HP compressor pressure ratio, P_3/P_2
(4) HP turbine entry temperature, T_4
(5) HP turbine pressure ratio, P_4/P_5
(6) LP turbine pressure ratio, P_5/P_6.

And the check vectors are:

(1) HP turbine flow compatibility $\left(\dfrac{W_4\sqrt{R_4T_4/\gamma_4}}{P_4}\right)$

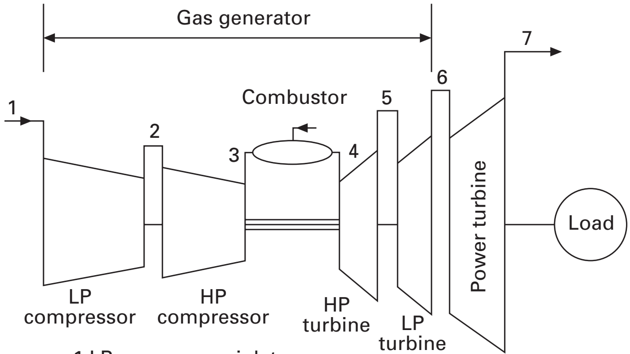

7.6 Schematic representation of a three-shaft free turbine gas turbine.

(2) HP turbine power balance $(W_2 \times cpa \times (T_3 - T_2) - W_3 \times cpg \times (T_4 - T_5))$

(3) LP turbine flow compatibility $\left(\dfrac{W_5\sqrt{R_5 T_5/\gamma_5}}{P_5}\right)$

(4) LP turbine power balance $(W_1 \times cpa \times (T_2 - T_1) - W_5 \times cpg \times (T_5 - T_6))$

(5) power turbine flow compatibility $\left(\dfrac{W_6\sqrt{R_6 T_6/\gamma_6}}{P_6}\right)$

(6) comparison between the power output from the power turbine and the power required.

The three-shaft free power turbine gas turbine has six estimated vectors and check vectors. *Note*: Instead of the power output check (6), LP speed or non-dimensional speed, LP compressor pressure ratio, HP spool speed or non-dimensional speed, HP compressor pressure ratio or fuel flow can be used.

7.6 Off-design performance prediction of a two-shaft gas turbine

The three-shaft gas turbine operating with a free power turbine can be modified into a two-shaft gas turbine. This is achieved by integrating the LP turbine with the power turbine. Therefore, the LP turbine now drives the LP compressor and the load. Such an engine configuration is again best suited for power generation where the load (i.e. electrical generator) operates at a constant speed. The advantages are similar to that of a single shaft gas turbine discussed previously. A schematic representation of a two-shaft gas turbine is shown in Fig. 7.7.

The off-design performance prediction of a two-shaft gas turbine requires only minor modification to that discussed in Section 7.5, where the off-design performance prediction of a three-shaft gas turbine operating with a free power turbine was considered.
The estimated and check vectors are:

(1) LP compressor inlet flow, W_1
(2) LP compressor pressure ratio, P_2/P_1
(3) HP compressor pressure ratio, P_3/P_2
(4) HP turbine entry temperature, T_4
(5) HP turbine pressure ratio, P_4/P_5.

And the check vectors are:

(1) HP turbine flow compatibility $\left(\dfrac{W_4\sqrt{R_4T_4/\gamma_4}}{P_4}\right)$
(2) HP turbine power balance $(W_2 \times cpa \times (T_3 - T_2) - W_4 \times cpg \times (T_4 - T_5))$
(3) LP turbine flow compatibility $\left(\dfrac{W_5\sqrt{R_5T_5/\gamma_5}}{P_5}\right)$
(4) speed compatibility between the LP compressor/turbine speed and the load
(5) comparison between the power output from the gas turbine and the power required.

The two-shaft gas turbine has five estimated vectors and check vectors. *Note*: Instead of the power output check (5), HP spool speed or non-dimensional speed, LP or the HP compressor pressure ratio or fuel flow can be used.

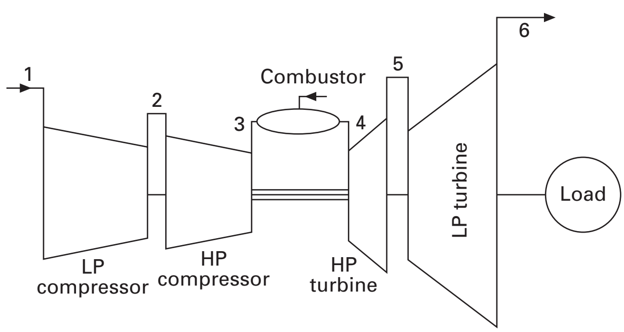

7.7 Schematic representation of a two-shaft gas turbine.

7.7 Off-design performance prediction of a three-shaft gas turbine

A three-shaft gas turbine is essentially a three-shaft gas turbine operating with a free power turbine where the power turbine drives a booster compressor and the load. Thus the booster compressor now becomes the LP compressor and the LP compressor and turbine becomes the intermediate (IP) compressor and IP turbine, respectively. This is illustrated in Fig. 7.8, which shows a schematic representation of a three-shaft gas turbine.

The vector data needed for the prediction of the off-design performance of a three-shaft gas turbine are as follows.

Estimated vectors are:

(1) LP compressor inlet flow, W_1
(2) LP compressor pressure ratio, P_2/P_1
(3) IP compressor pressure ratio, P_3/P_2
(4) HP compressor pressure ratio, P_4/P_3
(5) HP turbine entry temperature, T_4
(6) HP turbine pressure ratio, P_4/P_5
(7) IP turbine pressure ratio, P_6/P_7.

Check vectors are:

(1) HP turbine flow compatibility $\left(\dfrac{W_5\sqrt{R_5T_5/\gamma_5}}{P_5}\right)$

(2) HP turbine power balance $(W_3 \times cpa \times (T_4 - T_3) - W_5 \times cpg \times (T_5 - T_6))$

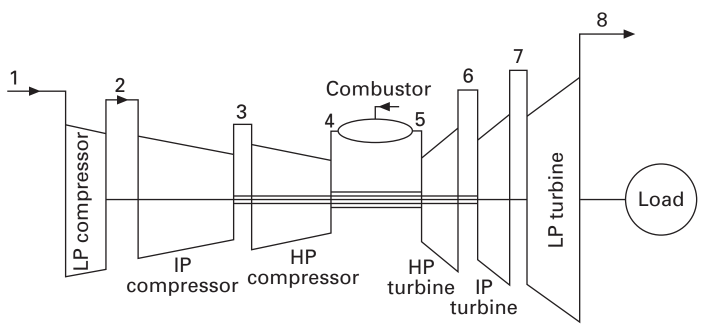

1 LP compressor inlet
2 IP compressor inlet
3 HP compressor inlet
4 HP compressor exit/combustor inlet
5 Combustor exit/HP turbine inlet
6 IP turbine inlet
7 LP turbine inlet
8 LP turbine exit

7.8 Schematic representation of a three-shaft gas turbine.

(3) IP Turbine flow compatibility $\left(\dfrac{W_6\sqrt{R_6T_6/\gamma_6}}{P_6}\right)$

(4) IP turbine power balance $(W_2 \times cpa \times (T_3 - T_2) - W_6 \times cpg \times (T_6 - T_7))$

(5) LP Turbine flow compatibility $\left(\dfrac{W_7\sqrt{R_7T_7/\gamma_7}}{P_7}\right)$

(6) speed compatibility between the LP compressor/turbine speed and the load

(7) comparison between the power output from the gas turbine and the power required.

The three-shaft gas turbine has seven estimated vectors and check vectors. *Note*: Instead of the power output check (7), the IP or HP spool speed or their non-dimensional speeds or pressure ratios, LP compressor pressure ratio or fuel flow can be used.

7.8 Off-design performance prediction of complex gas turbine cycles

In Chapter 3 was discussed the design point performance of complex cycles which incorporated intercooling to reduce the compressor power requirement, reheat to augment the turbine power output, and regeneration to decrease the thermal input in order to improve the thermal efficiency of the simple cycle gas turbine. Complex cycles may employ engine configurations such as multi-spooling compressors and turbines, including the use of free power turbines, as described, when discussing the methods for predicting the off-design performance of a simple cycle. These methods can also be used in predicting the off-design performance of complex cycles.

7.8.1 Off-design performance prediction of a single-shaft gas turbine employing an intercooler

The performance prediction of compressors, turbines and the combustion system has been discussed. The thermodynamic performance of an intercooler can be determined using the method described in Section 2.14. For an intercooler, the ratio of the thermal capacities of the heated and cooled fluid may be significantly different, and thus the ratio of thermal capacities for intercoolers could as low as 0.2. Referring to Fig. 2.18 in Chapter 2, the effectiveness of the intercooler can approach unity, particularly if water is employed as the cooling medium. This is primarily due to the higher specific heat of water compared with air, and the water flow rate through the intercooler can be greater than that of the air flow in the cooler. Thus the air temperature leaving the intercooler, T_3, can approach the ambient temperature, T_1 as shown in Fig. 7.9, which represents a single shaft intercooled gas turbine.

The pressure loss in the intercooler may be modelled using the loss coefficient, K_1, and the cooler inlet non-dimensional flow $W_2\sqrt{T_2}/P_2$, utilising the expression for the cooler non-dimensional pressure loss $\Delta P_{23}/P_2$ (Equation 7.17).

$$\frac{\Delta P_{23}}{P_2} = K_l \left(\frac{W_2 \sqrt{R_2 T_2 / \gamma_2}}{P_2} \right)^2 \gamma_2 \qquad [7.26]$$

The necessary estimates and checks can be developed as follows. The required power output, gas turbine speed, N_1, compressor inlet pressure, P_1, humidity, ω, and temperature, T_1, are specified. Ignoring bleeds, turbine cooling, inlet and exhaust losses and referring to Fig. 7.9, the estimate vectors are:

(1) compressor inlet mass flow, W_1
(2) LP compressor pressure ratio, P_2/P_1
(3) HP compressor inlet temperature, T_3
(4) HP compressor pressure ratio, P_4/P_3
(5) turbine entry temperature, T_3

The check vectors are:

(1) turbine flow compatibility $\left(\frac{W_3 \sqrt{R_3 T_3 / \gamma_3}}{P_3} \right)$
(2) speed compatibility (i.e. difference between the LP compressor speed and HP compressor speed)

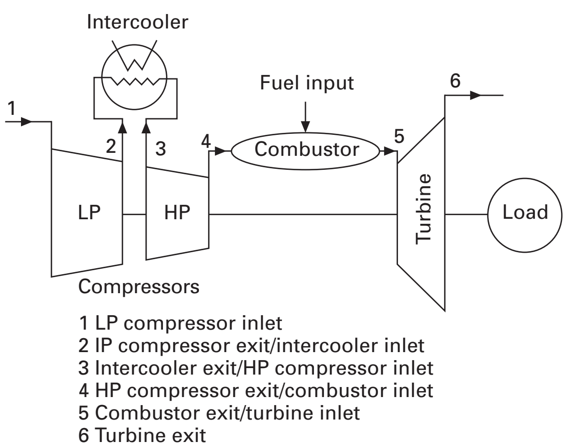

7.9 Schematic representation of an intercooled single-shaft gas turbine.

(3) power compatibility (i.e. difference between gas turbine calculated power and required power)
(4) speed compatibility (i.e. difference between gas turbine speed and the speed required by the load)
(5) difference between the estimated cooler exit temperature, T_3, and that calculated from the cooler effectiveness Equation 7.27:

$$\varepsilon_{\text{cooler}} = \frac{T_2}{T_2} - \frac{T_3}{T_c} \qquad [7.27]$$

where $\varepsilon_{\text{cooler}}$ is the effectiveness of the cooler and T_c is the coolant inlet temperature normally equal to T_1. It is assumed that the thermal capacity of the coolant is greater than that of the air being cooled, which would normally be the case.

Note: Required fuel flow can be specified rather than the required power output for the check vector (3), in which case the power output from the gas turbine will be calculated.

7.8.2 Off-design performance prediction of a single-shaft gas turbine employing intercooling and regeneration

The prediction of the off-design performance of an intercooled–regenerative gas turbine requires an additional estimate that corresponds to the heat exchanger air exit temperature, which now is the combustor inlet temperature. Referring to Fig. 7.10, the additional temperature estimate corresponds to T_5. The estimated vectors are:

(1) compressor inlet mass flow, W_1
(2) LP compressor pressure ratio, P_2/P_1
(3) HP compressor inlet temperature, T_3
(4) HP compressor pressure ratio, P_4/P_3
(5) heat exchanger exit air temperature, T_5
(6) turbine entry temperature, T_6

Check vectors are:

(1) turbine flow compatibility $\left(\dfrac{W_6\sqrt{R_6 T_6/\gamma_6}}{P_6}\right)$
(2) speed compatibility (i.e. difference between the LP compressor speed and HP compressor speed)
(3) power compatibility (i.e. difference between gas turbine calculated power and required power)

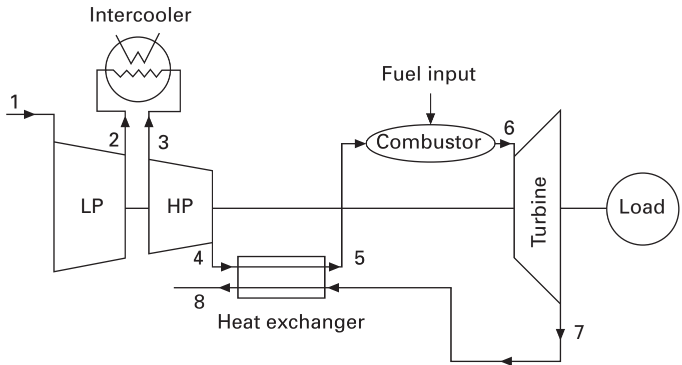

1 LP compressor inlet
2 IP compressor exit/intercooler inlet
3 Intercooler exit/HP compressor inlet
4 HP compressor exit/heat exchanger inlet (cold side)
5 Heat exchanger exit (cold side)/combustor inlet
6 Combustor exit/turbine inlet
7 Turbine exit/heat exchanger inlet (hot side)
8 Heat exchanger exit (hot side)

7.10 Schematic representation of an intercooled–regenerated gas turbine.

(4) speed compatibility (i.e. difference between gas turbine speed and speed required by the load)
(5) difference between the estimated cooler exit temperature, T_3, and that calculated from the cooler effectiveness in Equation 7.27
(6) difference between the estimated heat exchanger air exit temperature and that calculated by the heat exchanger in Equation 2.35 given in Chapter 2.

If we ignore intercooling and consider only regeneration, the vector data referring to Fig. 7.10 as follows:

(1) compressor inlet mass flow, W_1
(2) compressor pressure ratio, P_4/P_1, which is now the overall compressor pressure ratio
(3) heat exchanger exit air temperature, T_5
(4) turbine entry temperature, T_6

Check vectors are:

(1) turbine flow compatibility $\left(\dfrac{W_6\sqrt{R_6 T_6/\gamma_6}}{P_6}\right)$

(2) power compatibility (i.e. difference between gas turbine calculated power and required power)

(3) speed compatibility (i.e. difference between gas turbine speed and the speed required by the load)
(4) difference between the estimated heat exchanger air exit temperature and that calculated for the heat exchanger in Equation 2.35 given in Chapter 2.

7.8.3 Off-design performance prediction of a single-shaft gas turbine employing intercooling, regeneration and reheat

To predict the off-design performance of an intercooled–regenerative–reheat gas turbine an additional estimate is required to that described in Section 7.8.2 where the performance of the intercooled regenerative gas turbine was considered. This corresponds to the HP turbine pressure ratio, P_6/P_7, as shown in Fig. 7.11, which shows a schematic representation of an intercooled–regenerative–reheat gas turbine. It is also necessary to specify the reheat exit temperature, which also corresponds with the LP turbine entry temperature, T_8. The estimated vector data are:

(1) compressor inlet mass flow, W_1
(2) LP compressor pressure ratio, P_2/P_1
(3) HP compressor inlet temperature, T_3

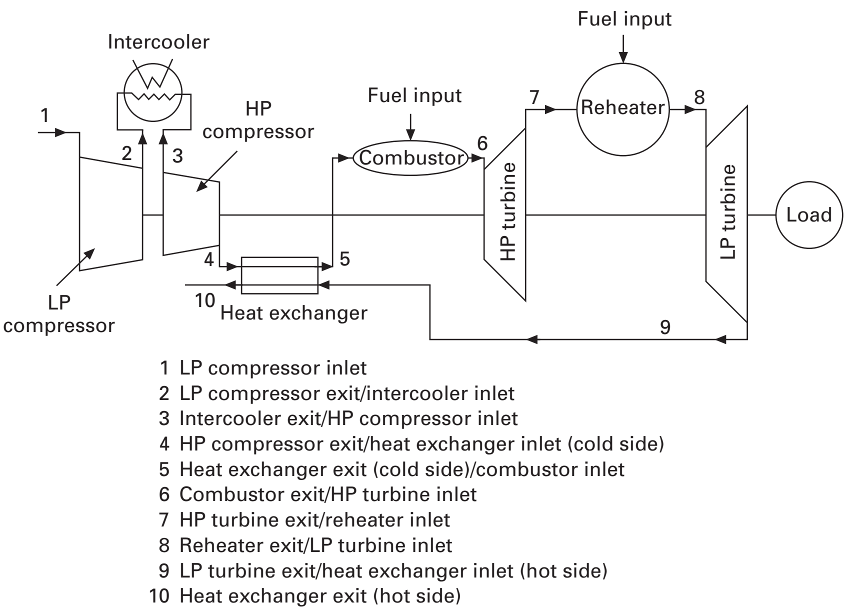

7.11 Intercooled–regenerative–reheat gas turbine.

(4) HP compressor pressure ratio, P_4/P_3
(5) heat exchanger exit air temperature, T_5
(6) turbine entry temperature, T_6
(7) HP turbine pressure ratio, P_6/P_7.

Check vectors are:

(1) HP turbine flow compatibility $\left(\dfrac{W_6\sqrt{R_6T_6/\gamma_6}}{P_6}\right)$

(2) LP turbine flow compatibility $\left(\dfrac{W_8\sqrt{R_8T_8/\gamma_8}}{P_8}\right)$

(3) speed compatibility (i.e. difference between the LP compressor speed and HP compressor speed)
(4) power compatibility (i.e. difference between gas turbine calculated power and required power)
(5) speed compatibility (i.e. difference between gas turbine speed and the speed required by the load)
(6) difference between the estimated cooler exit temperature, T_3, and that calculated from the cooler effectiveness in Equation 7.27
(7) difference between the estimated heat exchanger air exit temperature and that calculated by the heat exchanger in Equation 2.35 given in Chapter 2.

If intercooling is ignored, then the estimate vectors (3) and (4) and the check vectors (3) and (6) can be omitted. Similarly, if regeneration is ignored and only reheat considered, then estimate vectors (3), (4) and (5) and the check vectors (3), (6) and (7) can be omitted.

7.9 Off-design prediction of a two-shaft gas turbine using a free power turbine and employing intercooling, regeneration and reheat

The method applied to predict the off-design performance of a two-shaft gas turbine operating with a free power turbine (Section 7.3) may be modified to include intercooling, regeneration and reheating. Three more estimates need to be added, which correspond to the intercooler exit temperature (i.e. HP compressor inlet temperature), T_3, HP compressor pressure ratio, P_4/P_3, and the heat exchange exit or combustion inlet temperature, T_5, as shown in Fig. 7.12. The reheat exit temperature, T_8 also needs to be specified. Three more check conditions or vectors will now be needed. These correspond to the speed compatibility of the LP and HP compressor, a check against the intercooler

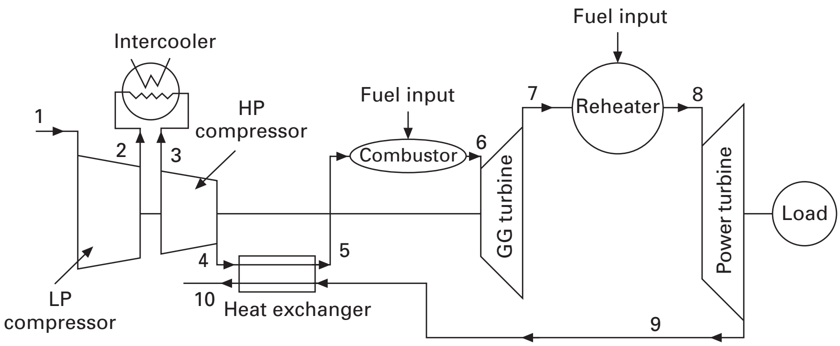

1 LP compressor inlet
2 LP compressor exit/intercooler inlet
3 Intercooler exit/HP compressor inlet
4 HP compressor exit/heat exchanger inlet (cold side)
5 Heat exchanger exit (cold side)/combustor inlet
6 Combustor exit/gas generator (GG) turbine inlet
7 GG turbine exit/reheater inlet
8 Reheater exit/power turbine inlet
9 Power turbine exit/heat exchanger inlet (hot side)
10 Heat exchanger exit (hot side)

7.12 Schematic representation of a two-shaft gas turbine including intercooling, regeneration and reheating operating with a free power turbine.

discharge temperature using Equation 7.27, and a check on the heat exchanger exit temperature, T_5, using Equation 2.35 in Chapter 2.
Therefore, the estimated vectors are:

(1) LP compressor inlet flow, W_1
(2) LP compressor pressure ratio, P_2/P_1
(3) HP compressor inlet temperature, T_3
(4) combustor inlet temperature, T_5
(5) HP compressor pressure ratio, P_4/P_3
(6) turbine entry temperature, T_3
(7) gas generator pressure ratio, P_3/P_4.

Check vectors are:

(1) gas generator flow compatibility $\left(\dfrac{W_6\sqrt{R_6 T_6/\gamma_6}}{P_6}\right)$

(2) power balance between the compressor and gas generator turbine
$W_1 \times cpa \times (T_2 - T_1) + W_2 \times cpa \times (T_4 - T_2)$ and
$W_6 \times cpg \times (T_6 - T_7) + W_7 \times cpg \times (T_7 - T_8)$ respectively

(3) power turbine flow compatibility $\left(\dfrac{W_8\sqrt{R_8T_8/\gamma_8}}{P_8}\right)$

(4) speed compatibility (i.e. difference between the LP compressor speed and HP compressor speed)
(5) difference between the estimated heat exchanger air exit temperature and that calculated by the heat exchanger in Equation 2.35 given in Chapter 2
(6) difference between the estimated cooler exit temperature, T_3 and that calculated from the cooler effectiveness in Equation 7.27
(7) the difference between the power output from the power turbine and the required power output.

7.10 Off-design prediction of a three-shaft gas turbine using a power turbine and employing intercooling, regeneration and reheat

For the prediction of the off-design performance of a three-shaft gas turbine operating with a free power turbine incorporating intercooling, a heat exchanger and reheat, only two more estimates are required in addition to the estimates needed for the corresponding simple cycle as described in Section 7.5. These estimates correspond to the intercooler discharge temperature, T_3, and the heat exchanger or combustion inlet temperature, T_5, as shown in Fig. 7.13. The corresponding checks are the intercooler discharge temperature calculated by Equation 7.27 and the heat exchanger exit temperature using Equation 2.35, described in Chapter 2. Again, the reheat or power turbine entry temperature needs to be specified.

Therefore, the estimate vectors needed to predict the off-design performance of a complex three-shaft gas turbine using a free power turbine as shown in Figure 7.13 are:

(1) LP compressor inlet flow, W_1
(2) LP compressor pressure ratio, P_2/P_1
(3) HP compressor inlet temperature, T_3
(4) HP compressor pressure ratio, P_3/P_2
(5) combustor inlet temperature, T_5
(6) HP turbine entry temperature, T_4
(7) HP turbine pressure ratio, P_4/P_5
(8) LP turbine pressure ratio, P_5/P_6.

Check vectors are:

(1) HP turbine flow compatibility, $\left(\dfrac{W_4\sqrt{R_4T_4/\gamma_4}}{P_4}\right)$

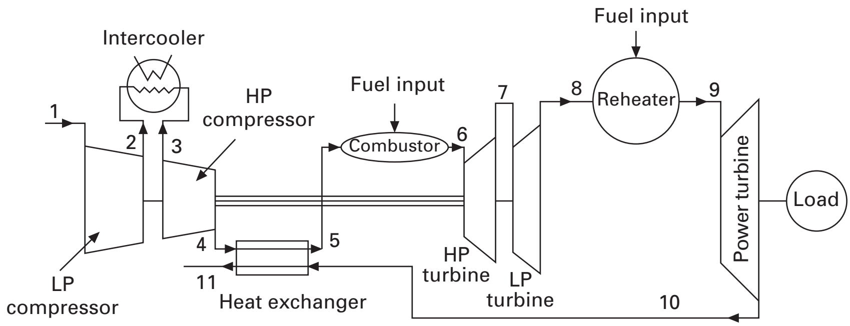

1 LP compressor inlet
2 LP compressor exit/intercooler inlet
3 Intercooler exit/HP compressor inlet
4 HP compressor exit/heat exchanger inlet (cold side)
5 Heat exchanger exit (cold side)/combustor inlet
6 Combustor exit/HP turbine inlet
7 LP turbine inlet
8 LP turbine exit/reheater inlet
9 Reheater exit/power turbine inlet
10 Power turbine exit/heat exchanger inlet (hot side)
11 Heat exchanger exit (hot side)

7.13 Schematic representation of a two-shaft gas turbine including intercooling, regeneration and reheating operating with a free power turbine.

(2) HP turbine power balance, $(W_2 \times cpa \times (T_3 - T_2) - W_3 \times cpg \times (T_4 - T_5))$

(3) LP turbine flow compatibility $\left(\dfrac{W_5\sqrt{R_5 T_5/\gamma_5}}{P_5}\right)$

(4) LP turbine power balance $(W_1 \times cpa \times (T_2 - T_1) - W_5 \times cpg \times (T_5 - T_6))$

(5) power turbine flow compatibility $\left(\dfrac{W_6\sqrt{R_6 T_6/\gamma_6}}{P_6}\right)$

(6) difference between the estimated heat exchanger air exit temperature and that calculated by the heat exchanger in Equation 2.35 given in Chapter 2

(7) difference between the estimated cooler exit temperature, T_3, and that calculated from the cooler effectiveness in Equation 7.27

(8) comparison between the power output from the power turbine and the power required.

Intercooling may be ignored, in which case estimated vector (3) and check vector (7) can be omitted. If intercooling and regeneration are ignored and only reheat considered, then the estimated and check vectors are the same as shown in Section 7.5.

Similarly, the off-design performance of two- and three-shaft gas turbines may be predicted as discussed in Sections 7.6 and 7.7 using intercooling and reheat, and the reader is left to develop the necessary vector data to predict the off-design performance of these cycles.

7.11 Variable geometry compressors

The use of variable geometry in compressors has been discussed in Chapter 4 (variable inlet guide vanes and stators, VIGVs and VSVs, respectively) to prevent compressor instabilities such as compressor stall and surge. Although the compressor characteristic will indeed change with the position of such variable geometry devices (guide vane angle), the control philosophy of these devices applied to a two- or three- shaft gas turbine operating with a free power turbine is such that the compressor non-dimensional speed is used in determining the position of the VIGV and VSV. Thus, for a given compressor non-dimensional speed, there is a unique VIGV and VSV position or guide vane angle which, in turn, fixes the compressor flow capacity, pressure ratio and efficiency. Provided the compressor characteristic employed in the prediction of the off-design performance of such engine configurations includes the effect of the position of these variable geometry devices in the compressor, then no change in the procedures given previously for predicting the off-design performance of such engines is necessary.

Single-shaft gas turbines, particularly generating large power outputs (above about 50 MW), also employ variable geometry in the compressor, usually VIGVs. The purpose of variable geometry in compressors employed by single-shaft gas turbines is to control the air flow through the compressor, such that the turbine exit temperature (also known as the exhaust gas temperature) is maintained at some predetermined value. Controlling the exhaust gas temperature by such means results in a reduction in the compressor flows at low power outputs, thus significantly decreasing the starting power requirements of the gas turbine. Variable geometry may also be employed to maintain the exhaust gas temperature at its design value at low power. Maintaining the exhaust gas temperature at the design value at low powers is particularly beneficial to the thermal efficiency at these powers when a heat exchanger is added or when the gas turbine is part of a combined cycle plant. Furthermore, the fuel–air ratio remains approximately constant at constant exhaust gas temperature operation, which is particularly useful in DLE combustion systems, as discussed in Chapter 6 on gas turbine combustion.

Unlike the case of a free power turbine discussed above, the compressor characteristic needs to be known for each VIGV and VSV setting (angle). Furthermore, an additional estimate and check is necessary when predicting the off-design performance of a single-shaft gas turbine operating with variable geometry compressors. This estimate and check corresponds to the guide vane angle and required exhaust temperature, respectively. Alternatively the compressor flow capacity of a fixed geometry compressor may be decreased by an amount depending on the guide vane angle of the VIGV and VSV. In this event it is important to adjust the compressor efficiency characteristic of the compressor due to the change in the guide vane angle.

7.12 Variable geometry turbines

Turbines may also incorporate variable geometry and this is usually applied to power turbines where the nozzle guide vanes (NGVs) are turned to alter the flow capacity and thus the turbine characteristic. Variable geometry has been employed in turbines operating with free power turbines to improve the off-design thermal efficiency (i.e. low power outputs), particularly when a heat exchanger is added. Variable geometry power turbines also provide improved acceleration when the NGVs are full opened and can also be used to provide substantial engine braking when the NGVs are rotated sufficiently, such that the gases leaving the NGV impinge on the turbine rotor in the opposite direction.

The prediction of the off-design performance of gas turbines employing variable geometry turbines requires an additional estimate and check vector, which correspond to the NGV angle and the required exhaust gas temperature, respectively. The exhaust gas temperature may be measured downstream of the gas generator turbine rather than at the power turbine exit. It is also necessary to know the change in the turbine characteristic with NGV angle, and the appropriate turbine characteristic must be used as the NGV angle changes during the iterations described above.

7.13 References

1. *Gas Turbine Theory*, 5th Edition, Saravanamuttoo, H.I.H., Rogers, C.F.G. and Cohen, H., Longman (2001).
2. *Gas Turbine Performance*, 2nd Edition, Walsh, P.P. and Fletcher, P., Blackwell Publishing (2004).
3. *Numerical Recipes in Fortran 77*, 2nd Edition, Press, W.H., Teukolsky, S.A., Vetting, W.T. and Flannery, B.P., Ch. 9, Sections 9.6 and 9.7, Cambridge University Press (1992).
4. *Applied Numerical Analysis*, 6th Edition, Gerald C.F. and Wheatly, P.O., Addison-Wesley.

8
Behaviour of gas turbines during off-design operation

It was stated in Chapter 7 that the change in ambient conditions and power demand from design conditions results in performance of the gas turbine deviating from its design point. In this chapter the concepts of component matching, discussed in the previous chapter, will be used to predict some of the behaviour of gas turbines during off-design operation. Some assumptions will be made as this will simplify the explanation of the behaviour of gas turbines during off-design operation.

8.1 Steady-state running line

Chapter 7 discussed the prediction of the off-design performance of various gas turbine configurations. Using these techniques, it is possible to determine the operating point for each non-dimensional speed line on the compressor characteristic. Joining these points will result in the steady-state running line on the compressor characteristic.

8.1.1 Single-shaft gas turbine

As stated, single-shaft gas turbines are used extensively in power generation; the gas turbine speed will be constant and will normally correspond to the generator speed. For a given ambient condition, this results in the running line aligning with a particular non-dimensional speed line. Before the generator can be loaded, the gas turbine speed is increased along the generator no-load line until it reaches the generator synchronous speed. Figure 8.1 shows this running line on the compressor characteristic. The effect of the change in ambient temperature, T_1, will result in the running line moving to another non-dimensional speed, as shown in Fig. 8.1. With lower ambient temperature, the non-dimensional speed, $N_1/\sqrt{T_1}$, will increase and conversely, the higher the ambient temperature, the lower will be the non-dimensional speed. Consequently, the compressor inlet non-dimensional flow increases with

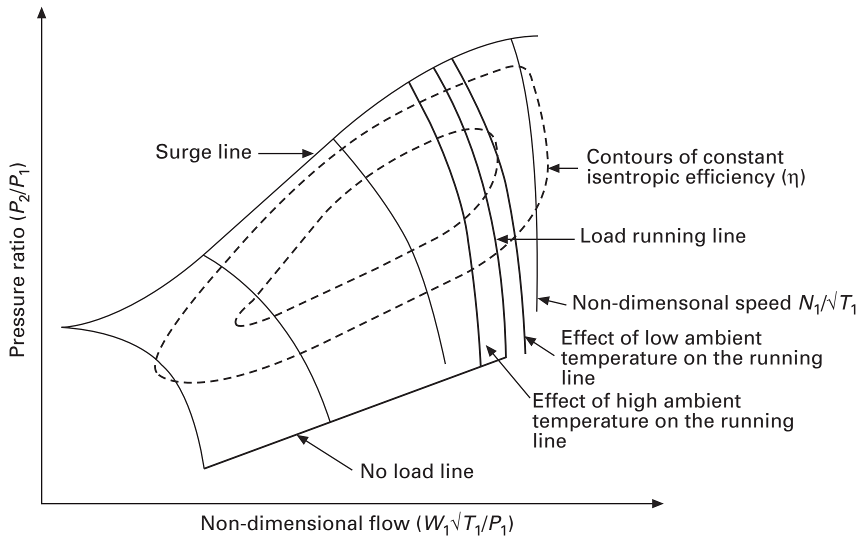

8.1 Steady-state running line for a single-shaft gas turbine.

decreasing ambient temperature and decreases with increase in ambient temperature.

Although the analysis of the off-design performance of a gas turbine is quite tedious, much useful insight may be obtained by considering a simplified analysis of the flow, work and speed compatibility equations.

Referring to Fig. 8.2 and ignoring the gas properties terms R and γ, as changes in these values are smaller compared with the changes in mass flows, pressures and temperatures, the flow compatibility equation may be written as discussed in Saravanamutto *et al.*[1] as:

$$\frac{W_3\sqrt{T_3}}{P_3} = \frac{W_1\sqrt{T_1}}{P_1} \times \frac{P_1}{P_2} \times \frac{P_2}{P_3} \times \sqrt{\frac{T_3}{T_1}} \times \frac{W_3}{W_1} \qquad [8.1]$$

If we assume that the turbine remains choked, particularly at high power, then $W_3\sqrt{T_3}/P_3$ will remain constant with turbine pressure ratio. If we also assume that the compressor speed line is near choke conditions, especially at high operating speeds, the variation of the compressor inlet non-dimensional flow $W_1\sqrt{T_1}/P_1$ with pressure ratio will be small. Furthermore, if the combustion pressure loss and bleeds are also assumed constant, then P_2/P_3 and W_3/W_1 will also be constant. Hence, an increase in compressor pressure ratio must be accompanied by an increase in T_3/T_1 to satisfy the flow compatibility in Equation 8.1.

Figure 8.3 shows a compressor characteristic, where the compressor non-dimensional temperature rise is plotted against the pressure ratio for a series of non-dimensional speeds. It can be seen that the non-dimensional temperature

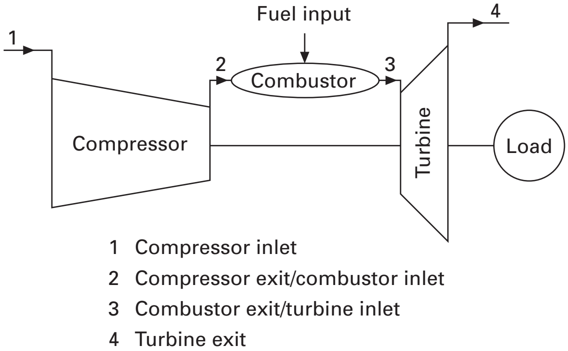

8.2 Schematic representation of a single-shaft gas turbine (simple cycle).

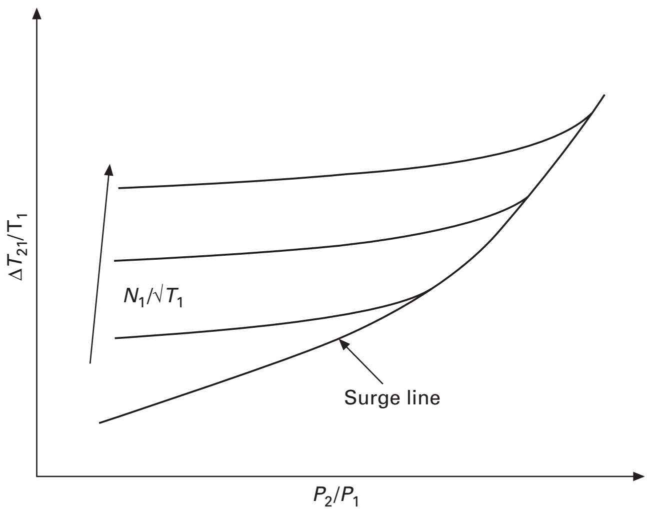

8.3 Compressor characteristic where the non-dimensional temperature rise varies with pressure ratio for a series of non-dimensional speeds.

rise for a given non-dimensional speed is approximately constant, particularly at low-pressure ratios. This is due to the fall in compressor efficiency as the operating point moves away from the design point. Therefore, for a given compressor non-dimensional speed and inlet temperature, the temperature rise $\Delta T_{21} = T_2 - T_1$ will be approximately constant, as discussed in Saravanamuttoo *et al.*[1]

The work compatibility equation gives us the net power output, p_{net}:

$$p_{net} = W_3 \times cpg \times (T_3 - T_4) - W_1 \times cpa \times (T_2 - T_1) \qquad [8.2]$$

The temperature drop across the turbine is:

$$(T_3 - T_4) = T_3 \times cpg \times \eta_t \times \left[1 - \left(\frac{P_4}{P_3}\right)^{\frac{\gamma g-1}{\gamma g}}\right]$$

where *cpa* and *cpg* are the mean specific heats at constant pressure during compression and expansion respectively and γg is the mean isentropic expansion index.

Unlike the compressor, the turbine efficiency does not vary very much with pressure ratio and non-dimensional speed. Therefore, as the turbine pressure ratio and turbine entry temperature, T_3, increase, there is an increase in turbine power output. Since the compressor power absorbed $W_1 \times cp_a \times (T_2 - T_1)$ is approximately constant, there is an increase in the gas turbine power output p_{net}. Thus, a series of running lines can be produced on the compressor characteristic, due to the increase in power and ambient temperature, T_1, as illustrated in Fig. 8.4.

In fact, the detailed analysis in determining the off-design performance of a gas turbine essentially solves these equations using detailed component characteristics. It also allows for the change in the thermodynamic properties of air and products of combustion due to temperature changes.

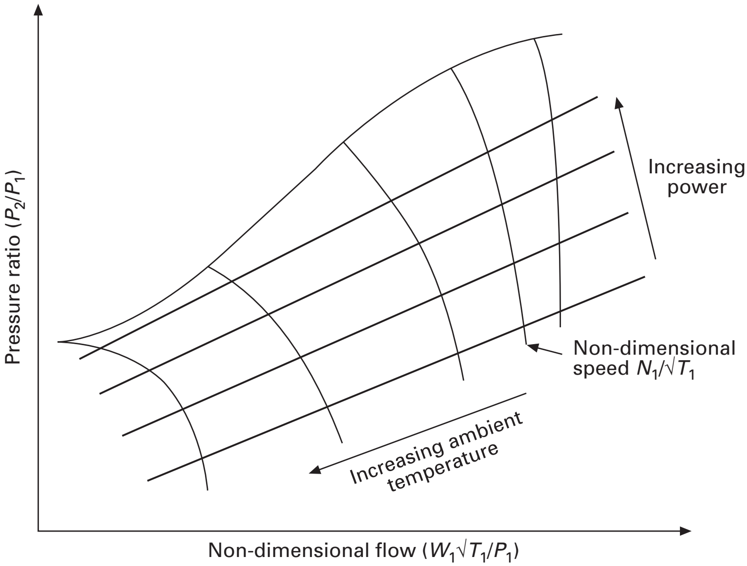

8.4 Series of running lines for various power and ambient temperature conditions for a single-shaft gas turbine.

8.1.2 Two-shaft gas turbine operating with a free power turbine

To predict the running line for a two-shaft gas turbine, it is necessary to consider the performance behaviour of turbines operating in series. Figure 8.5 shows the characteristics of two turbines operating in series. For example, the HP turbine and the LP turbine would represent the gas generator (GG) turbine and power turbine respectively when applied to a two-shaft gas turbine.

The GG turbine inlet non-dimensional flow increases initially with turbine pressure ratio until the GG turbine chokes, after which the inlet non-dimensional flow remains constant. However, the GG turbine outlet non-dimensional flow increases continuously with turbine pressure ratio as shown in Fig. 8.5. The power turbine inlet flow also increases with pressure ratio until it also chokes. The GG turbine exit flow must be 'swallowed' by the power turbine. Thus, the power turbine controls the GG turbine exit non-dimensional flow, and hence controls the GG turbine pressure ratio. The operating points 1, 2 and 3 in Fig. 8.5 illustrate this point.

When the power turbine operates unchoked, point (1) in Fig. 8.5, the gas generator turbine will be forced to operate at point (1) on its characteristic to satisfy the flow compatibility between these turbines. When the power turbine operates under choked conditions, points (2) and (3) on the power turbine characteristic, the gas generator turbine will be forced to operate at a fixed pressure ratio as shown by point (2, 3) on the gas generator characteristic.

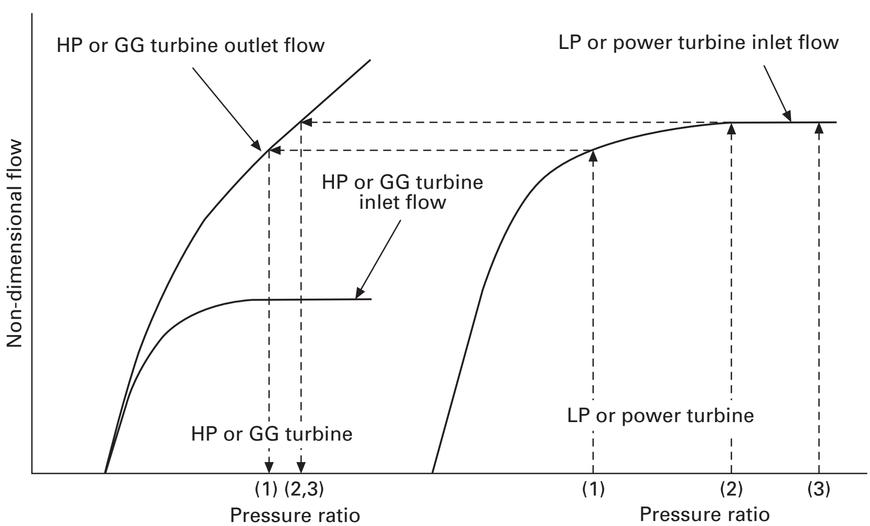

8.5 Turbines operating in series.

Thus, the operating point on the gas generator turbine characteristic is determined primarily by the swallowing capacity of the power turbine.

In this analysis, it has been assumed that the gas generator turbine efficiency remains constant for the three operating cases shown in Fig. 8.5 and this is usually the case. If there is a change in the gas generator turbine efficiency at these conditions, then the operating points (2) and (3) will not be coincident. However, this is usually small because of the small change in turbine efficiency with pressure ratio and non-dimensional speed.

Referring to Fig. 8.6 and ignoring the gas properties terms, R and γ, the flow compatibility equation for turbines operating in series can be written as:

$$\frac{W_4\sqrt{T_4}}{P_4} = \frac{W_3\sqrt{T_3}}{P_3} \times \frac{P_3}{P_4} \times \sqrt{\frac{T_4}{T_3}} \times \frac{W_4}{W_3} \quad [8.3]$$

where

$W_3\sqrt{T_3}/P_3$ is the non-dimensional flow at entry to the gas generator turbine

P_3/P_4 is the gas generator turbine pressure ratio

T_3/T_4 is the gas turbine temperature ratio

W_3/W_4 is the ratio of gas flow at inlet of gas generator turbine to gas flow at inlet of power turbine

$W_4\sqrt{T_4}/P_4$ is the power turbine inlet non-dimensional flow.

During power turbine choked conditions, the gas generator turbine pressure ratio and thus the non-dimensional temperature drop, $\Delta T_{34}/T_3$, will be constant provided the generator turbine efficiency is also constant.

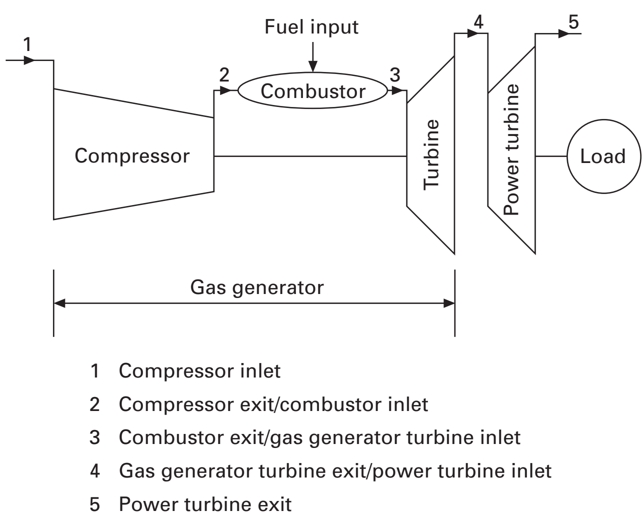

8.6 Schematic representation of a two-shaft turbine operating with a free power turbine.

Writing the power balance or work compatibility equation for the gas generator:

$$\frac{\Delta T_{21}}{T_1} = \frac{\Delta T_{34}}{T_3} \times \frac{T_3}{T_1} \times \frac{cpg}{cpa} \times \frac{W_3}{W_1} \qquad [8.4]$$

For a given compressor non-dimensional speed, $N_1/\sqrt{T_1}$, the compressor non-dimensional temperature rise, $\Delta T_{21}/T_1$ will be approximately constant (see Fig. 8.3). If compressor bleeds and the effect of fuel flow on W_3 are ignored, it can be assumed that W_3 equals W_1. For constant specific heats, Equation 8.4 indicates that, for a given compressor speed, there will be a unique value for T_3/T_1. To maintain the flow compatibility between the compressor and the gas generator turbine and referring to Fig. 8.6 we have:

$$\frac{W_3\sqrt{T_3}}{P_3} = \frac{W_1\sqrt{T_1}}{P_1} \times \frac{P_1}{P_2} \times \frac{P_2}{P_3} \times \sqrt{\frac{T_3}{T_1}} \times \frac{W_3}{W_1} \qquad [8.5]$$

$W_3\sqrt{T_3}/P_3$ will be fixed by the choking of the gas generator turbine as discussed. For a constant combustor pressure loss, P_2/P_3 will be constant. Although it is possible to find more than one solution for P_2/P_1 and $W_1\sqrt{T_1}/P_1$ from Equation 8.5, in practice, the shape of the compressor characteristic does not show a significant change in flow with pressure ratio, particularly at high speed, where $W_1\sqrt{T_1}/P_1$ is approximately constant. Thus only a single solution is possible.

At different compressor non-dimensional speeds, different values for $\Delta T_{21}/T_1$ would apply, resulting in different values for T_3/T_1 (Equation 8.4), hence giving unique operating points on each compressor speed line. Joining these points gives the (unique) running line on the compressor characteristic for a two-shaft gas turbine operating with a free power turbine. If gas property changes are considered, then the running line will change with ambient conditions but this is usually small, particularly at low ambient temperatures. For rigorous analysis, gas property changes need to be allowed for as discussed in Chapter 7. The compressor characteristic with the running line superimposed on it is shown in Fig. 8.7. This line differs from the case of a single-shaft gas turbine, where a series of running lines occurs, each of constant power output as shown in Fig. 8.4.

8.2 Displacement of running line (single- and two-shaft free power turbine gas turbine)

At low power and idle operating conditions, the running line may intersect with the surge line as shown in Fig. 4.23 (Chapter 4). This is primarily due to the stalling of the front stages as the compressor operates far from its design condition as discussed in Section 4.10. Therefore, it may not be possible to accelerate the engine without some remedial action being

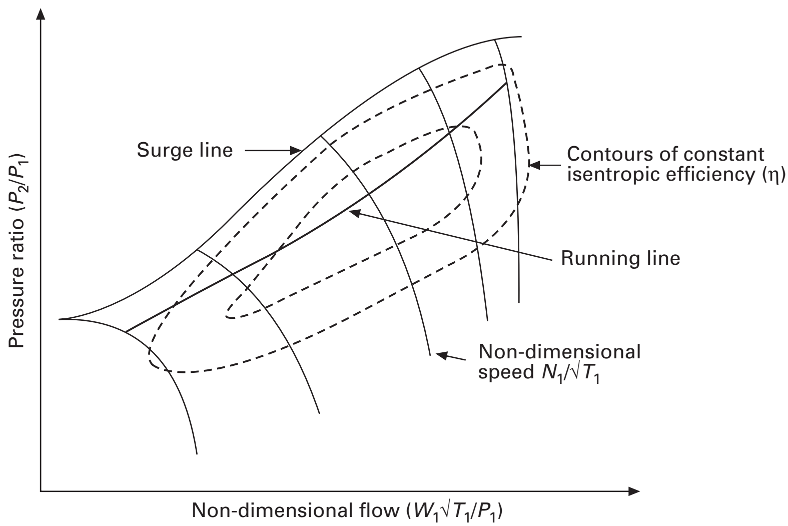

8.7 Running line on the compressor characteristic for a two-shaft gas turbine.

taken. Section 4.10 also discusses the remedies employed to overcome the problem. The impact that such remedies have on the running line will now be examined.

Blow-off

The impact of blow-off is to reduce the flow through the turbine section relative to the compressor. For simplicity, it will be assumed that the blow-off acts at the discharge of the compressor, although in practice the blow-off will be positioned at some intermediate point, so that the choking effect of the HP stages of the compressor are reduced during low compressor speed operation.

Referring to Fig. 8.8 and writing the power balance equation for the gas generator:

$$\frac{\Delta T_{21}}{T_1} = \frac{\Delta T_{34}}{T_3} \times \frac{T_3}{T_1} \times \frac{cpg}{cpa} \times \frac{W_3}{W_1} \qquad [8.6]$$

If it is assumed that the compressor continues to operate at a constant non-dimensional speed (by adjusting the fuel flow), the non-dimensional temperature rise $\Delta T_{21}/T_1$ will be approximately constant. When the blow-off valve is opened, W_3/W_1 will decrease. If it is also assumed that the turbines are choked, then from Section 8.1.2, $\Delta T_{34}/T_3$ will also be constant. From Equation 8.6, any reduction in W_3/W_1 must be compensated by a corresponding increase in T_3/T_1, that is T_3/T_1 is inversely proportional to W_3/W_1.

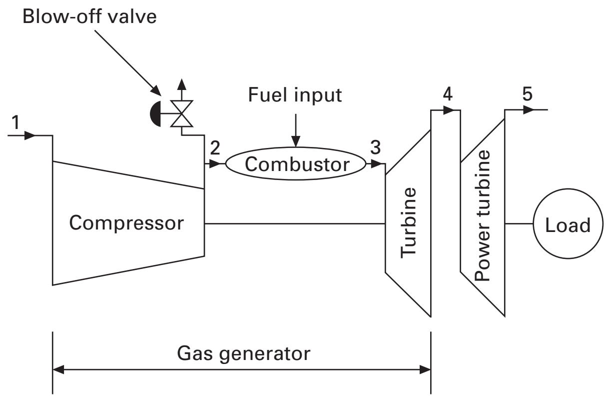

1 Compressor inlet
2 Compressor exit/combustor inlet
3 Combustor exit/gas generator turbine inlet
4 Gas generator turbine exit/power turbine inlet
5 Power turbine exit

8.8 Schematic representation of a two-shaft gas turbine operating with a blow-off valve.

Writing the flow compatibility equation for the gas generator:

$$\frac{W_3\sqrt{T_3}}{P_3} = \frac{W_1\sqrt{T_1}}{P_1} \times \frac{P_1}{P_2} \times \frac{P_2}{P_3} \times \sqrt{\frac{T_3}{T_1}} \times \frac{W_3}{W_1} \qquad [8.7]$$

If we assume $W_3\sqrt{T_3}/P_3$, $W_1\sqrt{T_1}/P_1$ and P_2/P_3 are approximately constant, then any reduction of W_3/W_1 must increase P_1/P_2 because the effect of the increase in T_3/T_1 will only be increasing by the value of its square root. Thus, during blow-off valve operation, the pressure ratio, P_2/P_1, for each non-dimensional speed line will decrease to satisfy the flow compatibility Equation 8.7. This is illustrated in Fig. 8.9, which shows the effect of blow-off valve operation on the running line on the compressor characteristic.

Variable stator vanes and inlet guide vanes (compressors)

Variable stators (VSVs)and variable inlet guide vanes (VIGVs) significantly alter the flow capacity of the compressor along a given speed line. However, they do not have a significant impact on the position of the running line. The change in compressor efficiency, on the other hand, does influence the running line. Closing the stator vanes will reduce the deflection in the corresponding rotors and result in a reduction in stage loading (Section 4.10.3 in Chapter 4). This would normally increase the efficiency of the compressor. The effect of increased compressor efficiency on the non-dimensional temperature rise,

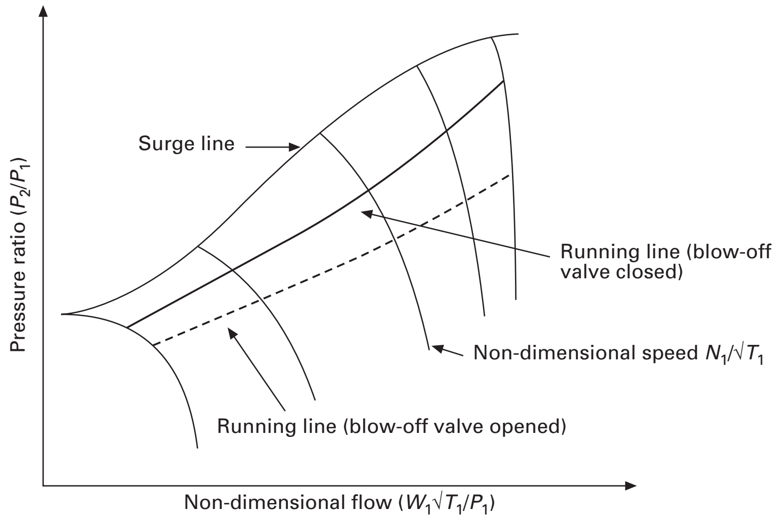

8.9 Effect of blow-off valve operation on the running line.

resulting in a reduction in non-dimensional temperature rise for a given non-dimensional speed, is shown in Fig. 8.10. Early work[2] on variable geometry compressors using VSV/VIGVs showed an improvement in efficiency at low compressor speeds, but that a notable loss in efficiency occurs at high compressor speeds due to the closure of the VSV/VIGVs. Thus, during high-speed operation, closure of the VSV/VIGVs will result in an increase in the compressor non-dimensional temperature.

If the gas generator of a two-shaft gas turbine employing a free power turbine is operating at low speeds, and we assume that the change in the efficiency of the compressor due to the closure of the VSV/VIGV is small, then the compressor non-dimensional temperature rise, $\Delta T_{21}/T_1$, for a given compressor non-dimensional speed, $N_1/\sqrt{T_1}$, will be unchanged due to the closure of the VSV/VIGV. Making the usual assumptions for turbines operating in series, the power balance or work compatibility in Equation 8.4 indicates that T_3/T_1 is constant. For a given compressor inlet non-dimensional flow, and from the flow compatibility, Equation 8.5, the compressor pressure ratio will be constant. Hence, the gas turbine power output remains constant due to VIGV/VSV closure. Therefore, these assumptions result in the operating point on the compressor characteristic remaining unaltered due to VSV/VIGV closure. However, the change in the compressor characteristic due to the closure of the VSV/VIGV will result in an increase in the compressor non-dimensional speed and thus an increase in the gas generator speed. This is illustrated in Fig. 8.11, which shows the operating point on the compressor characteristic due to VSV/VIGV closure. The figure also shows the change in the compressor characteristic due to VSV/VIGV closure.

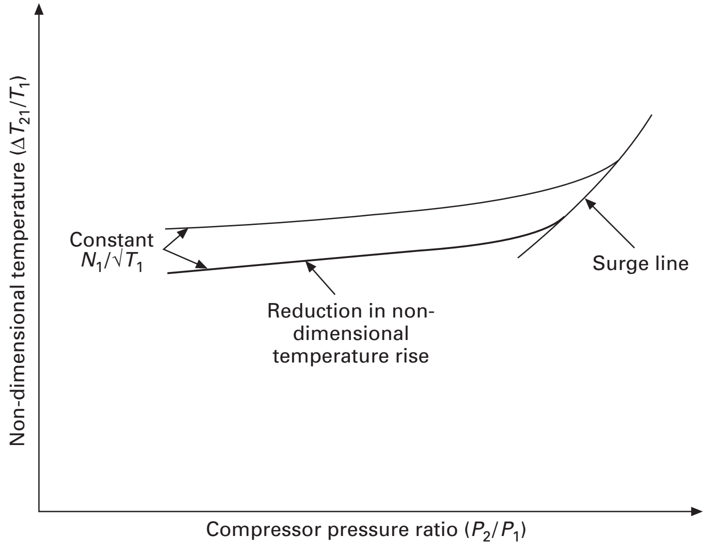

8.10 Effect of improved compressor efficiency on the non-dimensional temperature rise.

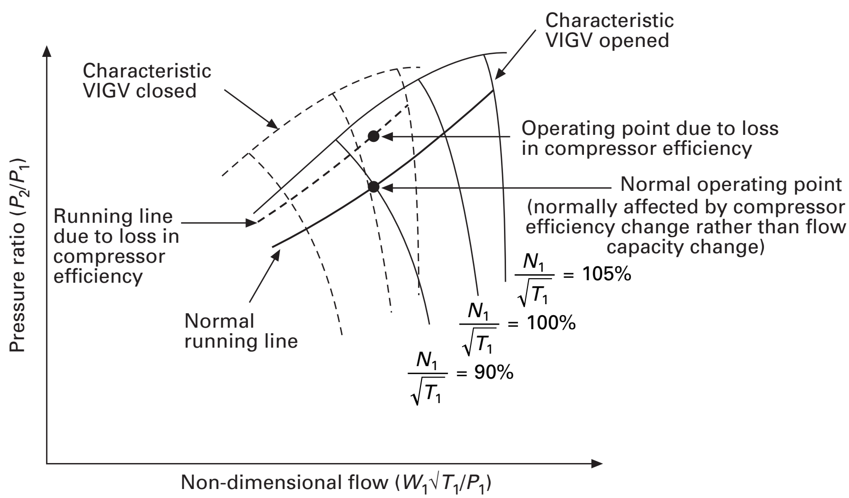

8.11 Effect of variable inlet guide vanes (VIGV) closure on the engine running line and operating point on the compressor characteristic.

It has been stated that the compressor efficiency may decrease at higher compressor speeds due to the closure of the VIGV. This would indeed increase the compressor non-dimensional temperature rise which, in turn, would increase T_3/T_1 to satisfy the power balance in the gas generator. For a given compressor inlet non-dimensional flow, the increase in T_3/T_1 will then increase the compressor pressure ratio P_2/P_1 in order to satisfy the flow compatibility of the gas generator. Hence, a loss in compressor efficiency will shift the operating line towards surge and the effects for VIGV closure and compressor efficiency loss are illustrated in Fig. 8.11. The figure shows the compressor speed is about 90% when the VIGV is opened and the speed increases to over 100% due to the closure of the VIGV. (*Note*: Whilst operating on a constant compressor speed line, the increase in T_3/T_1 due to a loss in compressor efficiency can indeed increase the power output of the gas turbine. But the drawback is the increased turbine creep life usage due to the higher turbine entry temperature.)

Variable stators and inlet guide vanes may also be applied to single-shaft gas turbines. Their application in single-shaft gas turbines is primarily to control the flow through the compressor. This is possible because a single-shaft gas turbine normally operates at a constant speed, thus any closure of the VSVs/VIGVs will result in a decrease in compressor flow. The control of the compressor flow by such means can result in constant turbine entry temperature operation at low powers. Considering the flow compatibility, Equation 8.1, for a constant T_3/T_1, any reduction in compressor flow and hence $W_1\sqrt{T_1}/P_1$, will result in a decrease in the compressor pressure ratio P_2/P_1. Thus the decrease in compressor flow and pressure ratio will result in a decrease in power output and thermal efficiency.

As stated in Section 7.11, constant turbine temperature operation is quite desirable because the combustion temperature can be maintained and thus the fuel–air ratio at low power, which makes the implementation of DLE combustion easier, as discussed in Chapter 6. The incorporation of a heat exchanger/regenerator, or if the gas turbine is part of a combined cycle plant, there will be a significant improvement in the off-design thermal efficiency. Furthermore, the reduction in compressor flows at low power, due to guide vane closure, also reduces the starting power requirements. However, the closure of these stators and VIGVs at high speeds will result in a decrease in compressor efficiency, and hence engine performance. All these effects are discussed in some detail later in the book where these issues will be illustrated using the gas turbine simulators.

Variable nozzle guide vanes (turbines)

Choking of the nozzle guide vanes (NGVs) normally controls the flow capacity of a turbine. Choking of the rotor is uncommon. Thus, any change in the nozzle guide vane flow area will affect the flow capacity. Changes in the flow areas of both the NGVs and rotors will affect the efficiency of the turbine and are usually due to the change in deflections across the NGVs and rotors. Early work on the development of such turbines was carried out by Ranhk.[3]

When turbines operate in series, as in a two-shaft gas turbine operating with a power turbine, any change in the turbine flow capacity will redistribute the pressure ratios across each turbine to satisfy the flow compatibility between the turbines. Thus, the gas generator and power turbine pressure ratio will be affected and the resultant change in the work done or power output by the gas generator turbine will displace the running line of the compressor characteristic. The effect of increasing the power turbine area will increase the gas generator pressure ratio. An increase in power turbine capacity can only be satisfied by increasing the gas generator (GG) turbine exit non-dimensional flow. This is achieved by increasing the gas generator turbine pressure ratio, as illustrated in Fig. 8.12.

The increase in GG turbine work will result in an increase in the non-dimensional temperature drop across the GG turbine, $\Delta T_{34}/T_3$. Considering the work compatibility across the gas generator, an increase in $\Delta T_{34}/T_3$ will result in a decrease in T_3/T_1 if operation is continued on a constant compressor non-dimensional speed line, as seen by the work compatibility Equation 8.4.

Considering the flow compatibility Equation 8.5, it can be seen that the pressure ratio P_2/P_1 along a constant compressor speed line should decrease. Thus, the running line will be shifted away from the surge line in a manner similar to that shown in Figure 8.9.

A decrease in power turbine area will therefore result in the running line being shifted towards the surge line. Also, T_3/T_1 will increase as the power turbine area is closed, so increasing the power turbine exhaust temperature. Gas turbines that employ variable geometry power turbines may increase the power turbine area during low power operations to shift the running line in

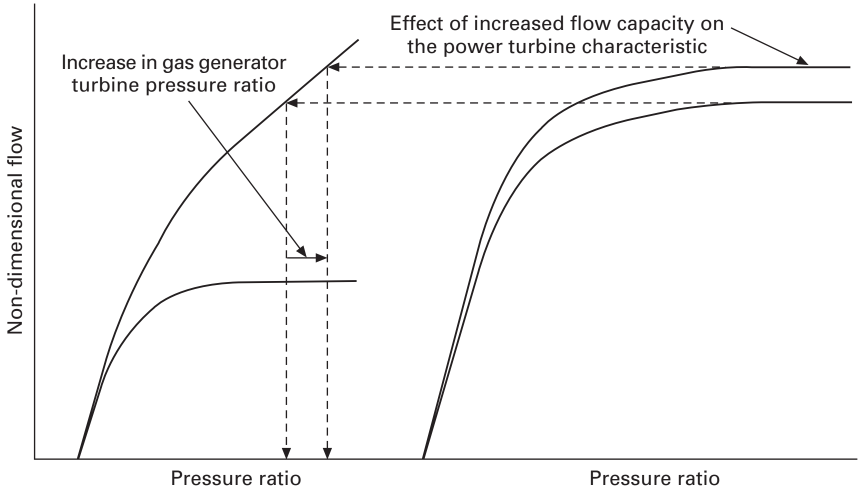

8.12 Effect of increasing the power turbine area on the gas generator (GG) pressure ratio.

order to prevent compressor surge during start-up and low power operating conditions. The advantage of using variable geometry power turbines is the prevention or reduction of wasteful blow-off, thus improving fuel efficiency at operating conditions where blow-off is needed to prevent compressor surge. When heat exchangers or waste heat boilers are used to recover gas turbine exhaust heat, the power turbine area may be reduced at low powers to optimise the exhaust heat recovery. They can also be used to provide substantial engine braking, as discussed in Chapter 7.

Reducing the gas generator turbine capacity will also increase the pressure ratio across the gas generator (GG) turbine as illustrated in Fig. 8.13. A reduction in the gas generator turbine flow capacity will necessarily reduce the outlet non-dimensional flow from the turbine. To maintain the same non-dimensional flow into the power turbine, the flow compatibility between the generator and power turbine will dictate an increase in the gas generator turbine pressure ratio.

The increase in gas generator turbine pressure ratio results in an increase in the GG turbine work done, or power output. The work compatibility between the GG turbine and compressor will therefore result in a reduction in T_3/T_1 as discussed above. From the flow compatibility, this reduction in T_3/T_1 will be compensated by a decrease in the compressor pressure ratio, P_2/P_1. However, the reduction in the flow capacity of the GG turbine, $W_3\sqrt{T_3}/P_3$ will require an increase in compressor pressure ratio to satisfy the flow compatibility of the gas generator. The reduction in the compressor pressure ratio, due to the reduction in T_3/T_1, will decrease only by the square root of T_3/T_1. However, the increase in compressor pressure ratio due to a decrease

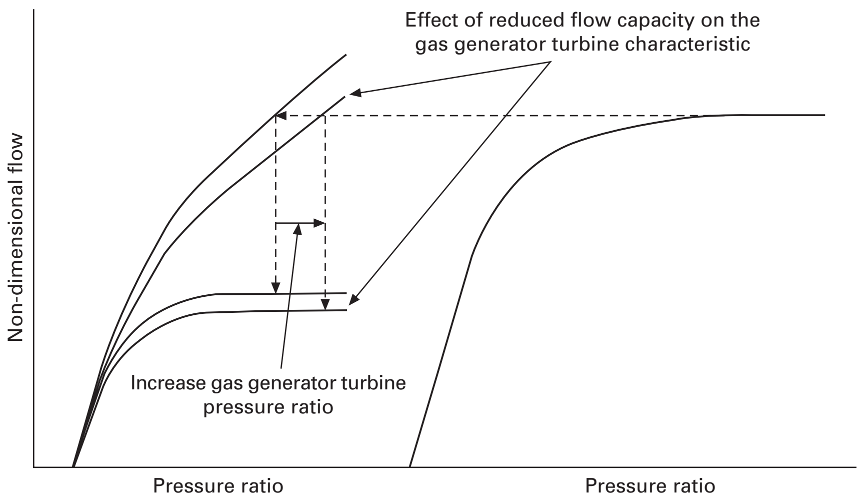

8.13 The matching of turbines operating due to a reduction of the gas generator (GG) turbine flow capacity.

in GG turbine flow capacity will be inversely proportional to the reduction in GG turbine flow capacity. Generally, the net effect of a reduced GG turbine flow capacity is an increase in compressor pressure ratio. Conversely, an increase in flow capacity of the gas generator turbine will result in an increase in T_3/T_1 (i.e. the engine will run hotter), but the compressor pressure ratio will decrease.

Variable geometry GG turbines are uncommon because of the high temperatures that prevail in the GG turbine. However, such effects (change in GG turbine pressure ratios) may be experienced due to deterioration of the turbine resulting in a change in capacity and will be discussed later.

By varying either the power turbine or GG turbine flow capacity, it is possible to plot the lines of constant T_3/T_1 on the compressor characteristic, as shown in Fig. 8.14. In practice, however, variable geometry power turbines are employed, and with such devices it is possible to operate under off-design conditions at constant T_3. However, the running line will drift towards surge on the compressor characteristic. At low power (low compressor speeds), it may be necessary to increase the power turbine flow capacity to prevent surge.

Variable geometry power turbines show little or no improvement at off-design conditions over simple cycle gas turbines when operating at constant T_3 (Bareau[4]). This is primarily due to the increased heat rejection at off-design conditions, which is very beneficial for a regenerative cycle. It would, however, be beneficial in DLE combustion engines using a two-shaft free power turbine configuration by maintaining a constant fuel–air ratio without incurring significant performance penalties due to overboard bleeds currently employed in such engine configurations.

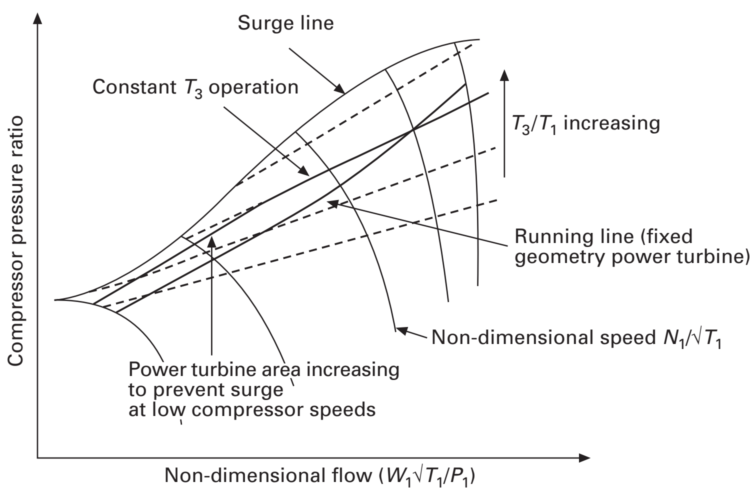

8.14 Lines for constant T_3/T_1 on the compressor.

Variable geometry power turbines, as stated, are also useful in improving the transient response of a two-shaft gas turbine operating with a free power turbine. Rapid acceleration is made possible by opening the power turbine to increase the surge margin. However, care is needed to prevent overheating of the gas generator turbine because of increased fuel flow, thus high turbine entry temperatures, lead to unacceptable loss in turbine blade creep life.

The off-design behaviour of single shaft gas turbines, due to changes in turbine flow capacity, is similar to that discussed above and can be established by considering the flow compatibility equation. For a constant T_3/T_1, any increase in the turbine flow capacity, $W_3\sqrt{T_3}/P_3$, will result in a decrease in the compressor pressure ratio P_2/P_1. Thus, the running line for a given power output will shift away from surge in a manner similar to that shown in Figure 8.9. However, with single-shaft engines, constant T_3 operation is best achieved by modulating a compressor variable inlet guide vane at off-design conditions as discussed earlier. The running line in this case will be similar to that shown in Fig. 8.14.

8.3 Three-shaft gas turbine operating with a free power turbine

A schematic representation of a three-shaft gas turbine operating with a free power turbine is shown in Fig. 8.15. The HP shaft, also known as the HP spool, which consists of the HP compressor driven by its own (HP) turbine, may be considered to act as the gas generator of a two-shaft gas turbine. The LP turbine will now be the corresponding power turbine. The LP turbine drives its own (LP) compressor, which acts as the load, and together they are referred to as the LP spool. Thus, a unique running line on the HP compressor characteristic will be determined by the swallowing and choking capacity of the LP turbine.

The LP turbine pressure ratio is now determined by the matching of the LP and power turbine characteristics. As discussed for a two-shaft engine, the power turbine swallowing capacity again determines the LP turbine pressure ratio. These details are shown in Figure 8.16. The matching of the turbines for a three-shaft gas turbine operating with a free power turbine will also establish a unique running line on the LP compressor characteristic.

Referring to Fig. 8.15, the power balance equation between the LP compressor and turbine may be written as follows:

$$\frac{\Delta T_{21}}{T_1} = \frac{\Delta T_{56}}{T_5} \times \frac{cpa}{cpa} \times \sqrt{\frac{T_5}{T_1}} \times \frac{W_5}{W_1} \qquad [8.8]$$

The choking of the power turbine will restrict the LP pressure ratio, P_5/P_6 as

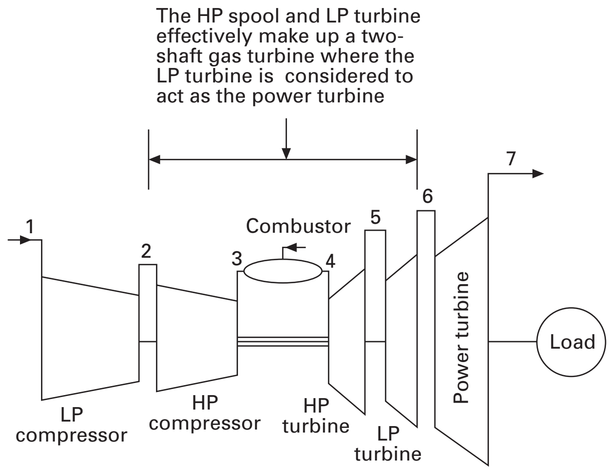

1 LP compressor inlet
2 HP compressor inlet
3 HP compressor exit/combustor inlet
4 Combustor exit/HP turbine inlet
5 LP turbine inlet
6 Power turbine inlet
7 Power turbine exit

8.15 Schematic representation of a three-shaft gas turbine highlighting the HP spool and LP turbine.

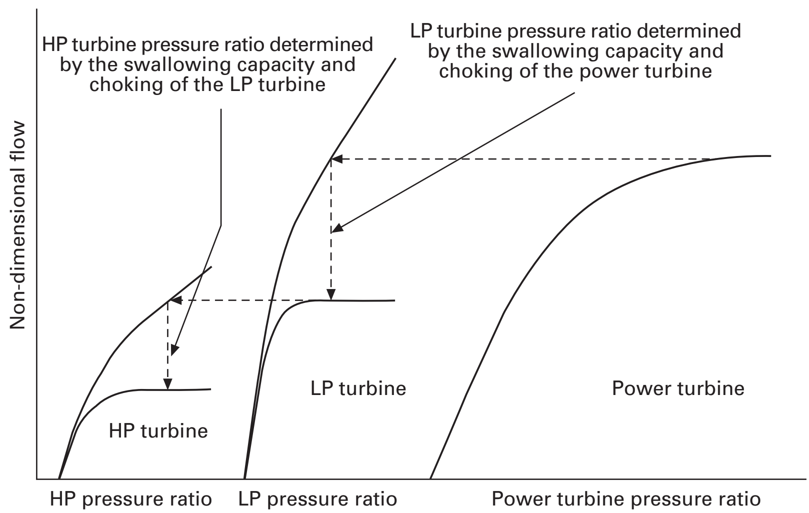

8.16 Matching of turbines for a three-shaft gas turbine operating with free power turbine.

shown in Figure 8.16. For a given LP turbine efficiency, the non-dimensional temperature drop, $\Delta T_{56}/T_5$, will therefore be constant. If a constant non-dimensional speed line on the LP compressor characteristic is operated on, then from the previous assumption and discussions, the LP compressor non-dimensional temperature rise, $\Delta T_{21}/T_1$, will also be constant. Ignoring the changes in specific heats (*cpa* and *cpg*) and any bleeds, $W_5 = W_1$; it may be concluded from the power balance Equation 8.8 that T_5/T_1 is also constant.

Similarly, the matching of the HP and LP turbine (Fig. 8.16) results in a constant non-dimensional temperature drop (i.e. $\Delta T_{45}/T_4$ = Constant) across the HP turbine (assuming constant HP and LP turbine efficiencies). Since T_5 is constant, it may be concluded that T_4 is also constant. For a given ambient temperature, T_1, a constant $\Delta T_{21}/T_1$ will result in a constant T_2. Thus T_4/T_2 is constant, which is the maximum to minimum temperature ratio for the HP spool in a three-shaft gas turbine. It has been stated that the HP spool behaves as a two-shaft gas turbine operating with a free power turbine, while the LP turbine acts as the power turbine. Thus the HP compressor will have a unique running line and the intersection of this running line with the corresponding T_4/T_2 line will fix the HP compressor inlet non-dimensional flow, $W_2\sqrt{T_2}/P_2$, and pressure ratio, P_3/P_2. Therefore, the LP compressor non-dimensional speed, $N_1/\sqrt{T_1}$, essentially fixes the operating point on the HP compressor characteristic. The flow compatibility between the LP and HP compressor may be written as:

$$\frac{W_2\sqrt{T_2}}{P_2} = \frac{W_1\sqrt{T_1}}{P_1} \times \frac{P_1}{P_2} \times \sqrt{\frac{T_2}{T_1}} \times \frac{W_2}{W_1} \qquad [8.9]$$

Since the flow along the compressor speed line is approximately vertical, and using the assumptions stated above, $W_1\sqrt{T_1}/P_1$ and T_2/T_1 will be approximately constant. Ignoring bleeds, $W_2 = W_1$, for a required $W_2\sqrt{T_2}/P_2$ (HP compressor inlet non-dimensional flow) will result in a unique LP compressor pressure ratio, P_2/P_1. Thus all LP compressor speed lines will have a unique pressure ratio, and joining these points will generate the unique running line on the LP compressor characteristic. This is illustrated in Fig. 8.17, which also shows the lines of constant temperature ratio, T_4/T_1, and T_4/T_2, on the LP and HP compressor, respectively. Unlike the HP compressor characteristic where the lines of constant temperature ratio, T_4/T_2, move towards surge as T_4/T_2 increases, the lines of constant temperature ratio, T_4/T_1, move away from surge on the LP compressor, as shown in Fig. 8.17. At low powers, the running line on the LP compressor characteristic may intersect the surge line and, in this case, a variable geometry LP compressor in the form of VIGVs may be necessary for satisfactory operation of a three-shaft gas turbine operating with a free power turbine.

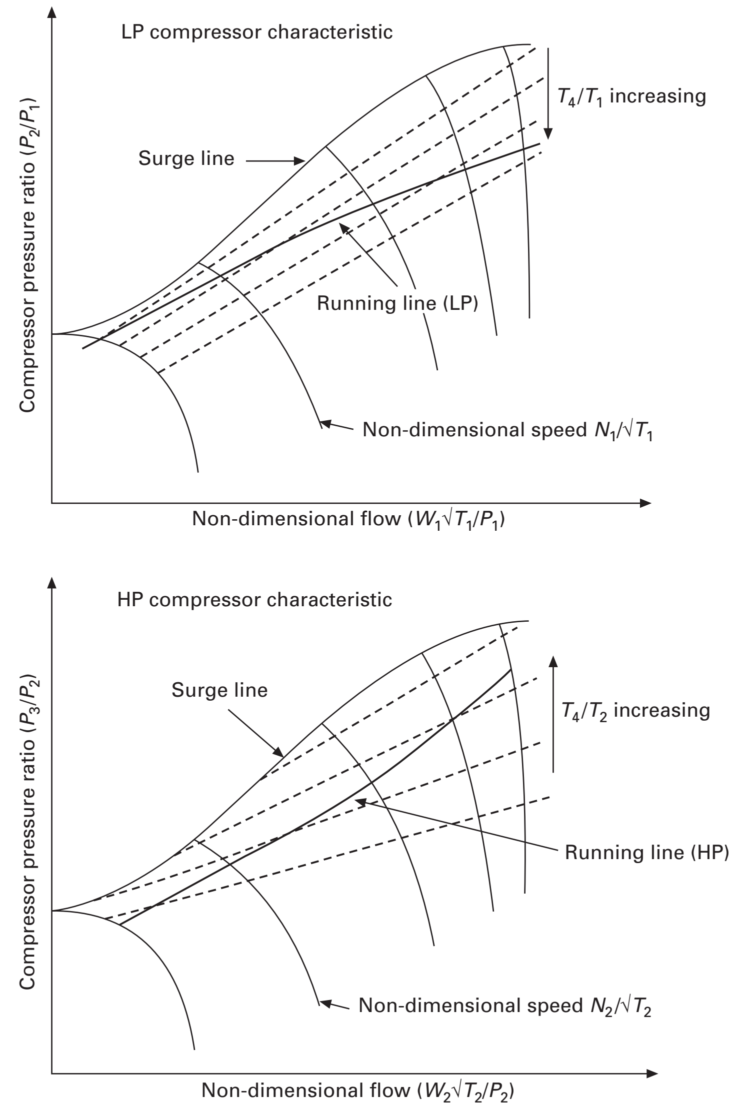

8.17 Running lines of the LP and HP characteristics for a three-shaft gas turbine operating with a free power turbine.

Since the lines of temperature T_4/T_1 on the LP compressor characteristic move away from surge, three-shaft engines using a free power turbine do not normally encounter surge during acceleration. However, during deceleration, the reduction of LP surge margin could give rise to LP compressor surge. Again, the incorporation of variable inlet guide vanes would prevent surge by improving the surge margin due to the closure of the VIGV.

8.4 Displacement of running line (three-shaft gas turbine)

A similar analysis as was discussed for a two-shaft engine can be carried out for a three-shaft gas turbine. However, discussion will be restricted to the effects of the changes in the power turbine flow capacity. Making the assumption that the turbines remain choked, the HP spool will be shielded from any change in the power turbine flow capacity due to the choked condition of the LP turbine. Therefore, the running line on the HP compressor characteristic will remain unaffected by any change in the flow capacity of the power turbine.

Increasing the power turbine flow capacity will result in an increase in the LP turbine pressure ratio, as illustrated in Fig. 8.18. This increase in LP turbine pressure ratio will increase the LP turbine power output. If we consider that the LP compressor continues to operate at a constant non-dimensional speed, the LP compressor discharge temperature will remain approximately constant. Since the non-dimensional speed lines describing the variation of flow with pressure ratio are steep, there is little variation in mass flow rate through the LP compressor with any change in LP compressor pressure. Thus, the power absorbed by the LP compressor will remain essentially constant with the change in power turbine flow capacity.

The turbine entry temperature, T_4, must therefore reduce to maintain the power LP spool balance. Since the HP compressor-running line is not affected by the change in the power turbine flow capacity due to the LP turbine choked conditions, and T_2 is approximately constant, T_4/T_2 will decrease.

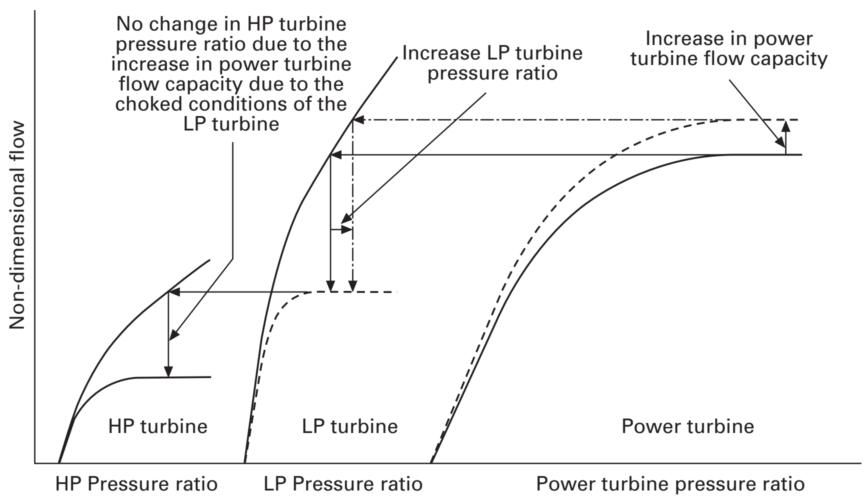

8.18 Matching of turbines due to an increase in power turbine flow capacity.

This will force the operating point on the HP compressor characteristic running line to fall to a lower pressure ratio and inlet non-dimensional flow, as illustrated in Fig. 8.19. The reduction in HP compressor inlet non-dimensional flow can only be satisfied by a reduction in LP compressor discharge non-

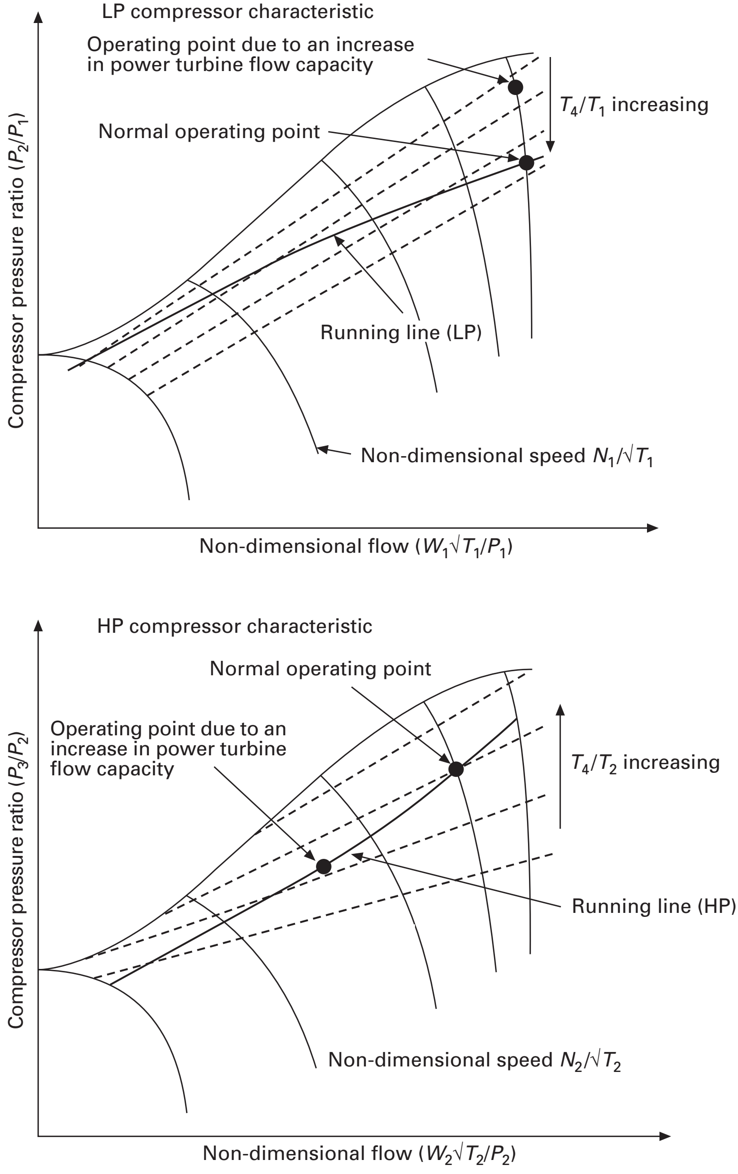

8.19 Effect of increasing power turbine capacity on the operating points of the LP and HP characteristics.

dimensional flow. Considering the flow identity between the inlet and discharge of the LP compressor, as described in Equation 8.9, since T_2/T_1 (constant non-dimensional speed), W_2/W_1 (no bleeds) and $W_1\sqrt{T_1}/P_1$ are constant (steep non-dimensional speed lines), any reduction in LP compressor non-dimensional discharge flow, $W_2\sqrt{T_2}/P_2$, must be accompanied by a reduction in P_1/P_2. This implies that the LP compressor pressure ratio, P_2/P_1 increases. Thus we see why the turbine entry temperature decreases and the LP compressor pressure ratio increases when the power turbine capacity is increased. This effect is illustrated on the LP compressor characteristic in Fig. 8.19.

Consequently, a reduction in the power turbine flow capacity will result in an increase in the turbine entry temperature, T_4, and causes the operating point to move along the HP compressor running line to a higher non-dimensional flow and pressure ratio. The effect on the LP compressor characteristic will be a decrease in pressure ratio along a given non-dimensional speed line.

8.5 Running line for a two-shaft gas turbine

The off-design performance prediction of a two-shaft gas turbine was discussed in Chapter 7. It was also stated that the two-shaft gas turbine case is similar to that of a three-shaft gas turbine operating with a free power turbine but with the LP and power turbine being integrated as one component (Fig. 7.7 in Chapter 7). Therefore, the LP turbine now drives both the LP compressor and load. It was also stated that such a configuration is quite suitable for driving a generator and therefore finds application in electrical power generation. Since the LP compressor, LP turbine and the load operate at a constant speed corresponding to the synchronous speed of the generator, for a given ambient temperature, T_1, the running line will be along a constant non-dimensional speed line on the LP compressor characteristic, as shown in Fig. 8.20. The matching of the HP and LP turbines is similar to that shown in Fig. 8.5.

Since the engine operates at a constant LP spool speed, for a given ambient temperature, T_1, the flow rate through the compressor and the LP compressor discharge temperature, T_2, remain approximately constant. Hence the increase in power output from the gas turbine must be accomplished by increasing the turbine entry temperature, T_4, and general overall pressure ratio, P_3/P_1 (i.e. increase in specific work). Since the LP compressor discharge temperature, T_2, which is also the HP compressor inlet temperature, is approximately constant, an increase in T_4 will result in an increase in T_4/T_2. From Fig. 8.20, the operating point would move along the HP running line from a low to a higher HP compressor inlet non-dimensional flow, $W_2\sqrt{T_2}/P_2$, and pressure ratio, P_3/P_2. Thus a higher HP compressor inlet non-dimensional flow must result in a decrease in the LP compressor pressure

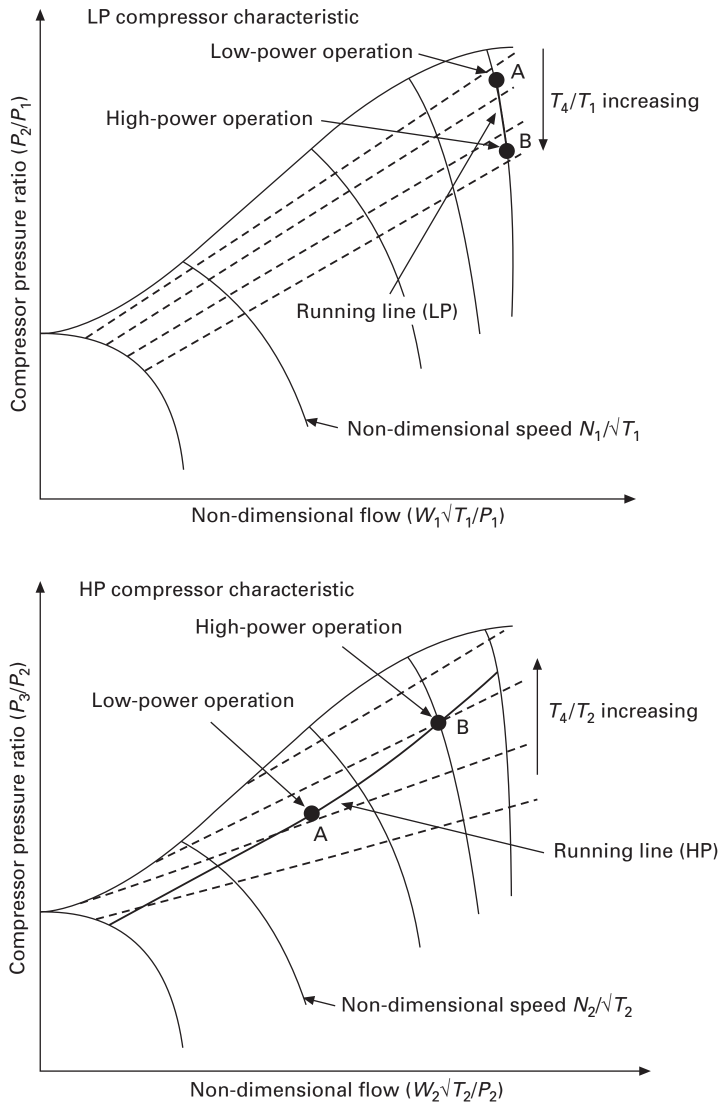

8.20 Operating point on the LP and HP compressor characteristics due to low and high power operation.

ratio to satisfy the flow compatibility between the LP and the HP compressor (Equation 8.9). Thus, as the power output from the gas turbine increases, the operating points on the respective compressor characteristics move from A to B (Fig. 8.20).

At different ambient temperatures, the operating point will switch to a different non-dimensional speed, increasing in speed as the ambient temperature falls. Hence lines of constant gas turbine power output can be produced on the LP compressor characteristic similar to those shown in Fig. 8.4, which presents the case for a single shaft gas turbine – the exception being that the lines of constant power move away from surge with increase in power as shown in Fig. 8.21. Unlike the case for the HP compressor, there is no unique running line on the LP compressor, and the running line is determined by the power output and ambient conditions.

Since the lines of constant power move away from surge as the power output from the gas turbine increases, it is possible that the zero load line on the LP compressor characteristic will be in the compressor surge region and therefore make the gas turbine impossible to start. Implementing blow-off at the LP compressor discharge will enable the starting of the engine. Considering the flow compatibility in Equation 8.9, blow-off will decrease W_2/W_1. For a given demand of HP compressor inlet non-dimensional flow (i.e. $W_2\sqrt{T_2}/P_2$ is constant), any decrease in W_2/W_1 must be accompanied by a decrease in the LP compressor pressure ratio, P_2/P_1, thus shifting the running line away from surge. The blow-off may remain open until adequate power demand has occurred, thereby shifting the running line sufficiently away from surge enabling the blow-off to be closed. Incorporating variable stators and VIGVs will also help shift the LP compressor running line away from surge. By closing these guide vanes during starting and low power operation, the turbine entry temperature is increased for a given LP compressor non-dimensional speed. As explained in Section 8.4, the LP compressor running line will move away from surge, thus easing the start-up of the gas

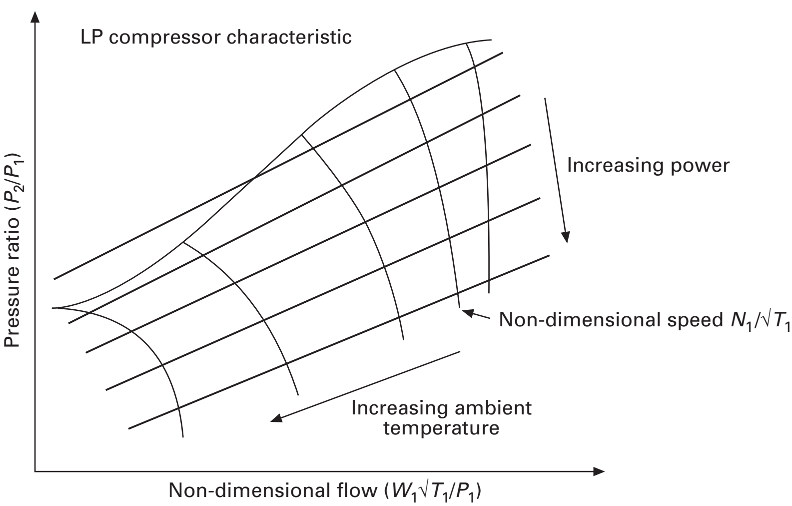

8.21 Running lines on the LP compressor characteristic of a two-shaft gas turbine illustrating effects of increases in power and ambient temperature.

turbine. Furthermore, VIGVs also shift the surge line to the left, thus increasing the surge margin.

8.6 Running lines of gas turbine complex cycles

The design point and off-design performance of complex cycles incorporating intercooling, regeneration and reheat have been discussed. The off-design performance of complex cycles using regeneration is very similar to that discussed above, the main difference being the increased pressure losses in the heating and exhaust part of the gas turbine cycle. Intercooling and reheat affect the off-design performance of the gas turbine differently from that discussed previously and depend on the engine configuration (i.e. single shaft, free power turbine, etc.). Discussion, however, will be restricted to only that which is noteworthy.

8.6.1 Intercooled single-shaft gas turbine

The off-design behaviour of an intercooled single-shaft gas turbine may be understood by dividing the process into two parts. The HP compressor and the turbine can be treated as a simple cycle single-shaft engine and therefore the off-design behaviour of this part of the gas turbine is similar to that discussed in Section 8.1.1. The HP compressor inlet temperature T_3 in Fig. 8.22, which shows a schematic representation of an intercooled single shaft gas turbine, will remain constant due to intercooling. Hence, the operating point on the HP compressor characteristic will approach surge along a line of

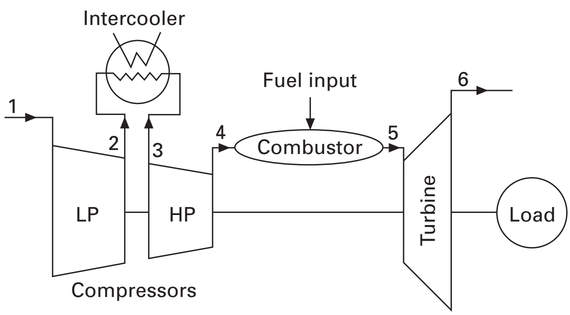

1 LP compressor inlet
2 LP compressor exit/intercooler inlet
3 Intercooler exit/HP compressor inlet
4 HP compressor exit/combustor inlet
5 Combustor exit/turbine inlet
6 Turbine exit

8.22 Schematic representation of a single-shaft gas turbine with intercooler.

constant non-dimensional speed as the engine load is increased. Since it is assumed that the constant speed line on the compressor characteristic is approximately vertical, the compressor inlet non-dimensional flow, $W_3\sqrt{T_3}/P_3$, will also be approximately constant. The flow compatibility between the inlet and exit of the intercooler gives:

$$\frac{W_3\sqrt{T_3}}{P_3} = \frac{W_2\sqrt{T_2}}{P_2} \times \frac{P_2}{P_3} \times \sqrt{\frac{T_3}{T_2}} \times \frac{W_3}{W_2} \qquad [8.10]$$

It has been shown that $W_3\sqrt{T_3}/P_3$ is approximately constant and T_3 is controlled by the intercooler and is also assumed to be constant. Since the gas turbine is constrained to operate at a constant speed, for a given LP compressor inlet temperature, T_1, the LP compressor non-dimensional speed will remain constant with engine load changes. It has been stated previously that, at a constant compressor non-dimensional speed, the compressor inlet non-dimensional flow and discharge temperature does not vary much and can be assumed to be approximately constant. Making these assumptions and also assuming a constant intercooler pressure loss, P_2/P_3, and ignoring bleeds (i.e. $W_3 = W_2$), we may conclude from Equation 8.10 that the LP compressor discharge non-dimensional flow, $W_2\sqrt{T_2}/P_2$ is also approximately constant.

The flow compatibility equation between the inlet and discharge of the LP compressor is:

$$\frac{W_2\sqrt{T_2}}{P_2} = \frac{W_1\sqrt{T_1}}{P_1} \times \frac{P_1}{P_2} \times \sqrt{\frac{T_2}{T_1}} \times \frac{W_2}{W_1} \qquad [8.11]$$

In Equation 8.11, the non-dimensional flows ($W_2\sqrt{T_2}/P_2$ and $W_1\sqrt{T_1}/P_1$), and temperature and flow ratios, T_2/T_1, and W_2/W_1 respectively, are approximately constant. Therefore from Equation 8.11, the LP compressor pressure ratio, P_2/P_1, is also approximately constant.

Change in the ambient temperature results in the LP compressor operating on a different non-dimensional speed. However, the operating point on this LP compressor non-dimensional speed will be unique for the reasons discussed. Thus it is possible to join these operating points and generate a unique running line on the LP compressor characteristic as shown in Fig. 8.23. The change in the ambient temperature will also result in a change in the intercooled discharge temperature, and hence a change in the HP compressor inlet temperature, T_3. Therefore, the operating line on the HP compressor characteristic will change with power output and ambient temperature in a manner similar to that of a simple cycle single-shaft gas turbine, as shown in Fig. 8.4. Thus, no unique running line exists for the HP compressor.

A variable inlet guide vane (VIGV) may be included in the LP compressor to control the air flow through the gas turbine, such that the turbine entry

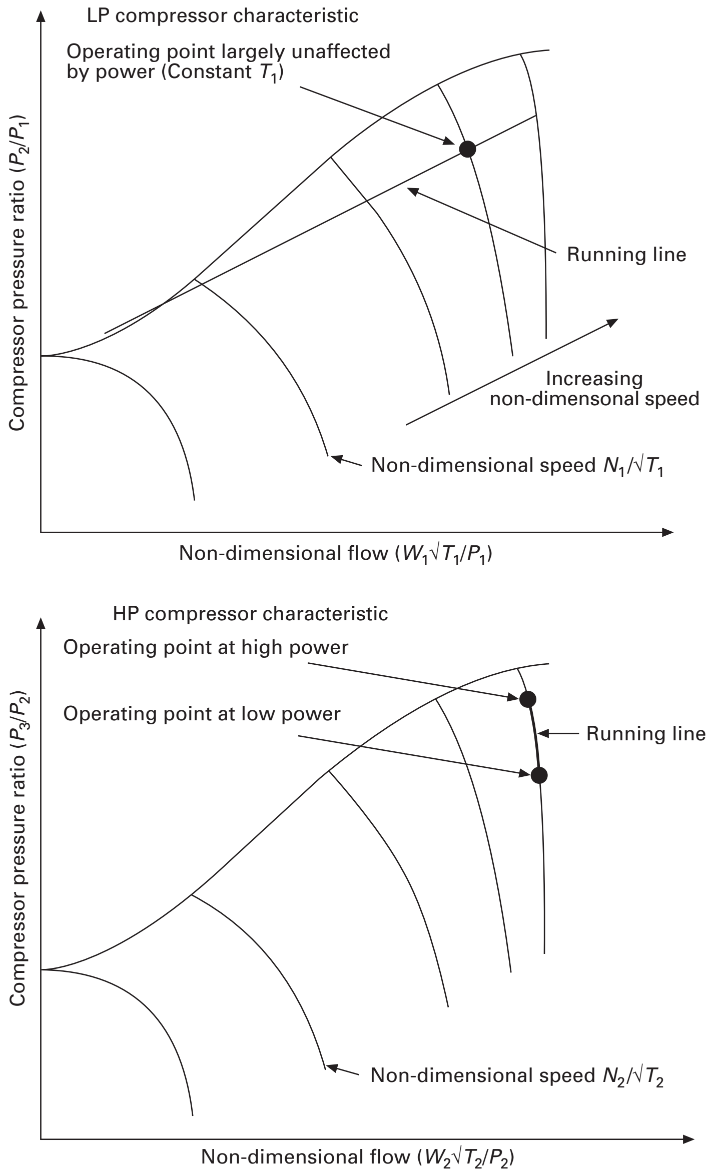

8.23 Operation points on the compressor characteristics with change in power output for an intercooled single-shaft gas turbine.

temperature remains constant with engine load (i.e. maximum cycle temperature T_5 remains constant as the power changes). Applying the flow compatible equation to the HP compressor and turbine gives:

$$\frac{W_5\sqrt{T_5}}{P_5} = \frac{W_3\sqrt{T_3}}{P_3} \times \frac{P_3}{P_4} \times \frac{P_4}{P_5} \times \sqrt{\frac{T_5}{T_3}} \times \frac{W_5}{W_3} \qquad [8.12]$$

Making the usual assumptions, $W_3\sqrt{T_3}/P_3$ and $W_5\sqrt{T_5}/P_5$ will be constant (vertical compressor speed lines and choked turbine nozzle, respectively). Assuming constant pressure losses and ignoring bleeds, P_4/P_5 will be constant and $W_5 = W_3$. Operating at the constant maximum cycle temperature, T_5, thus for a given minimum cycle temperature, T_3 (which would ideally be equal to the ambient temperature, T_1–perfect intercooler), the HP compressor pressure ratio must remain essentially constant as the engine load changes in order to maintain the flow compatibility between the HP compressor and turbine (Equation 8.12). Thus, for a given compressor inlet temperature, all the pressure ratio change takes place in the LP compressor, as illustrated in Fig. 8.24. This is in contrast with the previous case, (no VIGV), where it was determined that all the pressure ratio changes take place in the HP compressor rather than in the LP compressor.

A similar off-design behaviour occurs with an intercooled three-shaft gas turbine operating with a variable geometry free power turbine. When the power turbine capacity is adjusted such that the turbine entry temperature remains constant at part load conditions, the operating point on the HP compressor remains unchanged and all the pressure ratio change occurs in the LP compressor. It is assumed that the intercooling process takes place between the LP and HP compressors. This result is due to the LP turbine remaining choked and therefore forcing the HP turbine pressure ratio to be fixed. Thus the HP turbine non-dimensional temperature drop is also fixed. Due to the constant turbine entry temperature at off-design conditions, the HP turbine temperature drop will also remain constant. Since the HP compressor inlet temperature is maintained at a constant value due to intercooling the HP spool, the power balance between the HP compressor and turbine will maintain the HP compressor non-dimensional speed at a fixed value. As the turbine entry temperature and the HP compressor inlet temperature remain constant, due to the effect of the variable geometry power turbine and intercooling, respectively, the operating point on the HP compressor characteristic will be fixed where the HP compressor non-dimensional speed intersects the line of constant maximum to minimum temperature ratio on the HP compressor characteristic.

It must be pointed out that, when the design point performance is optimised for maximum thermal efficiency (i.e. approximately equal LP and HP compressor pressure ratio for a regenerative cycle), this optimum split in compressor ratios cannot be maintained at off-design conditions. Thus intercooled cycles may not achieve the maximum possible thermal efficiency at off-design conditions due to intercooling.

8.6.2 Reheat: two- and three-shaft gas turbine operating with a free power turbine

It has been discussed that the matching of turbines in series results in the low pressure turbine restrict the operating range of the high pressure turbine in

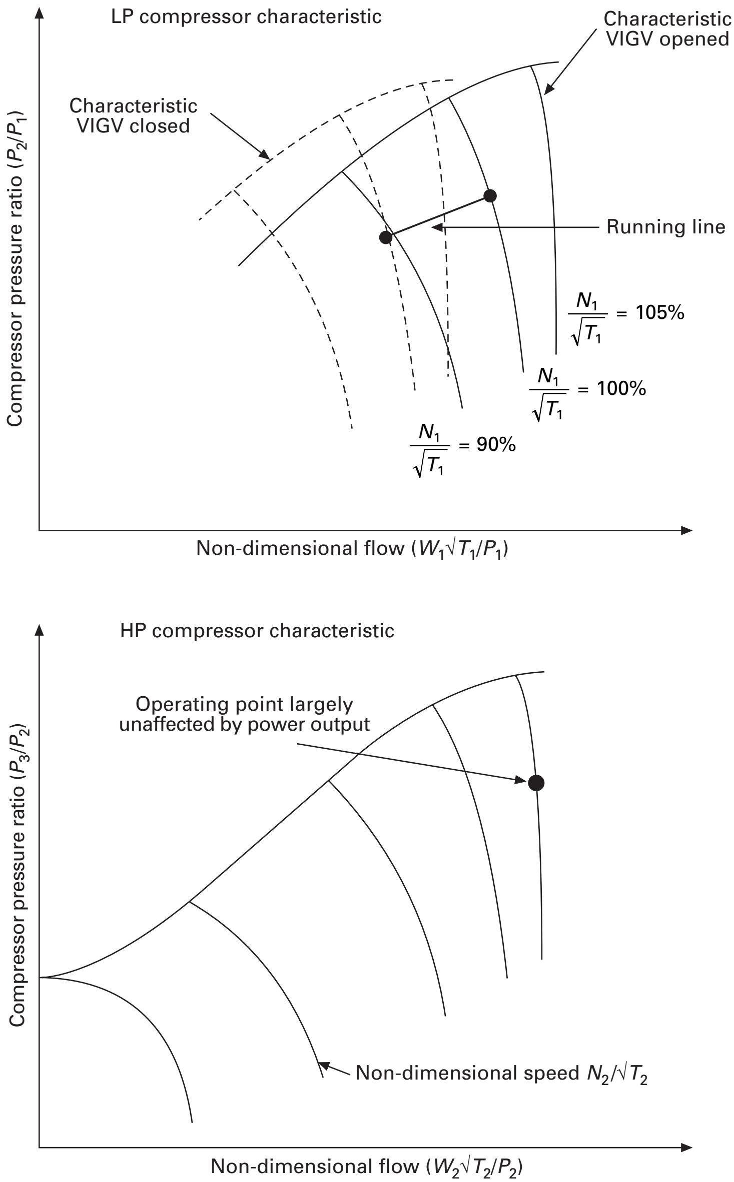

8.24 Running lines on the LP and HP compressor characteristics for an intercooled single-shaft gas turbine using a VIGV in the LP compressor.

order to maintain the flow compatibility between them. For a two-shaft gas turbine operating with a free power turbine, the power turbine characteristic controls the operating point on the gas generator (GG) turbine characteristic such that the flow demanded by the power turbine is satisfied. When we apply reheat to such an engine, as shown in Fig. 8.25, the reheat is usually applied between the gas generator and power turbine and this affects the matching of the turbines resulting in a redistribution of the turbine pressure ratios in order to satisfy the flow compatibility between them. Considering the flow identity (Equation 8.13), describing the non-dimensional flow at exit from the GG turbine:

$$\frac{W_4\sqrt{T_4}}{P_4} = \frac{W_3\sqrt{T_3}}{P_3} \times \frac{P_3}{P_4} \times \sqrt{\frac{T_4}{T_3}} \times \frac{W_4}{W_3} \qquad [8.13]$$

and the flow identity at the exit of the reheat chamber:

$$\frac{W_5\sqrt{T_5}}{P_5} = \frac{W_4\sqrt{T_4}}{P_4} \times \frac{P_4}{P_5} \times \sqrt{\frac{T_5}{T_4}} \times \frac{W_5}{W_4} \qquad [8.14]$$

The reheater exit non-dimensional flow, $W_5\sqrt{T_5}/P_5$, must be 'swallowed' by the power turbine. If it is assumed that the power turbine is choked, then $W_5\sqrt{T_5}/P_5$ will remain constant as the amount of reheat is varied, which is given by Tr (reheat temperature ratio) = T_5/T_4. Increasing reheat will increase T_5/T_4 and thus Tr. If we assume that the reheater pressure loss, P_4/P_5, is constant and ignore bleeds, any increase in reheat must be accompanied by a decrease in $W_4\sqrt{T_4}/P_4$ to satisfy the flow compatibility in the reheater (Equation 8.14). However, $W_4\sqrt{T_4}/P_4$ is the exit non-dimensional flow from the GG turbine. Assuming the GG turbine is choked and ignoring bleeds, the

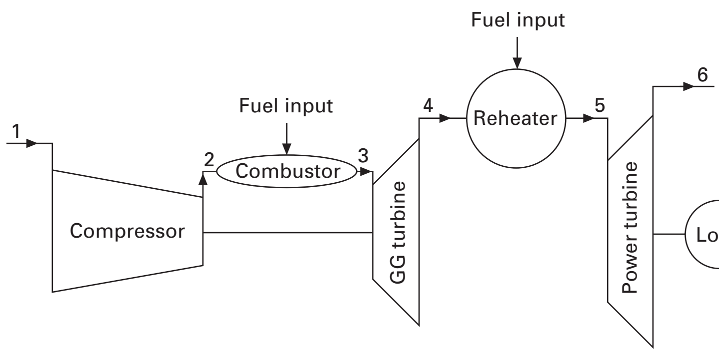

1 Compressor inlet
2 Compressor exit/combustor inlet
3 Combustor exit/gas generator (GG) turbine inlet
4 GG turbine exit/reheater inlet
5 Reheater exit/power turbine inlet
6 Power turbine exit

8.25 Schematic representation of a two-shaft reheat gas turbine operating with a free power turbine.

reduction in $W_4\sqrt{T_4}/P_4$ will result in a decrease in GG turbine pressure ratio, P_3/P_4, as required by Equation 8.13. (Although there is an increase in T_4/T_3 due to the decrease in P_3/P_4, the effect of the reduction in GG turbine pressure (P_3/P_4) is dominant). The effect of reheat on the GG turbine pressure ratio is illustrated in Fig. 8.26, which shows the matching of the GG and power turbine characteristics due to the application of reheat. The operating point on the GG turbine characteristic decreases in pressure ratio as the amount of reheat, Tr, is increased (from (1) to (2) in Fig. 8.26). Note the zero reheat line corresponds to the case when $Tr = 1$.

Reheat is usually applied when the gas generator is operating at its maximum speed or at the maximum turbine entry temperature. However, the decrease in the GG turbine pressure will decrease the non-dimensional temperature drop across the GG turbine, $\Delta T_{34}/T_3$. If we are continuously operating at the maximum compressor speed and a given compressor inlet temperature, T_1, the compressor non-dimensional speed, $N_1/\sqrt{T_1}$ will be constant during the application of reheat. From the discussion above, the compressor non-dimensional temperature rise, $\Delta T_{21}/T_1$, will be approximately constant. From the work compatibility equation or power balance Equation 8.4, the decrease in $\Delta T_{34}/T_3$ must result in an increase in T_3/T_1 and for a given T_1, will therefore increase the turbine entry temperature, T_3.

Assuming that the compressor speed lines are approximately vertical, therefore there is little variation in the compressor inlet non-dimensional flow, $W_1\sqrt{T_1}/P_1$ with compressor pressure, P_2/P_1. For a choked gas generator turbine, $W_3\sqrt{T_3}/P_3$, is a constant) and from Equation 8.5, which describes the

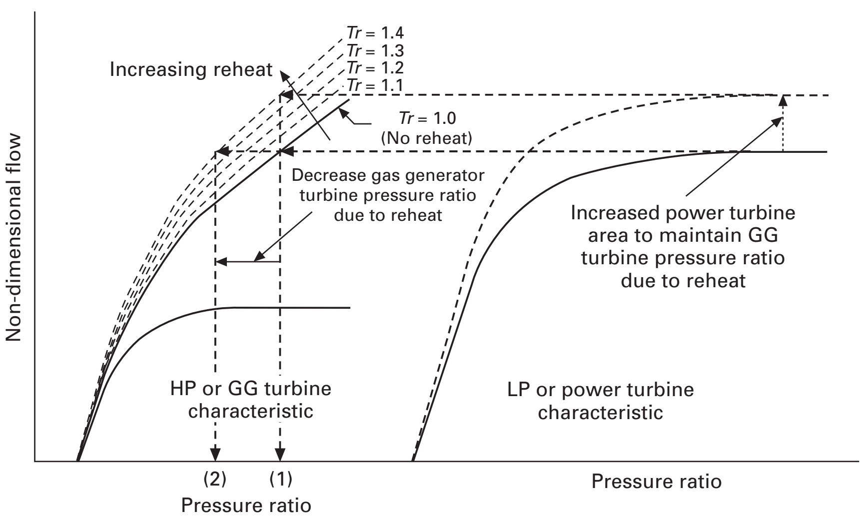

8.26 Matching of the GG and power turbines due to the application of reheat.

flow compatibility of the gas generator, an increase in T_3/T_1 will result in an increase in the compressor pressure ratio, P_2/P_1. Thus reheat increases the compressor pressure ratio as illustrated in Fig. 8.27, which shows the change in the operating point on the compressor characteristic due to reheat.

Thus reheat increases the turbine entry temperature and will contribute further in the increase in the power output of the gas turbine. However, the turbine creep life may be compromised severely and the application of reheat would normally require a variable geometry power turbine. It has been shown that increasing the power turbine capacity will increase the GG turbine pressure ratio as illustrated in Fig. 8.26. Thus by increasing the power turbine capacity sufficiently during reheat, it is possible to maintain the design turbine entry temperature and compressor pressure ratio. (It is worth pointing out that, when jet engines employ reheat or afterburning to augment the thrust, they often incorporate a variable geometry propelling nozzle, which is open during reheat operation.)

A three-shaft gas turbine operating with a free power turbine will usually apply reheat between the LP turbine and the power turbine. The redistribution of pressure ratio across the three turbines during the reheat operation is illustrated in Fig. 8.28. In this case, we observe the decrease in the LP turbine pressure ratio due to the application of reheat results in a decrease in LP turbine work. Hence a higher LP turbine inlet temperature is required to maintain the power balance of the LP spool when operating at a constant

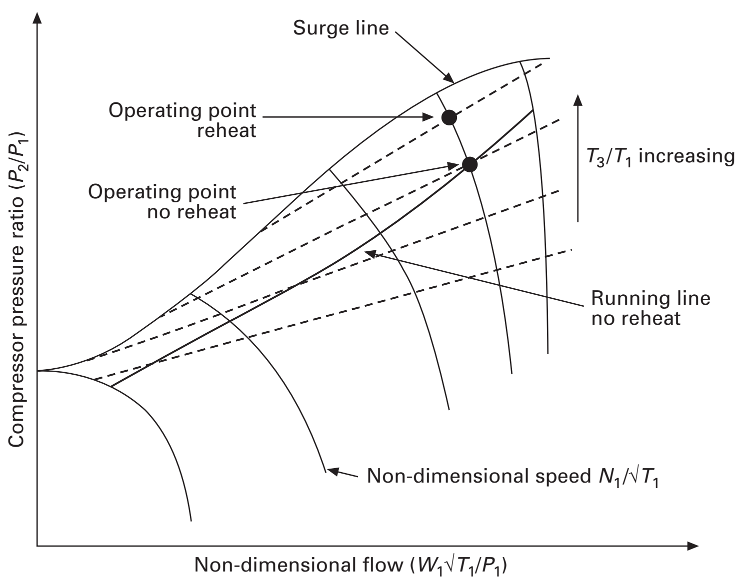

8.27 Change in the operating point on the compressor characteristic due to reheat.

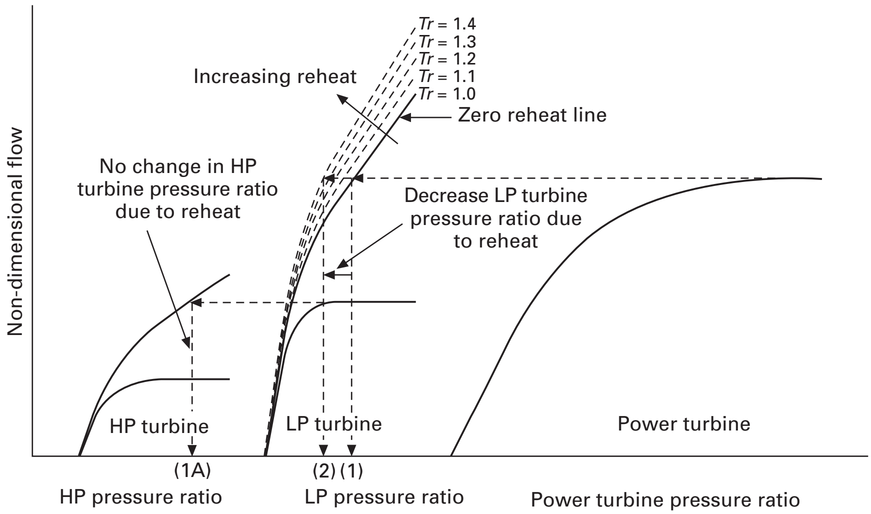

8.28 Turbine characteristics of a three-shaft gas turbine operating with a free power turbine during the application of reheat.

speed. Since the HP turbine is shielded from the effects of reheat due to the choking of the LP turbine, the increase in LP turbine entry temperature will result in an increase in the HP turbine entry temperature, thus increasing the work done by the HP turbine. The increase in HP turbine work is absorbed in the HP compressor by increasing the HP spool speed as illustrated in Fig. 8.29. Since we are operating at a constant LP compressor speed, the increase in HP compressor non-dimensional flow due to its increase speed can only be satisfied by decreasing the LP compressor pressure, as shown in Fig. 8.29. Thus the effect of reheat on the LP compressor is opposite to the previous case, where reheating was considered for a two-shaft gas turbine operating with a free power turbine.

Reheating a single-shaft gas turbine may also be considered by splitting the turbine into two parts. The matching of the flows between the turbines will be similar to that shown in Fig. 8.26. Although there will be a reduction in the HP turbine pressure ratio, and thus the work produced by the HP turbine, the two turbines are linked mechanically and therefore transfer of power from the LP to the HP turbine can occur. Hence, the compressor operating point and the turbine entry temperature can remain at the design value without the use of any variable geometry in the turbine.

In fact, power transfer has been applied to two-shaft gas turbines operating with a free power turbine, where controlled amounts of power are transferred from the GG turbine to the power turbine by the use of clutches (Turunen and Collman, 1965). Such techniques have been applied to regenerative automotive gas turbines to improve the part-load thermal efficiency. For

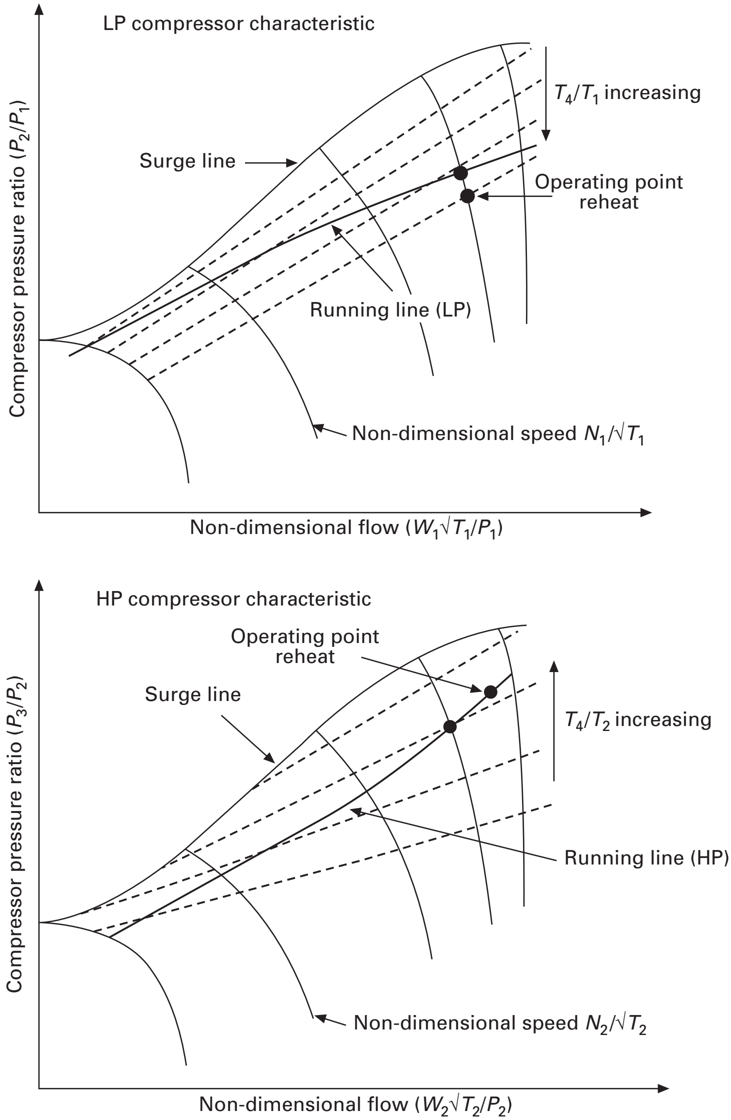

8.29 Change in the operating points on the LP and HP compressor characteristics due to reheating a three-shaft gas turbine incorporating a free power turbine.

naval applications, it is possible to consider a separate variable pitch propeller and shaft connected to the GG turbine. Thus it is possible to transfer power from the GG shaft such that the maximum turbine entry temperature is maintained at part-load operation. The incorporation of a heat exchanger and power transfer then can result in significant increase in off-design thermal efficiency of the gas turbine.

8.7 Running line, non-dimensional parameters and correcting data to standard conditions

The previous analysis on gas turbines using a free power turbine (without reheat) essentially describes a unique running line on the compressor and turbine characteristics. Therefore, for any given parameter, such as the compressor non-dimensional speed, there is a unique value for other parameters such as the compressor pressure ratio, temperature ratio, and non-dimensional mass flow. If these parameters are now plotted against compressor non-dimensional speed, we should obtain a unique line. The reason why these unique lines are obtained is because gas turbines behave non-dimensionally. Figure 8.30 shows such an example for the compressor inlet non-dimensional flow varying with compressor non-dimensional speed. Similar figures can be drawn for other parameters for each engine component such as compressors and turbines. Power and fuel flow can also be written in non-dimensional terms and these terms may be derived from the non-dimensional steady flow energy equation. The non-dimensional terms for power and fuel flow are Power/($P_1\sqrt{T_1}$) and Fuel flow/($P\sqrt{T_1}$), respectively.

8.7.1 Correction of data to standard conditions

Gas turbine performance is very sensitive to ambient conditions. Operators often require the engine performance at some standard atmospheric conditions

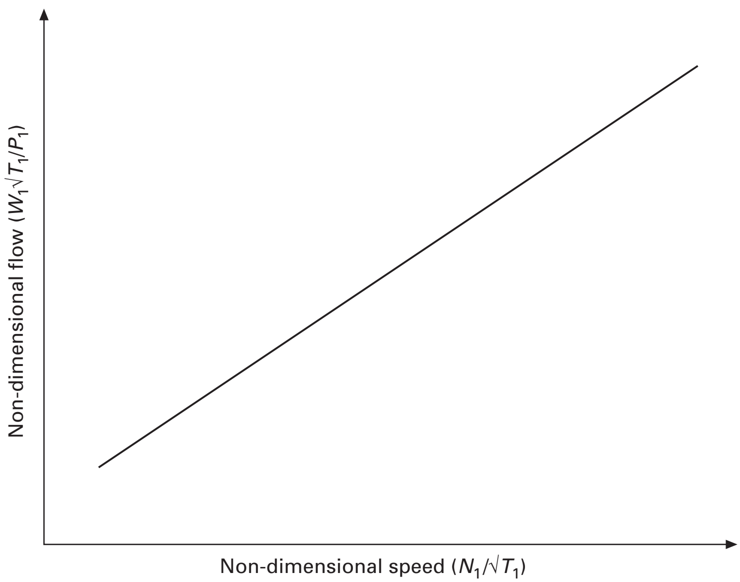

8.30 Variation of a compressor inlet non-dimensional flow with speed due to the non-dimensional nature of gas turbines.

so that the performance of different engines may be compared. Standard conditions normally refer to 1 standard atmosphere, usually 1.013 Bar, and 288.15 K or 15 degrees Celsius (also referred to as ISO conditions). However, for gas turbines operating in tropical environments, we have to correct the engine performance to an ambient temperature of 30 degrees Celsius. In Nordic countries, the average ambient temperature would be 0 degrees Celsius to give a more meaningful performance of the gas turbine.

The correction of data to these standard conditions is achieved by equating the respective non-dimensional parameters at the two different operating conditions. For example, when correcting power to standard conditions the non-dimensional power at the actual condition is equated to that of the standard condition as follows.

$$\frac{\text{Pow}}{P_1\sqrt{T_1}} = \frac{\text{PowCor}}{P_1\text{Cor}\sqrt{T_1\text{Cor}}}$$

thus

$$\text{PowCor} = \frac{\text{Pow}}{P_1\sqrt{T_1}} \times P_1\text{Cor}\sqrt{T_1\text{Cor}}$$

where Pow, T_1 and P_1 correspond to the actual power and ambient conditions and PowCor, T_1Cor and P_1Cor correspond to the standard ambient conditions. Similarly, we can correct fuel flow, airflow, speeds and other engine parameters such as pressures and temperatures to standard conditions by equating their respective non-dimensional parameters.

In fact, the corrected value for power may be determined directly using corrected parameters and corresponds to $\dfrac{\text{PowCor}}{\delta\sqrt{\theta}}$

where $\delta = \dfrac{P_1}{P_1\text{cor}}$ and $\theta = \dfrac{T_1}{T_1\text{cor}}$.

Similarly, corrected compressor flow, W_1Cor and speed, N_1Cor are determined by:

$$\frac{W_1\text{Cor}\sqrt{\theta}}{\delta} \text{ and } \frac{N_1\text{Cor}}{\sqrt{\theta}}$$

respectively. More information on non-dimensional groups may be found in Walsh and Fletcher.[6]

8.8 Power turbine curves

Power turbines are used to drive various loads. In power generation applications the power turbine (and generator) will run at a synchronous (mechanical) speed independent of the power output, whereas in mechanical drive applications, the power turbine runs at different speeds depending on the load, which is determined by the process conditions. However, the performance of the power turbine is not entirely determined by the mechanical speed but also by its non-dimensional speed, which is dependent on the power turbine inlet temperature and pressure ratio. Thus, the non-dimensional speed will vary with load even in power generation applications where the mechanical speed of the power turbine remains constant. However, operators often require such data in terms of mechanical speed rather than in terms of non-dimensional speed because it is easier to relate such data to their process conditions.

This is achieved by plotting the power turbine power output with speed for a series of gas generator speeds, as illustrated in Fig. 8.31. This shows the variation of power output with power turbine speed for a range of gas generator speeds and is normally drawn for ISO conditions. For a three-shaft engine operating with a free power turbine, the curves is drawn for a series of LP spool speeds.

For a given gas generator speed, there is a region where the power output increases with power turbine speed. This increase is primarily due to an increase in power turbine efficiency. Often, operators are concerned with the maximum power available from the gas turbine at various ambient temperatures. The above figure can be represented in terms of ambient temperature. Lines of constant gas generator speeds are shown in Fig. 8.31 and can be replaced by lines of constant ambient temperatures while maintaining the mechanical speed of the gas generator at 100%. It should be noted that each constant temperature line also corresponds to a particular compressor non-dimensional

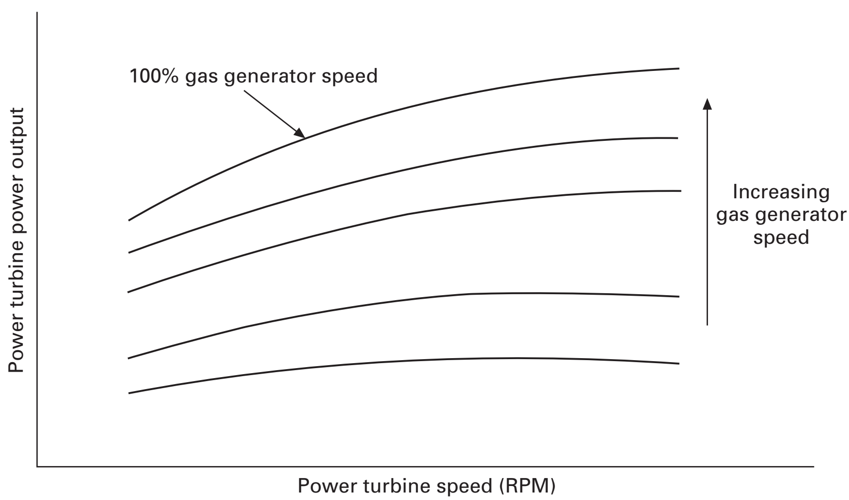

8.31 Variation of power turbine power output with power turbine speed for a series of gas generator speeds.

speed, although the mechanical speed of the gas generator remains at 100%, as illustrated in Fig. 8.32.

With aero-derived gas turbines, one manufacturer may build the gas generator while another, normally a package provider, will provide the power turbine. Providing the power turbine swallowing capacity matches that specified by the gas generator manufacturer, the performance of the gas generator should not be compromised. Having selected a gas generator, the user may consider various power turbines by comparing their performance as shown in Figures 8.31 and 8.32. The variations of thermal efficiency with power turbine speed can also be illustrated and will be similar in shape to the curves shown in Figures 8.31 and 8.32.

8.9 Gas power and gas thermal efficiency

Means of comparing the performance of power turbines have been discussed. The performance of gas generators may be compared by comparing the gas powers generated. The gas power is calculated by assuming that the expansion through the power turbine is isentropic (i.e. that the power turbine efficiency is 100%). The thermal efficiency of the gas generator is referred to as the gas thermal efficiency and is calculated from the gas power, thus enabling comparison of the performance of different gas generators. The comparison of gas generator performance may be carried out at various ambient temperatures and pressures, which the user is more likely to encounter during

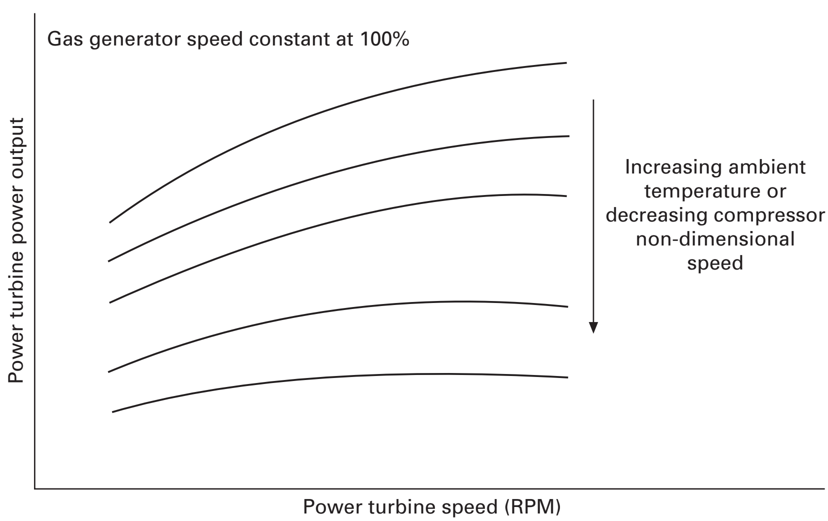

8.32 Variation of power turbine output with power turbine speed for a series of ambient temperatures.

operation rather than at ISO conditions. These are therefore more useful and are often referred to as site-rated conditions.

8.10 Heat rate and specific fuel consumption

The thermal efficiency of the gas turbine has been defined as the work done per unit input of heat. However, operators on occasions require the amount of heat per unit of work done and this is referred to as the heat rate of the engine. Thus, the heat rate is simply the reciprocal or the inverse of the thermal efficiency and is usually quoted in kJ of heat per kW hour. Thus the heat rate (HR) is given by:

$$\mathrm{HR} = \frac{3600}{\eta_{\mathrm{th}}} \quad [8.15]$$

where η_{th} is the thermal efficiency

An alternative means to determine the heat input per unit of work done is to express the heat input in terms of fuel consumption. This is referred to as the specific fuel consumption or SFC. It is usually quoted as kg of fuel per kW hour and is given by:

$$\mathrm{SFC} = \frac{3600}{\eta_{\mathrm{th}} \times Q_{\mathrm{net}}} \quad [8.16]$$

where Q_{net} is the lower heating value (LHV) of the fuel.

It is evident from Equations 8.15 and 8.16 that the heat rate and specific fuel consumption are related via the LHV of the fuel. Thus the heat rate can be expressed as:

$$\mathrm{HR} = \mathrm{SFC} \times Q_{\mathrm{net}} \quad [8.17]$$

8.11 References

1. *Gas Turbine Theory*, 5th Edition, Saravanamuttoo, H.I.H., Rogers, C.F.G., Cohen, H., Longman (2001).
2. Effect of variable-position inlet guide vane and inter-stage bleed on compressor performance of a high-pressure-ratio turbo jet engine. Huntly, S.C. and Braithwait, W.N, *NACA Research Memorandum*, December 1956.
3. The variable geometry power turbine. Ranhk, W.A., *Trans. SAE* (1969).
4. The performance of vehicular gas turbines, Bareau, D.E., *Trans. SAE* (1970).
5. The General Motors Research GT-309 gas turbine, Turunen, W.A. and Collman, J.S., *SAE Trans.*, 740[iv]. (1965), pp. 337–77.
6. *Gas Turbine Performance*, 2nd Edition, Walsh, P.P. and Fletcher, P., Blackwell Publishing (2004).

9

Gas turbine performance deterioration

Earlier chapters described the matching of engine component characteristics, namely compressors, combustors and turbines in determining gas turbine performance. In fact, it is the interaction of engine components that determines engine parameters such as pressures, temperatures, flows, speeds and power outputs. Any engine performance deterioration results from a change in the component characteristic of the deteriorated components. The interaction of these deteriorated characteristics results in a loss of power output and thermal efficiency. The measurable parameters such as pressures, temperatures, flows and speeds will also change for a given engine operating condition and the effect of performance deterioration is summarised in Fig. 9.1. Useful discussions are found in Ping and Saravanamuttoo[1] and Urban.[2]

The following conditions are typical causes of gas turbine performance deterioration:

- fouling
- variable inlet guide vane and variable stator vane problems

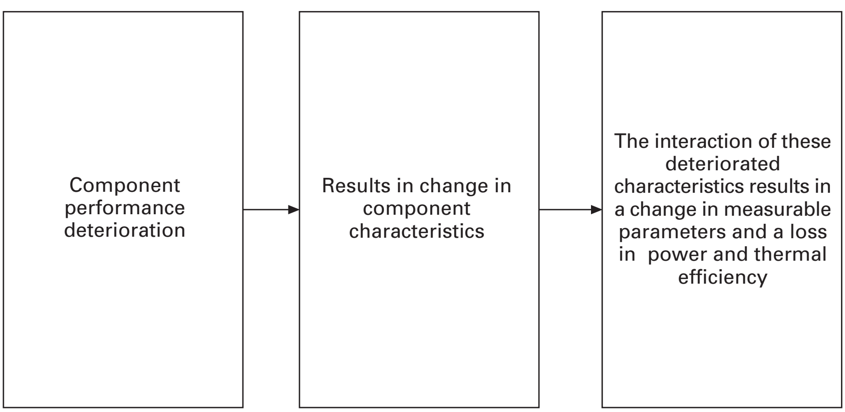

9.1 Effect of component performance deterioration on engine performance.

- hot end damage
- tip rubs
- vibration
- seal wear and damage
- foreign object damage (FOD) and domestic object damage (DOD)
- erosion
- corrosion
- control system malfunction.

A good general discussion on the causes and consequences of component performance deterioration on overall engine performance is given in Saravanamuttoo *et al*.[3]

9.1 Compressor fouling

Compressor fouling is probably the most common cause of performance deterioration. Compressor fouling results from the ingestion of dirt, dust, pollen, sap and general airborne debris. Filtration can only arrest fouling but cannot prevent it. Compressor fouling affects both compressor flow capacity and efficiency, but the effect on flow capacity is usually greater. The effect of fouling on the possible change in the compressor blade profile is shown in Fig. 9.2. The build-up of deposits will reduce the flow area, thus reducing the flow coefficient, and the change in blade profile will increase the tendency for the flow to separate, reducing the efficiency of the compressor.

The change in the compressor flow characteristic due to fouling is shown in Fig. 9.3 where the lines of constant non-dimensional speeds are shifted to the left, thus reducing the flow capacity of the compressor. Figure 9.4 shows the impact of fouling on compressor efficiency. Compressor fouling affects all stages; however, the biggest impact is on the front stages of the compressor. At normal operating speeds (high speeds), the compressor flow is controlled by the front stages of the compressor, thus fouling reduces the compressor flow capacity. However, at low compressor speeds, the choking of the HP

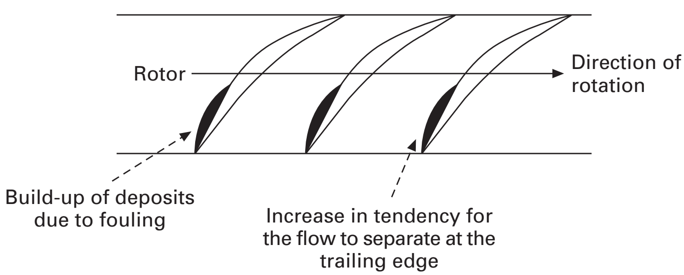

9.2 Build-up of deposits on the compressor blade profile during compressor fouling.

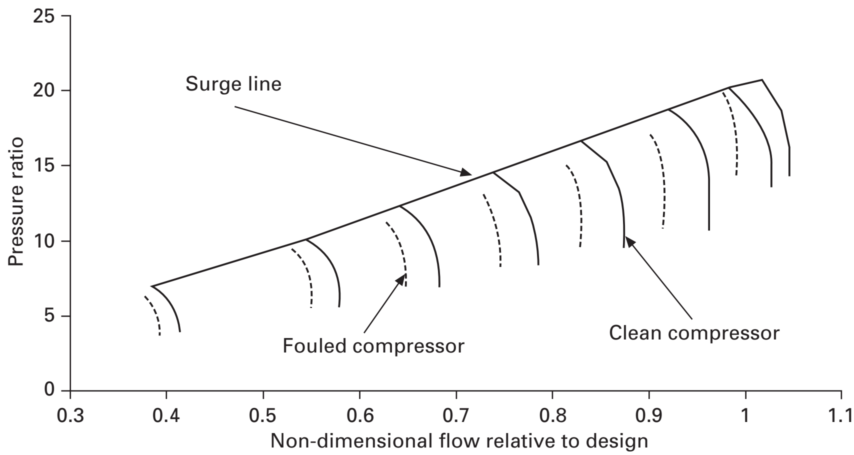

9.3 Impact of compressor fouling on the compressor flow characteristic.

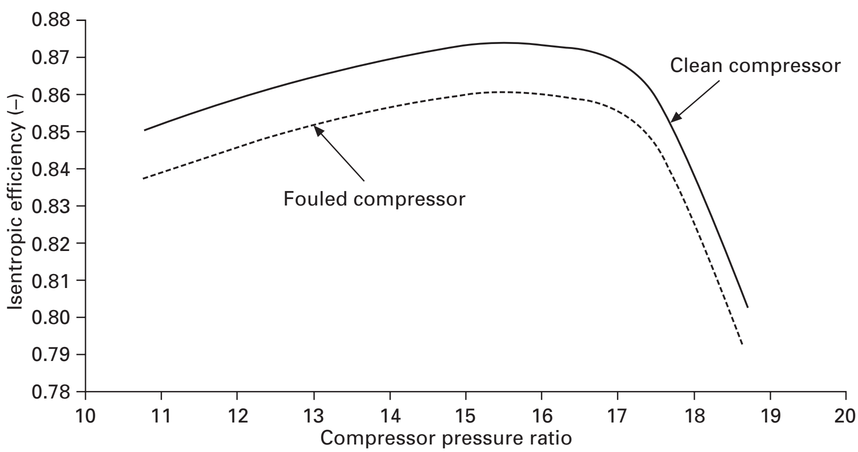

9.4 Effect of compressor fouling on the compressor efficiency characteristic for a given compressor non-dimensional speed.

stages normally controls the flow through the compressor where fouling is minimal. No change in the compressor flow characteristic will therefore be observed at these low speeds. Such low speed operation is usually at engine idle conditions and is of little importance. It is the high-speed part of the compressor characteristic that is important, as it is here that the engine spends most of its operating time and fouling effects are greatest. An excellent description of the effects of fouling on the compressor characteristic using computer simulations is given in Saravanamutoo and Lakshmiranasimha.[4]

In Section 8.2, under the heading ‘Variable stator vanes and inlet guide vanes (compressors)' the impact of improved compressor efficiency on the running line was discussed. It was shown that an improvement in the compressor efficiency moves the running line on the compressor characteristic away from surge (two-shaft gas turbine operating with a free-power turbine). When compressors foul, there is a loss of compressor efficiency, thus shifting the running line towards surge and reducing the surge margin, as illustrated in Fig. 9.5.

Since the change or reduction in flow capacity is usually greater than the effect on compressor efficiency, the compressor pressure ratio decreases with compressor fouling for a given compressor non-dimensional speed and this situation is illustrated in Fig. 9.6.

Although measuring the change in compressor pressure ratio with compressor non-dimensional speed gives an indication of compressor fouling, care is necessary as other performance-related faults can also influence the change in compressor ratio with non-dimensional speed. For instance, any change in the turbine areas can also give rise to a displacement in the running line and thus alter the relationship between the compressor pressure ratio and its non-dimensional speed. This has been illustrated in Section 8.2 'Displacement of running line (two-shaft gas turbine)'.

A better indication of compressor fouling can be obtained by plotting the variation of compressor non-dimensional speed with compressor inlet non-dimensional flow. The variation of the compressor non-dimensional speed

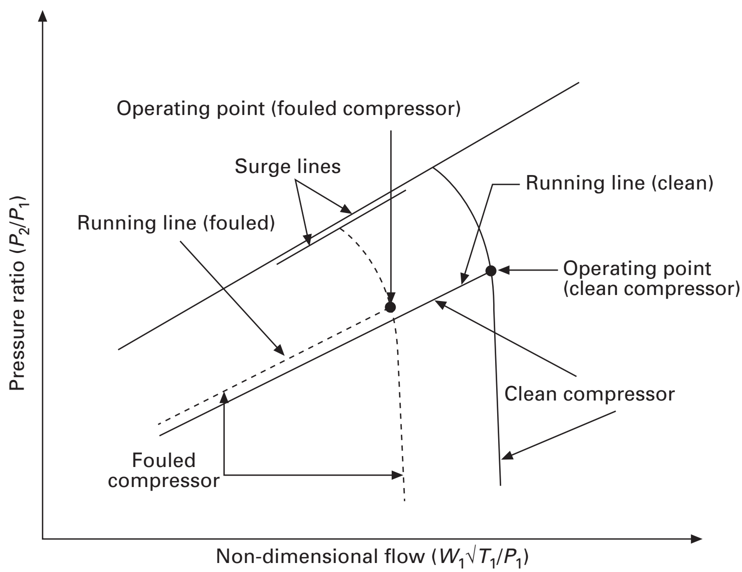

9.5 Effect of compressor fouling on the running line and operating point for a given compressor non-dimensional speed.

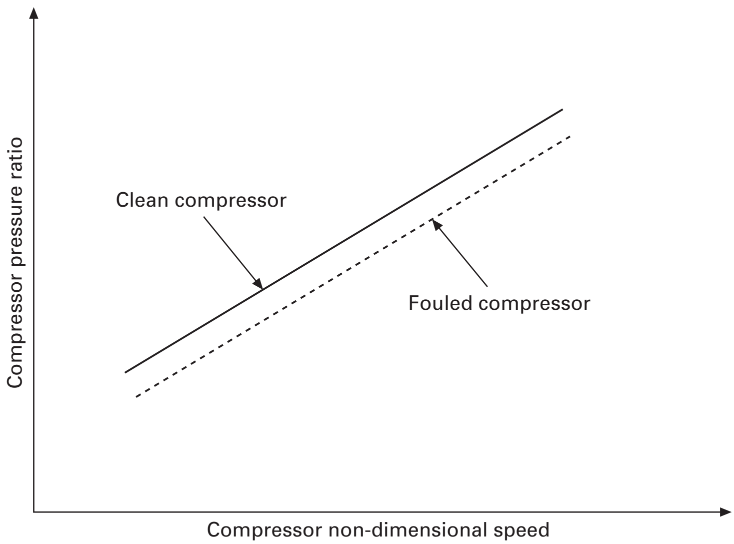

9.6 Effect of compressor fouling on compressor pressure ratio.

with inlet non-dimensional flow remains unaffected by other performance-related faults and is due to the steep flow line for a given non-dimensional speed. However, a measurement of the compressor flow is required and the accurate measurement of the compressor inlet flow on engines operating out in the field has yet to be achieved. The use of inlet depression measurements as an indication of compressor flow has been used by Diakunchak[5] to detect compressor fouling. Figure 9.7 shows the variation of non-dimensional flow with non-dimensional speed due to compressor fouling.

Performance deterioration due to compressor fouling is often recoverable after a compressor wash. The factors that determine when it is economical to wash the compressor are many. They include power demand, fuel cost, downtime for wash (and may include emissions taxes, e.g. CO_2). It is necessary to determine accurately the cost of compressor fouling, i.e. loss in power and increased heat rate, which can then determine the increase in operating cost (fuel cost) and lost revenue. A general strategy is to increase the wash frequency when power demand is high and decrease it at low power demands because, at low power demands, no loss in production should occur because the engine is not on a power limit under low power conditions. However, there will be an increase in fuel cost, but in applications where fuel cost is low or even zero, such as in oil and gas exploration and production, washes may be delayed significantly. Should emissions taxes be imposed, particularly on CO_2 emissions, the fuel cost in these industries will no longer be insignificant and optimising compressor washes will be of paramount importance. Online washing seems to be an effective method in combating fouling, but there are

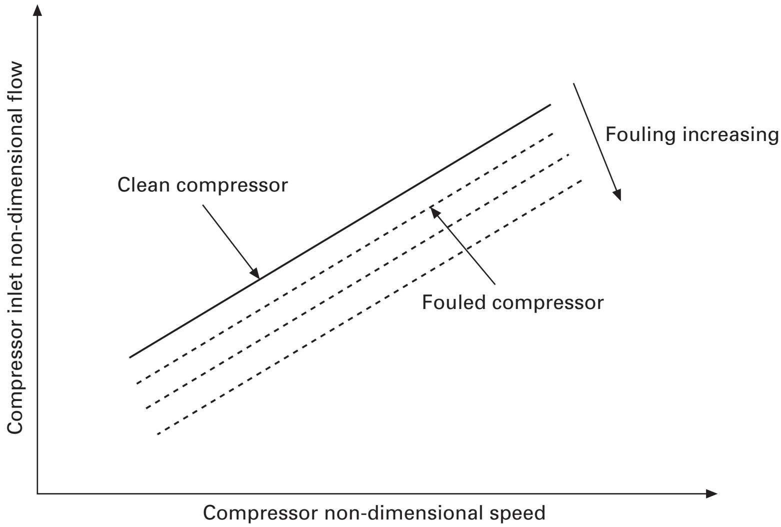

9.7 Variation of compressor inlet non-dimensional flow with compressor speed due to fouling.

many cases where online washing has done severe damage to compressor blades. However, current manufacturers of online wash systems claim they have resolved these issues. Details on the benefits of wash procedures are discussed in Meher-Homji[6] and methods to optimise compressor washing are discussed in Section 9.5.5.

9.2 Variable inlet guide vane (VIGV) and variable stator vane (VSV) problems

Multi-shaft free turbine gas turbines operating at high-pressure ratios often use variable inlet guide vanes and variable stators to ensure satisfactory and safe operation of the compressor, particularly at low speeds. The positions of the VIGV and VSV are normally functions of the compressor non-dimensional speed and Figure 9.8 shows the variation of the VIGV/VSV angle with non-dimensional speed. A region where operation is not possible is also shown, as compressor surge is very likely in this region. Any deviation of the operating point from the operating line (during steady-state operation) would imply a fault with the VIGV/VSV system.

In Section 4.10.3 under variable geometry compressors, the effect of VIGV and VSV on the compressor characteristic has been discussed. Closure of the VIGV will result in the non-dimensional flow decreasing and improving the surge margin. Thus, excessive closure of the VIGV/VSV will result in

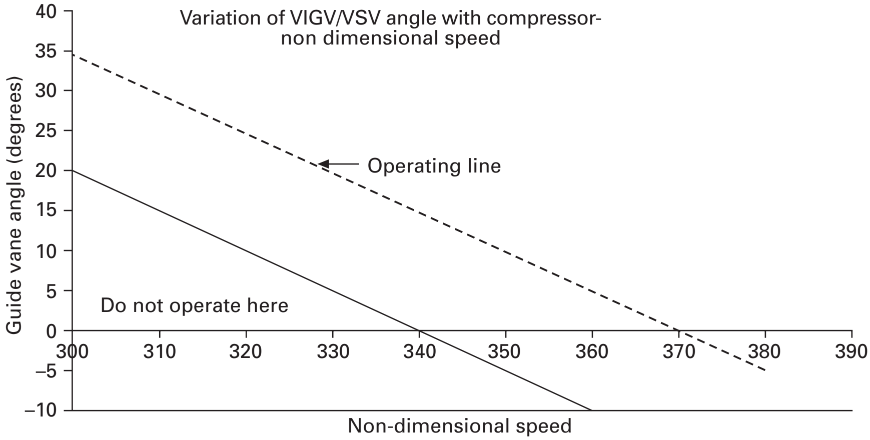

9.8 Variation of VIGV/VSV angle with compressor inlet non-dimensional speed.

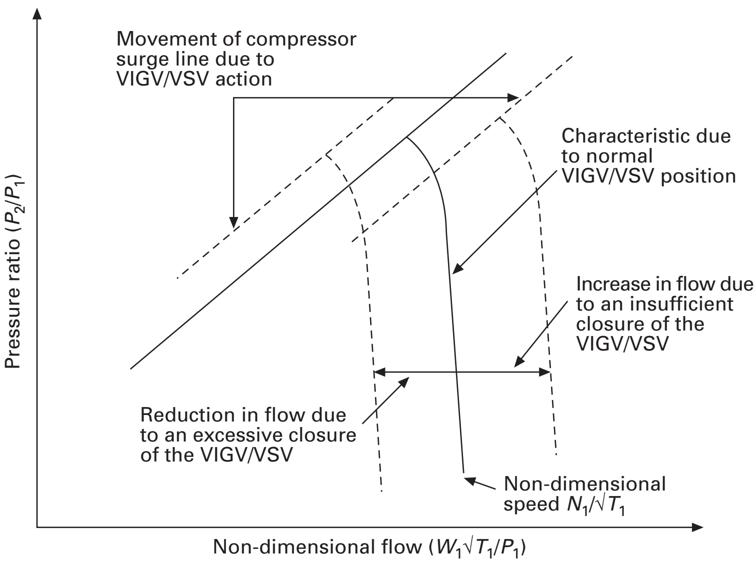

9.9 Effect of VIGV/VSV movement on the compressor characteristic.

the compressor behaving as if it is fouled. This is illustrated in Fig. 9.9, showing the effect of VIGV/VSV closure on the compressor characteristic. Thus, the variation of compressor non-dimensional flow with its non-dimensional speed will be similar to that shown in Fig. 9.7. However, compressor washing would have no effect on the displacement of this running line. The effect of excessive VIGV closure on compressor flow capacity has been investigated and described in Razak and Dosanjh.[7] If the VIGV/VSV is opened excessively, then the running line will move above the baseline in Fig. 9.7, where the baseline is shown as a bold line (clean compressors). Excessive opening of the VIGV/VSV is rather more serious, as the surge line may drift towards the running line and thereby increase the likelihood of compressor surge. The influence of VIGV/VSV on the compressor characteristic is also discussed in Muir *et al.*[8]

9.3 Hot end damage

Hot end damage is normally associated with turbines. Turbines operate at very high gas temperatures, often above the melting point of the turbine blade material. Extensive turbine cooling is therefore employed (as discussed in Section 5.7) to achieve satisfactory turbine creep life. The highest temperatures that occur are at the stagnation points which correspond to the leading and trailing edges of the turbine blade. The trailing edge of the turbine blade has little material and cooling is often difficult; thus, over a period of time, damage can occur to this part of the turbine blade. The flow capacity of the turbine is normally controlled by the nozzle guide vane (NGV) and is determined by the flow area defined by the trailing edge of the blade. Any change in the turbine blade profile involving the trailing edge of the blade will also have an impact on the turbine characteristic and thus on the performance of the engine.

Hot end damage will normally increase the turbine non-dimensional flow capacity and any change in the incidence of the gas on the turbine rotor will also affect its efficiency. Figure 9.10 shows a schematic representation of the nozzle guide vane, indicating trailing edge damage. The increase in turbine flow capacity does not reduce turbine performance necessarily. Under certain circumstances, for example, when the gas generator speed limits the power output of the gas turbine, an increase in power output is possible; however, an adverse impact on turbine life would occur. A reduction in turbine efficiency will always have a negative impact on the gas turbine performance and

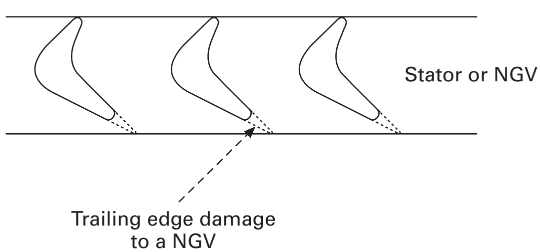

9.10 Change in the NGV profile due to hot end damage.

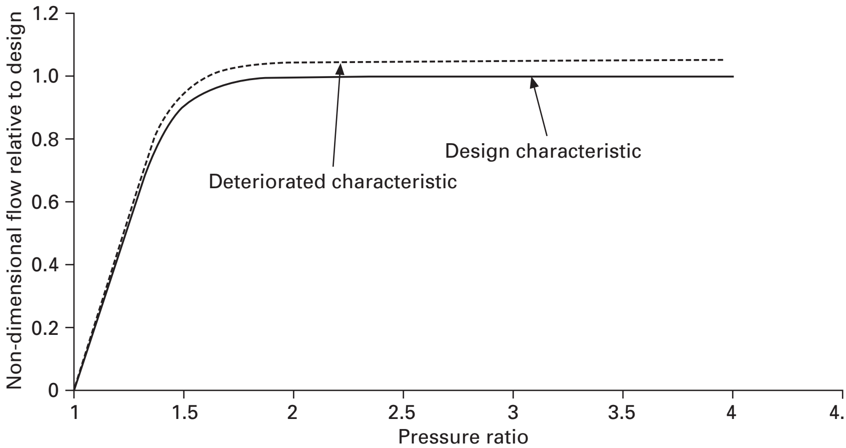

9.11 Effect of hot end damage on the turbine flow characteristic.

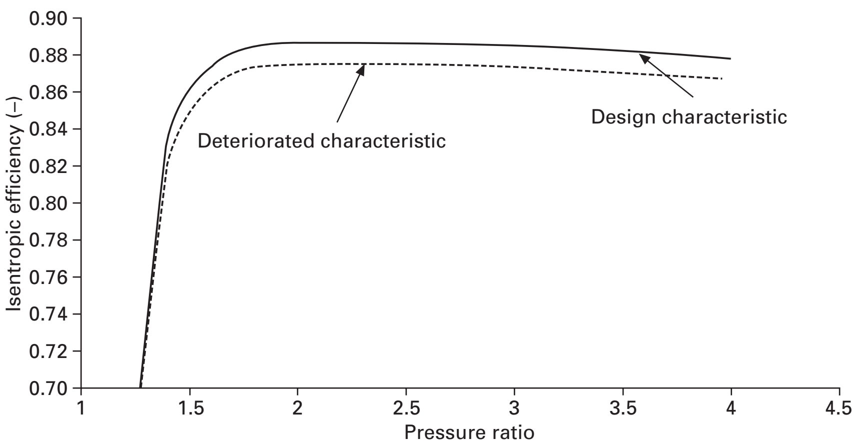

9.12 Effect of hot end damage on the turbine efficiency characteristic.

engine life. Figures 9.11 and 9.12 show the changes in the turbine flow and efficiency characteristics due to hot end damage, respectively.

The effect of hot end damage on the gas generator turbine of a two-shaft gas turbine (using a free power turbine) would be to move the running line away from surge, as discussed in Section 8.2, 'Displacement of running line (single- and two-shaft free power turbine gas turbine'. Thus, the variation of compressor pressure ratio with compressor non-dimensional speed would be similar to that observed during compressor fouling. Gas turbines that burn fuel containing high ash content may suffer from a reduction in the turbine flow capacity due to deposit of ash on the turbine components, and the variation of compressor pressure ratio with compressor non-dimensional speed will be the opposite to that due to hot end damage of the turbine. Regular cleaning of the turbine would be required to maintain the performance of the gas turbine. Means to detect turbine fouling can be developed where the variation of the turbine non-dimensional flow with its pressure ratio is plotted, as shown in Fig. 9.11.

9.4 Tip rubs and seal damage

The clearances between the rotor and the casing in turbomachinery should be kept to a minimum in order to minimise overtip leakages. In axial compressors, the stage pressure ratios are small compared with axial turbines. Thus, turbine rotors are usually provided with tip seals, in the form of a shroud to prevent such overtip leakages. Compressors normally do not have such shrouds; however, the clearances are kept to a minimum.

During normal operation, rubs occur during start-up and also, possibly, due to high vibration. Operation over a period of time will also increase these clearances due to wear. In axial compressors, an increase in tip clearance of the front stages would result in a change in both compressor flow capacity and efficiency, as it is the front stages of the compressor that control the flow. Increases in clearance of the HP stages of an axial compressor normally affect the compressor efficiency rather than the flow capacity. Thus, the change in capacity characteristic of the compressor due to front stages rubbing is similar to that of compressor fouling. However, unlike compressor fouling, this performance loss is not recoverable after an engine wash.

The effect of damage to the turbine shroud normally affects the efficiency of the turbine rather than the flow and this is mainly due to the flow capacity of the turbine being set by the choking of the nozzle guide vanes. Other seals are also provided in compressors and turbines to prevent or reduce internal leakages. One type of seal is called a labyrinth seal, which consists of knife-edges on a static or rotating component of the turbine or compressor assembly, as illustrated in Fig. 9.13. Other types of seals are honeycomb seals and ring seals. Damage to these seals normally affects the compressor/turbine efficiency rather than the flow capacity.

9.5 Quantifying performance deterioration and diagnosing faults

The above discusses performance deterioration in a qualitative manner and means to detect performance deterioration. However, we require methods to quantify performance deterioration. Such information is required on a component level basis. Additionally, since performance deterioration adversely affects gas turbine power output and heat rate/thermal efficiency, the impact of any performance deterioration on these performance parameters is also

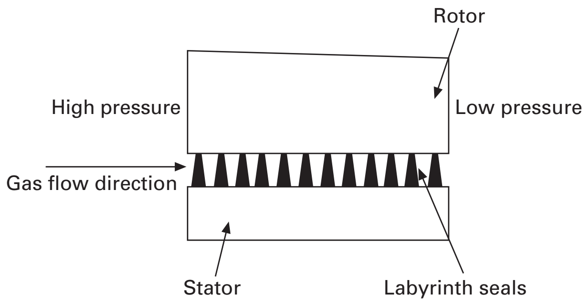

9.13 Schematic representation of a labyrinth seal arrangement.

required. It was stated at the beginning of this chapter that performance deterioration results from the change in component characteristics, namely compressors and turbines, as shown in Figs 9.3, 9.4 for compressors and Figs 9.11 and 9.12 for turbines. It was also stated that measurable parameters such as pressures, temperatures, flows and speeds are determined by the interaction of engine components and when performance deterioration occurs the change in these component characteristics results in the change in the measurable parameters, as summarised in Fig. 9.1. A performance-related fault can therefore be defined as a change in the component characteristic.

9.5.1 Fault indices

Fault indices are means of determining the deteriorated component characteristics. They represent the percentage change of the undeteriorated characteristic. Two fault indices can be defined for any component and they correspond to the fouling and efficiency fault index. For example, the fouled compressor flow characteristic, as shown in Fig. 9.3 is determined by reducing the compressor non-dimensional flow for any given non-dimensional speed line by 3%, and the deteriorated compressor efficiency characteristic shown in Fig. 9.4 is obtained by reducing the compressor isentropic efficiency for any given speed line by 1%. Thus, for a fouled compressor, the compressor fouling fault index and the compressor efficiency fault index is –3% and –1%, respectively, for this case.

Similarly, fault indices can be used to determine deteriorated turbine characteristics and these fault indices correspond to the turbine fouling fault index and turbine efficiency fault index. The deteriorated turbine characteristics shown in Figs 9.11 and 9.12 are obtained by applying a turbine fouling fault index of 3% and a turbine efficiency fault index of –1%, respectively.

9.5.2 Quantifying performance deterioration

Fault indices are quite powerful in quantifying performance deterioration as they provide a means of determining the deteriorated component characteristic. As a result, they also detect and quantify performance deterioration on a component by component basis. Thus, one of the objectives in performance monitoring and diagnostics is achieved by the use of fault indices. Since fault indices give us the deteriorated component characteristic, the engine model with deteriorated component characteristics can now be used to evaluate the loss in power output and increase in heat rate due to performance deterioration and therefore achieve the second objective of performance monitoring and diagnostics.

To determine fault indices, we need to be armed with an engine model representing the undeteriorated gas turbine that we wish to monitor. The model can be a steady-state model, built using the methods discussed in Chapter 7. In this event the measured data should also correspond to steady-state conditions. This can be achieved by filtering the measured data as done by Teukolsky *et al.*[9] and by Dole.[10] The engine model is run at the current operating conditions of the gas turbine and the measured data is compared with corresponding data determined by the model (expected or predicted measured values). If they do not match, fault indices are used to alter the component characteristics until they match. At the end of this iterative or implicit process, all the component fault indices are determined. This process for a single-shaft gas turbine is summarised in Fig. 9.14. The measurements required for a single-shaft gas turbine are as follows:

(1) compressor inlet temperature
(2) compressor inlet pressure
(3) compressor exit temperature
(4) compressor exit pressure
(5) turbine exit temperature (exhaust gas temperature, EGT)
(6) turbine exit pressure
(7) fuel flow
(8) gas turbine speed
(9) gas turbine power output
(10) variable inlet guide vane/variable stator vane position if applicable.

Single shaft gas turbines are often used in power generation and the gas turbine power output can be determined from the generator output. The total number of fault indices is four and they correspond to the compressor fouling and efficiency fault indices and to the turbine fouling and efficiency fault indices.

A similar approach can be used to determine the fault indices for other engine configurations discussed earlier. For a two-shaft gas turbine operating with a free power turbine the required measurements are:

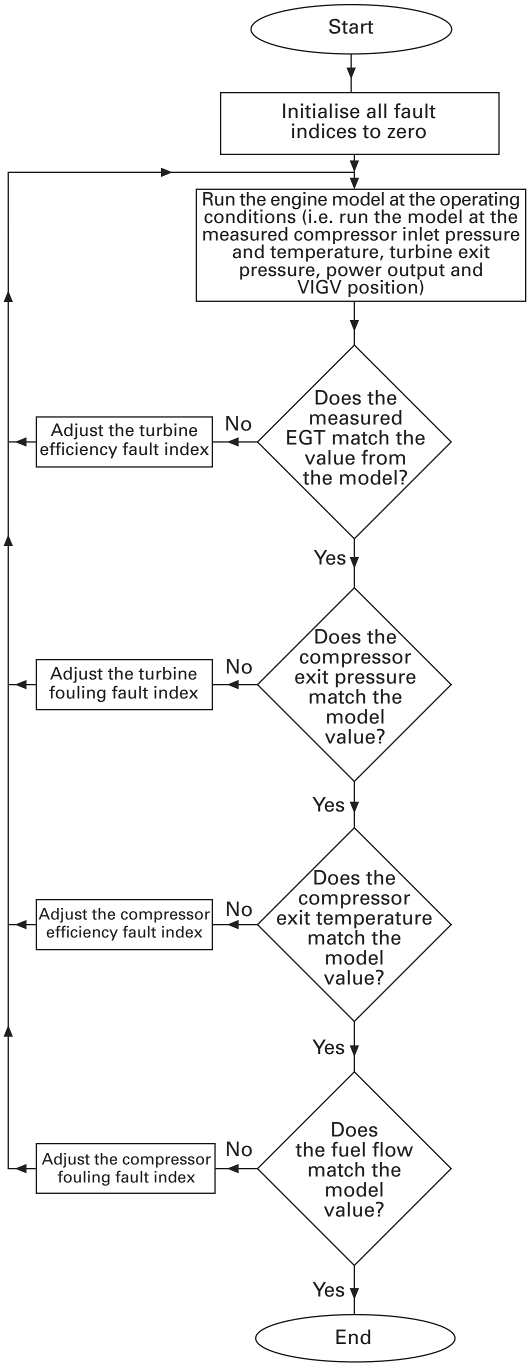

9.14 Procedure to determine fault indices by comparing the engine measured parameters with those obtained from the model.

(1) gas generator compressor inlet temperature
(2) gas generator compressor inlet pressure
(3) gas generator compressor exit temperature
(4) gas generator compressor exit pressure
(5) gas generator turbine exit temperature (EGT)
(6) gas generator turbine exit pressure
(7) power turbine exit temperature
(8) power turbine exit pressure
(9) fuel flow
(10) gas generator speed
(11) power turbine speed.

Note the absence of the power measurement for the case of the two-shaft gas turbine described above. Six fault indices can now be determined for a two-shaft gas turbine operating with a free power turbine. They correspond to the gas generator compressor fouling and efficiency fault index; gas generator turbine fouling and efficiency fault index; and the power turbine fouling and efficiency fault index.

The measurement of specific humidity should also be included, particularly at high ambient temperatures where the change in specific humidity with relative humidity is significant. As discussed in Chapter 2 (Section 2.11.1), a change in specific humidity will have a noticeable affect on the thermodynamic properties of air and products of combustion, hence influencing the engine performance, as shown in Fig. 11.30. Further details can be found in Mathioudakis and Tsalavoutas.[11]

Fault indices can also be determined using methods such as Newton–Raphson, in a manner similar to that discussed in Section 7.4 in Chapter 7. For a single-shaft gas turbine the estimated vectors are:

(1) compressor fouling fault index
(2) compressor efficiency fault index
(3) turbine fouling fault index
(4) turbine efficiency fault index

The corresponding check vectors are:

(1) difference between the measured EGT and the model
(2) difference between the measured compressor exit pressure and the model
(3) difference between the measured compressor exit temperature and the model
(4) difference between the measured fuel flow and the model.

For a two-shaft gas turbine operating with a free power turbine, the estimated vectors are:

(1) gas generator compressor fouling index
(2) gas generator compressor efficiency index

(3) gas generator turbine fouling index
(4) gas generator turbine efficiency index
(5) power turbine fouling index
(6) power turbine efficiency index.

The corresponding checks are:

(1) difference between the measured power turbine exit temperature and the model
(2) difference between the measured gas generator exit pressure and the model
(3) difference between the measured EGT and the model
(4) difference between the measured compressor exit pressure and the model
(5) difference between the measured compressor exit temperature and the model
(6) difference between the measured fuel flow and the model.

Similar methods are discussed by Esher[12] and earlier by Stamatis, Mathioudakis and Papailiou.[13] The simulators enclosed with this book are effectively virtual gas turbines and they enable the simulation of faulty engines using fault indices. Faults can be planted and therefore measurements generated due to performance-related faults using these simulators. Thus they can be used to develop performance-monitoring systems based on the discussion above.

9.5.3 Diagnostics

Fault indices, which represent the change in component (compressor and turbine) characteristics usually due to faults, indicate a faulty engine component. In diagnostics the cause of the fault needs to be determined. A number of causes have been stated that can result in gas turbine performance deterioration in the introduction of this chapter. Diagnostics attempts to detect one or more of these causes that is responsible for the deterioration of engine performance.

Trends in fault indices are an effective means of diagnosing performance-related problems as they show changes with component characteristics in time and satisfy the third requirement of gas turbine performance monitoring systems (diagnostics). For example, compressor fouling will display a trend similar to that shown in Fig. 9.15. If the low pressure (LP) stages of the compressor have also rubbed, resulting in increased clearance between the rotor tip and the casing, the trends in compressor fault indices would be similar to those shown in Fig. 9.16. Since the LP stage of an axial compressor controls the flow capacity at normal operating speeds, any increase tip casing clearance will affect the flow capacity and efficiency adversely, as discussed in Section 9.4. The trends in compressor fouling indices will leave an offset

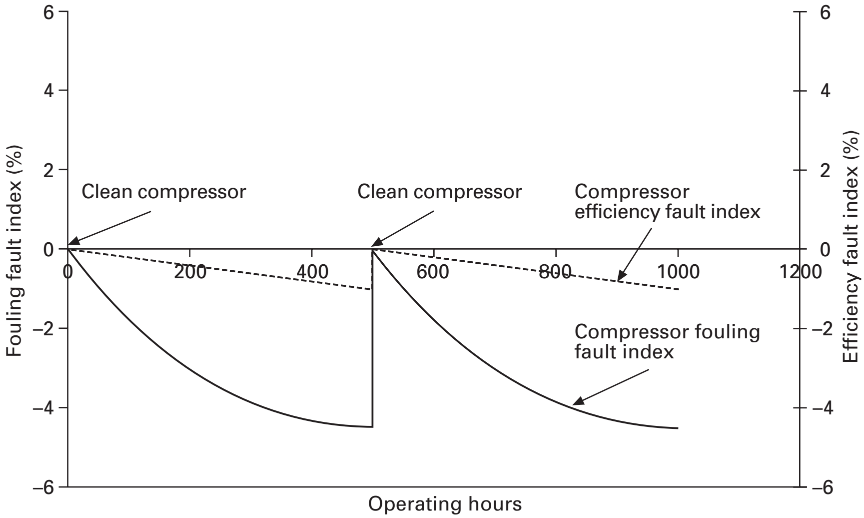

9.15 Expected trend in a compressor fault indices due to fouling only.

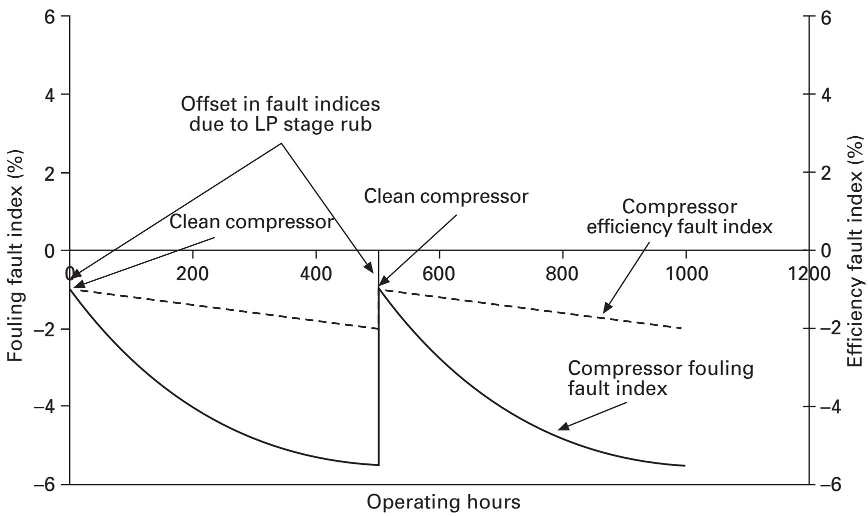

9.16 Expected trend in a compressor fault indices due to fouling and LP stage rubs.

after every wash, as shown in Fig. 9.16. Expected trends in turbine faults due to hot end damage and labyrinth seal damage are shown in Figs 9.17 and 9.18. Unlike hot end damage, labyrinth seal damage does not affect the turbine flow capacity.

In the above discussion and analysis it has been assumed that the measurements taken from the engine are correct. However, instrumentation/

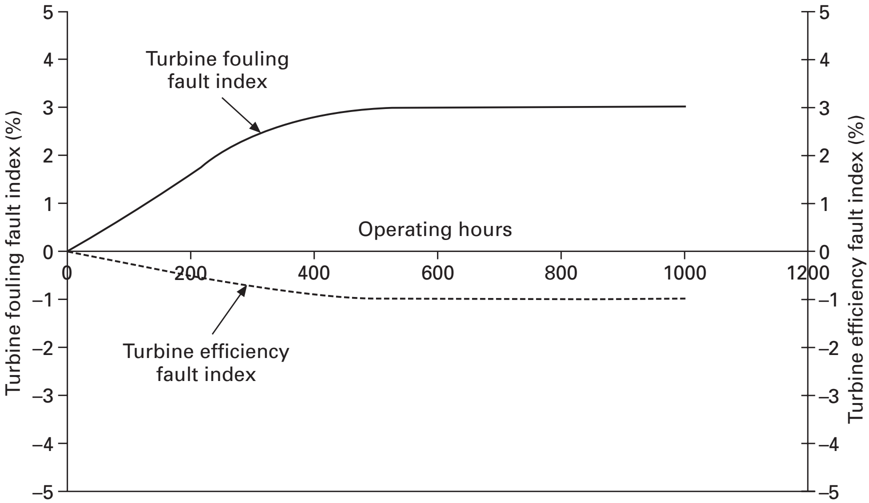

9.17 Expected trends in the turbine fault indices when hot end damage is present.

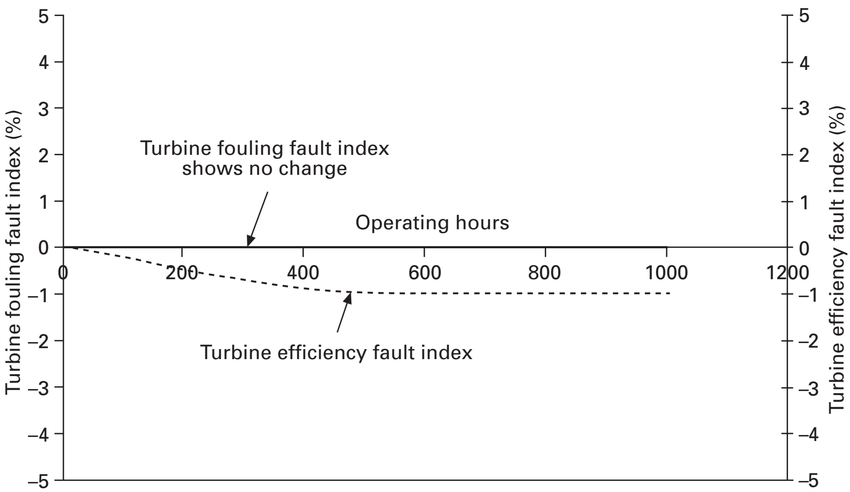

9.18 Expected trend in the turbine fault index due to tip rubs or if labyrinth seal damage is present.

measurement errors could result in incorrect diagnostics. An effective means to detect instrumentation errors is to build in instrumentation redundancy. For example, three sensors can be used to measure, say, the compressor exit pressure and compare these readings. Any significant deviation between these reading will highlight instrumentation errors.

Fault indices can also be used to detect measurement errors. When instrumentation faults are present, the values for the fault indices give rise to unreasonable values, especially where some inter-stage measurement is incorrect. For example, in a single-shaft gas turbine, if the compressor exit pressure is reading lower than expected, the non-dimensional flow into the turbine will increase while the entropy change during the expansion in the turbine will decrease. Also, the entropy change during compression will simultaneously increase. These changes, relative to the design values for flow and efficiencies, will result in an increase in the turbine fouling and efficiency fault index, while the compressor efficiency fault index decreases. Such patterns can be used to initiate an instrumentation calibration as discussed by Razak and Carlyle.[14]

9.5.4 Application of fault indices to root cause analysis (RCA)

Root cause analysis is a relatively new methodology for determining the actual cause of failures and then taking appropriate steps to prevent the occurrence of the failure. When performing root cause analysis, it is necessary to look beyond the reasons for the immediate reason for the failure. There can be many other reasons for the failure, including organisational structures and methods. To determine the root causes of failures, a significant amount of data has to be logged and analysed. The data logged will include operating conditions, events and any barriers or protection systems that have been exceeded.

It has been stated that fault indices indicate change in component characteristics due to faults, while examining the trends of fault indices gives diagnostics. Such data and information are invaluable in performing RCA, as the onset of damage and faults in gas turbines can be detected and action taken before engine failure occurs. For example, compressor fouling or seal wear shown in Figs 9.15 and 9.18 are expected during engine operation and would not normally result in engine failure. But blade rubs and hot end damage, as shown in Figs 9.16 and 9.17 are more serious. By examining such trends, action can be taken to prevent potential engine failures, therefore improving availability and profitability.

9.5.5 Compressor wash optimisation

Although we have stated that compressor fouling does not normally result in engine failure, the build-up of dirt and deposits during engine operation reduces the capacity and efficiency of the compressor as discussed. Thus a regular clean, normally by washing the compressor, is required to maintain production and profitability. If compressor washing is too frequent, the increase downtime for washing and cost will affect production adversely due to the unavailability of the engine. Infrequent washing will also reduce production and therefore profit due to the decrease in engine performance due to fouling. Thus there is a need to optimise the compressor wash frequency such that the loss in profit or revenue due to fouling and washing is minimised.

The downtime for engine washing will affect revenue directly. The cost of the wash needs to be added to this lost revenue to determine the total cost due to compressor washing. The lost revenue per annum due to engine washing will be equal to the lost revenue per engine wash, times the number of washes per annum, and will increase with wash frequency, as shown in Fig. 9.19. As stated above, compressor fouling will also reduce the revenue due to performance deterioration. This can be determined by using the compressor fault index profile (Fig. 9.15) due to fouling in conjunction with the engine model. The engine model is used to determine the loss in maximum power available and the loss in thermal efficiency at various times during fouling. The maximum power available from the engine is determined by running the model at some limiting condition such as the exhaust gas temperature (EGT) or speed limit imposed by the manufacturer. Issues on engine control limits are discussed in the next chapter, where engine control systems and the transient performance of gas turbines will be discussed. The fouling index profile, similar to that shown in Fig. 9.15, has to be determined by monitoring the compressor performance deterioration due to fouling. The lost revenue due to one fouling cycle can be used to extrapolate the lost revenue per annum due to fouling. Infrequent washing will result in increased

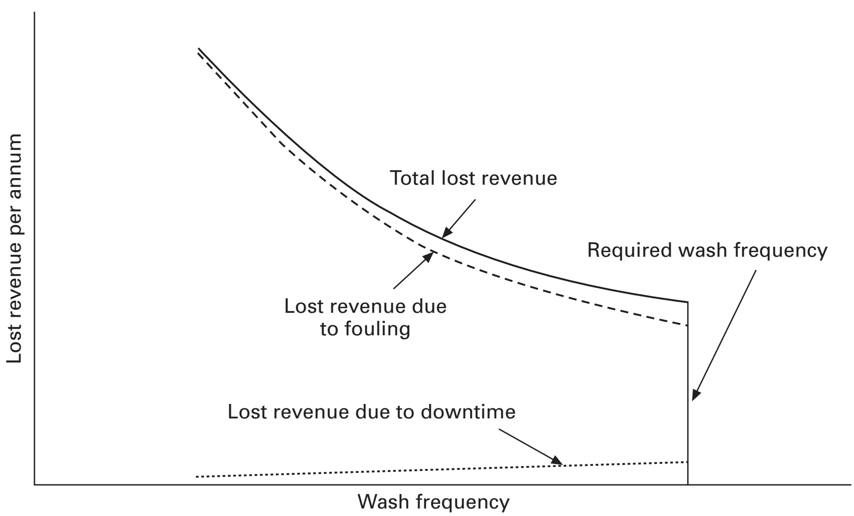

9.19 Optimised wash frequency when operating at high power.

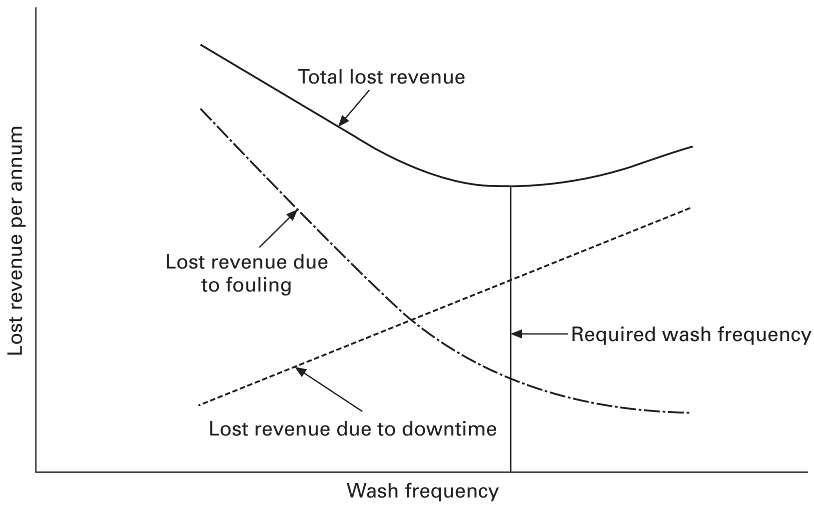

9.20 Optimised wash frequency when operating at low power.

lost revenue due to fouling, as shown in Fig. 9.19. The summation of these two sources of lost revenue will give the total lost revenue curve. The optimised wash frequency occurs when the total lost revenue is a minimum, as shown in Figs 9.19 and 9.20 for a high and low power case, respectively. Factors that influence wash frequency include the following:

- price of product (e.g. electricity unit price)
- production
- fuel cost
- emissions CO_2 taxes if applicable
- downtime and cost of wash (including the cost of disposal of wash material such as detergents).

Increase in unit price, fuel cost and emissions taxes will tend to increase the wash frequency, while increase in downtime and costs associated with the compressor wash activity will tend to reduce the wash frequency. The power demand will also influence the wash frequency. A higher power demand, where the engine has to operate near or at the engine operating limit such as the EGT, will tend to increase the wash frequency.

The method described above can be adapted to cover online wash systems. This is achieved by generating the compressor fouling profile due to online washing. It should be noted that online washing is not as effective as offline washes and the fouling fault index profile will look similar to that shown in Fig. 9.16, where there would be a small offset in the fault indices after each online wash. This offset would get progressively larger after each wash, due to residual fouling. However, there is no downtime penalty for washing and the engine availability is high. Thus, online wash frequencies would tend to be high. When the engine performance loss due to residual fouling is greater than the performance improvement due to an offline wash, then this will be an indication as to when an offline wash will be beneficial as discussed by Razak and Carlyle.[14] The benefits of online washing have yet to be clearly demonstrated and, as stated above, there have been reports of impact damage and erosion to compressor blades resulting from online washes. These effects would therefore have an effect on online wash frequency.

9.6 References

1. Ping, Z. and Saravanamuttoo, H.I.H., Simulation of an advanced twin-spool industrial gas turbine, *ASME paper 91-GT-34* (1991).
2. Urban, L.A., Gas path analysis applied to turbine engine conditioning monitoring, *AIAA/SAE paper 72-1082* (1972).
3. *Gas Turbine Theory*, 5th Edition. Saravanamuttoo, H.I.H., Rogers C.F.G. and Cohen, H., Longman (2001).
4. Saravanamutoo, H.I.H. and Lakshmiranasimha, A.N., A preliminary assessment of compressor fouling, *ASME paper 91-GT-153* (1991).
5. Diakunchak, I.S., Performance deterioration in industrial gas turbines, *ASME paper 91-GT-288* (1991).
6. Meher-Homji, C.B., Gas turbine axial compressor fouling: a unified treatment of its effects, detection and control, *International Journal of Turbo and Jet Engines*, 9, 1992, 311–34.
7. Razak, A.M.Y. and Dosanjh, M.S., Application of an advanced performance monitoring system to detect an implanted fault on a twin spool aero derived gas turbine, *ASME paper GT-2002-30022* (2002).
8. Muir, D.E., Saravanamuttoo, H.I.H. and Marshall, D.J., Health monitoring of variable geometry gas turbines for the Canadian Navy, *Transactions of ASME* pp. 244–250, April 1989.
9. *Numerical Recipes in Fortran 77*, Second Edition, Press, W.H., Teukolsky, S.A., Vetting, W.T. and Flannery, B.P., Cambridge University Press (1992).
10. Dole, D.L., Interpretation of weighted least squares gas path analysis results, *ASME Paper GT-2002-30025* (2002).
11. Mathioudakis, K. and Tsalavoutas, A., 'Uncertainty reduction in gas turbine performance diagnostics by accounting for humidity effects', ASME 2001-GT-0010, *ASME TURBO EXPO 2001*, New Orleans, Louisiana, June 2001.
12. Esher, P., Gas turbine data validation using gas path analysis, *ASME Paper GT-2002-30024* (2002).
13. Stamatis, A., Mathioudakis, K. and Papailiou, K.D., 'Adaptive simulation of gas turbine performance', *ASME Journal of Engineering for Gas Turbine and Power*, Vol. 112, No. 2, pp 168–175, 1990.
14. Razak, A.M.Y. and Carlyle, J.S., Methods, strategies and technologies to reduce total equipment ownership cost, *Aramco Conference Proceedings*, pp. 69–84, October 1997.

10
Principles of engine control systems and transient performance

The power output from a gas turbine is determined by fuel flow (thermal input), and the control system must ensure that the desired power output is achieved. However, the control system must also protect the engine from exceeding any design limits. These limits include component speeds, temperatures and operating regions which can result in compressor surge. The control strategy normally involves a set point and the control system drives the engine towards the set point. In the case of power generation, the set point will be the required power output from the generator. In mechanical drive applications such as a process compressor, the set point could be the discharge or suction pressure, compressor speed or inlet flow of the compressor. If the necessary power output or set point is not achieved, the control system will alter the fuel flow to the engine until the set point or required power is attained.

There are two groups of control systems, which are referred to as the open and closed loop control systems. In an open loop control system, the input (fuel flow) to the control system is independent of the output (generator output) and the input usually acts for a period of time after which the output is expected to have reached the required set point. In such a control system, the output seldom reaches the set point and the control system usually leaves an offset between the output and the set point.

In a closed loop control system, the offset left by the open loop control system is used as the input to the closed loop controller to generate the output. By such means, it is possible to eliminate the offset and the control system output will then correspond to the set point. In a closed loop control system the offset is converted to an error which is calculated as the percentage deviation from the set point and used as the input to the controller. For example, if the power output from the load, such as an electrical generator, is 10 MW and the set point is 15 MW, the error will be $(15 - 10)/15 \times 100 = 33.33\%$, which is used to control the fuel valves that alter the power output from the gas turbine, eventually reducing the error to zero (i.e. steady state). When the error is

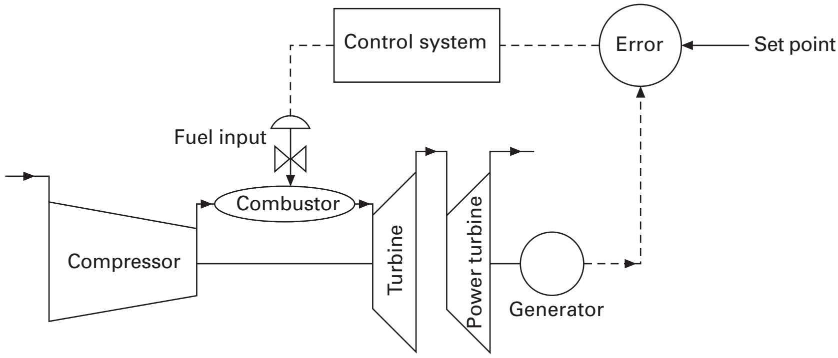

10.1 Simple gas turbine closed loop control system.

determined as a difference between the generator output and the set point as described above, the control system is said to operate as a negative feedback loop. A simple closed loop control system is shown in Fig. 10.1.

10.1 PID loop

A closed loop control system normally achieves the output using a proportional (P), integral (I) and derivative (D) action or a PID loop. Such a system is also known as a three-term controller.

10.1.1 Proportional (P) only controller

The proportional action results by producing an output which is proportional to the error plus a bias, and the output from a proportional only controller is given by Equation 10.1:

$$\mathrm{OP} = Kc \times \mathrm{err} + C \qquad [10.1]$$

where Kc is the proportional gain, err is the error between the process output (power output in this case) and the set point (which is the required power output from the gas turbine). C is the proportional bias.

The drawback of a proportional only controller is that it will leave a steady-state error known as the proportional offset, as illustrated in Fig. 10.2. The proportional offset can be eliminated by adjusting the fuel flow manually until the proportional offset (steady error) is zero.

10.1.2 Proportional and integral (PI) controller

The manual reset described above can be automated by including the integral component or action of the PID controller. The output from the integral controller is given by Equation 10.2.

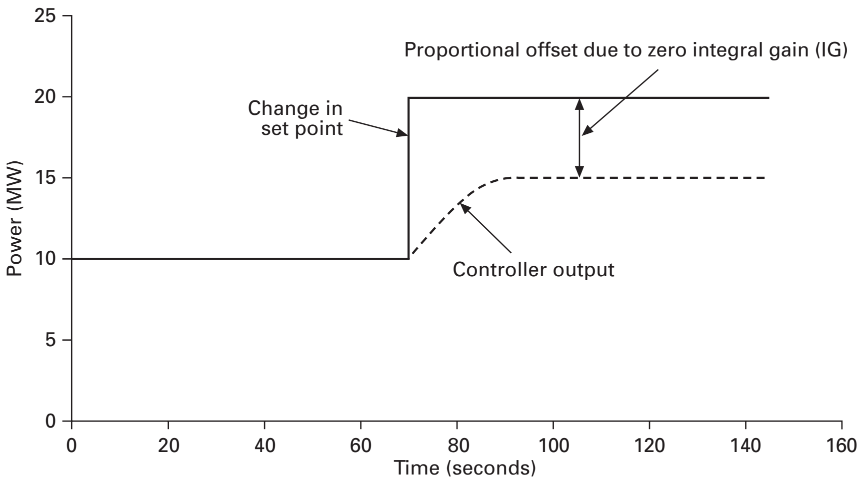

10.2 Proportional offset due to proportional action only.

$$OP = \frac{Kc}{Ti} \int err \cdot dt \qquad [10.2]$$

where *Ti* is the integral time or reset time.

The integral action occurs as a result of the error being integrated continuously or summed up. Thus, the proportional offset is eliminated when both proportional and integral control are employed and there is no need for resetting the proportional offset manually. This and is often referred to as automatic reset. The addition of integral action can also result in drawbacks and this is referred to as integral wind-up. Wind-up can occur when the conditions are such that the output from the process (in this case the gas turbine power output) is unaffected by the controller action. For example, it occurs when the fuel valve remains full open due to insufficient valve size before the power demand from the gas turbine is reached. In this event, the control system responds by increasing the integral output in an attempt to increase the fuel valve position, thus increasing the fuel flow to the engine. Since the fuel valve is fully opened, no further change in fuel flow is possible and power output from the engine remains unchanged. As long as this condition remains, the integral output will continue to increase, but with no change in the power output of the engine.

If the power demand is now reduced sufficiently (change in set point) so that the fuel valve will not be fully opened, the control system will still respond by keeping the valve fully opened because of the winding-up of the integral output. The valve will remain fully opened until the integral output has completely unwound itself before responding to the change in the set point. This rather unexpected response from the control system is referred to

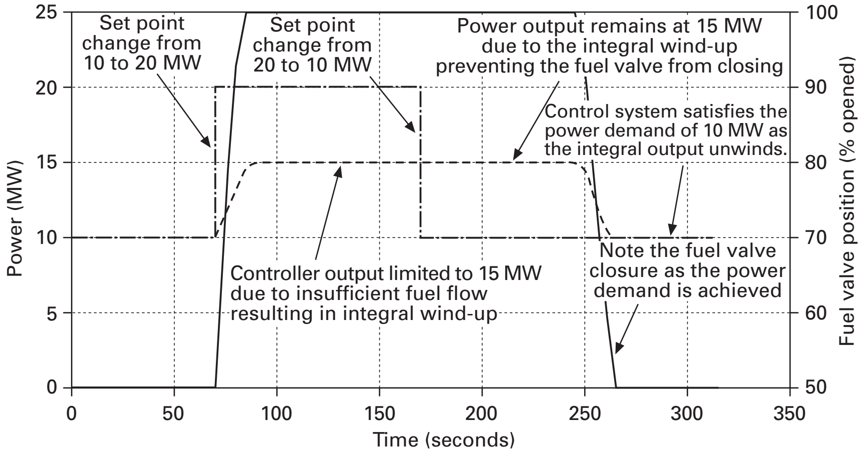

10.3 Effect of integral wind-up due to an insufficient fuel valve size.

as integral wind-up. The period of time the control system remains in this situation depends on the amount of wind-up. The means to rectify this problem are quite simple. The integral output is reset, normally to 100%, should the fuel valve reach a limiting condition such as a fully opened position. Figure 10.3 illustrates integral wind-up due to an insufficient fuel valve size.

10.1.3 Proportional, integral and derivative (PID) controller

The derivative output enhances the controller output during a transient response. It is normally used when the response of the system is very slow (e.g. furnaces), but is often omitted in gas turbine control systems. It should be noted that derivative control produces no action when a steady-state error occurs due to the proportional offset or integral wind-up, as the rate of change of the error under these conditions will be zero. The PID loop controller may be written as:

$$\mathrm{OP} = \mathrm{err} \times Kc + \frac{Kc}{Ti}\int \mathrm{err}\cdot \mathrm{d}t + Kc \times Td\,\frac{\mathrm{d}(\mathrm{err})}{\mathrm{d}t} \qquad [10.3]$$

where Td is the derivative time constant.

Some control manufacturers prefer to use the concept of proportional band, which is defined as the change in the input to cause a change in the output from zero to 100%. Thus, the proportional gain Kc is given by $Kc\,\frac{100}{\mathrm{PB}}$ where PB is the proportional band. The terms Kc/Ti and $Kc \times Td$ in Equation 10.3 can also be expressed as IG and DG, which correspond to the integral gain and derivative gain, respectively. Substituting PB, IG and DG into Equation 10.3:

$$OP = err\frac{100}{PB} + IG\int err \cdot dt + DG\frac{d(err)}{dt} \quad [10.4]$$

where OP is the controller output, PB is the proportional band, %, IG is the integral gain, and DG is the derivative gain.

Further details on control systems may be found in Shaw[1] and Sivanandam.[2]

10.2 Signal selection

It has been stated that the control system must achieve the necessary output, but it must also protect the gas turbine from exceeding any engine design limits. An engine has various limiting conditions, which prevent any damage to the engine. The following are the most common for a two-shaft gas turbine operating with a free power turbine.

(1) The exhaust gas temperature limit (EGT) is used to prevent the turbines from overheating and resulting in premature turbine blade failure.
(2) The gas turbine speed limit prevents the rotating parts from becoming over-stressed, resulting in failure.
(3) High performance engines operate at high compressor pressure ratios, and an upper limit on the aerodynamic or non-dimensional speed may be imposed so as to prevent stalling and surging of the compressor at high speeds.
(4) A power turbine speed limit is used to prevent the rotating parts of the power turbine from becoming over-stressed.

The control system shown in Fig. 10.1 has no means of preventing these engine limits from being exceeded. A continuous increase in power demand can be satisfied by a continuous increase in fuel flow. This could, of course, result in the engine over-speeding and overheating. Signal selection can be used to protect the engine by preventing such engine limits from being exceeded. With signal selection, further errors are calculated using the engine operating limits as the set point and comparing them with the current values. Figure 10.4 shows an engine control system with signal selection. The four engine limits discussed above are shown (aerodynamic speed limit, gas generator speed limit, EGT limit and the power turbine speed limit). The lowest error is used as the input to the control system and is often referred to as low signal select. Similarly, when the control system uses the highest error for control purposes, the signal selection is referred to as high signal select. High signal selection is used to prevent the gas generator and the power turbine speeds from reaching critical speeds, which occur at between 50% and 70% of the design speed, where high vibrations can occur resulting in engine damage.

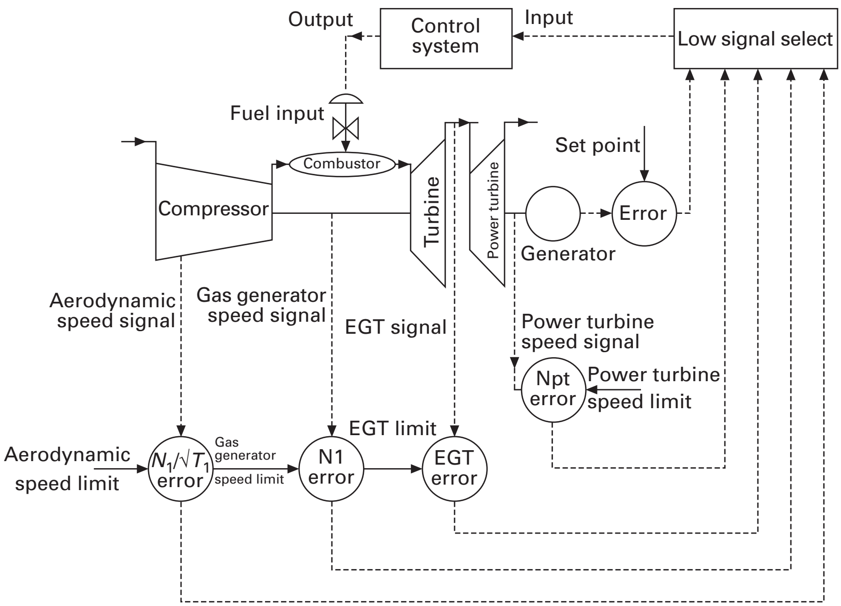

10.4 Simple engine control system with low signal select.

10.3 Acceleration–deceleration lines

It has been stated that a change in the power output from the gas turbine is achieved by varying the fuel flow. During transients, such as acceleration and deceleration, the operating points will shift or leave the steady-state running line, as shown in Fig. 10.5. If the change in fuel flow is very rapid, surge problems may be encountered during acceleration; and engine flameout during deceleration due to the fuel–air ratio being too weak. Flameout conditions may also be encountered during acceleration resulting from the fuel–air ratios becoming too rich and this situation may result in high turbine temperatures, thus compromising the turbine creep life.

It is therefore necessary to restrict the fuel flow rate during such transients, thereby preventing conditions that would lead to trips due to flameout and engine damage due to overheating and compressor surge. This is achieved by imposing limit lines on the compressor characteristic, thus preventing operating points from crossing these lines and hence avoiding conditions that would lead to the flameout and surge conditions discussed above. Figure 10.6 shows these lines on the compressor characteristic as acceleration and deceleration limit lines. The expected transient running lines during acceleration and deceleration are also shown in the Figure. Note that the transient running lines remain within these limit lines and therefore trips due to flameout conditions and compressor problems do not occur.

The implementation of such limit lines is impractical within engine control

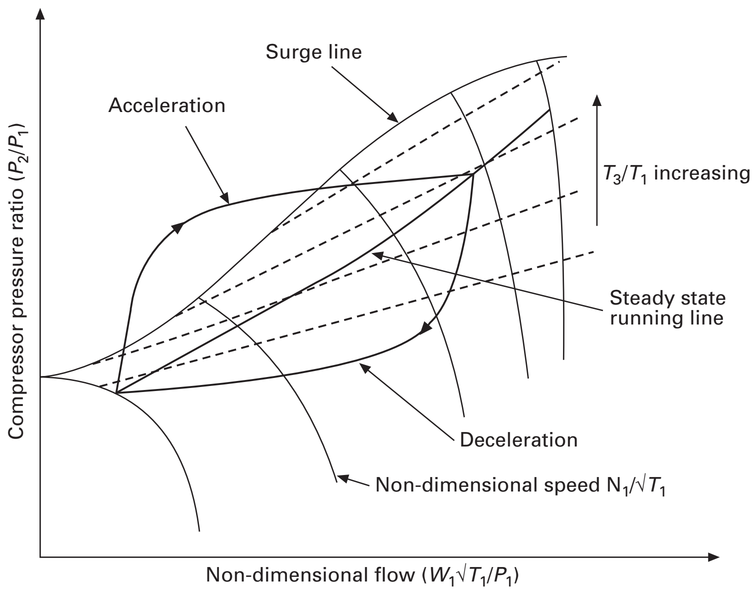

10.5 Transient running line on the compressor characteristic during acceleration and deceleration.

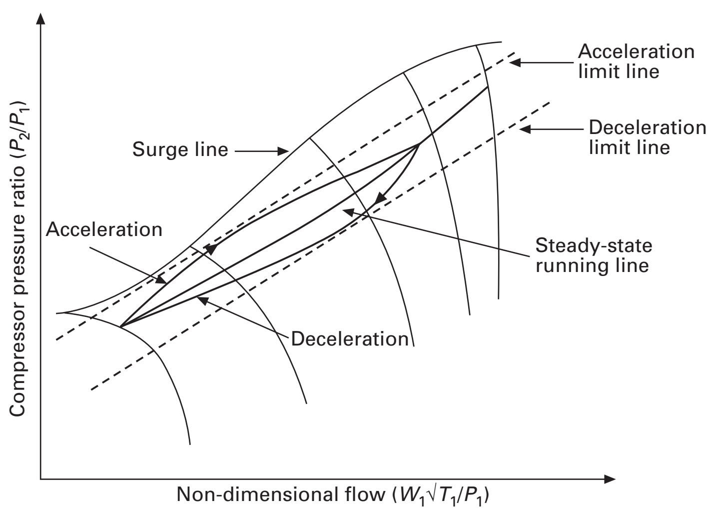

10.6 Transient performance on the compressor characteristic when acceleration and deceleration limit lines are present.

systems, especially if some of the necessary measured parameters are unavailable, such as compressor inlet airflow rate, W_1. Furthermore, the computation of the error is quite complex, especially on older hydro-mechanical engine control systems. However, the non-dimensional behaviour of gas

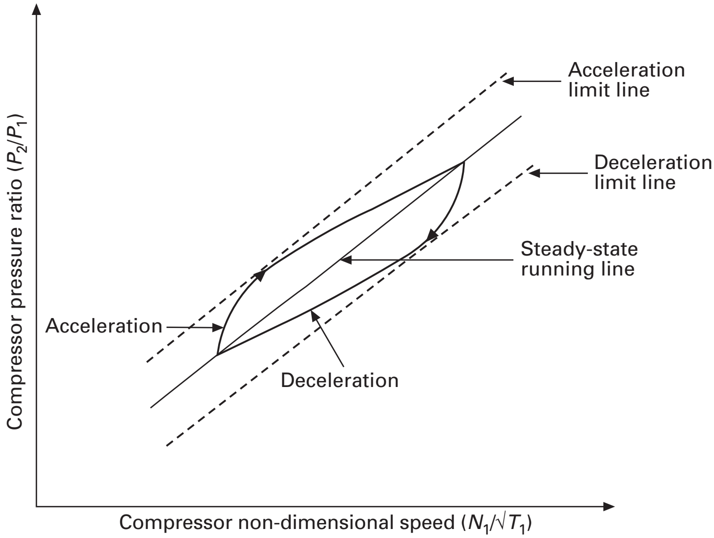

10.7 Transient running line of compressor pressure ratio and non-dimensional speed.

turbines enables such limit lines to be implemented on the basis of the compressor pressure ratio and compressor non-dimensional speed, as shown in Fig. 10.7. If the transient running lines are contained within such acceleration and deceleration limit lines, as shown in Fig. 10.7, this will ensure satisfactory transient performance from the gas turbine. Therefore, the acceleration limit line, often referred to as the *accel* line, is provided to prevent compressor surge, excessive high turbine entry temperatures and flameout due to too rich a fuel–air mixture during engine acceleration. Similarly, the deceleration limit line, often referred to as the *decel* line, is provided to prevent flameout conditions due to too lean a fuel–air ratio. In practice, manufacturers may use the compressor discharge pressure or fuel flow, with varying gas generator speed to implement the accel and decel limit lines.

The implementation of signal selection to protect the engine during steady-state operation and therefore prevent the engine from overheating and over-speeding has been discussed. The implementation of the acceleration and deceleration limit lines also uses signal selection. The error required by the control system for signal selection is calculated using the accel and decel lines as set points. This error is compared with the errors calculated using the gas generator speed, EGT, aerodynamic speed and power turbine speed limits as set points, as shown in Fig. 10.4. Thus, a low signal selection will ensure that the operating point will remain below the acceleration limit line and a high signal selection will ensure that the operating point will remain above the deceleration limit line during engine transients.

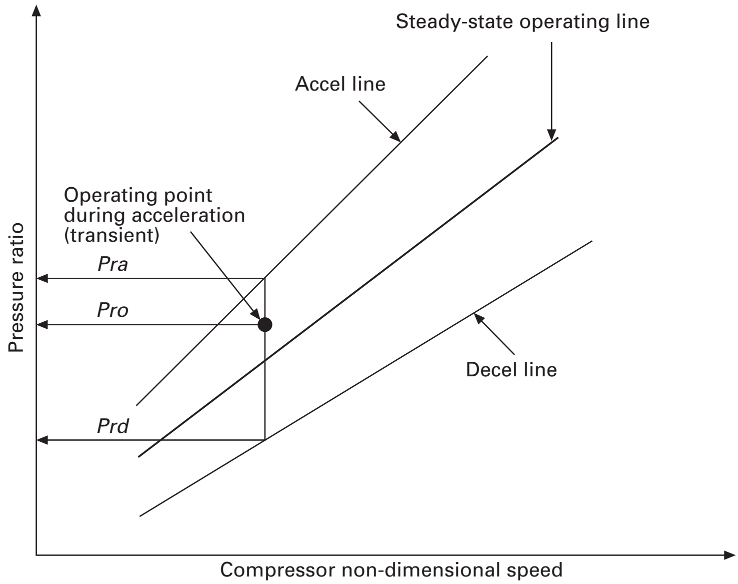

10.8 Typical acceleration–deceleration lines during an engine transient.

The calculation of the error is as follows. Referring to Fig. 10.8, the error based on the acceleration line (erra) is defined as:

$$\text{erra} = \frac{\text{Pra} - \text{Pro}}{\text{Pra}} \times 100 \qquad [10.5]$$

and the error based on the deceleration line (errd) is defined as:

$$\text{errd} = \frac{\text{Pro} - \text{Prd}}{\text{Prd}} \times 100 \qquad [10.6]$$

where Pra is the compressor pressure ratio limit during acceleration for a given compressor non-dimensional speed, Prd is the compressor pressure ratio limit during deceleration for a given non-dimensional speed and Pro is the operating compressor pressure ratio.

Alternatively, non-dimensional fuel flow may be used instead of compressor pressure ratio in setting the accel–decel line. The optimisation of these accel–decel lines will require the application of mathematical models to simulate the dynamic or transient behaviour of gas turbines.

10.4 Control of variable geometry gas turbines

It has been stated that the gas turbine may include variable geometry in the compressor for satisfactory compressor operation at off-design conditions and variable geometry turbines for improved off-design performance of the engine. The engine control system described above has to include the control of these variable geometry devices and this is discussed below.

10.4.1 Control of variable geometry compressor in free power turbine engines

Gas turbines employing free power turbines and operating with high compressor pressure ratios require variable geometry compressors in the form of variable inlet guide vanes (VIGVs) and stators (VSVs) to achieve satisfactory compressor surge margins as was discussed in Chapter 4. The operation of these devices results in the turning or rotating of the variable guide vanes via an actuator ring connected to a piston or ramp. Air or hydraulic pressure is applied to the ramp resulting in turning of the VIGVs and VSVs. The amount of turning of these devices is normally determined by the compressor non-dimensional speed, and these variable guide vanes open as the compressor non-dimensional speed increases. This process is shown in Fig. 10.9.

Early gas turbines, many of which are still in operation today, use an open loop system to actuate the variable guide vane. In other words, the amount of pressure applied to actuate the variable guide vanes is predetermined effectively by the value of the compressor non-dimensional speed. Although they generally operate satisfactorily, the control system performance is susceptible to wear and dirt in the guide vane and actuator system. As a result, such control systems seldom achieve the required guide vane angle (set point). Current gas turbines employ a closed loop system thus cancelling out any errors.

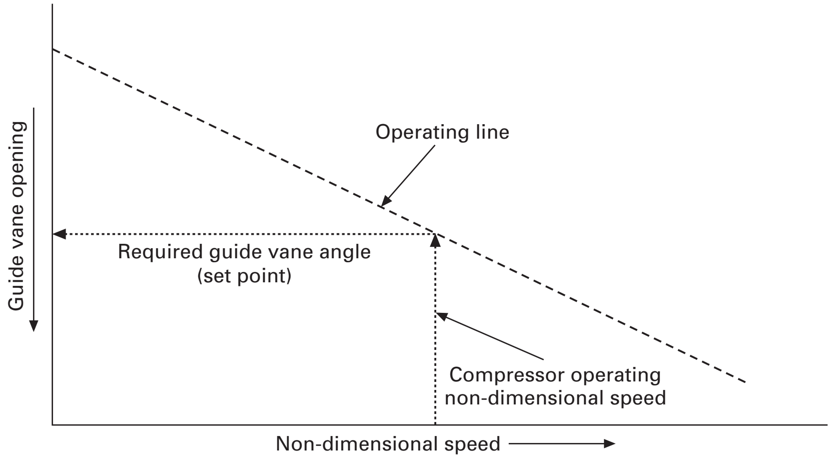

10.9 Variation of the required variable guide vane angle (set point) with compressor non-dimensional speed.

10.4.2 Control of variable geometry compressor in single shaft gas turbine

In Chapters 7 and 8 the off-design performance of gas turbines employing VIGVs and VSVs in order to maintain constant exhaust gas temperature (EGT) at off-design conditions was discussed. This was achieved by closing the variable stators at low power conditions, thereby reducing the mass flow rate through the engine, in turn requiring a higher turbine entry temperature to maintain the power required at these conditions. The control of the variable stators is achieved by employing a closed loop control system, as open loop systems may leave an offset resulting in too large a closure of the stators and may give rise to higher turbine entry temperatures than permitted, which would seriously compromise the turbine creep life.

One strategy for controlling the variable stator position is to employ two PID loops. The first PID loop controls the fuel flow using the power demand as a set point. The second loop controls the variable stator vane position to maintain the exhaust temperature (EGT) at the required value, which will be the set point for the second PID loop. This is described schematically in Fig. 10.10.

Such a strategy for VIGV control is suitable when the EGT set point for VIGV control is below the maximum EGT limit. It is normally employed primarily to reduce gas turbine starting power requirements for single-shaft gas turbines. Since the EGT set point for operating the VIGV is below the maximum EGT limit, the VIGV will be fully opened for most of the useful

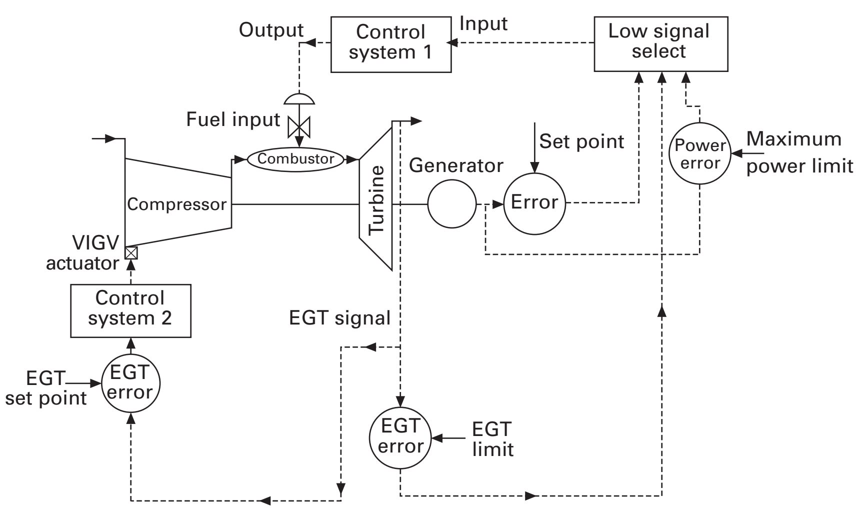

10.10 Control system strategy for VIGV control applied to a single-shaft gas turbine (EGT = exhaust gas temperature).

power output range of the gas turbine. Another strategy for controlling the VIGV is to maintain the EGT at the maximum or limiting value for reduced power outputs. If the above control strategy is attempted, an increase in power demand from the gas turbine will result in the EGT limit being reached before the VIGV is fully open. Thus the maximum power output from the gas turbine cannot be achieved. An open loop response may be incorporated into the control system of the VIGV to rectify this problem. The open loop response may be such that the VIGV is opened fully for a fixed time period when an increase in power demand is required. Provided this time period is sufficiently large, the desired power output from the gas turbine can be achieved. After the elapse of this time period, the control switches to close loop control so that the VIGV closes to maintain the EGT on its limit.

Inclusion of the open loop response resolves the difficulty of maintaining the power demand from the gas turbine at constant EGT operation, when such a control system is used in DLE engines, in the period when the VIGV is fully opened (open loop) the fuel–air ratio may exceed the lower extinction limit. This results in flameout and tripping of the engine. A better control strategy, in this instance, is to modulate the VIGV to maintain the power demand and to modulate the fuel valve to maintain the EGT on the required limit. By employing such a control strategy, the open loop response described above can be eliminated. A schematic representation of such a control strategy is shown in Fig. 10.11. Both these control strategies are discussed further when the use of the engine simulator to illustrate the control system behaviour is considered.

During starting and operating at low power outputs, the VIGV is fully closed (due to the EGT being below the limiting value). The control system strategy during this period of operation must be changed such that the power output is controlled by modulating the fuel flow. It is only when the EGT limit is reached that the switch is made to the control strategy described in Fig. 10.11.

A maximum power limit may be imposed on the engine. In this event, a low signal selection must be included in the control system, which operates the VIGV as shown in Fig. 10.11. Should the gas turbine power output exceed the maximum power limit, as could happen at low ambient temperature, the effect of low signal selection is to close the VIGV so as to maintain the gas turbine power output and the EGT on their maximum limits.

10.4.3 Control of variable geometry power turbine (two-shaft gas turbine)

It has been stated that a two-shaft gas turbine operating with a free power turbine can maintain the exhaust gas temperature (EGT) at off-design conditions by using a variable geometry power turbine. This is achieved by closing the

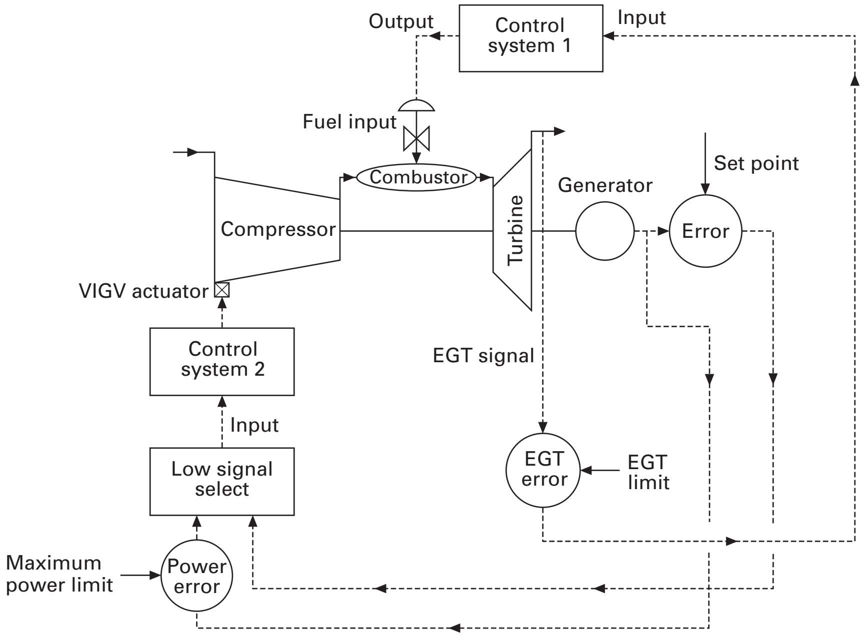

10.11 Control system strategy for maintaining the exhaust gas temperature (EGT) on the limiting value without the use of an open loop response.

nozzle guide vanes (NGVs) of the power turbine at low power conditions. If the choice is made to modulate the NGV to maintain the EGT, then it may not be possible to increase the power output of the gas turbine as the engine is already on the EGT limit. However, an open loop control response may be included to overcome the problem, similar to that discussed in Section 10.4.2. With such a control system the NGVs are opened fully for a fixed period of time, thus reducing the EGT. This will enable the engine power output to reach the increased power demand before the control system switches to the closed loop mode where the NGV is closed sufficiently to maintain the EGT on its limiting value.

Such a control strategy can maintain the EGT on the limiting value at off-design conditions; however, during transient operation, the EGT may be reduced and the use of such a control strategy in DLE combustion engines may lead to the fuel–air ratio exceeding the lower extinction limit, causing tripping of the engine. An alternative control strategy may be proposed, which is similar to that also discussed in Section 10.4.2, where the NGV is modulated to alter the power output from the gas turbine and the fuel flow is modulated to maintain the EGT on the limiting value. Such a control strategy will eliminate the need of an open loop response as discussed

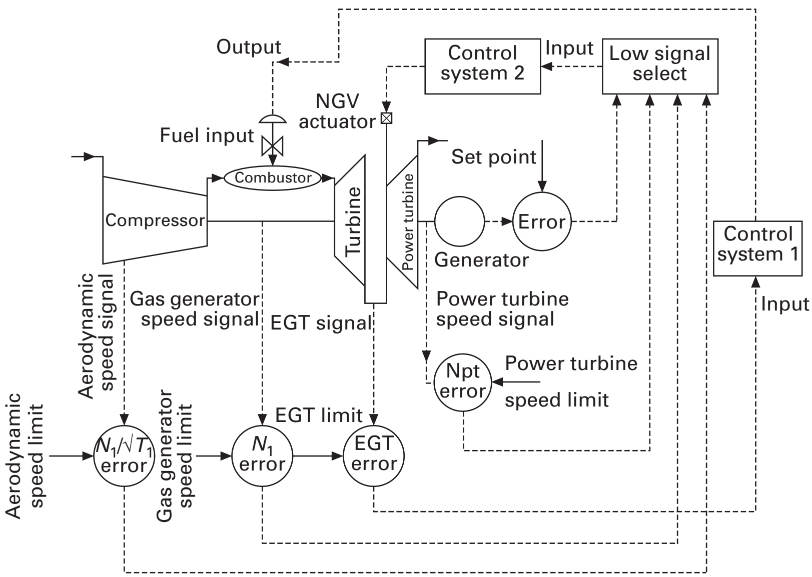

10.12 Control system strategy for maintaining the exhaust gas temperature (EGT) on the limiting value without the use of an open loop response (two-shaft free power turbine gas turbine).

previously. Figure 10.12 shows a schematic representation of such a control system applied to a two-shaft gas turbine operating with a free power turbine.

10.5 Starting and shutdown

Starting a gas turbine is probably one of the most difficult aspects of engine operation. The process begins with the turning or cranking of the engine using an external power source such as an electric starter motor. Other types of starters include air turbines and hydraulic motors.[3,4] The speed of the compressor must be high enough (about 20% of design speed) to build up sufficient mass flow and pressure in the combustion system so that ignition can be initiated. The igniters are initiated and the fuel is admitted into the combustion system. When ignition occurs, the increased turbine power will accelerate the engine. However, the starter motor will still be engaged, as the compressor speed is too low and the compressor efficiency is therefore poor. Thus, disengaging the starter motor too soon will result in the engine coasting down. Another problem during starting is ‘hanging’ and this is due to insufficient fuel flow or starter motor power. The failure of all the burners to light-up during starting will result in reduced heat input and this can result in a hanged start. Hanging therefore results in a very slow or even no acceleration of the engine during starting. This aspect is discussed further in Harman[3] and Walsh and Fletcher.[4]

Starting power demand must be minimised and this is achieved in multi-spooled engines by rotation of only one of the spools, usually the HP spool. Blow-off valves are opened to ensure satisfactory surge margin during starting. The power demand for starting large single-shaft gas turbines can be very large. The compressors of these engines are usually fitted with VIGVs to reduce the mass flow rate, thus decreasing the starting power demands of such gas turbines. These guide vanes are then fully opened during normal operation using a control strategy described in Section 10.4.2.

Although the above gives an overview of the starting process of a gas turbine, there are other sequences or phases that have to be passed before ignition can be initiated. One such sequence is purging where the cranking of the engine is carried without any combustion to clear the combustion system and the engine from fuel–air mixtures that can ignite in an uncontrolled manner and result in an explosion. This is particularly so for natural gas-fired engines where fuel gas can leak into the engine and present an explosive hazard. With liquid-fuelled engines using diesel or kerosene, purging is normally carried out after a trip, where fuel can be still flowing into the combustion system during coasting down after a flameout situation. The liquid fuel contacts the hot engine components and vaporises to forming an explosive mixture when mixed with the air stream.

After successful starting, the engine operates at idle conditions for a period, referred to as thermal soaking, when the engine components can achieve a new operating temperature. Thermal soaking is important in reducing the thermal stressing and minimising life usage. The idle speed is also important and must be above any critical speed to prevent resonance resulting in high engine vibration. A typical idle speed range for gas turbines is between 40% and 70% of the design speed and should be low enough to minimise idle power output of the engine. Figure 10.13 shows the speed–time display during the starting process for a single-shaft gas turbine. The figure also shows the major phases of the starting sequence. The starting torque required and turbine entry temperature (TET) during starting are shown in Fig. 10.14. Note the higher TET requirements at low speeds, which are due to low compressor and turbine efficiencies during low speeds.

It may be thought that shutting down a gas turbine is much simpler and more easily achieved by shutting off the fuel flow to the engine. However, such rapid shutdowns, which occur during engine trips, can cause rapid shrinkage of engine components resulting in temporary or even permanent seizure of the engine. The normal process of shutdown is to bring the engine to idle, where it remains for a suitable cooling down period, before the fuel flow is shut off to shutdown the engine. The cooling down period depends on the engine size, a large engine requiring a long idle period before shutdown.

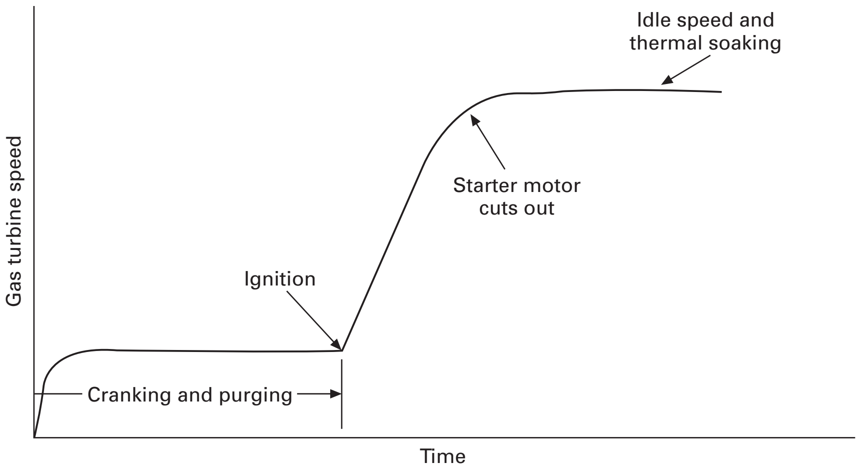

10.13 Gas turbine speed variation with time during starting.

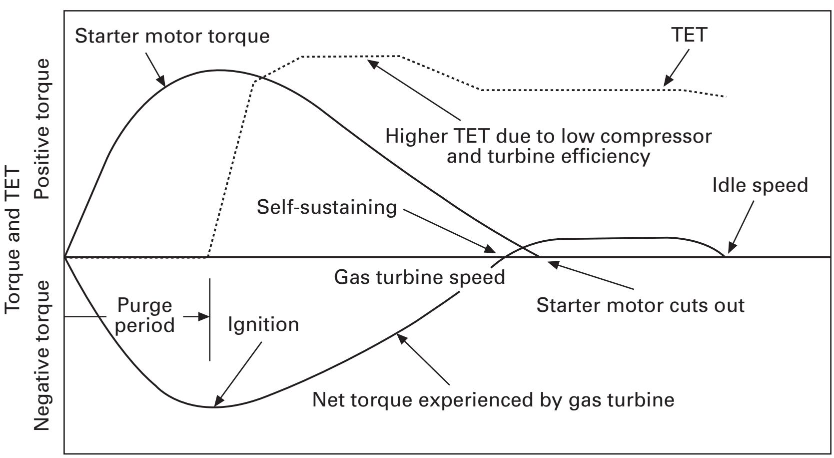

10.14 Torque and turbine entry temperature (TET) variation with gas turbine speed during starting.

10.6 Transient performance

In Chapters 7 and 8 the prediction and behaviour of the steady-state performance when gas turbines operate at off-design conditions were discussed. In this chapter we have also discussed that the change in fuel flow would result in the engine changing from one steady-state condition to another, resulting in a transient response from the gas turbine. During the transient response, the operating point will leave the steady-state operating condition and this condition will prevail until the new steady-state condition is reached. Problems such as compressor surge and flameout during these transient excursions have been highlighted and means to protect the engine during the transient period of operation were discussed. In this section, means of predicting the transient performance of the gas turbine will be discussed.

In predicting the steady-state performance of gas turbines only flow compatibility has been considered, which is effectively the steady-state law of continuity or conservation of mass and the power or energy balance between and within engine components such as compressors, turbines and combustors. Again, only the steady-state aspect of the law of conservation of energy has been considered. To simulate the transient performance of the gas turbine it is necessary to consider the dynamic terms present in these laws and also to consider the laws of conservation of momentum. If an engine element in general is considered at any instance in time as shown in Fig. 10.15, it would experience a fluid flow rate, W_1 and W_2, temperatures, Ts_1 and Ts_2, and pressures, Ps_1 and Ps_2, entering the element and leaving the element. Also, there would be external forces, F_{net}, on the element. Similarly, there would be net energy, E_{net}, either entering or leaving the element, as shown in Fig. 10.15. There would also be mass trapped within the element, M. It should be noted that the temperatures and pressures are static values rather than stagnation or total values. The element may represent a compressor, turbine, combustor or duct work such as a transition piece connecting the compressor, turbine and combustor.

10.6.1 Continuity

From the law of conservation of mass (continuity), the change in mass, M, trapped within the element is determined by the difference in amount of mass (of fluid) entering and leaving the element. Therefore, the rate of change in the mass trapped within the element is determined by the difference in the fluid flow rate at the inlet and exit of the element, W_1 and W_2, respectively. This can be represented mathematically by Equation 10.7:

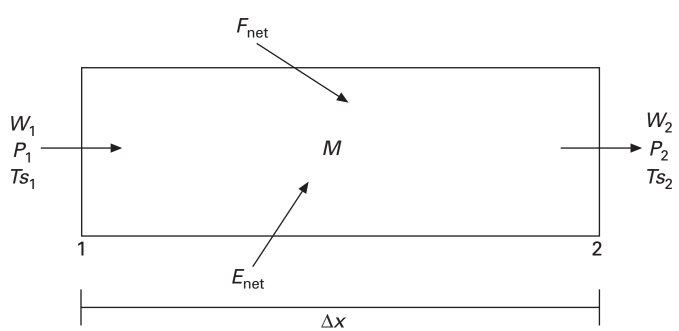

10.15 Generalised non-dimensional flow element.

$$\frac{dM}{dt} = W_1 - W_2 \qquad [10.7]$$

The density of the fluid within the element in differential form is given by:

$$d\rho = \frac{dM}{V} \qquad [10.8]$$

where ρ is the static density at some midpoint within the element and V is the volume of the element.

Substituting Equation 10.8 into Equation 10.7:

$$V\frac{d\rho}{dt} = W_1 - W_2 \qquad [10.9]$$

The equation of state for gases is given by $Ps = \rho \times R \times Ts$. For a given temperature and gas this equation in differential form is given by:

$$dPs = RTs \times d\rho \qquad [10.10]$$

Note: It has been assumed that the gas or fluid is perfect and this is usually the case for air and products of combustion at pressures and temperatures present in gas turbines. Since the methods developed here are applicable to all gases, the compressibility factor, Z, discussed in Chapter 2, should be included when appropriate.

Substituting Equation 10.10 into Equation 10.9 and rearranging:

$$\frac{dPs}{dt} = \frac{RTs}{V}(W_1 - W_2) \qquad [10.11]$$

Thus the rate of change of pressure at some midpoint within the element is given by Equation 10.11.

10.6.2 Momentum

In Section 10.6.1, the charging and discharging of the element due to flows entering and exiting the element were effectively considered and an equation was developed describing the rate of change of pressure within the element. It is also possible to consider the fluid within the element in motion. This can be achieved by forces acting on the element and these forces will correspond to the pressures surrounding the element and external forces, F_{net} acting directly on the element. Examples of such external forces could be friction in fluids flowing in pipes and ducts or the forces applied by the compressor rotor blade to the fluid. To develop equations to describe the effect of such forces on the movement of the element, the laws of conservation of momentum are used in the form of Newton's Second Law of Motion, which states that the rate of change of momentum is equal to the net force acting on an object or, in this case, the fluid element.

Restricting the discussion to a one-dimensional analysis and applying Newton's Second Law to the fluid trapped within the element:

$$M = \frac{\mathrm{d}u}{\mathrm{d}t} Am(Ps_1 - Ps_2 + F_{\mathrm{net}}) \qquad [10.12]$$

where u is the velocity of the element, Am is the mean flow area and F_{net} is the external pressure-force acting on the element. du/dt is the rate of change in velocity = acceleration or deceleration of the fluid trapped within the element.

Differentiating the continuity equation $W = \rho \times u \times Am$ with respect to time, t, for a given density and area:

$$\frac{\mathrm{d}W}{\mathrm{d}t} = \frac{1}{\rho \times Am}\frac{\mathrm{d}u}{\mathrm{d}t} \qquad [10.13]$$

Substituting Equation 10.13 into Equation 10.12 for the acceleration, du/dt:

$$\frac{M}{\rho Am}\frac{\mathrm{d}W}{\mathrm{d}t} = Am(Ps_1 - Ps_2 + F_{\mathrm{net}}) \qquad [10.14]$$

Since density $\rho = M/V$ and volume V can be expressed as $Am\Delta x$ where Δx is the element length, Equation 10.14 can be rearranged as:

$$\frac{\mathrm{d}W}{\mathrm{d}t} = \frac{Am}{\Delta x} = (Ps_1 - Ps_2 + F_{\mathrm{net}}) \qquad [10.15]$$

Thus an expression has been derived to describe the rate of change of flow rate at some mean position within the element due to external forces.

10.6.3 Energy

Using a similar argument to that above for continuity, the dynamics of the energy equation can be considered. The rate of change of the internal energy, U, of the element can be given by:

$$\frac{\mathrm{d}U}{\mathrm{d}t} = W_1 c_{p_1} T_1 - W_2 c_{p_2} T_2 + E_{\mathrm{net}} \qquad [10.16]$$

where E_{net} is the net external energy entering or leaving the element and T_1 and T_2 are the total or stagnation temperatures at inlet and exit of the element.

The internal energy for the element is given by:

$$U = Mc_v T \qquad [10.17]$$

where c_v is the specific heat at constant volume and T is the mean temperature of the element.

The rate of change of internal energy can be represented by:

$$\frac{\mathrm{d}U}{\mathrm{d}t} = \frac{\partial U}{\partial M}\frac{dM}{\mathrm{d}t} + \frac{\partial U}{\partial T}\frac{\mathrm{d}T}{\mathrm{d}t} \qquad [10.18]$$

From Equation 10.17, $\dfrac{\partial U}{\partial M} = c_v T$ and $\dfrac{\partial U}{\partial T} = Mc_v$. Substituting these partial derivatives into Equation 10.18:

$$\frac{dU}{dt} = c_v T \frac{dM}{dt} + Mc_v \frac{dT}{dt} \qquad [10.19]$$

Using Equation 10.19 in Equation 10.16:

$$c_v T \frac{dM}{dt} + Mc_v \frac{dT}{dt} = W_1 c_{p_1} T_1 - W_2 c_{p_2} T_2 + E_{\text{net}}$$

This can be rearranged to determine the rate of change of mean temperature in the element as follows:

$$Mc_v \frac{dT}{dt} = W_1 c_{p_1} T_1 - W_2 c_{p_2} T_2 + E_{\text{net}} - c_v T \frac{dM}{dt} \qquad [10.20]$$

Since $M = \rho V$ and from Equation 10.7 $\dfrac{dM}{dt} = W_1 - W_2$, Equation 10.20 becomes:

$$\frac{dT}{dt} = \frac{W_1 c_{p_1} T_1 - W_2 c_{p_2} T_2 + E_{\text{net}} - c_v T(W_1 - W_2)}{\rho V c_v} \qquad [10.21]$$

10.6.4 Linearly distributed and lumped model

The rates of change of pressures, flows and temperatures discussed above occur at some midpoint within the element. However, these rates of change are required either at the inlet or exit of the element. Two models can be used to determine these rates of change at the required element boundary and they correspond to the linearly distributed and lumped models.

The linearly distributed model assumes that these rates of change are linear across the element. Applying the linear distributed model to Equations 10.11, 10.15 and 10.21:

$$\frac{dP_1 s}{dt} + \frac{dP_2 s}{dt} = \frac{2RTs}{V}(W_1 - W_2) \qquad [10.22]$$

$$\frac{dW_1}{dt} + \frac{dW_2}{dt} = \frac{2Am}{\Delta x}(Ps_1 - Ps_2 + F_{\text{net}}) \qquad [10.23]$$

$$\frac{dT_1}{dt} + \frac{dT_2}{dt} = \frac{W_1 c_{p_1} T_1 - W_2 c_{p_2} T_2 + E_{\text{net}} - c_v T(W_1 - W_2)}{0.5 \rho V c_v} \qquad [10.24]$$

When applying the lumped parameter model, it is assumed that these mean values for the rates of change remain constant across the element. Therefore, Equations, 10.22, 10.23 and 10.24 become:

$$\frac{dP_2s}{dt} = \frac{RT_2s}{V}(W_1 - W_2) \qquad [10.25]$$

$$\frac{dW_1}{dt} = \frac{Am}{\Delta x}(P_1 - P_2 + F_{net}) \qquad [10.26]$$

$$\frac{dT_2}{dt} = \frac{W_1 c_{p_1} T_1 - W_2 c_{p_2} T_2 + E_{net} - c_v T_2 (W_1 - W_2)}{\rho_2 V c_v} \qquad [10.27]$$

10.6.5 Choice of model

Much of the early work on dynamic simulation of gas turbines was carried out by Corbett and Elder[5] and also by Elder and MacDougal.[6] They report that the simulated results for the lumped and linearly distributed models were in good agreement, but that the linear model required a significant increase in computational effort (some 2–3 times more computing time). Thus lumped models are often employed in the prediction of the transient performance of gas turbines. It should be pointed out that such models are equally applicable in the simulation of gas compression system present in the process industry.[7]

The equations described use static values for pressures and temperatures. However, total or stagnation values for these parameters are preferable in analysing engine performance in general. If element boundaries are chosen where the Mach number is low ($M_x < 0.3$), the differences between the static and total values will be small and the values computed using the equations described above could be treated as total or stagnation values. Examples of such boundaries are upstream and downstream of compressor stages rather than choosing boundaries between the rotor and stator of a compressor stage or close to the rotor inlet where the velocities are very high.

The assumption in the lumped parameter model imposes frequency limitations because second- or higher-order equations are being solved. Such systems of equations employed in predicting transient performance of gas turbines and gas compression systems are capable of simulating longitudinal waves. For air, the element length, Δx, in Equation 10.26 should be less than about 34 metres ($\Delta x << 34$ m) as determined by Corbett and Elder.[5] This is usually the case with gas turbine components.

It should be noted that these models are capable of simulating compressor surge cycles. Elder and Macdougal[6] developed a frequency parameter model to account for surge and pre-surge oscillations during the transient response of the compressor element. They related a frequency parameter to the phase change across the compressor element in terms of an expected error when comparing the lumped parameter model with the true solutions. Using an expected frequency of interest, f_x, and Mach number, M_x, of 0.3 or less, a suitable element length for the compressor could be determined using:

$$2\pi f_x \Delta x < a(1 - M_x) \tag{10.28}$$

where a is the velocity of sound

Although the above analysis improves the simulation, the elements do not communicate in a realistic manner if the adjacent element volumes are significantly different. In order for elements to interact in a realistic manner, a criterion of approximately equal volumes is used, in conjunction with the frequency parameter model.

Other researchers in the field of transient analysis of gas turbines include Greitzer[8] and Fawke and Saravamuttoo.[9] Although Greitzer used a similar approach to the one described by Elder and discussed above, Fawke and Saravamuttoo restricted their models to continuity only. Pre- and post-surge oscillations are unavailable using the continuity-only model.

10.6.6 Element definition

The starting values for pressures, flows, temperatures and speeds for transient analysis would be determined by a steady-state model of the gas turbine as discussed in Chapter 7. However, the force and energy terms F_{net} and E_{net} need to be defined in Equations 10.26 and 10.27, respectively. These are determined by applying the quasi-steady-state assumption, where the instantaneous values are used with the steady-state component characteristic to determine these terms, as discussed below.

Compressor

In the dynamic simulation of gas turbines, it is usual to employ compressor stage characteristics rather than overall characteristics as discussed in Chapter 7, where the prediction of the off-design performance of the gas turbine was considered. These stage characteristics are normally stacked together[10] to produce the overall characteristic used in the prediction of the steady-state performance of the gas turbine. A typical compressor stage characteristic is shown in Fig. 10.16. At any instance the flows, pressures, temperatures and speeds at the inlet to the compressor stage will be known. Given the compressor geometry (flow area), using the equation of state and the continuity equation, the axial velocity, Va, and blade velocity, U, at the reference point can be calculated (e.g. blade mid-height). Thus the flow coefficient, Va/U, can be determined. Using the stage characteristic and by interpolation, the stage loading coefficient, $\Delta h/U^2$, and the isentropic efficiency can be determined. Δh is the specific enthalpy rise.

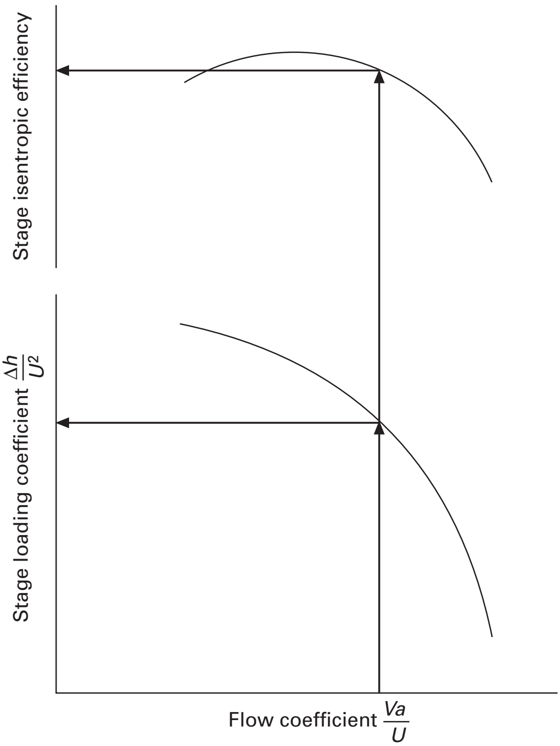

10.16 Typical axial compressor stage characteristic.

The stage pressure ratio, P_2/P_1 can now be calculated from

$$\Delta h = c_p T_1 \left(pr^{\frac{\gamma-1}{\gamma}} - 1 \right) / \eta_c ,$$

which will yield the compressor stage pressure ratio. c_p is the specific heat at constant pressure, γ is the isentropic index, T_1 is the stage inlet temperature and η_c is the stage isentropic efficiency. Note that pressures and temperatures are now assumed to be stagnation or total values.

The F_{net} term is defined as the pressure change (rise) across the compressor stage and is therefore given by:

$$F_{net} = P_2 - P_1$$

in terms of the stage pressure ratio:

$$F_{net} = P_1(pr - 1) \qquad [10.29]$$

Since the compression process is assumed to be adiabatic, the E_{net} term is equal to the rise in enthalpy, $\Delta h \times W_1$, where W_1 is the inlet compressor flow rate.

Transition ducts and combustors

The forcing term, F_{net}, for transition ducts and combustors can be determined by Equation 7.6 in Chapter 7. This equation gives the non-dimensional pressure loss across the combustor. For transition ducts, the temperature rise is zero. Therefore, the F_{net} term is simply the pressure loss across the transition duct or combustor.

The energy term, E_{net}, is zero for transition ducts because a thermodynamic process in such components is considered as adiabatic with no work transfer. However, for combustors the E_{net} term is calculated by the instantaneous flow, *mf*, times the lower heating value of the fuel, LHV. The work transfer for combustors is zero. Thus for combustors:

$$E_{net} = mf \times \text{LHV} \qquad [10.30]$$

Gas turbines often employ bleeds to prevent surge at starting conditions or when operating at low powers. This was discussed in Chapter 4. The dynamic modelling of such an element requires a modification to the continuity Equation 10.25. Referring to Fig. 10.17, which represents a blow-off valve element, Equation 10.25 becomes:

$$\frac{dP_2}{dt} = \frac{RT_2}{V}(W_1 - W_2 - W_3) \qquad [10.31]$$

where W_3 is the bleed or blow-off flow rate. Similarly, for combining flows, the term $-W_3$ becomes $+W_3$.

Turbines

As was found with compressors, the turbine characteristics can also be used to determine the necessary force and energy terms required to determine the

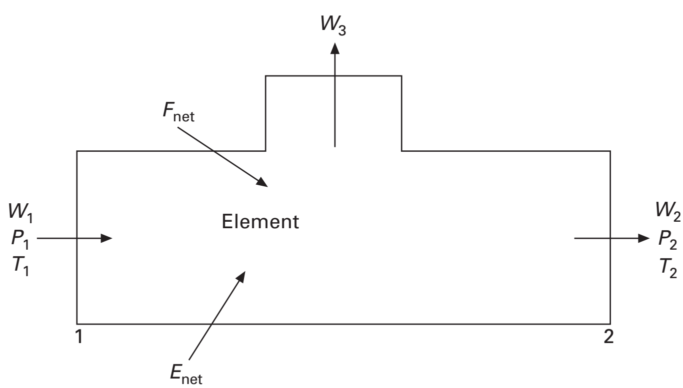

10.17 Dividing flow or blow-off element.

transient performance of turbines. Typical turbine characteristics are shown in Figs 5.8 and 5.10 in Chapter 5. Knowing the current values for inlet flow, pressure, temperature and turbine speed, these characteristics can be used to determine the pressure ratio and isentropic efficiency. The pressure ratio can then be translated to the F_{net} term using Equation 10.29. However, this is only applicable to the unchoked part of the turbine characteristic. When turbines operate in the choked part of the characteristic, the momentum Equation 10.26 is not applicable, and only the continuity and energy equations need to be considered (Equations 10.25 and 10.27, respectively).

Since the thermodynamic process in turbines is assumed to be adiabatic, the energy term, E_{net} can be determined from the turbine pressure ratio and isentropic efficiency as:

$$E_{\mathrm{net}} = W_1 c_p \eta_t \left(1 - \left(\frac{1}{Pr} \right)^{\frac{\gamma-1}{\gamma}} \right) \qquad [10.32]$$

10.6.7 Boundary conditions

Equations 10.25, 10.26 and 10.27 calculated the mass flow rate at the inlet of an element and pressure and temperature at the exit of an element. Therefore, a means of defining the inlet pressure and temperature into the first element in a simulation system and the mass flow rate at the exit from the last element of the system from boundary conditions is needed. In industrial gas turbines, the inlet pressure at the entry to the system, which is usually the filtration system, is the ambient pressure and therefore can be used as the inlet boundary condition. This is shown in Fig. 10.18, which is an elemental representation of a single shaft gas turbine. The inlet temperature at the entry to the system will also correspond to the ambient temperature.

The last element of an industrial gas turbine would normally be the exhaust system as shown in Fig. 10.18. This element incurs a small pressure loss, typically in the order of about 100 mm water gauge and can be used to determine the flow at the exit from the last dynamic element – the turbine as shown in Fig. 10.18. Since the pressure and temperature at the exit from the turbine element (which is the inlet to the exhaust system) are known, calculation of the mass flow rate at the exit from the turbine element is possible using the equation describing the pressure loss in the exhaust system. The pressure

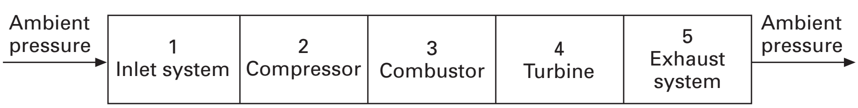

10.18 Elemental representation of a single-shaft gas turbine.

loss equation for the exhaust system is similar to Equation 7.6 in Chapter 7, but the temperature rise is zero. Since the pressure at the exit of the exhaust system is the ambient pressure, the pressure loss in the exhaust system is readily known. From Equation 7.6, the mass flow rate can be calculated.

10.6.8 Compressor–turbine speed calculation

During transients, the compressor–turbine and the driven load may vary in speed depending on the power absorbed by the compressor and load, and the power developed by the turbine. Also, the gas turbine configuration and control system performance will influence the changes in speed of these components. The power absorbed by the compressor and the power developed by the turbine are readily calculated as discussed previously. For a given compressor and turbine speed, the torque at the compressor and turbine are readily calculated using the relationship:

$$\text{power} = \text{torque} \times \text{angular velocity}$$

Therefore, at any instance the torque at the compressor and turbine can be calculated. Furthermore, for a given power output and load speed, the torque at the load is also known. For a single-shaft gas turbine rotor, as shown in Fig. 10.19, the net torque, T_{net}, is given by

$$T_{net} = T_{turb} - (T_{comp} + T_{load}),$$

where T_{turb}, T_{comp} and T_{load} are the torque at the turbine, compressor and load, respectively.

Applying Newton's second law of motion:

$$\alpha = \frac{d\omega}{dt} = \frac{T_{net}}{I} \qquad [10.33]$$

where α and I are the angular acceleration or deceleration of the rotor system and polar moment of inertia of the rotor, respectively.

Given an initial angular velocity, the current angular velocity can be calculated from the angular acceleration calculated from Equation 10.33. The analysis can be extended to other engine configurations discussed in Chapter 1.

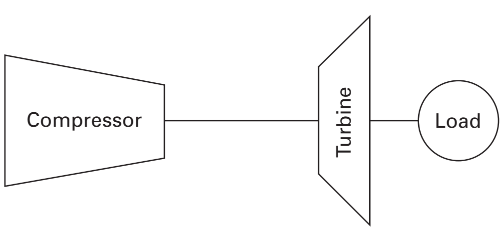

10.19 Rotor system for a single-shaft gas turbine.

10.6.9 Numerical solutions of differential equations

Equations 10.25, 10.26, 10.27 and 10.33 are referred to as first-order ordinary differential equations. These are non-linear differential equations and therefore no analytical solutions exist. In these situations the only means of finding a solution is numerically. Many such methods have been developed, from simple Euler to more advanced methods such as Rung–Kutta–Felberg and Gears methods.

Rung–Kutta–Felberg and Euler are referred to as the single-step methods because the current solutions and rates of change only are required to determine the solution at the next (time) step. Gears, on the other hand, requires previous solutions and rates of change and is known as a multi-step or predictor–corrector method. This method is generally more efficient compared with Rung–Kutta–Felberg, as fewer coefficients are needed to determine the next solution. However, single-step methods such as Rung–Kutta–Felberg are initially invoked to generate the necessary past solutions and rates of change before switching to multi-step methods. In this case, multi-step methods can be employed directly because steady-state conditions are always in place at the start. In this situation the previous solutions can be conveniently set to the current values and the previous rates of change set to zero.

Numerical methods have drawbacks where the solutions become unstable. For example, Euler would require very small time steps to achieve stable solutions and is rarely used. Rung–Kutta–Felberg and Gears can achieve stable solutions using larger steps and are therefore more efficient. Gears method is particularly suited because it is capable of overcoming a particular type of numerical instability referred to as stiff equations. Such instabilities occur when the general solution contains an exponential term such as Ce^{bx} where $b > 0$ with initial conditions $C = 0$, but the rounding off errors in the numerical computation produces a solution in which $C <> 0$. Further details on numerical methods for solving differential equations can be found in Press[11] and in Gerald and Wheatly.[12]

10.7 References

1. *PID Control Algorithm. How it Works, how to Tune it and how to Use it*, 2nd Edition, John A. Shaw, December 1 2003. E-book, http://www.jashaw.com/.
2. *Control Systems Engineering*, S.N. Sivanandam, Vikas Publishing, (2001).
3. *Gas Turbine Engineering*, Harman, R.T.C., Macmillan Press Ltd, (1981).
4. *Gas Turbine Performance*, 2nd Edition, Walsh, P.P. and Fletcher, P., Blackwell Publishing, (2004).
5. Stability of an axial compressor with steady inlet conditions, Corbett, A.G. and Elder, R.L, *J. Mech. Eng. Sci.*, 16 (6), 1975.
6. Simulation of centrifugal compressor transient performance for process plant application, Elder, R.L., MacDougal, I., *ASME Paper*, 1983.

7. Simulation of the transient performance of a compressor in a natural gas pumping station, Elder, R.L., Gill, M.E. and Razak, A.M.Y., *Third European Congress on Fluid Machinery*, The Hague, Netherlands, 18th–20th May, 1987.
8. Surge and rotating stall in axial compressors. Part II – Experimental results and comparison with theory, Greitzer, E.M., *J. Eng for Power*, April 1978.
9. Digital computer methods for prediction of gas turbine dynamic response, Fawke, A.J. and Saravamuttoo, H.I.H., *Transactions of the Society of Automotive Engineers*, 1971.
10. Effects of stage characteristics and matching on axial-flow compressor performance, Stone, A., *Transactions of the ASME*, 1958.
11. *Numerical Recipes in Fortran* 77, 2nd Edition, *The Art of Scientific Computing*, Press, W.H., Teukolsky, S.A., Vetting, W.T. and Flannery, B.P., Cambridge University Press (1992).
12. *Applied Numerical Analysis,* 6th Edition, Gerald, C.F., Wheatly, P.O., Addison-Wesley, (1997).

Part II

Simulating the performance of a two-shaft gas turbine

Much of what has already been discussed is rather complex, particularly engine off-design performance prediction. The use of a gas turbine simulator can illustrate eloquently these rather complex concepts. The gas turbine simulators will now be used to re-visit many of the preceding chapters, particularly off-design performance prediction, performance deterioration, gas turbine emissions, turbine creep life usage and the engine control system.

The gas turbine simulator is based on the quasi-steady-state model, using time constants to simulate the transient effects. Although such simulators are strictly only valid under steady-state conditions, much useful insight into engine operation can be achieved during transients using such simulators. They are excellent as training simulators. The concept of component matching, as discussed in Chapter 7, has been extensively used in building the simulator, thus making it capable of illustrating much of what has been discussed in Chapters 8, 9 and 10 in detail, including turbine creep life usage and engine emissions as discussed in Chapters 5 and 6.

Two engine simulators are used and they correspond to a single-shaft and a two-shaft gas turbine operating with a free power turbine. The single-shaft gas turbine simulator is also capable of simulating the performance of a single-shaft gas turbine when variable inlet guide vanes are incorporated. The single-shaft gas turbine is the most common engine configuration used in power generation and the use of the two-shaft gas turbine configuration operating with a free power turbine is widespread in mechanical drive applications. Although their use is widespread in mechanical drive, there are also a significant number of gas turbines using a two-shaft configuration employed in power generation. Thus, these two simulators cover the vast majority of gas turbines operating in the field. Simulation exercises provided in Chapter 21 are included to help readers to improve their understanding of gas turbine performance and operation.

11
Simulating the effects of ambient temperature on engine performance, emissions and turbine life usage

The engine simulator discussed here is based on a two-shaft gas turbine operating with a free power turbine. The engine corresponds to an advanced aero-derived industrial gas turbine having an ISO rating of about 20 MW. The simulator assumes that the driven load is an electrical generator.

11.1 Compressor running line

The reasons why an approximately unique running line occurs in a multi-shaft engine were discussed in Section 8.1.2. This can be demonstrated by producing the engine running line on the compressor characteristic using the simulator. This is achieved by running the simulator at different power and ambient conditions, increasing any engine limits such as exhaust gas temperature (EGT) and gas generator speed to produce the complete running line. Figure 11.1 shows the compressor characteristic with the running line

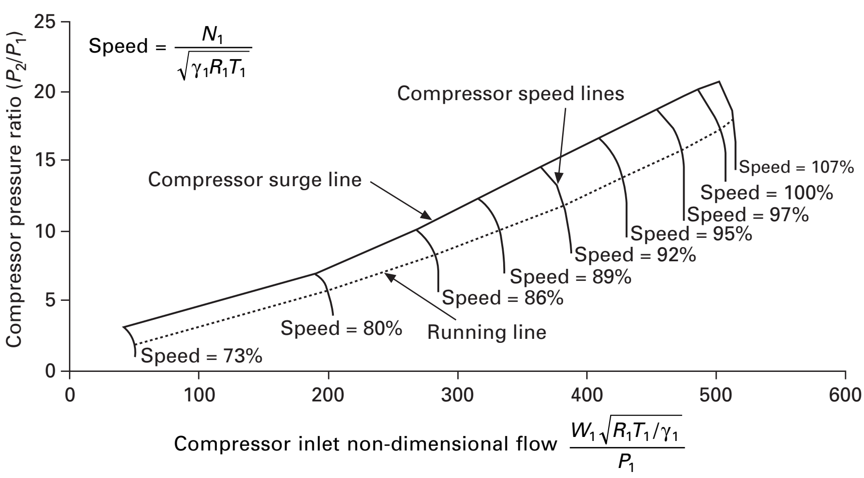

11.1 Running line on the compressor characteristic.

superimposed on it. The means of producing these characteristics and the operating points on the characteristics are found in the user guide on the CD, accompanying this book.

The reader is encouraged to run the simulations discussed below in order to become more familiar with these concepts. Instructions on how to use the simulator are also given in the user guide.

The pressure ratio of the compressor at design conditions is about 17.5. It was seen in Section 4.10.3 under variable geometry compressors that, at such high-pressure ratios, many stages of variable stator vanes are necessary to prevent compressor surge, particularly during low speed operation. In fact, this compressor has six variable stator vanes and one variable inlet guide vane to ensure satisfactory operation of the gas turbine. The variation of these guide vane positions with compressor (quasi) non-dimensional speed is shown in Fig. 11.2.

11.2 Representation of other non-dimensional parameters

Gas turbines behave in a non-dimensional manner and that is the reason why the unique running line is observed on the compressor characteristic when they operate with a free power turbine. Thus, the variation of non-dimensional parameters such as mass flow and pressure and temperature ratios can be compared with, say, compressor non-dimensional speed. Also any other non-dimensional parameter may be used instead of compressor non-dimensional speed.

Figure 11.3 shows the variation of the compressor non-dimensional flow with speed. Two kinks are observed in the display. One corresponds to the

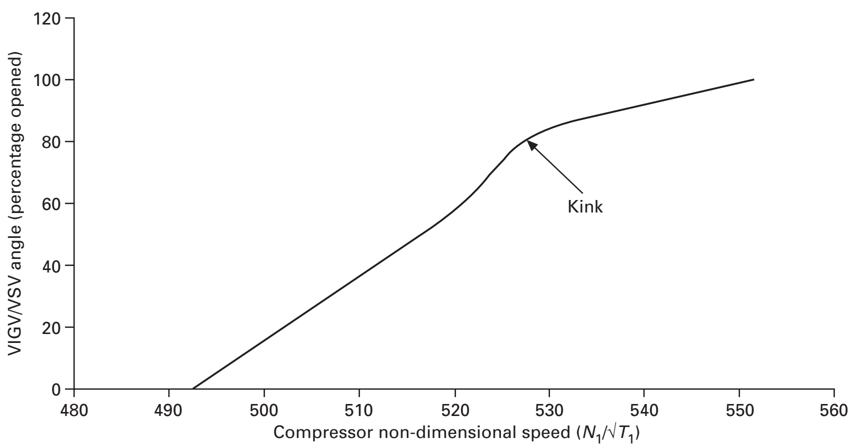

11.2 Variation of the variable stator vanes with compressor (quasi) non-dimensional speed. (It is usual to use quasi non-dimensional speed for this characteristic as the changes in R and γ are small.)

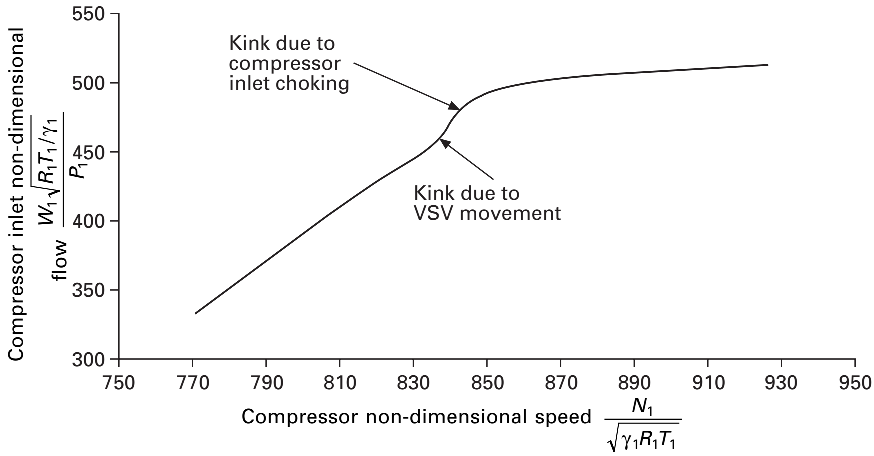

11.3 Variation of compressor non-dimensional flow with non-dimensional speed.

kink found in the VSV/VIGV movement shown in Fig. 11.2, which is due to the rapid opening of the VSV/VIGV as the compressor approaches its normal operating speed range. The other kink is due to the choking of the compressor inlet at high compressor non-dimensional speeds. This can also be observed in Fig. 11.1, where the increase in flow with speed is smaller at the high-speed part of the compressor characteristic when compared with the low speed part. Thus, as the compressor inlet chokes, the compressor non-dimensional speeds will collapse into a single line and no increase in non-dimensional flow is possible with any increase in compressor speed. Indeed, such a phenomenon has been observed with turbines, where the non-dimensional flow remains constant after the turbine chokes (see Fig. 5.8 in Chapter 5).

The variation of compressor pressure ratio and non-dimensional temperature rise with compressor non-dimensional speed is shown in Fig. 11.4. The kinks are observed again as described above when discussing the non-dimensional flow variation with speed. Because of the choking in the compressor inlet, the compressor pressure ratio flattens and imposes a maximum compressor pressure ratio of about 18. Thus, compressor inlet choking determines the maximum pressure ratio that a compressor can achieve.

Figures 11.5 and 11.6 show the variation of various turbine parameters with compressor non-dimensional speed, and Fig. 11.7 shows the variation of non-dimensional fuel flow and power with compressor non-dimensional speed. A similar picture emerges where the effects of the VSV/VIGV kink and the choking of the compressor inlet are observed. These non-dimensional parameters may be converted to corrected or standard conditions by using the equations described in Section 8.7.1 in Chapter 8.

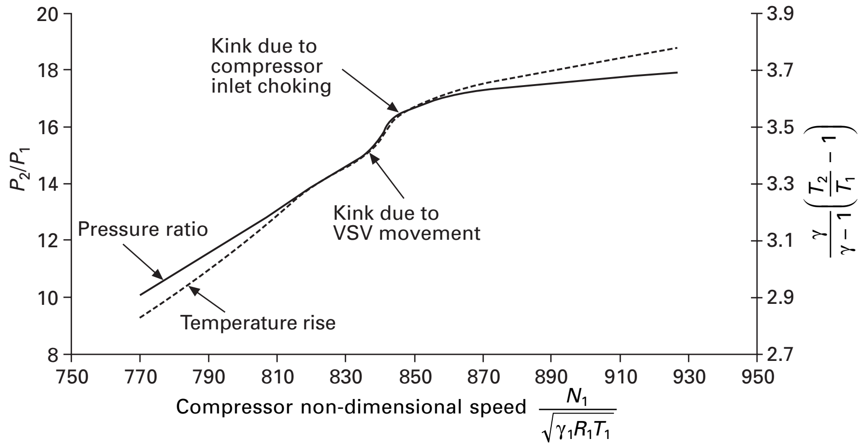

11.4 Variation of compressor pressure ratio and non-dimensional temperature rise with compressor non-dimensional speed.

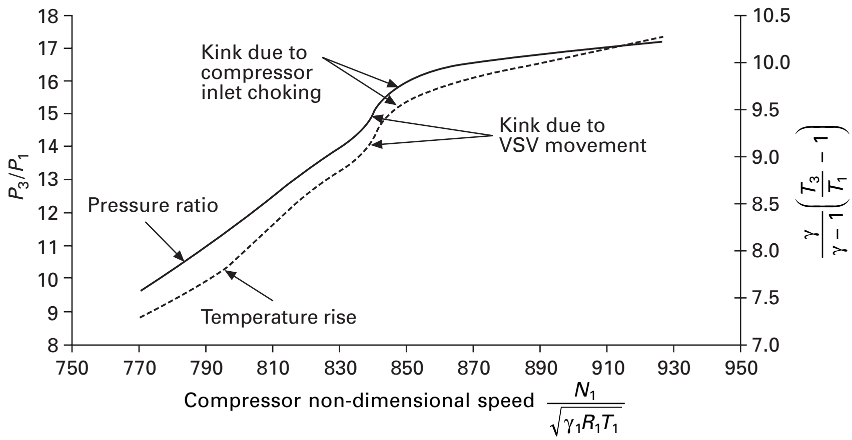

11.5 Variation of gas generation pressure ratio and non-dimensional temperature rise with compressor non-dimensional speed.

11.3 Effects of ambient temperature on engine performance (high-power operating case)

The engine model can be used to simulate the change in ambient temperature and its impact on engine performance. It has been stated that the simulator is based on a quasi-steady-state model, thus it is possible to subject the model to significant changes in ambient conditions. In practice, however, rapid changes in ambient conditions are not common and could lead to compressor surge.

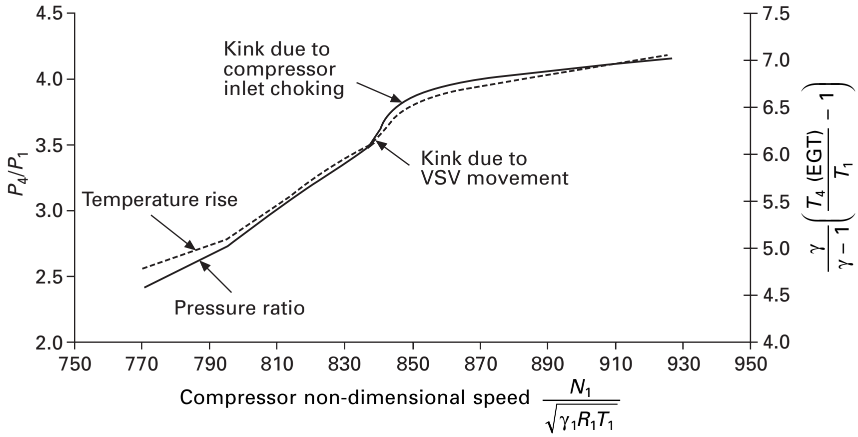

11.6 Variation of power turbine pressure ratio and non-dimensional temperature rise with compressor non-dimensional speed.

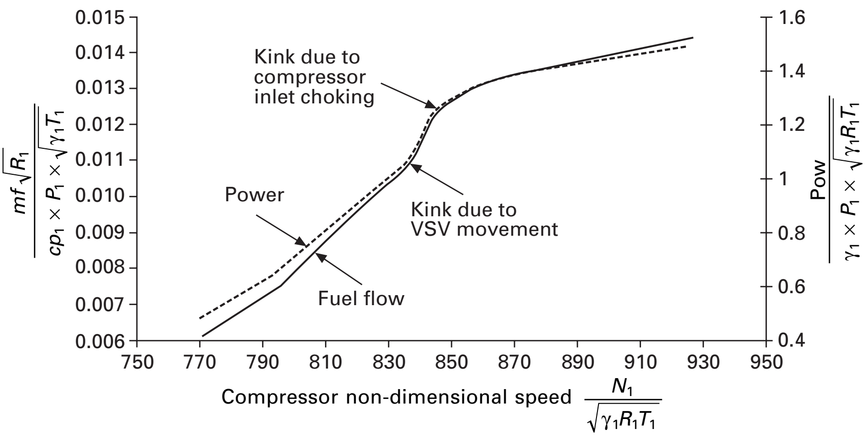

11.7 Variation of non-dimensional fuel flow and power with non-dimensional compressor speed.

In this simulation, the ambient temperature will be changed from +30 degrees Celsius to –30 degrees Celsius, linearly. The power demand from the simulator will be set to 25 MW throughout the simulation. The change in ambient temperature will take place over 60 minutes. The ambient pressure is set to 1.013 Bar during the change in ambient temperature. Also, the effects of the gas property terms R, c_p and γ will be ignored, as the changes in these parameters are small compared with the changes in temperatures and pressures.

During the simulation it will be observed that the power output from the gas turbine is limited by the exhaust gas temperature (EGT) at high ambient

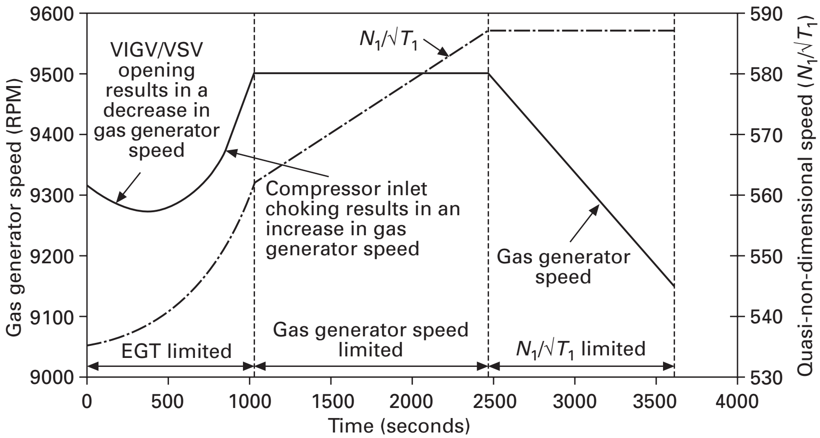

11.8 Variation of gas generator speed due to the reduction in ambient temperature.

temperatures (from 30 degrees C to about 12 degrees C) to prevent the turbine from overheating. As the ambient temperature decreases and operation is continued at the EGT limit, then the ratio of EGT to the ambient temperature, $T_4(\mathrm{EGT})/T_1$, will increase. From Fig. 11.6, an increase in $T_4(\mathrm{EGT})/T_1$ must therefore result in an increase in the compressor non-dimensional speed, $N_1/\sqrt{T_1}$. However, the gas generator speed, N_1, initially decreases with decrease in ambient temperature, T_1 before increasing at lower ambient temperature while power output is limited by the exhaust gas temperature. This condition is shown in Fig. 11.8. The initial decrease in gas generator speed is due primarily to the opening of VIGV/VSV as the compressor non-dimensional speed increases. At lower ambient temperatures, the increase in gas generator speed is due to the choking of the compressor inlet.

When the power output from the engine is limited by the gas generator speed (i.e. when N_1 is constant), as would occur at lower ambient temperatures, from about 12 degrees C to –12 degrees C, the drop in ambient temperature, T_1, will result in an increase in the $N_1/\sqrt{T_1}$. Thus as the ambient temperature decreases, the operating point on these characteristics (Figs 11.3 to 11.7) moves from left to right and becomes constrained to operate at the maximum permissible compressor non-dimensional speed, which occurs at ambient temperatures below –12 degrees C. At such low ambient temperatures, the power output is limited by the compressor non-dimensional speed, $N_1/\sqrt{T_1}$.

11.3.1 Trends in speed

The impact of the reduction in ambient temperature on gas generator speed is illustrated in Fig. 11.8. The change in gas generator speed with the reduction in the ambient temperature is observed until the gas generator speed reaches its 100% value of 9500 RPM (during constant EGT operation). The figure also shows the increase in non-dimensional speed of the compressor with a reduction in ambient temperature. The non-dimensional speed continues to increase even during the operating period, where the power output is restricted by the gas generator speed, N_1. At lower ambient temperature (below –12 degrees Celsius), the compressor non-dimensional speed reaches its operating limit as shown in Fig. 11.8. Note the continuous reduction in gas generator speed as the ambient temperature decreases during the period when the engine is constrained to operate at a constant compressor non-dimensional speed.

11.3.2 Compressor characteristic

Figure 11.9 shows the operating point on the compressor characteristic. As the ambient temperature decreases, the operation point moves up the characteristic closely following the running line. At an ambient temperature below –12 degrees Celsius, the operating point remains at the maximum non-dimensional speed line as the engine is now constrained to operate at the maximum, $N_1/\sqrt{T_1}$. The compressor pressure ratio is also approximately constant under these operating conditions. Thus the compressor pressure ratio and the non-dimensional mass flow increase with the decrease in ambient temperature, reaching a maximum when the engine performance is constrained by the compressor non-dimensional speed. The figure also shows the region where the compressor inlet starts to choke, resulting in the compressor non-

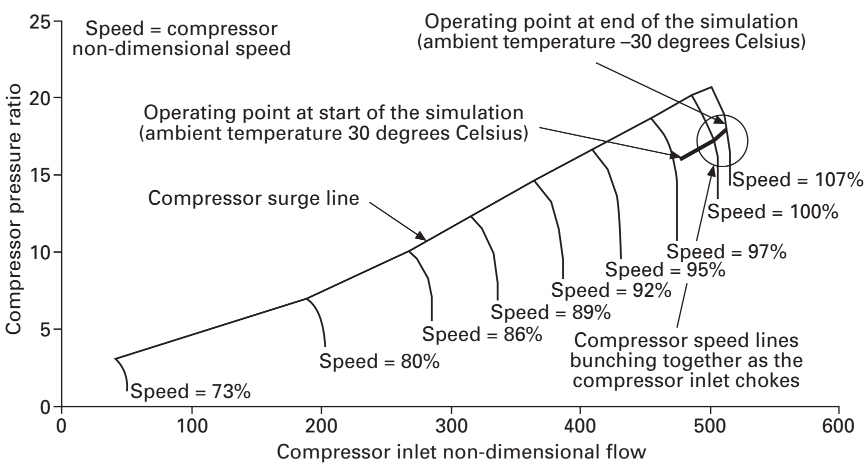

11.9 Change in operating point on the compressor characteristic as the ambient temperature decreases.

dimensional speed lines bunching together, thus restricting the increase in pressure ratio and mass flow in this region.

11.3.3 Trends in pressure ratio

The trends in the pressure ratios for the engine components are shown in Fig. 11.10 during the ambient temperature change. The Figure also shows the ratio of T_3/T_1, which is the ratio of the maximum cycle temperature (TET), to the compressor inlet temperature, T_1. Note that, as the compressor pressure ratio increases, the ratio of T_3/T_1 also increases. Also observe that the gas generator turbine pressure ratio remains essentially constant, although the power turbine pressures ratio increases as the ambient temperature decreases. This is due to the choked conditions of the power turbine restricting the gas generator turbine pressure ratio from changing. This was discussed in Section 8.1.2 where the matching of turbines operating in series was considered and it was established that the power turbine swallowing capacity controls the gas generator turbine pressure ratio. The Figure also shows the pressure ratios remaining constant when the engine is constrained to operate at a constant compressor non-dimensional speed.

11.3.4 Trends in flow

The trends in the compressor airflow rate, fuel flow rate, air–fuel ratio and the position of the fuel valve during the ambient temperature transient are shown in Fig. 11.11. (The simulator displays the trends of air–fuel ratio rather than the fuel–air ratio and this has been done for better clarity on the

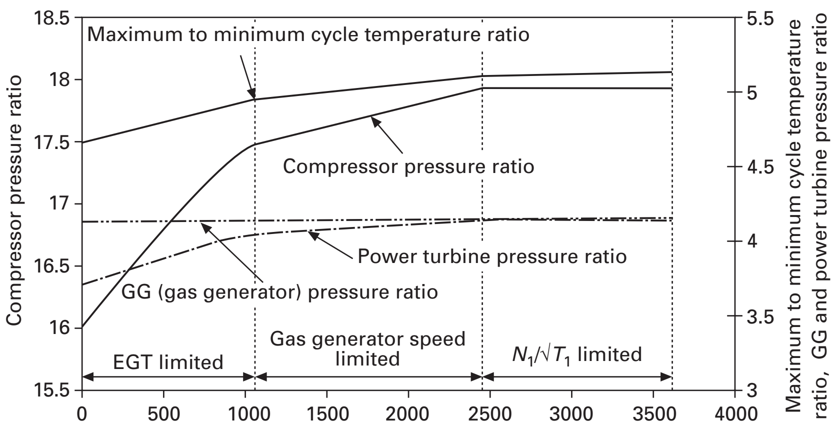

11.10 Trends in pressure ratio of the engine components during ambient temperature transient.

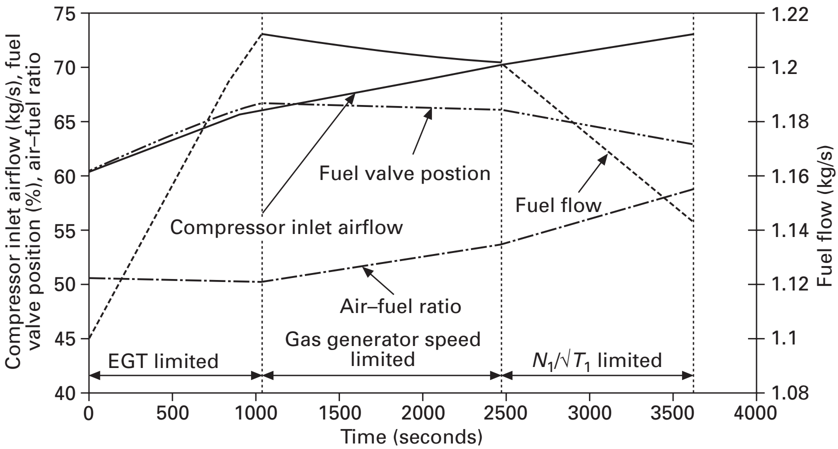

11.11 Variation of compressor airflow rate, fuel flow rate, air–fuel ratio and fuel valve position during ambient temperature transient.

display.) It has been established that the compressor non-dimensional speed increases as the ambient temperature falls for the ambient temperature transient case we are considering. From Fig. 11.3, it was observed that the compressor non-dimensional flow increases continuously with non-dimensional speed. Thus, the compressor airflow rate increases continuously with the reduction in ambient temperature because in general, as $W_1\sqrt{T_1}/P_1$ increases and as T_1 falls, W_1 must increase to compensate the reduction in $\sqrt{T_1}$. The rate of increase of airflow rate is the greatest when the engine performance is controlled by the exhaust gas temperature. During this period of operation, the compressor is farthest away from compressor inlet choking, as the lines of constant non-dimensional speed on the compressor characteristic are more spaced out, particularly at high ambient temperatures.

At low ambient temperatures, when the compressor operates under near-choked conditions, a flatter line describes the increase in compressor non-dimensional flow with its non-dimensional speed (Fig. 11.3). Thus, the rate of increase of compressor airflow rate decreases when the gas generator speed or the compressor non-dimensional speed controls the engine performance, which occurs at low ambient temperatures.

It is observed that the fuel flow rate increases during the period when the engine performance is controlled by the exhaust gas temperature, and decreases when the engine performance is controlled by the gas generator speed or the compressor non-dimensional speed. As the ambient temperature decreases, the power output and the thermal efficiency increase, particularly in the period when the power output from the gas turbine power output is controlled by EGT. This is due to the increase in compressor pressure ratio, maximum to minimum cycle temperature ratio and mass flow rate as discussed above.

However, the increase in power output is greater than the increase in thermal efficiency and is discussed in the next section. Hence, the fuel flow increases during the period when the EGT limits the gas turbine power output, as shown in Fig. 11.11.

At lower ambient temperature operation (+12 to –12 degrees Celsius), the power output of the gas turbine is controlled by the gas generator speed. The power output from the gas turbine during this period of operation remains essentially constant (see Fig. 11.12). However, the thermal efficiency of the gas turbine continues to increase due to the increase in pressure ratio and the maximum to minimum temperature ratio, T_3/T_1. Thus the increase in thermal efficiency and approximately constant power output from the gas turbine results in a decrease in the thermal input and hence fuel flow (Fig. 11.11).

At ambient temperatures below –12 degrees Celsius, the gas turbine power output is controlled by the compressor non-dimensional speed and therefore the engine operates at a constant compressor non-dimensional speed. From Fig. 11.7, which shows the variation of non-dimensional fuel flow and power, a constant compressor non-dimensional speed implies a constant gas turbine non-dimensional fuel flow, $Mf/P_1\sqrt{T_1}$, and power output, $\mathrm{Pow}/P_1\sqrt{T_1}$. Thus, a decrease in the ambient temperature, T_1, will result in a decrease in the fuel flow, Mf, in order to maintain the constant non-dimensional fuel flow. Hence, a decrease is observed in the fuel flow with the decrease in ambient temperature when the gas turbine is operating at a constant compressor non-dimensional speed.

It is observed that the air–fuel ratio decreases initially during the period when the engine performance is controlled by the exhaust gas temperature,

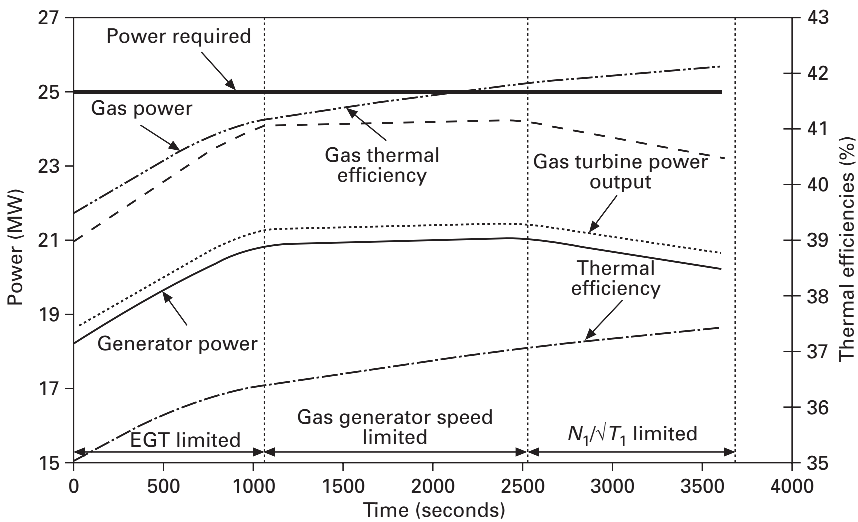

11.12 Trends in power and thermal efficiency during ambient temperature transient.

and then increases during the period when the engine performance is controlled by the gas generator speed and the compressor non-dimensional speed. In the period when the engine performance is controlled by the exhaust gas temperature, there is an increase in both compressor airflow and fuel flow (the increase in airflow must also increase the combustion airflow). The rate of increase in fuel flow is greater than the increase in combustion airflow thus resulting in a decrease in the air–fuel ratio and is due to an increase in the combustion temperature rise, as shown in Fig. 11.15. In the period when the engine performance is controlled by the gas generator speed and the compressor non-dimensional speed, the fuel flow rate decreases while the airflow rate increases. Thus, the air–fuel ratio increases during this period of operation.

11.3.5 Trends in power and thermal efficiency

Figure 11.12 shows the trends in power and thermal efficiency as the ambient temperature decreases from +30 degrees Celsius to –30 degrees Celsius. In the period when the engine performance is controlled by the exhaust gas temperature, the power output of the gas turbine and the thermal efficiency increase. The increase in power output results because of the increase in maximum to minimum cycle temperature ratio, T_3/T_1 (Fig. 11.10) and the increase in compressor airflow as discussed in Section 11.3.4. The increase in compressor pressure ratio will contribute only to an increase in power output provided design compressor pressure ratio is below the maximum cycle specific work, as discussed in Chapter 2. The power output of the gas turbine can be represented as the product of the airflow and the specific work as discussed in Chapter 2. The specific work is given by Equation 2.20. The increase in cycle temperature ratio always increases the specific work, whereas a change of the pressure ratio will increase only the specific work, provided that the compressor pressure ratio is below that which gives the maximum specific work. It should be noted that the specific work is proportional to the ambient temperature, T_1; thus, for a given pressure ratio and temperature ratio, T_3/T_1, the specific work will actually decrease as T_1 decreases. In the engine simulator, the maximum compressor pressure ratio is slightly above the case where the specific work is a maximum. Thus, the increase in specific work is due primarily to the increased maximum cycle temperature ratio, resulting in increased power output as the ambient temperature decreases, at ambient temperatures above 15 degrees Celsius. The increase in compressor pressure ratio and cycle temperature ratio, T_3/T_1, however, increases the thermal efficiency as discussed in Chapter 2 and as shown in Fig. 11.12. The increase in air flow (discussed above) also increases the power output of the gas turbine but has no direct effect on the thermal efficiency. The decrease in ambient temperature generally results in a larger increase in power output compared with the thermal efficiency of the gas turbine (during constant EGT operation).

Figure 11.12 also shows the trends in the gas power, which is effectively the power output of the gas generator and is calculated assuming that the isentropic efficiency of the power turbine is 100%. The gas thermal efficiency is also shown in Fig. 11.12 and is the thermal efficiency of the gas generator, which is calculated using the gas power output rather than the shaft power. Consequently, the gas power output and gas thermal efficiency will be higher than the gas turbine (shaft) power output and thermal efficiency of the gas turbine. The use of gas power and gas thermal efficiency is primarily to compare the performance of different gas generators and is included here only for completeness.

As the ambient temperature decreases below 12 degrees Celsius, the gas turbine performance becomes constrained by the gas generator speed. In the period of operation at constant gas generator speed, the power output increases very slightly. During this period of operation, the rate of increase of the maximum cycle temperature ratio, T_3/T_1, decreases due to near choked conditions at the compressor inlet. However, this temperature ratio and the compressor airflow have indeed increased, due to the increase in the compressor non-dimensional speed. The increase in these parameters will result in an increase in power output. But the impact of the lower ambient temperature reduces the specific work during the period of constant gas generator speed operation and this is shown in Fig. 11.13. Thus the net effect is only a modest or small increase in power output, as shown in Fig. 11.14, which represents the power and thermal efficiency trends shown in Fig. 11.12 on an ambient

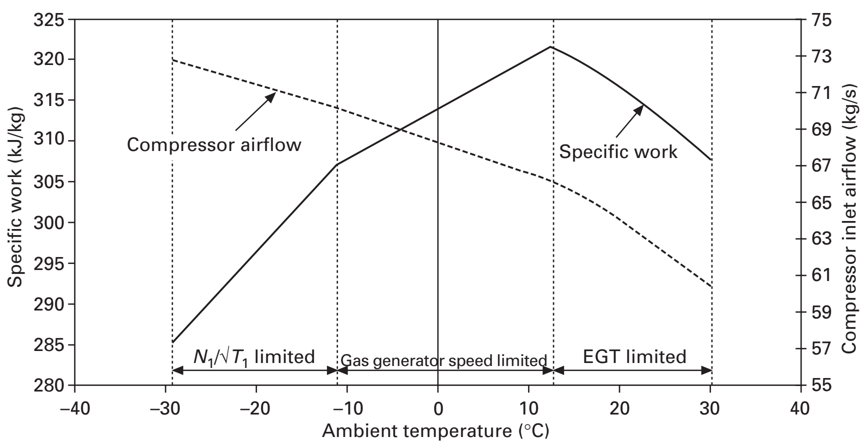

11.13 Variation of specific work and compressor airflow with ambient temperature.

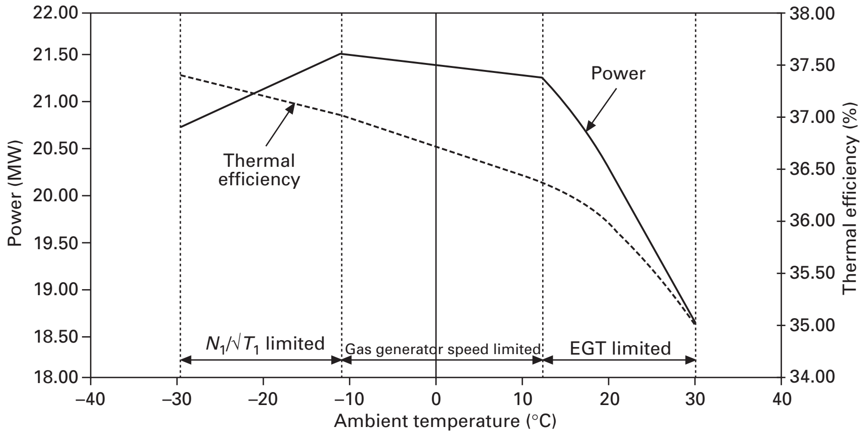

11.14 Variation of power output and thermal efficiency with ambient temperature.

temperature basis. When gas turbines are designed to operate at lower compressor pressure ratios, the compressor inlet choking is less severe. This will result in a larger increase in power output during constant gas generator speed operation, due to the larger increase in maximum to minimum temperature ratios and airflow rate as the ambient temperature decreases, particularly if the design compressor pressure ratio is below the maximum cycle specific work condition. In this case the resultant increase in pressure ratio will also contribute to an increase in gas turbine power output.

Figure 11.12 shows that, at lower ambient temperatures below –12 degrees Celsius, the gas turbine performance is constrained by the compressor non-dimensional speed, $N_1/\sqrt{T_1}$. The operating point on the compressor characteristic will now correspond to the –30 degrees Celsius case, as shown in Fig. 11.9. The compressor will continue to operate at this point, restricting the increase in compressor ratio and thus the maximum to minimum cycle temperature ratio, as shown in Figure 11.10. Therefore, as the ambient temperature decreases below –15 Celsius, the decrease in specific work will be more acute, as shown in Fig. 11.13. Although there is an increase in airflow during this period of operation, the net effect is a reduction in gas turbine power output, as shown in Fig. 11.14.

Another explanation as to why the power output falls as the ambient temperature decreases when the engine is constrained to operate at a constant compressor non-dimensional speed may be found in Fig. 11.7. This Figure shows the variation of non-dimensional power, Pow/$P_1\sqrt{T_1}$, with compressor non-dimensional speed, $N_1/\sqrt{T_1}$. Since the engine is constrained to operate at a constant non-dimensional speed, the non-dimensional power must also be constant. Thus, as T_1 decreases, the power must also decrease to maintain a constant non-dimensional power.

Figure 11.12 also shows the required power from the generator, which is set to 25 MW. It is observed that the generator power output never reaches this required power output. In practice, there will be a frequency shift as the generator slows down and this will result in a trip of the generation system. Thus it is very important for operators to know the capacity of their generation system. The simulators used here should prove an invaluable tool in predicting generating capacity, especially when engine deterioration is taken into account and this will be discussed later.

11.3.6 Trends in temperature

The temperature changes in the engine during the transient in the ambient temperature, T_1, are shown in Fig. 11.15. In the period of engine operation where the exhaust gas temperature is constant, it is observed that the turbine entry temperature is also essentially constant, thus preventing the gas generator turbine from overheating. Note that the power turbine exit temperature, T_5, decreases during the ambient temperature transient and this is due to the increase in the power turbine pressure ratio as shown in Fig. 11.10. The compressor discharge temperature also decreases slightly, although the compressor pressure ratio increases during this period (see Fig. 11.10). Although the compressor temperature ratio, T_2/T_1, increases, the decrease in T_1 during the ambient temperature transient is sufficient to decrease T_2. The Figure also includes the combustion primary zone temperature whose trend is very

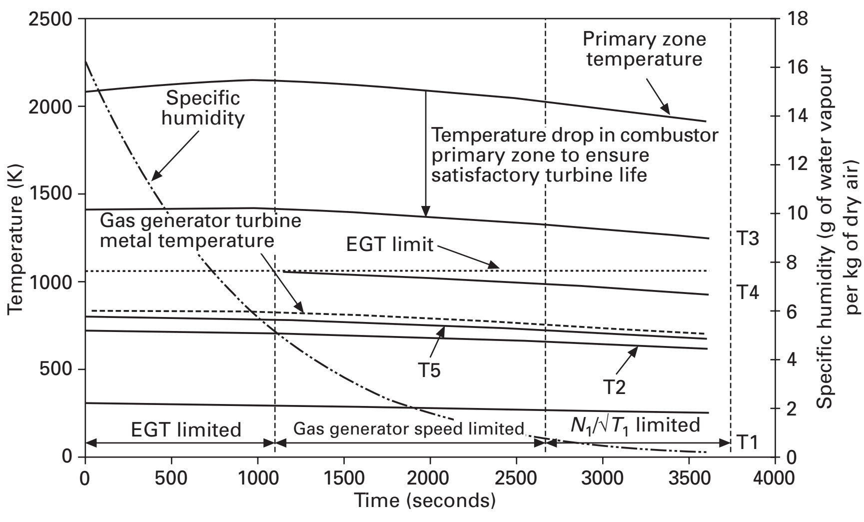

11.15 Trends in temperature and humidity during ambient temperature transient.

similar to that of the turbine entry temperature. The primary zone temperature is much too high for the turbine and the combustion dilution zone reduces the temperature of the products of combustion entering the turbine sufficiently to ensure satisfactory turbine creep life.

11.3.7 Trends in pressure

Figure 11.16 shows the trends in pressure at the inlet and exit of each engine component. The compressor discharge pressure and the turbine entry pressure, P_2 and P_3, respectively, increase during the periods of operation when the engine performance is controlled by the exhaust gas temperature and gas generator speed. During these periods of operation, there is an increase in compressor pressure ratio as discussed previously and shown in Fig. 11.10; thus there is an increase in these pressures as the ambient temperature falls. The Figure also shows that the gas generator turbine exit pressure or the power turbine inlet pressure, P_4 increases during the change in ambient temperature. Note from Fig. 11.10 that the gas generator pressure ratio remains essentially constant due to the choking conditions that prevail in the power turbine. Thus, as the gas generator turbine entry pressure increases, there will be an increase in P_4. At low ambient temperature when the engine performance is controlled by the compressor non-dimensional speed, the compressor pressure ratio remain constant. Thus the compressor discharge pressure, turbine entry pressure and the power inlet pressure also remain constant. Since the ambient pressure and the inlet and exhaust losses remain constant during the ambient temperature transient, the compressor inlet pressure,

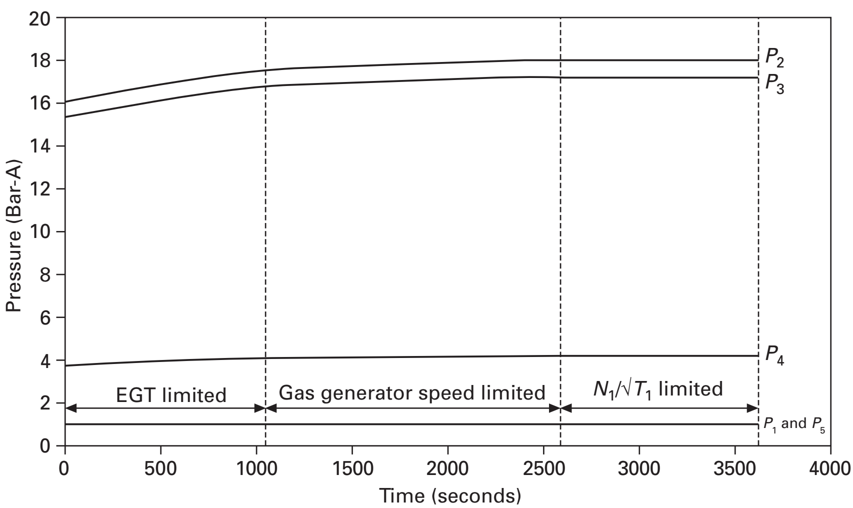

11.16 Trends in engine pressure during ambient temperature transient.

P_1, and the power turbine exit pressures, P_5, also remain constant. Due to the small inlet and exhaust losses, the trends in P_1 and P_5 are almost superimposed and are shown in Fig. 11.16.

11.3.8 Trends in turbine creep life

Turbine creep life analysis was discussed in Chapter 5 (Section 5.6), stating the importance of turbine blade temperature and stress on the plastic deformation of the turbine material when operating at elevated temperatures, even though the stresses in the blade material are below its yield point. The time for a given amount of plastic deformation defines the creep life of the turbine blade material. At the high temperatures that prevail in the gas generator turbine, the turbine creep life is about 20 000 hours operating at the design point and under ISO conditions. Significant turbine cooling is employed to maintain the blade temperature at about 1100 K. The corresponding turbine creep life for the power turbine is about 75 000 hours. The gas temperatures are much lower for the power turbine, which operates at about 1050 K. This compares with the gas entering the gas generator turbine, which may be at about 1400 K. Thus the simulator assumes that no turbine cooling is necessary for the power turbine blades.

Figure 11.17 shows the trends in the creep life usage for the gas generator and power turbines. The gas generator creep life usage remains essentially constant at ambient temperatures where the engine performance is controlled by the exhaust gas temperature. As the ambient temperature falls below 25

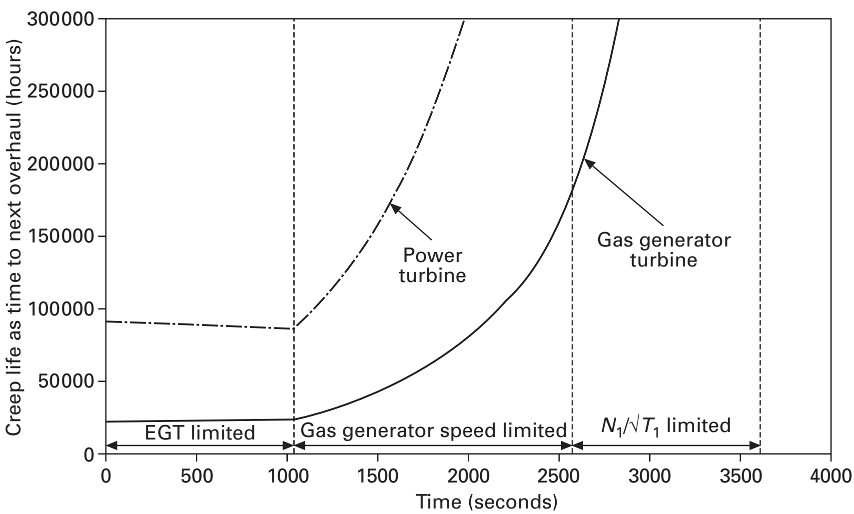

11.17 Trends in gas generator and power turbine creep life during ambient temperature transient.

degrees Celsius, the gas generator speed increases as seen in Fig. 11.8 during constant exhaust gas temperature operation. This increase in speed will indeed increase the (centrifugal) stresses in the turbine rotor blade. Furthermore, the gas generator turbine temperature drop will be constant due to the constant turbine pressure ratio resulting from the choked conditions that prevail in the power turbine and results in near-constant turbine entry temperature. The increase in mass flow rate through the engine (see Fig. 11.11) implies that the gas generator turbine power output is increasing and it is necessary to satisfy the increased power demand from the compressor as the ambient temperature decreases. Thus, the torque on the turbine rotor blades may also increase. The effect of the increased speed and torque will increase the stress on the rotor blades, thus having an adverse effect on the gas generator turbine creep life usage and reducing the time between overhauls during constant exhaust gas temperature operation. However, the cooling air temperature, T_2, decreases as the ambient temperature decreases, hence reducing the turbine blade temperature (see Fig. 11.15) as the ambient temperature falls during constant exhaust gas temperature operation. The net effect of these changes is that the change in gas generator creep life usage is minimal during constant exhaust gas temperature operation.

The impact on power turbine creep life usage is somewhat different. In the simulator the power turbine drives an electrical generator, which operates at constant (synchronous) speed. Thus the centrifugal stress remains constant. The power output from the gas turbine and thus the power generated increases as the ambient temperature falls during the period of constant exhaust gas temperature operation, as seen in Figs 11.12 and 11.14. This increase in power output at lower ambient temperatures increases the torque and stress on the rotor blades of the power turbine. It has been assumed that the power turbine is not cooled and therefore the power turbine blade temperature would be the same as the gas temperature (EGT), which is constant during this period of operation. Thus an increase in power turbine creep life usage is observed during the operating period when the exhaust gas temperature is constant.

When operating at lower ambient temperatures where the engine performance is governed by either the gas generator speed or compressor non-dimensional speed, the creep life usage of both turbines decreases significantly. The turbine entry temperature and exhaust gas temperature decrease during the period of operation when the gas generator speed is constant or when the compressor non-dimensional speed in constant (Fig. 11.15). Also note that the gas generator speed falls with decreasing ambient temperature when operating at constant compressor non-dimensional speed (Fig. 11.8). Irrespective of the changes in stress levels (due to restrictions in speed), the lower operating temperatures result in this significant decrease in turbine creep life usage. Figure 11.18 shows the creep life usage represented

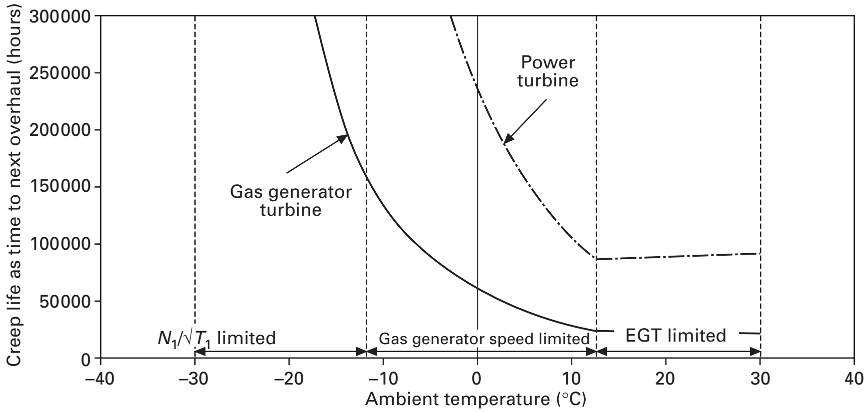

11.18 Turbine life changing with ambient temperature.

as time to next overhaul of the turbines plotted on an ambient temperature basis. At ambient temperatures below –12 degrees Celsius, hardly any creep life usage occurs.

Manufacturers often restrict the gas generator speeds at low ambient temperatures to achieve good creep life at high ambient operating conditions. The manufacturers assume a certain number of hours of engine operation at low and high ambient temperatures in determining turbine creep life and often refer to these operating cycles as rating curves. Rating curves find their origins in aero-engines, where the exhaust gas temperature limit may be raised on hot days to achieve adequate thrust for take-off. On cold days, the exhaust gas temperature limit would be reduced to compensate for the lost creep life when operating on hot days. The improved engine performance at low ambient temperatures would be adequate to ensure satisfactory engine performance for take-off. By restricting the power output at low ambient temperatures, such rating curves are normally universal and applicable to engines operating in any part of the world. Hence the manufacturer would guarantee the turbine creep life, no matter where in the world the engine operates.

11.3.9 Trends in emission

Gas turbine emissions such as NO_x and CO are dependent on the combustion pressure and temperature for a given fuel. In addition, NO_x is dependent on the specific humidity of the combustion air. The higher the specific humidity, the lower are the NO_x emissions due to the humidity suppressing the 'peak' combustion temperature. The higher the combustion pressure and temperature, the higher will be the NO_x emissions.

However, these conditions prompt the oxidation of CO to CO_2, thus reducing CO. Different operating conditions can give rise to significant changes in combustion pressures, temperatures and specific humidity, thus producing changes in such emissions. The simulator uses emission parametric models to predict the NO_x and CO emissions, which are discussed in Chapter 6 (Section 6.18). The NO_x emissions are predicted using the Bakken correlation and CO emissions are predicted using Rizk and Mongia's correlation.

Figure 11.19 shows the changes in NO_x and CO during the ambient temperature transient. As the ambient temperature decreases and the engine performance is limited by the exhaust gas temperature, NO_x increases while a small reduction in CO occurs. Figure 11.16 shows that the compressor discharge pressure increases during this period of engine operation, and thus an increase in the combustion pressure will occur. The mean primary zone temperature also increases and the specific humidity decreases (Fig. 11.15). These three factors result in an increase in NO_x and a reduction in CO. CO levels are much lower than NO_x and any significant increase in CO would imply a loss in combustion efficiency.

At lower ambient temperatures the engine performance is constrained by the gas generator speed, and there is an increase in NO_x and CO. During this period of engine operation, we note that the combustion pressure increases but at a lower rate of increase (Fig. 11.16). However, the combustion temperature (primary zone temperature) decreases but the specific humidity continues to decrease (Fig. 11.15). The effect of the decrease in combustion temperature and specific humidity gives a relatively flat NO_x curve during constant gas generator speed operation, as seen in Fig. 11.19. The decrease

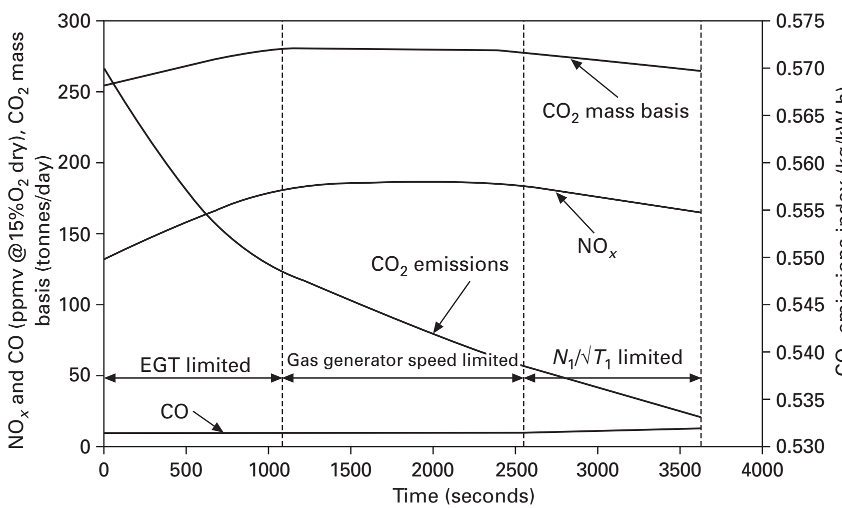

11.19 Trends in engine emissions and CO_2 during ambient temperature transient.

in combustion temperature increases the CO emissions during constant gas generator speed operation.

At ambient temperatures when the engine performance is controlled by the compressor non-dimensional speed, the compressor discharge pressure is essentially constant. However, the combustion temperature continues to fall, thus decreasing NO_x but also increasing CO. This is better illustrated in Fig. 11.20, where the emissions are shown to vary with ambient temperature.

Figure 11.19 also shows the trend in the production of CO_2 with the change in ambient temperature. The production of CO_2 is proportional to the fuel consumption and thus shows a very similar trend to the fuel flow illustrated in Fig. 11.11. CO_2, as stated previously, is not considered as a toxic pollutant but is a greenhouse gas, and is thought to contribute to global warming. Thus endeavours are made to reduce emissions of CO_2. Reductions in CO_2 can be achieved only by improving energy efficiency or burning fuels of low carbon content. Figure 11.19 also represents CO_2 emissions on an index basis, which is defined as the mass of CO_2 emissions per kWh of power produced. The increase in thermal efficiency at lower ambient temperatures reduces the fuel flow per unit of power generated. Thus, the CO_2 emission index decreases with decrease in ambient temperature. Reduction in emissions of NO_x, CO and UHCs have been achieved by the development of combustion technologies such as DLE combustors, where the emissions of NO_x and CO are below 25 ppm.

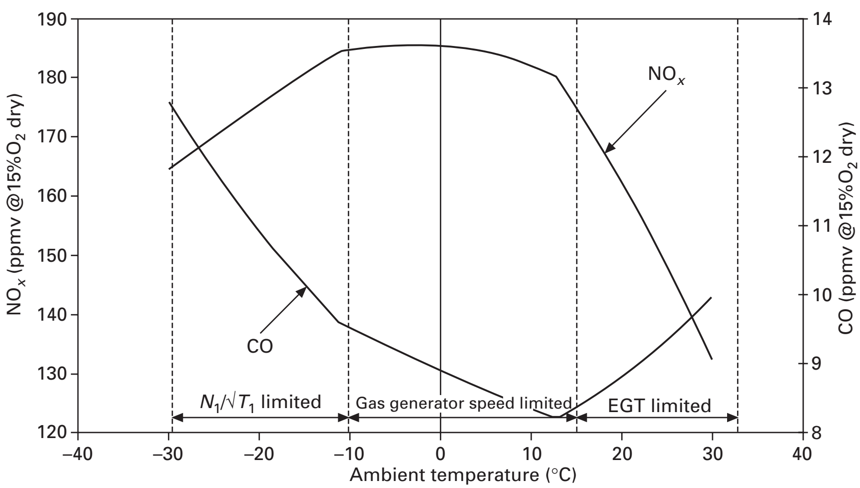

11.20 Variation of NO_x and CO with ambient temperature.

11.4 Effect of reduced power output during a change in ambient temperature

Preceding sections discussed the impact of ambient temperature on engine performance when the engine was operating on limits such as the exhaust gas temperature, gas generator speed and compressor non-dimensional speed. The case is now considered where the engine is operating at a low enough power output, such that no engine limit is reached during the same ambient temperature transient. To achieve this, the simulator is operated at an electrical power demand of 17.5 MW. As the ambient temperature decreases when operating at a constant power output (17.5 MW), the non-dimensional power (Power/$P_1\sqrt{T_1}$) will increase. Figure 11.7 shows that the non-dimensional power increases with the increase in compressor non-dimensional speed. Thus an increase in non-dimensional power implies an increase in compressor non-dimensional speed. This increase in non-dimensional speed will therefore result in an increase in compressor pressure ratio and temperature ratio, and other non-dimensional parameters, as shown in Figs 11.3 to 11.7.

11.4.1 Compressor characteristic

The operating point on the compressor characteristic during the ambient temperature transient is shown in Fig. 11.21. Due to the increase in compressor non-dimensional flow and pressure ratio, the operating point moves up the characteristic closely following the engine running line. Note that the movement of the operating point on the compressor characteristics is not as great as in the previous case when the engine was forced to operate on control system limits, as shown in Fig. 11.9.

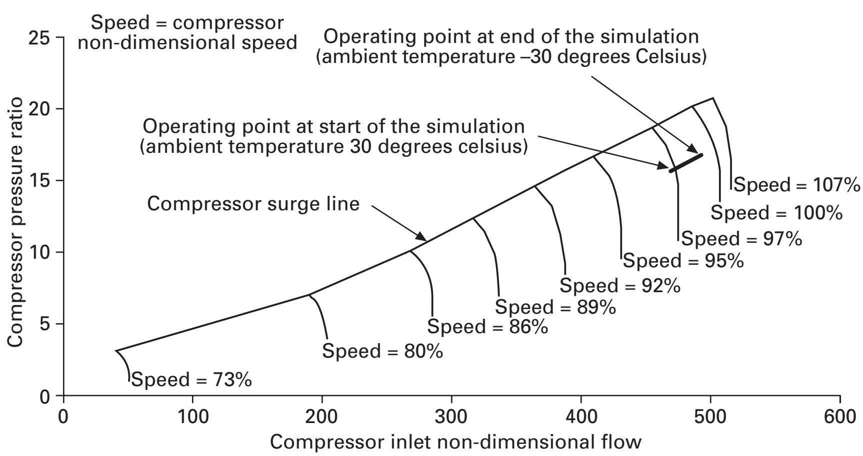

11.21 Operating points on the compressor characteristic during ambient temperature transient and low-power operation.

11.4.2 Trends in speed

The trends of the gas generator and compressor non-dimensional speed are shown in Fig. 11.22. Observe that the compressor non-dimensional speed increases, as explained in Section 11.4. The gas generator speed, however, decreases with the decrease in ambient temperature. Note that the increase in compressor non-dimensional speed is not as great as was observed when the engine power output was constrained by a control system limit. Thus, the increase in compressor non-dimensional speed is smaller for a given fall in ambient temperature. The interaction of the component characteristics (compressor and turbines) and the shape of the compressor characteristic (including VIGV position) result in a continuous fall in the gas generator speed with decreasing ambient temperature. $N_1/\sqrt{T_1}$ increases as T_1 falls, but requires a drop in N_1 to maintain the required $N_1/\sqrt{T_1}$ as dictated by component matching between the compressor and turbines (speed compatibility). Thus this trend differs from the previous case where the gas generator speed was observed to increase as the ambient temperature decreased during constant EGT operation, as shown in Fig. 11.8.

11.4.3 Trends in pressure ratio

Figure 11.23 shows the trends in the pressure ratios of the engine components (compressor and turbines). The compressor pressure ratio is observed to increase due to the increase in compressor non-dimensional speed. The trend in the pressure ratio of the gas generator turbine is essentially constant and

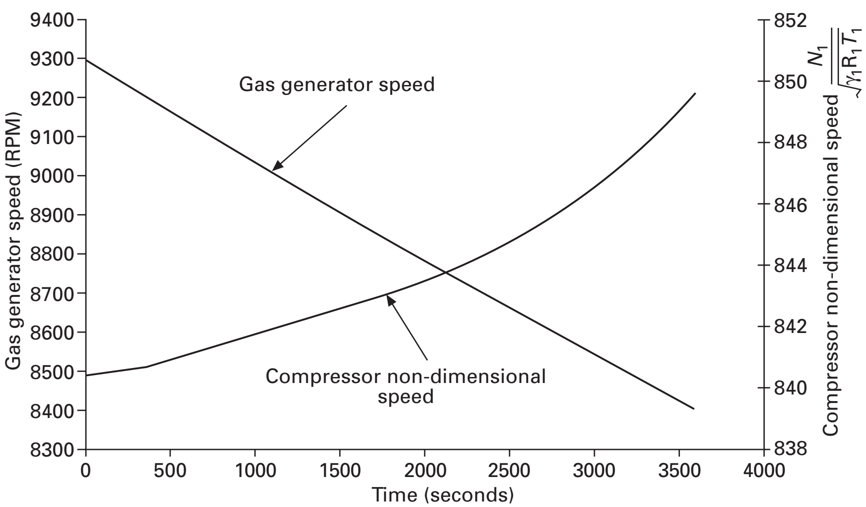

11.22 Trends in speed during ambient temperature transient and low-power operation.

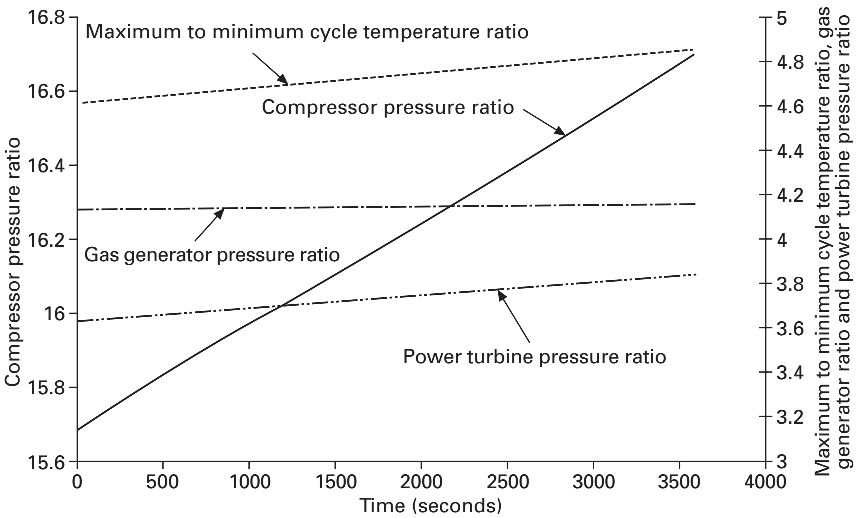

11.23 Trends in pressure ratio during ambient temperature transient and low-power operation.

is due to the choked conditions that prevail in the power turbine. Hence an increase in the power turbine pressure ratio is observed. The figure shows that the ratio of the maximum to minimum cycle temperature, T_3/T_1 also increases as the ambient temperature decreases.

11.4.4 Trends in power and thermal efficiency

As no engine limits are exceeded, the engine is capable of delivering the required power demand by the generator (17.5 MW) during the ambient temperature transient. The gas power also remains essentially constant, although a very slight decrease in gas power is observed, as seen in Fig. 11.24. Note in Fig. 11.26 that the exhaust gas temperature decreases with ambient temperature and this will be discussed later. Since the power turbine speed is constant, the power turbine non-dimensional speed $Npt/\sqrt{T_4}$, where Npt is the power turbine speed and T_4 is the exhaust gas temperature), actually increases as the ambient temperature decreases. The increase in non-dimensional speed would improve the power turbine efficiency, hence requiring slightly lower gas power for a given shaft power demand.

The thermal efficiency and the gas thermal efficiency increase as the ambient temperature decreases. It was seen in Fig. 11.23 that the compressor pressure ratio and maximum to minimum cycle temperature increase as the ambient temperature decreases. It was seen in Chapter 2 that increases in these parameters would increase the thermal efficiency of the gas turbine.

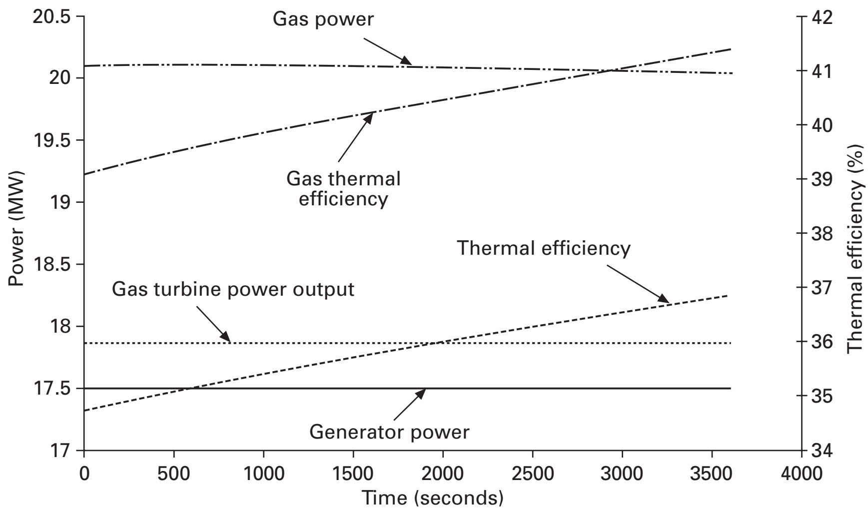

11.24 Trends in power and thermal efficiency during ambient temperature transient and low-power operation.

11.4.5 Trends in flow

The increase in compressor non-dimensional flow will require an increase in compressor inlet mass flow as the ambient temperature decreases. The improvement in thermal efficiency at lower ambient temperature will result in a lower fuel flow for a constant power output. These effects are seen in Fig. 11.25, which shows the trends in compressor mass flow and fuel flow. The fuel valve position is also shown and follows the fuel flow closely. The trend in air–fuel ratio will increase and is due to the increase in air flow and the reduction in fuel flow.

11.4.6 Trends in temperature

The trends in the temperatures at inlet and exit of each engine component are shown in Fig. 11.26. All the temperatures are observed decreasing with the fall in ambient temperature. The fall in the exhaust gas temperature occurs because the engine performance improves. Similarly, the turbine entry temperature, T_3, also decreases with a fall in ambient temperature, although T_3/T_1 increases with the reduction in ambient temperature, as shown in Fig. 11.23.

11.4.7 Trends in pressure

The trends in the pressure during the ambient temperature transient are shown in Fig. 11.27. The compressor discharge pressure and the combustion pressure

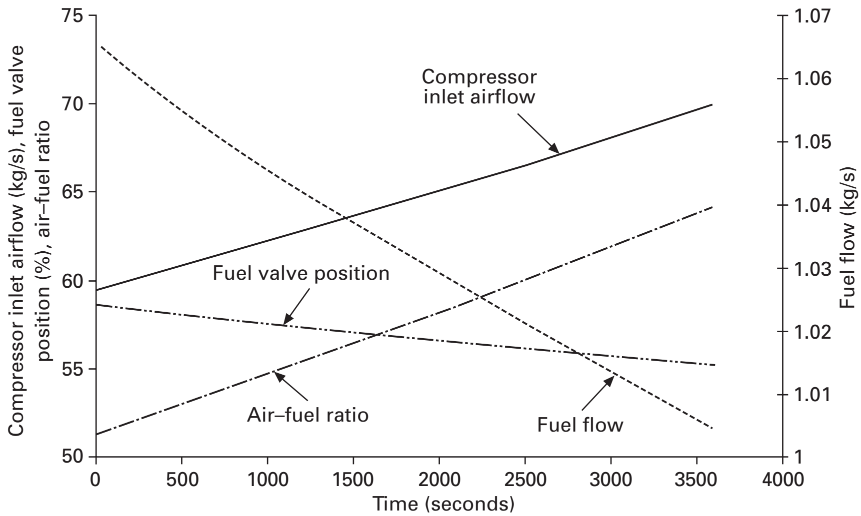

11.25 Trends in flow during ambient temperature transient and low-power operation.

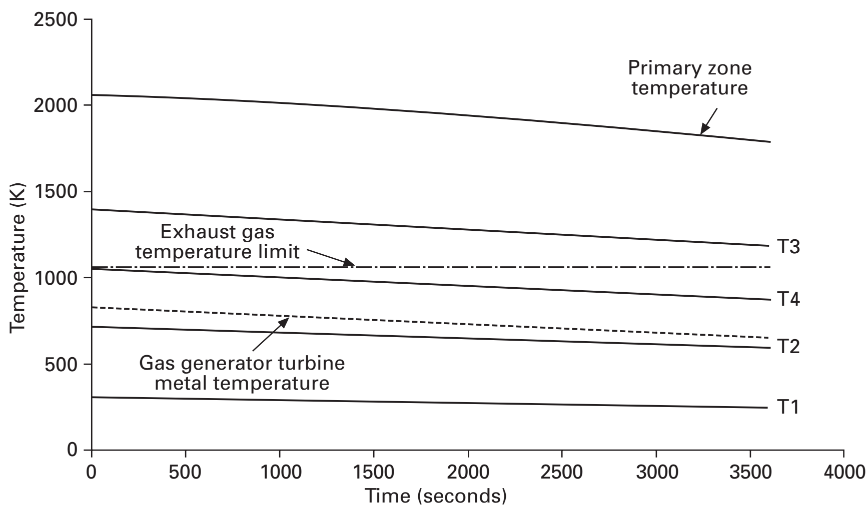

11.26 Trends in temperature due to ambient temperature transient during low-power operation.

increase as the ambient temperature decreases, due to the increase in compressor pressure ratio, as observed in Fig. 11.23. The power turbine inlet pressure, P_4, also increases during the transient and this is a result of the increase in compressor pressure ratio and constant gas generator pressure ratio, due to choking conditions that prevail in the power turbine.

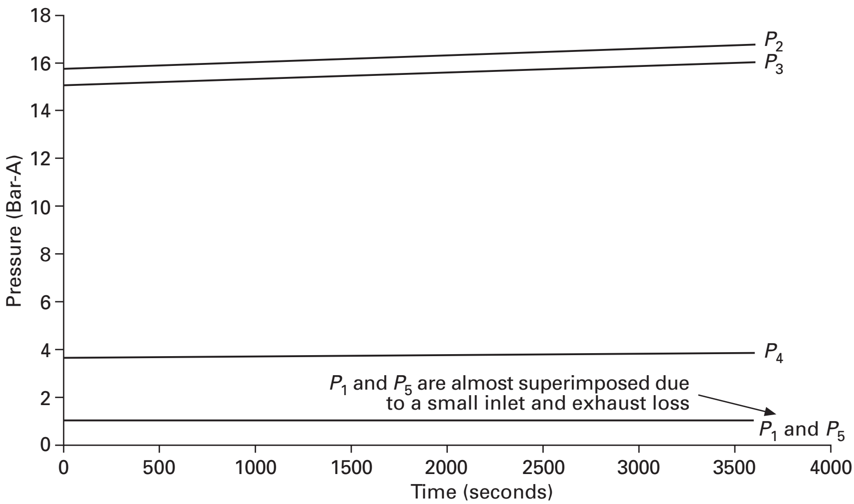

11.27 Trends in pressure during ambient temperature transient.

11.4.8 Trends in turbine creep life

From the trends in speed and temperature (Figs 11.22 and 11.26, respectively) it is observed that the speed and turbine entry temperature decrease during the ambient temperature transient. It is also observed that the compressor discharge temperature decreases, thus resulting in a lower cooling air temperature.

All these factors decrease the gas generator creep life usage and this can be seen in Fig. 11.28, which shows the trends in the gas generator and power turbine creep life usage. Since the exhaust gas temperature also decreases, the power turbine creep life usage decreases and this can also be seen in Fig. 11.28. Since turbine creep lives are dependent on load and ambient conditions, proper monitoring of turbine creep life can increase periods between turbine overhaul and reduce the engine maintenance costs, thus improving engine life cycle costs.

11.4.9 Trends in emissions

The trends in NO_x, CO and CO_2 during the ambient temperature transient are shown in Fig. 11.29. The sensitivity of combustion pressure in the formation of NO_x has been discussed. It is observed that the combustion pressure increases during this simulation, as shown in Fig. 11.27. Although the combustion temperature decreases in Fig. 11.26, the specific humidity decreases exponentially with ambient temperature, as shown in Fig. 11.15. The decrease in specific humidity increases the formation of NO_x, which results in an increase in NO_x as the ambient temperature decreases. However, at low ambient temperatures, which occur towards the end of the simulation, the

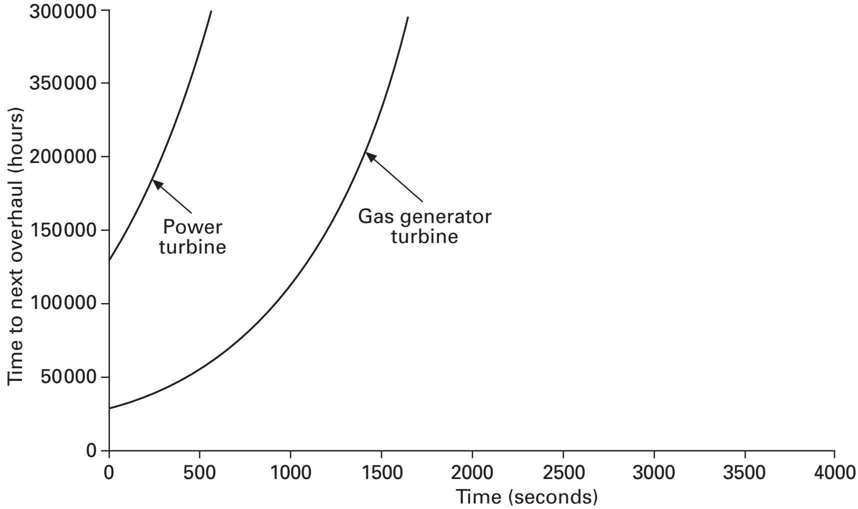

11.28 Increase in turbine creep life during ambient temperature transient and low-power operation.

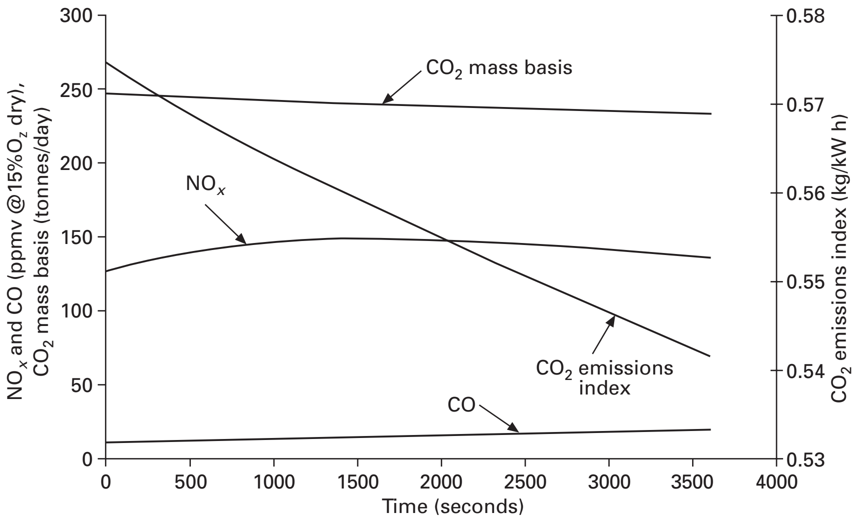

11.29 Trends in emissions due to ambient temperature transient and low-power operating conditions.

specific humidity is small and the decrease in combustion temperature dominates, resulting in a decrease in NO_x emissions. This can be seen in Fig. 11.29, which shows the trend in emissions when the engine is operating at low power. The figure also shows that CO increases during this transient. It has been discussed that CO formation is more sensitive to combustion temperature than combustion pressure, thus the decrease in combustion temperature results in an increase in CO as the ambient temperature decreases. The figure also shows the trends in CO_2. A reduction in CO_2 is observed and is due to the reduction in fuel flow, because of the better thermal efficiency, as the ambient temperature decreases.

11.5 Effect of humidity on gas turbine performance and emissions

It was stated in Chapter 2 that it is the specific humidity which affects the performance of gas turbines. Also the effects of humidity on emissions have been discussed, particularly NO_x. Increasing the specific humidity increases the gas constant, R, and specific heat at constant pressure, c_p, while the ratio of specific heats, γ, decreases. These trends are shown in Fig. 11.30, which shows the variation of these gas properties with specific humidity. Also observe that the variation in γ is small compared with c_p and R.

For a given ambient temperature and pressure, an increase in relative humidity will increase the specific humidity, as can be seen from Fig. 2.16 in Chapter 2. During maximum power demand and operating at high ambient temperatures, the power output of the gas turbine is limited by the exhaust gas temperature (EGT). For a given ambient temperature, the ratio of exhaust gas temperature to compressor inlet temperature, T_4(EGT)/T_1, is fixed (note the change in γ is small as discussed above). From Fig. 11.6, the compressor non-dimensional speed, $N_1/\sqrt{(\gamma R_1 T_1)}$ is also fixed, which in turn would fix the non-dimensional power output (see Fig. 11.7). Referring to Fig. 11.7, any increase in the gas constant, R, results in an increase in the gas turbine power output in order to maintain the non-dimensional power output of the gas

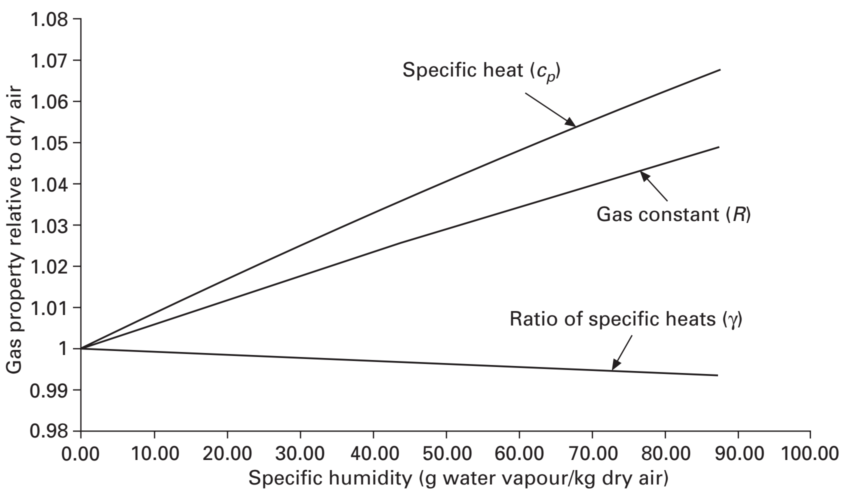

11.30 Variation of c_p, R and γ relative to dry air with specific humidity.

turbine. This is illustrated in Fig. 11.31, which shows the gas turbine power output with ambient temperature for a series of values for relative humidity. However, the increase in specific humidity reduces the thermal efficiency, due to the additional fuel required to heat the water vapour to the required turbine entry temperature. The variation of gas turbine thermal efficiency with ambient temperature for a series of values of relative humidity, is shown in Fig. 11.32. At high ambient temperatures (30 degrees Celsius), the increase in gas turbine power output due to the increase in relative humidity (from 0% to 100%) can be about 1.5% and this increase in power increases with ambient temperature. Thus, at high ambient temperature, an increase in humidity will result in a worthwhile increase in power output. Operating at constant compressor non-dimensional speed, $N_1/\sqrt{(\gamma RT)}$, an increase in the gas constant, R, due to the increase in specific humidity, will require an increase in the gas

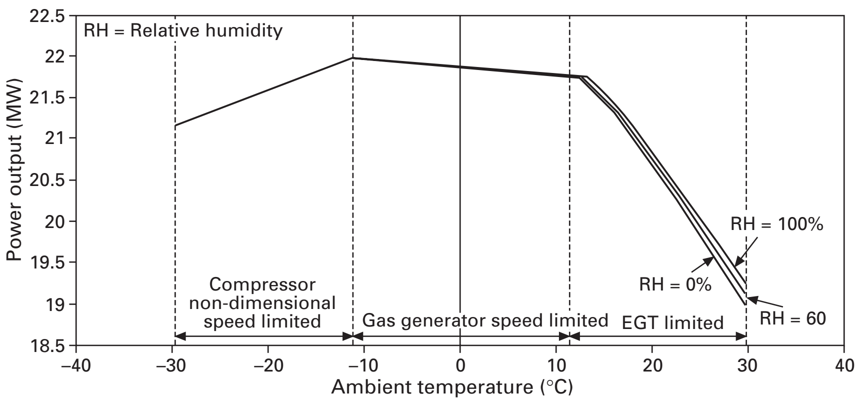

11.31 Impact of relative humidity on gas turbine power output.

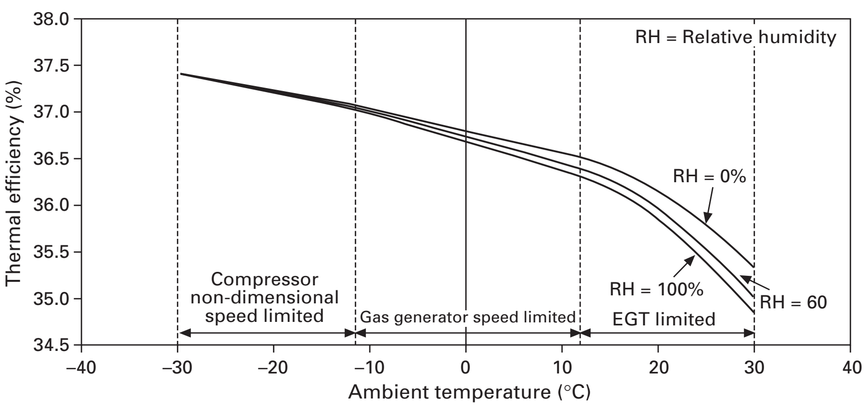

11.32 Impact of relative humidity on gas turbine thermal efficiency.

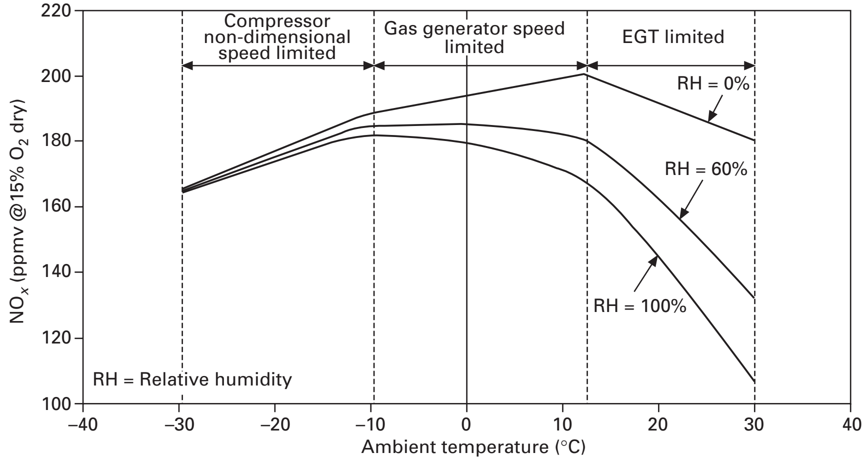

11.33 Impact of relative humidity on NO_x emissions

generator speed, N_1. Therefore, the gas generator speed limit is reached at a higher ambient temperature as the relative humidity increases, as observed in Fig. 11.31. Furthermore, from Fig. 11.3, it is evident that the compressor inlet mass flow rate, W_1, would decrease with increased humidity.

At low ambient temperatures, the gas turbine power output is limited by the gas generator speed or $N_1/\sqrt{T_1}$. Thus, an increase in the gas constant, R, results in a decrease in compressor non-dimensional speed, $N_1/\sqrt{(\gamma RT)}$. This, in turn, would reduce the turbine entry temperature, T_3, as seen in Fig. 11.5. Therefore, the specific work decreases due to the decrease in T_3. Although the increase in R and therefore c_p to increase the specific work, the decreases in T_3 and W_1 result in a decrease in gas turbine power output. The decrease in power output is small due to the low ambient temperatures, when the gas turbine power output is limited by the gas generator speed or $N_1/\sqrt{T_1}$. At such low ambient temperatures, the change in specific humidity with the relative humidity is small as can be seen in Fig. 2.16. Thus the changes in gas properties such as R and c_p are also small. Hence, there is a very small loss in power output with increase in relative humidity at low ambient temperatures when the gas generator speed or $N_1/\sqrt{T_1}$ limit the power output of the gas turbine.

The impact of humidity on NO_x emissions is more profound. High specific humidity results in increased presence of water vapour in the combustor, thus suppressing the 'peak' combustion temperature. This decrease in temperature results in a significant decrease in NO_x with the increase in humidity, as illustrated in Fig. 11.33.

12

Simulating the effect of change in ambient pressure on engine performance

The impact of the change in ambient temperature on engine performance was considered in Chapter 11, where the negative impact of high ambient temperatures on performance was observed. Another factor that affects engine performance is the ambient pressure, where low ambient pressure reduces maximum power output from the engine. The two-shaft gas turbine simulator will now be used to investigate the effects of the change in ambient pressure on engine performance. The ambient pressure may change quite significantly at a given elevation. At sea level it may vary from 1.04 Bar to 0.96 Bar for a high pressure day and a low pressure day, respectively. This represents about an 8% change in ambient pressure corresponding to those days. Gas turbines that operate at high elevations, where the ambient pressure is lower than at sea level will show a reduced power output. For example, at an elevation of 1000 metres, the ambient pressure would be about 0.9 Bar on an ISA (International Standard Atmosphere) day. However, the ambient temperature at this altitude will be lower, thus partly compensating for the reduced power output.

To cover this ambient pressure range, the ambient pressure will be varied from 1.03 Bar to 0.9 Bar in 1 hour (3600 seconds). Also considered will be two operating cases, which correspond to high power and low power operating conditions. The high power operating condition will be represented by setting the power demand from the generator such that the engine will always be on an operating limit. This is simulated by setting the generator power demand to 25 MW. The low power case will be simulated by setting the power demand from the generator such that an engine operating limit is never reached (low power case power demand is set to 17.5 MW). To investigate the impact of ambient pressure changes on engine performance, the ambient temperature will be assumed to remain constant at 15 degrees Celsius. This will result in the engine power output being limited by the exhaust gas temperature (EGT) limit rather than by the speed limits from the gas turbine. The inlet and exhaust losses will be set to 100 mm water gauge during these simulations. Again we shall ignore the gas properties terms (γ and R) present in the non-dimensional parameters for flows and speeds, and we shall make reference to them when relevant.

12.1 Effect of ambient pressure on engine performance (high-power case)

During high power operation, the exhaust gas temperature limits the engine performance. Since the ambient temperature remains constant and the engine operates on the EGT limit, the ratio of T_4 (EGT)/T_1 also remains constant as the ambient pressure decreases from 1.03 Bar to 0.9 Bar. Figure 11.6 shows the running line describing the variation of T_4 (EGT)/T_1 with the compressor non-dimensional speed, ($N_1/\sqrt{T_1}$). A constant T_4 (EGT)/T_1, implies that the compressor non-dimensional speed will also remain constant. Thus, the non-dimensional speed of the compressor remains constant throughout the simulation. A constant compressor non-dimensional speed will mean that other engine non-dimensional parameters will remain constant throughout the simulation (see Figs 11.3 to 11.7). Hence the pressure ratios, temperature ratios, non-dimensional flows and non-dimensional power will all remain constant during the simulation.

12.1.1 Trends in compressor characteristic and flow

Since the pressure ratio and compressor non-dimensional flow remain constant, the operating point does not move on the compressor characteristic during the ambient pressure transient, as shown in Fig. 12.1.

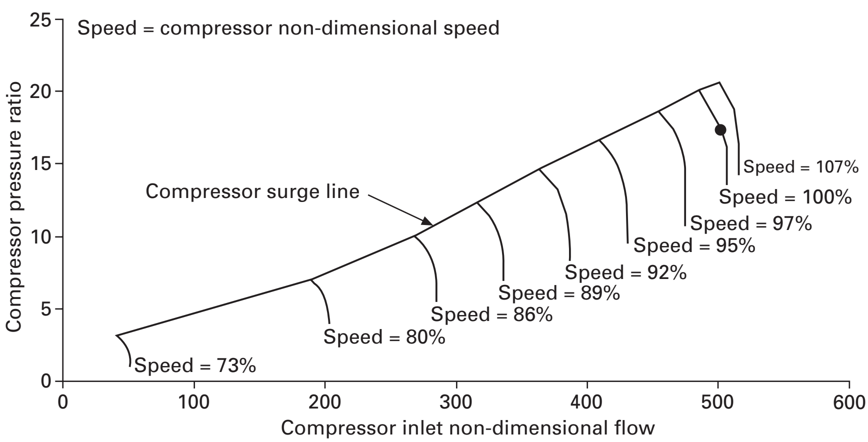

12.1 Operating point on the compressor characteristic during ambient pressure transient.

Since the compressor inlet non-dimensional flow $W_1\sqrt{T_1}/P_1$ is constant during this transient, the compressor inlet flow W_1 decreases proportionally with P_1 due to the fall in the ambient pressure. This can be seen in Fig. 12.2, which shows the trends in flow and fuel valve position during the ambient pressure transient. The temperature rise across the combustion system and the combustion inlet temperature, T_2, also remain constant during this ambient pressure transient. Figure 2.17 in Chapter 2, which shows the variation of the air–fuel ratio as a function of the combustor inlet temperature and temperature rise, indicates that the air–fuel ratio is also constant. Since the compressor airflow is decreasing, the amount of combustion air also reduces. As the air–fuel ratio is constant, a decrease in combustion airflow will result in a decrease in fuel flow as can be seen in Figure 12.2. The figure also shows the trend in the fuel valve position and this trend is similar to the trend in fuel flow.

12.1.2 Trends in power and thermal efficiency

As the compressor non-dimensional speed is constant during the ambient pressure transient, the non-dimensional power also remains constant. Thus any reduction in P_1 requires a corresponding reduction in power output to maintain the constant non-dimensional power and results in a lower power output (shaft and gas power) due to the decrease of ambient pressure, as shown in Fig. 12.3. Hence, the negative impact of low ambient pressure on maximum engine power output is illustrated, a problem often encountered by gas turbines operating at high elevations.

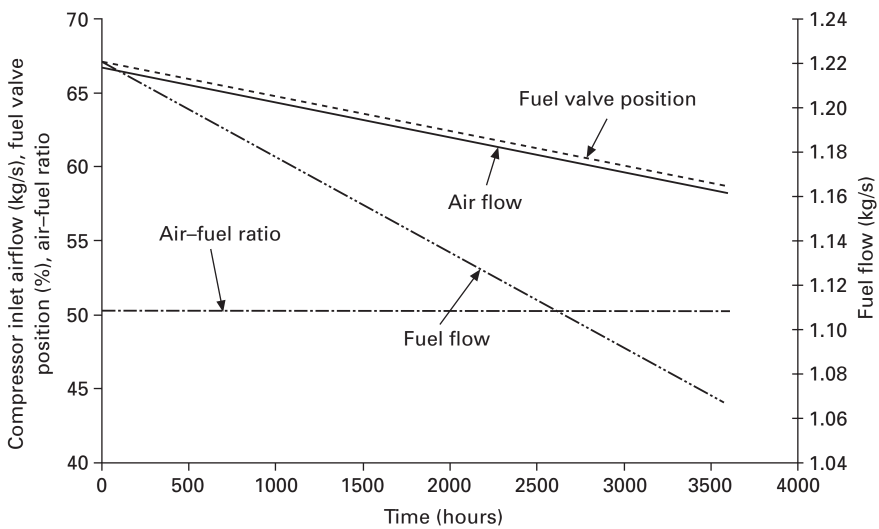

12.2 Trends in flow during ambient pressure transient.

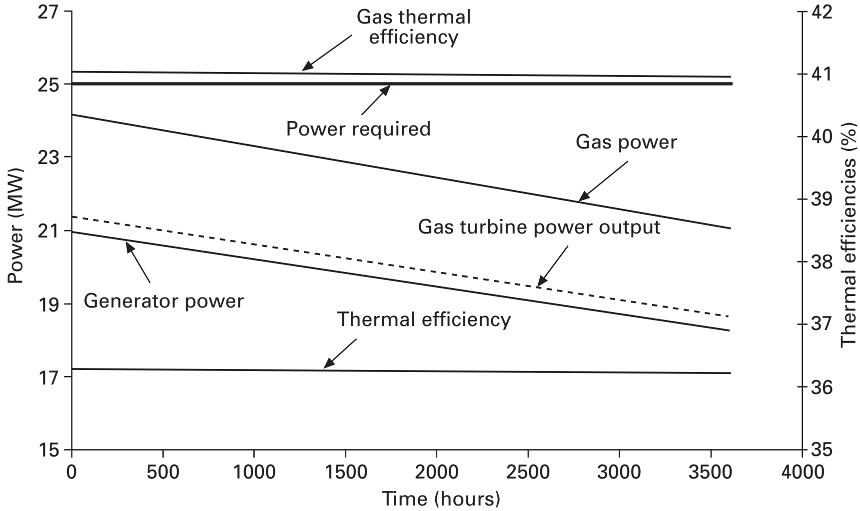

12.3 Trends in power output and thermal efficiency during ambient pressure transient.

The thermal efficiencies are affected by the compressor pressure ratio, P_2/P_1, and temperature ratio, T_3/T_1. These parameters remain constant due to the constant compressor non-dimensional speed, thus the thermal efficiencies do not change very much for the current operating conditions. The slight decrease in thermal efficiency is largely attributed to the increase in specific humidity due to the decrease in ambient pressure.

12.1.3 Trends in pressure

The compressor and turbine pressure ratios are constant during the decrease in the ambient pressure, and any fall in ambient pressure will result in a decrease in compressor discharge pressure. The decrease in the compressor discharge pressure will be directly proportional to the ambient pressure. Similarly, the gas generator and power turbine inlet and exit pressures also fall proportionally with the ambient pressure, as shown in Fig. 12.4.

12.1.4 Trends in creep life

The trends in creep life usage of the gas generator and power turbines during the ambient pressure transient are shown in Fig. 12.5. Observe that the creep life usage of the gas generator and power turbine decreases as the ambient pressure decreases. Note from Fig. 12.3 that the power output also decreases with the decrease in ambient pressure. Therefore, the torque acting on the power turbine blades must decrease, as the power turbine speed is constant.

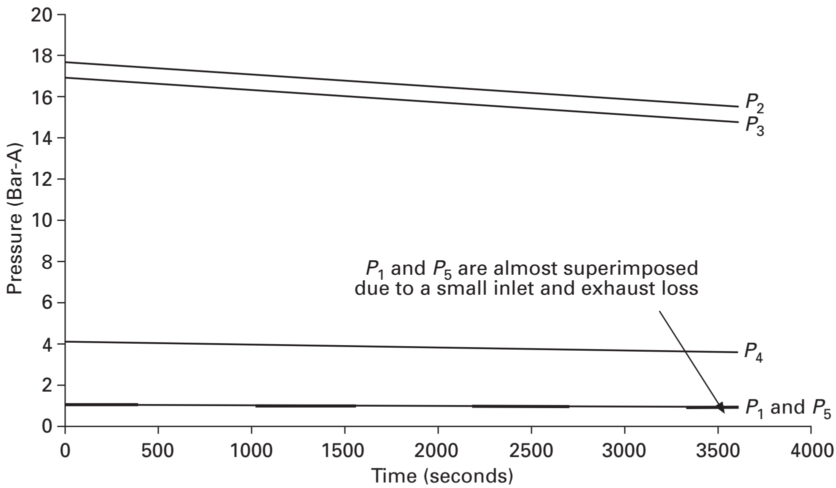

12.4 Trends in pressure during ambient pressure transient.

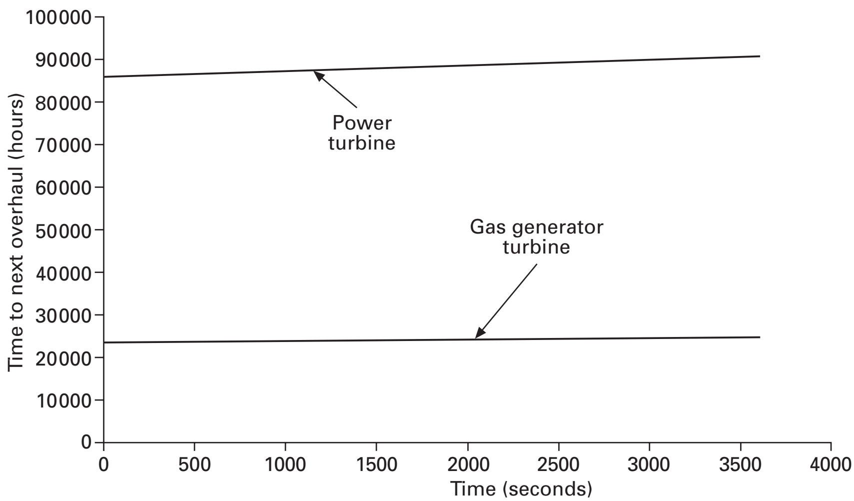

12.5 Trends in creep lives of gas generator and power turbine blades during ambient pressure transient.

This reduction in torque will result in a lower total stress level on the blades, although the centrifugal stress is constant. Since the exhaust gas temperature remains constant, the lower stress levels result in a decrease in creep life usage of the power turbine.

A similar situation exists for the gas generator turbine. Because of the constant compressor non-dimensional speed, the gas generator speed and the turbine entry temperature will also remain constant. Furthermore, the compressor discharge temperature and hence the cooling air temperature will also remain constant. Since the airflow through the compressor decreases with the ambient pressure, the power absorbed by the compressor will also reduce. All the power required by the compressor is provided by the gas generator turbine, so the power produced by the gas generator turbine will also reduce. Although the gas generator turbine speed and temperature are constant during the ambient pressure transient, the reduced compressor power demand results in less torque in the gas generator turbine blades. The lower stresses in the gas generator turbine blades due to the lower torque requirements result in a decrease in the gas generator turbine creep life usage and can be seen in Fig. 12.5.

12.1.5 Trends in emissions

Figure 12.6 shows the trends in NO_x, CO and CO_2 emissions. Observe that the compressor discharge pressure decreases with ambient pressure, leading to a decrease in combustion pressure. The combustion temperature remains constant due to the constant compressor non-dimensional speed. Thus, the decrease in combustion pressure results in a decrease in NO_x emission and an increase in CO emissions. Also, the increase in specific humidity due to the decrease in ambient pressure will contribute to the reduction in NO_x.

Since the fuel flow decreases with ambient pressure, the CO_2 emissions on a mass basis also decrease with reduced ambient pressure and follow the fuel flow trend. The thermal efficiency decreases slightly as discussed above,

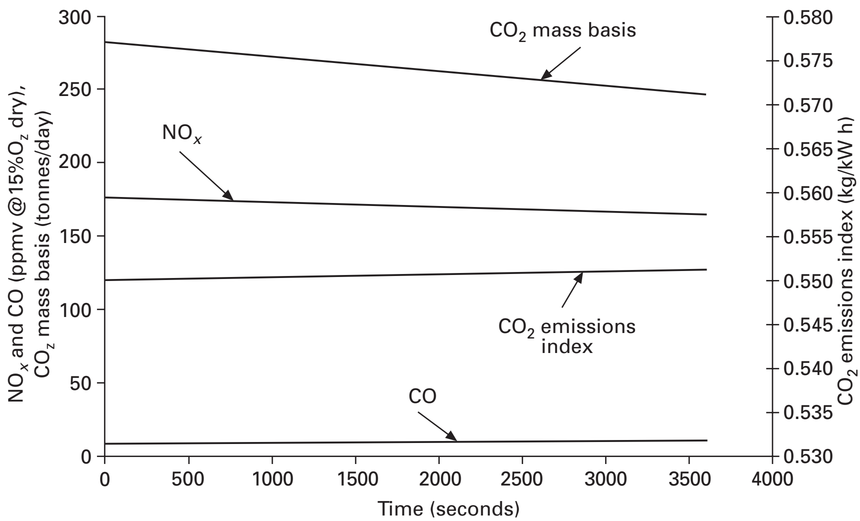

12.6 Trends in gas turbine emissions during ambient pressure transient.

so the CO_2 emission index also increases slightly. The trends in these emission parameters are shown in Fig. 12.6.

12.2 Effect of ambient pressure changes on engine performance at lower power outputs

Section 12.1 considered the impact of ambient pressure changes on engine performance when the engine performance is constrained by an engine operating limit, as would be encountered at high-power output levels. Consider now the impact of change in the ambient pressure when the engine is operating at lower power such that no engine operating limits are encountered. The same ambient pressure transient used previously will be repeated (i.e. reducing the ambient pressure from 1.03 to 0.9 Bar in 1 hour), with the ambient temperature set to 15 degrees Celsius, and inlet and exhaust losses set to 100 mm water gauge. The generator power demand is set to 17.5 MW throughout the simulation to represent the low power case.

Since the power output of the gas turbine will be constant throughout the simulation as no engine limits are reached, the non-dimensional power, Power/$(P_1\sqrt{T_1})$, will increase as the ambient pressure P_1 decreases. Referring to Fig. 11.7, which shows the variation of non-dimensional power with compressor non-dimensional speed, any increase in non-dimensional power must be accompanied by an increase in compressor non-dimensional speed. Thus the increase in non-dimensional speed will result in increases in other non-dimensional parameters such as pressure ratios, temperature ratios and non-dimensional flows.

12.2.1 Compressor characteristic

The operating point on the compressor characteristic for the low power case is shown in Fig. 12.7. The operation point is observed moving up the running line from a lower compressor non-dimensional flow and pressure ratio to a higher compressor non-dimensional flow and pressure ratio. This is due to the increase in compressor non-dimensional speed as the ambient pressure decreases.

12.2.2 Trends in speed

The ambient pressure transient results in an increase in compressor non-dimensional speed, $N_1/\sqrt{T_1}$ and therefore an increase in gas generator speed due to a constant ambient temperature, T_1. This is shown in Fig. 12.8, which illustrates the changes in the gas generator and compressor non-dimensional speed during the ambient pressure transient.

It is also observed that the rate of increase in gas generator speed increases

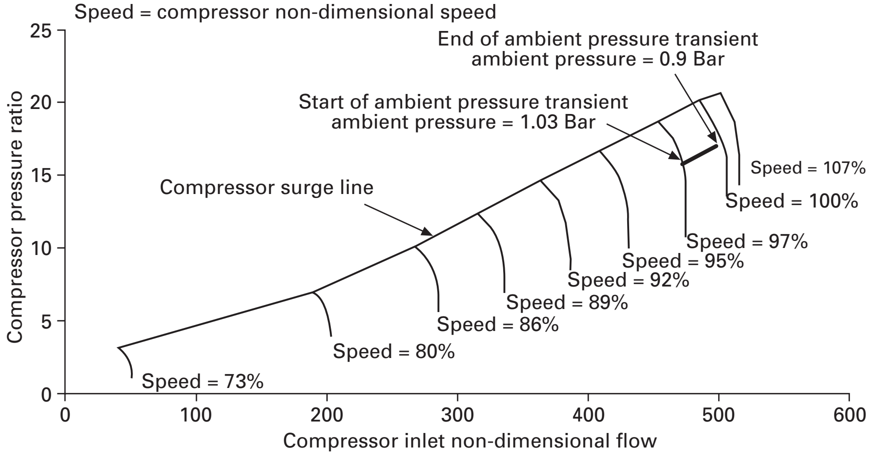

12.7 Operating point on the compressor characteristic during ambient pressure transient.

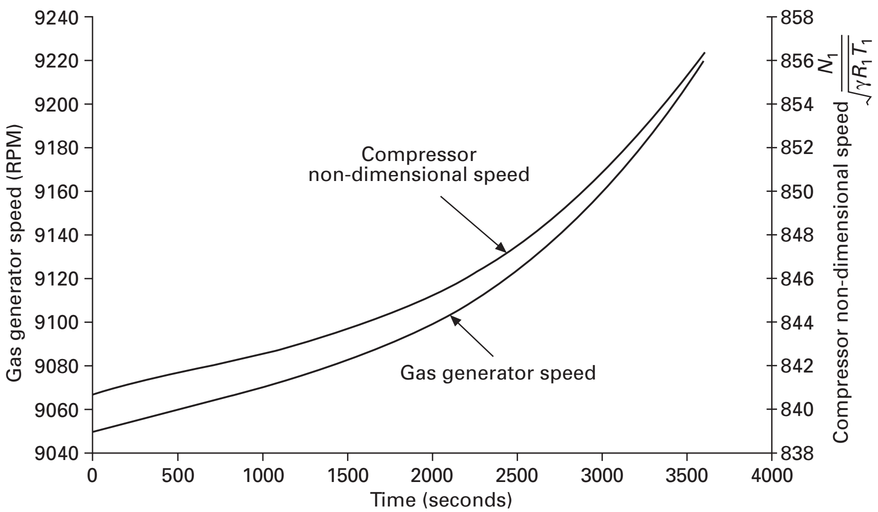

12.8 Compressor speed changes during ambient pressure transient.

as the ambient pressure falls. This is due to higher compressor non-dimensional speeds forcing the compressor to operate closer to compressor inlet choke conditions. Note that the speeds do not reach or exceed any limiting values during this transient.

12.2.3 Trends in pressure ratios

The trends in pressure ratios for the compressor, gas generator turbine and power turbine are shown in Fig. 12.9. The increase in compressor non-

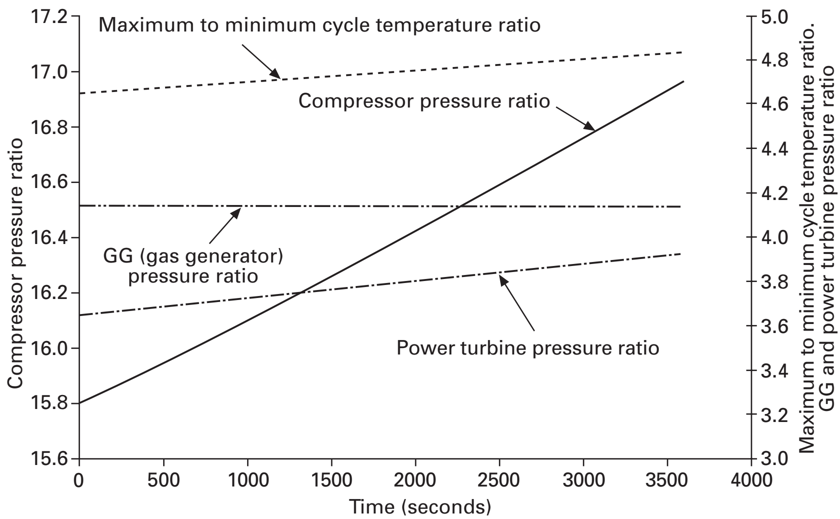

12.9 Trends in pressure ratios for compressor, gas generator turbine and power turbine.

dimensional speed results in an increase in compressor pressure ratio, as can be observed in Fig. 11.4. The gas generator turbine pressure ratio remains essentially constant, due to the choking conditions that prevail in the power turbine. Thus an increase in compressor pressure ratio results in an increase in the power turbine pressure ratio.

The figure also shows the trend in the maximum to minimum cycle temperature ratio, T_3/T_1. An increase in T_3/T_1 is necessary because of the increase in compressor non-dimensional speed, as illustrated in Fig. 11.5.

12.2.4 Trends in power and thermal efficiency

Since no engine operating limits are exceeded during the ambient pressure transient, the power required by the generator will always be provided by the gas turbine. Thus the generator power output trend remains on the power demand set point. Hence, the gas turbine power output and the gas power also remain essentially constant during this ambient pressure transient, as can be seen in Fig. 12.10, which shows the trends in powers and thermal efficiencies during the ambient pressure transient. The slight increase in gas power is due primarily to a small decrease in the power turbine isentropic efficiency. As the ambient pressure decreases, the exhaust gas temperature increases to maintain the generator power demand. The power turbine non-dimensional speed now decreases (note that the power turbine speed is constant), resulting in a small decrease in power turbine efficiency. Thus a

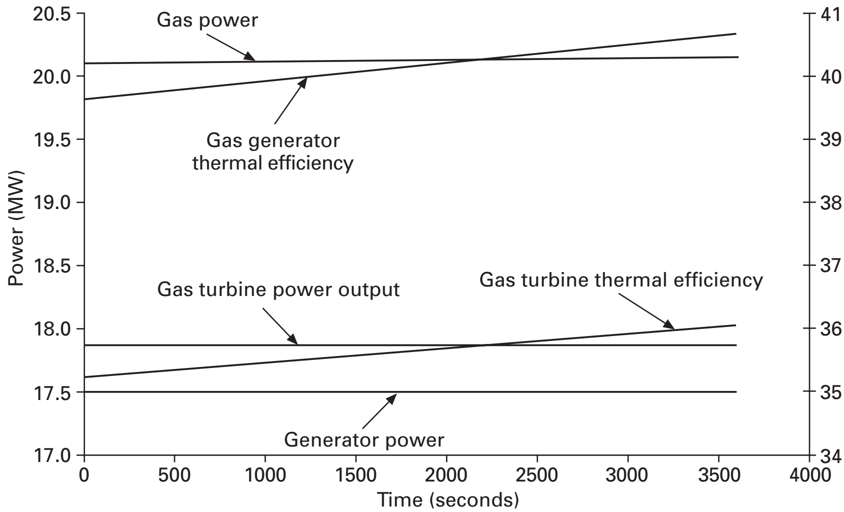

12.10 Trends in the power and thermal efficiency during ambient pressure transient.

corresponding increase in gas power output occurs to maintain the power demand from the generator as observed in Fig. 12.10.

The gas turbine thermal efficiency and the gas thermal efficiency, which represents the efficiency of the gas generator, increase as the ambient pressure decreases. As was seen in Fig. 12.9, the compressor pressure ratio and the maximum to minimum cycle temperature ratio, T_3/T_1 increase as the ambient pressure decreases. The thermal efficiencies essentially are functions of these ratios and independent of ambient pressure as discussed in Chapter 2. Thus the increases in the compressor pressure ratio and temperature ratio, T_3/T_1, result in increases in the gas turbine thermal efficiency and the gas generator thermal efficiency. Therefore, when the power demand is below the maximum capacity of the engine, a low ambient pressure is desirable because it results in an increase in thermal efficiency. It is worth pointing out that this is indeed the principle of a closed cycle gas turbine where we reduce the cycle working pressure to reduce the load, thus maintaining a constant thermal efficiency at lower loads. Such closed cycle gas turbines have been built and operated as a means of overcoming the poor thermal efficiencies of gas turbines at low loads.

12.2.5 Trends in flow

Figure 12.11 shows the trends in compressor inlet flow, fuel flow and the air–fuel ratio during the ambient pressure transient. The figure also shows the position of the fuel valve during this transient. It has been observed that

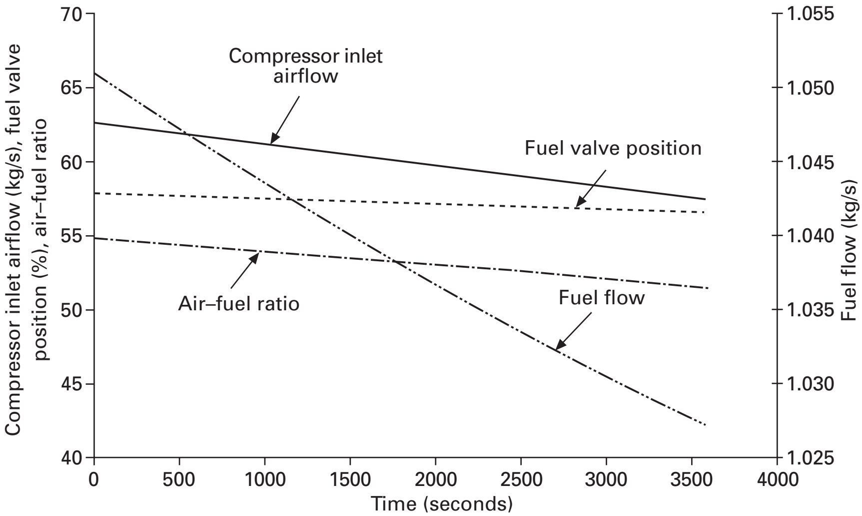

12.11 Trends in flow during ambient pressure transient.

the compressor pressure ratio and the temperature ratio, T_3/T_1, increase during the ambient pressure transient. The specific work will increase and this is due to the increase in T_3/T_1. As the power output remain constant (see Fig. 12.10), the increase in specific work will result in a decrease in compressor inlet air flow as shown in Fig. 12.11.

It is worth noting that the decrease in compressor flow, compared with the previous case, where the engine was operating on an exhaust gas temperature limit (Fig. 12.2), is smaller. This is due to the resultant increase in the compressor non-dimensional flow and speed for this case, whereas in the previous case the compressor non-dimensional flow remained constant as the ambient pressure decreased.

The trends in the fuel flow and fuel valve position also show a decline. This is due primarily to the increased thermal efficiency. Since the power output remains constant, any increase in the thermal efficiency must result in a decrease in fuel flow, as shown in Fig. 12.11. The air–fuel ratio decreases because of the increase in T_3/T_1, as shown in Fig. 12.9. This results in an increase in the turbine entry temperature, T_3, as the ambient temperature, T_1 is constant during this transient. Although there is an increase in the compressor discharge temperature, thus also an increase in combustion inlet temperature, due to the increase in compressor pressure ratio (see Fig. 12.9), the increase in T_3 is greater, as shown in Fig. 12.12. Hence, the combustion temperature rises as the ambient pressure decreases. The net effect of the increase in combustion temperature rise is a decrease in the air–fuel ratio, as observed in Fig. 12.11.

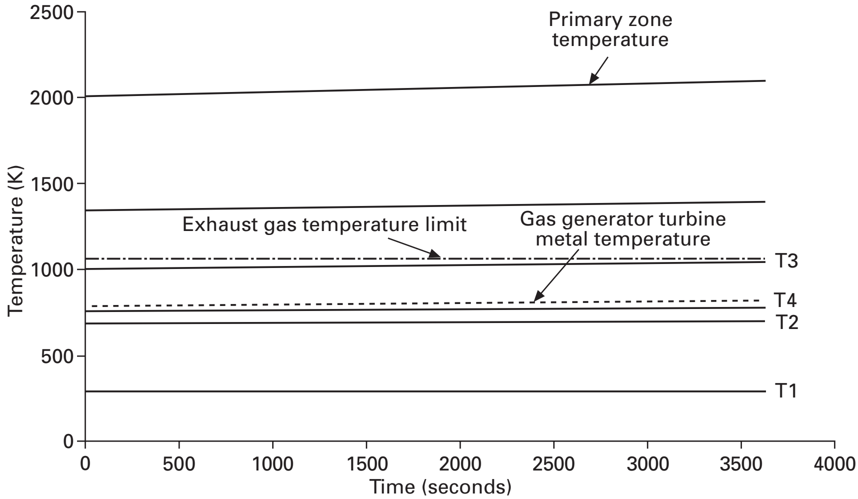

12.12 Trends in temperature during ambient pressure transient.

12.2.6 Trends in temperature

Figure 12.12 shows the trends in temperature during the ambient pressure transient. The increase in compressor non-dimensional speed results in an increase in the temperature ratios, T_2/T_1, T_3/T_1, and T_4 (EGT)/T_1). Since the ambient temperature, T_1, remains constant during this transient, an increase in all the other temperatures is observed during this ambient pressure transient. Note that the exhaust gas temperature, T_4, remains below its limiting value during this transient.

12.2.7 Trends in pressure

Although the compressor pressure ratio increases during the decrease in ambient pressure, the fall in ambient pressure is greater than the increase in compressor pressure ratio. Thus the net result is a fall in compressor discharge pressure during the ambient pressure transient, as shown in Fig. 12.13, which illustrates the pressure trends during the ambient pressure transient. The gas generator turbine inlet pressure trend closely follows the compressor discharge pressure and shows a reduction in the gas generator turbine inlet pressure. Since the gas generator turbine pressure ratio remains essentially constant due to the choked conditions that prevail in the power turbine, a decrease in the compressor discharge pressure results in a decrease in the power turbine inlet pressure. The power turbine exit pressure, which is very similar to the compressor inlet pressure, decreases in line with the transient being simulated.

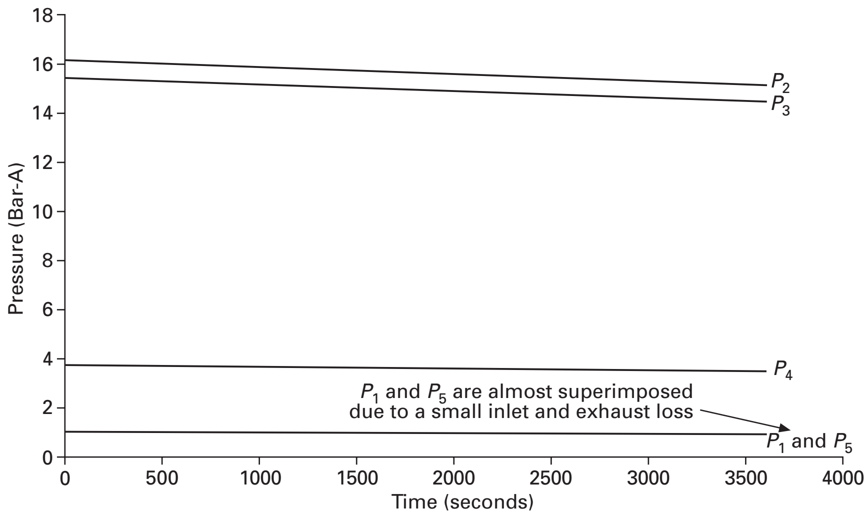

12.13 Trends in pressure during ambient pressure transient.

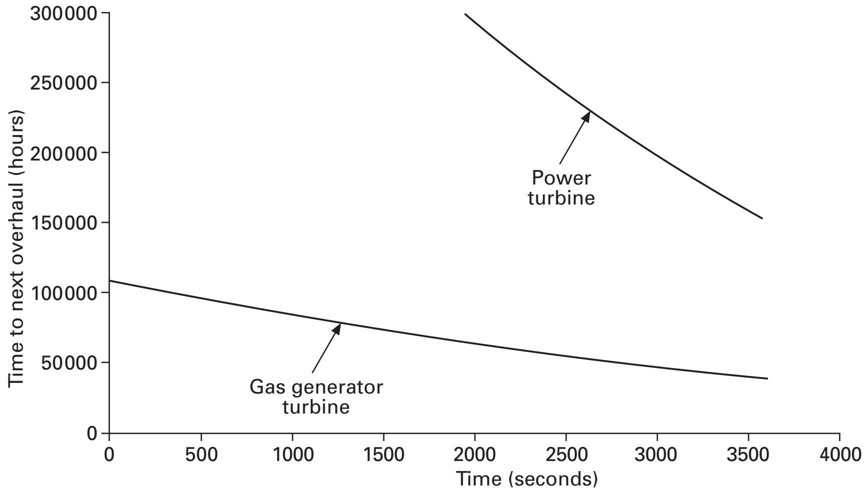

12.14 Trends in gas generator and power turbine creep life during ambient pressure transient.

12.2.8 Trends in turbine creep life

The trends in the gas generator and power turbine creep life usage change during the ambient pressure transient are shown in Fig. 12.14. It has been observed that the gas generator speed, turbine entry temperature and hence the exhaust gas temperature increase during the decrease in ambient pressure. This also results in an increase in the gas generator turbine metal temperature.

Thus, the creep life usage of the gas generator turbine and power turbine increase as the ambient pressure falls, resulting in a reduction in the time between overhauls. At the start of the ambient pressure transient, the power turbine operating life is in excess of 300 000 hours; thus it is outside the scale of the trend shown in Fig. 12.14 and is set by the speeds and temperature that prevail at the start of this simulation.

12.2.9 Trends in gas turbine emissions

During the ambient pressure transient, the compressor discharge pressure has been observed to decrease, although the compressor pressure ratio increases. It was also observed that the primary zone temperature increases. In this case the influence of the increase in primary zone temperature is greater than the resultant decrease in combustion pressure, thus increasing the NO_x, as shown in Fig. 12.15, where the trends in emissions during this transient are illustrated. The emission of CO remains essentially constant and is due to the increase in primary zone temperature compensating for the decrease in combustion pressure during the production of CO.

The production of CO_2 decreases and follows the fuel flow trend, thus showing a decrease in CO_2 production during this ambient pressure transient due to the improved thermal efficiency. Hence, at low engine power outputs, low ambient pressures are very beneficial in reducing CO_2 emissions; CO_2 is considered a greenhouse gas and is thought to be responsible for global warming.

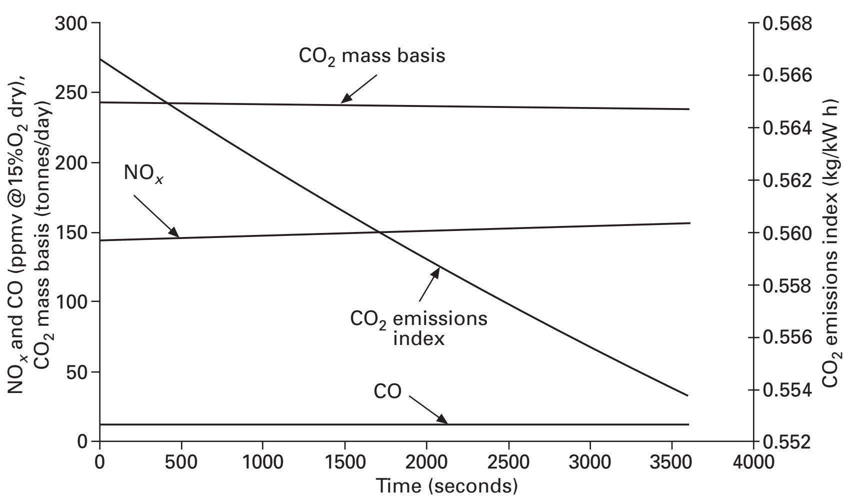

12.15 Trends in gas turbine emissions during ambient pressure transient.

13
Simulating the effects of engine component deterioration on engine performance

In Chapter 9 the impact of component deterioration on engine performance and the undesirable effect on power output and thermal efficiency were discussed. The factors that affect engine performance deterioration were also discussed. In this chapter the engine simulator will be used to simulate many of these faults to investigate the impact they have on engine performance and the change in running line characteristics. Some simple methods to detect engine performance deterioration will also be discussed, particularly compressor fouling, which is the most common cause of performance deterioration. Two operating cases will be considered and they correspond to a high power output and a low power output condition, respectively.

13.1 Compressor fouling (high operating power)

As stated above, compressor fouling is the most common form of engine performance deterioration and it affects all open cycle gas turbines. The level of fouling depends on many factors. The main factors are the level of dirt and particles in the atmosphere, quality of air filtration and, to a certain extent, the power output of the gas turbine, particularly in multiple shaft gas turbines such as that represented by this simulator. As explained above, compressor fouling occurs because of the deposit of dirt and dust particles on the compressor blades, thus altering the shape of the compressor characteristic. An example of the change in compressor characteristic is shown and discussed in Chapter 9, Section 9.1.

Compressor fouling is simulated using this simulator by reducing the compressor non-dimensional flow linearly with time for any given non-dimensional compressor speed. (It should be noted that compressor fouling is not linear. Experience has shown that the rate of fouling decreases with time as deposits of dirt and dust collect on the compressor blades, changing the profile of the blade.) Thus the compressor non-dimensional speed line shifts to the left due to the reduction in capacity as shown in Fig. 9.3. Fouling also reduces the efficiency of the compressor and this is simulated by decreasing the compressor efficiency linearly and simultaneously with non-dimensional flow. The reduction in compressor non-dimensional flow and compressor efficiency for a moderately fouled compressor is about 3% and 1% respectively.

Fault indices are used to represent engine component performance deterioration. Fault indices simply represent the changes in the component characteristics. There are two fault indices per engine component and these are referred to as the fouling fault index and the efficiency fault index. The fouling fault index represents the change in the non-dimensional flow capacity of the engine component and the efficiency fault index represents the change in the efficiency of the engine component. The simulation of compressor fouling is achieved by displaying the gas turbine degradation page and typing in –3% for the compressor fouling fault index and –1% for the compressor efficiency fault index. A suitable ramp time is selected, which represents the time for compressor fouling to take effect. Compressor fouling takes weeks or months but the process will be accelerated and a ramp time of 1 hour (3600 seconds) used.

As the current interest is in the impact of compressor fouling at high powers, such that the engine is on an engine-operating limit, the power from the generator is set to 25 MW. The ambient pressure, temperature and relative humidity will be set to 1.013 Bar, 15 degrees Celsius and 60%, respectively, and the inlet and exhaust losses will both be set to 100 mm of water gauge. The simulation is carried out for 4000 seconds.

13.1.1 Trends in fault indices

The trends in fault indices are shown in Fig. 13.1, which displays the changes in the compressor fouling and efficiency fault indices, respectively. The compressor fouling fault index varies linearly from 0% to –3% in 3600 seconds and this is, of course, the input made to the model. Similarly, the compressor efficiency fault index varies linearly from 0% to –1% in 3600 seconds.

These changes in compressor fault indices affect the compressor characteristic by reducing the non-dimensional flow and compressor efficiency, thus simulating compressor fouling. No other fault is present and this is indicated by the fault indices for the turbine components remaining at zero throughout the simulation.

13.1.2 Compressor characteristic

The movement of the operating point on the compressor characteristic is shown in Fig. 13.2. The operating point moves down the characteristic as the

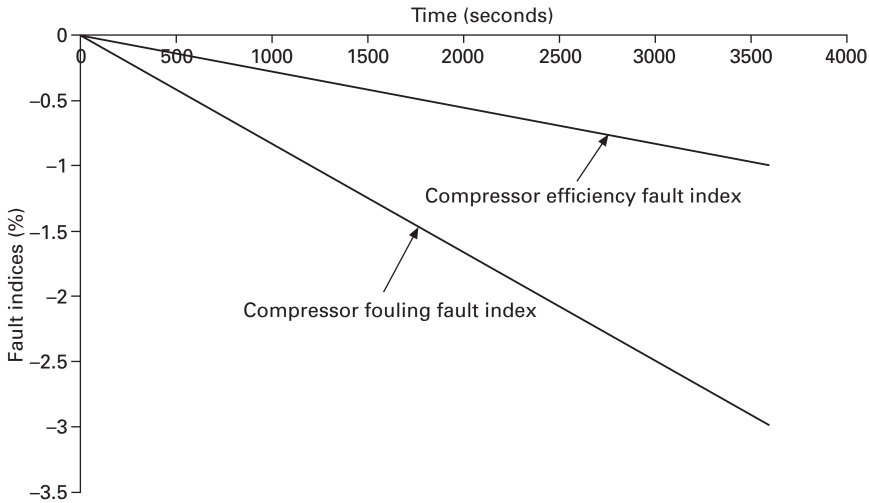

13.1 Trends in compressor and turbine fault indices during compressor fouling.

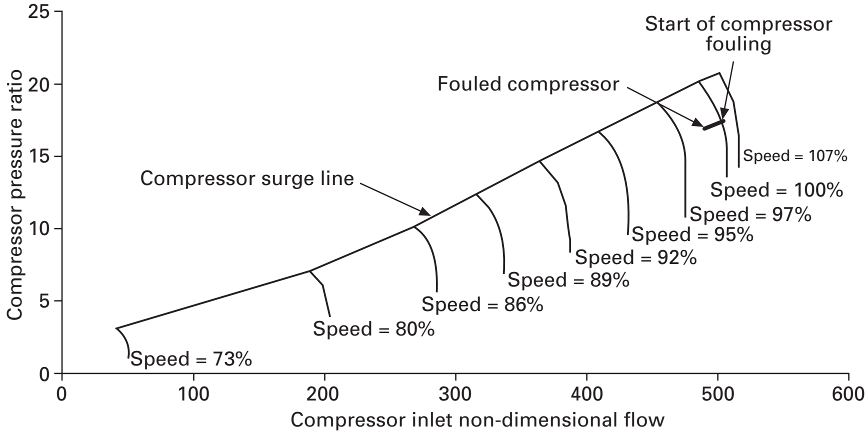

13.2 Operating point on the compressor characteristic during compressor fouling when the engine is operating at a control limit.

compressor speed lines shift to the left during fouling (the characteristic displayed is for a clean compressor). Thus a reduction in compressor non-dimensional flow and pressure ratio is observed during fouling.

The non-dimensional speed of the compressor remains essentially constant during fouling when the engine is operating on a control limit – EGT limited (high power operation). Thus compressor fouling at these operating conditions will result in a decrease in compressor discharge pressure and compressor inlet mass flow.

13.1.3 Trends in pressure ratio

The trends in pressure ratio during compressor fouling are shown in Fig. 13.3. As discussed previously, a decrease in compressor pressure ratio is observed. The choked conditions that prevail in the power turbine prevent the gas generator turbine pressure ratio from changing, as seen in Section 8.1.2. The constant gas generator turbine pressure ratio now results in a decrease in the power turbine pressure ratio. However, the decrease in power turbine pressure ratio is smaller than the decrease in the compressor pressure ratio.

The figure also shows the trend in the maximum to minimum cycle temperature, T_3/T_1, which remains constant during fouling. This is because the engine is operating on an exhaust gas temperature limit. Since the ambient temperature is constant during this simulation, T_3/T_1 is therefore essentially constant.

13.1.4 Trends in pressure

Figure 13.4 shows the trends in pressure during compressor fouling. The decrease in compressor pressure ratio during fouling results in a decrease in the compressor discharge pressure. The decrease in compressor discharge pressure also results in a decrease in the power turbine inlet pressure because the gas generator turbine operates at a constant pressure ratio. The gas generator turbine inlet pressure decreases with the compressor discharge pressure, as the combustion system pressure loss does not change very much.

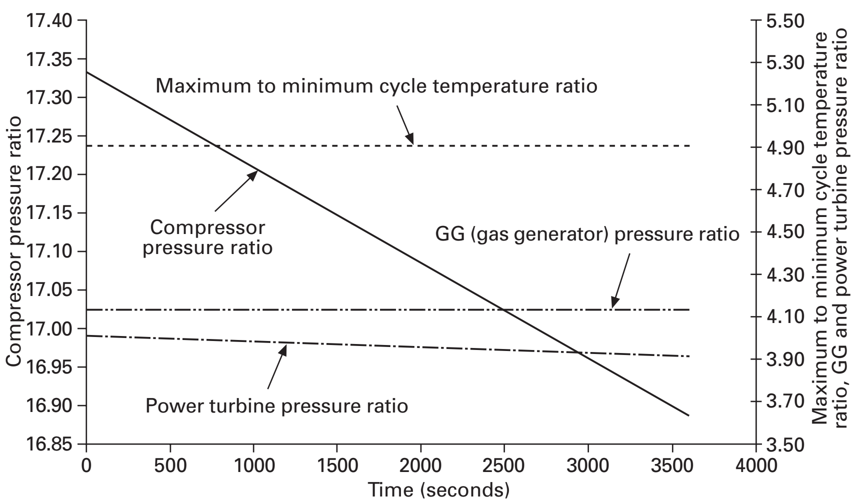

13.3 Trends in compressor and turbine pressure ratios during compressor fouling when the engine is operating at a control limit.

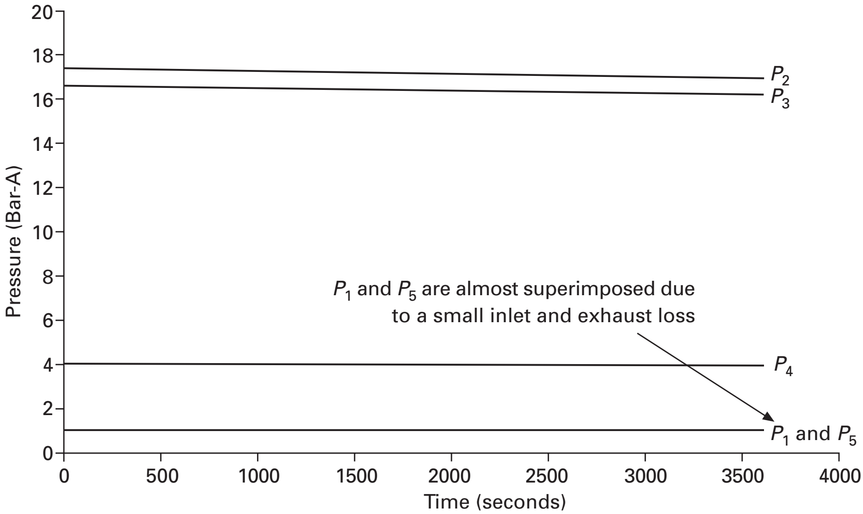

13.4 Trends in pressure during compressor fouling when engine is operating at a control limit.

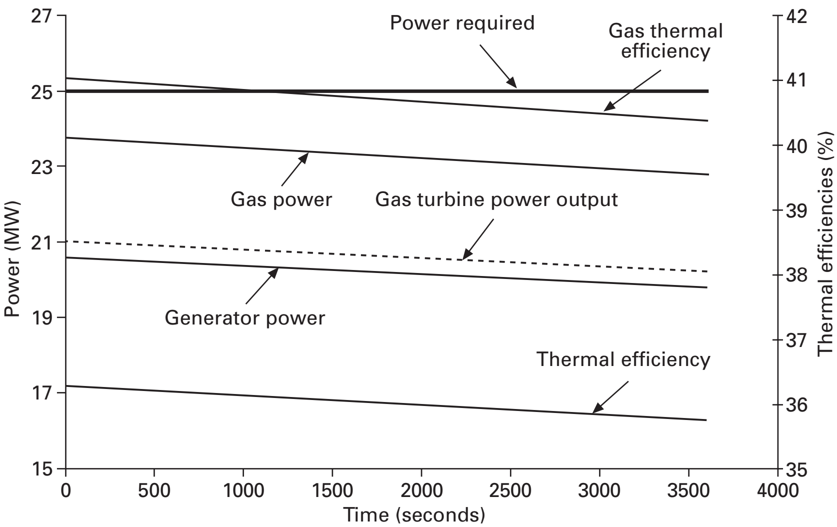

13.5 Trends in power and thermal efficiency during fouling when engine is operating at an engine limit.

13.1.5 Trends in power and thermal efficiency

The most important aspects of engine performance are power output and thermal efficiency. The impact of compressor fouling has an adverse effect on these performance parameters and, in Fig. 13.5 the power output from the gas turbine is observed decreasing from about 21 MW to about 20 MW. Although this only represents a 1 MW drop in power output, it corresponds to about a 5% loss in power output and thus a loss of 5% in revenue. It is also observed that the thermal efficiency decreases from 36% to about 35.5%, which represents about 1.5% increase in fuel flow and therefore a 1.5% increase in fuel cost. Although these numbers appear small, they represent a significant loss in revenue and increase in operating costs. Thus the detection and management of compressor fouling is of paramount importance in maintaining the profitability of industries that use gas turbines as a source of power. The figure also shows the trends in gas power and gas thermal efficiency and these follow a similar trend to the gas turbine power output and gas turbine thermal efficiency.

13.1.6 Trends in flow

The trends in flow during compressor fouling are shown in Fig. 13.6. The compressor inlet mass flow is observed to decrease and this is due to the decrease in the compressor non-dimensional flow during fouling.

Since the compressor inlet pressure and temperature remain constant in this simulation, any decrease in the compressor non-dimensional flow $W_1\sqrt{T_1}/P_1$ results in a proportional decrease in compressor inlet mass flow, W_1. Since the power loss due to compressor fouling is greater than the efficiency loss, the fuel flow decreases. The air–fuel ratio remains constant because the combustion system temperature rises and the compressor exit temperature remain essentially constant during fouling, as shown in Fig. 13.7.

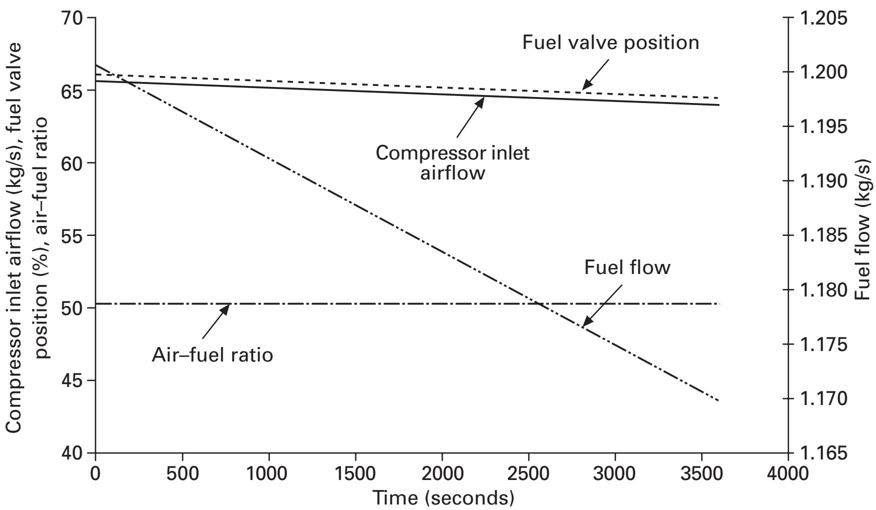

13.6 Trends in flow during compressor fouling when engine is operating at a control limit.

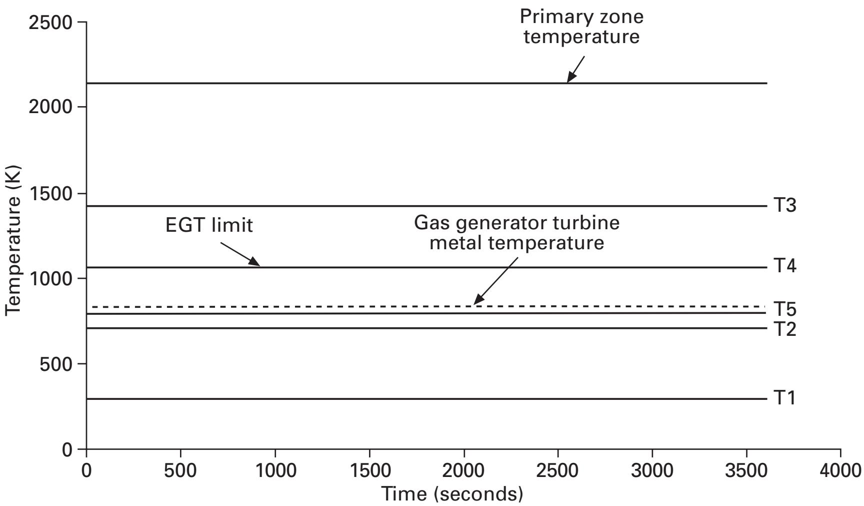

13.7 Trends in temperature during compressor fouling.

13.1.7 Trends in temperature

The trends in the temperature at the inlet and exit of each engine component are shown in Fig. 13.7. The temperature trends remain essentially constant during compressor fouling for this case. Although the compressor pressure ratio decreases, the loss in compressor efficiency results in a near constant compressor exit temperature.

The choked conditions that prevail in the power turbine prevent the gas generator turbine pressure ratio from changing. Thus the temperature ratio across the gas generator turbine is approximately constant as discussed in Section 8.1.2. Since the engine operates at a constant exhaust gas temperature, T_4, the turbine entry temperature, T_3 and the combustion temperature remain essentially constant.

As the exhaust gas temperature remains constant and there is only a small decrease in the power turbine pressure ratio that occurs during this transient, as shown in Fig. 13.3, the increase in the power turbine exit temperature is small.

13.1.8 Trends in speed

Figure 13.8 shows the trends in the gas generator and compressor non-dimensional speeds during compressor fouling. These speeds are observed to remain essentially constant during compressor fouling. This is because the engine performance is controlled by the exhaust gas temperature limit and therefore there is no significant margin to increase or alter the speed during fouling.

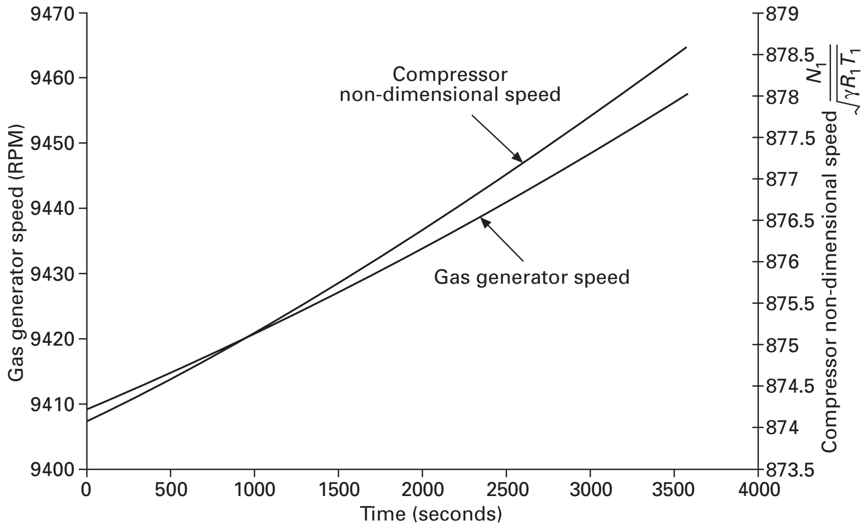

13.8 Trends in speed during compressor fouling when engine is operating at a control limit.

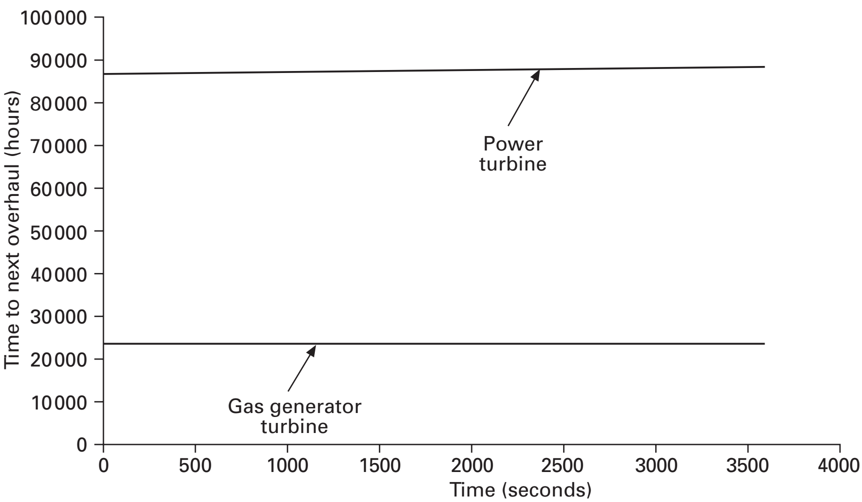

13.9 Trends in turbine creep life during compressor fouling when engine is operating at a control limit.

13.1.9 Trends in turbine creep life

The trends in the gas generator and power turbine creep life usage during compressor fouling are shown in Fig. 13.9. A slight decrease is observed in both the gas generator and power turbine creep life usage during compressor fouling. It was observed that the compressor mass flow decreases during compressor fouling and the compressor temperature rise is essentially constant. Thus the power absorbed by the compressor decreases during fouling. Since the compressor power is provided by the gas generator turbine, the gas generator turbine power also decreases during fouling. Thus the torque produced by the gas generator turbine blades will decrease. It was also observed that the gas generator speed and turbine temperatures remain essentially constant during fouling. The constant gas generator speed will result in a constant centrifugal stress, but the reduction in the torque acting on the turbine blade will result in a lower bending stress. The net effect reduces the stresses in the gas generator turbine blades and therefore decreases the gas generator turbine creep life usage.

The power turbine speed remains constant at 3000 RPM during the simulation. The decrease in power output from the gas turbine due to compressor fouling will therefore reduce the stress in the power turbine blades (lower torque). As the exhaust gas temperature remains constant during this simulation, the creep life usage of the power turbine also decreases due to the lower stresses that prevail in the power turbine blades. However, for a given exhaust gas temperature, compressor fouling results in reduced power output from the gas turbine and therefore, in real terms, there is an increase in creep life usage due to fouling. The reader can illustrate this by running the simulator at reduced power outputs typical of fouling, but when no compressor fouling is present.

13.1.10 Trends in gas turbine emissions

It has been observed that the compressor discharge pressure, and hence the combustion pressure, decreases during compressor fouling. However, the primary zone temperature remains constant during the simulation of fouling. Thus a decrease in NO_x is observed during compressor fouling, due to the lower combustion pressure. The emission of CO, on the other hand, remains essentially constant, as the formation of CO is more sensitive to primary zone temperature than combustion pressure. These trends can be seen in Fig. 13.10. The figure also shows the decrease in CO_2, which is proportional to the fuel flow. Since the fuel flow during fouling decreases, we also observe a decrease in CO_2. However, the increase in the CO_2 index (also shown in Fig. 13.10) implies an increase in CO_2 emissions in real terms.

It has been stated that the NO_x emissions decrease during fouling, and this effect seems to indicate that fouling has a beneficial effect on gas turbine emissions. However, this is somewhat misleading as the power output from the gas turbine has also decreased. The correct picture only appears when the simulator is run at the reduced power output caused by fouling and when no performance deterioration is present. It is only then that the emissions due to a fouled compressor are indeed observed to be higher than those from a clean engine and the user is left to simulate this case.

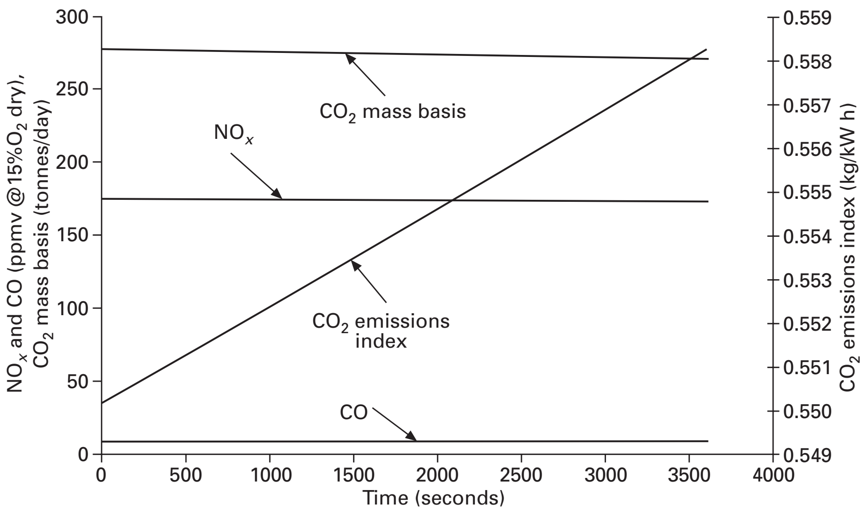

13.10 Trends in gas turbine emissions due to compressor fouling when engine is operating at a control limit.

13.1.11 Effect of ambient temperature and compressor fouling on engine performance

The previous discussions on compressor fouling considered the case when the ambient temperature was 15 degrees Celsius. The effect of a change in ambient temperature during compressor fouling is now considered by summarising the effect on gas turbine power output.

Figure 13.11 shows the variation of power output with ambient temperature for both a clean and fouled compressor, respectively. The loss in gas turbine power at different ambient temperatures has also been shown. Simulating the compressor fouling discussed above at different ambient temperatures produced this figure. Note that the loss of power is most significant at lower ambient temperatures when the power output from the gas turbine is limited by speed rather than by the exhaust gas temperature. Furthermore, at high ambient temperatures, the compressor flow tends to be controlled by the HP stages of the compressor as the operating point moves down the compressor characteristic similar to that shown in Fig. 11.9 (lower compressor non-dimensional speed). However, fouling affects the LP stages of the compressor compared with the HP stages. Thus, the impact of fouling will be more important at low ambient temperatures. A very interesting discussion of the effects of compressor fouling at different compressor non-dimensional speeds is given in Saravanamutoo and Lakshmiranasimha.[1]

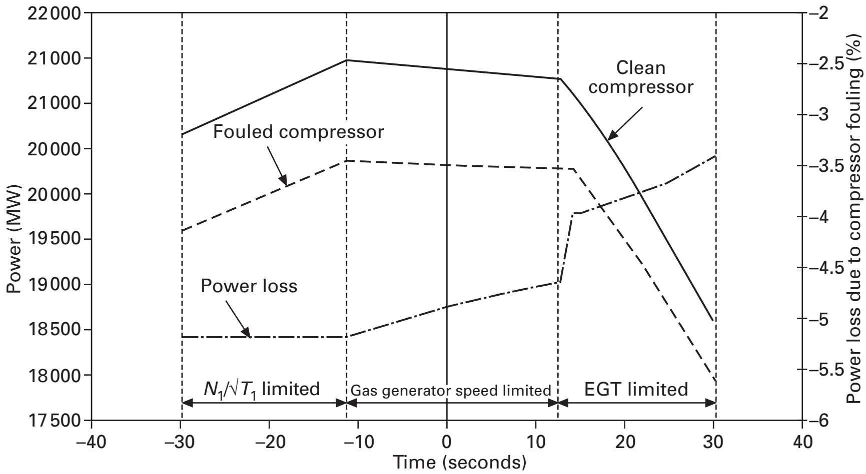

13.11 Variation of gas turbine power output with ambient temperature for a clean and fouled compressor, respectively.

13.1.12 Displacement of running lines due to compressor fouling

The variation of non-dimensional parameters was discussed in Chapter 11, Section 11.1 and it was stated that the running lines are essentially an invariant of operating conditions (Figs 11.3 to 11.7). When engine performance deterioration takes place due to compressor fouling, these running lines change and the changes may be used to detect performance-related faults such as compressor fouling. Compressor fouling as stated earlier reduces the compressor non-dimensional flow and efficiency for a given non-dimensional speed.

These deteriorated compressor characteristics have been used to simulate the effect of compressor fouling on engine performance. The effect fouling has on these running lines can also be represented. Figure 13.12 shows the running line on the compressor characteristic for both a clean and a fouled compressor. The running line for the case when the compressor is fouled shows only a slight displacement towards surge, and is primarily due to the reduction of the compressor efficiency. The efficiency reduction is only 1% (compressor efficiency fault index), thus resulting in a small shift in the running line. Figure 13.12 also shows the operating points for the clean and fouled cases for the high-power operation cases just discussed.

The displacement of the running line on the compressor characteristic is only small, and, at lower power, the operating points for the two cases will be almost coincident; as will be demonstrated later. A better strategy is to

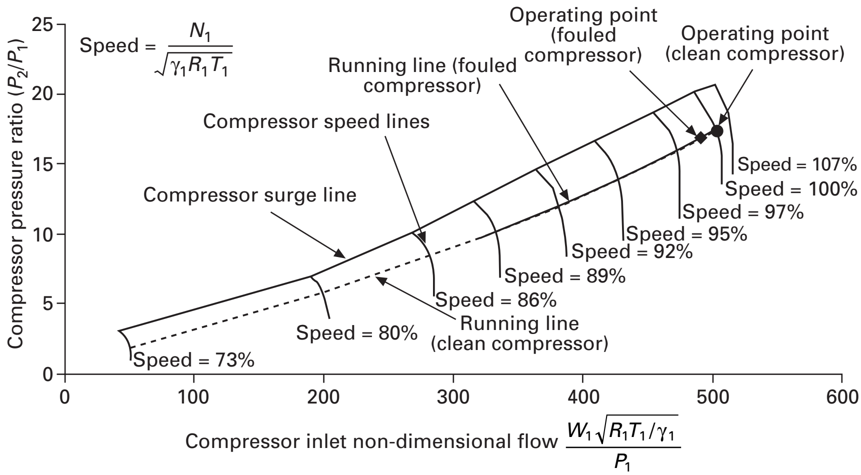

13.12 Running lines on the compressor characteristic for a clean and fouled compressor operating at high power.

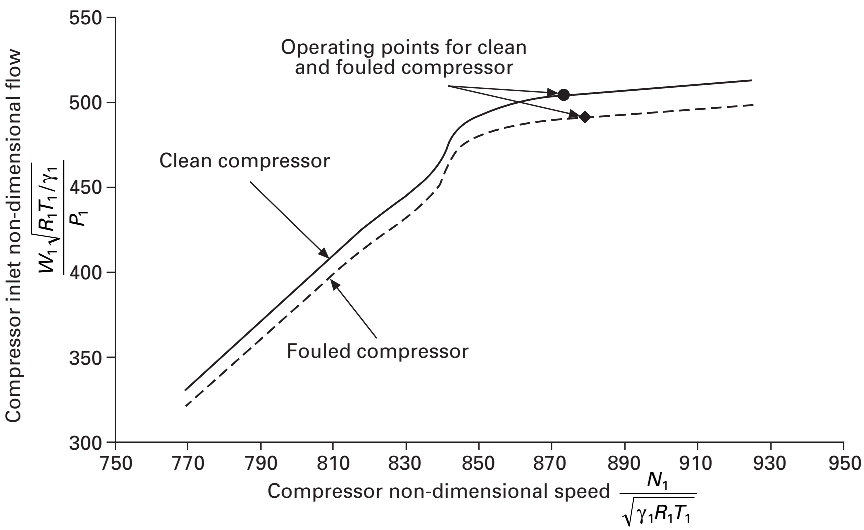

13.13 Variation of compressor non-dimensional flow with non-dimensional speed.

represent these running lines on a compressor non-dimensional flow versus non-dimensional speed basis, as shown in Fig. 13.13. The displacement of the running line due to compressor fouling is shown clearly. The shift in the running line is dependent only on the compressor fouling fault index, which represents the level of compressor fouling.

The reduction in compressor non-dimensional flow for a given compressor non-dimensional speed during compressor fouling not only shifts the running line on the compressor characteristic but the compressor pressure ratio will also decrease as the compressor fouls, as shown in Fig. 13.3. This effect is best illustrated by displaying the variation of the compressor pressure ratio with its non-dimensional speed, as shown in Fig. 13.14, where the displacement in the running line is clearly shown. Unlike the variation of the compressor non-dimensional flow with its non-dimensional speed, which is only influenced by compressor fouling, the variation of compressor pressure ratio will also be influenced by other engine faults, as will be seen later when damage to turbines is considered.

Similarly, the running lines based on other non-dimensional parameters may be produced. The user can generate these running lines with the respective operating points for a clean and fouled compressor.

13.2 Compressor fouling (low operating power)

The effect of compressor fouling when the gas turbine is operating at high enough powers such that the engine is always on an operating limit has been discussed. The effect of fouling on engine performance will now be considered when the power demand from the generator is sufficiently low enough (17.5 MW) to prevent the engine from reaching an operating limit during compressor fouling. The simulation of the compressor fouling is the

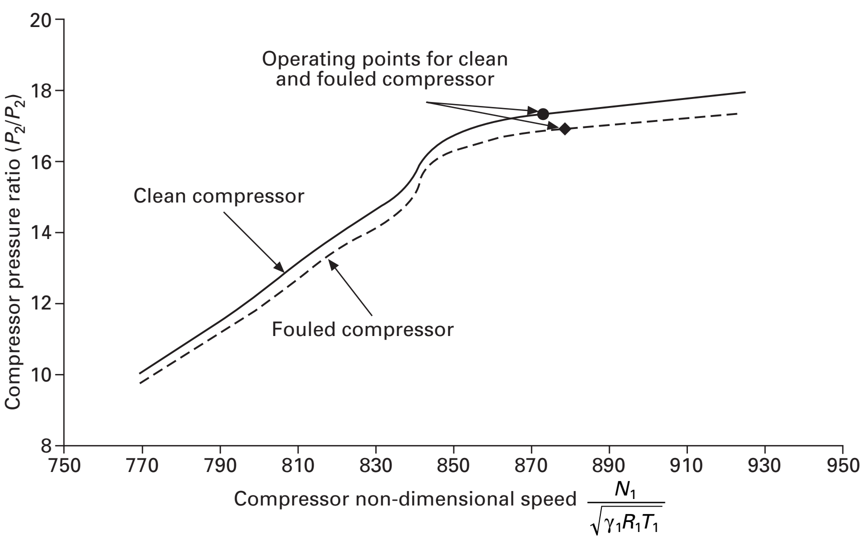

13.14 Variation of compressor pressure ratio with compressor non-dimensional speed.

same as that discussed for the case previously where the effect of compressor fouling at high operating power was discussed.

13.2.1 Compressor characteristic

The movement of the operating point on the compressor characteristic during fouling when operating at low power is shown in Fig. 13.15. The movement of the operating point in this case is significantly less when compared with the case of high operating power (see Fig. 13.2). This is due to the engine being able to increase the gas generator speed and exhaust gas temperature to maintain the generator power demand.

13.2.2 Trends in speed

Since the engine is not on an operating limit during low power operation, compressor fouling will result in an increased gas generator speed in order to maintain the power demand, which is met by increasing the fuel flow. Since the compressor inlet temperature does not change, the increase in gas generator speed results in an increase in the compressor non-dimensional speed. This is illustrated in Fig. 13.16, which shows the trends in the gas generator and compressor non-dimensional speeds during fouling when operating at low power.

13.2.3 Trends in temperature

The trends in temperature during compressor fouling when operating at low power are shown in Fig. 13.17. Note that the exhaust gas temperature, turbine

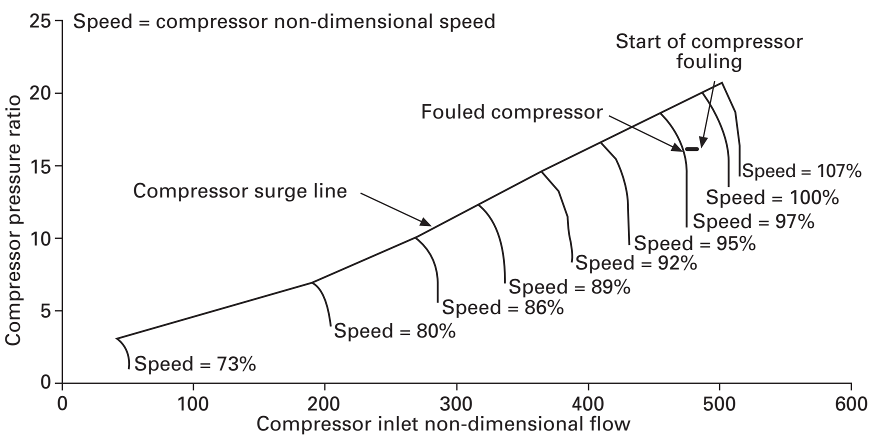

13.15 Movement of operating point on compressor characteristic during compressor fouling when operating at low power.

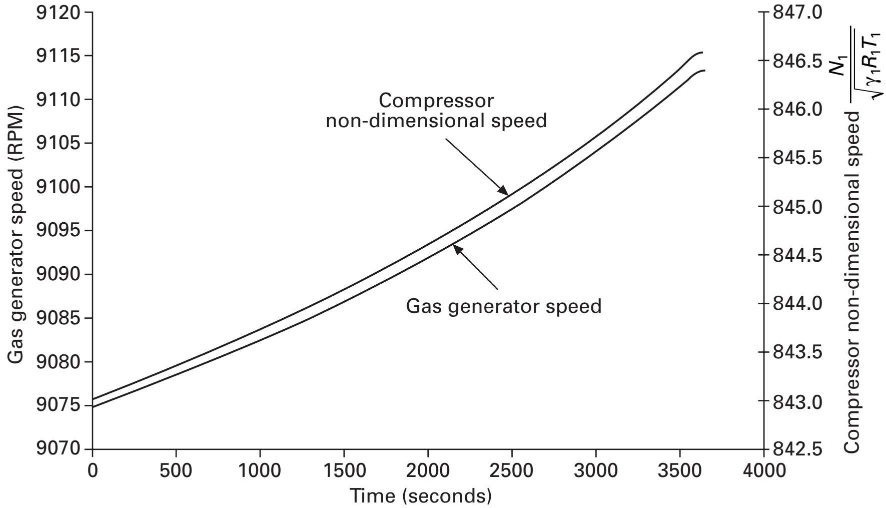

13.16 Trends in speed during compressor fouling when operating at low power.

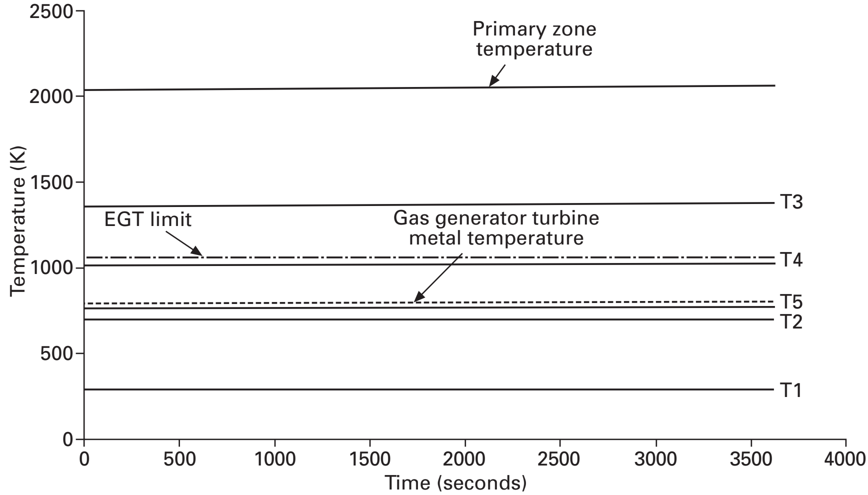

13.17 Trends in temperature during compressor fouling when operating at low power.

entry temperature and the primary zone temperature are all increasing during fouling. This is due to the loss in engine performance, thus requiring higher operating temperatures to maintain the generator power demand. However, the compressor exit temperature remains essentially constant during compressor fouling and any slight increase is due to the loss in compressor efficiency.

13.2.4 Trends in power and efficiency

The trends in power and thermal efficiency are shown in Fig. 13.18. The generator power output remains on the set point (17.5 MW), thus the gas turbine power output and the gas power also remain constant during fouling. The gas turbine thermal efficiency and the gas thermal efficiency decrease during compressor fouling and this is due to the loss in engine performance. Thus, compressor fouling at low power has no effect on revenue, as the power demand can be met, since no engine limits are reached. However, the loss in thermal efficiency will result in increased fuel costs.

In industries where fuel costs are minimal, such as in oil and gas exploration and production, compressor fouling is of little consequence if engines operate at relatively low powers. Thus, compressor washes can be infrequent. However, if dirt and debris are allowed to accumulate on the compressor blades, particularly on the high pressure stages where such debris can become baked on due to the higher temperatures in these compressor stages, subsequent washing of the compressor may not return the compressor back to its best performance.[2] This will result in reduced revenue when maximum power demand is required. Thus frequent washing is important but has to be balanced with the loss of production due to downtime during washing.

13.2.5 Trends in flow

Figure 13.19 shows the trends in flow during compressor fouling. Observe that the compressor inlet flow decreases slightly since the movement of the

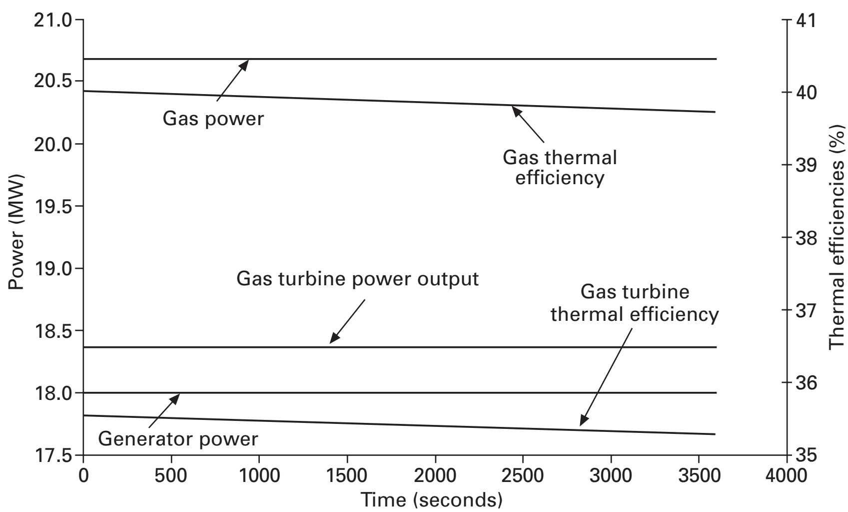

13.18 Trends in power and thermal efficiency during compressor fouling when operating at low power.

compressor operating point is small compared with the case when the effect of fouling on engine performance at high operating powers is considered. There is an increase in fuel flow and fuel valve position during fouling and this is due to the lower thermal efficiency as discussed before. Since there is an increase in fuel flow and a decrease in compressor inlet flow, the reduction in combustion airflow causes the air–fuel ratio to decrease during fouling.

13.2.6 Trends in pressure ratio and pressure

The trends in the pressure ratio during compressor fouling are shown in Fig. 13.20. Due to little movement in the operating point on the compressor characteristic during fouling when operating at low power, only a small change in the compressor pressure ratio occurs during fouling at these power output conditions. There is a slight increase in the maximum to minimum cycle temperature ratio, T_3/T_1, and this is due to the increase in turbine entry temperature during compressor fouling. As there is only a small change in these pressure ratios, the changes in pressure trends during compressor fouling are also small and are shown in Fig. 13.21.

13.2.7 Trends in turbine creep life

It has been observed that the gas generator speed and the turbine entry temperature increase with compressor fouling when operating at low power

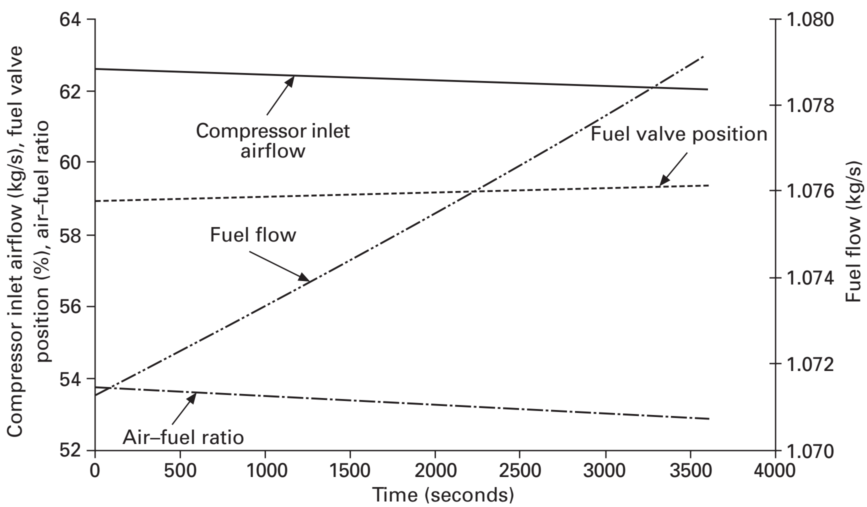

13.19 Trends in compressor inlet air and fuel flow during compressor fouling when operating at low power.

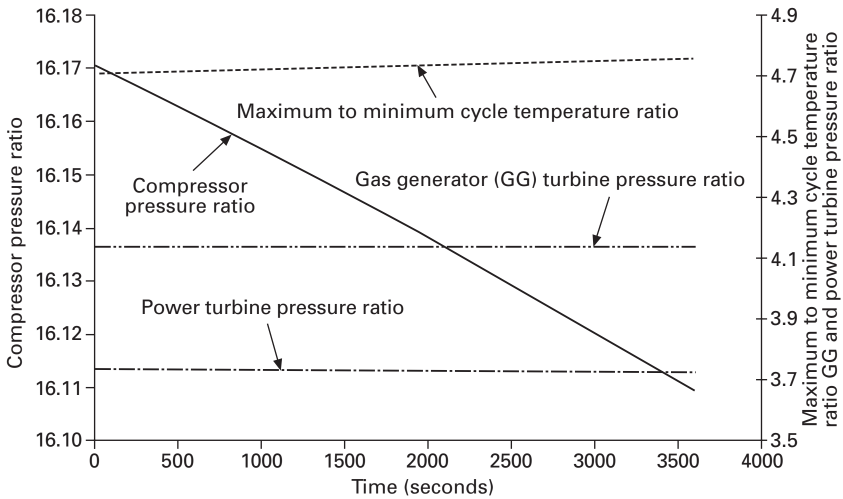

13.20 Trends in pressure ratio during compressor fouling at low power.

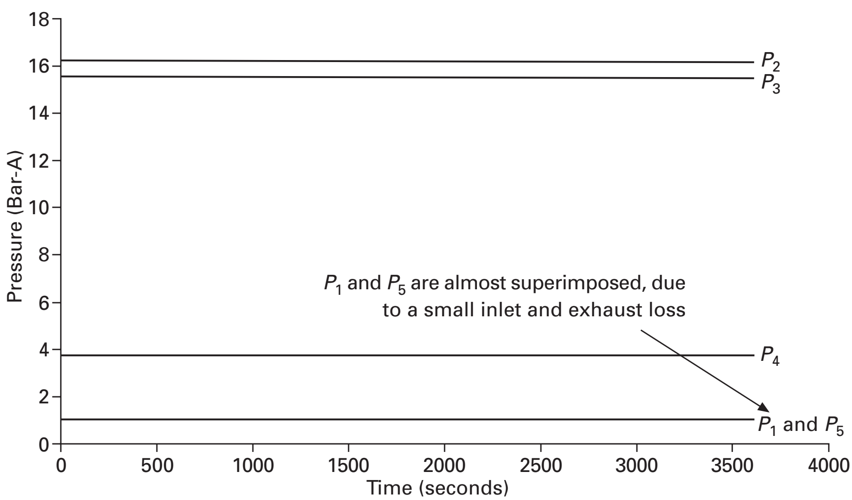

13.21 Trends in pressure during compressor fouling at low power.

outputs. The increase in gas generator speed results in an increase in the centrifugal stress of the rotor blades, and the increase in turbine entry temperature results in the increase in the turbine blade temperature. These two factors have an adverse effect on the gas generator turbine creep life such that the gas generator turbine creep life usage is observed to increase significantly as the compressor fouls. This is shown in Fig. 13.22 and is clearly different from the high power operating case (see Fig. 13.9).

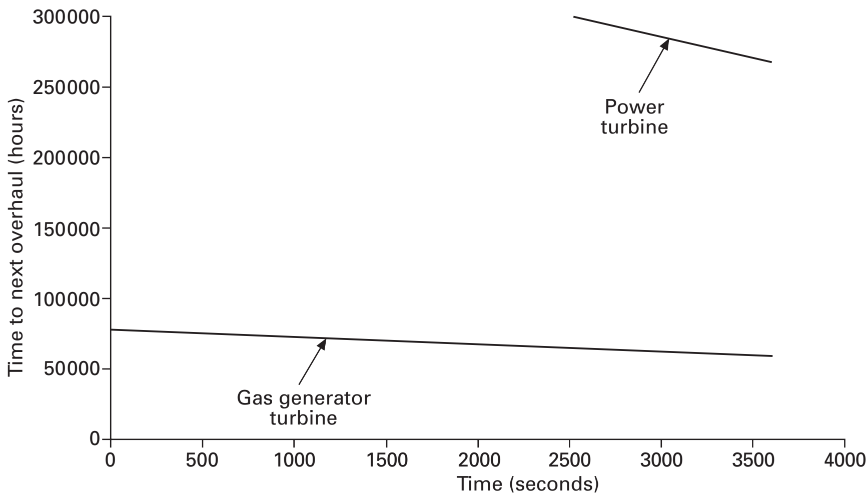

13.22 Trends in creep life during compressor fouling.

The power turbine operates at a constant speed as dictated by the generator with the load being constant, thus the stress in the power turbine blades will also remain constant. However, the increase in the exhaust gas temperature due to compressor fouling results in an increase in the power turbine blade temperature leading to an increase in power turbine creep life usage. Note that the gas generator turbine time to overhaul decreases from about 75 000 hours at the start of compressor fouling to about 35 000 hours at the end of compressor fouling. The power turbine time to overhaul is in excess of 300 000 hours at the start of compressor fouling and decreases to about 240 000 hours at the end of compressor fouling. The creep life for both turbines at the end of compressor fouling is still in excess of the hours when engine overhauls take place (about 20 000 hours). Thus decreases in turbine creep life are of little consequence unless the actual turbine creep life is monitored. As the creep life is in excess of 20,000 hours at low gas turbine power outputs, proper monitoring of turbine creep life usage can result in a significant increase in time between overhauls resulting in reduced maintenance costs.

13.2.8 Trends in emissions

The increase in primary zone temperature during compressor fouling, as shown in Fig. 13.17, results in an increase in NO_x during fouling, although there is a slight decrease in compressor discharge pressure and therefore in combustion pressure. The effect of the changes in these parameters on CO is small. The increase in fuel flow due to the reduction in gas turbine thermal efficiency results in an increase in CO_2 emission and this is seen in Fig.

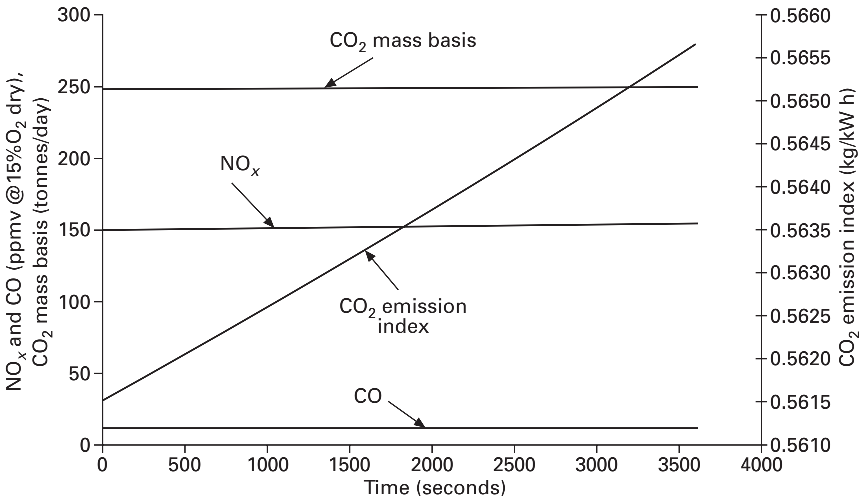

13.23 Trends in gas turbine emissions during compressor fouling at low power.

13.23, which shows the trends in gas turbine emissions during compressor fouling at low power.

It has been stated that in industries where the fuel cost is relatively low, the impact of compressor fouling on revenue is small when operating at low power. However, if emissions become important, the operators may be taxed on the amount of emissions produced by their gas turbines. Then, compressor fouling at low power output becomes important as increased emissions would have an adverse effect on profitability.

13.2.9 Displacement of running lines due to compressor fouling (low power)

The displacement of the running line is no different from that shown in Fig. 13.13, as the amount of compressor fouling for the high and low power cases are the same. All that changes are the operating points, as shown in Fig. 13.24, which illustrates the change in compressor non-dimensional flow with its non-dimensional speed due to compressor fouling.

Figure 13.25 shows the displacement of the compressor pressure ratio with its non-dimensional speed. It is again observed that the displacement of the running line is the same as that shown for the high power case (Fig. 13.14), since the compressor fouling simulation is no different. The two operating points are shown for the clean and fouled cases, respectively, when the engine is operating at low power. The high power operating points are also shown for comparison.

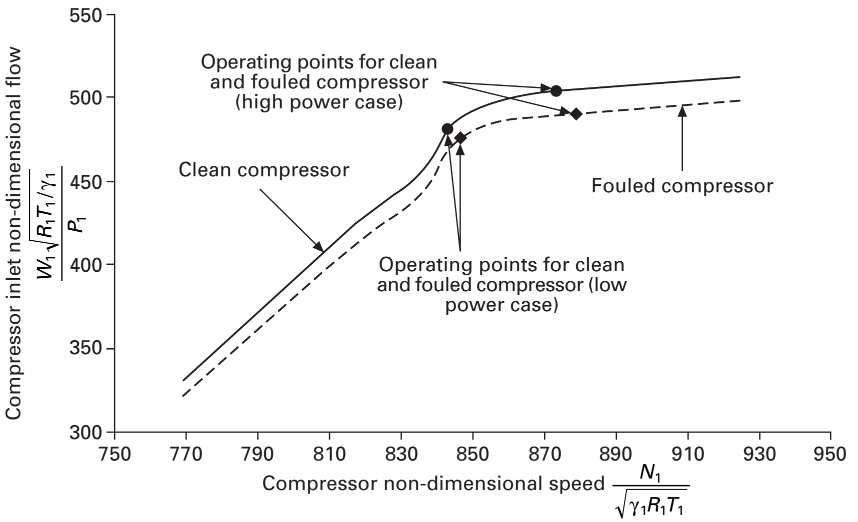

13.24 Displacement of compressor non-dimensional flow running line and operating points due to compressor fouling for high power and low power cases.

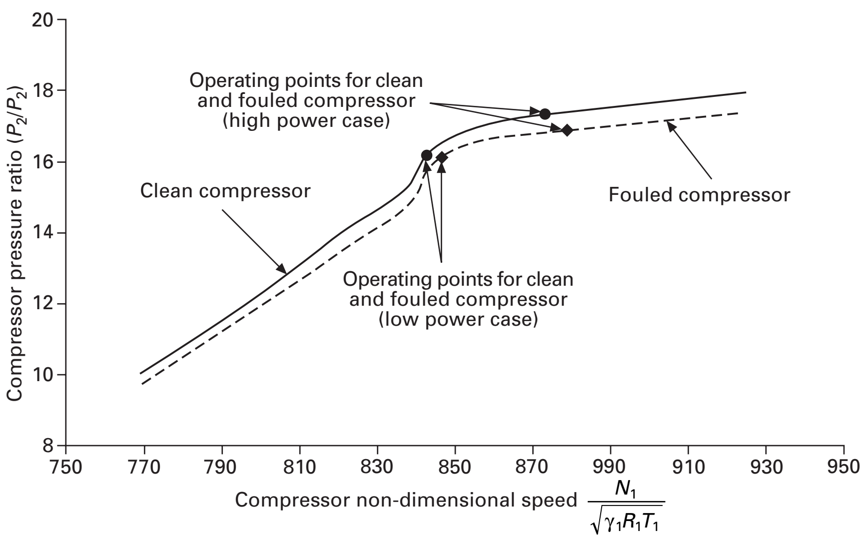

13.25 Displacement of compressor pressure ratio running line and operating points for low and high power cases.

13.3 Turbine damage

Turbines are exposed to very high temperatures, particularly the gas generator turbine, and these turbines often employ cooling to achieve satisfactory creep life. However, during exposure to high temperatures over prolonged periods, damage can occur resulting in a change in performance of the turbines. Two cases of deterioration for turbines will be considered. First, the effect of hot end damage as discussed in Section 9.3 will be simulated. Hot end damage will be applied to the gas generator turbine, as this is where hot end damage is most likely to occur. Secondly, the effect of turbine rotor tip rub will be simulated and this deterioration applied to the power turbine, although such deterioration could occur with either turbine.

13.3.1 Hot end damage

Hot end damage results in an increase in non-dimensional flow of the turbine. Thus, the effects of hot end damage are simulated by increasing the gas generator turbine fouling fault index to 3%. Since such damage is likely to reduce the turbine efficiency, the gas generator turbine efficiency fault index is also reduced by 2% simultaneously. Hot end damage may occur over a long period due to prolonged exposure of the turbine to high temperature combustion gases, or it may occur in a short period of time due to combustion problems that result in a poor combustor temperature traverse.

Since slow deterioration was considered when compressor fouling was discussed, turbine deterioration will be introduced over a short period of time, where these changes in the fault indices are applied in a 10-second time period. To see the impact of this deterioration on engine performance at high power output conditions, the generator power demand is set to 25 MW. The ambient pressure, temperature and relative humidity are set to 1.013 Bar, 15 degrees Celsius and 60%, respectively, and the engine performance will be limited by the exhaust gas temperature limit. Figure 13.26 shows the trends in the fault indices where it can be seen that the gas generator turbine fouling fault index increases from 0 to 3% and its efficiency fault index decreases simultaneously from 0 to –2% in 10 seconds.

Trends in speed

In Section 8.2, the displacement of the running line on the compressor characteristic due to the reduced gas generator turbine non-dimensional flow caused by closing the NGV of the turbine was discussed. This resulted in an increase in the gas generator pressure ratio, as shown in Fig. 8.13, to maintain the required non-dimensional flow into the power turbine. The non-dimensional flow into the gas generator turbine has now been increased in order to simulate the impact of hot end damage on engine performance. As a result, the gas generator turbine pressure ratio decreases.

This reduction in gas generator turbine pressure ratio will reduce work done by the gas generator turbine and thus the power output from the turbine.

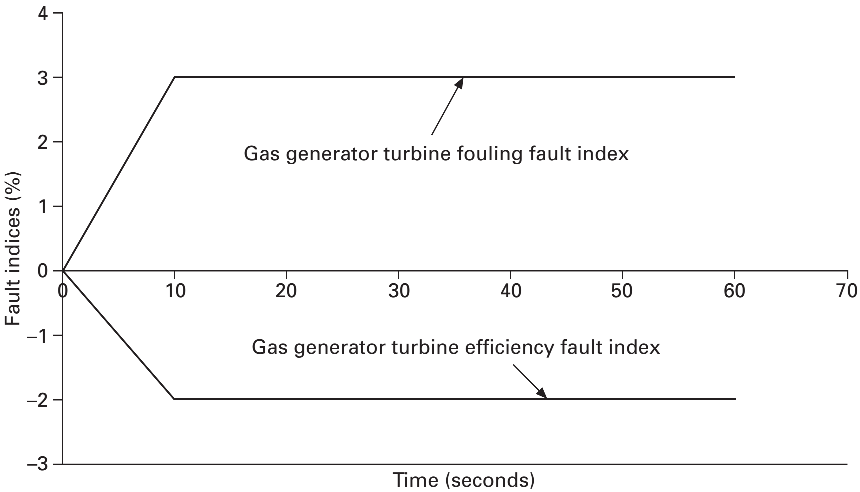

13.26 Trends in gas generator turbine fault indices due to hot end damage in the power turbine.

Since the power output from the gas generator turbine drives the compressor, the gas generator will slow down, as seen in Fig. 13.27, where the speed trends are shown. The compressor non-dimensional speed will also decrease due to the reduction in the gas generator speed.

Trends in pressure ratio and pressure

The reduction in gas generator speed due to hot end damage will reduce the compressor pressure ratio as the operating point on the compressor characteristic moves down. The effect of increased non-dimensional flow through the gas generator turbine due to hot end damage will also move the compressor running line away from surge, thus further reducing the compressor pressure ratio. This can be seen in Fig. 13.28, which shows the trends in pressure ratios due to the effect of hot end damage to the gas generator turbine. The trends also show a reduction in maximum to minimum cycle temperature ratio, T_3/T_1.

It is also observed that the gas generator turbine pressure ratio decreases due to increasing non-dimensional flow through the gas generator turbine, as discussed previously. The compressor pressure ratio decreases from about 17.3 to 15.8, whereas the gas generator turbine pressure ratio decreases from about 4.1 to about 3.9. Since the fall in compressor pressure ratio is greater than the fall in gas generator turbine pressure ratio, a decrease in the power turbine pressure ratio is observed.

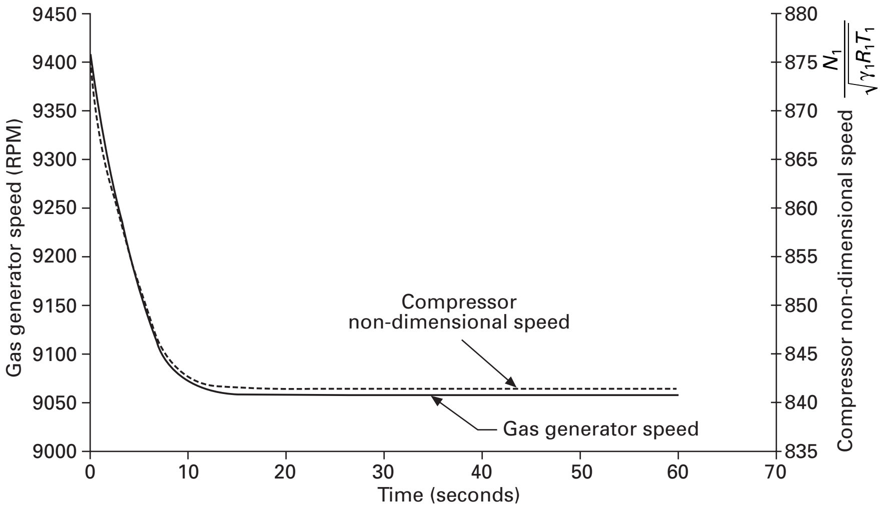

13.27 Trends in speed due to hot end damage of the gas generator turbine.

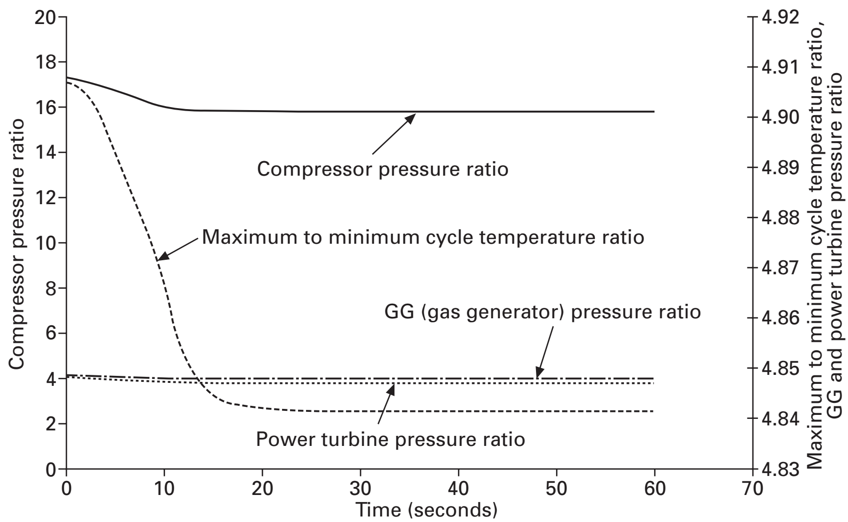

13.28 Trends in pressure ratios due to hot end damage in the gas generator turbine.

The decrease in the pressure ratios now results in decreases in the compressor discharge pressure, combustion pressure and power turbine inlet pressure, as shown in Fig. 13.29.

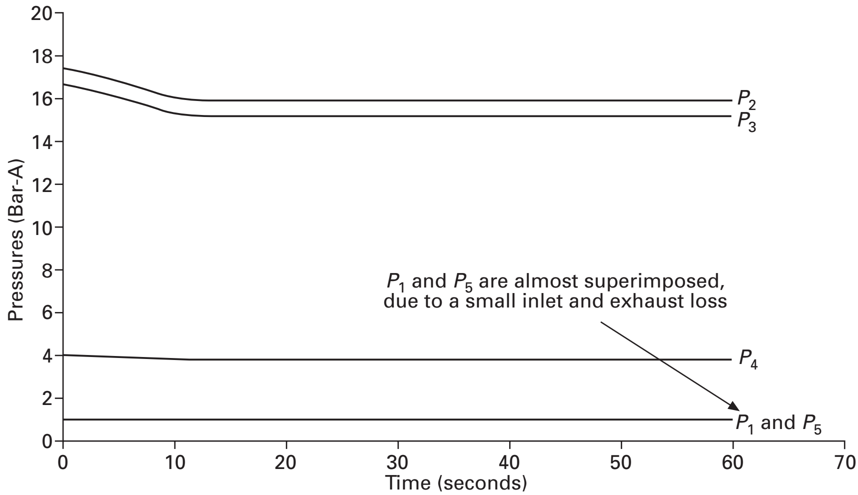

13.29 Trends in pressure due to gas generator turbine hot end damage.

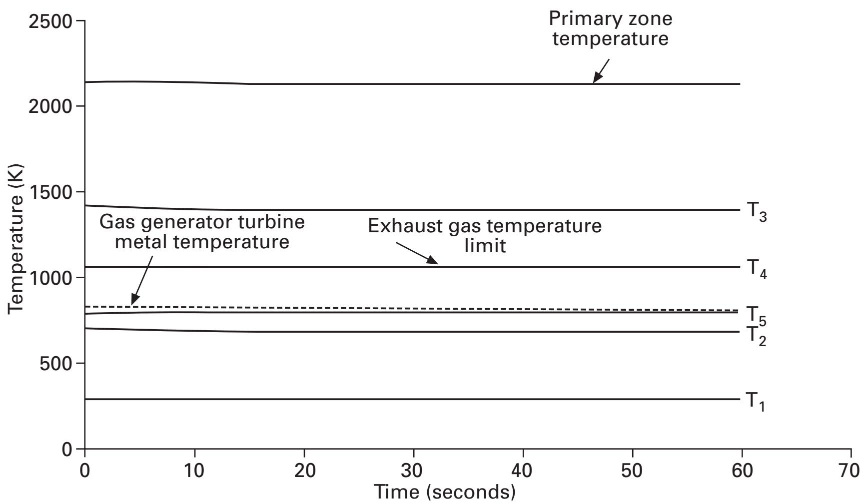

13.30 Trends in temperature due to hot end damage in the gas generator turbine.

Trends in temperature

The trends in temperature due to hot end damage in the gas generator turbine are shown in Fig. 13.30. The reduction in compressor pressure ratio results in a decrease in the compressor discharge temperature. Since the exhaust gas temperature limits the engine performance (constant EGT), the decrease in the gas generator turbine pressure ratio, as explained, will decrease the turbine entry temperature, the primary zone temperature and T_3/T_1, as seen in Fig. 13.28. However, the decrease in the power turbine pressure ratio will increase the power turbine exit temperature, T_5, as seen in Fig. 13.30.

Trends in power and thermal efficiency

The decrease in the gas generator turbine efficiency and the maximum to minimum cycle temperature ratio, T_3/T_1, reduces the specific work. Furthermore, the compressor inlet airflow will also decrease as can be seen in Fig. 13.32, resulting in a decrease in the gas power and the gas turbine power output. The decreases in compressor pressure ratio, gas generator turbine efficiency and the cycle temperature ratio, T_3/T_1, result in a decrease in the thermal efficiency. Thus the decrease in powers and thermal efficiencies are observed as shown in Fig. 13.31, where the trends in power and thermal efficiency due to hot end damage in the gas generator turbine are illustrated. The generator power output decreases from about 20.5 MW to 18.1 MW, representing nearly a 12% loss in generation power and thus revenue. The gas turbine thermal efficiency decreases from about 36% to 34.6%, this representing nearly 4% increase in fuel cost in real terms.

Trends in flow

Figure 13.32 shows the trends in compressor inlet airflow, fuel flow and the air–fuel ratio due to hot end damage in the gas generator turbine. The figure

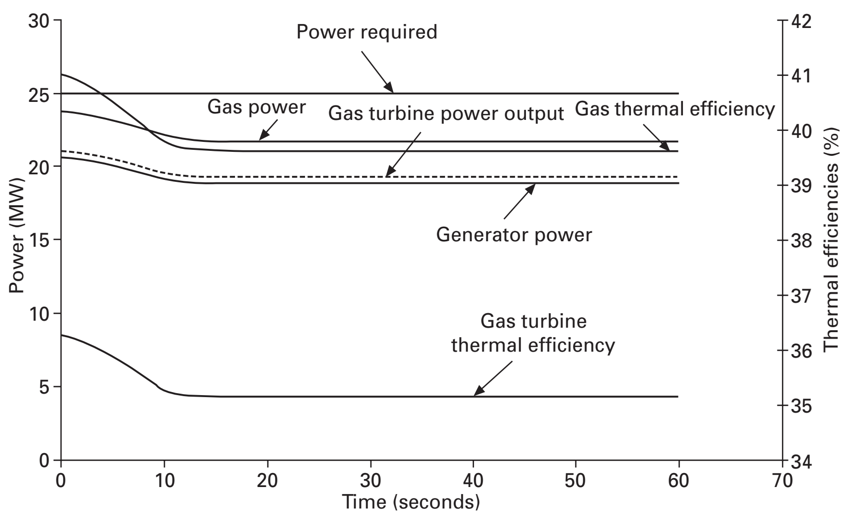

13.31 Trends in power and thermal efficiency due to gas generator turbine hot end damage.

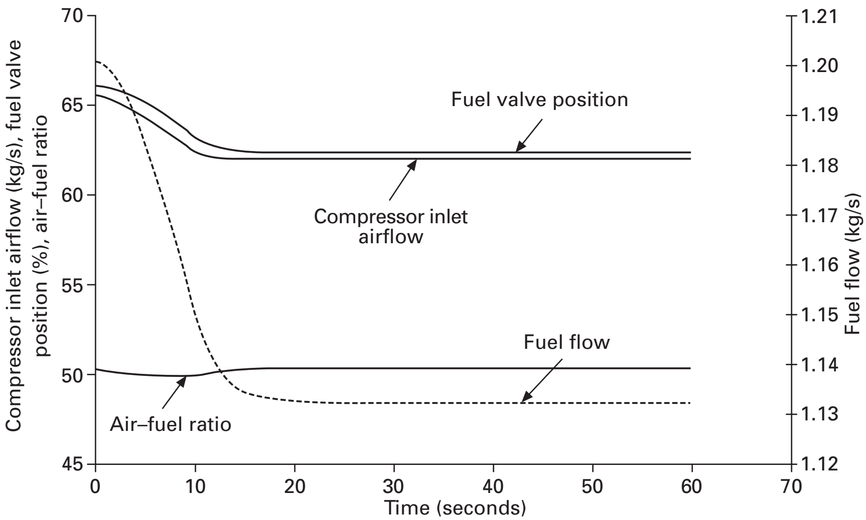

13.32 Trends in flow due to gas generator hot end damage.

also shows the trend in the fuel valve position. The decrease in compressor speed, as observed in Fig. 13.27, forces the operating point down along the running line on the compressor characteristic and thus we observe a decrease in compressor inlet mass flow. Although the gas turbine thermal efficiency decreases, the loss in power output is greater than the loss in gas turbine thermal efficiency and therefore a reduction in fuel flow is observed. (If the simulator is run at low power level such that the engine is not on an operating limit, an increase in fuel flow would then be observed for the same turbine deterioration.)

The decrease in the compressor inlet airflow and thus the combustion airflow is similar to the decrease in fuel flow. Furthermore, the combustion temperature rise remains essentially unchanged before and after hot end damage (Fig. 13.30). Thus, only a slight change in the air–fuel ratio is observed due to hot end damage in the gas generator turbine.

Trends in turbine creep life

The trends in turbine creep life due to hot end damage are shown in Fig. 13.33. It is interesting to note that the gas generator turbine creep life usage actually decreases due to this deterioration. The time to overhaul for the gas generator turbine increases from about 22 000 hours to 45 000 hours. In the above figures it has been observed that the gas generator speed and turbine entry temperature decrease due to hot end damage, resulting in lower stress and blade temperature during hot end damage. These factors therefore decrease

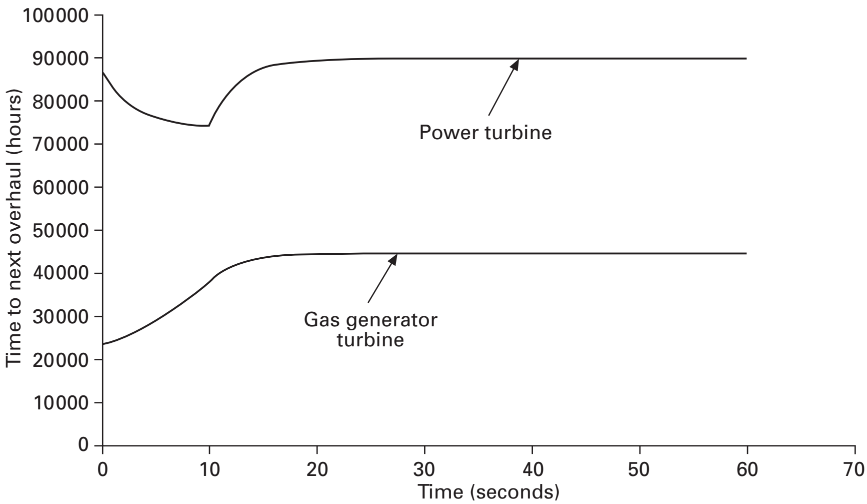

13.33 Trends in gas generator and power turbine creep life due to gas generator turbine hot end damage.

the gas generator turbine life usage due to this deterioration. However, this decrease in turbine creep life usage is very misleading. To obtain the complete picture the simulator needs to be run at the maximum power available when hot end damage is present and with no performance deterioration (i.e. at a generator power of 18.8 MW). The gas generator turbine time to overhaul would then be observed increasing to about 55 500 hours. Thus, hot end damage actually results in a loss in gas generator turbine creep life.

Figure 13.33 also shows the trend in the power turbine creep life. Observe that the power turbine creep life usage increases during the period when hot end damage to the gas generator turbines first occurs. The power turbine creep life usage is observed to decrease apparently above that before hot end damage was applied to the gas generator turbine. This is due to the transient as the control system responds by closing the fuel valve, hence reducing the fuel flow, in an attempt to keep the exhaust gas temperature within the control limits. This action results in a slight over-shoot of the exhaust gas temperature, as seen in Fig. 13.30, and results in the increased power turbine creep life usage during the transient. If the hot end damage was applied to the gas generator turbine over a longer time period, greater than 500 seconds, a continuous decrease in the power turbine creep life usage would be observed. This decrease in power turbine creep life usage occurs mainly due to the reduction in power output from the power turbine resulting in lower stress in the power turbine blades.

Again, this increase in power turbine life is misleading. The simulator needs to be run at the limiting power due to hot end damage, but when no turbine deterioration is present, to determine the actual effect of hot end damage on the power turbine creep life usage. Then a decrease in creep life usage would be seen, thus indicating the negative impact on power turbine creep life due to hot end damage. The user is left to demonstrate this difference in creep life.

Trends in gas turbine emissions

The trend in gas turbine emissions due to hot end damage to the gas generator turbine is shown in Fig. 13.34. Observe that NO_x and CO_2 decrease, while a slight increase in CO occurs. It has been observed that the compressor discharge pressure, hence combustion pressure and primary zone temperature, decrease due to this degradation, thereby resulting in a decrease in NO_x and an increase in CO. The decrease in CO_2 is primarily due to the decrease in fuel flow resulting from hot end damage to the gas generator turbine. However, the increase in CO_2 emission index implies an increase in CO_2 emission in real terms.

The maximum power available from the engine, due to the gas generator turbine hot end damage, is about 18.8 MW. If the engine was run at this power, but when no engine degradation is present, then a further decrease in NO_x would be observed. Thus, in real terms, hot end damage does result in an increase in these emissions, particularly of NO_x and CO_2.

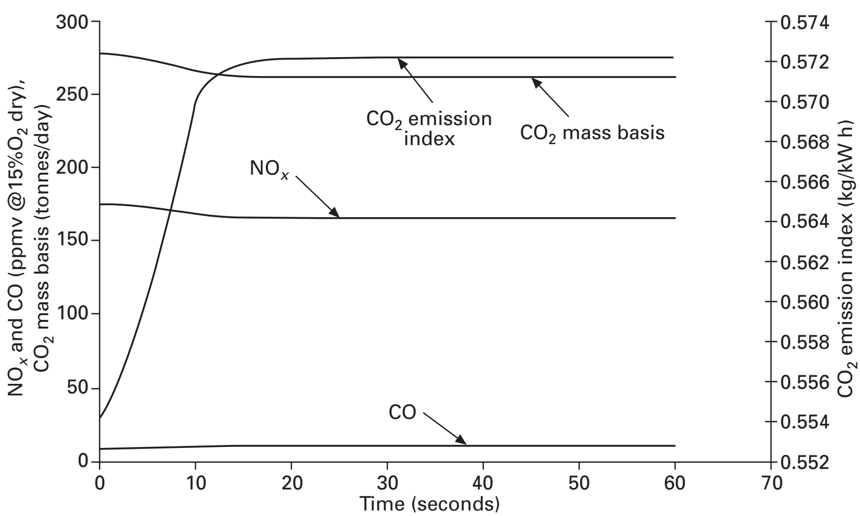

13.34 Trends in gas turbine emissions when hot end damage is present in the gas generator turbine.

Displacement of running line due to hot end damage in the gas generator turbine

It was discussed in Section 8.2 that decreasing the swallowing capacity (non-dimensional flow) of the gas generator turbine would shift the running line on the compressor characteristic towards surge. Conversely, an increase in the capacity of the gas generator turbine would shift the running line away from surge. However, the effect of reducing the gas generator turbine efficiency would shift the running line towards surge. This can be demonstrated by running the simulator where only the effect of reducing the gas generator turbine efficiency fault index by 2% is considered.

The effect of increasing the capacity of the turbine dominates because the shift in the running line due to the fall in gas generator turbine efficiency is small. Thus, the net effect on the running line of the compressor characteristic is a slight shift away from surge.

This is seen in Fig. 13.35, which shows the running line on the compressor characteristic when hot end damage is present in the gas generator turbine. The running line when no performance deterioration is present is also shown in the figure. The figure also shows the operating points for both these cases.

The variation of the compressor non-dimensional flow with its non-dimensional speed is shown in Fig. 13.36. The figure shows the curves when no engine faults are present and also the case when hot end damage is present. No shift is observed in this running line when hot end damage is

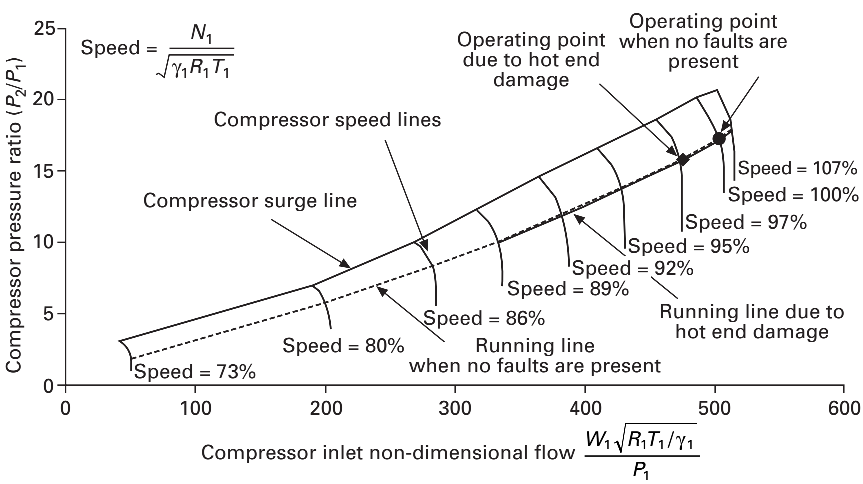

13.35 Running line and operating points in the compressor characteristic with and without hot end damage in the gas generator turbine.

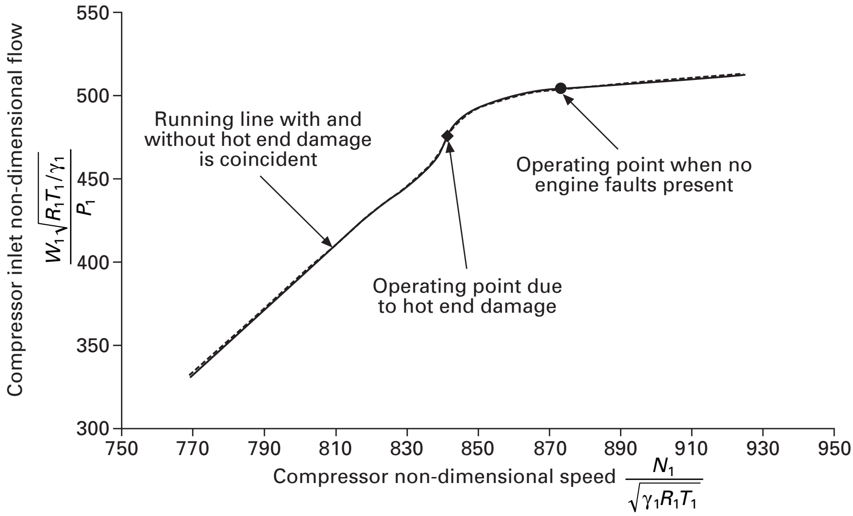

13.36 Variation of compressor non-dimensional flow with non-dimensional speed when hot end damage is present in the gas generator turbine.

present, unlike the case when compressor fouling was considered (Fig. 13.24). The operating points on this figure have also been shown for the cases with and without hot end damage. The effect of hot end damage results in a reduction in compressor speed and compressor inlet flow for a given compressor inlet temperature and pressure. Since compressor fouling influences only the displacement of this running line, it is a good indication of compressor fouling.

The variation of the compressor pressure ratio with its non-dimensional speed when hot end damage is present is shown in Fig. 13.37. The case when no damage is present is also shown in the Figure. Unlike the previous case when the effect on compressor non-dimensional mass flow varying with its non-dimensional speed due to hot end damage was considered, here the running line is shifted down when hot end damage is present. It has also been observed that the variation of compressor pressure ratio with its non-dimensional speed is influenced by compressor fouling, as shown in Fig. 13.25. Thus the variation of the compressor pressure ratio with its non-dimensional speed is not a good indication of compressor fouling as this running line is influenced by other fault conditions.

The above fault condition may be simulated for a low power condition where no engine operating limits are reached. The user is left to carry out this simulation where the power demand from the generator may be set to 18.5 MW to represent the low power case.

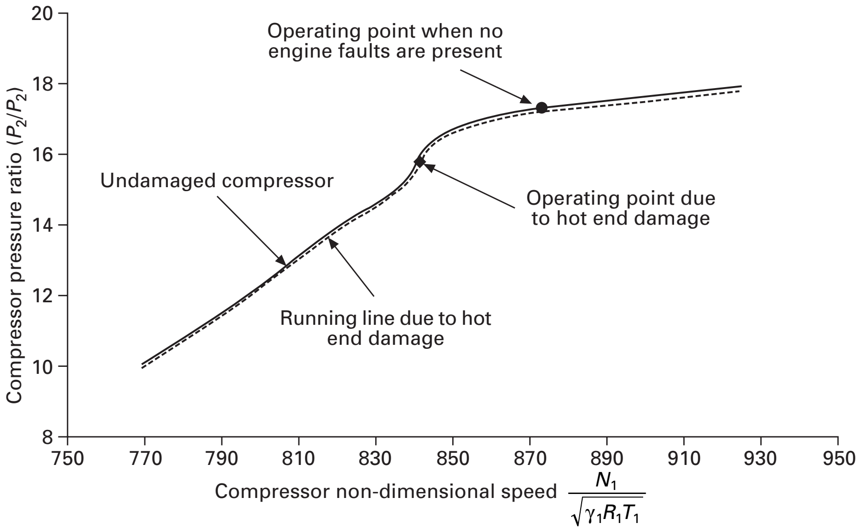

13.37 Variation of compressor pressure ratio with compressor non-dimensional speed when hot end damage is present in the gas generator turbine.

13.3.2 Turbine damage due to rotor tip rub

In Section 9.4, the importance of maintaining the clearances between the turbine rotor tip and the casing was discussed. Turbine blade rubs may result from high vibration, thus increasing the clearance between the turbine rotor and casing. The impact of such damage largely affects the turbine efficiency, rather than the non-dimensional flow capacity. Thus, this fault condition is simulated by decreasing the turbine efficiency fault index and thereby reducing the turbine efficiency.

Such faults may happen in either the gas generator or power turbine. The effect of turbine rotor tip rubs on the power turbine will be simulated on this occasion. Furthermore, a low power case will be considered where the engine does not reach an operating limit such as the exhaust gas temperature limit. This may be achieved by setting the power demand from the generator to 18 MW. The reader is left to consider the high power case when engine-operating limits are reached. The power turbine rotor tip damage is simulated by reducing the power turbine efficiency fault index by 2% over a 10-second period.

Figure 13.38 shows the trend in this fault index. The power turbine efficiency fault index is observed changing from 0% to –2% in 10 seconds, as this is the fault being simulated.

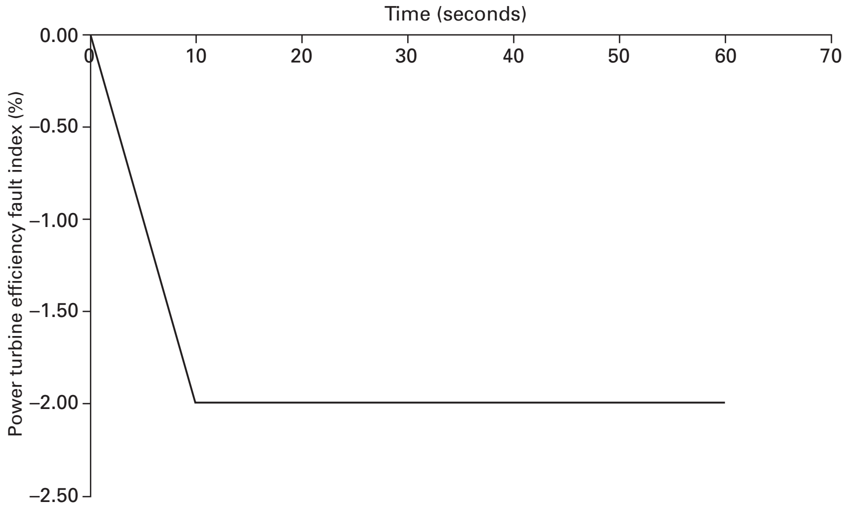

13.38 Trend in fault indices due to power turbine tip rub.

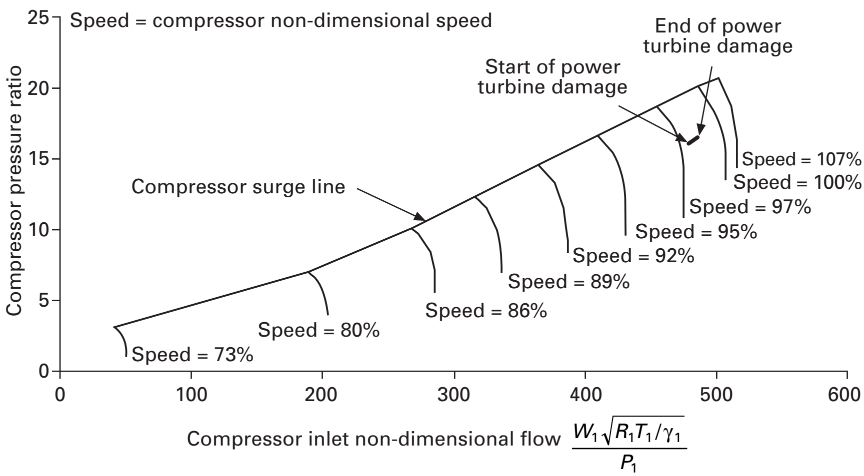

13.39 Operating point on the compressor characteristic due to power turbine damage.

Compressor characteristic

Figure 13.39 shows the operating point on the compressor characteristic. The operating point is observed moving up the characteristic, thus increasing the compressor pressure ratio, non-dimensional flow and non-dimensional speed. Since the engine is not operating on an engine limit, the fuel flow will increase to meet the power demanded by the generator, thus producing these changes on the compressor characteristic.

Trends in pressure ratio and pressure

The trends in the compressor and turbine pressure ratios are shown in Fig. 13.40. Increases in the compressor and the power turbine pressure ratios are observed. The gas generator turbine pressure ratio remains constant because of the choke conditions that prevail in the power turbine. Thus any increase in the compressor pressure ratio results in an increase in the power turbine pressure ratio.

Since the operating point on the compressor characteristic moves up due to this fault condition, the maximum cycle temperature ratio, T_3/T_1 will also increase as shown in Fig. 13.40. Figure 13.41 shows the trends in pressure for the compressor and turbines.

Trends in temperature

The trends in temperature due to power turbine damage are shown in Fig. 13.42. An increase in exhaust gas temperature, turbine entry temperature and the primary zone temperature are observed. This is due to the loss in the power turbine efficiency, thus requiring a higher firing temperature to maintain the generator power demand. The increase in power turbine exit temperature results from the increase in exhaust gas temperature and the loss in power turbine efficiency, although the power turbine pressure ratio has increased slightly, as shown in Fig. 13.40.

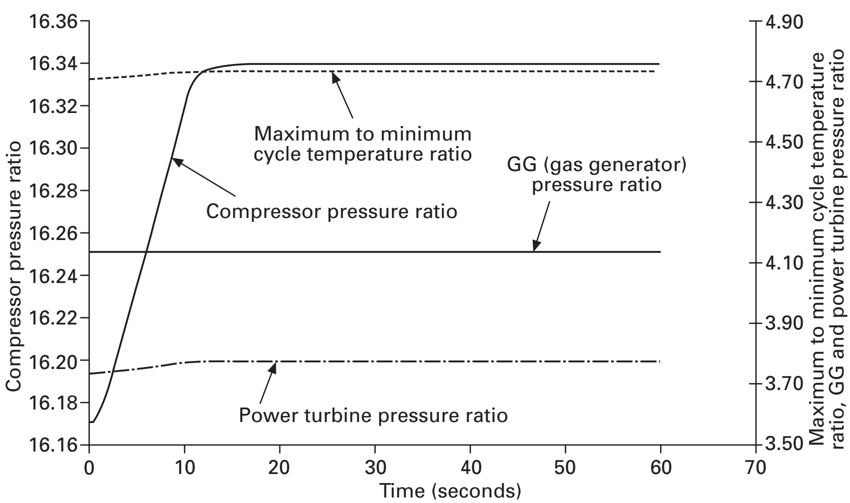

13.40 Trends in compressor and turbine pressure ratios due to power turbine damage.

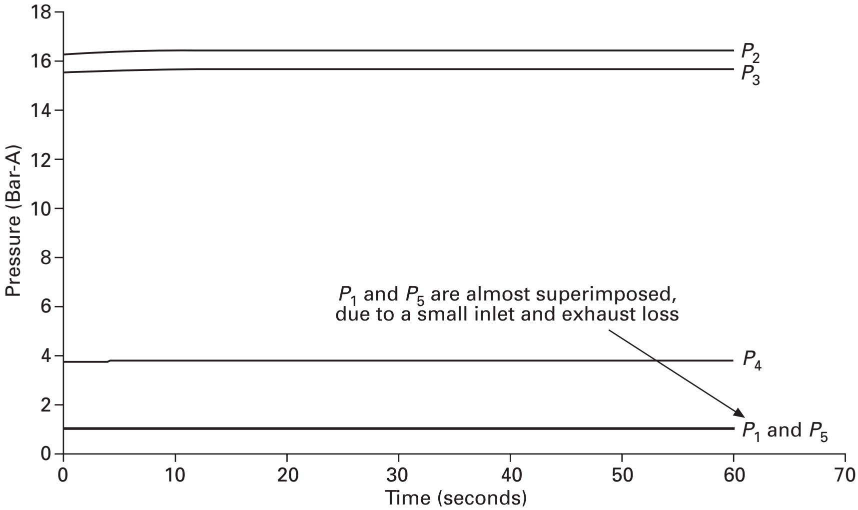

13.41 Trends in pressure due to power turbine damage.

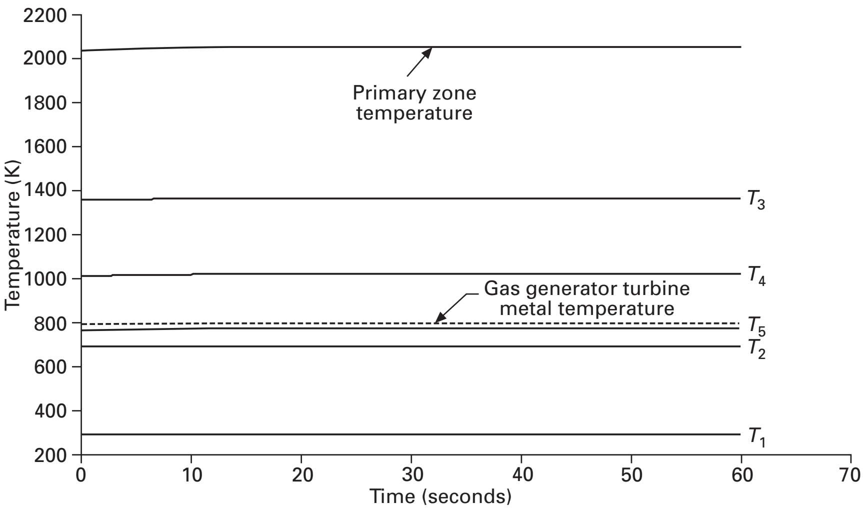

13.42 Trends in temperature due to power turbine damage.

Trends in flow

The trends in compressor inlet airflow, fuel flow and air–fuel ratio are shown in Fig. 13.43. The figure also shows the trend in the fuel valve position, which is very similar to the fuel flow trend. The increase in airflow results because of the increase in compressor non-dimensional flow due to the operating point moving up the running line on the compressor characteristic, as shown in Fig. 13.39.

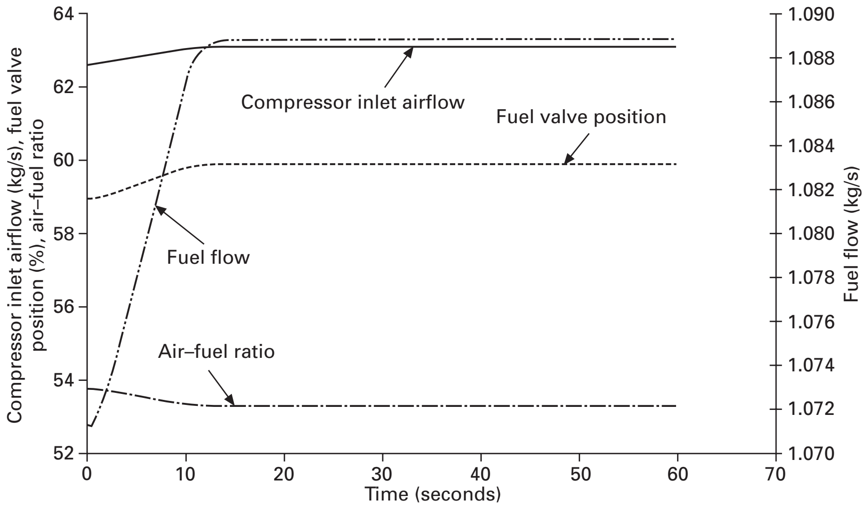

13.43 Trends in flow due to power turbine damage.

The combustor temperature rise, $T_3 - T_2$, has been observed to increase due to the power turbine damage, as shown in Fig. 13.42, and results from the higher firing temperature, T_3, needed to maintain the power demand, due to power turbine damage. Thus, the increase in combustion temperature results in a decrease in air–fuel ratio.

The loss in gas turbine thermal efficiency due to power turbine damage results in an increase in fuel flow to maintain the required power output. The fuel valve position increases in order to allow an increase in fuel flow to the gas turbine, enabling the power output demand to be maintained.

Trends in speed

The trends in the gas generator and compressor non-dimensional speeds are shown in Fig. 13.44. As the operating point moves up the compressor characteristic due to the power turbine damage, the compressor non-dimensional speed must increase, as seen in Fig. 13.39. Since the compressor inlet temperature remains constant, there must be an increase in the gas generator speed to satisfy the required compressor non-dimensional speed, $N_1/\sqrt{T_1}$.

Trends in power and efficiency

The trends in power and thermal efficiency are shown in Fig. 13.45. It is observed that the gas turbine power output and the generator power demand remain constant due to the power turbine damage. Since the engine is not

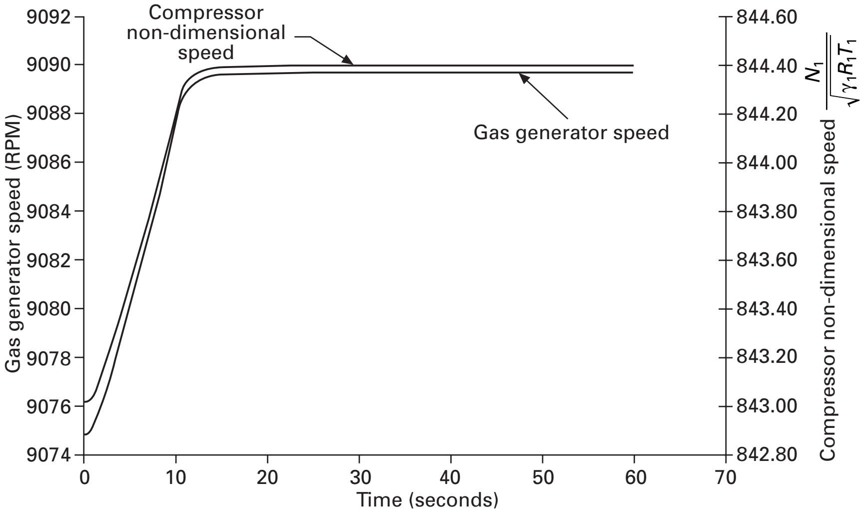

13.44 Trends in speeds due to power turbine damage.

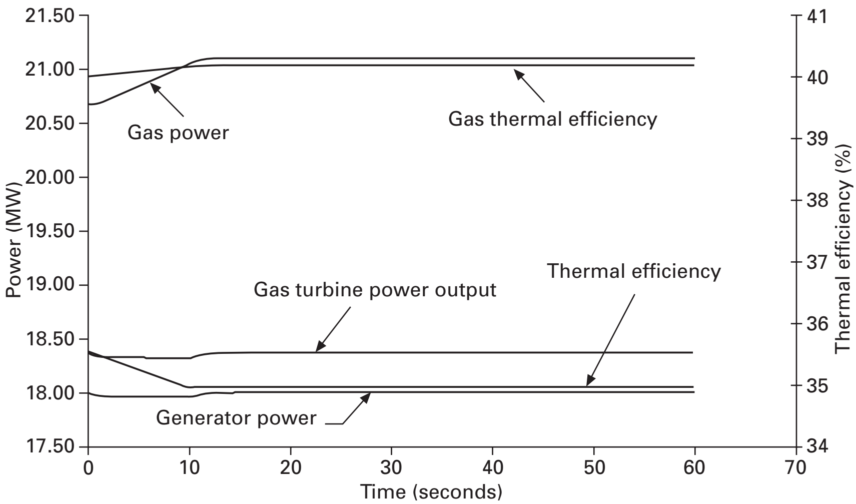

13.45 Trends in power and thermal efficiency due to power turbine damage.

operating on an engine limit, the fuel flow can increase to satisfy the generator power demand, thereby resulting in increases in pressures, temperatures, flows and speeds, as seen in previous figures.

Notice that the gas power has indeed increased due to the power turbine damage. Since the power turbine fault resulted only in a loss in power turbine efficiency, the gas generator performance is unaffected by this degradation. The loss in power turbine efficiency thus results in an increase in gas power to maintain the same gas turbine power output, hence the increase in the gas power output (as seen in Fig. 13.45 where the generator power output remains on the set point). This increase in gas power output improves the gas thermal efficiency due to the increase in compressor ratio and maximum to minimum cycle temperature ratio. The increase in gas power demands an increase in fuel flow; however the gas turbine power output remains the same. Hence the gas turbine thermal efficiency decreases due to the power turbine damage.

Trends in turbine creep life usage

The trends in creep life usage for the gas generator turbine and power turbine due to power turbine damage are shown in Fig. 13.46. An increase in creep life usage is observed for both these turbines. Power turbine damage results in an increase in gas generator speed and turbine entry temperature. The increase in stress due to the increase in speed, and the higher turbine blade temperature due to the increase in turbine entry temperature, result in an increase in the gas generator turbine creep life usage. The increase in the exhaust gas temperature also results in an increase in the power turbine blade temperature, thus increasing the power turbine creep life usage.

Trends in gas turbine emissions

The trends in gas turbine emissions due to power turbine damage are shown in Fig. 13.47. The increase in combustion pressure and temperature due to

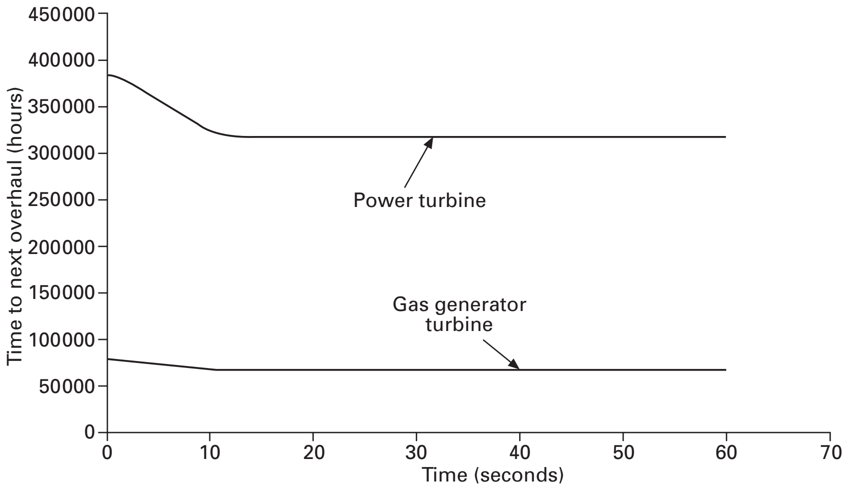

13.46 Trend in gas generator and power turbine creep life usage due to power turbine damage.

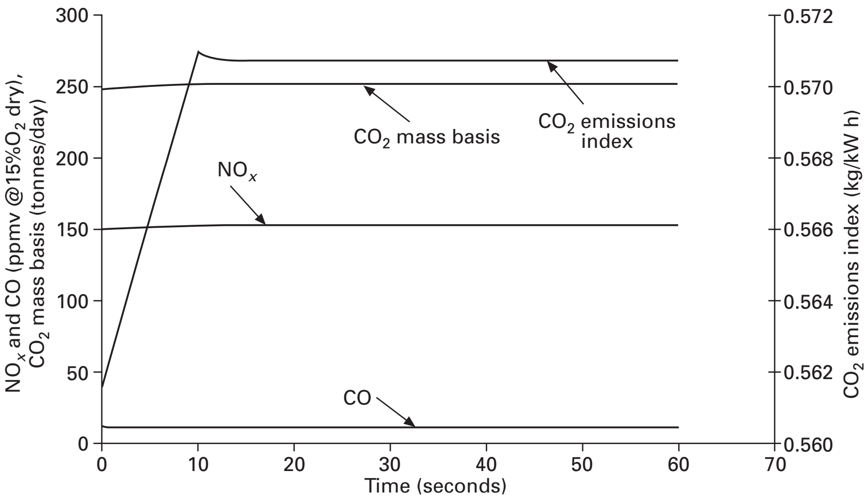

13.47 Trends in gas turbine emissions due to power turbine damage.

power turbine damage results in an increase in NO_x, while the effect on CO is small. The increase in fuel flow and loss in thermal efficiency, due to power turbine damage, results in an increase in CO_2 emissions on a mass and index basis.

Displacement of the running line

Since the power turbine efficiency loss due to rotor blade tip rubs does not affect the performance of the gas generator, there is no shift in the running lines. The reader is left to plot the running lines and compare them with the case when no faults are present to demonstrate that there is no displacement in the running line. However, if the power turbine suffered from hot end damage, thus changing the non-dimensional flow of the power turbine, there would be a displacement in the running line. Again, the reader is left to run this simulation to demonstrate the effect of power turbine hot end damage on the running lines. Setting the power turbine fouling fault index and efficiency fault index to 3% and –2%, respectively can simulate hot end damage of the power turbine over a suitable ramp rate.

13.4 References

1. Saravanamutoo, H.I.H. and Lakshmiranasimha, A.N., A preliminary assessment of compressor fouling, *ASME paper 91-GT-153*, 1991.
2. *Gas Turbine Theory*, 5th Edition, Saravanamuttoo, H.I.H., Rogers, C.F.G. and Cohen, H., Longman (2001).

14
Power augmentation

The power output of the gas turbine is limited, as has been seen, by the exhaust gas temperature, gas generator speed and the compressor non-dimensional speed. The exhaust gas temperature limit prevents the turbine from overheating thus preventing the excess usage of turbine creep life. The gas generator speed limit prevents the over-stressing of the rotating members such as compressor/turbine blades and discs. Any increase in stress levels due to speed excursions will also contribute to a reduction in turbine creep life. The compressor non-dimensional speed limit prevents the compressor from stalling and surging at high compressor speeds due to choke conditions at the inlet of the compressor.

It has been observed that, at different ambient temperatures, the performance of the gas turbine is limited by different limiting parameters. At high ambient temperatures above 15 degrees Celsius, it is the exhaust gas temperature that limits the engine performance. At ambient temperatures between +15 and –15 degrees Celsius, the engine performance is controlled by the gas generator speed and at ambient temperatures below –15 degrees Celsius, the engine performance is controlled by the compressor non-dimensional speed. The values for these parameters are as follows and are referred to as the continuous rating or base rating:

- exhaust gas temperature limit 1058 K
- gas generator speed limit 9500 RPM
- compressor non-dimensional speed limit 587.

At high ambient temperatures, when the engine performance is restricted by the exhaust gas temperature limit, the performance of the gas turbine may be improved by increasing the limit by about 20 degrees Celsius. However, there will be a significant reduction in turbine creep life due to the higher operating blade temperatures and stress. Augmenting the power by increasing the exhaust gas temperature limit is often referred to as peak rating.

The gas generator speed limit is normally the base-rated condition, which corresponds to its 100% value of 9500 RPM. However, manufacturers often offer a maximum continuous rating value, which usually corresponds to 105% gas generator speed. Thus at ambient temperatures when the engine performance is restricted by the gas generator speed, the gas generator speed limit can be increased to the maximum continuous rating value, thereby improving the performance of the engine. Operating at the maximum continuous rating will have an impact on the turbine creep life, due to the increased stress and turbine blade temperatures resulting from higher gas temperatures required to achieve the increased gas generator speed. Thus the manufacturer will require major engine overhauls on a more frequent basis, which result in increasing maintenance costs.

At very low ambient temperatures, when the engine performance is limited by the compressor non-dimensional speed, it may not be possible to improve the engine performance by increasing the compressor non-dimensional speed limit because compressor surge could be encountered, which should be avoided.

However, when operating is at low ambient temperatures for significant periods, it may be possible to increase the engine performance by reducing the power turbine non-dimensional flow capacity. The net effect of reducing the power turbine non-dimensional flow capacity is to increase the compressor pressure ratio and the maximum to minimum cycle temperature ratio, T_3/T_1, when the engine performance in limited by the compressor non-dimensional speed. Thus a significant increase in both thermal efficiency and power output results and this will be discussed later in this chapter. However, the increase in T_3/T_1 will increase T_3, resulting in a higher turbine blade temperature, which reduces the turbine creep life, and hence increases maintenance cost.

The engine simulator will now be used to augment the power output from the gas turbine using each of these methods and the effect on performance, emissions and loss in creep life will be determined.

14.1 Peak rating

The simulator is run by setting the generator power demand at 25 MW, thus ensuring the engine is always on an engine limit. The exhaust gas temperature limit is increased by 20 degrees Celsius to 1078 K (peak rating value) and then the ambient temperature changed from 30 degrees to –30 degrees Celsius in steps of 10 degrees. The increase in the exhaust gas temperature limit will result in an increase in $T_4(\mathrm{EGT})/T_1$. From Fig. 11.6, which shows the variation of $T_4(\mathrm{EGT})/T_1$ with the compressor non-dimensional speed ($N_1/\sqrt{T_1}$), an increase in compressor non-dimensional speed will result. Thus an increase in compressor pressure ratio, turbine entry temperature and power output will also occur. For a given ambient temperature, T_1, the increase in $N_1/\sqrt{T_1}$ will also result in an increase in the gas generator speed, N_1, due to peak rating.

At high ambient temperatures above 20 degrees Celsius, a significant increase in power output may be achieved (Fig. 14.1). The higher the ambient temperature, the larger is the increase in power due to peak rating. For example, at an ambient temperature of 30 degrees Celsius, the power output from the gas turbine would increase from about 18.2 MW to 19.4 MW, representing nearly a 7% increase in power output due to peak rating. However, at about 20 degrees Celsius, the power output from the gas turbine increases from about 20 MW to 21 MW during peak rating, which represents only about 5% increase in power output. At lower ambient temperatures, the gain in power output is even smaller as the gas generator speed limit is reached. In fact, at ambient temperatures below 15 degrees Celsius, no peak rating is possible as the gas generator speed would have reached its limiting value, therefore forcing the exhaust gas temperature to decrease.

The increase in maximum to minimum cycle temperature ratio, T_3/T_1, and compressor pressure ratio, results in an increase in the gas turbine thermal efficiency during peak rating and this is shown in Fig. 14.2. Thus a useful reduction in fuel costs will also result because of peak rating.

The increase in gas generator speed and turbine blade temperature during peak rating results in an increase in the turbine creep life usage. This can be seen in Fig. 14.3 where the change in the gas generator and power turbine creep life usage with ambient temperature is shown. The increase in the turbine creep life usage during peak rating is approximately constant over a range of ambient temperatures when the EGT limits the performance of the gas turbine. The loss in the gas generator turbine creep life is about 40%, whereas the loss in the power turbine creep life is about 45%. Thus peak rating almost doubles the turbine creep life usage.

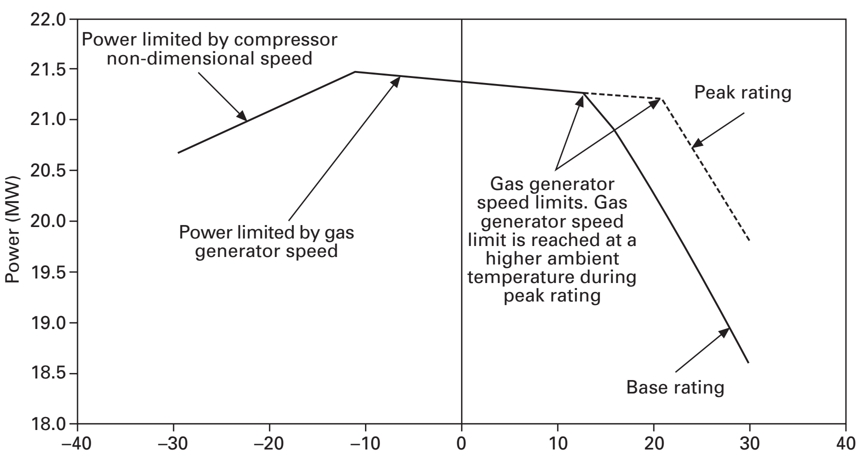

14.1 Effect of peak rating on power output.

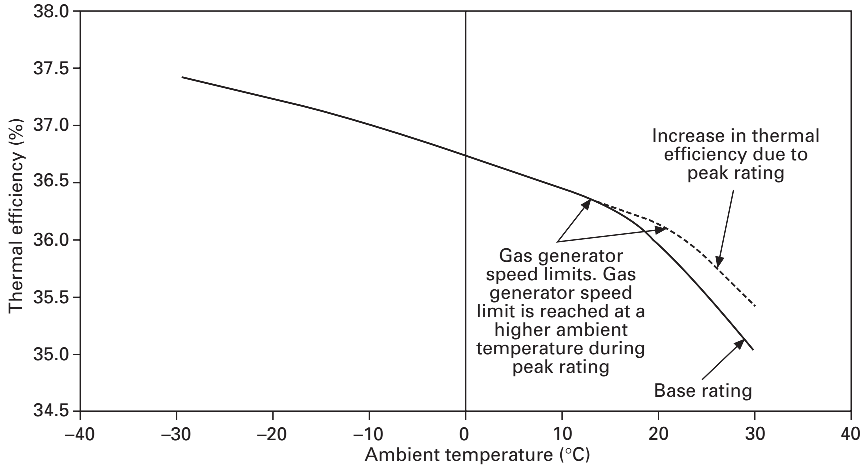

14.2 Effect of peak rating on thermal efficiency.

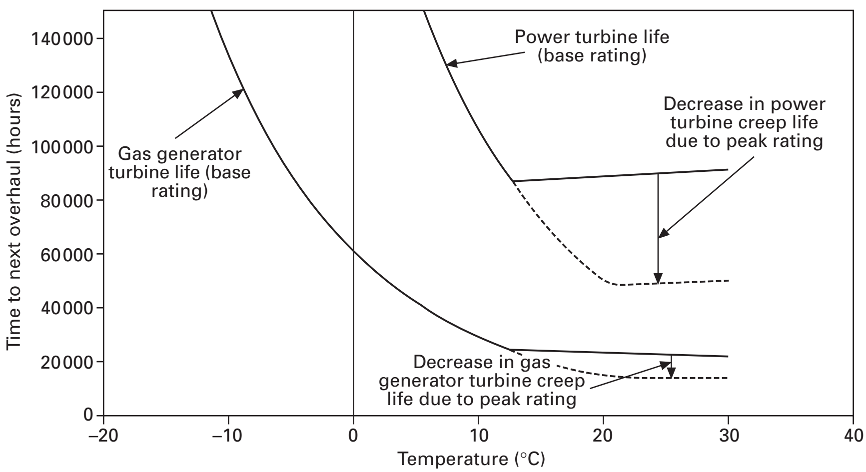

14.3 Effect of peak rating on turbine creep.

The impact of peak rating on gas turbine emissions is shown in Fig. 14.4. Since the compressor pressure ratio, the combustion pressure and the combustion temperature have increased during peak rating, the NO_x emissions will increase. However, an increase in these parameters will result in a reduction of CO. CO_2 emissions will also increase due to the increased power output during peak rating because of increased fuel flow.

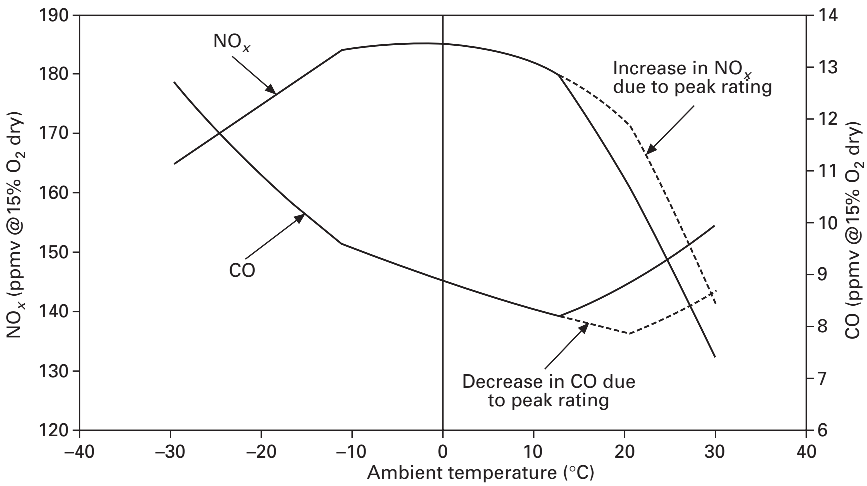

14.4 Change in gas turbine emissions during peak rating.

Although a significant increase in creep life usage occurs during peak rating, on occasions, increased revenue due to the increased power generation capacity will justify the increased maintenance costs.

Thus the business case for peak rating should be evaluated carefully, taking into consideration the increased capacity, better thermal efficiency and increased maintenance costs, particularly at high ambient temperatures, where the increase in power output is the greatest for a given loss in turbine creep life.

14.2 Maximum continuous rating

It has been stated that the base rating of the engine restricts the gas generator speed to 100%. However, manufacturers may allow a maximum continuous rating of 105% gas generator speed, provided the impact on turbine creep life is not too excessive. This may be the case at low ambient temperatures where the engine power output is limited by the gas generator speed, resulting in reduction in turbine creep life usage due to the reduction in turbine temperatures (Section 11.3). Increasing the gas generator speed limit to the maximum continuous rating value will result in an increase in the compressor non-dimensional speed for a given ambient temperature. This will result in an increase in compressor pressure ratio, turbine entry temperature and compressor inlet mass flow rate, and therefore an increase in thermal efficiency and power output from the gas turbine will occur.

The increased power output during maximum continuous rating is shown in Fig. 14.5. The maximum increase in power occurs at an ambient temperature

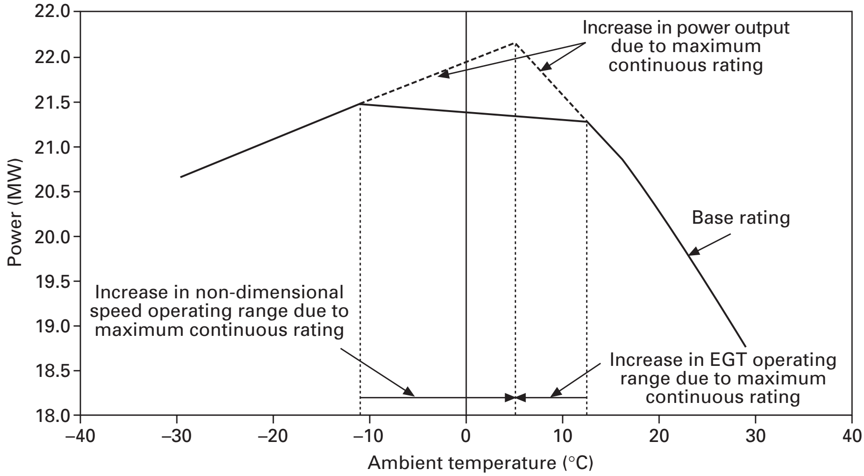

14.5 Effect of maximum continuous rating on power output.

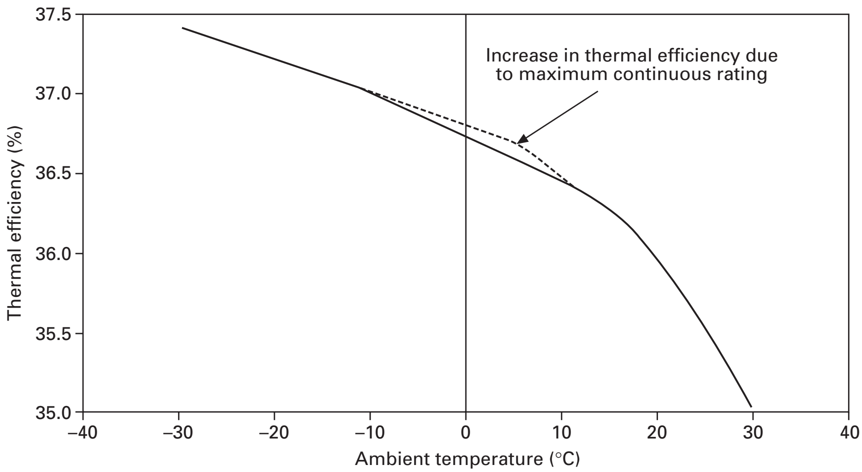

14.6 Effect of maximum continuous rating on gas turbine thermal efficiency.

of about 5 degrees Celsius. The power output from the gas turbine increases from about 21.3 MW to about 22 MW, representing about a 3% increase in power output. Thus, a useful increase in power output can be achieved during maximum continuous rating. Figure 14.6 shows the change in thermal efficiency during maximum continuous rating. There is also a useful increase in thermal efficiency during maximum continuous rating due to the higher compressor pressure ratio and turbine entry temperature. The increase in the gas generator speed limit results in an increase in ambient temperature range where the engine power output is limited by the exhaust gas temperature. Operating at maximum continuous rating also results in an increase in the ambient temperature range where the engine power output is limited by the compressor non-dimensional speed. In fact, there is no operation at constant gas generator speed on this engine when operating at maximum continuous rating.

The impact of maximum continuous rating on turbine creep life is shown in Fig. 14.7. An increase in turbine life usage is observed to occur during maximum continuous rating operation. However, this increase is not as dramatic as with the case of peak rating. Nonetheless, the manufacturer may require an increase in engine maintenance frequency to allow for the reduction in turbine creep life. It would be possible to maintain the same maintenance frequency but to accept a reduced exhaust gas temperature limit at higher ambient temperatures, resulting in a loss in power output at these ambient temperatures. Although, at first sight, it may appear unacceptable to the operator to reduce the exhaust gas temperature limit at higher ambient temperatures, in temperate countries where maximum power demand is often at low ambient temperatures, such a compromise may result in more revenue and thus more profit.

Figure 14.8 shows the change in gas turbine emissions when operating at the maximum continuous rating. The increase in compressor pressure ratio and combustion temperature results in an increase in NO_x and a decrease in CO.

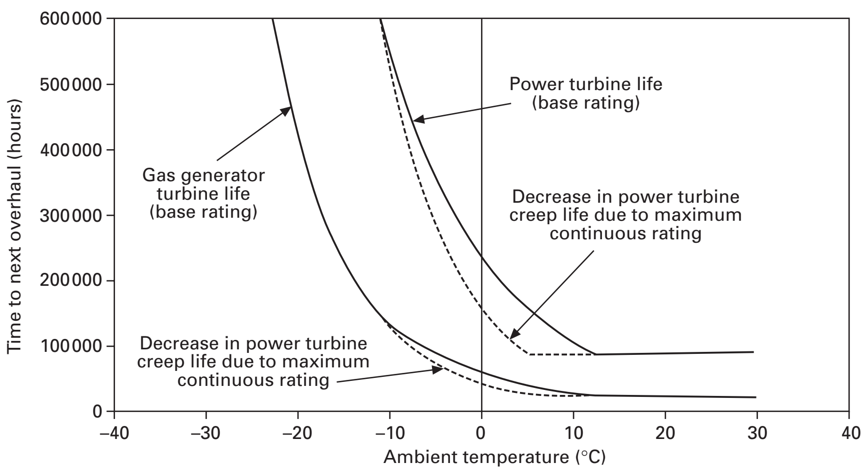

14.7 Effect of maximum continuous rating on turbine creep life.

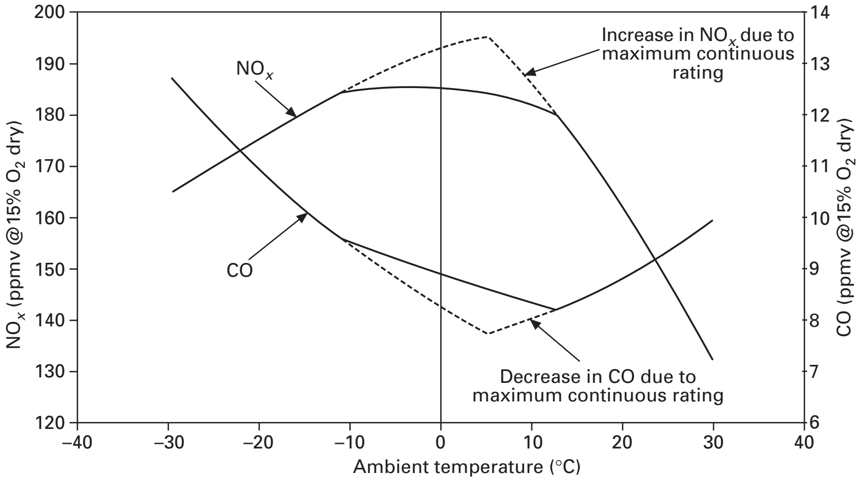

14.8 Change in gas turbine emissions due to operation at maximum continuous rating.

14.3 Power augmentation at very low ambient temperatures

At ambient temperatures below –15 degrees Celsius it has been observed that the gas turbine power output is limited by the compressor non-dimensional speed, and the maximum non-dimensional speed of the compressor cannot be increased due to the likelihood of compressor surge. It has also been observed that, as the ambient temperature falls, the gas generator speed increases and eventually becomes the factor that limits the engine performance. To increase the power output at such low temperatures, a method of increasing the turbine entry temperature is required whilst the compressor non-dimensional speed is not increased.

From the discussion of the component matching process for turbines operating in series in Section 8.2 (Fig. 8.12), the effect of reducing the power turbine area, and thus its non-dimensional flow capacity, will decrease the gas generator turbine pressure ratio. If operation is continued at a constant compressor non-dimensional speed, the power balance between the compressor and gas generator turbine will result in an increase in turbine entry temperature. Furthermore, the flow compatibility between the compressor and the gas generator turbine will also result in an increase in compressor pressure ratio. Thus, by reducing the power turbine area, at ambient temperatures where the power output from the gas turbine is limited by the compressor non-dimensional speed, an increase in thermal efficiency and power output will occur due to the higher compressor pressure ratio and turbine entry temperature.

At high ambient temperatures, where the exhaust gas temperature limits the gas turbine power output, a loss in power output and thermal efficiency will occur. Since the exhaust gas temperature limit cannot be increased, any reduction in the gas generator turbine pressure ratio due to the reduction of the power turbine capacity results in a decrease in the compressor non-dimensional temperature rise in order to satisfy the power balance between the compressor and the gas generator turbine. Thus a decrease in turbine entry temperature, compressor pressure ratio and inlet mass flow rate will occur (i.e. for a given EGT a decrease in the gas generator turbine pressure ratio results in a decrease in the turbine entry temperature, T_3). These three factors will result in a decrease in power output and thermal efficiency when operating at high ambient temperatures.

It may thus be argued that an increase in power turbine capacity will help improve the gas turbine performance at high ambient temperatures. However, an increase in compressor non-dimensional temperature must occur due to the increased gas generator turbine pressure ratio and therefore an increase in gas generator speed and turbine entry temperature results. The increase in gas generator speed and turbine entry temperature will result in an increase in turbine creep life usage, which may be unacceptable.

Figure 14.9 shows the change in power due to a decrease in power turbine capacity. The power turbine capacity was reduced by 3%, achieved by setting the power turbine fouling fault index to –3%. The range of ambient temperature when the exhaust gas temperature limits the gas turbine power output has now increased. The ambient temperature range for constant exhaust gas

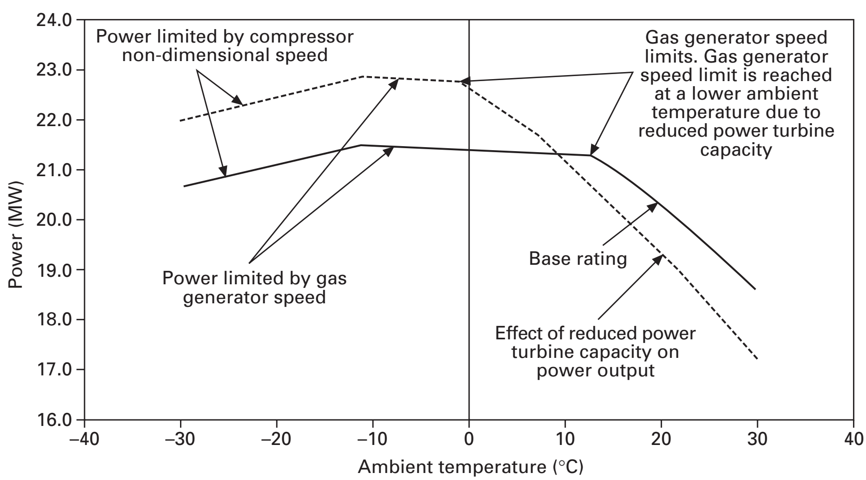

14.9 Change in power output with ambient temperature due to a decrease in power turbine capacity.

temperature operation for the base rated case is from 30 to about 15 degrees Celsius, below which the power output is limited by the gas generator speed. Where there is a reduction in the power turbine capacity, the ambient temperature range for constant exhaust gas temperature operation now increases to 30 to about 0 degrees Celsius.

It is observed that the power output due to the decrease in power turbine capacity exceeds the base-rating case when the ambient temperature decreases to below 10 degrees Celsius. This is due to the higher exhaust gas temperature and therefore higher turbine entry temperature. At an ambient temperature of –5 degrees Celsius, the power output increases from about 21.4 MW to about 22.7 MW, which is a 6% increase. At lower ambient temperatures, the increase in power output is even greater. However, at ambient temperatures above 15 degrees Celsius, a loss in power output results due to the decrease in turbine entry temperature as explained above. Thus a significant increase in power output is possible by optimising the power turbine capacity at low ambient temperatures, when the engine performance is limited by the gas generator speed. This results in increased revenue and profit.

The increases in compressor pressure ratio and turbine entry temperature at low ambient temperatures result in an increase in the gas turbine thermal efficiency. Thus a reduction in fuel costs in real terms will occur, leading to lower operating costs. At high ambient temperatures, of course, a decrease in thermal efficiency would be incurred, due to the reasons discussed above and thus fuel costs would increase. Figure 14.10 shows the effect of reduced power turbine capacity on thermal efficiency for a range of ambient temperatures.

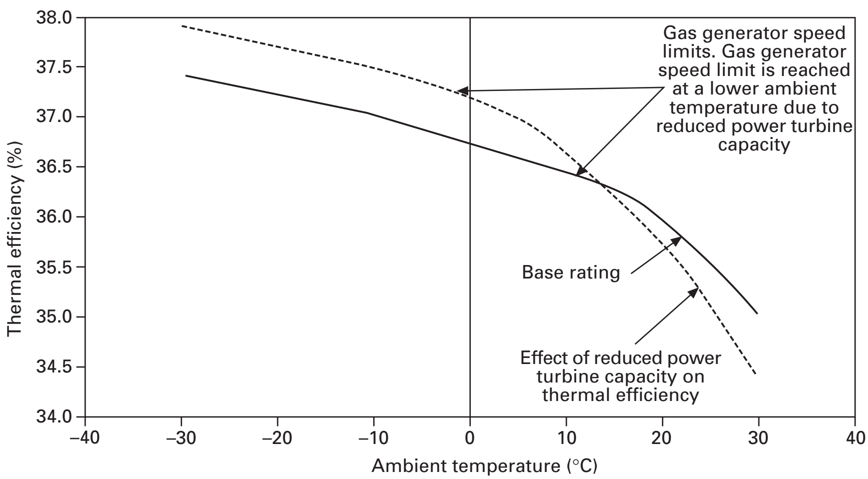

14.10 Variation of gas turbine thermal efficiency due to reduction in power turbine capacity.

The impact of reduced power turbine capacity on turbine creep life is shown in Fig. 14.11. At ambient temperatures above 12 degrees Celsius, the gas generator turbine creep life usage is actually smaller compared with the base-rating case. This is due to the reduction in the gas generator speed and turbine entry temperature when the exhaust gas temperature limits the engine power output. There is also a slight reduction in the power turbine creep life usage above an ambient temperature of about 12 degrees Celsius. This is due to the lower stress in the turbine blades resulting from less torque due to the reduction in gas turbine power output.

At ambient temperatures below 12 degrees Celsius, the gas turbine creep life usage increases and this increase is due to the increase in turbine entry temperature that arises from the reduced power turbine capacity. At ambient temperatures below 12 degrees Celsius, the power turbine life also decreases and this is due to the higher exhaust gas temperature compared with the base-rating case. This is shown in Fig. 14.11, which illustrates the effect of reduced power turbine capacity on turbine creep life.

Although a significant increase in turbine creep life usage occurs at low ambient temperatures, the creep life is still above 20 000 hours, when normally engine overhauls are necessary. However, manufacturers may want an increased frequency of engine overhaul but the improvement in creep life usage at high ambient temperature should be considered before agreeing to any such increase in engine maintenance. Clearly, a worthwhile increase in power output at low ambient temperatures is possible without any significant change in maintenance cost. Furthermore, the increase in the thermal efficiency will

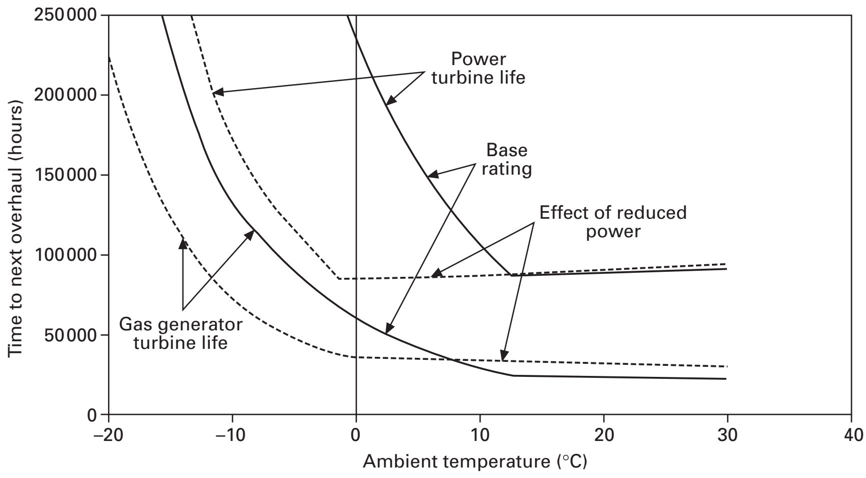

14.11 Change in turbine creep life due to reduction in power turbine capacity.

reduce fuel costs resulting in lower operating costs. However, the drawback is lower power output and thermal efficiency at high ambient temperatures. If demand for power is important during winter months, then such optimisation of the power turbine capacity will result in higher profits during these months. The increase in fuel costs during the summer months would have to be carefully evaluated before deciding whether such optimisation results in reduced life cycle costs.

A similar improvement in engine performance at low ambient temperatures may be obtained by increasing the gas generator turbine swallowing capacity. The reader is left to run the simulator to demonstrate the impact of increasing the gas generator turbine capacity on engine performance at low ambient temperatures.

Figure 14.12 shows the effect of reduced power turbine capacity on engine emissions. At high ambient temperatures, the decrease in turbine entry temperature, compressor pressure ratio, and thus combustion pressure, results in a decrease in NO_x and an increase in CO. At low ambient temperatures the increase in combustion pressure and temperature, results in the increase of NO_x and decrease in CO.

Figure 14.13 shows the shift of the running line on the compressor characteristic. It is observed that the running line has indeed shifted towards surge, thereby reducing the surge margin. However, this shift in the running line is small. The VIGV/VSV schedule may be changed if necessary so that the variable stators do not open as much. This could increase the surge margin, but reduce the flow capacity of the compressor, and the resultant loss in compressor capacity should be taken into account. Alternatively, the

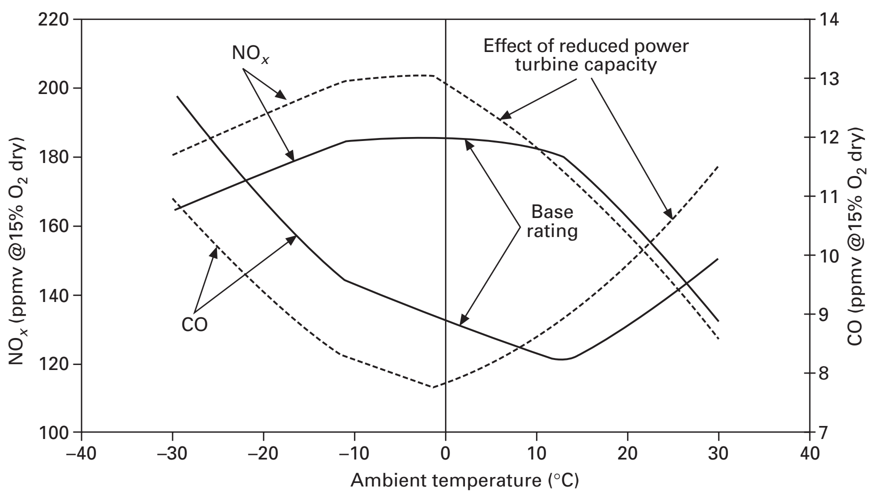

14.12 Effect of reduced power turbine capacity on engine emissions.

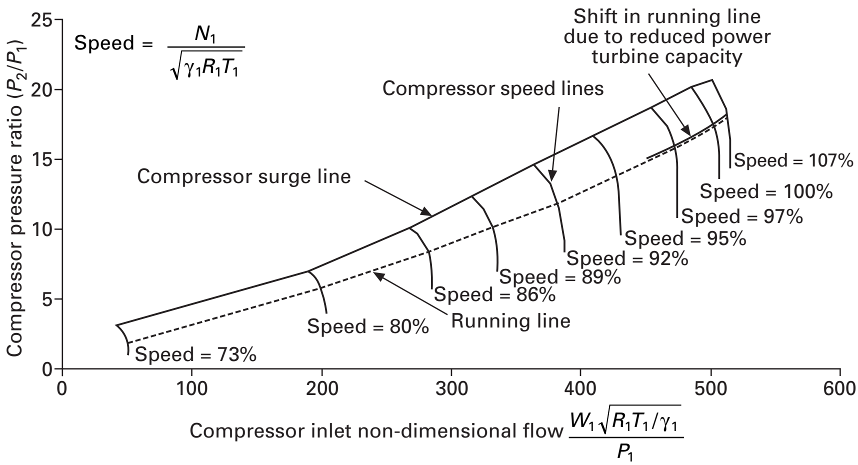

14.13 Shift in the running line on compressor characteristic due to reduction in power turbine capacity.

acceleration line may be reduced, thus reducing the transient response of the engine and this condition will be discussed in the next chapter.

14.4 Power augmentation by water injection

Gas turbine power output may be augmented by water injection. Water may be injected into the inlet of the compressor or directly into the primary zone of the combustion system. When water is injected into the inlet of the compressor, the reduction of the compressor inlet temperature due to the evaporation of the water is primarily responsible for the increase in power output. The amount of water that can be evaporated depends on the humidity of the air. The lower the humidity, the larger is the amount of water that can be evaporated, resulting in a greater decrease in the compressor inlet temperature. Such means of power augmentation is, in fact, referred to as turbine inlet cooling and is only applicable where the relative humidity of the air is low and the ambient temperature is high. Turbine inlet cooling will be discussed in the next section.

Direct injection of water into the primary zone augments the power output by increasing the flow through the turbines. The ambient temperature and humidity have no influence on how much water can be injected, but injection is limited by the increase in emission of CO and UHC. In this section the impact of direct injection of water into the combustion system on engine performance is considered.

The increase in gas turbine power output due to water injection into the combustion system is shown in Fig. 14.14. The water–fuel ratio is maintained

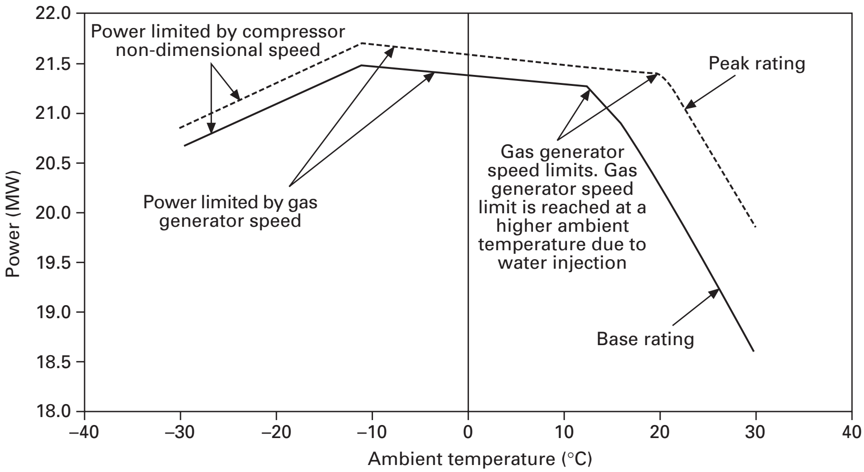

14.14 Increase in gas turbine power output due to water injection.

at unity during the change in the ambient temperature range. At high ambient temperatures, a significant increase in power output is achieved by water injection. The gas turbine power output increases by about 6% and 7% above the base rating for ambient temperatures of 20 and 30 degrees Celsius, respectively. As the ambient temperature falls below 20 degrees Celsius, the power output starts to flatten out and is due to the gas generator speed reaching its operating limit (continuous rating limit), which now occurs at an higher ambient temperature compared with the base-rated base.

At zero degrees Celsius, the power increase due to water injection is only about 1%. At such low ambient temperatures, the gas generator speed limits the power output of the gas turbine. Direct water injection into the combustor would increase the mass flow rate through the gas generator turbine, thus increasing the power output of the gas generator turbine and this would increase the gas generator speed as observed at high ambient temperatures when the exhaust gas temperature limits the power output of the gas turbine. At low ambient temperatures, when the gas generator speed or compressor non-dimensional speed limits the performance of the gas turbine, a decrease in turbine entry temperature, T_3, is necessary to maintain the power balance between the compressor and gas generator turbine. The reduction in turbine entry temperature reduces the specific work, while water injection increases the gas generator turbine power output. The net effect is a small increase in power output at low ambient temperatures due to water injection when speeds limit the power output of the gas turbine.

The effect of water injection on the gas turbine thermal efficiency is shown in Fig. 14.15. Water injection results in a reduction in thermal efficiency.

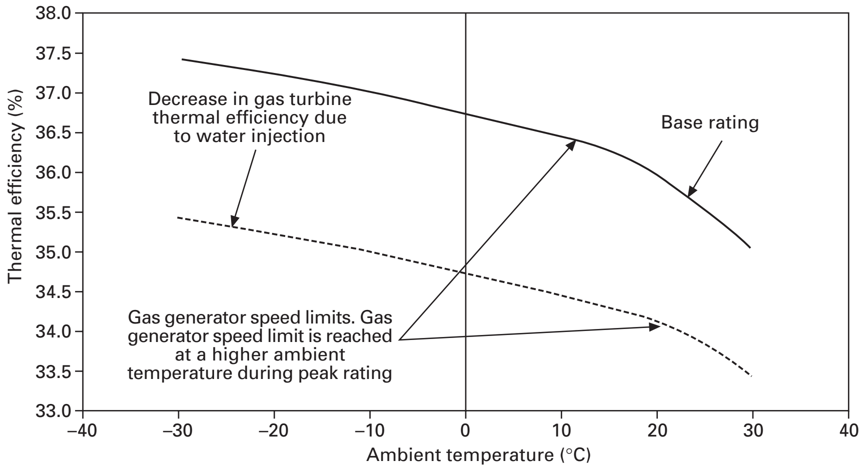

14.15 Decrease in gas turbine thermal efficiency due to water injection.

Additional fuel input is necessary to evaporate the water and heat the steam to the required turbine entry temperature. However, the latent heat of evaporation of water required to evaporate the water cannot be used by the engine because the power turbine exhaust temperature is well above the boiling point of water (i.e. it is not possible to condense the steam and retrieve the latent heat).

Thus the latent heat supplied is wasted in the exhaust system, resulting in a decrease in the gas turbine efficiency. At ambient temperatures below 20 degrees Celsius, a greater loss in thermal efficiency occurs because the turbine entry temperature decreases due to constant speed operation. The loss in thermal efficiency at an ambient temperature of 30 degrees Celsius is about 4%, whereas the loss in thermal efficiency at 0 degrees Celsius is about 6%. Thus, water injection at low ambient temperatures, where the power output from the gas turbine is limited by the gas generator speed or compressor non-dimensional speed, may be uneconomical because of the increase in fuel cost, unless the fuel is relatively inexpensive. However, water injection can suppress NO_x emissions significantly and would be used for reducing emissions at such low ambient temperatures. This is discussed later in this section.

Figure 14.16 shows the variation of turbine creep life usage with ambient temperature, as affected by water injection. A loss in gas generator turbine creep life occurs at ambient temperatures above 20 degrees Celsius. The increase in gas generator speed at these ambient temperatures is responsible for the increase in creep life usage. At ambient temperatures below 20 degrees

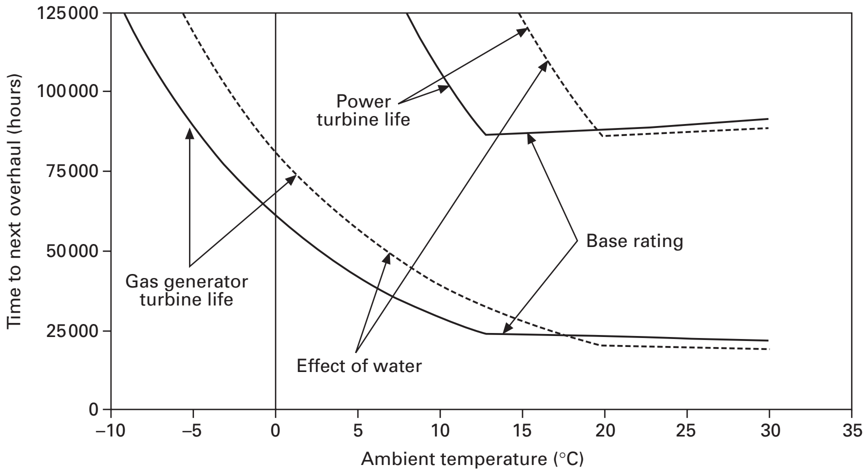

14.16 Effect of water injection on turbine creep life.

Celsius, the gas generator creep life usage reduces and this is primarily due to the decrease in the turbine entry temperature.

The power turbine creep life also decreases for ambient temperatures above 20 degrees Celsius and this is because of the increase in power output from the power turbine, resulting in increased stresses due to the increase in torque in the blades. At ambient temperature below 20 degrees Celsius, the reduction in power turbine creep life usage is due to the decrease in the exhaust gas temperature, when the gas turbine power output is limited by the gas generator speed.

Since water injection gives rise only to a small increase in power output at low ambient temperatures, it is unlikely that water injection would be employed at these temperatures when the increase in fuel cost, due to the marked reduction in thermal efficiency, is significant. Thus it may not be possible to exploit the decreased creep life usage at low ambient temperature to compensate for the loss in creep life at high ambient temperatures, where the power output from the gas turbine is limited by the exhaust gas temperature. Therefore, an increase in engine overhaul frequency will lead to increased maintenance costs. Water injection also results in damage to the combustion system due to the significant chilling of the flame, resulting in increased thermal stress cycles and corrosion, hence adding further maintenance costs. It must be noted that demineralised water must be used and this adds to the operating cost.

The greatest effect of water injection directly into the primary zone of the combustion system is a significant suppression of NO_x emissions as discussed in Section 6.9. The impact of water injection on NO_x and CO emissions is shown in Fig. 14.17. About 80% reduction in NO_x has occurred. However, the CO emissions have increased by a factor of 3.5. Also note that the increase in CO is the greatest at lower ambient temperatures. Thus the degree of NO_x suppression by water injection may be limited at low ambient temperatures if the CO emissions exceed any alarm levels. The emissions of CO_2 will also increase as a result of water injection and this effect is shown in Fig. 14.18. This is because of the loss in thermal efficiency and increased power output, which require increased fuel consumption.

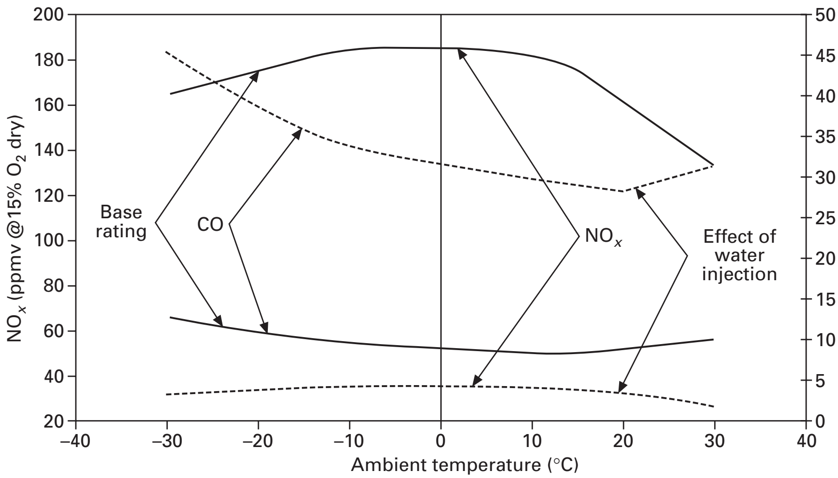

14.17 Effect of water injection on gas turbine emissions.

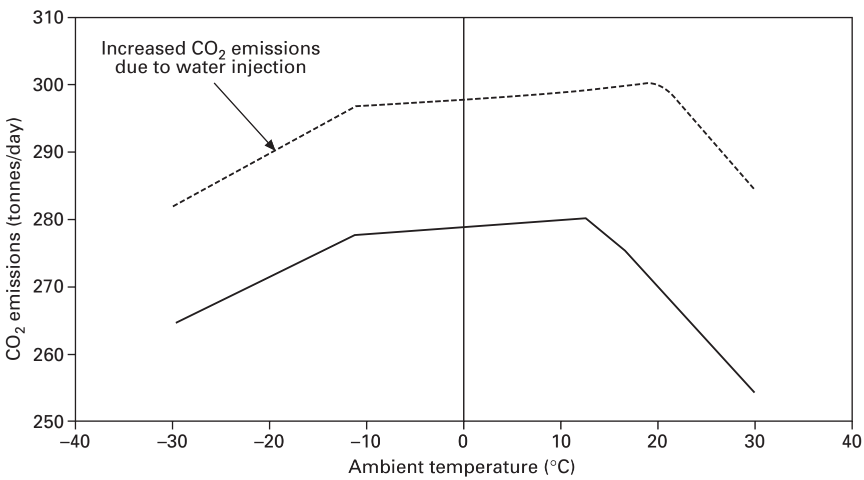

14.18 Impact of water injection on CO_2 production.

If water injection is used for NO_x suppression, then the decrease in turbine creep life usage at low ambient temperatures should be considered when determining mean time between turbine overhauls. This should result in a useful reduction in maintenance costs of the turbine.

14.5 Turbine inlet cooling

The adverse effect that high ambient temperature has on power output and thermal efficiency has been observed. Means to improve gas turbine power output at high ambient temperatures using methods such as peak rating and water injection have also been discussed. However, they invariably have some disadvantages such as increased creep life usage and lower thermal efficiencies with direct water injection. As stated in Section 14.4, the turbine inlet can be cooled, thereby reducing the compressor inlet temperature to augment the power output at high ambient temperatures. This is referred to as turbine inlet cooling or TIC. There are two main technologies available to reduce the compressor inlet temperature and they are known as evaporative (wetted media and inlet fogging) and chilling.[1]

Wetted media cooling and fogging operate on the same principles, where the evaporation of water absorbs latent heat of evaporation, thus cooling the turbine inlet air. With wetted media, the media is saturated with water, is exposed to the compressor inlet air, and the resultant evaporation reduces the compressor inlet temperature thus increasing the gas turbine power output. Alternatively, the water can be introduced into the inlet as a very fine spray. The evaporation of the fine water droplets similarly cools the compressor inlet air and is known as fogging. The design issues regarding fogging systems are discussed by Meher-Homji and Mee.[2]

Wetted media can operate on raw water; however, the mineral and salt content has to be controlled in order to prevent damage to the wetted media. Over time, the concentration of these minerals and salts will increase in the wetted media, resulting in blockage and damage to the wetted media. This reduces the effectiveness of the cooling media. With media cooling using raw water, a sufficient amount of water recirculation is necessary to prevent the concentration of minerals and salts in the evaporative media. Unlike wetted media evaporative cooling, which can operate with raw water, fogging systems require demineralised water. It should be noted that demineralised water is quite aggressive and will attack certain metals, and the inlet systems should use materials such as stainless steel or coatings that are resistant to attack from demineralised water.

The amount of water that can be evaporated depends on the relative humidity of the air. The lower the humidity, the more water can be evaporated and this results in a greater degree of turbine inlet temperature cooling. Another factor that limits the amount of cooling is the effectiveness of the cooling system. The more efficient the cooling, the closer the dry bulb temperature (which is effectively the ambient temperature) approaches the web bulb temperature. For evaporative cooling systems using wetted media, the effectiveness can vary from 0.85 to 0.95, which is a measure of the difference between the final dry bulb and wet bulb temperature. There is an additional inlet loss due to the presence of the wetted media. This is considered small and can vary between 5 mm water gauge and 10 mm water gauge, depending on the effectiveness of the cooling media.

For a fogging system, the effectiveness can approach unity. In this case the dry bulb temperature approaches the wet bulb temperature and the compressor inlet air will be saturated. In fact, evaporative cooling occurs at a constant wet bulb temperature. Therefore, if the ambient wet bulb temperature is close to the dry bulb temperature (i.e. high relative humidity), only a little turbine inlet cooling is possible. There is no noticeable increase in inlet loss with fogging systems.

Another evaporative cooling technique is wet compression or overspray. Here, additional water is added as a fine spray directly into the inlet of the compressor. This water evaporates in the compressor due to the high temperatures that occur during adiabatic compression, thus cooling the air within the compressor. This is similar to isothermal compression, but to a lesser degree, and it reduces the compression power demand, therefore increasing the power output of the gas turbine. Hence this method of power augmentation is also referred to as fog intercooling. Since water is added directly into the compressor as a spray, there is an increased risk of compressor damage due to erosion, which can result in severe engine damage. It is argued that such damage is more than justified, considering the increased production. However, such compressor blade damage could easily result in surge, which can destroy the engine. In the event of such damage and reduced availability, any benefit from a wet compressor could easily be lost. As with a fogging system, demineralised water should be used for wet compression and should be applied in conjunction with evaporative cooling such as fogging.

Unlike evaporative cooling which is adiabatic, with inlet chilling heat is removed from the inlet air using some form of refrigeration. Thus inlet chillers are not limited by the wet bulb temperature, and the compressor inlet air can be cooled down to any desired temperature provided the cooling capacity is available. However, when the inlet temperature decreases below 10 degrees Celsius, there is an increased risk of ice formation in the inlet, which can break away and enter the engine, thereby damaging the engine. Thus turbine inlet cooling, whether evaporative or chilling is limited to compressor inlet temperatures of about 10 degrees Celsius. Refrigeration systems for chillers can be either vapour compression or vapour absorption systems. The power demand from vapour compression systems is significant and is referred to as parasitic loss. In spite of such losses, there is still a useful gain in engine performance and so these have been employed to augment the power output at high ambient temperatures. Absorption refrigeration systems require a heat source, which can be provided from waste heat. Thus their parasitic losses are very small; however their performance is much poorer than vapour compression systems. If waste heat is readily available, the poor performance of vapour absorption refrigeration systems is of little consequence.[3] Vapour compression systems can be part of a thermal storage system (TES) where low cost (off-peak electricity) is used to drive the chillers to produce ice or chilled water. During peak demand, the TES is used to provide the necessary turbine inlet cooling using ice or chilled water. Other sources for chilling include LNG evaporation systems where the turbine inlet air is used as a heat source for the evaporation of LNG.

14.5.1 Wet bulb temperature, dry bulb temperature and cooling effectiveness

Wet bulb temperature is the lowest temperature to which air can be cooled by the evaporation of water into the air at a constant pressure. It is therefore measured by wrapping a wet wick around the bulb of a thermometer and the measured temperature corresponds to the wet bulb temperature. The dry bulb temperature is the ambient temperature. The difference between these two temperatures is a measure of the humidity of the air. The higher the difference in these temperatures, the lower is the humidity. Given the wet bulb temperature, dry bulb temperature and ambient pressure, the humidity of the air can be calculated as follows:.

$$p = pw - 0.00066P(Ta - Tw)(1 + 0.00115Tw) \qquad [14.1]$$

where p is the vapour pressure of water vapour, pw is the saturated vapour pressure of water vapour at the wet bulb temperature, P the ambient pressure, Ta is the ambient or dry bulb temperature, and Tw is the wet bulb temperature.

The saturated vapour pressure of water vapour at the wet bulb temperature, pw is given by:

$$pw = 6.112 \times \mathrm{e}^{\frac{17.67 \times Tw}{T + 243.5}} \qquad [14.2]$$

Also the saturated vapour pressure of water vapour at the dry bulb temperature is:

$$ps = 6.112 \times \mathrm{e}^{\frac{17.67 \times Ta}{T + 243.5}} \qquad [14.3]$$

Using Equations 14.1 and 14.3, the relative humidity, ϕ, is calculated by:

$$\phi = \frac{p}{ps} \times 100 \qquad [14.4]$$

The specific humidity, ω, can also be determined and is given by:

$$\omega = 0.622 \frac{p}{P - p} \tag{14.5}$$

The dew point can also be determined from:

$$Td = \frac{243.5 \times \ln\left(\frac{p}{6.112}\right)}{17.67 - \ln\left(\frac{p}{6.112}\right)} \tag{14.6}$$

The pressures in Equations 14.1 to 14.6 are in millibars (mb) and the temperatures are in degrees Celsius.

Figure 14.19 shows a schematic representation of an evaporative cooling system. The ambient (warm, dry) airflow enters the wetted media/fogging chamber, where water is added and evaporated. The resultant cooled, moist air leaving the wetted media/fogging chamber enters the engine inlet. As stated above, the cooling effectiveness is a measure of how close the temperature of the moist, cooled, T_{cool}, air approaches the wet bulb temperature, T_w. The cooling effectiveness, ε, is defined as:

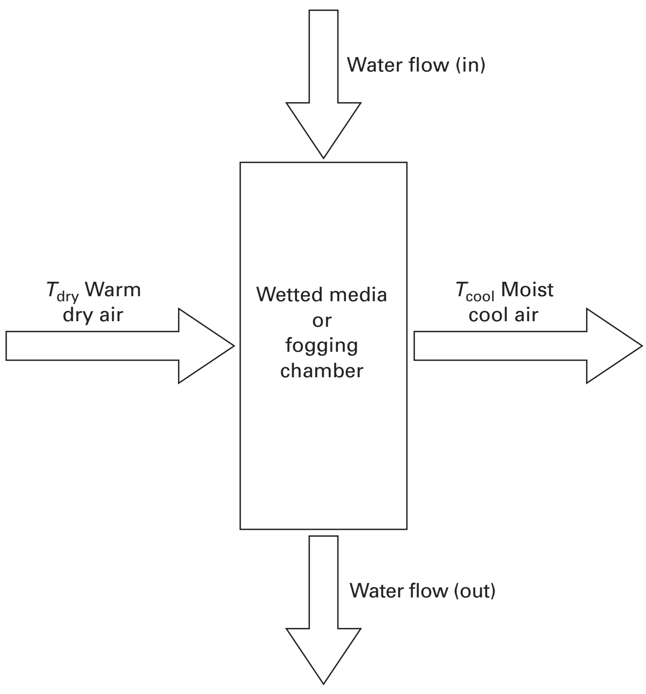

14.19 Schematic representation of a (wetted media) evaporative cooling system.

$$\varepsilon = \frac{Ta - T_{cool}}{Ta - Tw} \qquad [14.7]$$

Wetted media and chillers may be positioned either upstream or downstream of the gas turbine inlet filter/plenum. If they are positioned upstream of the inlet system, the filters have to be made of synthetic material. If paper filters were to be employed, the cool high humidity air would cause these filters to swell and become damaged.

14.5.2 Power augmentation using turbine inlet cooling

The amount of turbine inlet cooling using the three types of technologies, for a range of ambient temperatures, is shown in Fig. 14.20. The most significant cooling is achieved using chillers followed by fogging and wetted media cooling. This Figure has been produced assuming a constant relative humidity of 60%, and cooling effectiveness for fogging and wetted media are assumed to be 1.0 and 0.85, respectively. The amount of cooling is observed to increase with ambient temperature. With wetted media and fogging, the potential to cool the compressor inlet decreases with ambient temperature, due to the divergence of the lines of constant relative humidity on the psychrometric chart, as shown in Fig. 14.21. With chillers, this decrease is more acute, as seen in Fig. 14.20. Turbine inlet cooling using chillers is not restricted by the humidity of the air and therefore more cooling is possible at high ambient temperatures compared with evaporative cooling, provided the cooling capacity

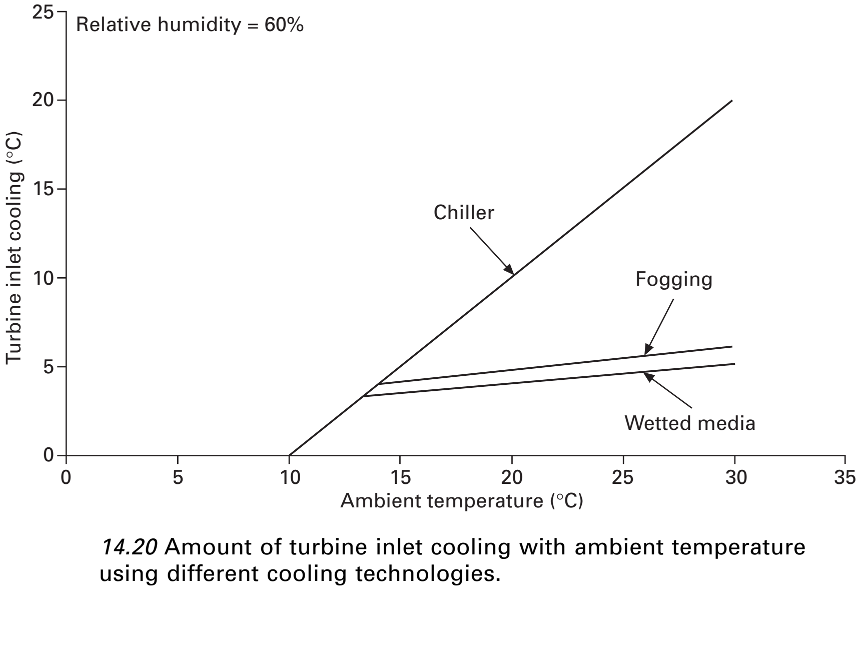

14.20 Amount of turbine inlet cooling with ambient temperature using different cooling technologies.

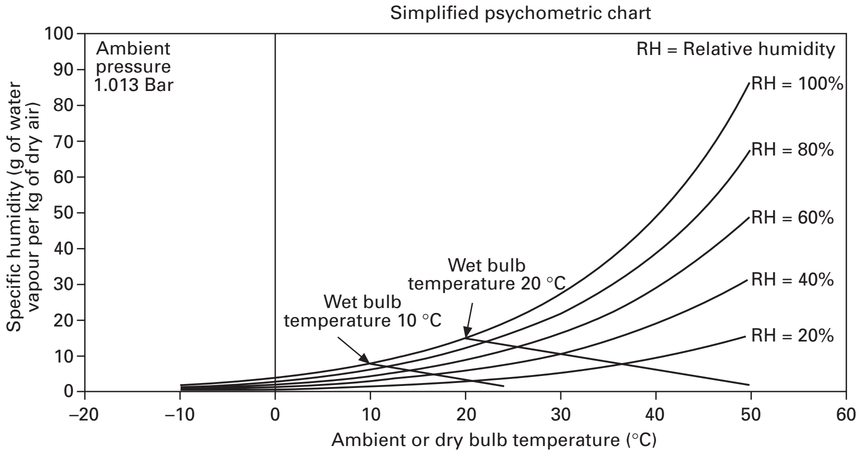

14.21 Variation of humidity with ambient temperature.

is available. The maximum cooling capacity of 4.5 MW has been assumed, which is sufficient to maintain the compressor inlet temperature at 10 degrees Celsius for the ambient temperature range considered in Fig. 14.20. It has been stated that the relative humidity does not limit the amount of turbine inlet cooling using chillers, but high relative humidity will result in a significant amount of water condensation occurring. Since the latent heat of evaporation is given up by the condensing water, much of the cooling load is used up in producing the condensation rather than in cooling the inlet air. Thus the parasitic load increases at high humidity, requiring larger chiller capacity to achieve a given level of turbine inlet cooling. The reader should reproduce this figure for various levels of relative humidity using the gas turbine simulator to illustrate the impact of humidity on turbine inlet cooling.

The resultant decrease in compressor inlet temperature increases the power output of the gas turbine and thus the generator power output. This is shown in Fig. 14.22 for each of the above-mentioned cooling technologies. It can be seen that chillers produce the largest gain in power output, followed by fogging and wetted media. The figure also shows the effect of the cooling technology employed by chillers. With vapour compression chillers, the impact of power demand by the chiller on generator output is significant and appears as a parasitic loss. Nevertheless, there is still a significant increase in power output at the generator terminals. With vapour absorption chillers, this parasitic loss is small and is ignored by the simulator as the simulator represents an open cycle gas turbine, and the heating required by the absorption refrigeration system can be provided from the gas turbine exhaust heat.

The decrease in compressor inlet temperature due to turbine inlet cooling also increases the thermal efficiency of the gas turbine, which the user should

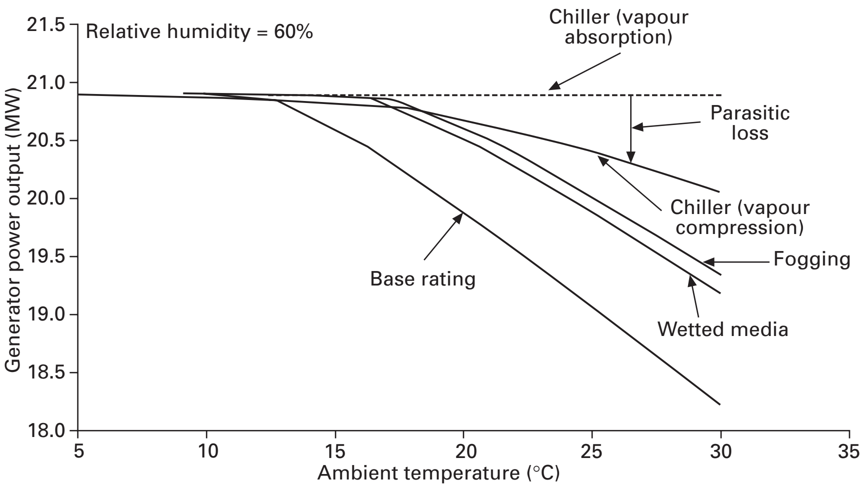

14.22 Generator power output with ambient temperatures using various turbine inlet cooling technologies.

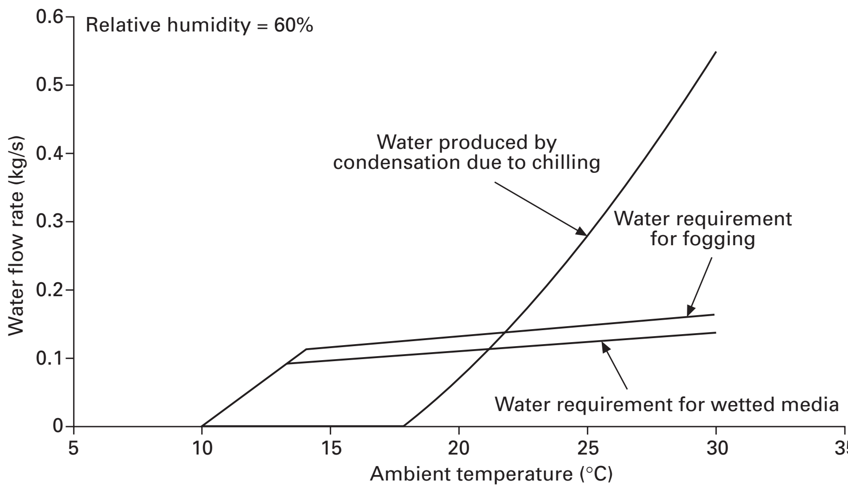

14.23 Water requirements for turbine inlet cooling systems.

produce as an exercise. The increase in compressor airflow and therefore increased exhaust flow rate due to turbine inlet cooling also increases the heat rejection from the gas turbine and is beneficial to combined cycle power plants.

Turbine inlet cooling using wetted media and fogging requires water for evaporation and water requirements are shown in Fig. 14.23. The simulator is a useful calculator to determine the water requirements for a given level of turbine inlet cooling. The information can be scaled to suit any gas turbine engine. Details are given in the simulation user guide. With chillers, condensation can occur when the relative humidity reaches 100% due to cooling and condensation produced is also shown in Fig. 14.23. At high ambient temperatures, the condensation can be about three times that required by evaporative cooling systems. For example, at an ambient temperature of 30 degrees Celsius, the condensation flow rates can be as much as 50 tonnes per day. Thus, means to remove this water must be provided when chillers are employed. The cooling loads and power demand for chillers using vapour compression systems are shown in Fig. 14.24. Note that the cooling loads and power demand increase exponentially when condensation occurs. This is primarily due to the absorption of the latent heat of evaporation for water by the chillers. For example, when turbine inlet cooling of about 8 degrees Celsius is required, the cooling loads and power demand are about 0.5 MW and 0.1 MW, respectively (assuming a coefficient of performance of refrigeration of 5.0). If the turbine inlet cooling required is doubled (16 degrees Celsius), the cooling load and power demand from the chiller increase to nearly 2.75 MW and 0.55 MW, respectively. This is due to the formation of condensation at the higher levels of turbine inlet cooling.

The application of turbine inlet cooling using evaporative cooling results in an increase in relative and specific humidity, as illustrated in Fig. 14.25. It should be noted that the wet bulb temperature remains constant. The ambient temperature and relative humidity are held constant at 30 degrees Celsius and 60%, respectively. The increase in specific humidity suppresses the increase in NO_x emissions, which are due to the increase in combustion temperature and pressure as the compressor inlet temperature decreases.

With chillers, the relative humidity increases and the wet bulb temperature decreases, while the specific humidity remains constant, provided no

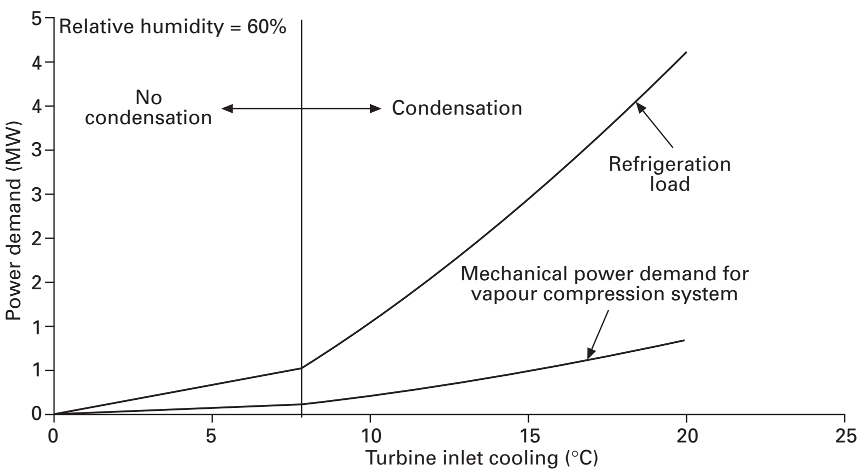

14.24 Cooling loads and power demand for vapour compression refrigeration system due to turbine inlet cooling.

condensation occurs. When relative humidity reaches 100%, any further cooling produces condensation and this decreases the specific humidity, as shown in Fig. 14.25. Thus, the decrease in specific humidity and the increase in combustion temperature and pressure result in an increase in NO_x emissions. These effects can be simulated and the reader should use the simulator to illustrate these issues. As with wetted media cooling and fogging, it should be noted that the simulator is a useful calculator to determine the cooling load requirements for a given level of turbine inlet cooling. The information can be scaled to suit any gas turbine with either single- and multi-shaft engines.

The choice of cooling technology is not defined very clearly and it depends on the site ambient conditions. Lower humidity tends to favour evaporative cooling technologies such as wetted media and fogging systems, as the amount of turbine inlet air cooling will be significant. Conversely, a high humidity environment will tend to favour chillers; however, parasitic losses will be high. Also, low humidity and very high ambient temperature (above 35 degrees Celsius), as found in desert conditions, will tend to favour chillers. Under these ambient conditions, more inlet air cooling is possible with chillers compared with evaporative cooling and the parasitic loss will be low. Turbine inlet cooling is also applicable in temperate climates, where summertime temperatures and humidity will justify turbine inlet cooling.[4] Ideally, the increase in engine performance due to turbine inlet cooling needs to be analysed on a day-by-day basis over a long enough period, typically a year, for each type of cooling technology. Another important factor is the capital cost of the turbine inlet cooling system. The capital cost of chillers can be

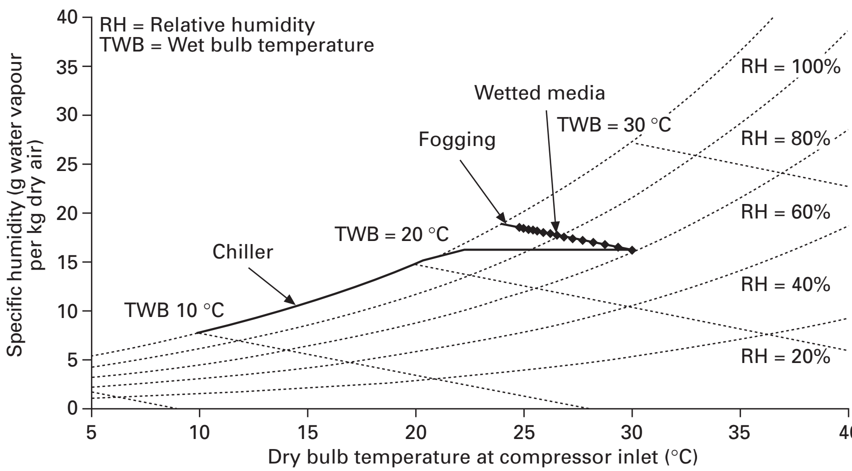

14.25 Running line on psychrometric chart for various turbine inlet cooling technologies.

orders of magnitude greater (as much as ten or more) than that of evaporative cooling systems. Further information on the selection of turbine inlet cooling systems can be found in Ameri *et al.*[5]

14.6 Power turbine performance

The performance of the power turbine is of paramount importance, as this component is responsible for converting the energy at the exit from the gas generator into shaft power. The power developed from the power turbine is dependent on the pressure ratio across the power turbine, which is determined by the gas generator performance and the power turbine efficiency. For a given power turbine pressure ratio, the efficiency is dependent on the non-dimensional speed of the turbine, as shown in Fig. 7.3. The power turbine speed (mechanical speed) is determined by the driven load, and therefore the driven load has a direct impact on the power turbine non-dimensional speed. In our simulator, it has been assumed that the power turbine drives an electrical generator, which requires the power turbine speed to remain constant with the change in load to maintain the required frequency. However, in other cases such as mechanical drive applications (process compressors and pumps), the speed of the process compressor may be low during dense phase operation due to high suction pressures in the process compressor. The process compressor speed and therefore the power turbine speed may be as low as 70% of the rated (100%) speed. Hence it is important to determine the power output of the gas turbine at different power turbine speeds.

Figure 14.26 shows the variation of the power developed by the power turbine with power turbine speed at ISO conditions and zero inlet and exhaust losses. The power output has been drawn for different gas generator speeds and of particular interest is the 100% gas generator (GG) speed, as this situation normally corresponds to the maximum gas power generated by the gas generator. At a power turbine of 70% speed, which corresponds to a power turbine 2100 RPM, the power output decreases by about 11%, hence illustrating the importance of the power turbine performance. At high power turbine speeds, there is little variation of power turbine efficiency with the power turbine non-dimensional speed, thus resulting in a relatively flat power curve when operating at these speeds. It will therefore be necessary for our loads to operate at relatively high speeds or a very flat power turbine curve will be required if a significant loss in power is not to be incurred at low power turbine speeds (similar in shape to the curve describing the 85% GG speed in Fig. 14.26). The figure also shows the effect of the gas generator speed on power output. There is a loss in power output at lower gas generator speeds due to the reduction in air mass flow and turbine entry temperature and generally in pressure ratio (i.e. reduced gas power).

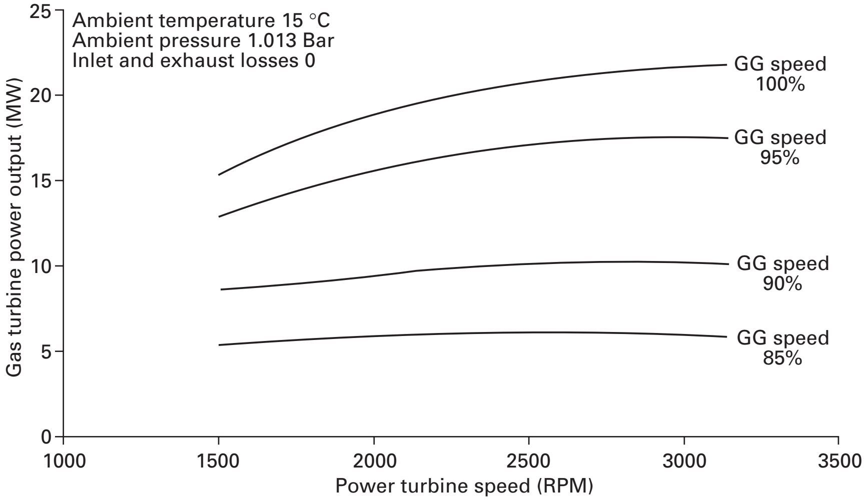

14.26 Variation of power output with turbine speeds at different gas generator speeds.

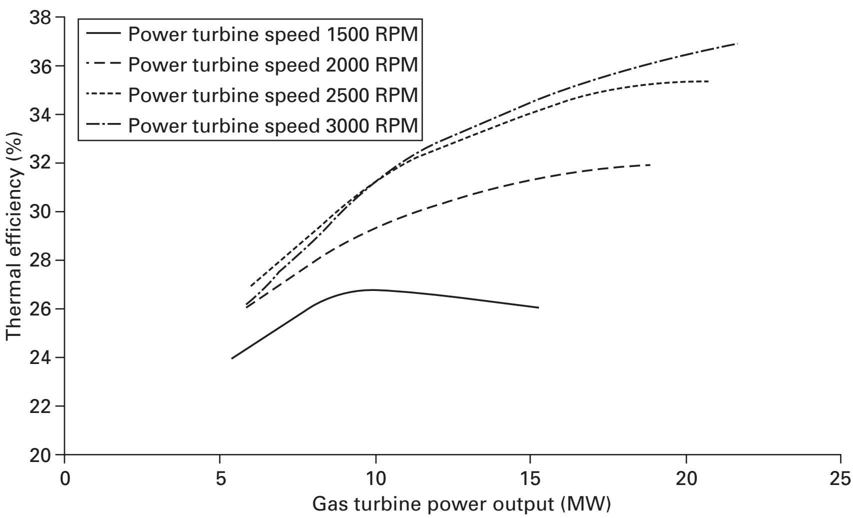

14.27 Variation of gas turbine efficiency with power output for different power turbine speeds.

The variation of the gas turbine thermal efficiency with power output for different power turbine speeds is shown in Fig. 14.27. The decrease in thermal efficiency with power for a given power turbine speed is due to the reduction in the gas generator speed, resulting in lower compressor pressure ratio and turbine entry temperature. However, for a given power output, the thermal efficiency improves with the increase in power turbine speed and this is due to the improvement in the power turbine efficiency. At high power turbine speeds (around 3000 RPM), there is only a small variation in the thermal efficiency with the power turbine speed and this is due to minimal variation in power turbine efficiency at these speeds. Thus the loss in performance in the power turbine at low speeds is responsible for the low thermal efficiency at these power turbine speeds.

Furthermore, gas turbines are most efficient at high load conditions and, if a significant turndown in power is required, it is best to employ two smaller engines, where each engine operates near its design condition at any given load condition. This is the principle of Combination Of Gas turbine Or Gas turbine (COGOG)/Combination Of Gas turbine And Gas turbine (COGAG) where one engine is used at low powers and either or both engines operate at higher power requirements.

The principle of COGOG and COGAG is often used in naval applications where the cruise speed of the ship is about half the boost speed. Due to the propeller law, which states that the power required is proportional to the cube of the speed, the cruise power requirement is only about 12.5% of the boost power requirements. At such low powers, the thermal efficiency of the gas turbine will be very poor. The thermal efficiency at cruise conditions is improved by employing a smaller gas turbine to operate at cruise conditions and switching to a larger gas turbine for boost conditions. The power output of the cruise gas turbine is about 30% of the total propulsive power requirement. It is worth noting that naval ships spend a significant time (about 95%) at cruise conditions.

For naval applications, the use of a variable pitch propeller would enable the power turbine speed to be varied independently of the power requirements. By employing a variable pitch propeller, it would be possible to operate at the maximum thermal efficiency for a given gas generator speed resulting in a useful improvement in thermal efficiency, particularly at low power operation, typical of cruise conditions. This is illustrated in Fig. 14.28, where the gas turbine thermal efficiency is displayed as a function of power turbine speed for different gas generator speeds. The figure shows the load lines for a fixed pitch propeller and also for an electrical generator. The optimum line indicates what could be achieved by using a variable pitch propeller for naval propulsion. At low power, a 4% improvement in thermal efficiency may be possible using a variable pitch propeller and this corresponds to a significant reduction in fuel cost.

14.7 The effect of change in fuel composition on gas turbine performance and emissions

All of the simulations discussed above were carried out using natural gas, whose lower heating value (LHV) is about 48 MJ/kg. Gas turbines can

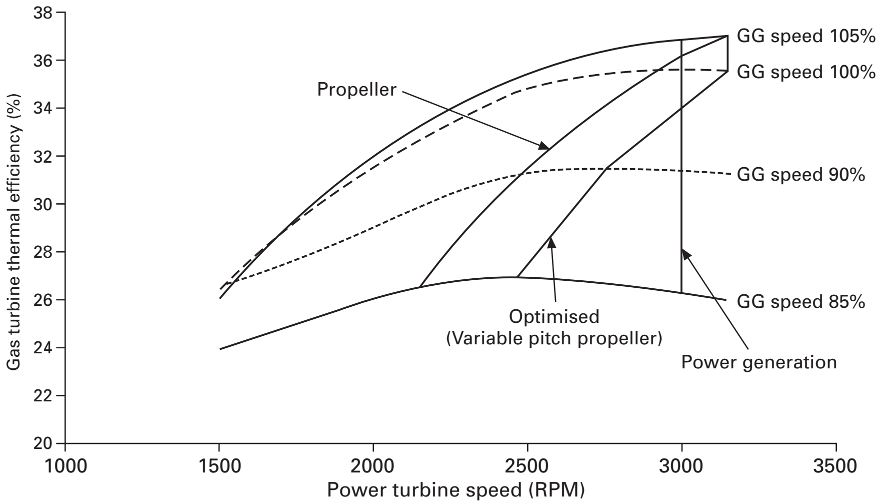

14.28 Load lines for a propeller and electrical generator, superimposed on the power turbine performance curves.

Table 14.1 Exhaust gas composition when operating with natural gas

Exhaust gas composition as mole %				
CO_2	H_2O	N_2	O_2	Ar
3.120	7.032	74.994	13.961	0.893

Table 14.2 Exhaust gas composition when operating with diesel fuel

Exhaust gas composition as mole %				
CO_2	H_2O	N_2	O_2	Ar
4.128	5.091	75.738	14.141	0.902

operate on a range of fuels, which include liquid fuels such as diesel, kerosene, naphtha, crude oil and residual fuels. This simulator can operate on either natural gas, methane or diesel fuel. The impact of the change in fuel from natural gas to diesel on gas turbine performance will now be considered.

Table 14.1 shows the tabulated output of the exhaust gas composition as mole percentages when the gas turbine is operating with natural gas. Table 14.2 shows the tabulated output for the case when the gas turbine is operating with diesel fuel. Note that the exhaust gas composition has changed in that the amount of CO_2 has increased and the amount of H_2O has decreased when diesel fuel is employed. The decrease in H_2O results in a decrease in the specific heat of the products of combustion, c_p. However, the impact of the isentropic index, $\gamma = c_p/c_v$, is small when changing from natural gas to diesel. The isentropic index, γ, relates to c_p by the expression $1/\gamma = 1 - R/c_p$, where $R = R_o$/MW is the gas constant of the products of combustion, and R_o and MW are the universal gas constant and molecular weight, respectively. An increase in R when operating with natural gas is due to its lower molecular weight compared with diesel fuel, but this is compensated by the increase in c_p. Hence only a small change in γ occurs when switching from natural gas to diesel. However, the increase in c_p results in an increase in the power developed by the turbine and hence an improvement in gas turbine performance occurs when natural gas is used. The improvement in performance depends on the fuel gas composition. An increase in power output and thermal efficiency of about 1 to 2 per cent is possible when operating with natural gas compared with diesel.

In this simulator, about 1 per cent increase in engine performance was obtained when the switch was made from diesel oil to natural gas and the reader is left to demonstrate this effect of the change in fuel on engine performance.

The effect of switching from natural gas to diesel fuel has a significant impact on engine emissions, as shown in Fig. 14.29. It is observed that NO_x has increased from 175 ppmv to nearly 300 ppmv, representing about 70% increase in NO_x. A significant increase in CO is also observed when changing

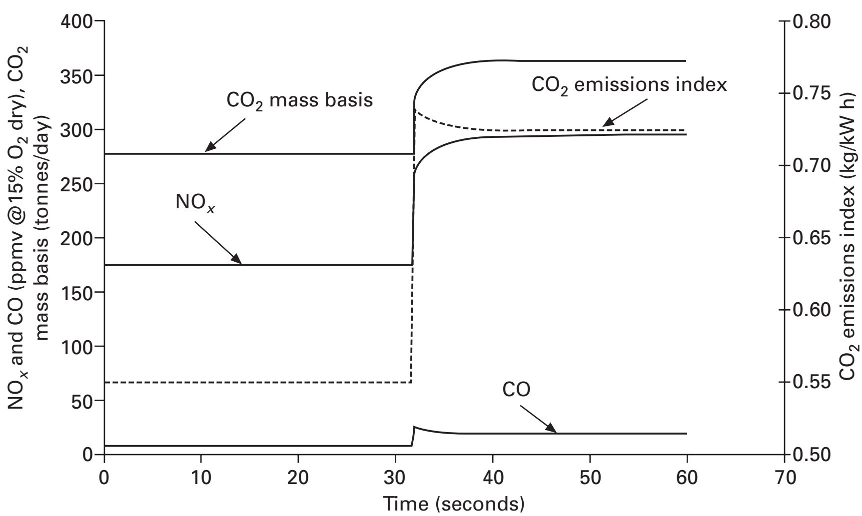

14.29 Trends in gas turbine emissions when switching from natural gas fuel to diesel fuel.

from natural gas to diesel fuel, when the CO increases from 8 ppmv to 18 ppmv, thus more than doubling the emission of CO.

When operating with diesel fuel, the atomisation process results in localised air–fuel mixtures nearer to stoichiometric compared with the case of natural gas fuel, although the overall air–fuel ratio would be much higher. Thus the higher flame temperatures that prevail in the vicinity of the burning liquid fuel droplets result in higher NO_x emissions when burning liquid fuels such as diesel. Furthermore, the adiabatic flame temperature achieved when using diesel fuel is greater than that with natural gas due to the reduced presence of H_2O and this also contributes to higher NO_x when burning diesel fuel. In Section 6.5, the importance of good atomisation and mixing in arresting the formation of CO was discussed. With gaseous fuels, good mixing is easily achieved compared with liquid fuels and therefore the formation of CO is reduced when burning natural gas.

The increase in CO_2 is largely due to the higher carbon–hydrogen ratio and low LHV of diesel fuel compared with natural gas fuel. Figure 14.29 shows the trends in gas turbine emissions when the change is made from natural gas fuel to diesel fuel, where an increase in gas turbine emissions occurs. Figure 14.30 shows the trends in the fuel flow and valve position when the switch is made to diesel fuel operation. The figure also shows the trends in the air–fuel ratio and compressor inlet airflow.

The increase in fuel flow and fuel valve position is primarily due to the lower LHV of diesel fuel, thus resulting in a decrease in the air–fuel ratio.

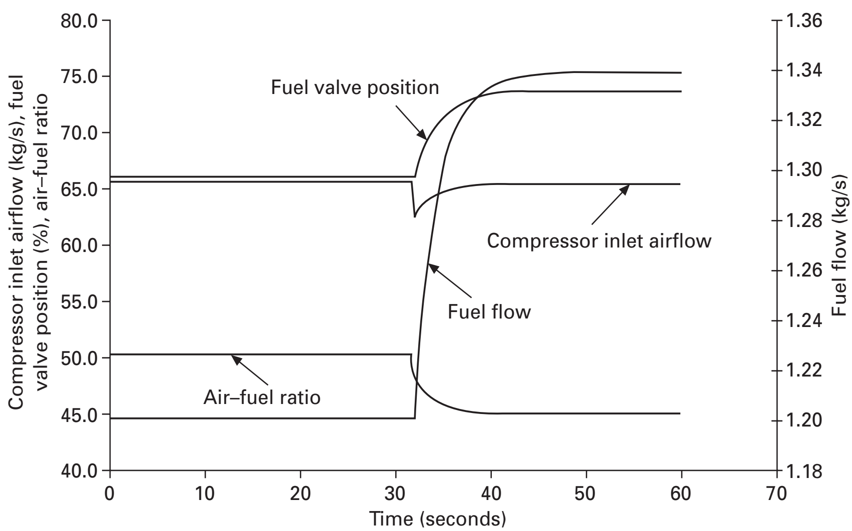

14.30 Trends in the change of fuel flow and air–fuel ratio due to diesel fuel operation.

14.8 References

1. Gas turbine inlet air cooling and the effect on a Westinghouse 501D5 CT, Kohlenberger, C., *ASME Paper 95-GT-284*, 1995.
2. Inlet fogging of gas turbine engines Part A: Theory, psychometrics and fog generation, Meher-Homji C.B. and Mee III T.I.L., *ASME Paper 2000-GT-307*, 2000.
3. Analysis of a combined gas turbine and absorption–refrigeration cycle, Nagib, M.M., *Journal of Engineering for Power*, January 1971.
4. Inlet fogging of gas turbine engines: climate analysis of gas turbine evaporative cooling potentials of international locations, Chaker, M. and Meher-Homji, C.B., *ASME Paper GT-2002-30559*, 2002.
5. Gas turbine power augmentation using fog inlet air-cooling system, Ameri, A., Nabati, H. and Keshtgar, A. *Proceedings of ESDA04*, 7th Biennial Conference on Engineering Systems Design and Analysis, July 19–22, 2004, Manchester, United Kingdom, ESDA2004-58101, 2004.

15
Simulation of engine control system performance

In Chapter 10, the principles of gas turbine control were discussed where it was stated that the change in engine power is accomplished by altering the energy input to the gas turbine. This is achieved by varying the fuel flow into the combustion system until the desired power output is reached. It has also been stated that this change in power output from the gas turbine should be accomplished without any detrimental effect to the gas turbine. The principle of a simple PID control system was introduced, together with the concept of low signal select. Such a simple control system has been implemented in this gas turbine simulator and much of what was discussed in Chapter 10 will be simulated to illustrate the principles of gas turbine control systems. The two-shaft gas turbine simulator will now be used to illustrate some of the features of control systems applied to gas turbine control. A PID control system contains the P – proportional, I – integral and D – derivative terms and is often referred to as a three-term control system.

15.1 Proportional action

Pure proportional action results in the proportional band acting on the error that is determined by the difference of the power output from the electrical generator and the set point, which represents the power required by the generator. Pure proportional action leaves an offset as illustrated by Fig. 15.1, which shows the trends in power due to a step change in the required power output of the generator from 1 MW to 19 MW. Pure proportional action is achieved in the simulator by switching off the integral output in the engine control setting option.

The trends in power as shown in Fig. 15.1 have been generated for three values of proportional band and correspond to 100%, 75% and 50%. As the proportional band decreases, which corresponds to an increase in proportional gain, there is an increase in output from the process, which in this case is the electrical generator power output. However, the set point of 19 MW is never

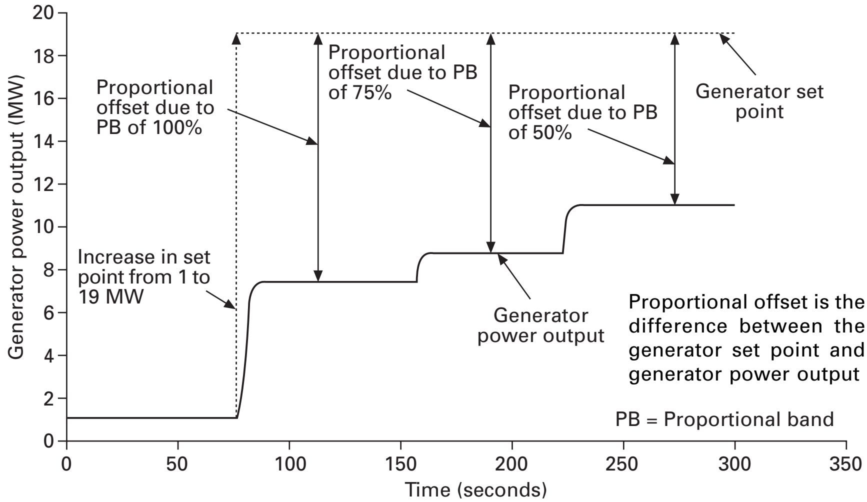

15.1 Trends in generator power output due to proportional action only. (PB = proportional band).

reached by the generator output and pure proportional action normally leaves a difference between the generator output and the set point. This difference is referred to as the proportional offset, which reduces as the proportional band decreases. The manual reset discussed in Chapter 10 may be applied to remove the proportional offset (not available in the simulator).

15.2 Proportional and integral action

Integral action is essentially a summation or integration process on the residual error left by the proportional action (proportional offset). This action (automatic reset as discussed in Chapter 10) results in reducing the error to zero and therefore achieving the required generator output as specified by the set point. Hence both proportional and integral actions are required in control systems if the specified set point and therefore the desired power output is to be achieved. The value of the integral gain is very important, as a small gain will result in prohibitively long time periods before the set point is reached. Too large an integral gain will result in excessive oscillatory response, again resulting in too long a time period before the required set point is reached. Such oscillatory response will also have a detrimental effect on turbine creep life due to overshoots in speeds and temperatures above the steady-state values and can cause unexpected trips in order to protect the engine.

The trend in power due to the integral action for a set point change from 1 MW to 19 MW is shown in Fig. 15.2. Initially, only proportional action is applied, resulting in the proportional offset as shown in Fig. 15.2. The proportional band is set at 100%. After about 100 seconds, the integral action is switched on and the power output from the gas turbine is observed approaching the set point of 19 MW. The integral gain is set to 0.1 and a long time period results (about 100 seconds) before the required set point is reached and this delay is due to the small value of the integral gain.

Increasing the integral gain to 2 results in a very rapid increase in power output, as observed in Fig. 15.3. The oscillatory response is clearly seen and the control system reaches the set point of 19 MW in about 15 seconds, thus representing a significant improvement in transient response of the engine compared with the previous case, which represented a small integral gain of 0.1. (It is necessary to inactivate the engine trips during this type of simulation exercise – see the user guide on the CD for instructions to inactive engine trips.)

Reducing the integral gain to about 0.4 still maintains a rapid response in power output but virtually eliminates the overshoots, as shown in Fig. 15.4. Such optimisation is necessary in tuning control systems and the optimisation process is a specialist area, which is outside the scope of this book but is discussed in Shaw[1] and in Sivanandam.[2]

It has been stated above that an oscillatory response due to poor control system performance has a detrimental effect on turbine creep life. This is illustrated in Fig. 15.5, which shows the trend in turbine creep life usage when the integral gain is set to 2. The creep life usage is observed for both gas generator and power turbines where the creep lives undershoot the steady-

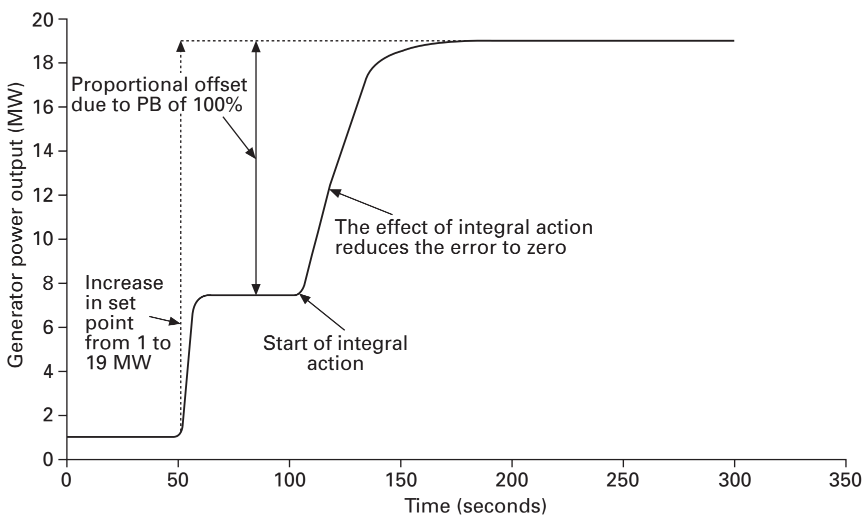

15.2 Trends in generator power output due to proportional and integral action. (PB = proportional band).

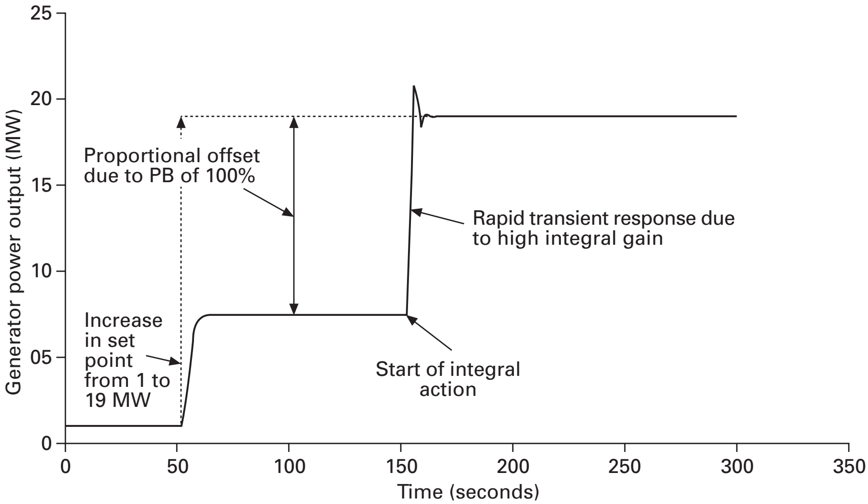

15.3 Trends in generator power due to high integral gain. (PB = proportional band).

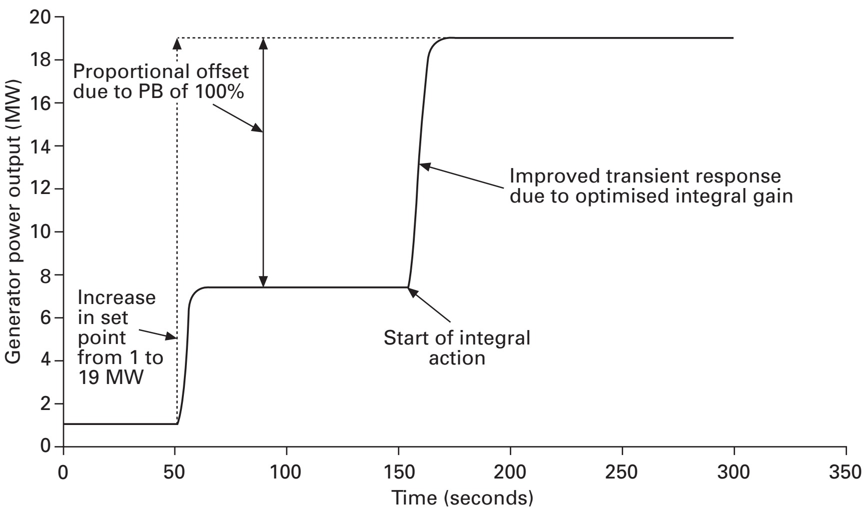

15.4 Trends in generator power output due to optimised control system.

state values by significant amounts. The gas generator turbine creep life undershoots the steady-state creep life by about 30000 hours and the power turbine creep life undershoots the steady-state value by about 150000 hours. The decrease in creep life occurs due to the fuel flow overcompensating because of the poor performance of the control system. This results in

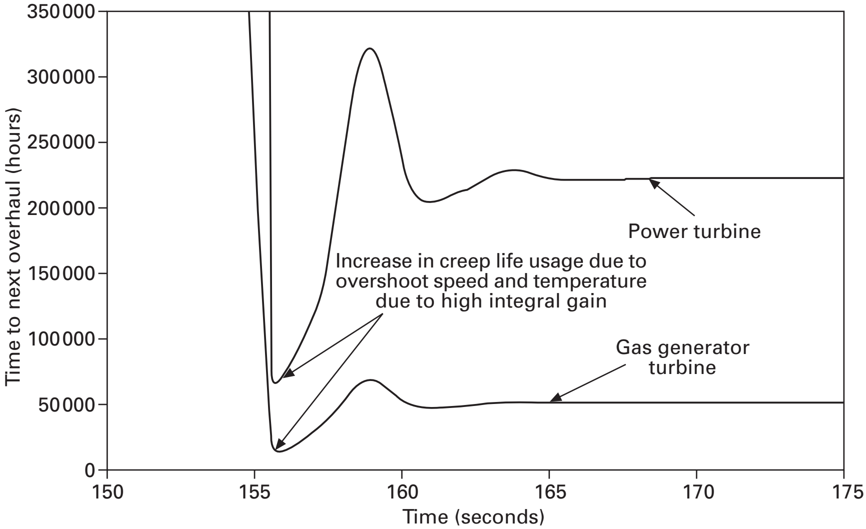

15.5 Trends in turbine creep life due to integral gain.

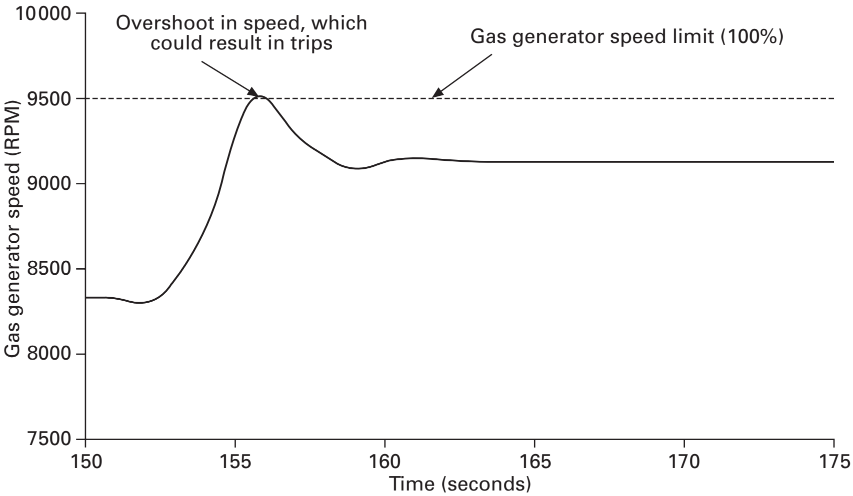

15.6 Trends in speed due to high integral gain.

overshoots in the gas generator speed and turbine entry temperature, as shown in Figs 15.6 and 15.7, respectively. The increase in speed and turbine entry temperature during the overshoot is always greater than the decreases in speed and turbine entry temperature during the corresponding undershoot as the control system endeavours to attain steady state conditions. Furthermore, the non-linear nature of the Larson–Miller curve (see Fig. 5.11), which describes the average creep life of the turbine blades, results in a greater decrease in

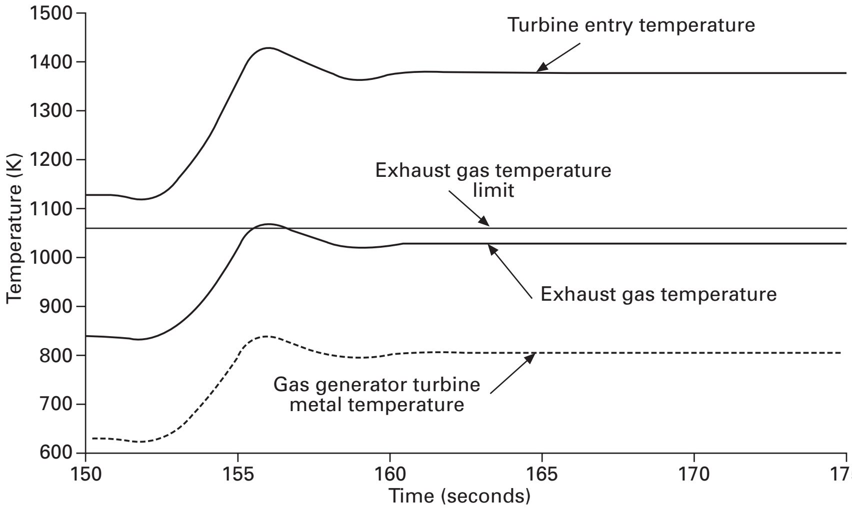

15.7 Trends in temperature due to high integral gain.

the Larson–Miller parameter during the overshoot than the increase in this parameter during the undershoot in speed and temperature. Thus both these effects result in a decrease in creep life.

Although the significant loss in creep life occurs for only a very short period of time, the decrease in creep life of the turbines will accumulate if such oscillatory response is allowed to continue, leading to a reduced engine life and increased engine overhauls and therefore increasing maintenance costs.

The trend for speeds and temperatures for the optimised case, where the integral gain was set to 0.4, is shown in Figs 15.8 and 15.9, respectively. Virtually no oscillatory response is observed. Consequently, a satisfactory trend in turbine creep life is obtained, as shown in Fig. 15.10.

15.3 Signal selection

In Section 10.2 the use of signal selection to prevent any operating limits such as exhaust gas temperature and gas generator speeds being exceeded was described. This action protects the engine from damage and achieves suitable turbine creep life. In fact, signal selection was used when the effect of ambient temperature on engine performance was considered in Section 11.3, where the power output of the gas turbine becoming limited by either the exhaust gas temperature, gas generator speed or compressor non-dimensional speed limits was demonstrated. Hence these figures are reproduced here for a discussion of signal selection.

Referring to Fig. 15.11, at high ambient temperatures, the exhaust gas

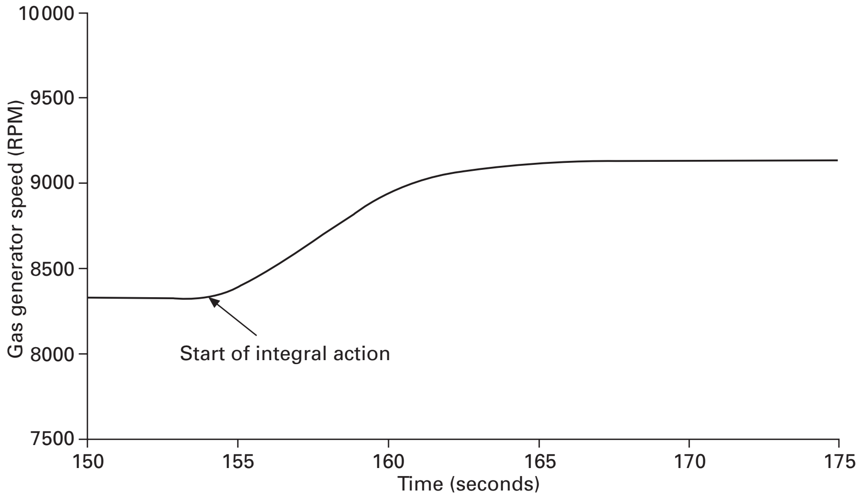

15.8 Trends in speed when the control system is optimised.

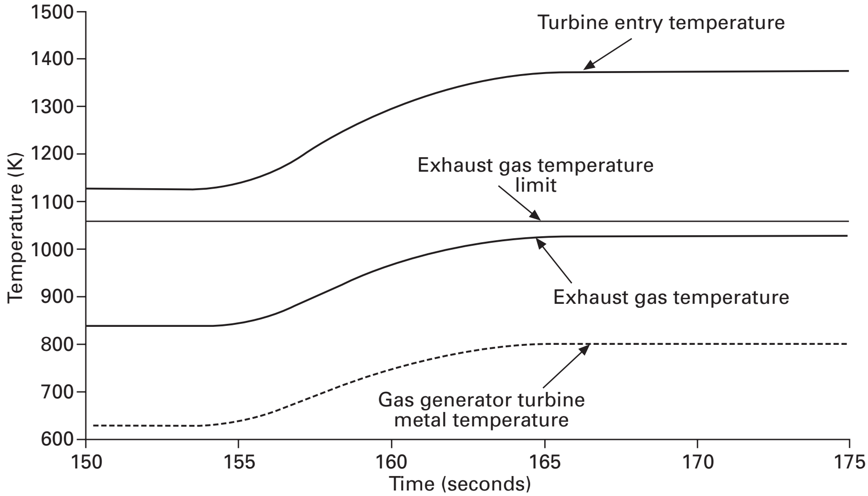

15.9 Trends in temperature when the control system is optimised.

temperature limits the power output, as the gas generator speed and compressor non-dimensional speed are below their limiting condition. This is observed in Fig. 15.12, which shows the trends in speeds during the ambient temperature transient (+ 30 to –30 degrees over one hour).

As the ambient temperature decreases, the gas generator speed and the compressor non-dimensional speed increase until the ambient temperature reduces to about 12 degrees Celsius, at which point the gas generator speed limit is reached. At ambient temperatures below 12 degrees Celsius, the

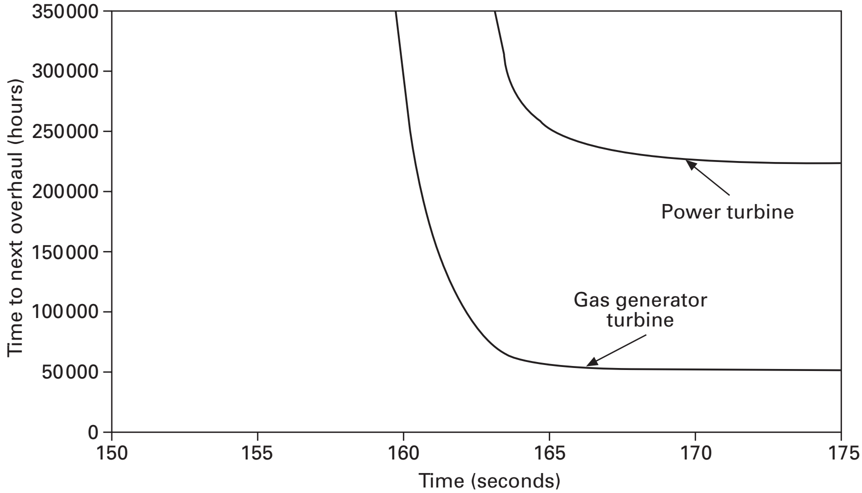

15.10 Trends in turbine creep life when the control system is optimised.

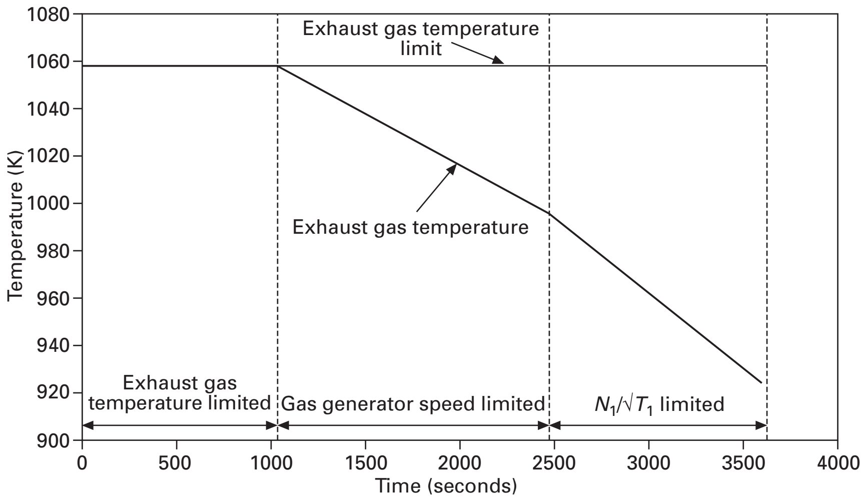

15.11 Trends in temperature during ambient temperature transient.

signal selection switches from exhaust gas temperature control to gas generator speed control, when the gas generator speed will remain constant at its 100% speed, or a continuous rating value until the ambient temperature reduces to about –11 degrees Celsius (Fig. 15.12).

Note that the exhaust gas temperature decreases (Fig. 15.11) during constant gas generator speed operation and the compressor non-dimensional speed continues to increase. At ambient temperatures below –11 degrees Celsius,

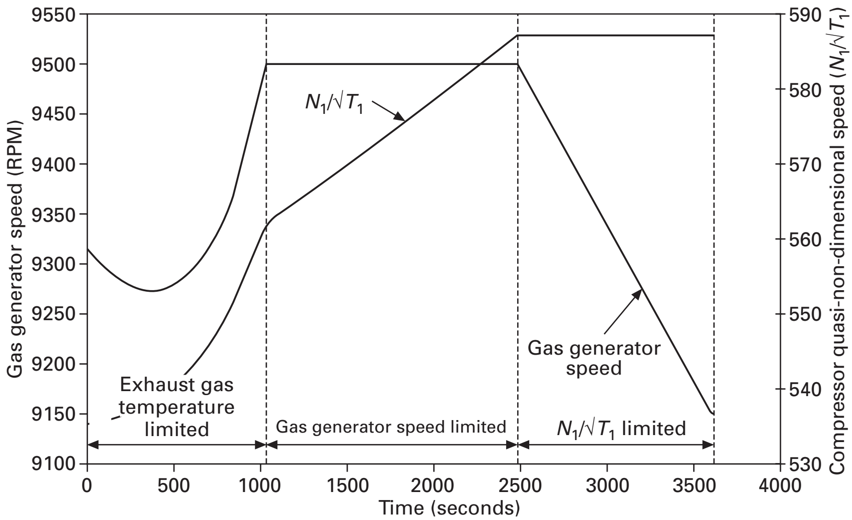

15.12 Trends in speed during ambient temperature transient.

the compressor non-dimensional speed limit is reached and the signal selection now switches to compressor non-dimensional speed control. At an ambient temperature below –11 degrees Celsius, both the exhaust gas temperature and gas generator speed are observed to continue to decrease. Thus, this is how signal selection protects the engine from over-speeding or overheating.

15.4 Acceleration and deceleration lines

Signal selection discussed above considered only limits on the exhaust gas temperature and speed. Although these would be the limiting values during steady-state and slow transient conditions, a means is needed of preventing conditions that would occur during fast transients, such as rapid acceleration and deceleration, resulting in flameout or compressor surge. It is the variation of the air–fuel ratio that is important, as flameout occurs when the air–fuel ratio is outside the combustion stability limits. The computation of the air–fuel ratio is not practical, as the combustion airflow value is needed and is often unavailable.

Figure 15.13 shows the variation of fuel flow with gas generator speed for a series of ambient temperatures, T_1 varying from –30 degrees Celsius to 30 degrees Celsius. The figure also shows the acceleration and deceleration limits. Figure 15.14 shows the variation of air–fuel ratio with ambient temperature, T_1, and gas generator speed. Note that the variation of the air–fuel ratio with ambient temperature is small for a limited range of gas generator speed (from about 8000 RPM to 10000 RPM). Referring to Fig. 15.13, at

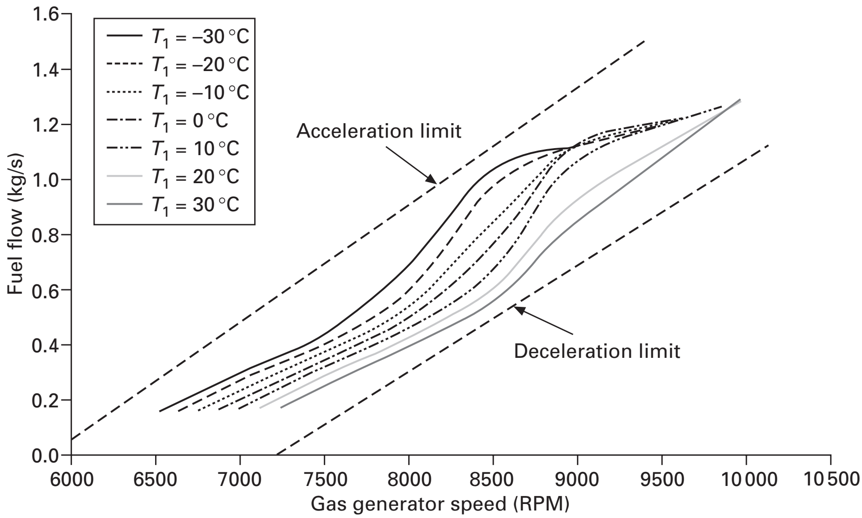

15.13 Variation of fuel flow with gas generator speed for a series of ambient temperatures.

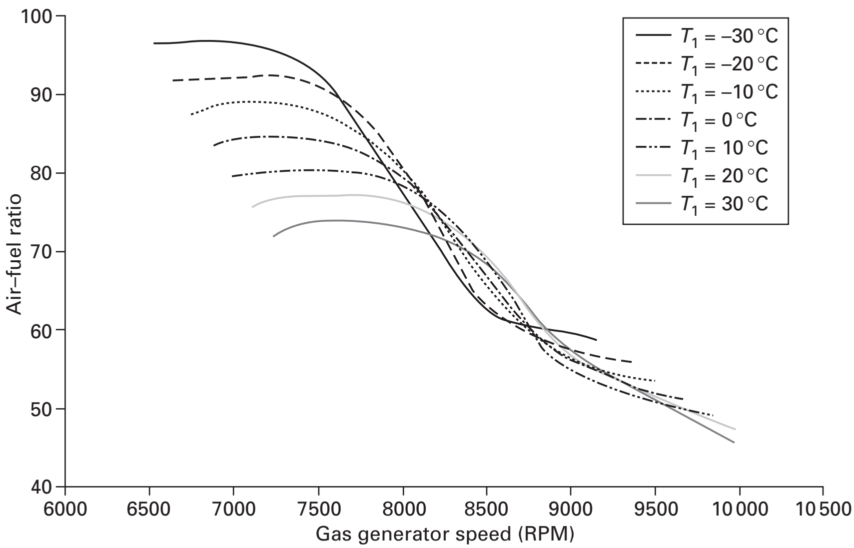

15.14 Variation of air–fuel ratio with gas generator speed for a series of ambient temperatures.

low ambient temperatures, the margin for acceleration will decrease and the margin for deceleration will increase. Thus the transient response during acceleration will be poor and the increased deceleration margin could result in flameout during deceleration. Conversely, at high ambient temperatures the acceleration margin will increase, whereas the deceleration margin will decrease. Thus at high ambient temperatures, the increased acceleration margin could result in flameout due to low air–fuel ratios. Low air–fuel ratios can also result in high turbine temperatures and compressor surge. The reduced deceleration margin at high ambient temperatures will result in poor transient response of the gas turbine during deceleration. These problems may be overcome by implementing the acceleration–deceleration ('accel–decel') schedules, also known as the fuel schedule curves, using non-dimensional parameters as discussed in Section 10.3. Because of the non-dimensional behaviour of gas turbines resulting in unique running lines, as shown in Figures 11.3 to 11.7 in Section 11.2, the accel–decel schedules are applicable for all ambient temperatures and pressure. The non-dimensional parameters considered in Section 10.3 were the compressor pressure ratio and non-dimensional speed. However, the variation of these non-dimensional parameters exhibit a kink and this is due to the VIGV/VSV movement as discussed in Section 11.2 and shown in Fig. 15.15, which also displays the accel and decel lines.

The implementation of the accel and decel lines would be simpler if the kink is eliminated and this can be achieved by using the non-dimensional parameters for fuel flow and compressor pressure ratio, as shown in Fig. 15.16. The figure also shows the accel and decel lines. Thus, in the simulator the variation of non-dimensional fuel flow is used with compressor pressure ratio to implement the accel–decel lines. In practice, manufacturers may omit the temperature term present in the non-dimensional fuel flow as it is a weaker function compared with the pressure term.[3]

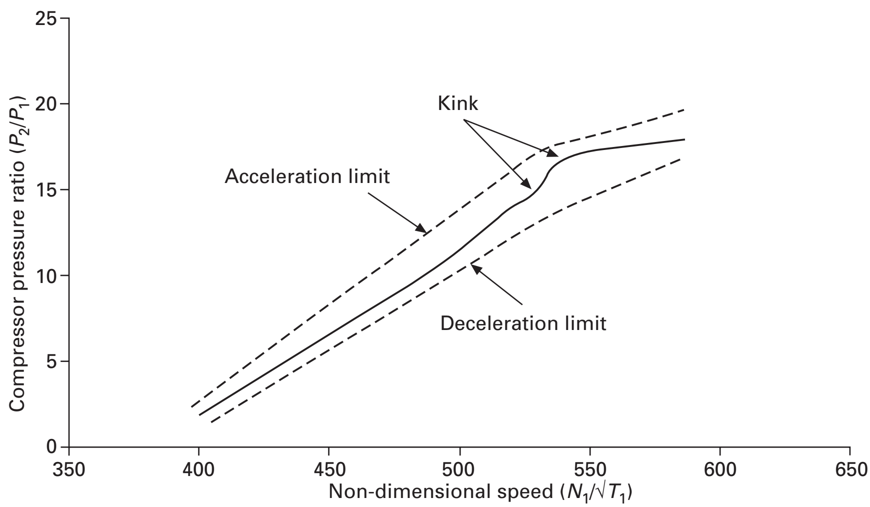

15.15 Acceleration and deceleration line on the compressor pressure ratio versus speed characteristic.

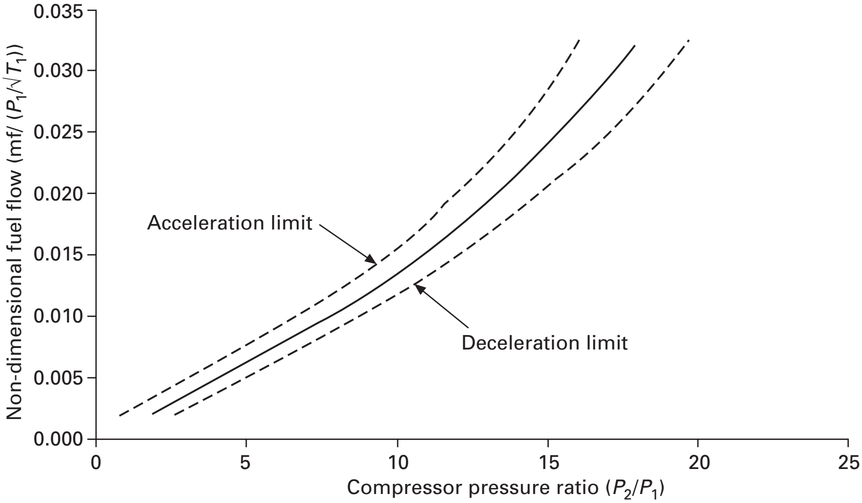

15.16 Acceleration and deceleration line on the non-dimensional fuel flow versus compressor pressure ratio characteristic.

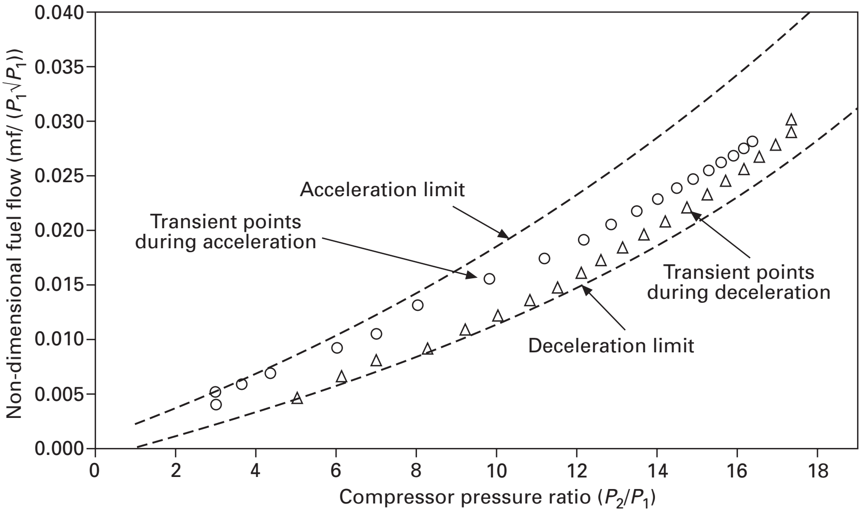

15.17 Transient operating points on acceleration–deceleration lines.

The transient operating points due to a step increase in power demand from 1 MW to 19 MW on the acceleration–deceleration curve are shown in Fig. 15.17. The figure also shows the transient operating points due to a step decrease in power demand from 19 MW to 1 MW. All the transient operating points during both acceleration and deceleration are observed to remain within the acceleration–deceleration limit lines, thus ensuring satisfactory transient operation of the engine. Fig. 15.18 shows the transient operating points on the compressor characteristic during acceleration and deceleration. Note that all the transient operating points do not cross the compressor surge line during acceleration, thus preventing compressor surge during acceleration.

In the absence of acceleration and deceleration lines, the operating points during engine transient may cross these limiting lines, resulting in compressor surge or flameout conditions. This is illustrated in Fig. 15.19, which shows the operating points for the same transient described above on the acceleration–deceleration curve when the acceleration and deceleration lines are inactive. It is observed that the operating points cross the acceleration and deceleration lines during the transient, particularly during deceleration, and could result in flameout due to the air–fuel ratio exceeding the weak flammability limit. The operating points crossing the acceleration line would result in compressor surge, as shown in Fig. 15.20, which displays the operating points on the compressor characteristic during these transients.

15.5 Integral wind-up

The size of the fuel valve is of paramount importance in ensuring satisfactory fuel flow to the engine and thus achieving the required power output subject to engine operating limits such as exhaust gas temperature and speed limits as discussed previously, particularly during transient operation. Inadequate fuel valve capacity will result in unexpected behaviour of the control system

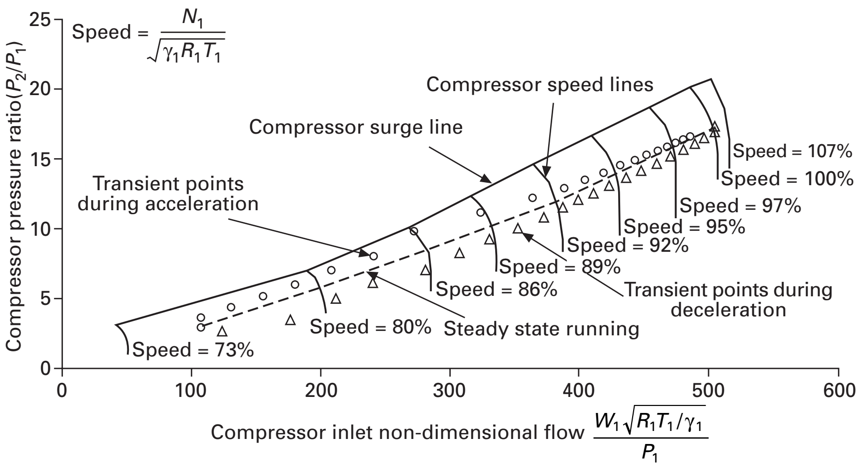

15.18 Transient operating points on compressor characteristic due to a step change in power demand.

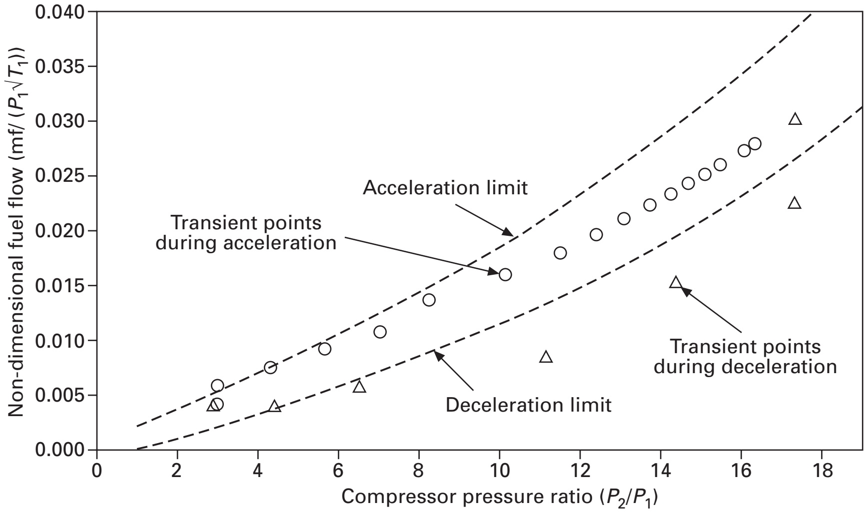

15.19 Operating points during step changes in power demand when acceleration–deceleration lines are inactive.

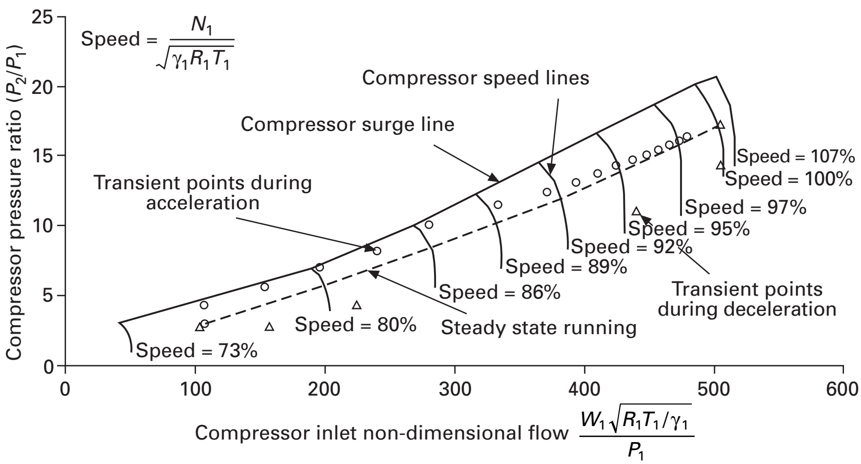

15.20 Operating points due to step changes in power on the compressor characteristic when acceleration–deceleration lines are inactive.

and one such behaviour is due to the continuous increase in the integral output, often referred to as integral wind-up, due to the fuel valve becoming fully opened, as discussed in Section 10.1.2. It should also be noted that, if the fuel pressure is low due to a fault in the fuel system, the fuel valve could become fully opened. Integral wind-up will now be illustrated using the gas turbine simulator. (It is necessary to ensure that the integral reset wind-up is switched off for this simulation exercise – see the user guide on the CD for instructions on switching off the reset wind-up.)

The valve flow coefficient (CG) is reduced to half its design value from 1100 to 550. If the power demand from the electric generator is increased from 1 MW to 20 MW, the fuel valve will open fully (100%). However, the power output will not meet the generator power demand due to insufficient fuel flow. The power output from the generator would be about 14.8 MW, which is well short of the required power demand of 20 MW. The important point to note is that no engine operating limits such as the exhaust gas temperature or speed limit have been reached. Under these conditions the integral output would be observed to continue to increase and exceed 100% output as the control system attempts to open the fuel valve to meet the generator power demand. Since the fuel valve is fully opened, no further increase in fuel flow can occur and thus no increase in power output from the gas turbine is possible. As long as these conditions prevail, the integral output continues to increase or wind up and should be observed in the main display screen of the gas turbine simulator.

If we reduce the generator set point from 20 MW to, say, 12 MW, which is below the current power output from the generator, it is observed that the generator power output will remain at 14.8 MW. This unexpected result occurs because the integral output is above 100% but will then be observed to start winding down and this can be seen on the main screen of the simulator. The power output from the generator will remain at 14.8 MW until the integral output has completely wound down (below 100%), after which the power output from the electrical generator will decrease and eventually match the set point value of 12 MW.

The above is summarised in Figs 15.21 and 15.22, which show the trends in power and fuel flow/valve position, respectively. Figure 15.21 shows the generator power output remaining at 14.8 MW until the integral output has wound down, although the generator set point has decreased from 20 MW to 12 MW after about 100 seconds. Figure 15.22 shows the trend in the fuel valve position, which remains at 100% until the integral output has wound down. The fuel valve then closes so that the power output from the generator matches the required power as stipulated by the generator set point.

To prevent the integral output from winding up, so resulting in this unexpected response from the engine control system, the output from the PID controller is reset to 100% if the output from the control system exceeds 100% and the fuel valve is concurrently fully open. This is achieved with the simulator by clicking the reset wind-up option to 'Reset Wind-up On' with the engine control setting display (see user guide). The above simulation is run again and the generator power output set point reduced to 12 MW as above. However, on this occasion the power output from the generator responds

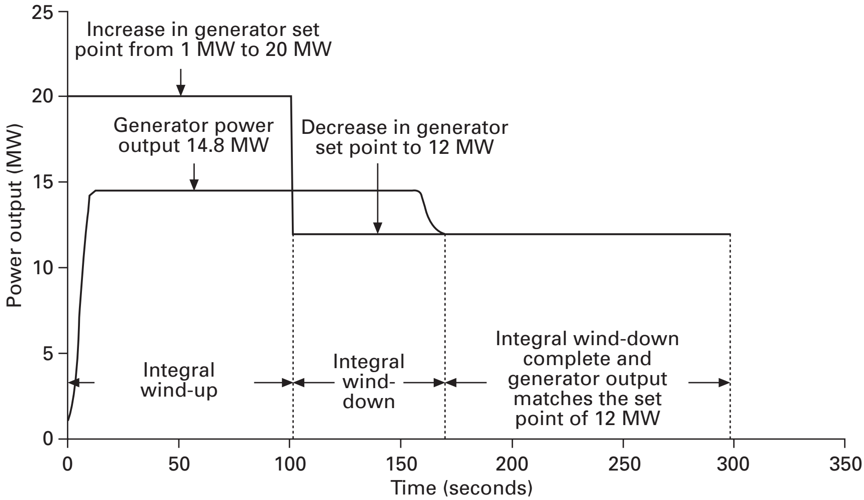

15.21 Trends in power due to integral wind-up.

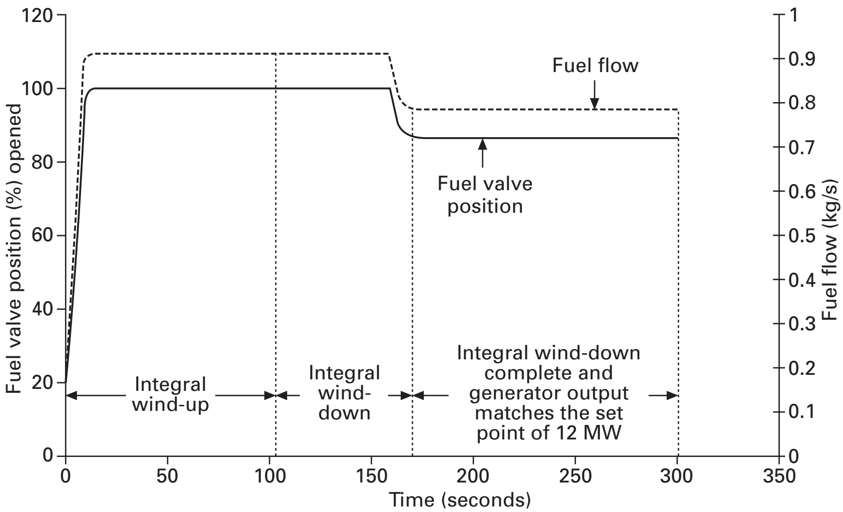

15.22 Trend of the fuel valve position due to integral wind-up.

almost immediately and achieves the required power output of 12 MW. Figure 15.23 displays the trends in power when reset wind-up is active and the power output from the gas generator is observed responding to the change in set point to 12 MW. The trend in flows and fuel valve position are shown in Fig. 15.24. Again, the fuel valve is observed responding to the change in power demand from the generator almost immediately when the reset wind-up option is active.

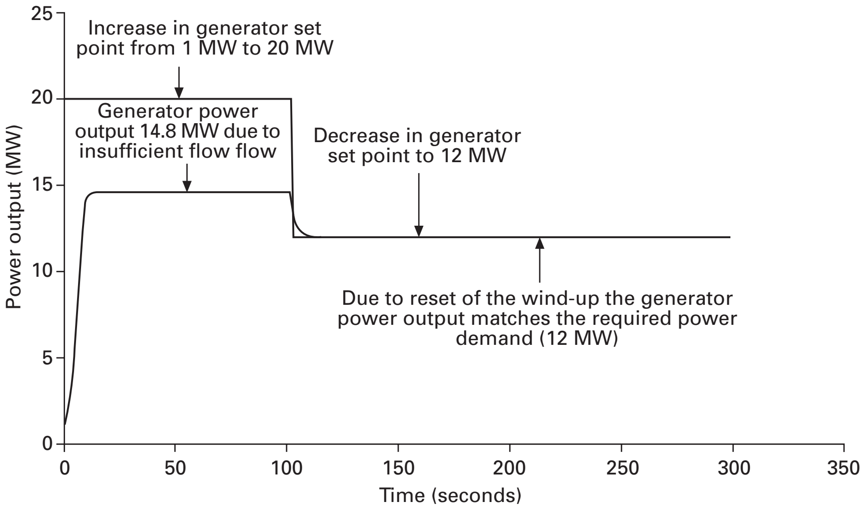

15.23 Trends in power when reset wind-up is active.

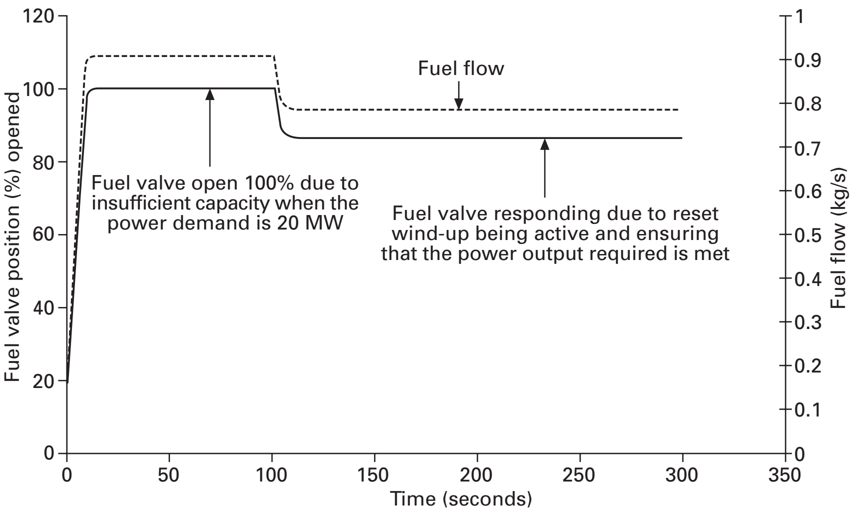

15.24 Trend in the fuel valve position due to the reset wind-up being active.

15.6 Engine trips

In Section 15.2, the likelihood of trips due to poor control system performance was discussed, where excursions in exhaust gas temperature and speeds can occur, thereby exceeding their trip levels. A well-tuned control system would prevent such excursions and hence engine trips. However, in certain situations the control system may not be able to respond adequately and will result in trips. Although trip levels are important to protect the engine from damage, their frequent occurrence is indicative of faults either in the control system or in the operating procedure, resulting in increased unscheduled downtime and reduced availability. Some engine faults, such as compressor VIGV/VSV schedule problems, may also result in trips. These problems affect revenue and profits and thereby increase life cycle costs.

One such trip is illustrated, where water injection to augment the power output of the gas turbine is considered. The injection of water results in a decrease in thermal efficiency and thus, for a given power output, requires an increase in fuel flow. If water injection is ceased then care must be taken not to reduce the water injection rate rapidly as the fuel flow rate may not decrease sufficiently, thus injecting too much fuel resulting in a very high gas temperature (due to the absence of water). Such increases in gas temperature may result in engine trips.

The simulator is run at an ambient temperature of 30 degrees Celsius where water injection for power augmentation is most beneficial and the generator power demand (power set point) is set to 25 MW. After 10 seconds of operation, water is injected over a period of 10 seconds (ramp time) to achieve a water–fuel ratio of 1.5. Figure 15.25 shows the trends in power and the generator power is observed to be increasing when water injection is present. After about 50 seconds water injection is ceased by reducing the ramp time to just 1 second, so reducing the water injection very rapidly. The engine is observed to trip very shortly after 50 seconds.

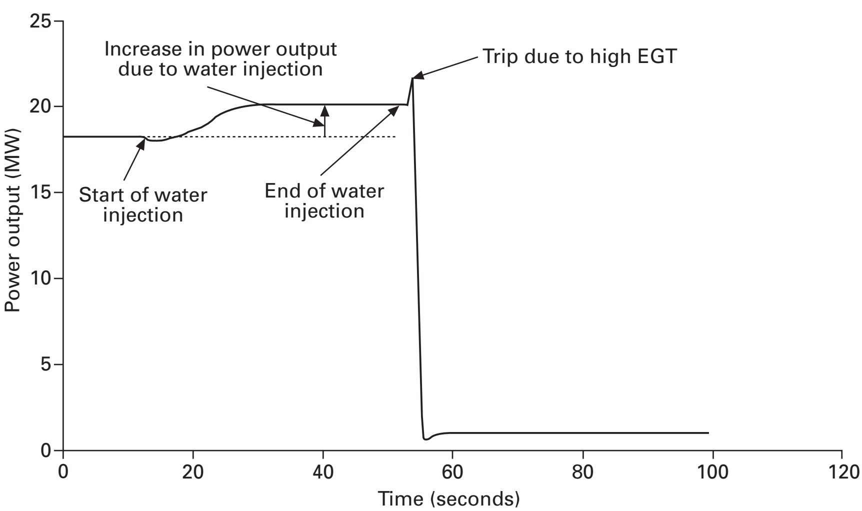

15.25 Trend in power when the engine trips due to high exhaust gas temperature (EGT).

This is illustrated more clearly in Fig. 15.26, which show the corresponding trends in exhaust gas temperature (EGT). The exhaust gas temperature is observed to rise and it reaches its trip level, resulting in the engine trip. Figure 15.27 shows the trends in speed and it is noted that an increase in gas generator speed occurs but that this increase in speed is insufficient to initiate a trip. (*Note*: In the simulator, a trip is simulated by reducing the power output of the gas turbine to its idle power output, which is set to 1 MW.) However, the solution in preventing this trip condition is quite simple. The

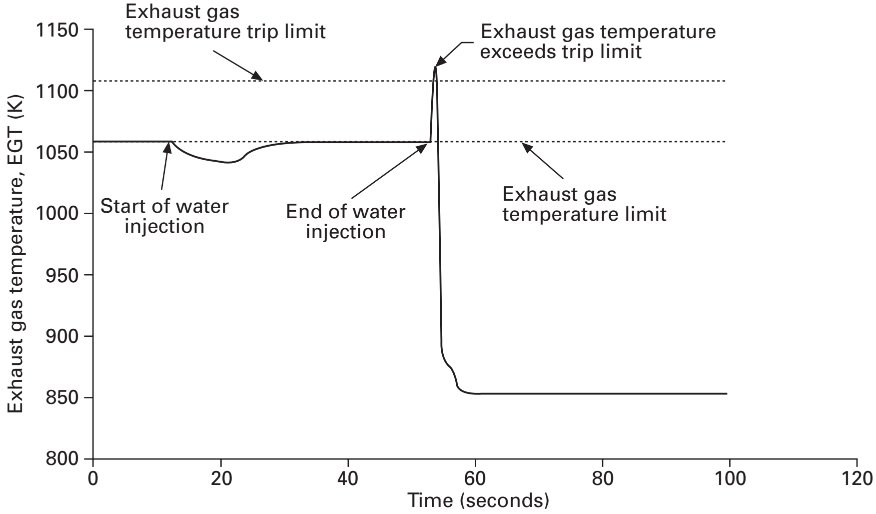

15.26 Trends in exhaust gas temperature during engine trip.

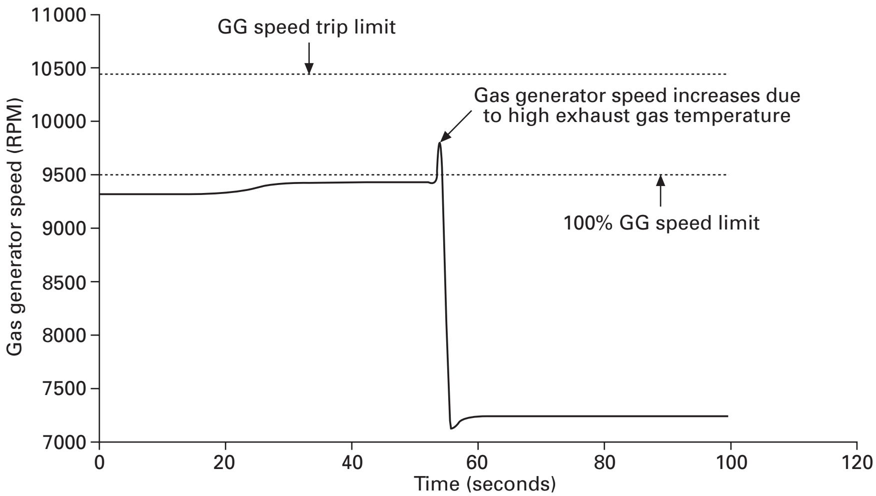

15.27 Trends in speed during engine trip.

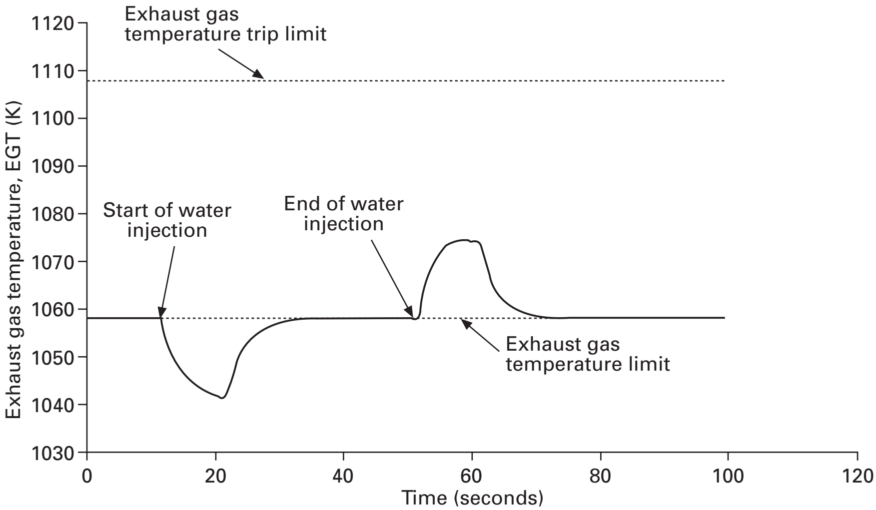

15.28 Trends in temperature with and without water injection.

ramp time is increased sufficiently when water injection cessation is desired, thus preventing the exhaust gas temperature from rising rapidly. To use a short ramp time, it would be necessary to reduce the power demand before shutting off the water injection. The case is illustrated where the ramp time is increased when shutting off the water injection. The ramp time is increased from 1 second to 10 seconds in this case.

Figure 15.28 shows the trend in exhaust gas temperature when the ramp time is increased to 10 seconds, and it can be seen that the exhaust gas temperature rises, but not sufficiently to cause a trip condition. Thus, increasing the ramp time representing the time period for switching off the water reduces the increase in exhaust gas temperature. In the simulation, the user should also note the change in primary zone temperature due to water injection. It is left to the user to vary the ramp time to investigate its influence on the change in exhaust gas temperature due to shutting off the water injection.

15.7 References

1. *PID Control Algorithm. How it Works, How to Tune it and How to Use it*, 2nd Edition, Shaw, J. A., December 1, 2003. E-book, http://www.jashaw.com/.
2. *Control Systems Engineering*, Sivanandam, S. N., Vikas Publishing (2001).
3. *Gas Turbine Performance*, 2nd edition, Walsh, P. and Fletcher, P., Blackwell Publishing (2004).

Part III

Simulating the performance of a single-shaft gas turbine

In Part II the two-shaft gas turbine simulator was used to illustrate the performance, turbine life usage and engine emissions of a two-shaft gas turbine operating with a free power turbine. The simulator was also used to illustrate the behaviour and performance of the engine control system applied to such an engine.

In Part III the single-shaft gas turbine simulator will be used to illustrate these effects and repeat many of the simulations carried out in Part II. The single-shaft gas turbine simulator can be operated in two modes and both modes of operation will be considered in this part of the book. The first of these modes refers to the variable inlet guide vane (VIGV) remaining fully opened during the normal power output range, while in the second mode of operation the VIGV is modulated to maintain the exhaust gas temperature (EGT) on its limiting value as the power output from the gas turbine is reduced. Control of the VIGV is usually achieved using a PID loop as discussed in Chapter 10, Section 10.4.2 and will also be discussed later in Chapter 20.

Unlike the case of the two-shaft gas turbine operating with a free power turbine, there are no unique running lines for a single-shaft gas turbine. The only exception is the variation of the compressor inlet non-dimensional flow with its speed, particularly if the compressor flow speed lines are vertical on the compressor characteristic. This was discussed in Chapter 8.

16
Simulating the effects of ambient temperature on engine performance, emissions and turbine life usage

The single-shaft gas turbine simulator is based on an industrial gas turbine having an ISO rating of about 40 MW and a maximum power limit of 45 MW at low ambient temperatures. As already stated, single-shaft gas turbines are widely used in power generation and therefore the driven load is assumed to be an electrical generator that operates at the synchronous speed determined by the frequency. Thus the gas turbine also operates at a constant speed as the load and ambient conditions change.

The reader is encouraged to run the simulations discussed below to become more familiar with concepts of engine performance, turbine life usage, gas turbine emissions and the behaviour of the engine control system. The single gas turbine simulator user guide gives details on how to use the simulator.

16.1 Configuration of the single-shaft simulator

The configuration of the single-shaft gas turbine simulator is similar to that shown in Fig. 2.3 except that the compressor is fitted with VIGV. One of the purposes of the VIGV is to reduce gas turbine starting power requirements (mode 1 as discussed previously, where the fuel flow is varied to maintain the generator output and the VIGV is modulated to maintain the exhaust gas temperature). This is achieved by closing the inlet guide vane during starting and low power operation. The closure of the inlet guide vane results in a reduction in airflow rate through the compressor, thus reducing the starting power demands. The normal operating power range of the gas turbine is between 60% and 100% when the VIGV is fully open. Control of the VIGV is achieved by maintaining the exhaust gas temperature (EGT) on a set point by modulating the inlet guide vane. Thus, when the EGT is below the set point temperature, the guide vane will be fully closed in an attempt to maintain the EGT on the set point, hence reducing starting power requirements. When the EGT is above the set point temperature, the inlet guide vane will therefore be fully opened, which corresponds to the normal operating power range.

Thus, the set point temperature for modulating the inlet guide vane needs to be below the maximum exhaust gas temperature limit (EGT limit). The values for the EGT limit and the (exhaust gas) set point temperature for VIGV modulation used by the simulator correspond to 825 K and 650 K respectively.

When regenerative cycles are employed in single-shaft gas turbines, the use of the VIGV is useful in maintaining constant maximum EGT during part-load operation. This results in a much improved thermal efficiency at part-load operation due to near constant maximum to minimum cycle temperature ratio, T_3/T_1, at these operating conditions. Similarly, the use of VIGV improves the part-load performance of combined cycle plants. Maximum EGT operation can be achieved at part-load by setting the temperature set point for variable inlet guide vane operation to the maximum EGT limit (i.e. the EGT for VIGV operation is increased from 650 K to 825 K) – mode 2 as discussed previously. Up to about 65% reduction in power output can be achieved at the maximum EGT by the use of VIGV.

With such VIGV operation, the air–fuel ratio remains approximately constant, resulting in approximately constant combustion temperature with the change in power output. In Section 6.11 it was seen that, if the combustion temperature is kept within certain limits (1700 K to 1900 K), the emissions of NO_x and CO are small and this approach is the basis of dry low emission (DLE) combustion systems. Thus the application of VIGV (mode 2 operation) in single-shaft gas turbines can achieve DLE combustion without having to resort to multi-staged combustion. In fact, such a combustion system will have similar characteristics to the variable geometry combustion system discussed in Section 6.12.

16.2 Effect of ambient temperature on engine performance at high power

The simulator can be used to investigate the effect of change in ambient temperature on engine performance. It has been stated in Part II that the simulators are based on a quasi-steady-state model, thus it is possible to subject the model to significant changes in ambient conditions. In practice, however, rapid changes in ambient conditions are not common and could lead to compressor surge.

In the simulation, the ambient temperature will be changed from +35 degrees Celsius to –30 degrees Celsius linearly over a period of 3600 seconds. The power demand from the simulator will be set above the ISO rating to 60 MW throughout the simulation. This action simulates the effects of the changes in ambient temperature on engine performance when the engine continuously operates on an engine operating limit such as the EGT or power limit. It should be noted that such high power demands from the generator would result in trips due to the frequency shift. However, in a simulator this can be considered as it is a convenient means of maintaining the engine on a limiting condition, such as the EGT or maximum power, as the ambient temperature changes. The ambient pressure is held constant at 1.013 Bar during the change in ambient temperature and the inlet and exhaust pressure losses are set to 100 mm water gauge. The relative humidity is also held constant at 60%. For simplicity, the gas property terms, R and γ, will be omitted from any non-dimensional terms such as flow and speed but reference will be made to them when relevant.

16.2.1 Trends in power, pressure and temperature ratios and compressor characteristics

The gas turbine speed and thus the compressor speed, N_1, remain constant as the electrical generator speed (synchronous speed) remains constant with the change in load. The reduction of ambient temperature will therefore result in an increase in the compressor non-dimensional speed, $N_1/\sqrt{T_1}$. This is seen in Fig. 16.1, which depicts the operating point on the compressor characteristic during this ambient temperature transient.

The increase in compressor non-dimensional speed will increase the compressor inlet non-dimensional flow, $W_1\sqrt{T_1}/P_1$. If at first it is assumed

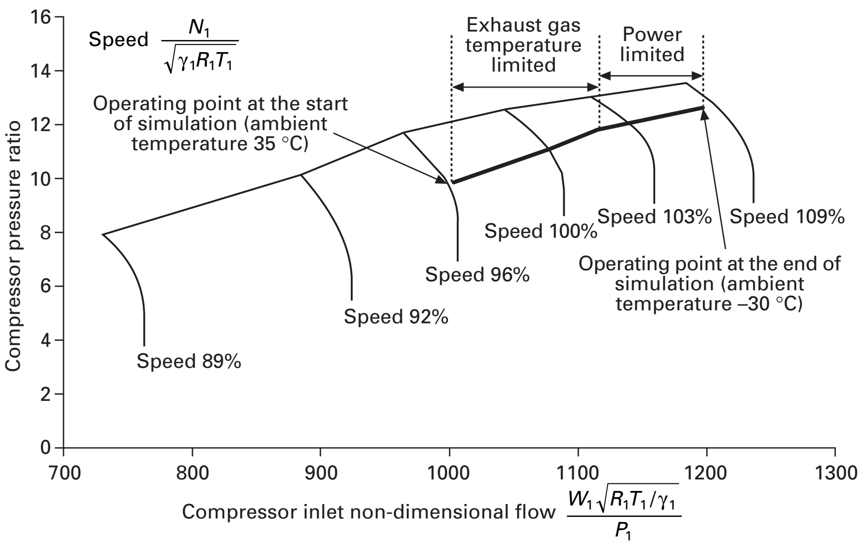

16.1 Operating point on compressor characteristic during temperature transient.

that the maximum to minimum temperature, T_3/T_1, remains constant (by adjusting the power output as the ambient temperature decreases), the compressor pressure ratio, P_2/P_1, must increase to satisfy the flow compatibility (Equation 8.1 assuming a choked turbine, i.e. $W_3\sqrt{T_3}/P_3$ is constant). The higher compressor pressure ratio will also result in a higher turbine pressure ratio. Also, at high ambient temperatures, the engine power output will be limited by the EGT limit. Thus, an increase in turbine pressure ratio must necessarily increase the turbine entry temperature, T_3. The decrease in ambient temperature will therefore result in an increase in the temperature ratio, T_3/T_1, which in turn further increases the compressor pressure ratio in order to satisfy the flow compatibility (Equation 8.1). This results in a steep operating line on the compressor characteristic, as shown in Fig. 16.1. The higher compressor pressure ratio and temperature ratio, T_3/T_1, will improve the thermal efficiency, as seen in Fig. 16.2.

The higher T_3/T_1 will also increase the specific work, but at these operating pressure ratios the increase in T_3/T_1 will have a greater influence on specific work than will pressure ratio (see Chapter 2, Section 2.15). The higher compressor inlet non-dimensional flow with the reduction in ambient temperature, T_1, will result in an increase in the compressor inlet air flow rate. Both the increased specific work and airflow rate increase the power output from the gas turbine as the ambient temperature decreases, as shown in Fig. 16.2.

The steep running line on the compressor characteristic may intersect the compressor surge line, which must be avoided for reasons discussed in Section 4.8. Adequate margin between the surge line and the operating point must be

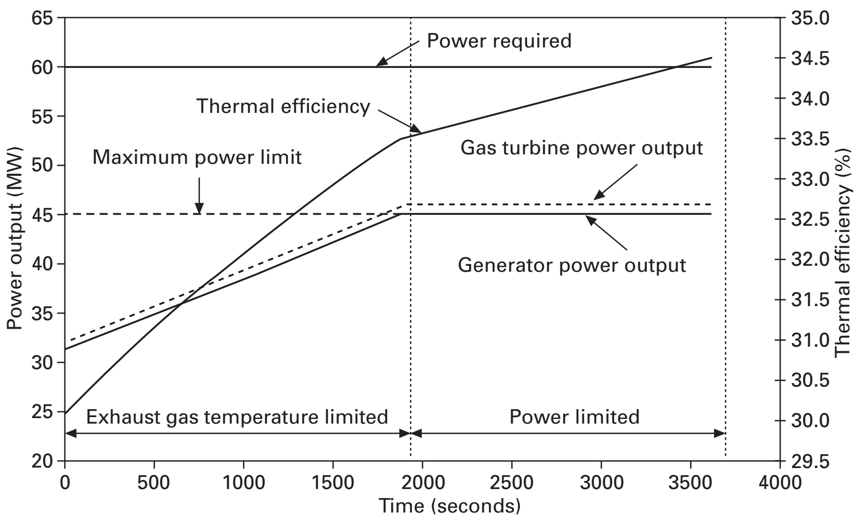

16.2 Changes in gas turbine power output and thermal efficiency during temperature transient.

maintained to allow for transient conditions. This is achieved by limiting the maximum power output from the gas turbine at low ambient temperatures to 45 MW. Limiting the power output at low ambient temperatures will decrease the turbine entry temperature, T_3. This is necessary to reduce the specific work in order to maintain the power output from the gas turbine at the maximum power limit of 45 MW. As a result, the rate of increase in the compressor pressure ratio decreases as can be seen in Figs 16.1 and 16.3. The reduction in T_3 will reduce the turbine creep life usage at these ambient temperatures. Thus manufacturers may impose the maximum power limit to ensure satisfactory turbine creep life at low ambient temperatures in a manner similar to that discussed in Section 11.3.8 (rating curves).

The rate of increase in thermal efficiency also decreases when operating at constant power output (Fig. 16.2), as the ambient temperature lowers. This is primarily due to the effect on compressor pressure ratio and the (slight) decrease in T_3/T_1 (Fig. 16.3). There is also a reduction in compressor efficiency under these conditions as the compressor operates in a region on the compressor characteristic where the compressor efficiency is lower.

The trends in compressor and turbine powers are shown in Fig. 16.4. The increase in the turbine power output is due to the increase in turbine entry temperature, pressure ratio and mass flow rate through the turbine. The increase in compressor power absorbed is due primarily to the increase in mass flow rate through the compressor and pressure ratio. The figure also shows the trends in the isentropic efficiencies of the compressor and turbine.

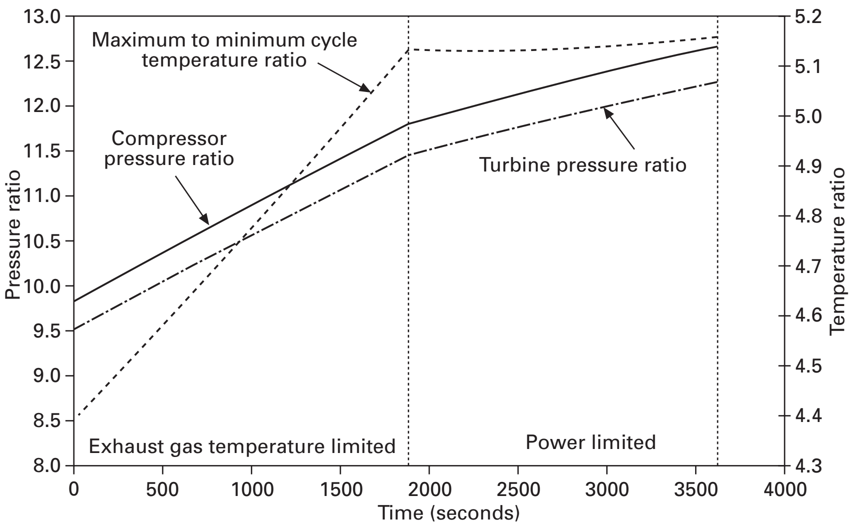

16.3 Trends in pressure and temperature ratios during temperature transient.

The compressor efficiency initially increases slightly before decreasing as the compressor operates in a lower efficiency part of its characteristic at low ambient temperatures. The turbine efficiency decreases slightly before increasing slightly, due to the change in the turbine non-dimensional speed. During constant EGT operation the turbine entry temperature increases (Fig. 16.8), resulting in a decrease in the turbine non-dimensional speed, thus giving a slight reduction in turbine efficiency. During constant power operation, the turbine entry temperature decreases, hence increasing the turbine non-dimensional speed resulting in a slight gain in the turbine efficiency.

The changes in power and thermal efficiency trends can be displayed on an ambient temperature basis and these are shown in Figs 16.5 and 16.6, respectively. Figure 16.6 also shows the change in specific work where the increase in specific work is noted during constant EGT operation and a decrease in specific work during constant power operation.

16.2.2 Trends in pressure and temperatures

During constant EGT operation it has been shown that the compressor pressure ratio and thus the turbine pressure ratio increase. This results in an increased compressor discharge pressure, P_2, and turbine entry pressure, P_3, during the transient as shown in Fig. 16.7. However, when operating at constant power output a decrease in rate of pressure rise is observed, which is due to a decrease in the rate of compressor pressure ratio increase (Fig. 16.3). Since

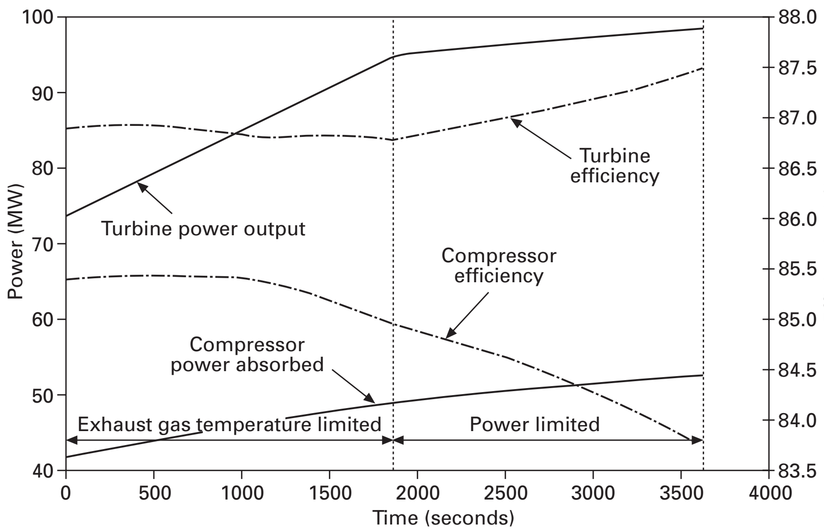

16.4 Trends in compressor and turbine power efficiency during ambient temperature transient.

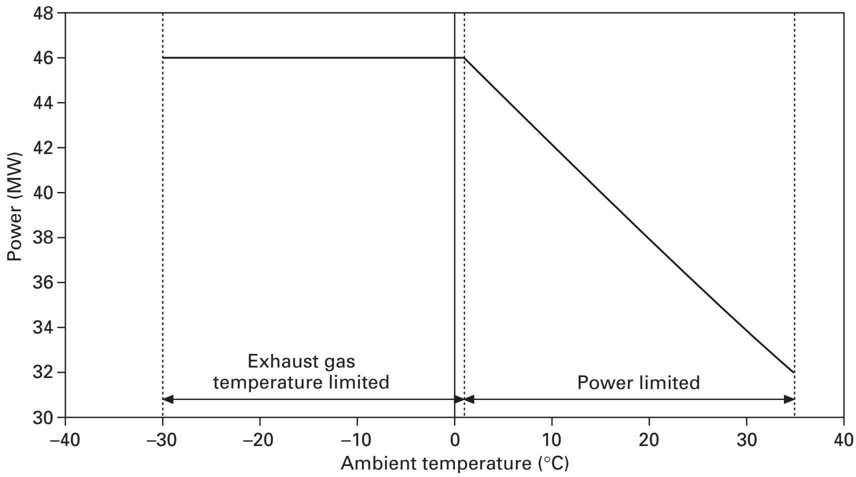

16.5 Variation of gas turbine output on an ambient temperature basis.

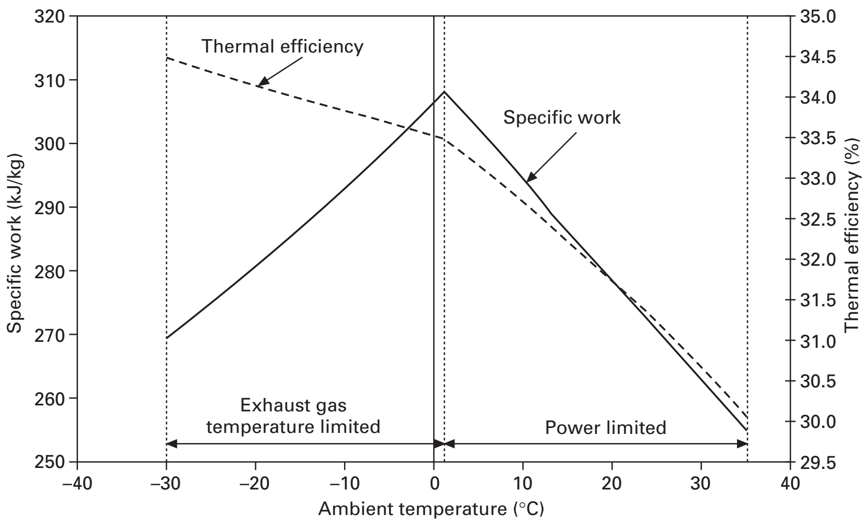

16.6 Variation of thermal efficiency and specific work on an ambient temperature basis.

the ambient pressure does not change during this transient, the compressor inlet and turbine exit pressures do not change during this transient.

The trends in temperature are shown in Fig. 16.8. The turbine entry temperature, T_3, rises as mentioned earlier and this also results in an increase in primary zone temperature during the period when the engine power output is limited by the EGT. These temperatures decrease as the engine becomes

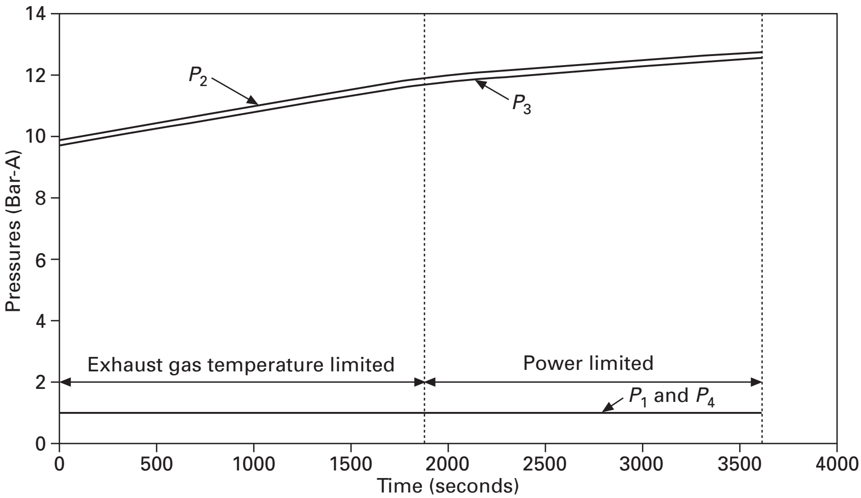

16.7 Trends in pressure during ambient temperature transient.

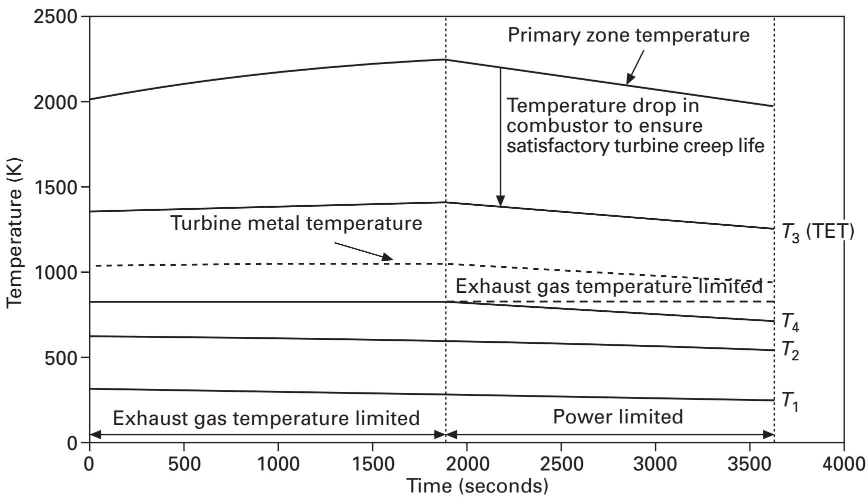

16.8 Trends in temperature during ambient temperature transient

power limited. The trend in the EGT, T_4, remains constant until the engine becomes power limited, after which the EGT decreases. The increase in compressor non-dimensional speed increases the compressor non-dimensional temperature rise, $\Delta T_{21}/T_1$, as shown in Fig. 8.3 in Chapter 8. However, the decrease in ambient temperature, T_1, results in a reduction in the compressor discharge temperature, T_2.

The figure also shows the turbine blade metal temperature, and an increase in the turbine blade metal temperature occurs during the period when the engine is EGT limited. This is due primarily to the increase in turbine entry temperature, T_3, although the cooling air temperature, T_2, is decreasing. The reduction in cooling air temperature during this transient reduces the rate of increase in the turbine blade metal temperature. When the engine power is limited, the turbine blade temperature decreases and this is due to the decrease in turbine entry and cooling air temperatures.

16.2.3 Trends in flow

The trends in air flow, fuel flow, fuel valve position and the air–fuel ratio are shown in Fig. 16.9. The air flow increases continuously due to the increase in compressor inlet non-dimensional flow, $W_1\sqrt{T_1}/P_1$, and the decrease in ambient temperature, T_1. The fuel flow increases during the period when the power output is controlled by the EGT. During this period, the power output from the gas turbine and its thermal efficiency increase.

However, the increase in power output is greater than the increase in thermal efficiency, thus the fuel flow increases to satisfy the increased power output. During the period when the gas turbine is power limited, the fuel flow decreases. This is because the thermal efficiency increases while the power output remains constant. The fuel valve position follows a similar trend to the fuel flow. The air–fuel ratio decreases during the period of constant EGT operation due to the combustor temperature rise, $T_3 - T_1$, during this period of operation (Fig. 16.8). Conversely, the air–fuel ratio increases during the period when the engine is power limited because of a decrease in combustor temperature.

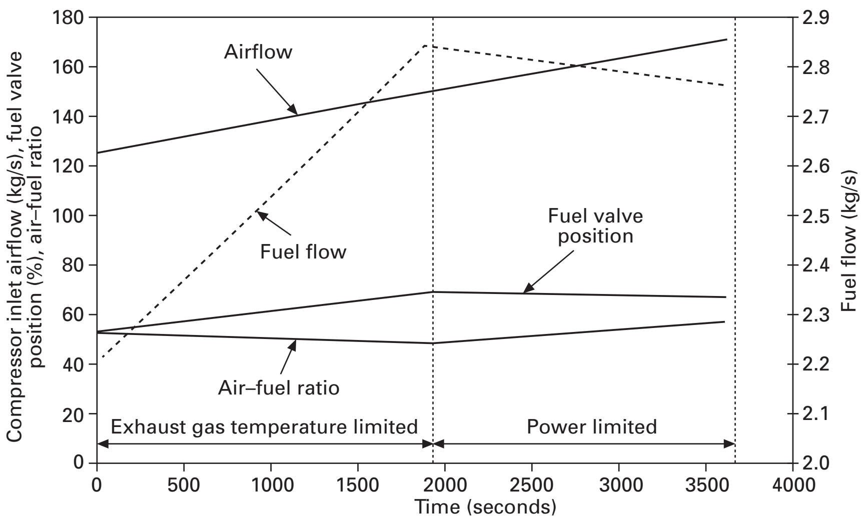

16.9 Trends in flow, fuel valve position and air-fuel ratio during ambient temperature transient.

16.2.4 Trends in turbine creep life

The trend in turbine creep life usage, which is shown as the time to next overhaul, decreases during the period when the engine power output is limited by the EGT (Fig. 16.10). The increase in turbine blade temperature has been observed (Fig. 16.8) and an increase in turbine power output (Fig. 16.4).

The increased power developed by the turbine increases the stress in the blades due to the increased torque (note turbine speed is constant). Thus, together with the increase in blade temperature, the creep life usage increases. During the period when the engine power output is constant, the turbine blade metal temperature decreases. Although the turbine power output increases during constant power operation, it increases at a lower rate (Fig. 16.4). The reduction in turbine blade metal temperature has a greater effect on reducing creep life usage than the increased torque, which produces increased stress in the turbine blade material. The net effect is a decrease in turbine creep life usage (Fig. 16.10). Figure 16.11 shows the creep life usage on an ambient temperature basis during this transient.

The turbine creep life usage has been seen to be lower at high ambient temperatures and this is due to the lower turbine pressure ratios resulting in lower turbine entry temperatures while operating at the EGT limit. It is therefore possible to increase the turbine creep life usage under these conditions by increasing the EGT limit as the ambient temperature increases and this is often the case with single-shaft gas turbines. This will improve the engine performance due to the increase in compressor pressure ratio and maximum

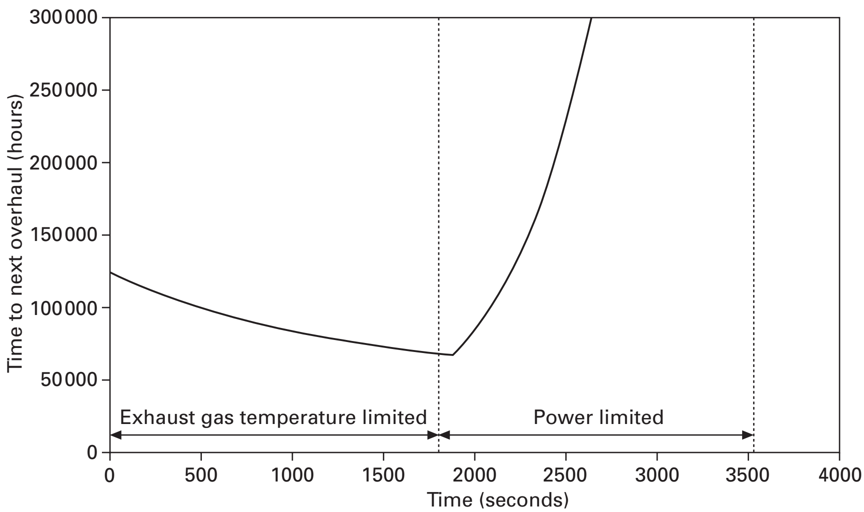

16.10 Trends in turbine creep life usage during ambient temperature transient.

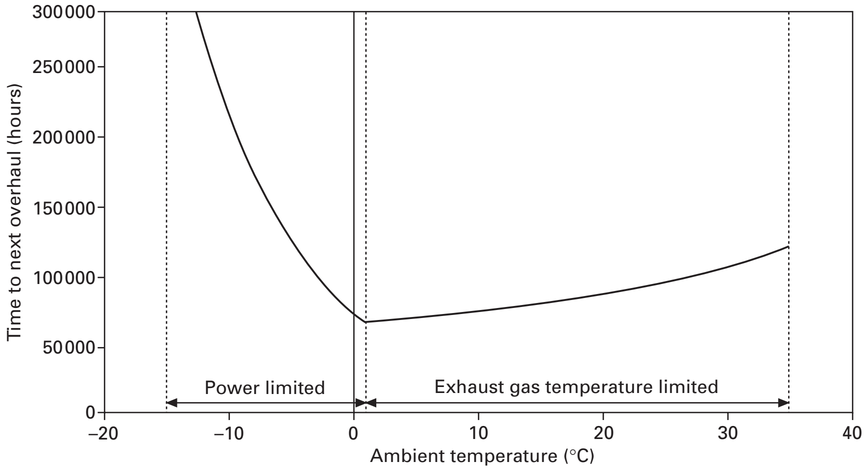

16.11 Creep life usage as time to next overhaul on an ambient temperature basis.

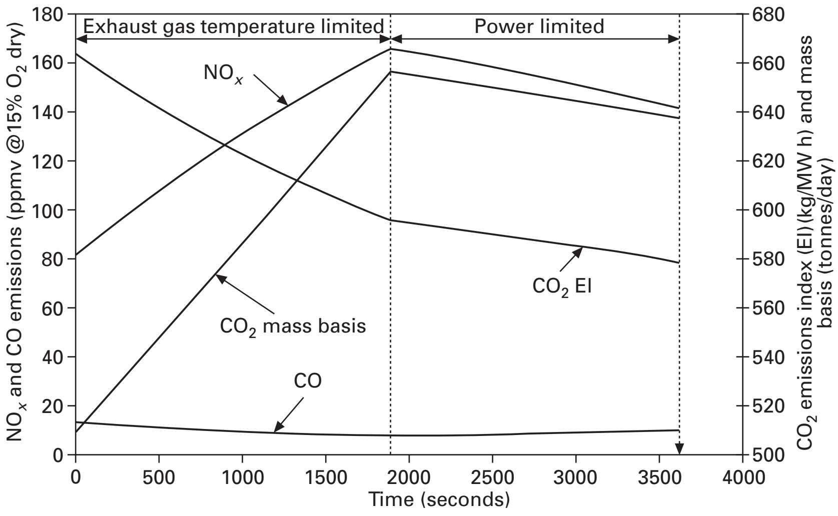

16.12 Trends in gas turbine emissions during temperature transient.

to minimum cycle temperature, T_3/T_1, at high ambient temperatures and is discussed further in Chapter 20.

16.2.5 Trends in gas turbine emissions

The trends in gas turbine emissions during the ambient temperature transient are shown in Fig. 16.12. NO_x is observed to be increasing while operating on the EGT limit. Note also that the compressor pressure ratio, as well as the combustion pressure, increases during this period of operation. It is also observed that the primary zone temperature increases during this period of engine operation. Also, the specific humidity of the ambient air decreases as the ambient temperature decreases, as seen in Fig. 11.15. The change in these parameters with ambient temperature results in an increase in NO_x as discussed in Section 6.8. However, an increase in these parameters also results in a decrease in CO (Section 6.8). Thus it is observed that NO_x increases while CO decreases when operating on the EGT limit.

When the engine is constrained to operate on the power limit, it is observed that the combustion temperature falls. Although the compressor discharge pressure and the combustion pressure continue to increase, they do so at a decreased rate. The fall in combustion temperature is greater and a decrease in NO_x is observed, although the fall is not as great as the rise in NO_x during constant EGT operation because of the continuous rise in the combustion pressure. These factors also give rise to an increase in CO when the engine is constrained to operate at constant power.

The trend in CO_2 emissions is also shown in Fig. 16.12. The mass flow rate of CO_2 is observed to increase during constant EGT operation and this is due to the increase in fuel flow during this period of operation. During constant power operation the fuel flow falls, thus a decrease in CO_2 flow rate is observed. The figure also shows the CO_2 emissions as an emissions index, kg/MW h, and represents the emission of CO_2 on a mass basis per unit of power produced. Note that the emissions index falls continuously during this transient. This index is similar to the specific fuel consumption and, for a given fuel, it is proportional to the specific fuel consumption. Since the specific fuel consumption is inversely proportional to the thermal efficiency, the continuous increase in thermal efficiency results in a continuous decrease in the CO_2 emissions index. Thus less CO_2 is generated at constant power if the ambient temperature falls. Figure 16.13 shows the NO_x and CO emissions on an ambient temperature basis while Fig. 16.14 shows the CO_2 emissions index on an ambient temperature basis. It must be noted that the NO_x and CO emissions are predicted using Bakken's and Rick and Mongia's correlation at discussed in Sections 6.18.1 and 6.18.2, respectively.

16.2.6 Speed and VIGV position trends

The gas turbine speed remains constant and the speed is determined by the generator, depending on the required frequency. As the ambient temperature falls during this transient, the compressor non-dimensional speed, $N_1/\sqrt{T_1}$, increases. This is observed in Fig. 16.15, which shows the trends in compressor non-dimensional speed and the trend in the VIGV position during this transient.

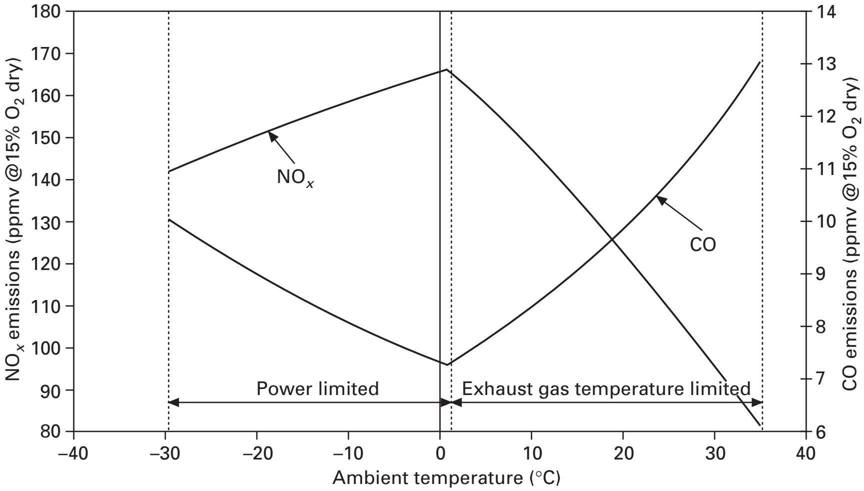

16.13 NO_x and CO emissions on an ambient temperature basis.

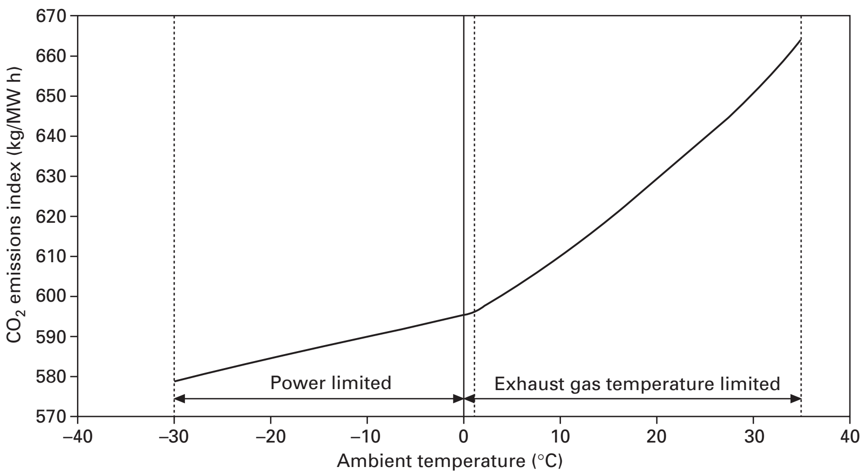

16.14 CO_2 emissions index on an ambient temperature basis.

The figure also shows the trend in the turbine non-dimensional speed, $N_1/\sqrt{T_3}$). It is observed that the turbine entry temperature, T_3 increases during the period when the EGT limits the power output and then decreases during the period when the power output from the gas turbine is limited (Fig. 16.8). Thus it is observed that the turbine non-dimensional speed decreases during the period when the engine power output is limited during constant EGT

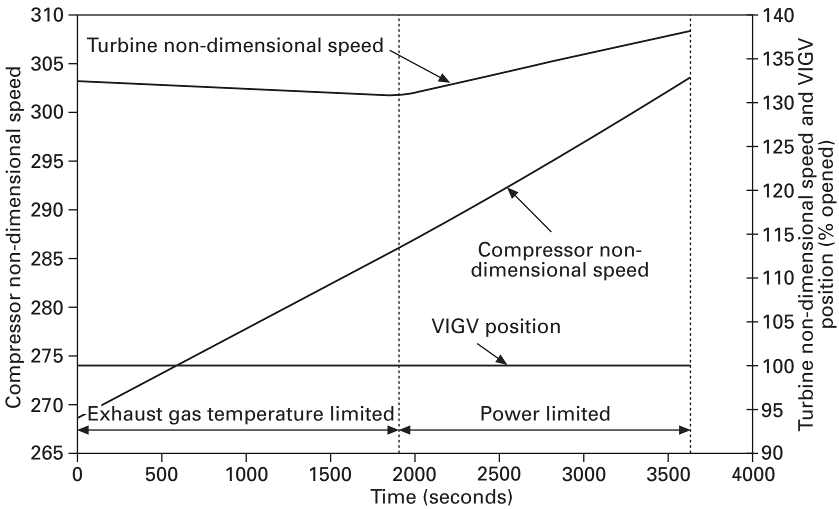

16.15 Trends in non-dimensional speeds and VIGV position.

operation. However, when the power output limit operates, the turbine non-dimensional speed increases.

Since the EGT always remains above the temperature set point for VIGV modulation, the VIGV stays fully opened during this transient.

16.3 Effect of ambient temperature on engine performance at low power

The effect of varying the ambient temperature has been considered when the gas turbine is always on an engine limit, which would be encountered at high power operating conditions. The same ambient temperature transient is now considered but at lower power such that the engine never reaches an engine-limiting condition. This is achieved by setting the power demand from the generator to 30 MW. Again, the pressure is maintained at 1.013 Bar, the inlet and exhaust losses at 100 mm water gauge and relative humidity at 60%.

16.3.1 Trends in temperature and pressure ratio

Since no engine limit is reached or exceeded during this ambient temperature transient, the power output remains constant. The increased mass flow rate at lower ambient temperatures leads to a reduction in specific work due to maintaining the required (constant) power output from the generator. Thus a reduction in the maximum to minimum cycle temperature, T_3/T_1, occurs in order to reduce the specific work, (in the period of constant VIGV operation) as seen in Figure 16.16. The reduction in T_1 and T_3/T_1 will result in a decrease in turbine entry temperature, T_3. Since the turbine pressure ratio increases (to satisfy the flow compatibility between the compressor and turbine), the decrease in T_3 results in a decrease in EGT. This is shown in Fig. 16.17, which displays the trends in temperature during this ambient temperature transient.

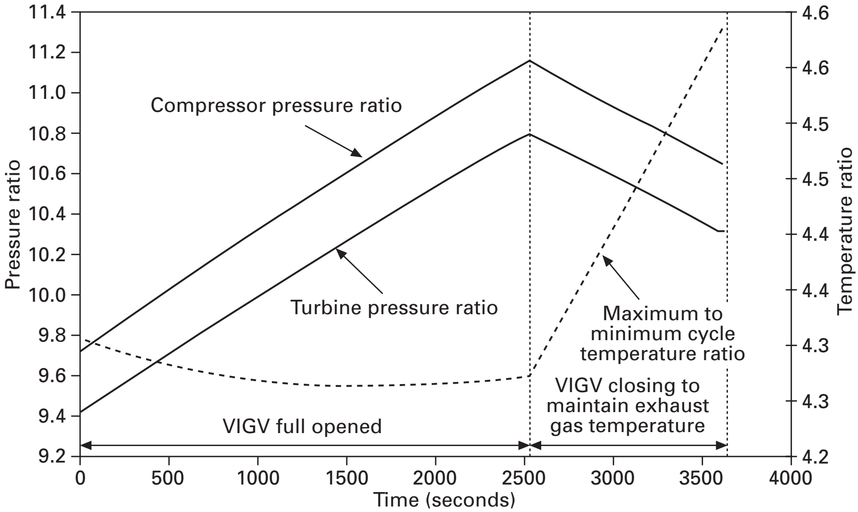

16.16 Trends in compressor and turbine pressure ratios. Also shown is the trend in T_3/T_1.

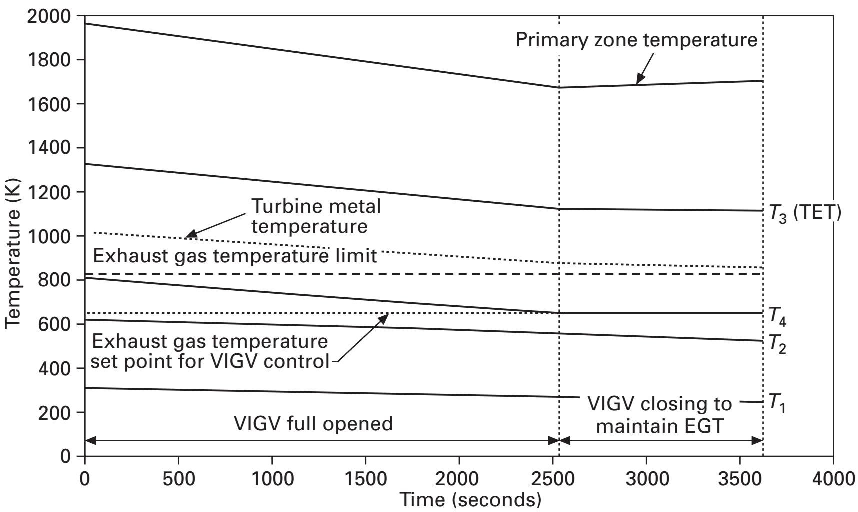

16.17 Trends in gas turbine temperature during ambient temperature transient.

During this transient, the decrease in EGT is significantly large such that it decreases below the EGT limit of 650 K, which is the set point for VIGV control. The VIGV control system responds by closing the VIGV so that the EGT remains at its set point of 650 K as shown in Fig. 16.17. Thus, during the period when the VIGV is closing, the EGT remains constant. The closure of the VIGV, for a given compressor non-dimensional speed, $N_1/\sqrt{T_1}$), will reduce the compressor inlet non-dimensional flow, ($W_1\sqrt{T_1}/P_1$). For a given T_3/T_1, the reduction in $W_1\sqrt{T_1}/P_1$ requires a decrease in compressor pressure ratio, P_2/P_1, to satisfy the flow compatibility Equation 8.1 (Chapter 8). Although the ambient temperature and thus the compressor inlet temperature is decreasing, and therefore resulting in an increase in the compressor non-dimensional speed, the closure of the VIGV is sufficient to reduce the compressor inlet non-dimensional flow, resulting in a decrease in compressor pressure ratio to satisfy the flow compatibility equation. The reduction in compressor pressure ratio also results in a reduction in turbine pressure ratio. Since the EGT remains constant during the period of VIGV operation, this results in a decrease in the turbine entry temperature, T_3. Thus the trend in T_3 shows a small decrease, as shown in Fig. 16.17.

Although the compressor non-dimensional temperature rise, $\Delta T_{21}/T_1$, increases due to the increase in the compressor non-dimensional speed, $N_1/\sqrt{T_1}$, and compressor pressure ratio, P_2/P_1, a decrease in T_1 results in the reduction in the compressor discharge temperature, T_2. The decrease in the temperatures T_3 and T_2 results in a decrease in turbine blade metal temperature, even during the period of VIGV operation (Fig. 16.17).

16.3.2 Trends in pressure

During the period when the VIGV is fully opened, the increase in compressor ratio results in an increase in compressor discharge pressure and turbine inlet pressure. This can be seen in Fig. 16.18, which shows the trends in pressures during this transient. It is also observed that the compressor discharge pressure and turbine inlet pressure decrease during the period of VIGV closure. This is due to the decrease in compressor pressure ratio when the VIGV closes. The figure also shows the trends in the compressor inlet and turbine exit pressures. Since it has been assumed that the inlet and exhaust losses are small, the trends for these two pressures are almost superimposed.

16.3.3 Compressor characteristic

It has been explained that, to satisfy flow compatibility, the compressor inlet non-dimensional flow and compressor pressure ratio increase when the ambient temperature decreases during operation at a constant gas turbine power output (high power output case in Section 16.2.1). This is illustrated in Fig. 16.19,

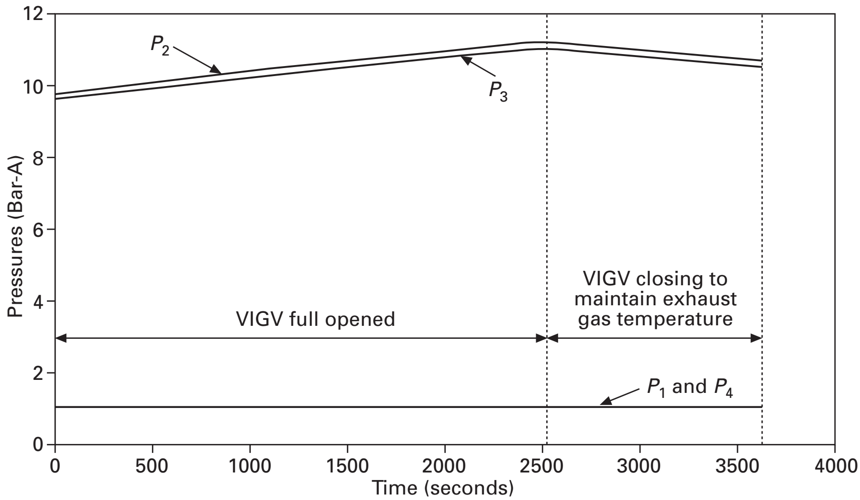

16.18 Trends in pressure during ambient temperature transient.

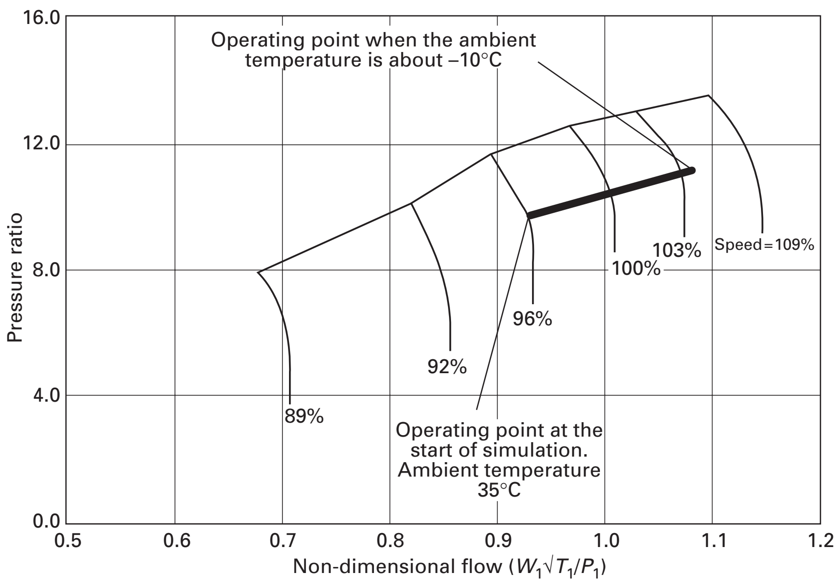

16.19 Operating point on compressor characteristic for period when the VIGV remains open during ambient transient.

which shows the operating point on the compressor characteristic during the period when the VIGV remains fully opened. The VIGV remains fully open until the ambient temperature has decreased to about –10 degrees Celsius. As the ambient temperature falls below this temperature, the VIGV starts to close because otherwise the EGT would fall below the EGT set point for

VIGV control. The closure of the VIGV endeavours to maintain a constant EGT at its corresponding set point as shown in Fig. 16.17. Figure 16.20 shows the change in the compressor characteristic due to the closure of the VIGV and the operating point on the compressor characteristic at the end of this ambient temperature transient. The figure shows the change in compressor speed lines as patches due to the closure of the VIGV. The shift in the compressor surge line due to the closure of the VIGV is also shown. The shift in the surge line is only approximate.

The effect of the VIGV closure on the compressor characteristic is illustrated schematically in Fig. 16.21. The closure of the VIGV shifts the lines of constant non-dimensional speed and the surge line to the left. This results in a reduction in the compressor inlet non-dimensional flow for each compressor non-dimensional speed. The running line is also superimposed on the compressor characteristic. Note that the running line tends to match the compressor characteristic at lower efficiency contours when the VIGV is closed. It must be pointed out that the shift of the surge line due to the closure of the VIGV is generally less distinct at the high speed part of the compressor characteristic. This is because the surge conditions are produced by the stalling of the HP stages rather than by the LP stages at high compressor speeds. At low compressor speeds, it is the stalling of the LP stages that cause surge, and therefore the closure of the VIGV under low speed conditions

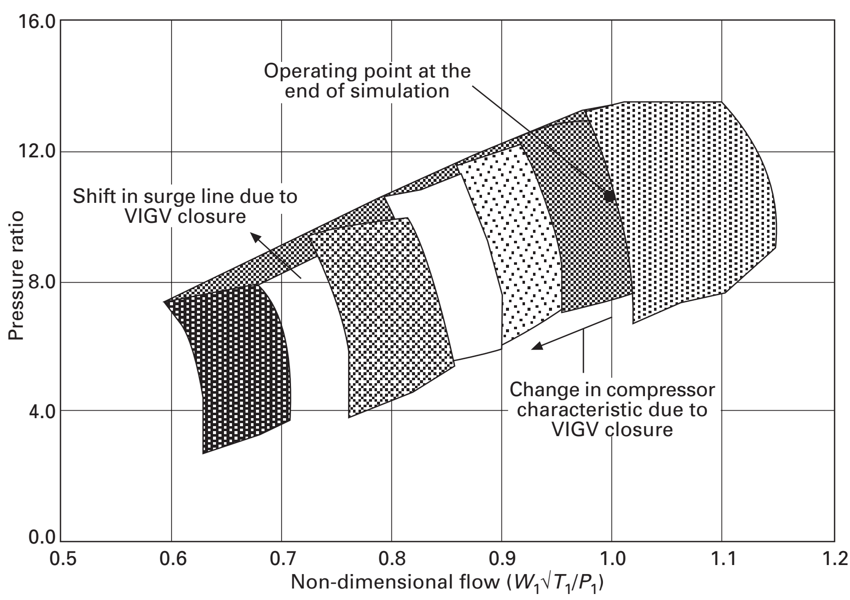

16.20 Operating point on compressor characteristic for period when VIGV closes to maintain constant EGT.

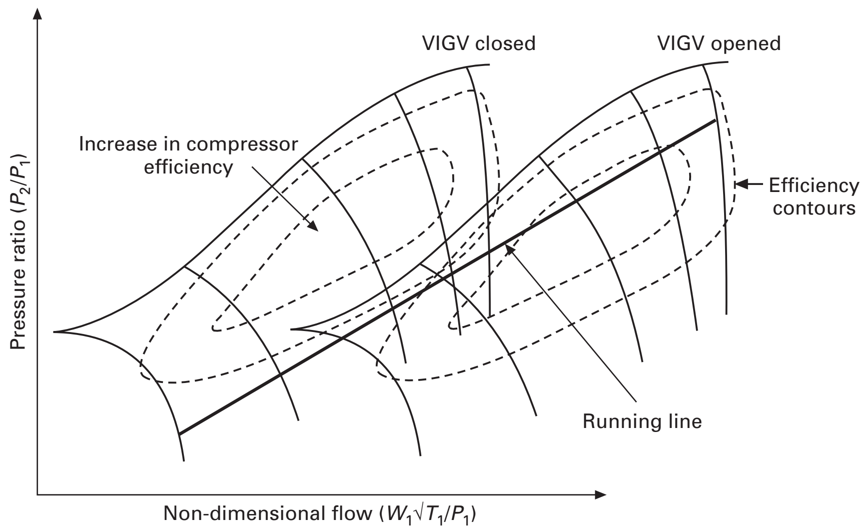

16.21 Shift in the compressor characteristic due to closure of VIGV.

delays stall and results in a greater shift of the surge line to the left-hand side of the compressor characteristic, hence improving the surge margin. This was discussed in Section 4.10.3.

16.3.4 Trends in speed and VIGV position

The constant speed of the gas turbine and the reduction in ambient temperature results in a continuous increase in the compressor non-dimensional speed as observed in Fig. 16.22, which shows the trends in non-dimensional speeds and VIGV position during this transient. The turbine entry temperature, T_3 is also observed to decrease during the period when the VIGV is fully opened, as discussed in Section 16.3.1. Since the gas turbine speed is constant, the turbine non-dimensional speed increases. However, the turbine entry temperature remains essentially constant to maintain a constant EGT during the period when the VIGV closes. Thus the turbine non-dimensional speed remains approximately constant during this period of engine operation.

The figure also shows the trend of the VIGV position. It is observed that VIGV starts to close as the EGT attempts to fall below the temperature set point (650 K) when VIGV control is active. The VIGV is about 43% opened at the end of the ambient temperature transient.

16.3.5 Trends in flow

During the period when the VIGV remains fully open, it is observed that the compressor inlet non-dimensional flow, $W_1\sqrt{T_1}/P_1$, increases. Since the ambient

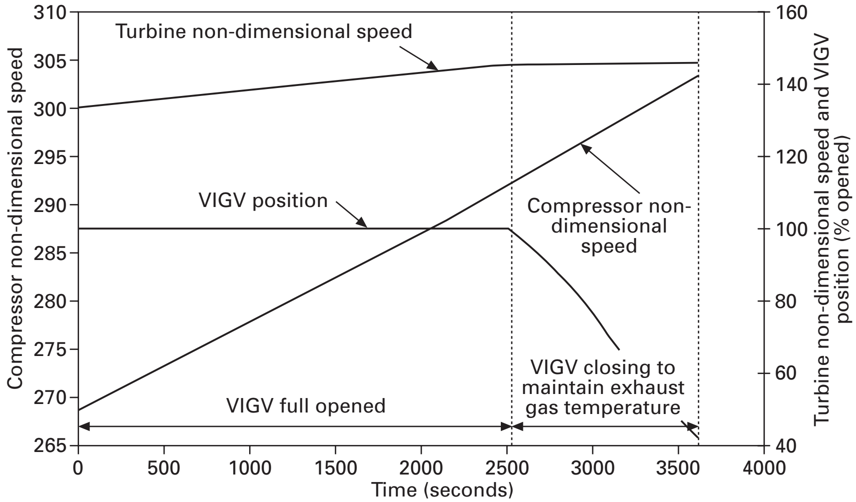

16.22 Trends in non-dimensional speeds and VIGV positions during ambient temperature transient.

temperature, T_1, decreases during this transient, the mass flow rate through the compressor increases. It is also observed that, during the period when the VIGV is fully opened, the compressor pressure ratio increases while the maximum to minimum cycle temperature, T_3/T_1, decreases as shown in Fig. 16.16. The net effect is a small increase in thermal efficiency which is due to the increase in compressor pressure ratio. Since the gas turbine power output remains constant, the increased thermal efficiency results in the fuel flow and the fuel valve position decreasing during this transient. The increase in airflow and the decrease in fuel flow result in an increase in the air–fuel ratio as shown in Fig. 16.23, which displays the trends in flow and fuel valve position for this transient.

In the period when the VIGV closes, the compressor inlet mass flow rate decreases, although the compressor non-dimensional speed continues to increase (Fig. 16.22). There is a decrease in compressor pressure ratio while the maximum to minimum temperature ratio, T_3/T_1, increases. Furthermore, the operating point on the compressor characteristic is in a region where the compressor efficiency is lower (Figure 16.21). The net effect of these changes is that the thermal efficiency remains essentially constant. Since the power output from the gas turbine remains constant during this transient, the fuel flow and fuel valve position also remain constant as seen in Fig. 16.23. Note that compressor airflow and thus combustion airflow decrease slightly while the fuel flow remains constant. Thus the air–fuel ratio decreases slightly during this transient.

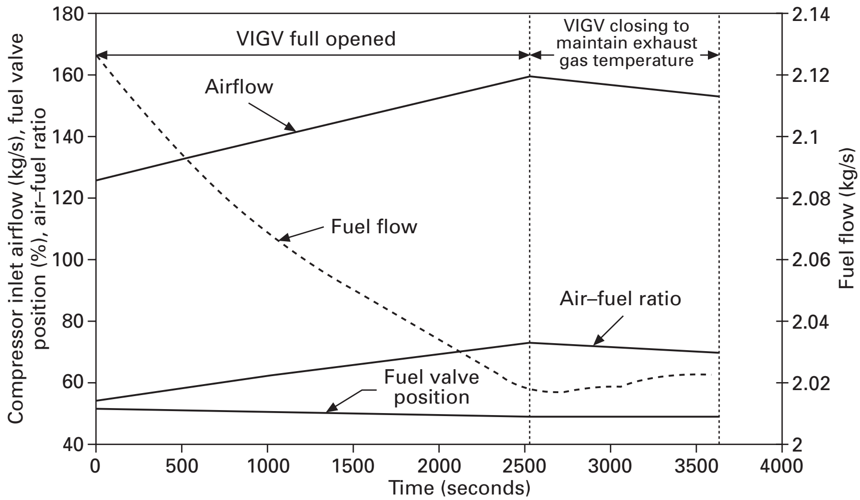

16.23 Trends in flow and fuel valve position due to ambient temperature transient.

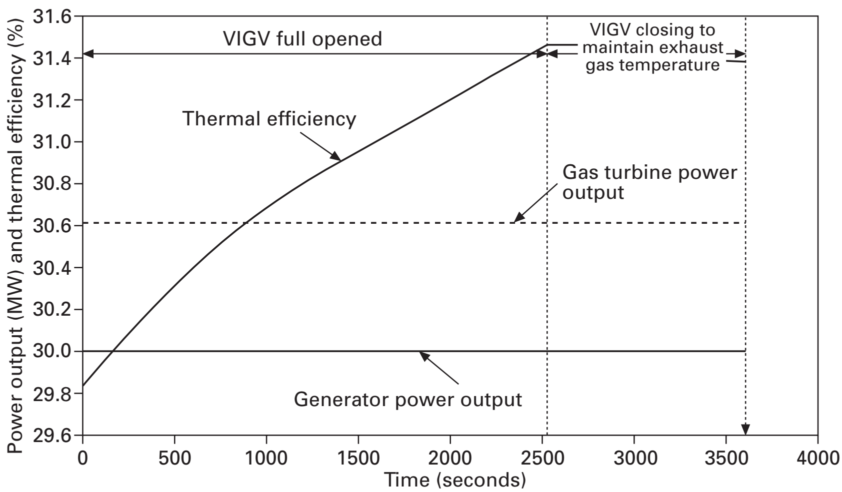

16.24 Trends in gas turbine power output and thermal efficiency during ambient temperature transient.

16.3.6 Trends in power and efficiency

The gas turbine and generator power remain constant because no engine operating limits are exceeded during this transient. The gas turbine thermal efficiency increases during the period when the VIGV is fully opened and remains essentially constant during the period when the VIGV closes. This is explained in Section 16.3.5 and these trends are shown in Fig. 16.24.

The trends in compressor and turbine isentropic efficiencies are shown in Fig. 16.25. There is a slight increase in turbine isentropic efficiency during the period when the VIGV remains fully open, and this effect is associated with the increased turbine non-dimensional speed as shown in Fig. 16.22. During the period when the VIGV closes, the turbine efficiency remains approximately constant and this is due largely to the approximately constant turbine non-dimensional speed during this period of operation.

The trend in the compressor isentropic efficiency shows an increase in the compressor efficiency followed by a decrease during the period when the VIGV is fully opened. As the ambient temperature decreases, the compressor operating point moves through regions on the compressor characteristic where the efficiency is high and then through regions (at low ambient temperatures) where the compressor efficiency is low. This is shown schematically in Fig. 16.21 for the case when the VIGV is fully opened.

During the period of engine operation when the VIGV closes, the compressor efficiency decreases more rapidly and this is due to the compressor operating on the part of the compressor characteristic that is further away from surge as explained in Section 16.3.3. Thus the isentropic efficiency of the compressor is lower in this region and this is also shown in Fig. 16.21 for the case when the VIGV is closed.

The increase in compressor power absorbed (Fig. 16.25), during the period when the VIGV remains fully opened, is due to the increase in mass flow rate through the compressor as shown in Fig. 16.23. Conversely, the decrease in compressor power absorbed during the period when the VIGV closes is due to the decrease in mass flow rate through the compressor as can be seen in Fig. 16.23.

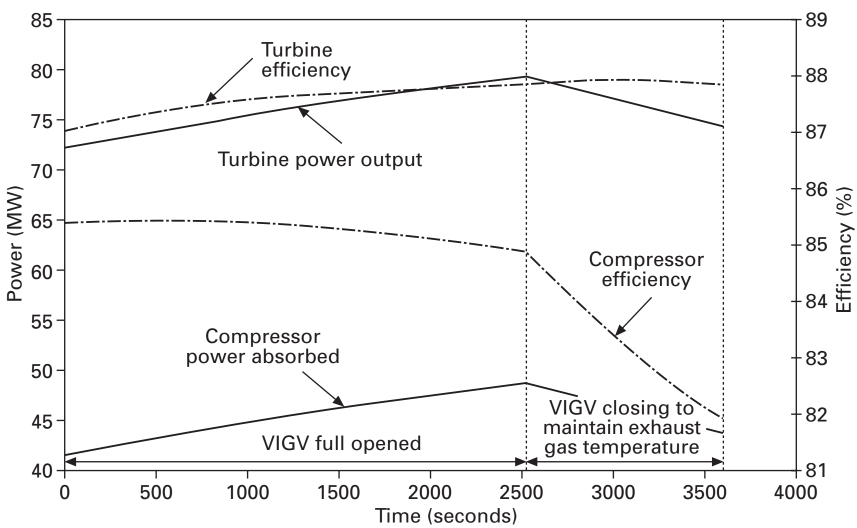

16.25 Trends in compressor and turbine efficiency and power.

Since the power output from the gas turbine remains constant during this transient, the change in compressor power absorbed results in a change in turbine power output to maintain the power compatibility. Thus, the turbine power output increases during the period when the VIGV is fully opened and decreases when the VIGV closes, as is shown in Fig. 16.25.

16.3.7 Trends in turbine creep life

The turbine blade metal temperature decreases during the transient (Fig. 16.17) and this reduction is due to the decrease in the turbine entry temperature, T_3, and compressor discharge temperature, T_2, which is also the cooling air temperature. Although the turbine power output increases and therefore the stress in the turbine increases due to the extra torque, the reduction in turbine blade metal temperature dominates, thus decreasing the turbine creep life usage. This is shown in Fig. 16.26 as an increase in the time to next engine overhaul, which increases to over 500 000 hours, which means that the usage of turbine creep life is minimal during this transient.

16.3.8 Trends in gas turbine emissions

The trends in gas turbine emissions during this transient are shown in Figure 16.27. Although there is an increase in compressor discharge pressure and hence the combustion pressure increases (Fig. 16.18) during the period when the VIGV is fully opened, there is also a reduction in combustion temperature (Fig. 16.17). However, the specific humidity decreases exponentially with

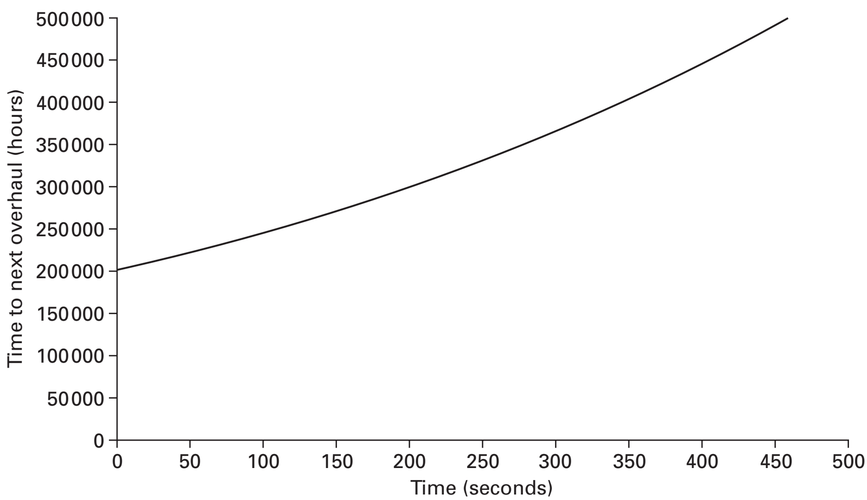

16.26 Trend in turbine creep life usage during ambient temperature transient.

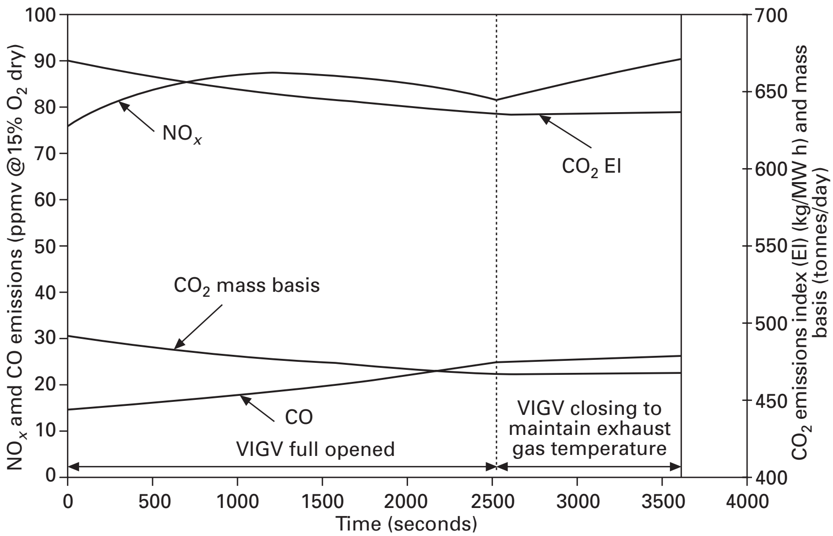

16.27 Trends in gas turbine emissions during ambient temperature transient.

ambient temperature. The net effect is an initial increase in NO_x emissions due to the decrease in specific humidity followed by a decrease in NO_x emissions due to the decrease in combustion temperature. The decrease in combustion temperature results in an increase in CO emissions during the period of operation when the VIGV is fully opened. During the period when the VIGV closes, there is an increase in combustion temperature while the combustion pressure decreases. The ambient temperature when the VIGV closes is also low (about –10 degrees Celsius) and therefore the specific humidity is low. This results in a small increase in NO_x emissions, while the CO emissions remain essentially constant.

There is a decrease in CO_2 emissions during the period when the VIGV remains fully opened due to the increase in the gas turbine thermal efficiency. Since the thermal efficiency is essentially constant during the period when the VIGV closes, the CO_2 emissions also remain approximately constant during this period of engine operation.

16.4 Effect of ambient temperature on engine performance at high power (single-shaft gas turbine operating with an active variable inlet guide vane)

The simulator used to describe the performance of the single-shaft gas turbine in Sections 16.2 and 16.3 assumed that the VIGV remained opened during the normal operating power range (60% to 100%) of the gas turbine. It was stated in Section 16.1 that it is possible to operate the gas turbine when the VIGV is active during the normal operating power range. This is achieved by setting the EGT limit (set point) for VIGV control to that of the maximum EGT limit for the engine. In this case the EGT will remain at the limiting value at low power outputs from the gas turbine provided the VIGV is not fully closed. Such operation of the gas turbine results in approximately constant air to fuel ratio and is a suitable means of implementing dry low emissions (DLE) combustion systems.

While operating at low powers (say 70%) the EGT will be maintained at the maximum/limiting value and the VIGV will be partly closed. Any attempt to increase the power output (greater than 70%) will now require the EGT to exceed its limiting value. The control system will prevent this in order to protect the turbine from overheating. This is achieved by the control system using low signal selection where the lowest error is used to change the fuel flow as discussed in Section 10.2. Thus, it will not be possible to increase the power output of the gas turbine unless some remedial action is taken. One method of overcoming this problem is to employ an open loop control system, when the power demand is increased as discussed in Section 10.4.2. The open loop response has been implemented in the simulator, resulting in the opening of the VIGV fully for a fixed period. During this period the EGT will decrease, thus providing the necessary EGT margin or error (i.e. the difference between the EGT limit and EGT) in the engine control system to increase the fuel flow and thus the power output from the gas turbine. In practice, the EGT limit for VIGV control would also be set to be slightly lower, by say 2 degrees, than the maximum EGT limit. This will prevent unnecessary VIGV operation as the ambient temperature changes during maximum power operation.

The ambient temperature transient has been repeated as described in Section 16.2, where the ambient pressure, inlet and exhaust losses and relative humidity were held constant at 1.013 Bar, 100 mm water gauge and 60% relative humidity. The trends in the parameters discussed are the same during the period when the engine power output is limited by the EGT (i.e. high ambient temperature operation when the VIGV is fully opened). It is only when the engine performance is power limited that the differences in performance are seen when compared with the case discussed in Section 16.2 above.

16.4.1 Trends in temperature

As stated above, the trends in temperature during the period when the EGT limits the power output from the gas turbine are the same as those shown in Fig. 16.8. When the engine is limited by power output, and the VIGV closes

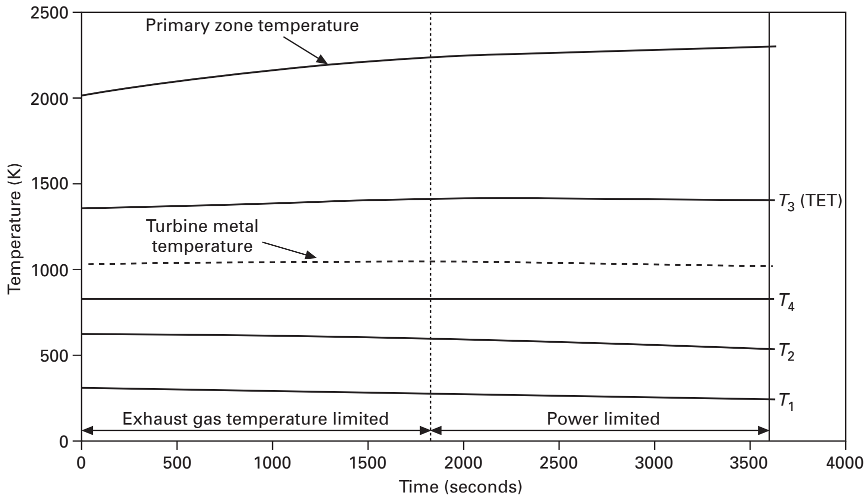

16.28 Trends in temperature during the ambient temperature transient when VIGV is operational at normal operating power range.

to maintain the EGT, the trends in temperature now differ from those shown in Fig. 16.8. Accordingly, it is observed that the EGT remains constant throughout the transient, as shown in Fig. 16.28.

The closure of the VIGV also results in an increase in the combustion temperature, whereas the combustion temperature falls when the VIGV is fully opened, as is shown in Fig. 16.8. Similarly, the turbine entry temperature, T_3, remains essentially constant during the period when the VIGV closes. The compressor discharge temperature decreases for the reason given in Section 16.2.2. Due to a higher turbine entry temperature, T_3, as the VIGV closes, there is a smaller decrease in the turbine blade metal temperature compared with the case when the VIGV remains opened (Fig. 16.8).

16.4.2 Trends in speed and VIGV position

The effect of the closure of the VIGV during the period when the gas turbine performance is power limited can be seen in Fig. 16.29. The VIGV closes from 100% to about 15% at the end of the ambient transient. The figure also shows the change in the compressor and turbine non-dimensional speed during this transient. The increase in compressor non-dimensional speed is similar to that discussed in Section 16.2.6. The turbine non-dimensional speed remains essentially constant because the turbine entry temperature remains virtually constant during this transient.

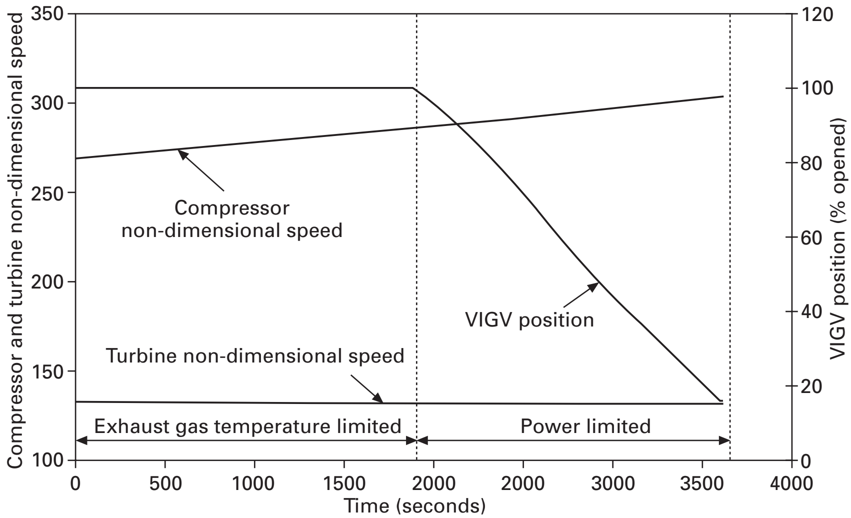

16.29 Trends in non-dimensional speed and VIGV position during ambient temperature transient.

16.4.3 Trends in temperature ratio and pressure ratio

When the VIGV closes, the trends in temperature and pressure ratios differ from the case described in Section 16.2.1. It is observed that the compressor and thus the turbine pressure ratio decrease during the period when the engine is power limited, resulting from the closure of the VIGV, as shown in Fig. 16.30. It is also observed that the maximum to minimum cycle temperature ratio increases due to the turbine temperature, T_3, remaining constant while the ambient temperature and thus the compressor inlet temperature decreases.

The decrease in pressure ratio is necessary to satisfy the flow compatibility between the compressor and turbine as discussed in Section 16.3.1, where a similar response was observed from the engine when the VIGV closes at low ambient temperatures and low power outputs to maintain the EGT on its set point for VIGV control.

16.4.4 Trends in power, efficiency and compressor characteristic

The trend in power output from the gas turbine is the same as discussed in Section 16.2.1. The trend in the thermal efficiency of the gas turbine is, however, different during the period when the engine reaches the power limit. This can be seen in Figure 16.31, where the thermal efficiency remains essentially constant during this period. It is observed in Figure 16.30 that the compressor pressure ratio decreases while the maximum to minimum cycle

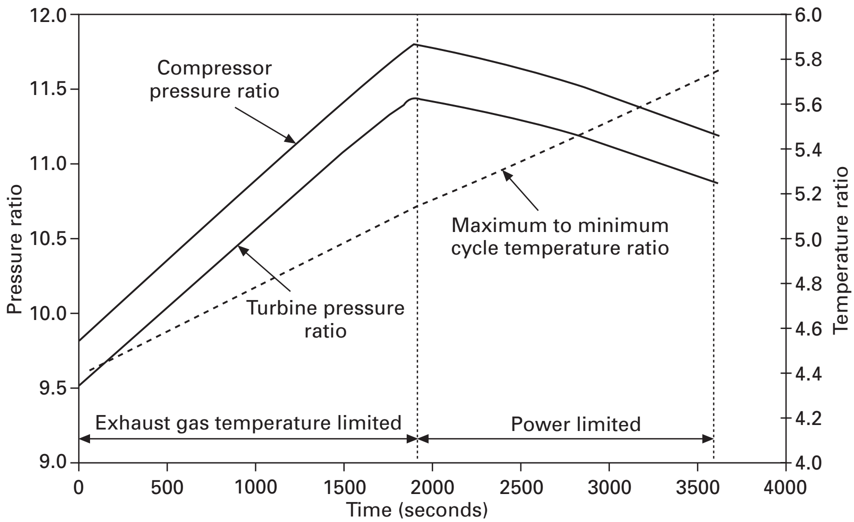

16.30 Trends in pressure and temperature ratios during ambient temperature transient.

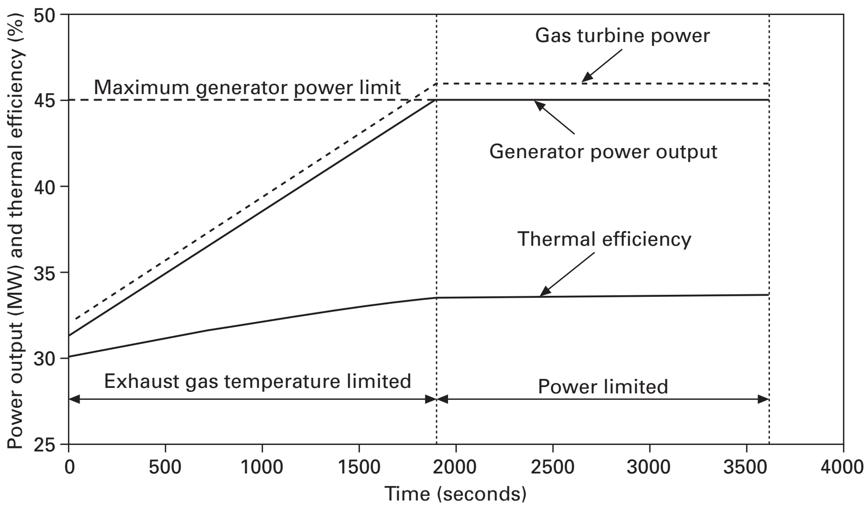

16.31 Trends in power output and thermal efficiency.

temperature, T_3/T_1, increases when the power output limits the engine performance. There is also a decrease in the compressor isentropic efficiency as the VIGV closes and this is explained in Section 16.3.3. The net effect of these factors results in virtually no change in thermal efficiency during this period of engine operation.

Figure 16.32 shows the trends in the compressor and turbine powers and isentropic efficiencies. Again, it is the period when the engine power limit is reached that is of interest. The compressor power is observed decreasing as the VIGV closes and this is largely due to a reduction in mass flow rate through the compressor. A reduction in turbine power output also results, in order to maintain the power output from the gas turbine at its limiting value of 45 MW. The compressor efficiency is observed to reduce and this is associated with the closing of the VIGV as explained in Section 16.3.3. The trend in turbine isentropic efficiency is similar to the case described in Section 16.2.1, where the turbine efficiency remains essentially constant. This is due to approximately constant turbine non-dimensional speed (Fig. 16.29).

The performance of the gas turbine when the engine power output is limited by the EGT is not different to that discussed in Section 16.2.1. Thus the movement of the operating point on the compressor characteristic is the same as that shown in Fig. 16.1 when the VIGV remains fully opened. It is only when the gas turbine becomes power limited that the difference in compressor performance is seen, which is due to the closure of the VIGV in order to maintain the exhaust gas temperature on its set point. This results in the change of the compressor characteristic as shown in Fig. 16.33. It is similar to that discussed in Section 16.3.3, when the EGT decreased below the EGT set point for VIGV movement, which was then set at 650 K.

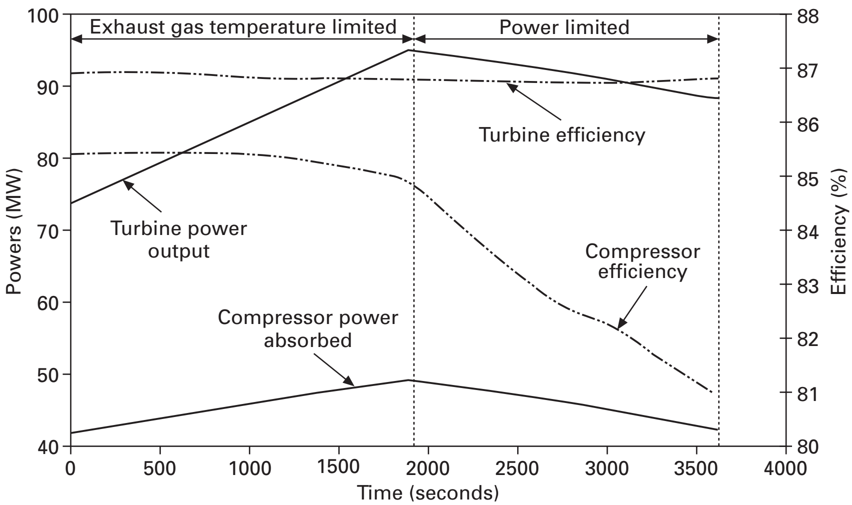

16.32 Trends in compressor and turbine power and isentropic efficiency during transient when VIGV operates during normal operating power range.

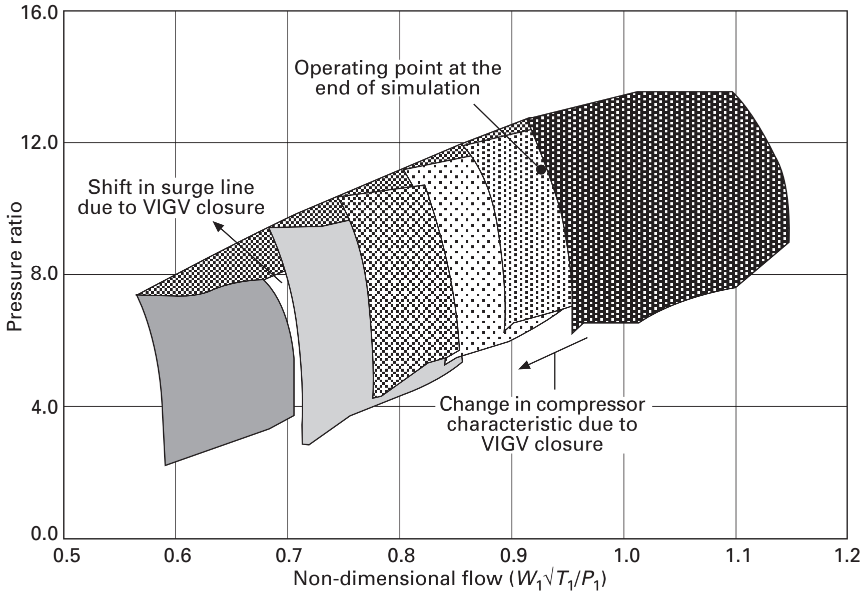

16.33 Change in compressor characteristic due to VIGV closing.

16.4.5 Trends in flow

During the period when the power limit of the gas turbine is reached, the compressor flow decreases due to the closure of the VIGV (Fig. 16.34). The fuel flow and the fuel valve position remain essentially constant due to the thermal efficiency remaining approximately constant as shown in Fig. 16.31. The small decrease in compressor air flow and approximately constant fuel flow results in a slight decrease in the air–fuel ratio.

16.4.6 Trends in pressure

The trends in pressure during this transient are shown in Figure 16.35. During the period after the gas turbine power limit is reached, the compressor discharge and turbine inlet pressures decrease. This is due to the decrease in the compressor pressure ratio, as shown in Fig. 16.30, in order to satisfy the flow compatibility between the compressor and turbine.

16.4.7 Trends in turbine creep life

The trend in turbine creep life usage is similar to the case when the VIGV remains fully open, as discussed in Section 16.2.4. However, the turbine creep life usage is greater during the period of constant power output, as

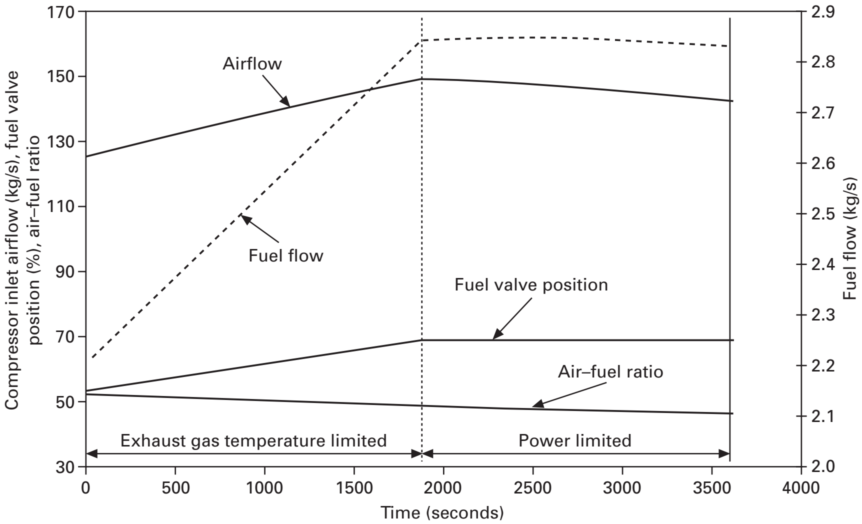

16.34 Trends in flow during temperature transient when VIGV closes at low ambient temperatures.

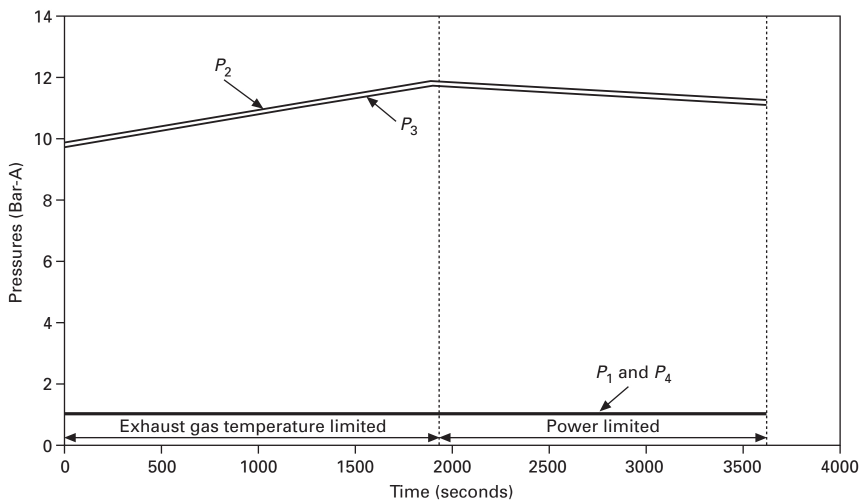

16.35 Trends in pressure during temperature transient where VIGV closes at low ambient temperatures.

shown in Fig. 16.36. This is due primarily to the higher turbine entry temperature during this period of engine operation, resulting in higher turbine blade metal temperatures, as shown in Fig. 16.28.

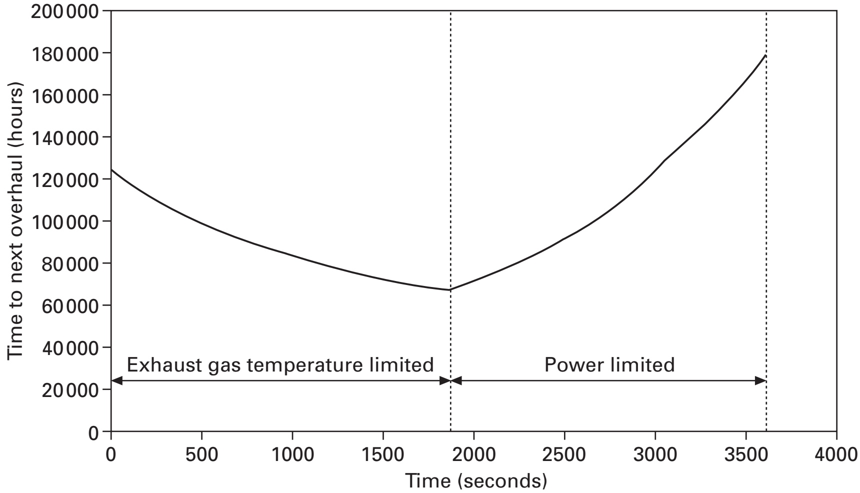

16.36 Trends in turbine creep life usage during temperature transient where VIGV closes at low ambient temperatures.

16.4.8 Trends in gas turbine emissions

Although the combustion pressure decreases during the period when the gas turbine power limits the performance of the engine, the combustion temperature increases during this period of operation (Fig. 16.28). The increase in combustion temperature is sufficient to result in an increase in NO_x. CO emissions, however, remain approximately constant, whereas an increase in CO was previously observed during the period of constant power operation (Fig. 16.12). This is due to the higher primary zone temperature compared with the previous case (Fig. 16.8). The emissions of CO_2 on a mass flow basis and as an emission index remain essentially constant during the period when the gas turbine is power limited. This is because the thermal efficiency does not vary much during this period, as shown in Figure 16.31. These trends in emissions are shown in Fig. 16.37.

This simulation may be repeated at lower powers when no engine operating limit is reached. The results will be similar to that discussed when the engine is operating on a power limit. However, at lower powers, the VIGV will close further, in order to maintain the EGT on the control set point, and may become fully closed, depending on the power demand from the generator and the change in the ambient temperature during the transient. The reader is left to carry out these simulations and confirm the similarity.

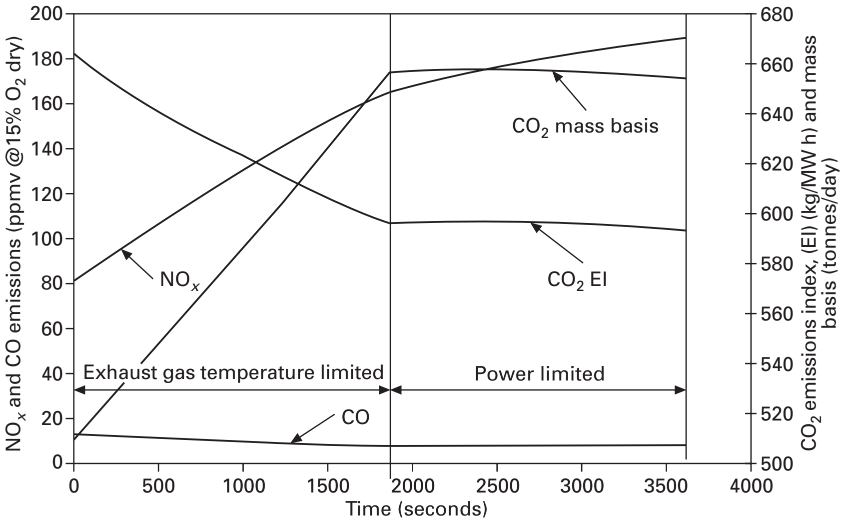

16.37 Trends in gas turbine emissions during temperature transient where VIGV closes at low ambient temperatures.

16.5 Effect of humidity on gas turbine performance and emissions

In Chapter 2, it was stated that it is the specific humidity that affects the performance of gas turbines. Also the effects of humidity on emissions have been discussed, particularly on NO_x. Increasing the specific humidity increases the gas constant, R, and specific heat at constant pressure, c_p, while the ratio of specific heats, γ, decreases. These trends are shown in Fig. 11.30, which shows the variation of these gas properties with specific humidity. The variation in γ is also observed to be small compared with c_p and R. These issues were discussed and illustrated for a two-shaft gas turbine operating with a free power turbine in Chapter 11, Section 11.5. The impact of humidity on the performance and emissions of a single-shaft gas turbine are now considered.

At any given ambient temperature and pressure, an increase in relative humidity increases the specific humidity. This results in an increase in the gas constant, R, and specific heat at constant pressure, c_p, for air, while decreasing its isentropic index, γ. As stated in Section 11.5, the increase in R and c_p is greater than γ. For Equation 2.19 in Chapter 2, which describes the specific work of an ideal gas turbine cycle, it is seen that the specific work is directly proportional to the specific heat at constant pressure, c_p. For a given compressor ratio and maximum to minimum cycle temperature ratio, T_3/T_1, any increase in humidity will increase the specific work of the gas turbine cycle. This is due to the corresponding increase in c_p. However, the compressor non-dimensional speed, $N_1/\sqrt{(\gamma_1 R_1 T_1)}$ decreases due to the increase the increase in R (note the compressor speed is constant for the single-shaft gas turbine. Also, only the effect of humidity is being considered and thus a constant ambient pressure P_1 and temperature T_1 are assumed).

The increase in humidity will therefore result in the compressor operating at a lower speed on the compressor characteristic. The decrease in compressor non-dimensional speed will also decrease the compressor non-dimensional flow $\dfrac{W_1\sqrt{R_1 T_1/\gamma_1}}{P_1}$. The decrease in compressor non-dimensional flow and the increase in the gas constant, R_1, due to the increase in humidity, will result in a decrease in the airflow rate through the compressor. As discussed earlier in the chapter, the decrease in the compressor non-dimensional flow will also decrease the maximum to minimum temperature cycle temperature ratio, T_3/T_1. Although the increase in c_p due to the increase in humidity increases the specific work, the decrease in T_3/T_1 will decrease the specific work. The decrease in airflow rate through the compressor will also reduce the power output from the gas turbine. The net effect of these changes is a small decrease in power output due to the increase in humidity. This is illustrated in Fig. 16.38, which shows the variation of gas turbine power output with ambient temperature for relative humidity zero and 100%. The effect of humidity on the thermal efficiency of a single shaft gas turbine is illustrated in Figure 16.39. The decreases in the parameters that decrease the power output also contribute to a lower thermal efficiency. The decrease in compressor pressure due to the decrease in compressor non-dimensional speed, and the heat addition due to the increased water content of the air, also contribute to a lower thermal efficiency.

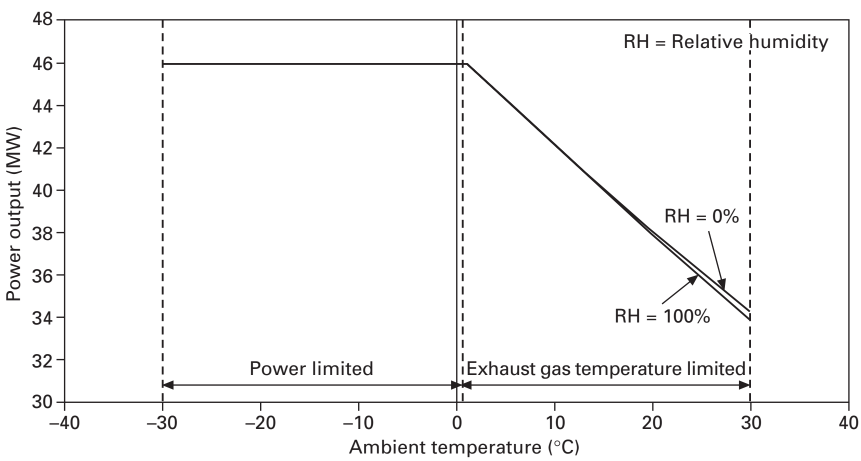

16.38 Effect of relative humidity on gas turbine power output.

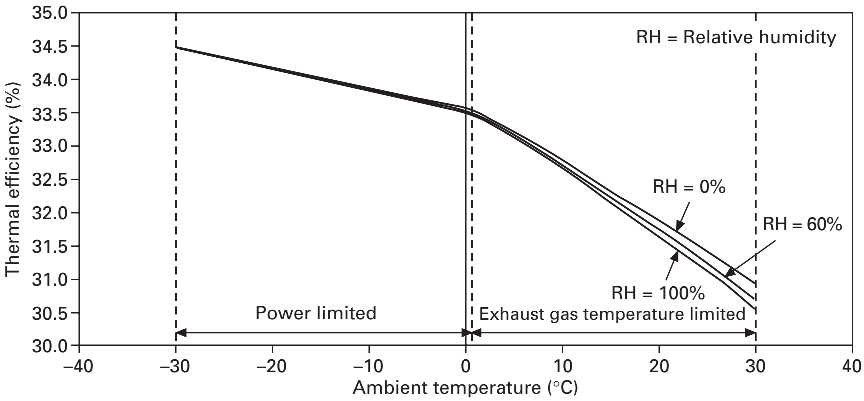

16.39 Effect of relative humidity on gas turbine thermal efficiency.

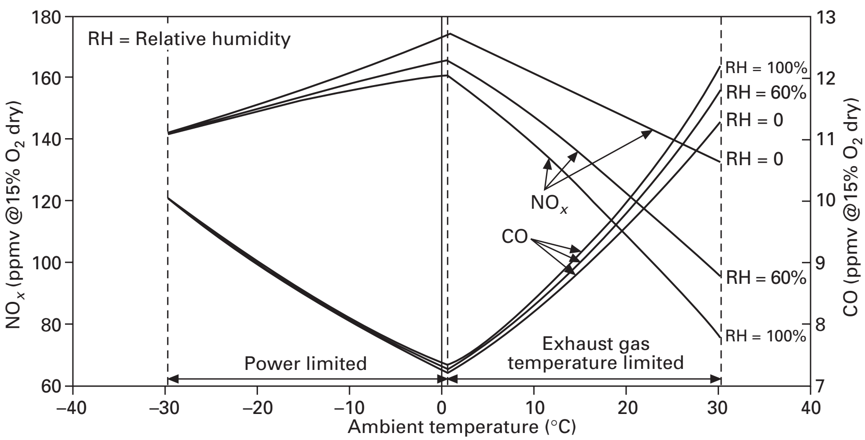

16.40 Effect of relative humidity on gas turbine emissions.

At high ambient temperatures, when the EGT limits the power output of the gas turbine, the effect of humidity on gas turbine power output differs from the two-shaft gas turbine operating with a free power turbine, which shows a worthwhile increase in power output from the gas turbine with humidity, particularly at high ambient temperatures. However, the impact of thermal efficiency is similar.

The impact of humidity on NO_x emissions is more profound. High specific humidity results in increased presence of water vapour in the combustor, thus suppressing the ‘peak’ combustion temperature. This decrease in temperature results in a significant decrease in NO_x with the increase in humidity, as illustrated in Fig. 16.40.

17

Simulating the effect of change in ambient pressure on engine performance

The impact of the change in ambient temperature on engine performance was considered in Chapter 16, where the negative impact of high ambient temperatures on performance was observed. Another factor that affects engine performance is the ambient pressure. The single-shaft gas turbine simulator will now be used to investigate the effects of the change in ambient pressure on engine performance. The ambient pressure may change quite significantly at a given elevation. At sea level it may vary from 1.04 Bar to 0.96 Bar for a high pressure and a low pressure day, respectively. This represents about an 8% change in ambient pressure corresponding to these days. Gas turbines that operate at high elevations, where the ambient pressure is lower than at sea level, will show a reduced power output. For example, at an elevation of 1000 metres, the ambient pressure would be about 0.9 Bar on an ISA (International Standard Atmosphere) day. However, the ambient temperature at this altitude will be lower in general, thus partly compensating for the reduced power output.

To cover this ambient pressure range, the ambient pressure will be varied from 1.03 Bar to 0.9 Bar in 1 hour (3600 seconds). Two operating cases will also be considered, which correspond to a high-power and low-power operating condition. The high-power operating condition will be represented by setting the power demand from the generator such that the engine will always be on an operating limit. Conversely, the low-power case will be simulated by setting the power demand from the generator such that an engine operating limit is never reached. Since the impact of ambient pressure changes on engine performance is to be investigated, it will be assumed that the ambient temperature remains constant at 15 degrees Celsius. This results in the engine power output being limited by the exhaust gas temperature (EGT) limit rather than by the power limit from the gas turbine. The inlet and exhaust losses will be ignored during these simulations.

Again, the gas property terms from the various non-dimensional parameters will be omitted for simplicity but reference will be made to them when relevant.

17.1 Effect of ambient pressure on engine performance at high power

In this section the change in gas turbine performance due to the ambient pressure transient will be considered when the engine is operating at high power. A constant ambient temperature of 15 degrees Celsius has been selected and therefore the power output from the gas turbine is always limited by the exhaust gas temperature during this transient.

17.1.1 Compressor characteristic

Since the gas turbine speed and the compressor inlet temperature remain constant (constant ambient temperature), the compressor non-dimensional speed, $N_1/\sqrt{T_1}$, will also remain constant. If it is assumed that the turbine entry temperature, T_3, is constant, then the maximum to minimum cycle temperature, T_3/T_1, will remain constant. For a given compressor non-dimensional speed, the compressor inlet non-dimensional flow, $W_1\sqrt{T_1}/P_1$, will not vary very much with compressor pressure ratio, due to nearly vertical speed lines. Furthermore, the choked conditions that prevail in the turbine will maintain a constant turbine inlet non-dimensional flow, $W_3\sqrt{T_3}/P_3$. To satisfy the flow compatibility Equation 8.1, the compressor pressure ratio will also be nearly constant. A constant compressor ratio also implies an approximately constant turbine pressure ratio and a constant compressor exit temperature, T_2. If operation is at a constant turbine entry temperature, the exhaust gas temperature (EGT) will also be constant.

Since the engine performance is limited by the EGT (high-power case), from the above analysis, any decrease in the ambient pressure and thus compressor inlet pressure, P_1, will not have any effect on the operating point on the compressor characteristic, provided an EGT limit is maintained as the ambient pressure changes. This can be seen in Fig. 17.1, which shows the operating point on the compressor characteristic during this transient. Since the compressor pressure ratio and the maximum to minimum cycle temperature ratio is fixed, from Equation 2.20, the specific work output from the gas turbine cycle will also remain constant.

17.1.2 Trends in power and efficiency

As the compressor inlet non-dimensional flow, $W_1\sqrt{T_1}/P_1$, remains constant during this transient, the compressor air flow rate decreases proportionally with the ambient pressure. Since the specific work does not change with ambient pressure, a decrease in air flow rate results in a decrease in power output from the gas turbine and thus from the generator. This can be seen in

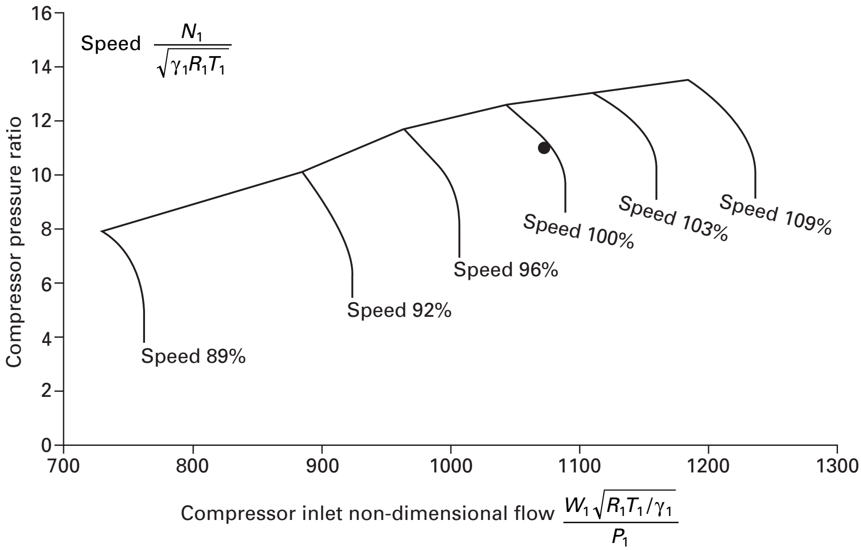

17.1 Operating point on compressor characteristic during ambient pressure transient.

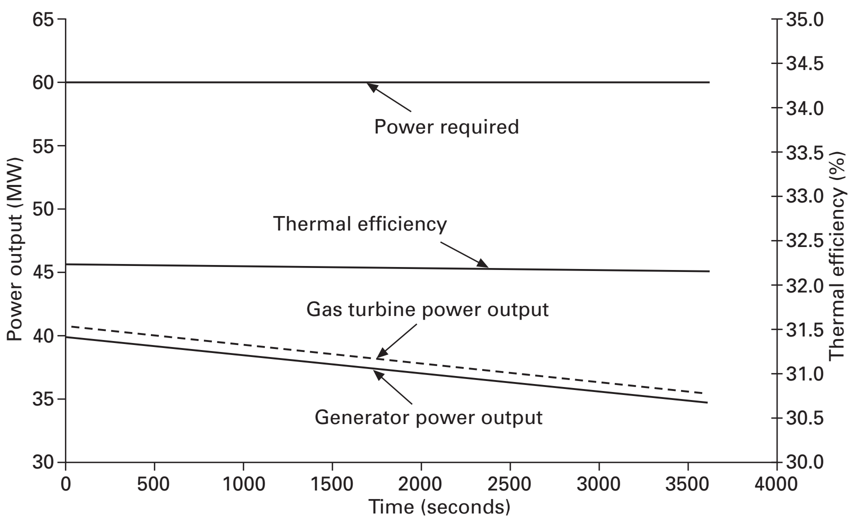

17.2 Trends in power output and thermal efficiency during ambient pressure transient.

Fig. 17.2, which shows the trends in power output from the gas turbine and the generator. As the thermal efficiency is dependent largely on the compressor pressure ratio and the maximum to minimum cycle temperature ratio, and as these parameters remain constant during this transient, the thermal efficiency of the gas turbine also remains nearly constant during this transient. This can be seen in Fig. 17.2, which also shows the trend in the thermal efficiency of the gas turbine during this transient. The slight decrease in thermal efficiency is due primarily to the slight increase in specific humidity as the ambient pressure decreases.

Since the compressor pressure ratio and consequently the turbine pressure ratio remain constant, the power associated with these components also decreases due to the reduction in mass flow rate through these components. This can be seen in Fig. 17.3, which shows the trends in the powers associated with the compressor and turbine. As the operating points on the compressor and turbine characteristics do not change very much, their efficiencies also remain constant during this transient as shown in Fig. 17.3.

17.1.3 Trends in pressure

The constant pressure ratios that prevail in the compressor and turbine result in a decrease in the compressor discharge pressure and in the turbine inlet pressure. The decrease in these pressures is proportional to the decrease in the ambient pressure during this transient, as shown in Fig. 17.4. The figure also shows the trends in compressor inlet pressure and the turbine exit pressure. The decrease in these pressures is due to the introduction of the ambient pressure transient.

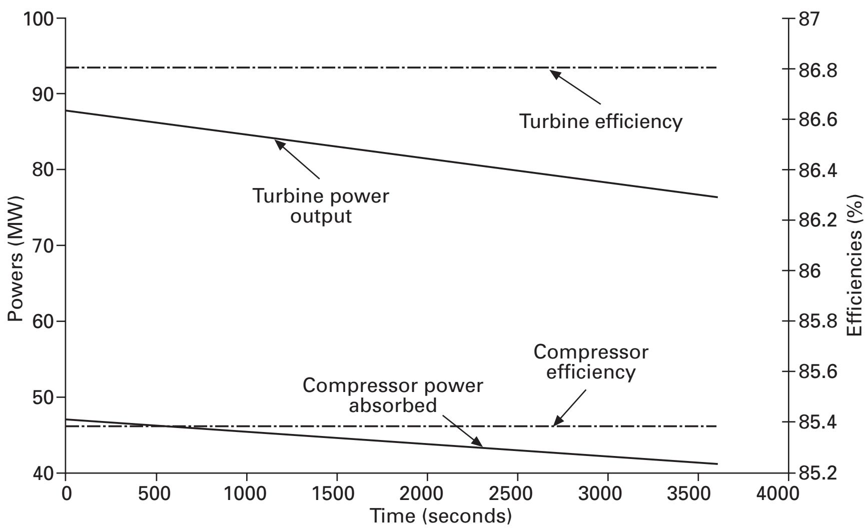

17.3 Trends in power and isentropic efficiency associated with compressor and turbine during ambient pressure transient.

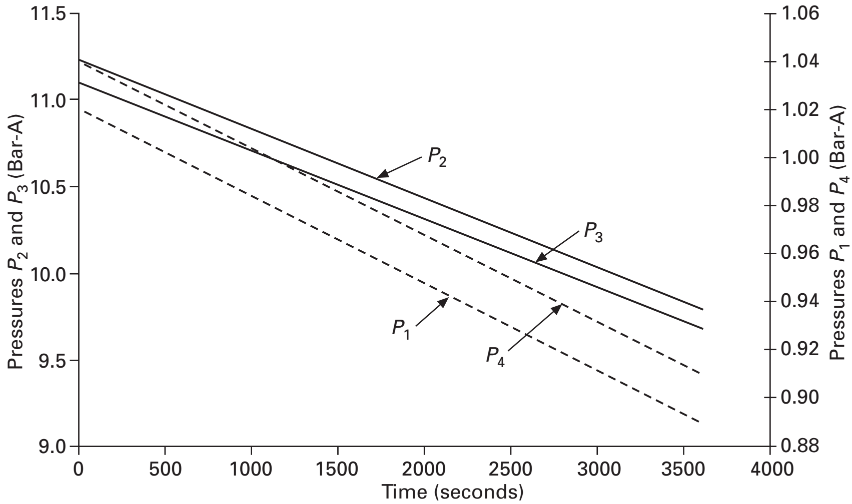

17.4 Trends in pressure during the ambient pressure transient.

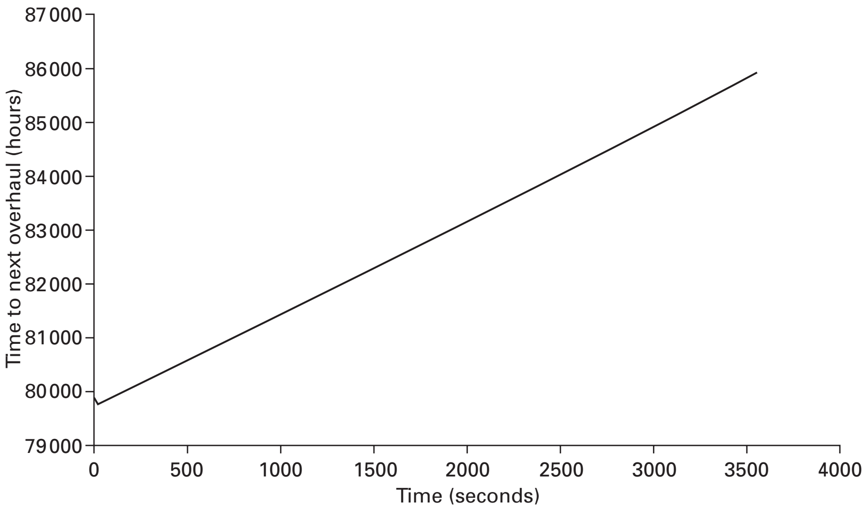

17.5 Trend in turbine creep life usage during ambient pressure transient.

17.1.4 Trends in creep life

Figure 17.5 shows the trend in turbine creep life usage during this transient. It has been stated that the ambient temperature does not change during this transient and therefore the turbine entry temperature, T_3, and the turbine cooling air temperature, T_2, remain constant. Thus the turbine blade metal temperature also remains constant during this transient. Since the gas turbine speed is constant, the radial stress will not vary. However, we see that the turbine power output decreases due to the reduction in the mass flow rate through the turbine. This results in a decrease in stress in the turbine blade material due to the reduced torque. The consequent reduction in the stress and the constant blade metal temperature result in a slight decrease in the turbine creep life usage as illustrated in Fig. 17.5, which shows the trend in the turbine creep life usage as time to next overhaul.

17.1.5 Trends in flow

The reduction in the mass flow rate due to the decrease in the ambient pressure is shown in Fig. 17.6. The figure also shows the trend in the fuel flow rate during this transient. Since the power output from the gas turbine decreases and the thermal efficiency remains approximately constant, the fuel flow decreases. Consequently, the fuel valve position also decreases due to the reduction in fuel flow. Since the temperature rise across the combustor remains constant, the air–fuel ratio also remains constant, as shown in Fig. 17.6.

17.1.6 Trends in emissions

The constant combustion temperatures and the decrease in the compressor discharge pressure referred to above, and thus the combustion pressure,

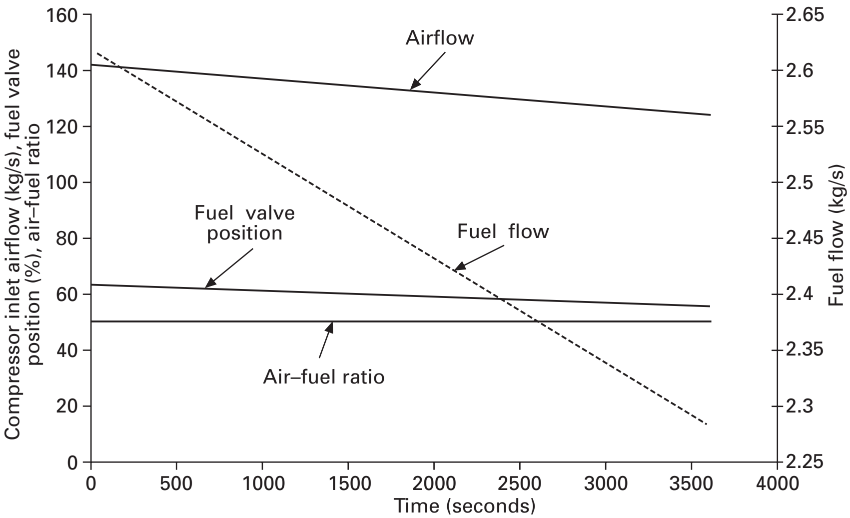

17.6 Trends in flow and air-to-fuel ratio during ambient pressure transient.

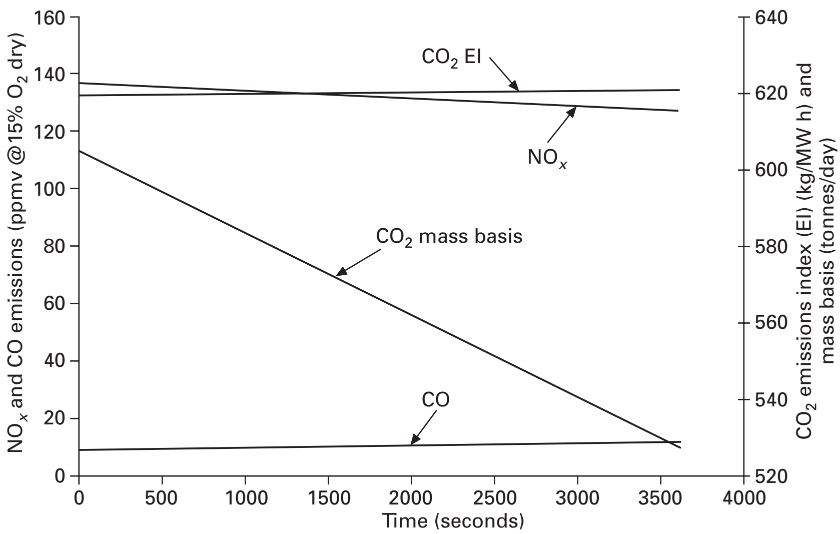

17.7 Trends in gas turbine emissions due to ambient pressure transient.

result in a decrease in NO_x but an increase in CO during this transient, as shown in Fig. 17.7. The decrease in fuel flow causes a decrease in the mass flow rate of CO_2, which is proportional to the decrease in fuel flow as shown in Fig. 17.7. The CO_2 emissions index remains constant because the thermal efficiency remains constant. Thus there is no change in CO_2 emission per unit of power produced.

17.2 Effect of ambient pressure on engine performance at low power

Simulating the effect of the change in ambient pressure at low operating power is based on the same assumptions as were stated as in Section 17.1. However, the power demand from the generator is reduced to 34 MW, ensuring that no engine operating limits will be encountered during the ambient pressure transient.

It has been seen that the decrease in ambient pressure results in a decrease in power output from the gas turbine when the engine is subjected to an engine operating limit as discussed in Section 17.1. When the engine is operating at a reduced power output, the specific work increases to compensate for the decrease in mass flow rate due to the decrease in ambient pressure, such that the power output remains constant. This is possible because the engine is not constrained by an operating limit such as the exhaust gas temperature (EGT). The increase in specific work results in an increase in the maximum to minimum temperature ratio, T_3/T_1. The increase in T_3/T_1 also increases the compressor pressure ratio to satisfy the flow compatibility between the compressor and the turbine. The increase in these parameters then raises the thermal efficiency of the gas turbine.

17.2.1 Compressor characteristic

The necessity to increase the specific work to maintain the power demand from the generator results in an increase in the maximum to minimum cycle temperature ratio and thus compressor pressure ratio. As the gas turbine speed and the compressor inlet temperature remain constant, the operating point on the compressor characteristic is forced to operate at a constant compressor non-dimensional speed, $N_1/\sqrt{T_1}$. Thus the increase in compressor pressure ratio is achieved by the operating point moving up the constant non-dimensional speed line on the compressor characteristic, as shown in Fig. 17.8.

17.2.2 Trends in pressure ratio and temperature ratio

The increase in compressor pressure ratio is shown as a trend in Fig. 17.9. The figure also shows the trend in the maximum to minimum cycle temperature ratio, T_3/T_1. It has been stated that the increase in specific work results in an

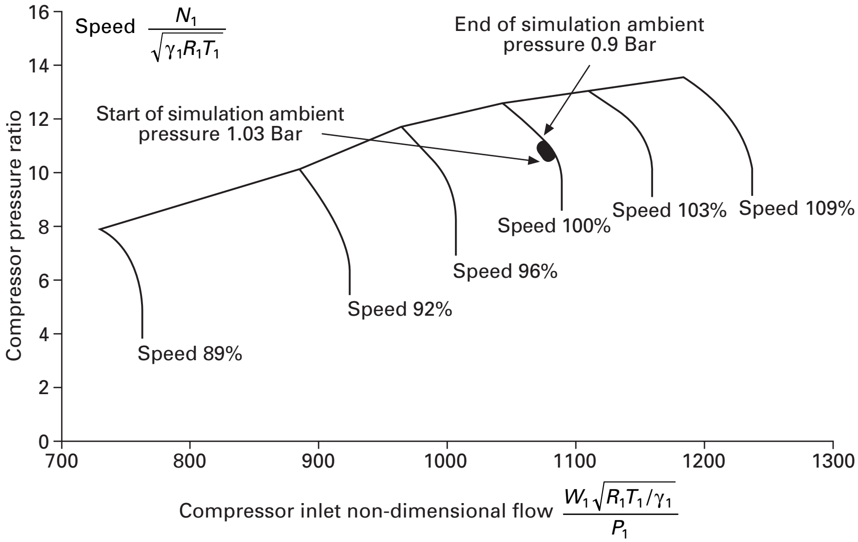

17.8 Operating point on compressor characteristic during ambient pressure transient.

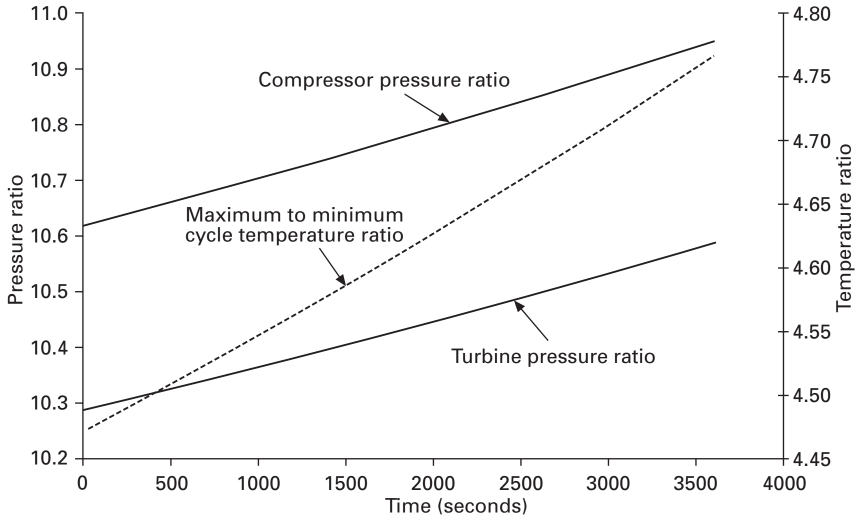

17.9 Trends in pressure and temperature ratios during ambient pressure transient.

increase in turbine entry temperature, T_3. Since the ambient temperature, thus the compressor inlet temperature, T_1, is constant, T_3/T_1 will increase. Since the turbine is choked and the speed line on the compressor characteristic is steep, the compressor and turbine inlet non-dimensional flows remain essentially constant. If a constant combustion pressure loss is assumed, then, from Equation 8.1, any increase in T_3/T_1 must result in an increase in the compressor pressure ratio, P_2/P_1. Thus an increase in P_2/P_1 is seen as the ambient pressure falls (see Fig. 17.9). The figure also shows the trend in turbine pressure ratio, which is similar to that of the compressor pressure ratio.

17.2.3 Trends in power and efficiency

The increases in the compressor pressure and temperature ratios result in an increase in the thermal efficiency, as seen in Fig. 17.10. Thus, low ambient pressures are beneficial when the power demand from the gas turbine does not subject it to an engine operating limit. A similar conclusion was drawn when the ambient pressure transient was considered using the two-shaft gas turbine simulator (Section 12.2). The principle of the closed cycle gas turbine was also discussed, where the system pressure is varied to reduce the power output of the gas turbine while maintaining the thermal efficiency. Closed cycle gas turbines are equally applicable to single-shaft gas turbines and were first implemented using such an engine configuration.

Figure 17.10 also shows the trends in the gas turbine and generator power

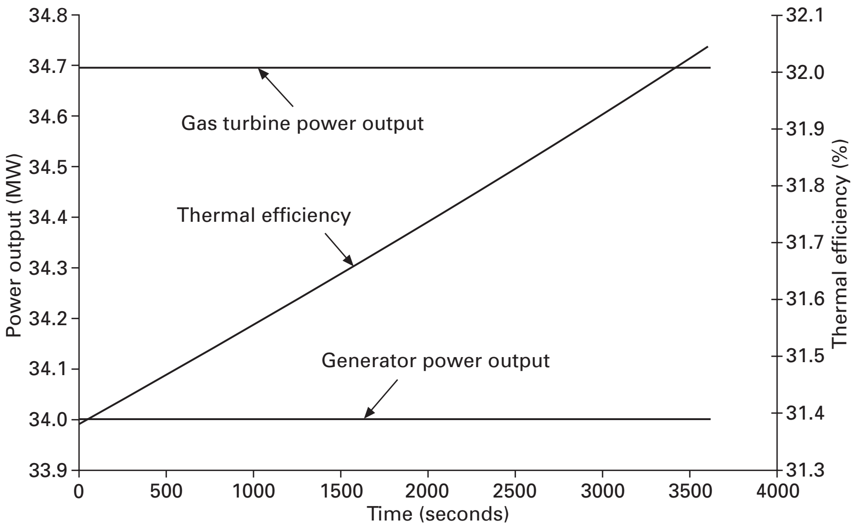

17.10 Trends in power output and thermal efficiency during ambient pressure transient.

outputs. These remain constant because the engine is not subjected to an operating constraint. Since the compressor is constrained to operate at a constant compressor non-dimensional speed, the compressor non-dimensional temperature rise, $\Delta T_{21}/T_1$ also remains approximately constant, as discussed in Section 8.1.1. Therefore, for a given compressor inlet temperature, T_1, the compressor temperature rise, ΔT_{21} will be approximately constant. Thus the decrease in the compressor mass flow rate results in a decrease in the compressor power absorbed. This can be seen in Fig. 17.11, which shows the trend in the compressor power absorbed during the ambient pressure transient. As the power output from the gas turbine remains constant, the power developed by the turbine section/component also falls, to maintain the power demand from the generator as shown in Fig. 17.11.

The trends in compressor and turbine isentropic efficiency are also shown in Fig. 17.11. The small movement of the operating point on the compressor characteristic results in little or no change in the compressor efficiency. The turbine efficiency also shows a similar trend, and the small fall in turbine efficiency is associated with the small decrease in the turbine non-dimensional speed due to the increase in T_3 as the ambient pressure falls.

17.2.4 Trends in flow

The trends in flows, air–fuel ratio and the fuel valve position during this transient are shown in Fig. 17.12. The decrease in air flow rate is due to the decrease in ambient pressure and near constant compressor non-dimensional

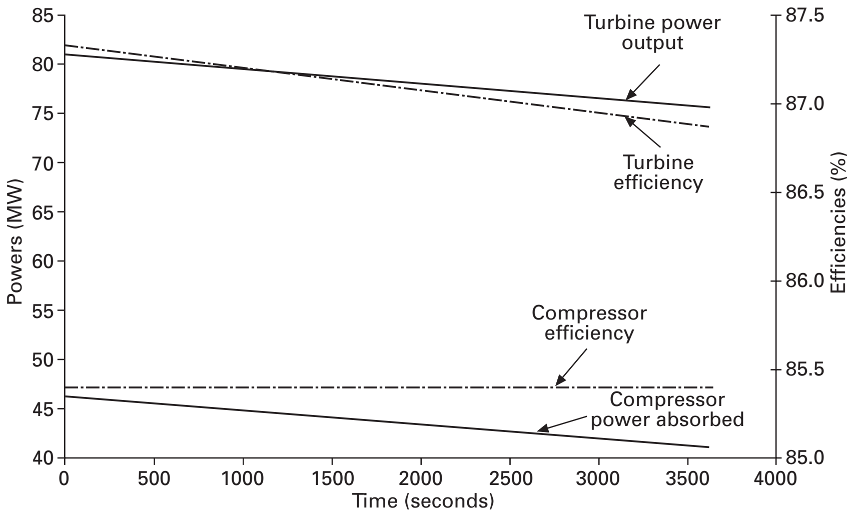

17.11 Trends in compressor and turbine power and efficiency changes during ambient pressure transient.

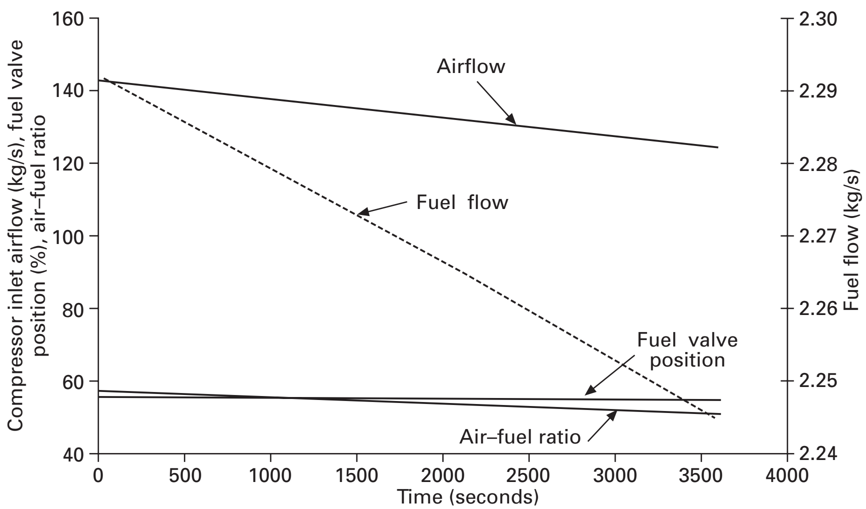

17.12 Trends in flow, air–fuel ratio and fuel valve position during ambient pressure transient.

flow, $W_1\sqrt{T_1}/P_1$ due to the steepness of the speed line. The change in mass flow during this transient is similar to that of the high-power case and is due to the same compressor inlet conditions and a similar change in the compressor non-dimensional flow during the transient.

Since the thermal efficiency improves and the power output from the gas turbine is constant, a decrease in fuel flow is observed as the ambient pressure falls. A similar downward trend in the fuel valve position is also observed. The air–fuel ratio decreases due to the increase in the temperature rise across the combustor, $T_3 - T_2$, as shown in Fig. 17.13.

17.2.5 Trends in temperature

Since the compressor inlet temperature, T_1 remains constant during this transient, the increase in the maximum to minimum cycle temperature ratio results in an increase in the turbine entry temperature, T_3. Due to the constant compressor inlet temperature and constant compressor non-dimensional speed, the compressor non-dimensional temperature rise, $\Delta T_{21}/T_1$, is approximately constant, as discussed in Section 8.1.1. Thus the compressor discharge temperature, T_2 remains essentially constant. The increase in T_3 results in an increase in the primary zone temperature as shown in Fig. 17.13, which displays the trends of these temperatures. For a given turbine entry temperature, the increase in turbine pressure ratio will decrease the exhaust gas temperature. However, the increase in the turbine entry temperature is sufficiently large to result in an increase in exhaust gas temperature, T_4. Also, the increase in the turbine entry temperature results in an increase in the turbine blade metal temperature.

17.2.6 Trends in pressure

Although there is an increase in the compressor ratio, the decrease in the ambient pressure during this transient results in a decrease in the compressor

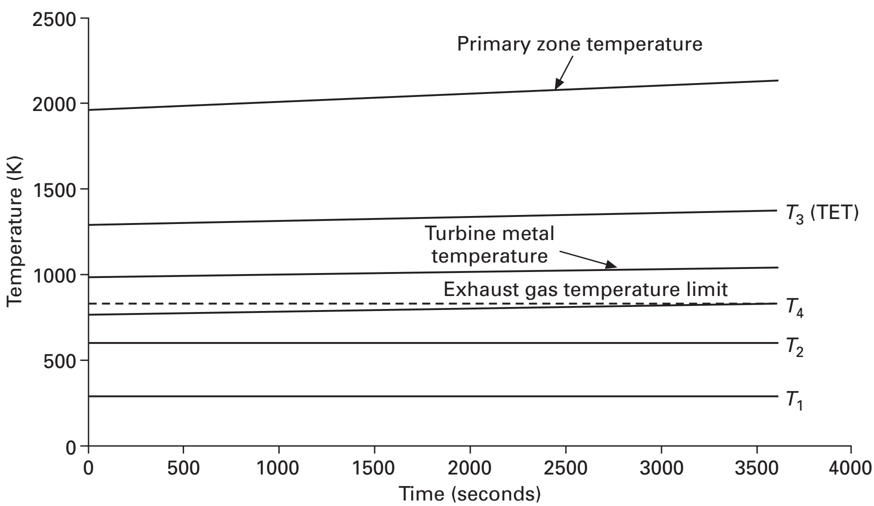

17.13 Trends in temperature during ambient pressure transient.

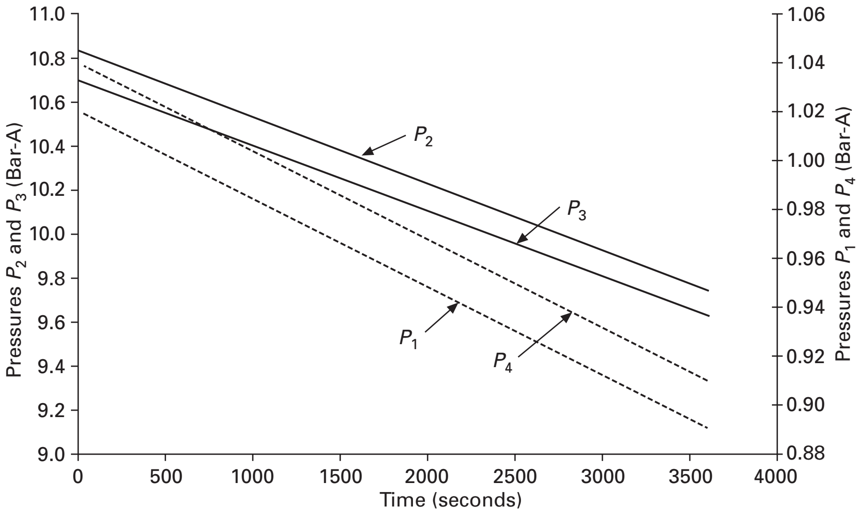

17.14 Trends in pressure during ambient pressure transient.

discharge and turbine inlet pressure, as seen in Fig. 17.14. The decrease in the compressor inlet and turbine exhaust pressures is due to the transient (decreasing ambient pressure) which is being simulated.

17.2.7 Trends in creep life

It is observed that the turbine blade metal temperature increases during this transient, and this is shown in Fig. 17.13. It is also observed that the turbine power developed decreases (Fig. 17.11), hence the torque is reduced, which lowers the stresses in the turbine blade material. However, the effect of the increase in turbine metal temperature prevails and this results in an increase in turbine creep life usage, as is shown in Fig. 17.15.

At the beginning of this transient, the temperatures and stress in the turbine blades result in a creep life exceeding 500 000 hours. Although the thermal efficiency of the gas turbine is improved under these conditions, the penalty paid is an increased creep life usage where the time to next overhaul is reduced from over 500 000 hours to just over 100 000 hours. Since the creep life usage is still over 75 000 hours, when overhauls are due for this engine, the increase in creep life usage is of little consequence unless creep life monitoring is implemented, in which event it is necessary to track such changes in creep life usage carefully. With such monitoring, the time between overhauls may be increased to over 75 000 hours, thus resulting in a useful reduction in maintenance costs.

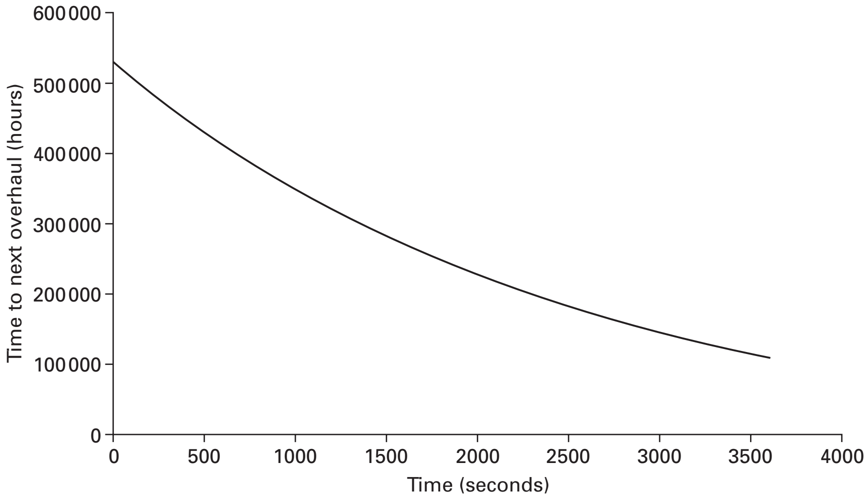

17.15 Turbine creep life usage during ambient pressure transient.

17.2.8 Trends in gas turbine emissions

It is observed in Figure 17.13 that the primary zone temperature has increased and will increase the NO_x emissions while decreasing CO emissions. But the combustion pressure decreases (Figure 17.14) and this change has the opposite effect on these emissions. However, it is also observed that the compressor pressure ratio increases and tends to suppress the full effect of the decrease in ambient pressure on the combustion pressure. Hence, the net effect is an increase in NO_x, while decreasing CO, as shown in Fig. 17.16.

The increase in thermal efficiency has resulted in a decrease in fuel flow. The increase in thermal efficiency and reduced fuel flow therefore reduces both the CO_2 mass flow rate and the emissions index as shown in Fig. 17.16, thus reducing greenhouse gas emissions.

17.3 Effect of ambient pressure on engine performance at low power (single-shaft gas turbine operating with an active variable inlet guide vane)

The effect of varying ambient pressure on engine performance has been simulated for a single-shaft gas turbine. The VIGV control system was set, in that case, such that the VIGV remained fully opened for most of the useful operating power range. The effect of varying the ambient pressure on the engine performance is now considered when the VIGV operates in the useful power range. This is achieved by setting the EGT set point to that of the EGT limit, as discussed in Section 16.4. The low power operating case will now

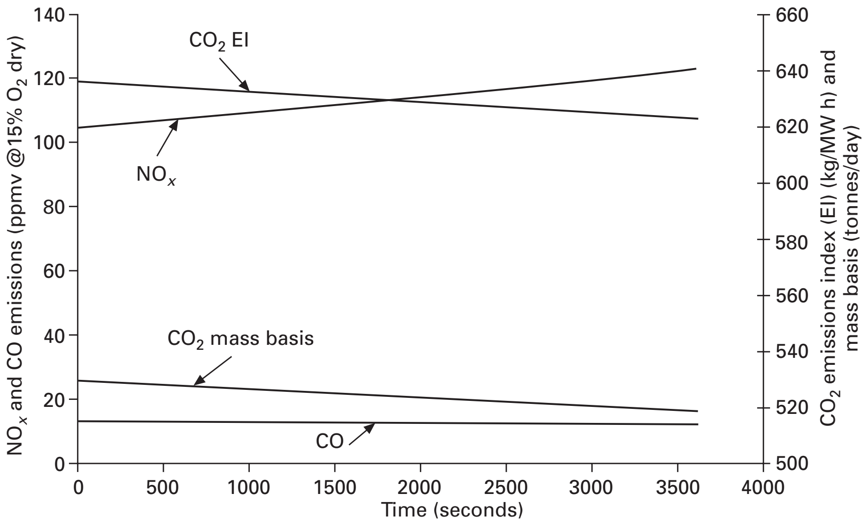

17.16 Trends in gas turbine emissions during ambient pressure transient.

be considered as the high-power case will not differ from that discussed in Section 17.1. If the ambient temperature is low enough, such that the engine performance is limited by the power limit, then varying the ambient pressure will result in a different engine performance from that discussed in Section 17.1 when operating at high power. However, the performance will be similar to the case being considered here, as the power output from the gas turbine remains constant during the ambient pressure transient.

The power demand from the generator is set to 34 MW and the ambient pressure is decreased from 1.03 Bar to 0.9 Bar in 3600 seconds. The ambient temperature and relative humidity are maintained at 15 degrees Celsius and 60%, respectively. The inlet and exhaust losses are each set to 100 mm water gauge.

17.3.1 Compressor characteristics and trends in pressure and temperature ratios

As the ambient pressure decreases and the VIGV remains fully opened, it is observed that the air flow rate through the engine decreases (Section 17.2.4). This results in an increase in specific work to compensate for the loss in air flow rate in order to maintain the power output from the gas turbine. The increase in specific work is achieved by increasing the turbine entry temperature, T_3, thus increasing the maximum to minimum cycle temperature ratio, T_3/T_1. The increase in turbine entry temperature also increases the EGT and, in this case, the VIGV control system responds by opening the VIGV to maintain the EGT at its set point, thus altering the compressor characteristic. The change in the compressor characteristic due to the opening of the VIGV is shown in Fig. 17.17. The resultant increase in the compressor non-dimensional flow increases the compressor pressure ratio to satisfy the flow compatibility, as indicated by the operating points on the compressor characteristic. The effect of the change in the turbine entry temperature and thus the increase in the maximum to minimum cycle temperature ratio, T_3/T_1, which is smaller in this case, is shown in Fig. 17.18 as a trend. The figure also shows the trend in compressor and turbine pressure ratio.

17.3.2 Trends in power and efficiency

The opening of the VIGV increases the compressor non-dimensional flow, as shown in Fig. 17.17. The decrease in ambient pressure and thus the compressor inlet pressure are sufficient to decrease the mass flow rate through the compressor. Although there is a small increase in the compressor discharge temperature, the decrease in air flow rate results in a reduction in the compressor absorbed power, as shown in Fig. 17.19. However, the decrease in the compressor power absorbed is smaller than in the case when the VIGV remained opened, as shown in Fig. 17.11. This is due to the decrease in mass flow rate through the compressor being greater in the previous case

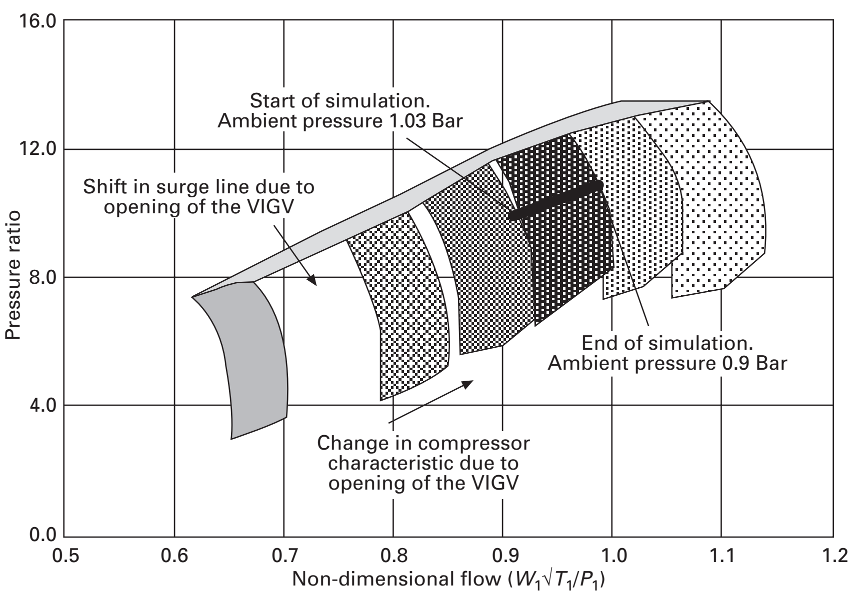

17.17 Change in compressor characteristic due to opening of VIGV.

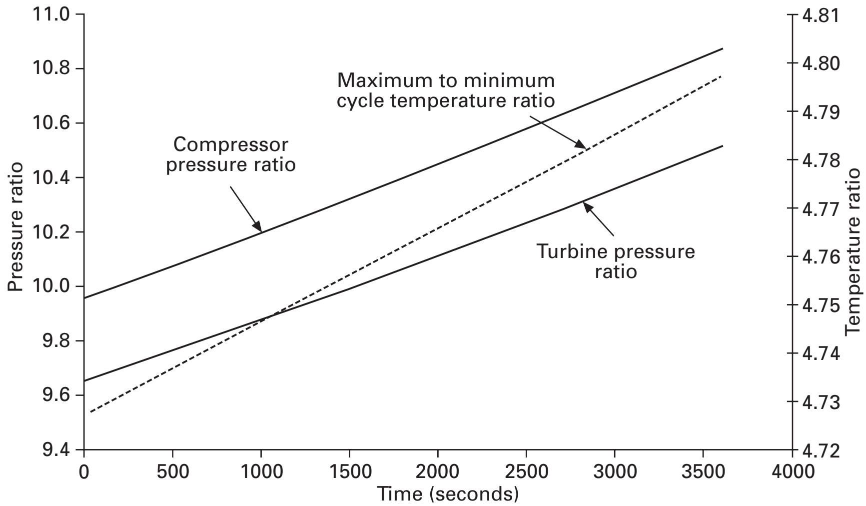

17.18 Trends in pressure and temperature ratios for compressor and turbine during ambient pressure transient.

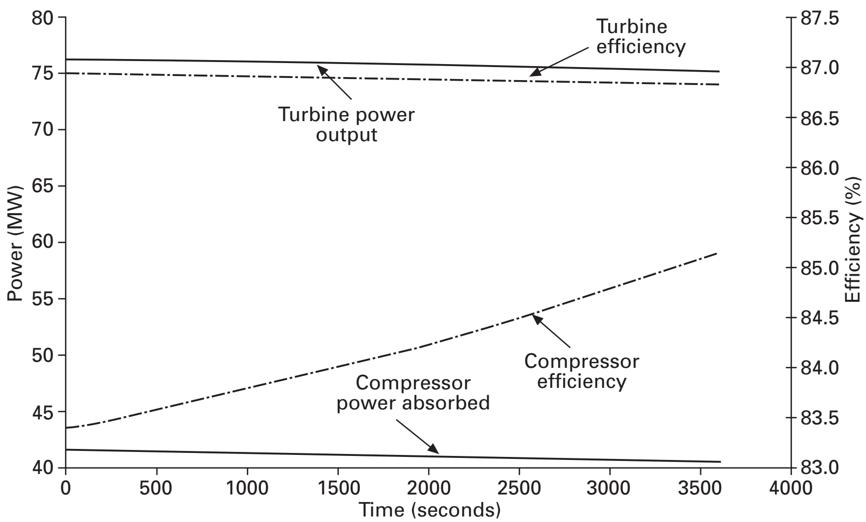

17.19 Trends in compressor and turbine power and efficiency.

(see Figs 17.12 and 17.24). To maintain the constant power demand from the generator, the turbine power also decreases with the ambient pressure. The smaller decrease in mass flow rate results in a smaller increase in T_3/T_1 to maintain the required power out from the gas turbine (i.e. the specific work increase in this case is smaller compared with the previous case discussed in Section 17.2). The compressor efficiency increases and this is due to the opening of the VIGV. The turbine efficiency remains essentially constant due to the small change in turbine entry temperature.

The increase in the compressor pressure ratio and maximum to minimum cycle temperature ratio increases the thermal efficiency of the gas turbine. This is shown in Fig. 17.20. The power output from the generator remains on the required set point of 34 MW as no engine operating limit is reached during this transient. The benefit on thermal efficiency is also seen at low ambient pressures when the engine is not subjected to an engine operating limit. The increase in thermal efficiency, as the ambient pressure falls, will result in lower fuel consumption, and thus operating costs.

17.3.3 Trends in temperature and pressure

The trends in temperature due to the decrease in ambient pressure during this transient are shown in Fig. 17.21. It is observed that the EGT remains constant throughout the transient and this is due to the opening of the VIGV as the ambient pressure decreases to maintain the EGT in the set point. The increase in specific work results in the increase in the turbine entry temperature, T_3. The increase in T_3 is smaller compared with the previous case, and this is due primarily to a small decrease in compressor flow rate during the transient caused by the increase in compressor non-dimensional flow, resulting from the opening of the VIGV. The increase in compressor pressure ratio also results in a small increase in the compressor discharge temperatures. The increase in the turbine entry temperature and compressor discharge temperature,

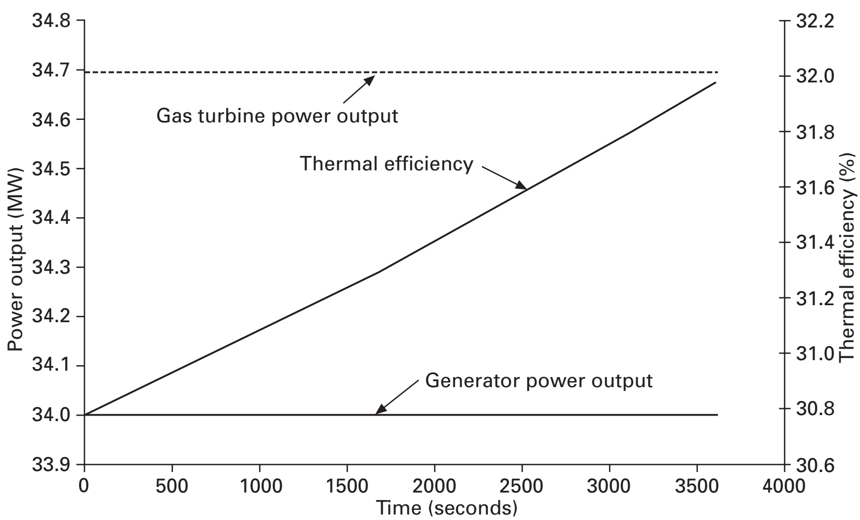

17.20 Trends in gas turbine efficiency and power output during ambient pressure transient.

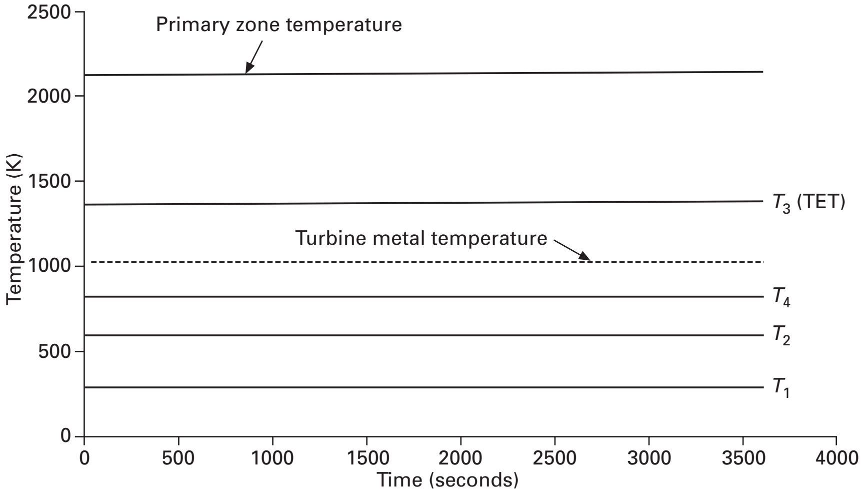

17.21 Trends in temperature during ambient pressure transient.

which is also the cooling air temperature, increase the primary zone and turbine metal temperatures.

It has been observed that the compressor pressure ratio increases during the transient, as shown in Fig. 17.18. But whether the compressor discharge pressure, and hence the turbine inlet pressure, decrease during the transient depends on the compressor characteristic changes due to the opening of the VIGV and to the decrease in ambient pressure. Since the change in the maximum to minimum temperature ratio, T_3/T_1, is small in this case, the increase in compressor non-dimensional flow due to the opening of the VIGV results in the increase in compressor pressure ratio, as shown in Fig. 17.18. This is necessary to satisfy the flow compatibility between the compressor and turbine (Equation 8.1). It is also observed that the increase in the compressor pressure ratio is greater compared with the previous case (Fig. 17.9), where the increase in compressor ratio resulted largely from the increase in T_3/T_1 (i.e. the compressor inlet non-dimensional flow is approximately constant in the previous case). However the pressure ratio in the previous case is affected only by the factor $\sqrt{T_3/T_1}$, thus the increase in pressure ratio in this case is greater. The decrease in the ambient pressure is sufficient to decrease the compressor discharge pressure and turbine inlet pressure in spite of the increase in compressor pressure ratio, but the decrease in these pressures is smaller compared with the previous case (Section 7.2), as shown in Fig. 17.22 and 17.14, respectively.

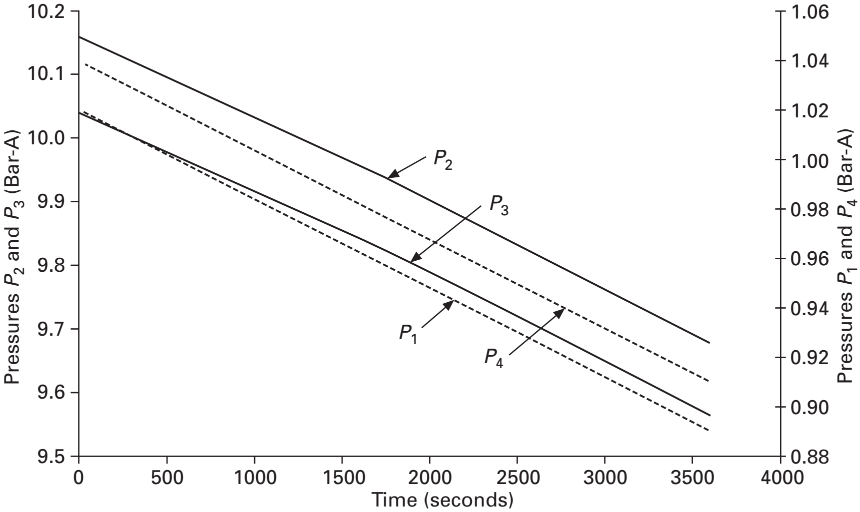

17.22 Trend in pressure during ambient pressure transient.

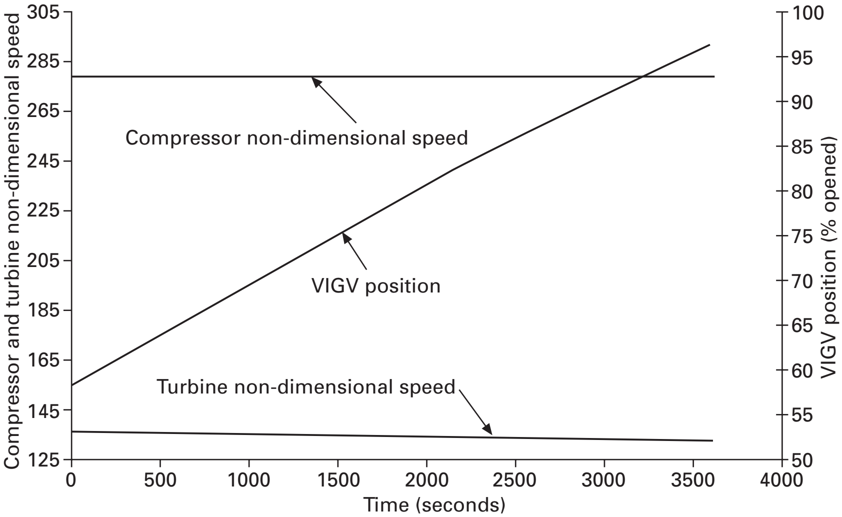

17.23 Trends in VIGV position and compressor and turbine speed during ambient pressure transient.

17.3.4 Trends in VIGV position and speed

The opening of the VIGV due to the decrease in the ambient pressure is shown in Fig. 17.23. The VIGV opens from about 60% to about 95% as the ambient pressure decreases. The compressor non-dimensional speed remains constant during this transient because the ambient temperature and gas turbine speed also remain constant. Similarly, the turbine non-dimensional speed also remains essentially constant and any variation is due to the small variation in the turbine entry temperature, as shown in Fig. 17.21.

17.3.5 Trends in flow

Although the compressor non-dimensional flow increases during the transient, the decrease in compressor inlet pressure results in a decrease in compressor flow as the ambient pressure reduces. This is shown in Fig. 17.24, which gives the trends in flow, fuel valve position and air–fuel ratio during the ambient pressure transient. It has been seen that the thermal efficiency increases and this is due to the increase in the compressor pressure ratio and the maximum to minimum cycle temperature ratio.

Since the gas turbine power output remains constant, the fuel flow decreases during the transient. The fuel valve also closes due to the decrease in fuel flow. The small increases in the compressor discharge temperature and turbine entry temperature result in the air–fuel ratio remaining essentially constant. Thus the suitability of the use of a VIGV compressor in DLE engines is again observed where the air–fuel ratio can be maintained during a change in load.

17.3.6 Trends in creep life

It has been seen that the turbine entry temperature and the compressor discharge temperature (which is also the turbine cooling air temperature) increase only

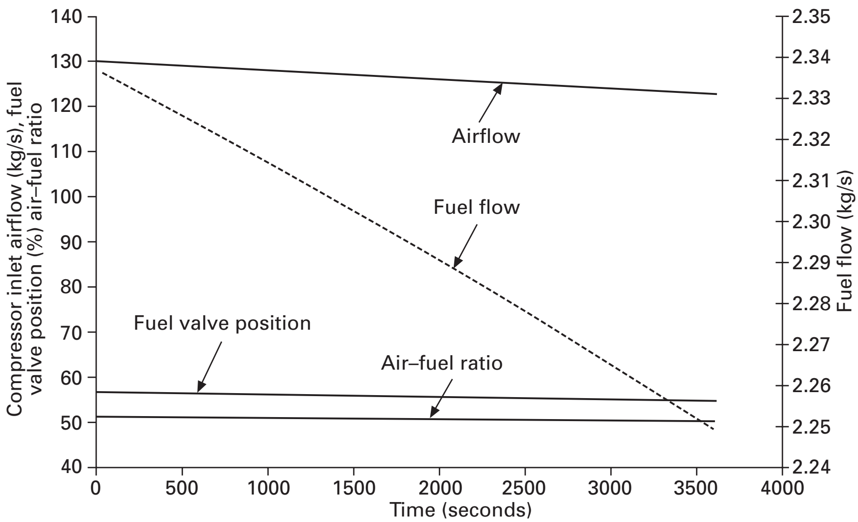

17.24 Trends in flow and air–fuel ratios during ambient pressure transient.

slightly. Therefore, there is only a slight increase in the turbine blade metal temperature. However, the turbine creep life usage is very sensitive to the turbine blade metal temperature and this increase results in higher turbine creep life usage, as shown in Fig. 17.25.

Although the creep life usage in the present case is greater compared with the previous case when the VIGV remained fully opened (Fig. 17.15), the

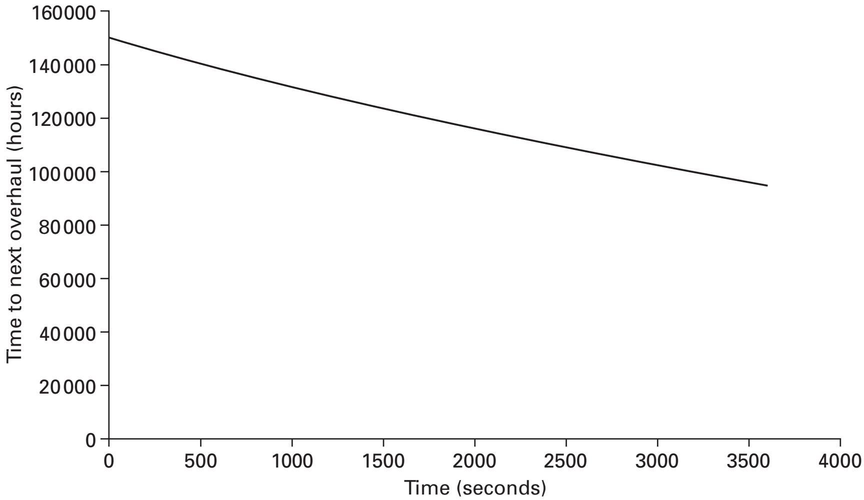

17.25 Turbine creep life usage during ambient temperature transient.

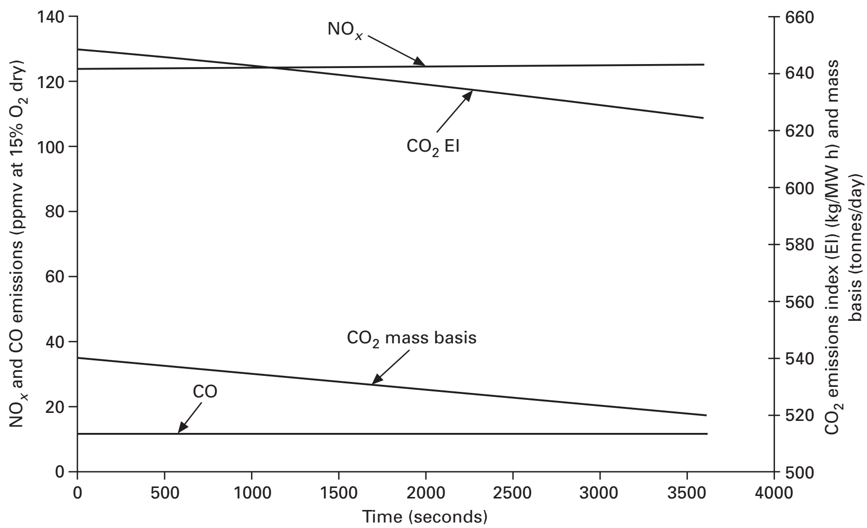

17.26 Trends in gas turbine emissions during ambient pressure transient.

change in the creep life usage with ambient pressure is greater in the previous case and this is due to the larger increase in the turbine entry temperature during the transient. This can be seen by comparing Figs 17.15 and 17.25.

17.3.7 Trends in gas turbine emissions

The combustion pressure and temperature changes are quite small during in this case. Thus the changes in NO_x and CO emissions are also small as shown in Fig. 17.26. The increase in gas turbine thermal efficiency leads to a decrease in the fuel flow as the gas turbine power output remains constant during the decrease in ambient pressure. The decrease in fuel flow therefore reduces the CO_2 emissions on a mass basis and the increase in the turbine thermal efficiency also results in the decrease in CO_2 emissions index as shown in Fig. 17.26.

18
Simulating the effects of engine component deterioration on engine performance

The effects of component performance deterioration on engine performance were discussed in Chapter 9 and these deteriorations applied to the two-shaft gas turbine. These deteriorations are now applied to investigate the impact of component performance deterioration on a single shaft gas turbine. The engine performance is deteriorated or degraded by applying fault indices as discussed when the two-shaft gas turbine was considered. However, there are only four fault indices, due to the absence of the power turbine in the single-shaft gas turbine. These indices correspond to the compressor fouling and efficiency fault indices and the turbine fouling and efficiency fault indices, respectively.

18.1 Compressor fouling (high-power operation)

As stated, compressor fouling is the most common form of performance deterioration and compressor fouling is simulated by reducing the flow capacity and efficiency of the compressor through the use of fault indices. Again, moderate compressor fouling is considered and this is simulated by setting the compressor fouling fault index and the compressor efficiency fault index to –3% and –1%, respectively, to change over 1 hour (3600 seconds) linearly. It is also assumed that the ambient pressure, temperature and relative humidity remain constant during compressor fouling at 1.013 Bar, 15 degrees Celsius and 60%, respectively. The inlet and exhaust losses are assumed to be at 100 mm of water gauge. As the impact of compressor fouling at high power is to be investigated, the generator power demand is set at 60 MW. At the assumed ambient conditions, the engine will always remain on the EGT limit during the simulation.

18.1.1 Trends in fault indices

The trend in fault indices is shown in Fig. 18.1 and the changes in the compressor fouling and efficiency fault indices due to compressor fouling

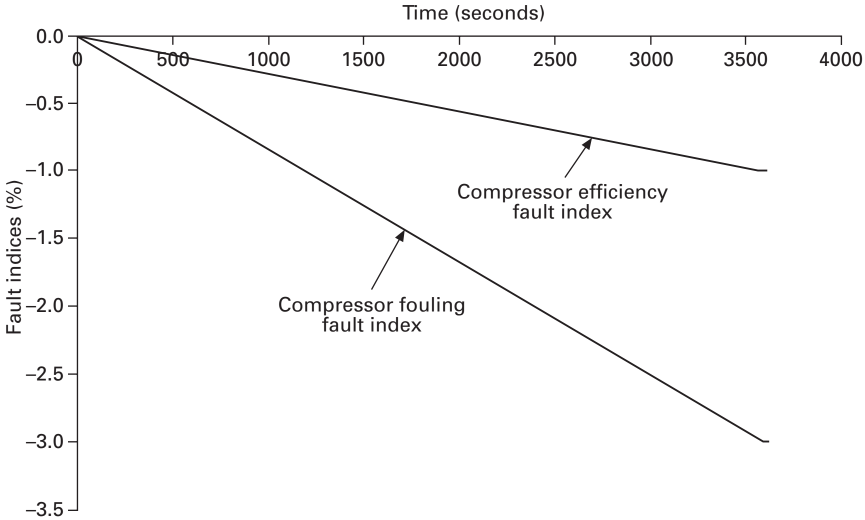

18.1 Trends in fault indices during compressor fouling.

are observed. These changes in compressor fault indices affect the compressor characteristic by reducing the non-dimensional flow and compressor efficiency, thus simulating compressor fouling. No other fault is present and this is indicated by the fault indices for the turbine component remaining at zero throughout the simulation.

18.1.2 Compressor characteristic and pressure and temperature ratios

Since the ambient temperature, and hence the compressor inlet temperature, remain constant and the compressor speed does not change (determined by the frequency of the electrical generator), the compressor non-dimensional speed, $N_1/\sqrt{T_1}$, remains constant. Due to the shift in the compressor non-dimensional speed line during fouling, the operating point on the compressor characteristic shifts to the left. This is shown in Fig. 18.2, where the movement of the operating point is shown on the compressor characteristic during compressor fouling. Thus compressor fouling will result in a decrease in compressor non-dimensional flow. The reduction in compressor non-dimensional flow will also result in a decrease in compressor pressure ratio, as shown in Fig. 18.3. This is due to the effects of re-matching between the compressor and turbine due to compressor fouling.

In a single-shaft gas turbine, the turbine pressure ratio is influenced directly by the compressor pressure ratio, so a decrease is also observed in the turbine pressure ratio (Fig. 18.3). Since the operation is on an EGT limit and the

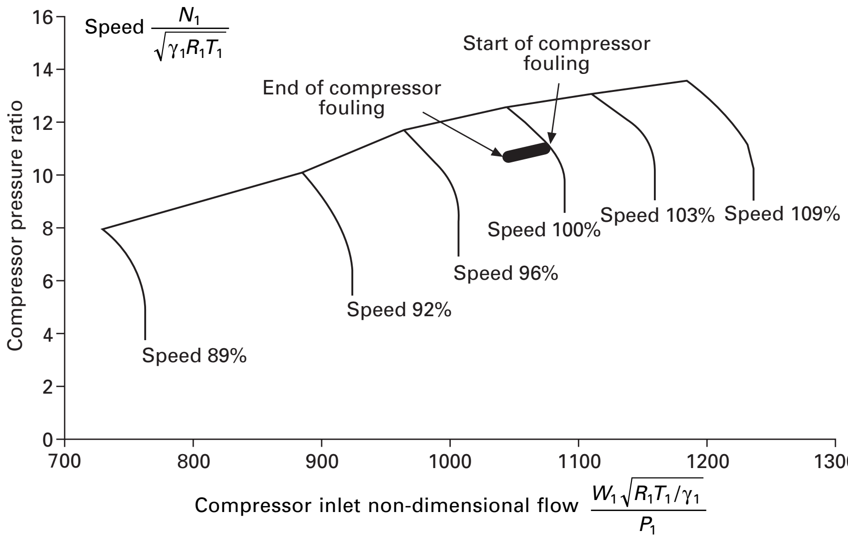

18.2 Operating point on compressor characteristic during compressor fouling.

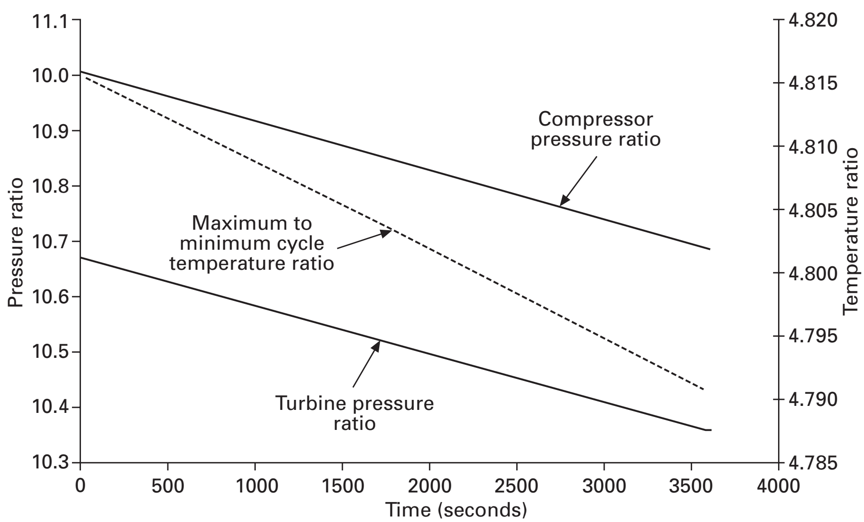

18.3 Trends in pressure and temperature ratios during compressor fouling.

ambient temperature remains constant, the decrease in turbine pressure ratio also results in a decrease in the turbine entry temperature and thus the reduction in the maximum to minimum cycle temperature ratio, T_3/T_1.

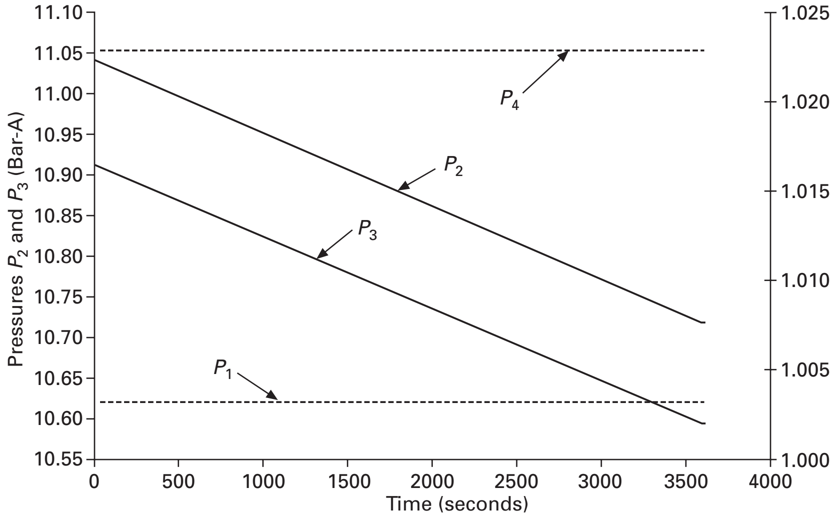

18.4 Trends in pressure during compressor fouling.

18.1.3 Trends in pressure and temperature

The decrease in the compressor discharge pressure and turbine inlet pressure is due to the decrease in the compressor pressure ratio. As the ambient pressure and the inlet and exhaust losses remain constant during compressor fouling, the compressor inlet and turbine exit pressures do not change much during compressor fouling. The trends in these pressures are shown in Fig. 18.4.

Although the compressor pressure ratio decreases, the loss in compressor efficiency during fouling, and the constant compressor non-dimensional speed, result in an approximately constant compressor discharge temperature, as shown in Fig. 18.5. The decrease in the turbine pressure ratio results in a decrease in the turbine entry temperature since the EGT remains constant on its operating limit. The reduction in the turbine entry temperature and the near-constant compressor discharge temperature also result in a small decrease in the turbine metal temperature, and this can be seen in Fig. 18.5. The decrease in the turbine entry temperature during compressor fouling also reduces the combustor primary zone temperature.

18.1.4 Trends in flow

The trends in flow during compressor fouling are shown in Fig. 18.6. The decrease in the compressor air flow rate is primarily due to the decrease in the compressor non-dimensional flow. The decrease in the turbine entry temperature and constant compressor discharge temperature, and thus

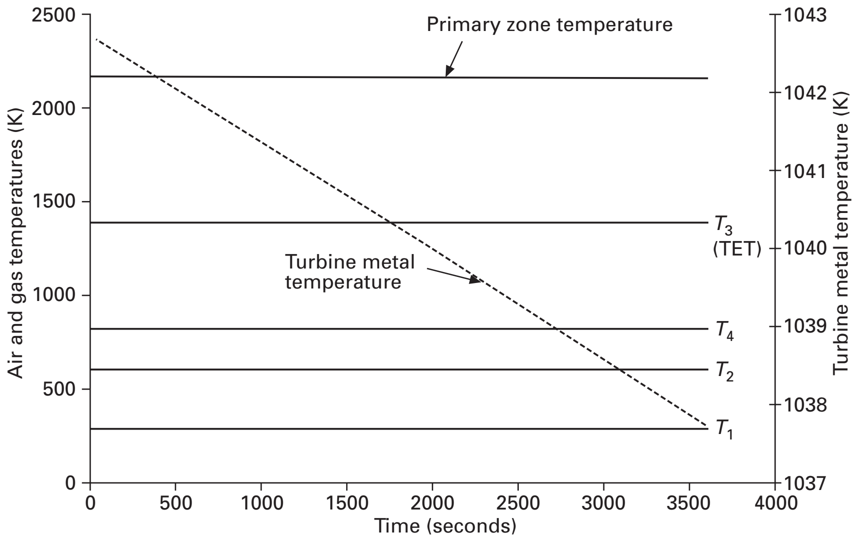

18.5 Trends in temperature during compressor fouling.

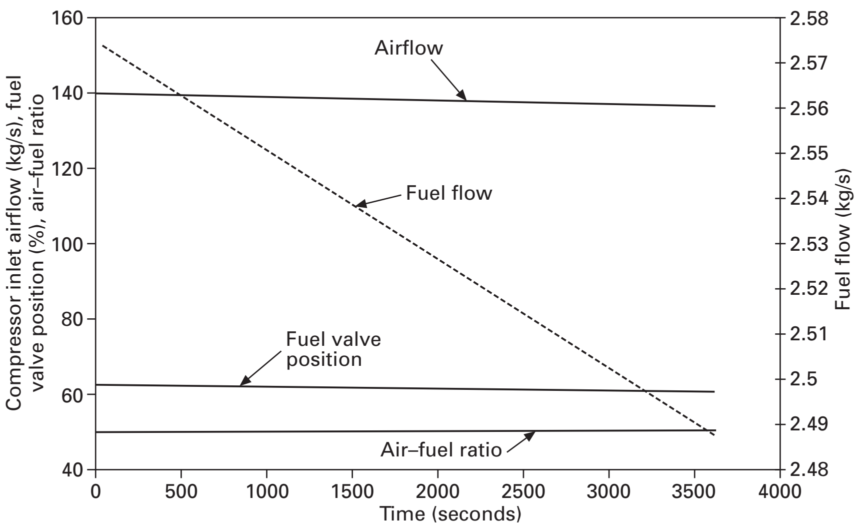

18.6 Trends in flow during compressor fouling.

combustor inlet temperature, result in an increase in the air–fuel ratio. The decrease in the combustion air flow due to the decrease in the compressor air flow rate, and the increase in air–fuel ratio, result in a decrease in the fuel flow during compressor fouling. The fuel valve position also decreases to satisfy the reduction in fuel flow.

18.1.5 Trends in power and efficiency

Since the compressor temperature rise remains essentially constant, the specific work absorbed by the compressor also remains constant. However, the reduction in the compressor mass flow rate through the compressor due to fouling results in a decrease in the power absorbed by the compressor and this is shown in Fig. 18.7, as is the decrease in the compressor efficiency. The turbine power output also decreases due to the decreases in the turbine pressure ratio, mass flow rate through the turbine and the turbine entry temperature. The small decrease in the turbine entry temperature does not affect the turbine efficiency and this is also shown in Fig. 18.7. The decrease in the above parameters also results in a decrease in the gas turbine thermal efficiency, gas turbine power output and hence a reduction in the power output from the generator (Fig. 18.8).

Unlike the case of the two-shaft gas turbine where the gas generator speed may increase, thereby increasing the air flow rate to partly compensate for the loss in power output due to compressor fouling, the fixed gas turbine speed of a single-shaft gas turbine generally has a more adverse effect on engine performance when compressor fouling occurs.

18.1.6 Trends in turbine creep life

The decrease in the turbine metal temperature as seen in Fig. 18.5 and the reduced power developed by the turbine result in a decrease in creep life

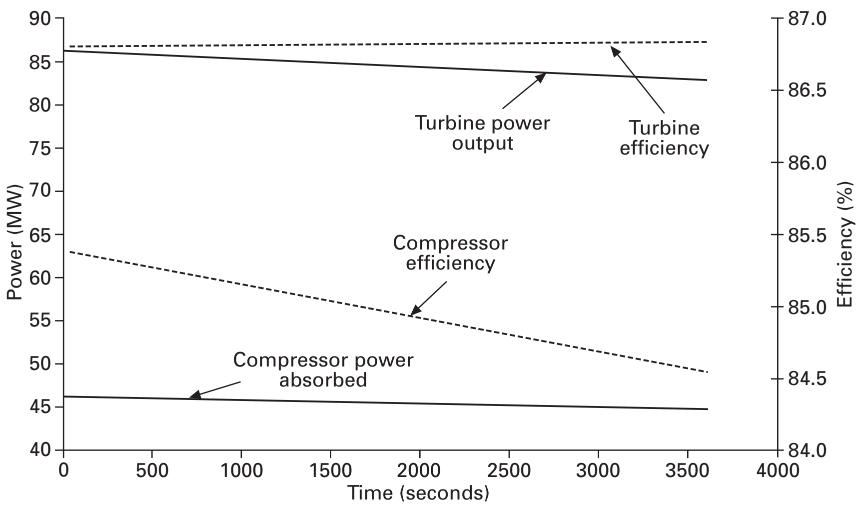

18.7 Trends in compressor and turbine power and efficiencies due to compressor fouling.

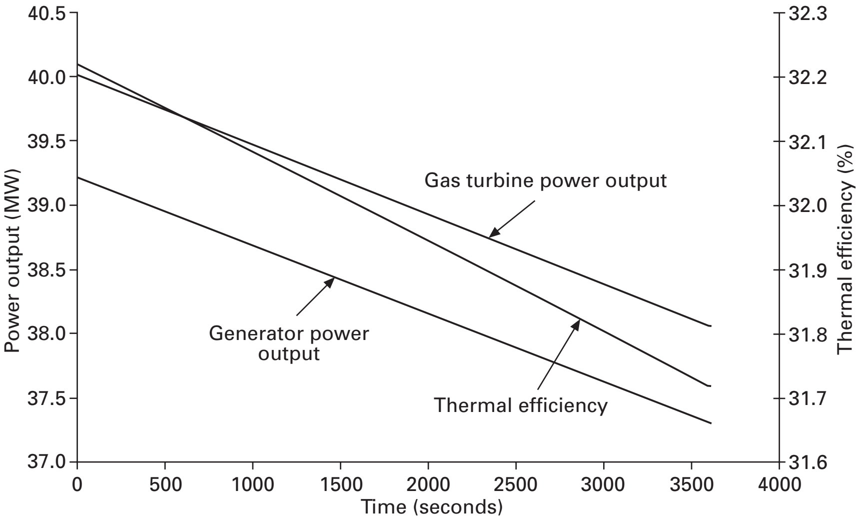

18.8 Trends in gas turbine thermal efficiency, power and generator output due to compressor fouling.

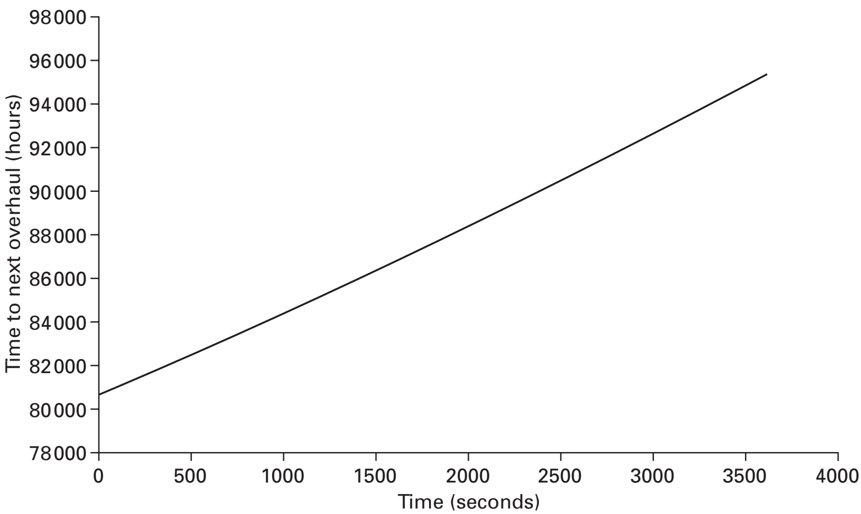

18.9 Trends in creep life usage due to compressor fouling.

usage. This can be seen in Fig. 18.9, where the trend in the creep life usage, as the time to next overhaul, is shown when compressor fouling occurs. However, this decrease in creep life usage is somewhat misleading and the true picture emerges only when the simulator is run at the reduced gas turbine power available due to fouling (at about 37.3 MW), but when no fouling is present. It is only then that the creep life usage is observed to decrease further, thus illustrating the actual impact of compressor fouling on turbine creep life usage. The reader is left to run the necessary simulation to determine the actual increase in the turbine creep life usage due to compressor fouling.

18.1.7 Trends in gas turbine emissions

The decrease in the combustion pressures and temperatures due to compressor fouling results in a decrease in NO_x and an increase in CO, as shown in Fig. 18.10. Again, it is when the simulator is run at the reduced power available due to fouling, but when no fouling is present, that we observe an actual increase in NO_x due to compressor fouling. The decrease in fuel flow results in the decrease in CO_2 on a mass flow basis. However, the decrease in the thermal efficiency results in an increase in the CO_2 emissions index as shown in Fig. 18.10. Thus, in real terms, fouling increases NO_x and CO_2 emissions. The reader should run the simulator at the power available due to compressor fouling but when fouling is absent and determine the true impact of compressor fouling on NO_x, CO and CO_2 emissions.

18.1.8 Displacement of running line due to compressor fouling

It has been stated that no unique running line exists for a single-shaft gas turbine. However, due to the steepness of the non-dimensional speed lines

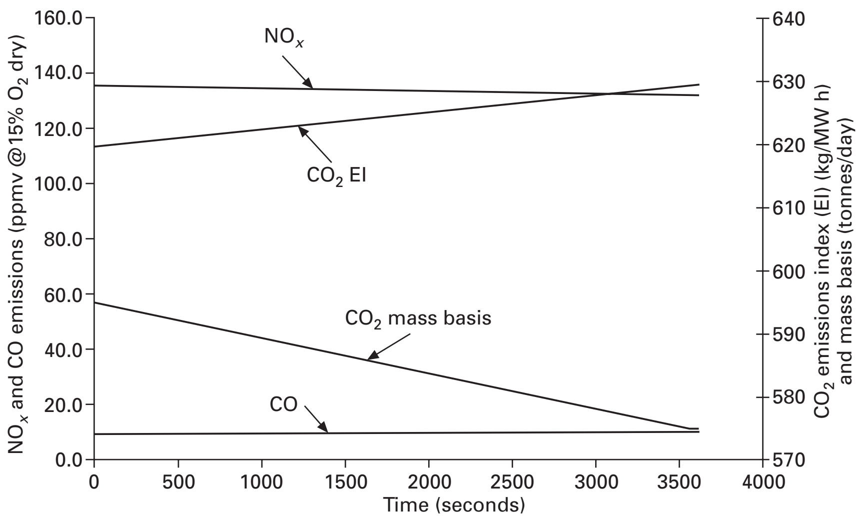

18.10 Trends in gas turbine emissions due to compressor fouling.

on the compressor characteristic, the change in the compressor non-dimensional flow with its pressure ratio is usually small and can be used to detect compressor fouling for a fixed geometry compressor. This was discussed in Section 9.1, where the change in compressor non-dimensional flow with its non-dimensional speed due to compressor fouling was considered. Figure 18.11 shows the variation of the compressor non-dimensional flow with its speed. The figure also shows the change in this running line, which is shifted downwards due to compressor fouling. The compressor operating points for the clean and fouled cases are also shown on this figure. Such a plot is useful in detecting compressor fouling and is similar to that discussed previously where the effects of compressor fouling on a two-shaft gas turbine were considered.

18.2 Compressor fouling (low-power operation)

In Section 18.1 the effects of compressor fouling on the performance of a single-shaft gas turbine were considered when operating at high power so that the engine is always on an operating limit such as the EGT. The effects of compressor fouling are now considered when the gas turbine power demand is sufficiently low such that the engine never reaches an operating limit. This is achieved by setting the generator power demand to 35 MW and subjecting the engine to compressor fouling with ambient operating conditions as described in Section 18.1. As the compressor is being subjected to the same level of compressor fouling as when operating at high power levels, the trends in the

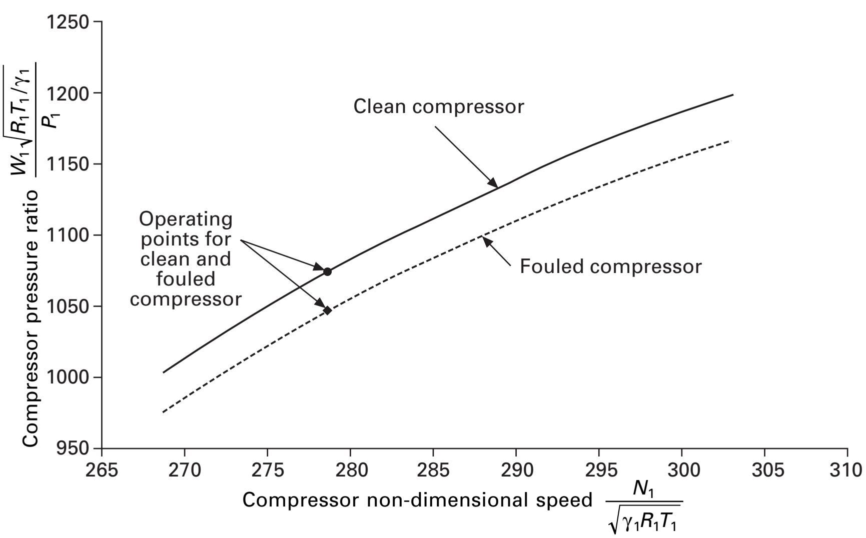

18.11 Effect of fouling on variation of compressor non-dimensional flow with speed.

fault indices for this case are the same as those described in Section 18.1.1 and shown in Fig. 18.1.

18.2.1 Compressor characteristic, pressure and temperature ratios

As gas turbine speed and compressor inlet temperature do not change, the compressor non-dimensional speed remains constant during this simulation. Thus the movement of the operating point on the compressor characteristic due to fouling is similar to that shown in Fig. 18.2. The main difference when operating at lower power is that the compressor pressure ratio is lower. However, the decrease in the compressor ratio due to fouling is smaller because operation is at a constant (lower) power output and the turbine entry temperature increases to maintain the power output of the gas turbine. This can be seen in Fig. 18.12. It is also observed that this differs from the corresponding case for the two-shaft gas turbine where the gas generator speed increases, thus partly compensating for the effects of compressor fouling by maintaining the compressor operating point on the compressor characteristic.

The decreases in the compressor and turbine pressure ratios are shown in Fig. 18.13. To maintain the power output of the gas turbine, the specific work must therefore increase as the mass flow rate decreases. This is achieved

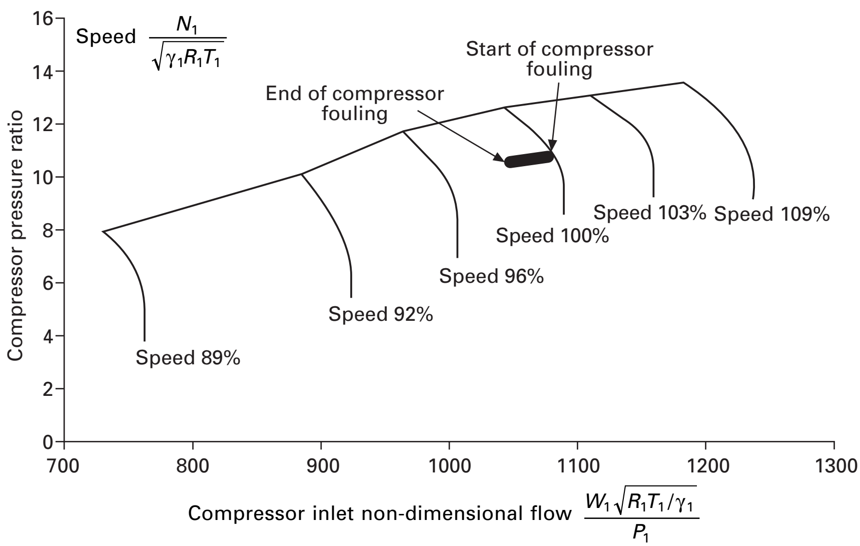

18.12 Operating point on compressor characteristic due to fouling and operating at low power.

by increasing the maximum to minimum cycle temperature ratio, T_3/T_1, and an increase in T_3/T_1 is observed, as shown in Fig. 18.13.

18.2.2 Trends in pressure and temperature

It has been seen that the compressor and turbine pressure ratios decrease and therefore there is a decrease in the compressor discharge pressure and turbine inlet pressure during compressor fouling, as shown in Fig. 18.14. Compared with the case for the two-shaft gas turbine, these pressures remain essentially constant due to the increase in the gas generator speed during compressor fouling. The compressor inlet and turbine exit pressures do not change and this is due to maintaining constant ambient pressure during this simulation.

To maintain the power output of the gas turbine, the turbine entry temperature and thus the EGT increases. The compressor discharge temperature remains constant and this is due to the constant compressor non-dimensional speed and the decrease in compressor pressure ratio and efficiency caused by fouling. Since the compressor discharge temperature and thus the cooling air temperature remain constant, the increase in turbine entry temperature results in the increase in turbine blade metal temperature. The increase in the turbine entry temperature also results in an increase in the combustion primary zone temperature. The trends in these temperatures can be seen in Fig. 18.15. Comparing the trends in these temperatures with the case when operating at the EGT limit (Fig. 18.5), it is observed that the trends in temperature for this case are the opposite, with the exception of that for the compressor discharge temperature.

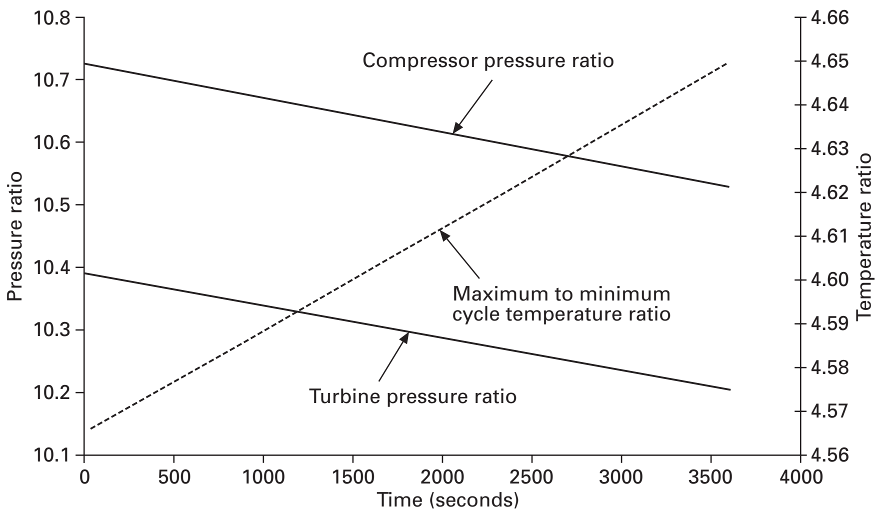

18.13 Trends in pressure and temperature ratio.

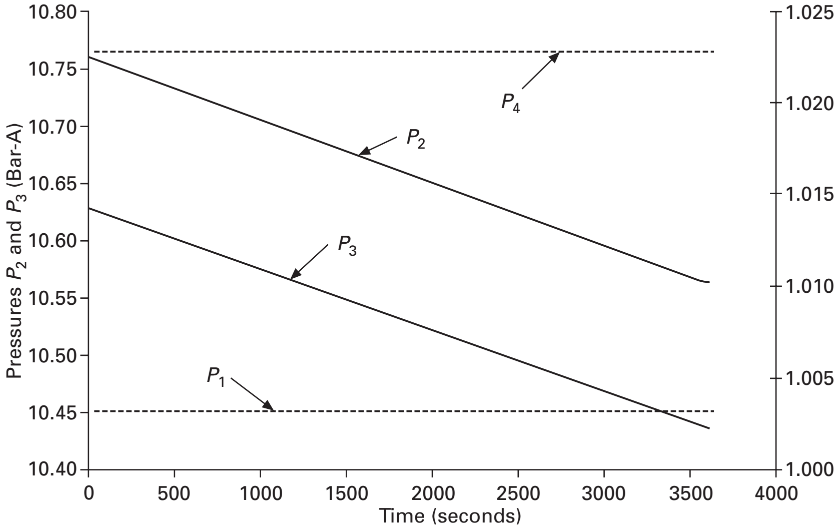

18.14 Trends in pressure due to compressor fouling when operating at low power.

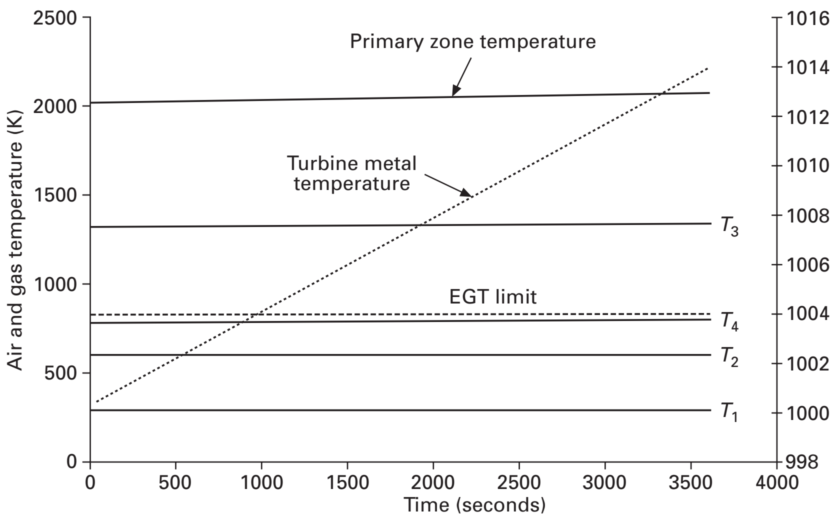

18.15 Trends in temperature due to fouling and operating at low power.

18.2.3 Trends in flow

The decrease in the compressor non-dimensional flow and the constant compressor inlet pressure and temperature result in a decrease in the compressor airflow, as shown in Fig. 18.16. Since operation is at a constant compressor

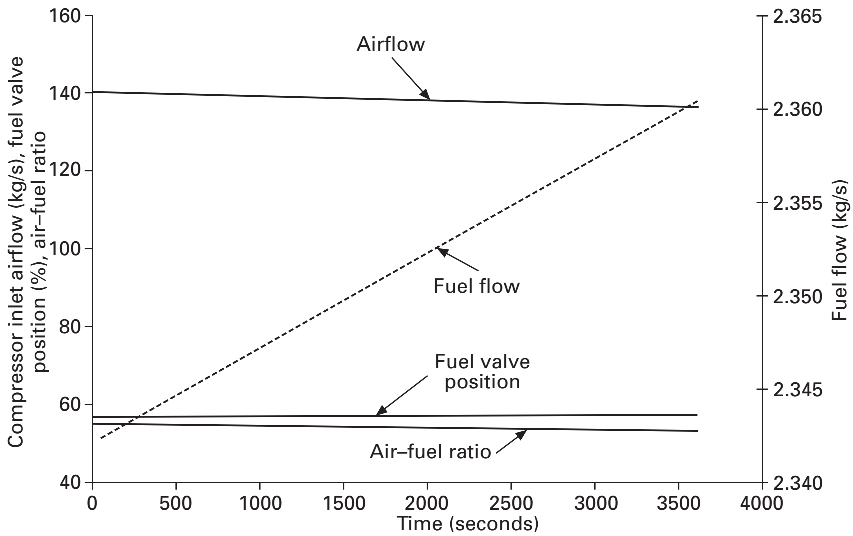

18.16 Trends in flow due to compressor fouling and operating at low power.

non-dimensional speed, the decrease in the compressor airflow is very similar to that when operating at the EGT limiting condition (Fig. 18.6). Since the power output from the gas turbine remains constant in this case and the gas turbine thermal efficiency decreases due to fouling, the fuel flow increases. As a result, the fuel valve position also follows a similar trend to that shown in Figure 18.6. The increase in the temperature rise across the combustor and the approximately constant combustion inlet temperature, T_2, result in a decrease in the air–fuel ratio. Again, these trends differ from the maximum power case discussed in Section 18.1.4.

18.2.4 Trends in power and efficiency

The decrease in the compressor airflow rate results in a decrease in the compressor power absorbed. Similarly, the reduction in the turbine flow also results in a decrease in turbine power. The compressor efficiency decrease is due primarily to the effects of compressor fouling. Any reduction in the turbine efficiency is due to the decrease in the turbine non-dimensional speed resulting from the increase in the turbine entry temperatures, as observed in Fig. 18.15. The trends in compressor and turbine powers with their efficiencies are shown in Fig. 18.17.

The trends in the gas turbine thermal efficiency and power output are shown in Fig. 18.18. The figure also shows the trend in the generator power output, which remains constant on the generator set point. The decrease in the thermal efficiency is due to the decrease in the compressor efficiency and pressure ratio.

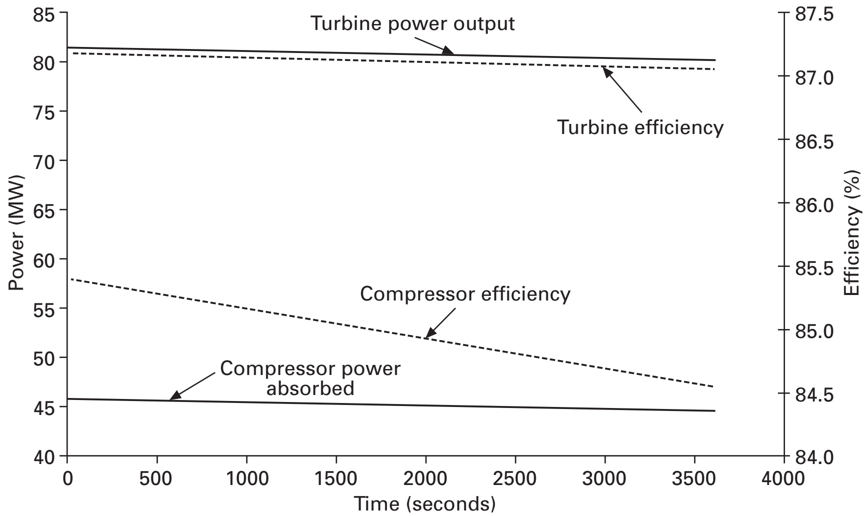

18.17 Trends in compressor and turbine power and efficiency due to compressor fouling at low power.

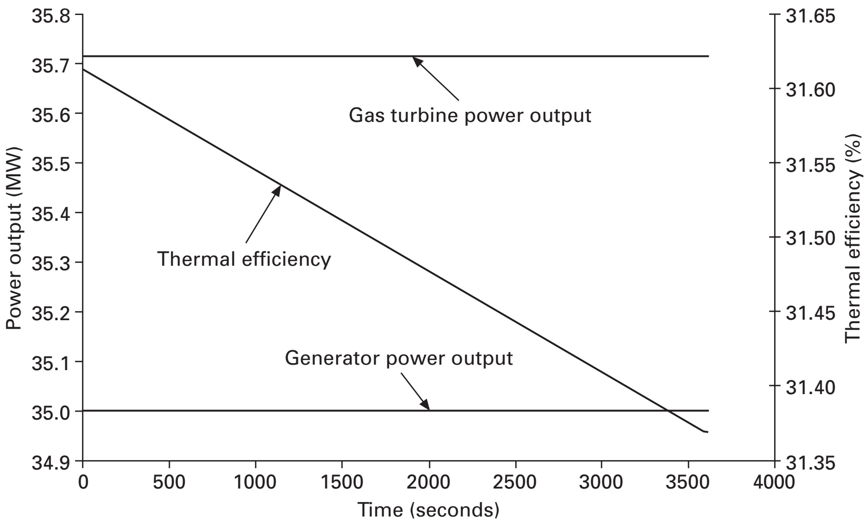

18.18 Trends in gas turbine power and thermal efficiency due to compressor fouling when operating at low power.

18.2.5 Trends in turbine creep life

It has been shown that the turbine metal temperature increases during this simulation of compressor fouling, mainly because of the increase in the turbine entry temperature (Fig. 18.15). Although there is a reduction in the turbine power resulting in a reduction in stress in the turbine blade material, the increase in temperature dominates and increases the creep life usage as shown in Fig. 18.19.

18.2.6 Trends in gas turbine emissions

The combustion primary zone temperature increases while the combustion pressure decreases, as discussed in Section 18.2.2. Although the decrease in combustion pressure would reduce NO_x the increase in combustion temperature is sufficient to result in an increase in the NO_x emissions. These changes in combustion pressures and temperatures have little effect on CO emissions, which remain essentially constant.

The decrease in the gas turbine thermal efficiency results in an increase in the CO_2 emissions index. The increase in the fuel flow to maintain the power required also results in an increase in CO_2 emissions on a mass basis. The trends in these emissions are shown in Fig. 18.20.

18.2.7 Displacement of running line due to compressor fouling

Since the level of compressor fouling in this case is the same as that applied to the high-power operating case, the shift in the running line is very similar. As operation is at the same compressor non-dimensional speed and the steepness of the compressor speed lines are the same, therefore, the operating points

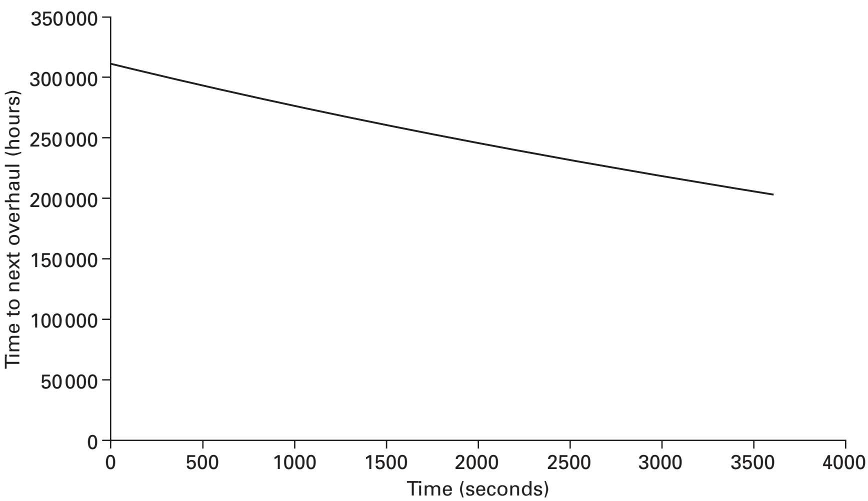

18.19 Trends in turbine creep life usage due to compressor fouling when operating at low power.

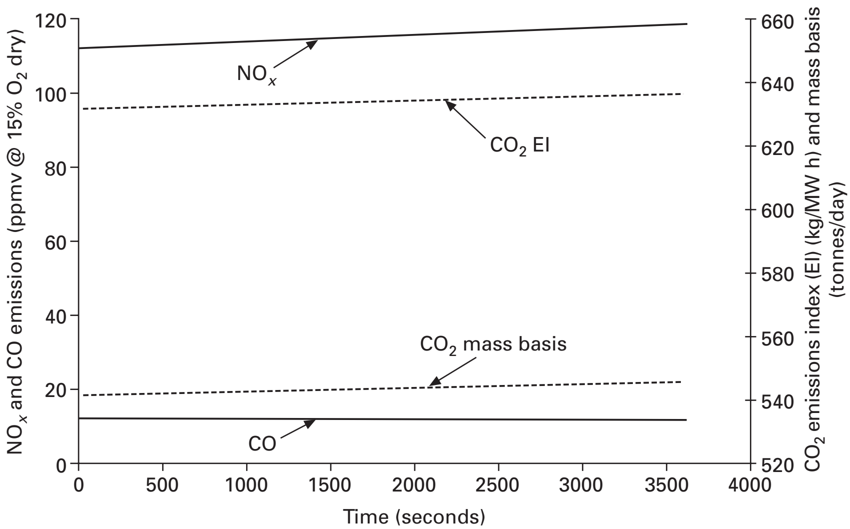

18.20 Trends in gas turbine emissions due to compressor fouling when operating at low power.

due to fouling for the high- and low-power cases are similar, as shown in Fig. 18.21. It is only when the ambient temperature changes that the operating point moves along the respective lines, depending on whether the compressor is fouled or not.

18.3 Compressor fouling at low-power operation (single-shaft gas turbine operating with an active variable inlet guide vane)

In Section 18.2 the effects of compressor fouling when operating at low powers were considered such that no engine operating limit was reached during the simulation. Furthermore, these cases assumed that the VIGV remained open during compressor fouling. The effects of compressor fouling on engine performance are now considered when the VIGV is active during the normal power range of the gas turbine. Means to achieve active VIGV operation during the normal power range have been discussed in Chapter 16 and in this chapter, and are described in the simulator user guide on the CD.

Compressor fouling is introduced via fault indices as discussed earlier in this chapter and the fouling and ambient conditions are the same as that discussed previously. The power demand is set to 35 MW for the low power case. The case of maximum power can be considered, but this would be the same as that discussed in Section 18.1 as the VIGV would remains open since the engine power output is limited by the EGT.

At low ambient temperatures, the performance of the gas turbine will be different, as the engine is power limited rather than EGT limited. The response

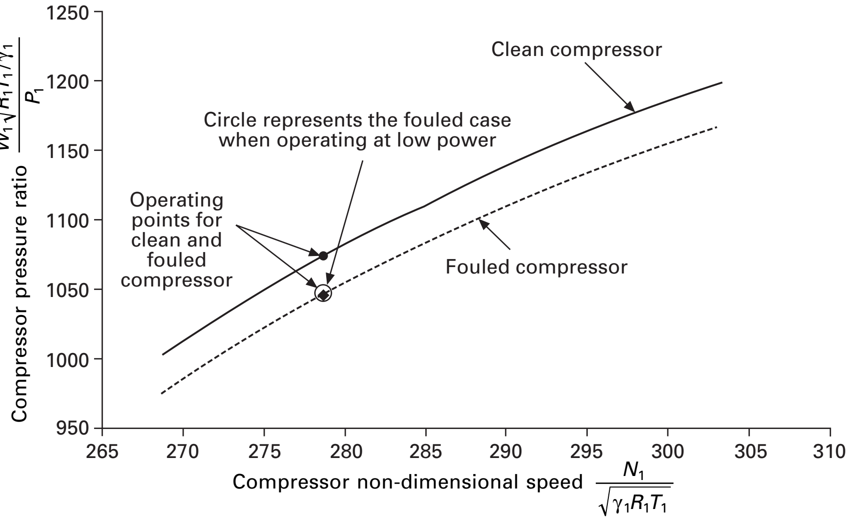

18.21 Operating points for the fouled compressor when operating at low and high power.

of the engine will then be similar to that discussed here, since power output of the generator is held constant during this simulation. The reader is left to simulate the effect of compressor fouling when the engine power is limited, as will happen at low ambient temperatures. The generator power demand for this maximum power case should be set to 60 MW.

Since the level of fouling over the time period of 1 hour is the same as that discussed in Section 18.1, the trends in the fault indices will be the same as shown in Fig. 18.1. When operating at low power, compressor fouling will increase the EGT if the VIGV remains open as was found in Section 18.2.2. In this case, the VIGV control system will open, the VIGV to maintain the EGT at its set point. The opening of the VIGV increases the compressor non-dimensional flow, thus compensating for the reduced flow capacity of the compressor due to fouling. Hence, the operating point on the compressor characteristic remains essentially unchanged as shown in Fig. 18.22. Furthermore, the opening of the VIGV improves the compressor efficiency due to the operating point matching on the compressor characteristic where the efficiency is higher. The compensates for the loss in compressor efficiency due to fouling and is discussed in Section 16.3.3.

As a result, there is very little change in the trends in powers, efficiencies (see Fig. 18.23), pressures, temperature, etc. with the exception of the VIGV trend. This shows an increase during compressor fouling, as shown in Fig. 18.24, where the VIGV position increases from 72% to about 86%.

It should not be thought that compressor washing and cleaning can be deferred because of the very small loss in engine performance resulting from

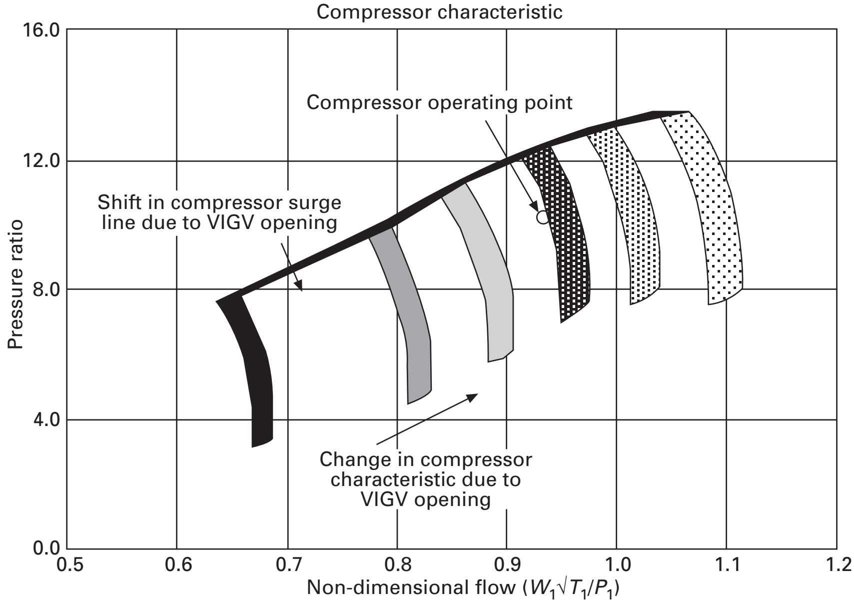

18.22 Operating point due to compressor fouling, at low power and with VIGV operation.

the opening of the VIGV due to compressor fouling. It is only when the maximum power demand from the gas turbine is required that the loss in power output and thermal efficiency is observed. Thus it is always necessary to clean the compressor on a regular basis if lost production and increased fuel costs are to be avoided at high-power conditions. Certainly, some delay in the washing of the compressor may occur when operating at low power; however, such wash optimisation should take into careful consideration the increased life cycle costs when maximum power output from the gas turbine is required.

18.3.1 Displacement of the running line during compressor fouling

Also discussed in Section 18.2.7 was the effect of compressor fouling on the running line as shown in Fig. 18.21. The compressor characteristic was fixed, due to the VIGV being fully opened, thus an approximate unique running line (describing the variation of compressor non-dimensional flow with compressor non-dimensional speed, as shown in Figures 18.11 and 18.21) is observed and the shift of this running line is affected only by compressor fouling. When the VIGV is active in the normal operating power

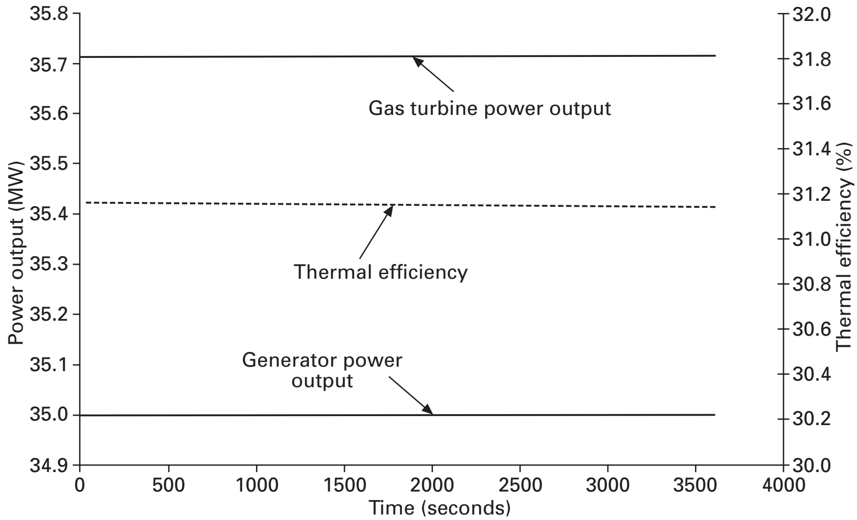

18.23 Trends in power and thermal efficiency. Note the very slight drop in thermal efficiency due to compressor fouling at low power and with VIGV operation.

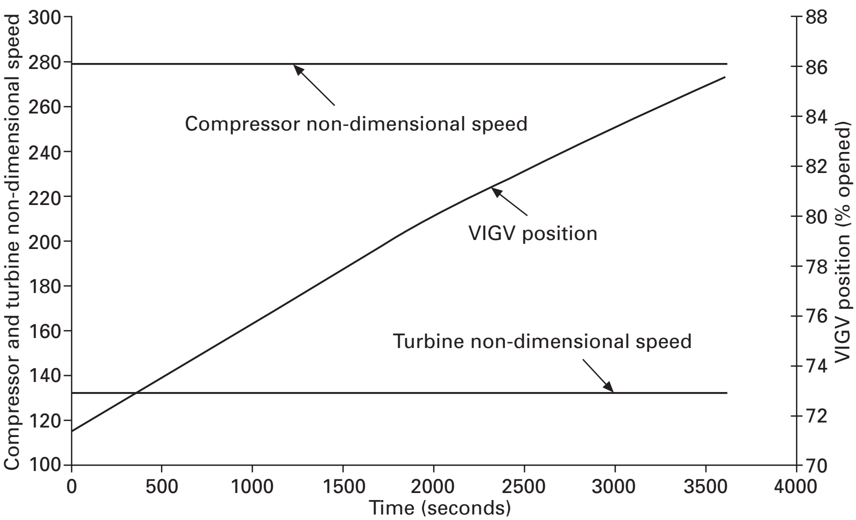

18.24 Trend in VIGV position due to compressor fouling at low power and with VIGV operation.

range, the characteristic is continuously changing, thus the running line for a clean compressor will also change. Hence, compressor fouling cannot be detected due to the shift of the running line as shown in Fig. 18.21, and there is no simple means of detecting compressor fouling for a single shaft gas turbine when the VIGV is active. In this instance, gas turbine models are needed such as that used in building this simulator in conjunction with gas path analysis techniques to detect compressor fouling.

It should be pointed out that the compressor of the two-shaft gas turbine also uses VIGV and VSV to achieve satisfactory performance of the engine and the concept of unique running lines was applied to detect compressor fouling. In this case, the movement of the VIGV and VSV is determined by the compressor non-dimensional speed rather than by the EGT. Thus, for a given compressor non-dimensional speed, there is a unique VIGV/VSV position and this results in a unique compressor characteristic for a given compressor non-dimensional speed. Therefore, the displacement of the unique running lines can be used to detect compressor fouling for a two-shaft gas turbine and this has been discussed in Section 13.1.12.

18.4 Turbine damage (hot end damage) at high-power outputs

As discussed previously, turbines are exposed to high temperatures and the turbine blades are often cooled to achieve satisfactory life. Over a period of time, turbine damage may occur where the bowing and erosion of the nozzle guide vanes (NGV) increases the non-dimensional flow capacity of the turbine (hot end damage). The change in incident and deflection of the gas through the turbine stages, due to damage of the turbine blades, will also affect the turbine efficiency. Turbine blade rubs also result in reduced engine performance and such damage normally affects the turbine efficiency rather than the flow capacity of the turbine. The effect of hot end damage on engine performance will be considered and the reader left to simulate the effects of turbine blade rubs on engine performance. The simulation of hot end damage is achieved by increasing the turbine fouling fault index by 3%, while decreasing the turbine efficiency fault index by 2%. On this occasion hot end damage which occurs over a 1-hour period will be simulated.

The effect of hot end damage will be considered when the engine is operating at two power output conditions. The first is at a power level such that the engine is always on an operating limit such as EGT. The second case is at reduced power, when no engine operating limit is reached during hot end damage; but the case of the VIGV being active at reduced operating power will be considered so that the EGT is maintained on the set point, which corresponds to the maximum EGT limit. The ambient pressure and temperature is set at 1.013 Bar and 15 degrees Celsius, respectively. Inlet and exhaust losses of 100 mm water gauge are also assumed. The high-power case is simulated by setting the power demand from the generator to 60 MW. At an ambient temperature of 15 degrees Celsius, the engine is constrained to operate on the EGT limit.

18.4.1 Trends in fault indices

Hot end damage has been implemented by increasing the turbine capacity and decreasing its efficiency via fault indices. This is shown as a trend in Fig. 18.25, where it is observed that the turbine fouling fault index increases from 0% to 3%, while the efficiency fault index decreases from 0% to – 2% over a period of 1 hour.

18.4.2 Compressor characteristic and trends in pressure and temperature ratios

The increase in the turbine fouling fault index results in increased turbine non-dimensional flow capacity. If it is assumed that the maximum to minimum cycle, temperature ratio T_3/T_1, remains constant, then from the flow compatibility equation (Equation 8.1) the compressor pressure ratio, P_2/P_1, decreases. This is because the compressor non-dimensional flow remains essentially constant due to the steepness of the compressor non-dimensional speed lines.

Since the engine is on an EGT limit, any decrease in the compressor pressure ratio, and therefore in the turbine pressure ratio, causes the turbine entry temperature to decrease, which requires a further reduction in the compressor pressure ratio to maintain the flow compatibility between the compressor and the turbine. This is shown in Fig. 18.26.

The decrease in the compressor pressure ratio due to hot end damage is also shown on the compressor characteristic, where a change in the operating

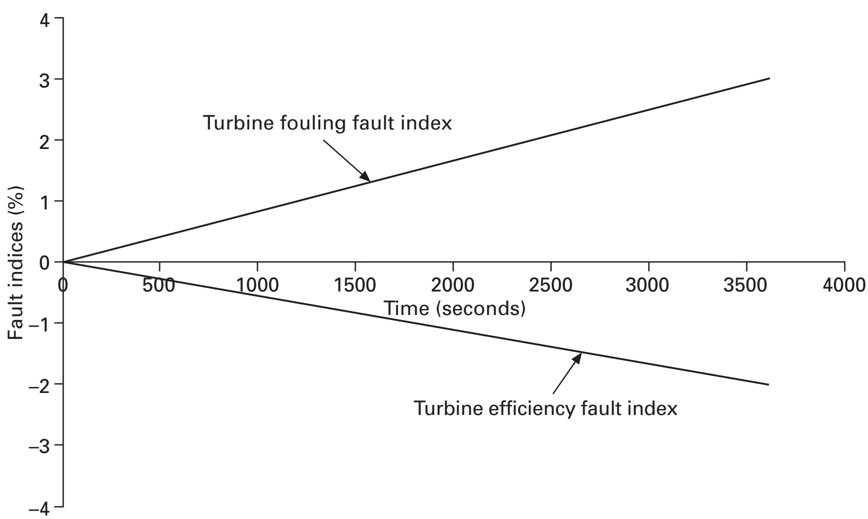

18.25 Trends in turbine fault indices due to hot end damage.

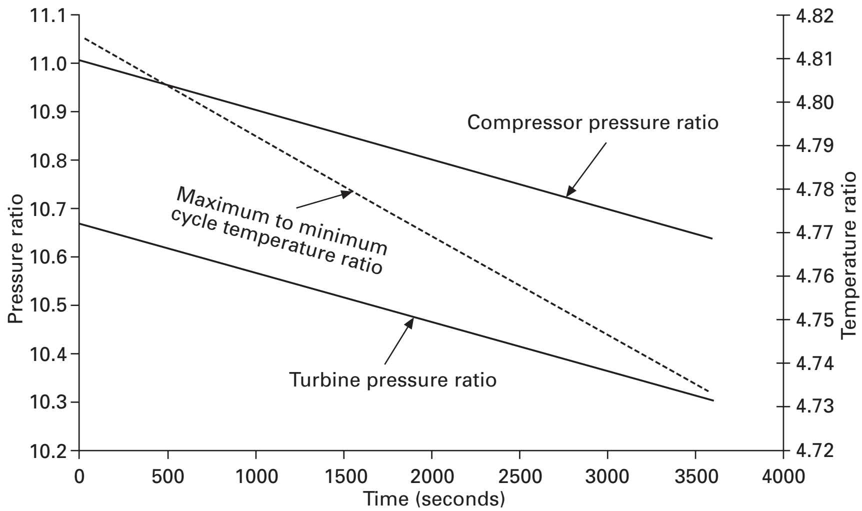

18.26 Trends in compressor, turbine and maximum-to-minimum cycle temperature are shown due to hot end damage.

point on the compressor characteristics is shown in Fig. 18.27. The operating point is constrained to operate on a fixed compressor non-dimensional speed as the ambient temperature (which is also the compressor inlet temperature), and the compressor speed remain constant. As stated this results in little change in the compressor non-dimensional mass flow and is due to the steepness of the compressor non-dimensional speed line.

18.4.3 Trends in power and efficiency

The decrease in T_3/T_1 and the compressor pressure ratio result in the reductions in the gas turbine thermal efficiency and power output. At the operating compressor pressure ratios, the loss in power output is largely due to the reduction in T_3/T_1 rather than the decrease in the compressor pressure ratio. However, the decrease in the gas turbine thermal efficiency is affected by both these parameters. Furthermore, the decrease in the turbine efficiency also affects both the power output and thermal efficiency quite adversely, as shown in Fig. 18.28 (where the trends in gas turbine power and thermal efficiency is shown to be due to hot end damage).

The loss in turbine power due to hot end damage is evident and is shown in Fig. 18.29 (which shows the trends in compressor and turbine powers and efficiencies). The change in compressor power absorbed is much smaller, compared to the change in the turbine power and is primarily due to the significant loss in the turbine efficiency.

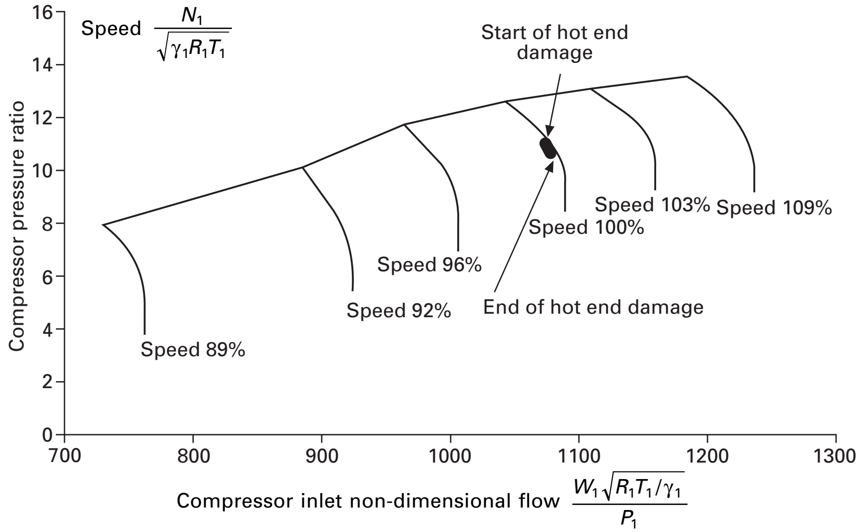

18.27 Change in the operating point on the compressor characteristic due to hot end damage.

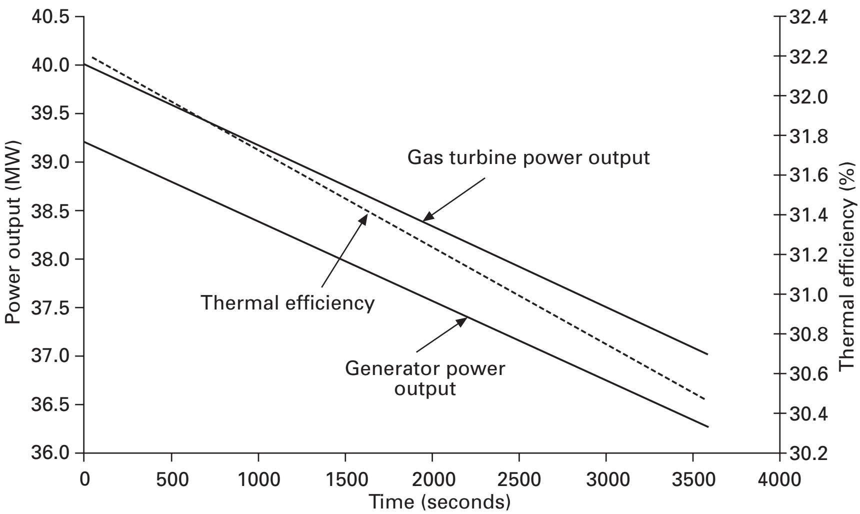

18.28 Trends in gas turbine and generator power outputs, and thermal efficiency due to the effect of hot end damage.

18.4.4 Trends in pressure and temperature

As the ambient pressure and thus the compressor inlet pressure remain constant, the decrease in compressor pressure ratio and the turbine pressure ratio result in decreases in the compressor discharge pressure and turbine inlet

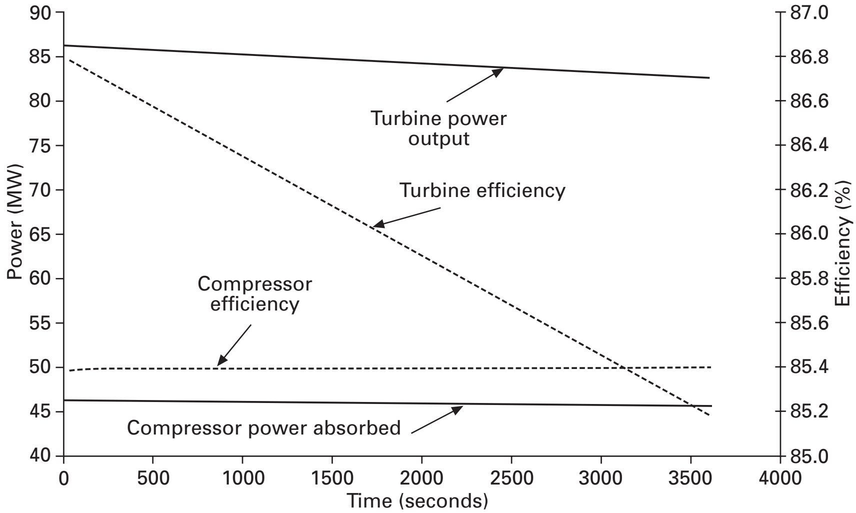

18.29 Trends in compressor and turbine power and efficiency due to the effect of hot end damage.

pressure. This can be seen in Fig. 18.30 which shows the trends in pressure due to hot end damage.

The decrease in T_3/T_1 shown in Fig. 18.26 results in a decrease in the turbine entry temperature, T_3, since the compressor inlet temperature remains constant during this simulation. The EGT remains on the limit as it prevents the engine from overheating the turbine during high-power operation. Since the compressor is operating at a constant non-dimensional speed, the non-dimensional temperature rise across the compressor does not change much and hence no significant change is seen in the compressor discharge temperature due to hot end damage. The decrease in the turbine entry temperature also results in decreases in the combustor primary zone temperature and in the turbine metal temperature. The trends in these temperatures due to hot end damage are shown in Fig. 18.31.

18.4.5 Trends in flow

Since the compressor non-dimensional speed remains constant during this simulation, the compressor non-dimensional flow also essentially remains constant. As the compressor inlet temperature and pressure remain constant, there is little change in the compressor airflow rate due to hot end damage, as shown in Fig. 18.32. As a result, the combustion air flow also remains essentially constant. The loss in power output due to hot end damage is greater than the loss in the gas turbine thermal efficiency and therefore a

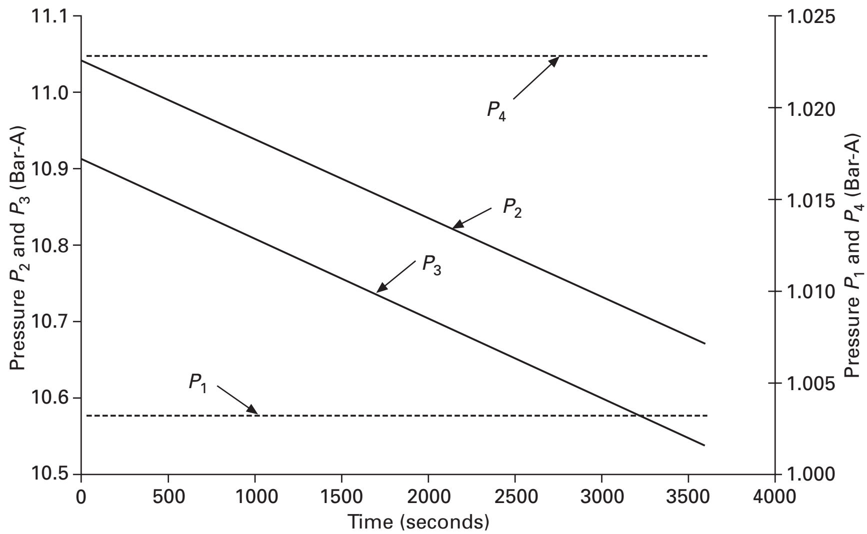

18.30 Trends in pressure due to hot end damage.

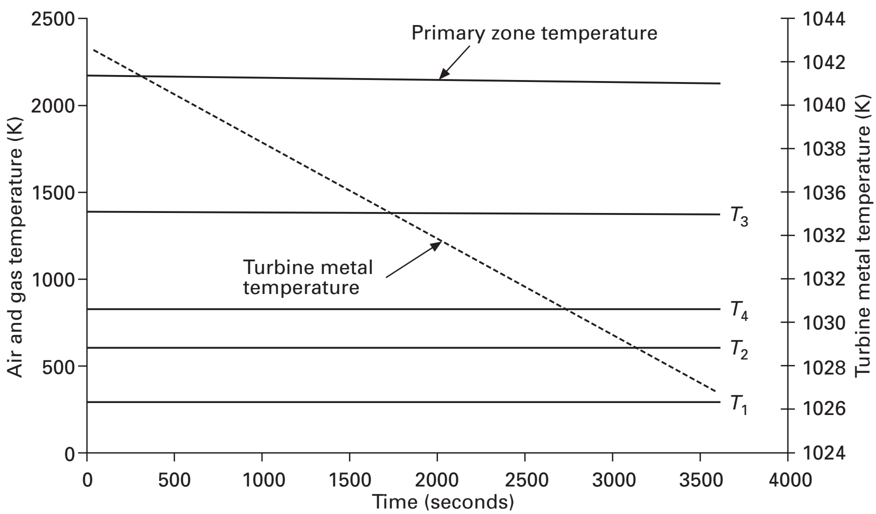

18.31 Trends in temperature due to hot end damage.

decrease in the fuel flow is observed. The air–fuel ratio now increases and this is due to the decrease in fuel flow, while the combustion air flow remains essentially constant. The fuel valve position follows the fuel flow trend and therefore shows a decrease in the fuel valve position during this simulation.

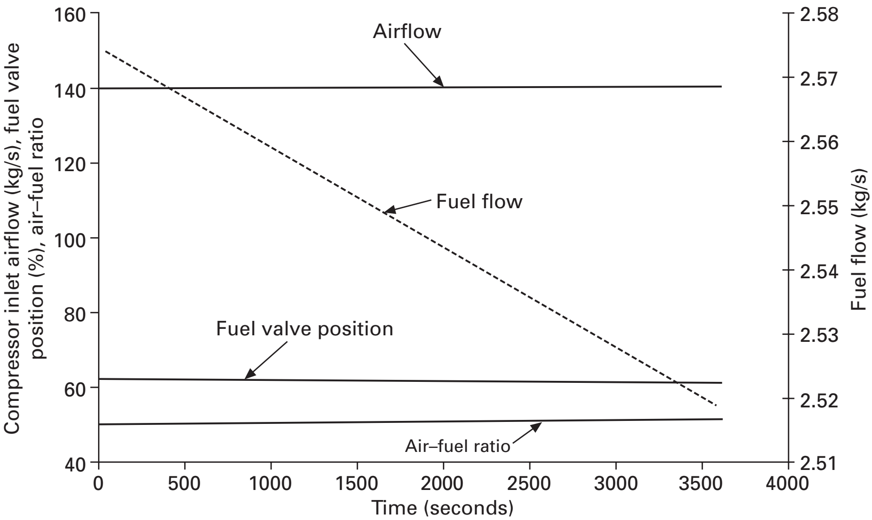

18.32 Trends in flow, air-to-fuel ratio and fuel valve position due to the effect of hot end damage.

18.4.6 Trends in turbine creep life

During the simulation of hot end damage when operating at high power, a decrease in the turbine blade metal temperature is observed, as shown in Fig. 18.31. It is also observed that the turbine power decreases (Fig. 18.29), which results in a decrease in the turbine blade torque, hence reducing stress in the turbine blade material. These two factors reduce the turbine creep life usage as shown in Fig. 18.33. It must again be pointed out that the power output has also reduced. Thus it is only when the simulator is run at this reduced maximum power and when no performance deterioration is present that an increase in creep life usage is seen in real terms due to hot end damage. This is left as a simulation exercise for the reader to demonstrate the actual creep life usage due to hot end damage.

18.4.7 Trends in gas turbine emissions

The decrease in combustion pressure (Fig. 18.30) and temperature (Fig. 18.31) result in a decrease in NO_x emissions, while CO emissions increase. To determine the true picture of the impact of hot end damage on these emissions, it is necessary to run the simulator at the reduced power available due to this performance deterioration, but when no hot end damage is present. It is then that an increase in NO_x emissions will be observed in real terms.

The reduction in fuel flow results in the decrease in CO_2 emission on a mass basis but, due to the decrease in the gas turbine thermal efficiency, an

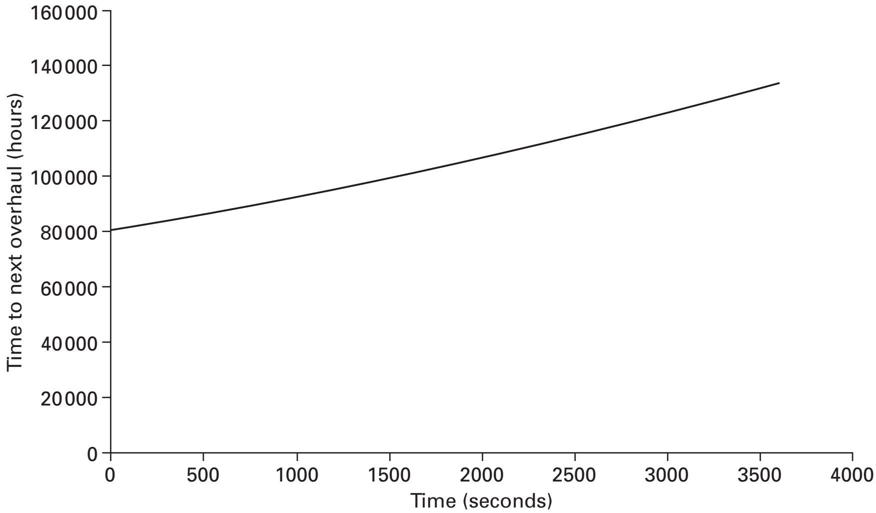

18.33 Turbine creep life usage due to hot end damage and operating at high power.

increase in the CO_2 emissions index is observed, as can be seen in Fig. 18.34. This shows the trends in gas turbine emissions due to hot end damage when operating at high power. Thus, in real terms, there is an increase in CO_2 emissions due to hot end damage.

18.5 Hot end damage at low power with active VIGV operation

The effect of hot end damage on the engine performance has been discussed when operating at high power and the reader left to simulate the case when operating at low power, when the VIGV remains fully opened. The impact of hot end damage at low operating power (e.g. 35 MW) with the VIGV fully opened is an increase in the EGT so that the power demand can be maintained. This results in an increase in turbine entry temperature, and thus an increase in T_3/T_1, but a decrease in compressor pressure ratio.

The impact of hot end damage is now investigated when the VIGV is active to maintain the EGT on its set point (maximum EGT limit) during the normal operating power range. The method of implementation of hot end damage using the simulator and the ambient conditions are the same as those discussed in Section 18.4. Thus the trends in the fault indices are the same as those shown in Fig. 18.25. However, the power demand from the generator is reduced to 35 MW, as the case is being simulated when the power demand is below the maximum available from the gas turbine.

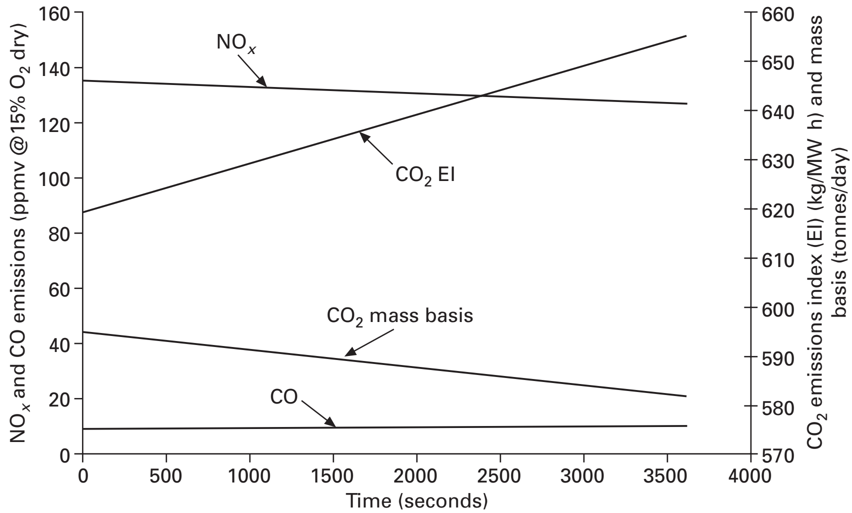

18.34 Trends in gas turbine emissions due to hot end damage when operating at high power.

18.5.1 Compressor characteristic and trends in pressure and temperature ratio

The increase in the EGT due to hot end damage results in the opening of the VIGV, such that the EGT remains on the EGT limit, which is also the set point for the VIGV control system, during this simulation. The opening of the VIGV results in an increase in the compressor non-dimensional flow capacity. The effect of hot end damage also results in an increase in the turbine non-dimensional flow capacity. The increase in the turbine non-dimensional flow is almost compensated by the increase in the compressor non-dimensional flow due to the opening of the VIGV. As a result, only a small change (increase) in the compressor pressure ratio is needed to satisfy the flow compatibility between the compressor and turbine. This can be seen in Fig. 18.35, which shows the operating points on the compressor characteristic during the simulation of hot end damage. Furthermore, the change in the maximum to minimum cycle temperature ratio, T_3/T_1, is also small, although a slight decrease is observed in the trend of T_3/T_1, as shown in Fig. 18.36. This is due to the increase in mass flow rate through the engine, resulting from the increase in compressor non-dimensional flow (due to the opening of the VIGV), thus compensating for the loss in specific work due to hot end damage. Figure 18.36 also shows the changes in compressor and turbine pressure ratios and, as stated, there are only small increases in these pressure ratios.

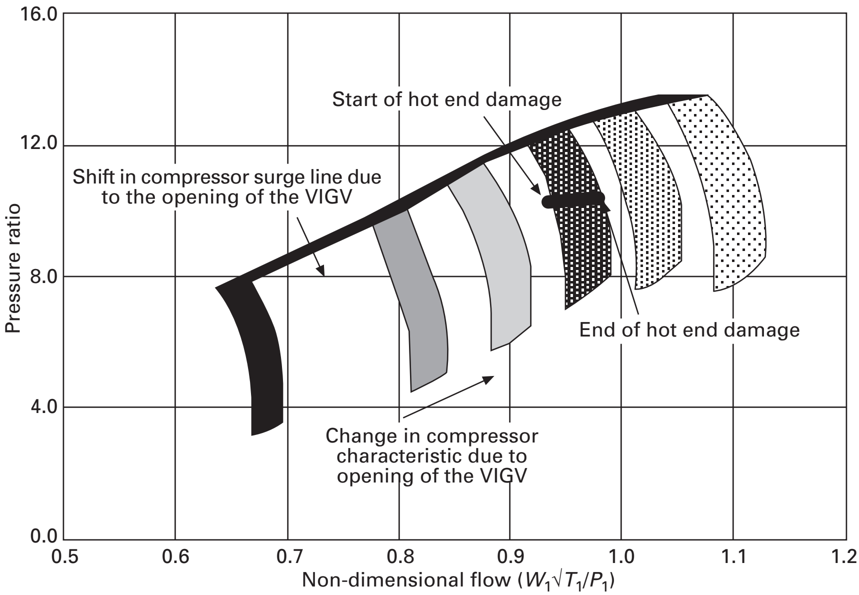

18.35 Operating point on the compressor characteristic due to hot end damage at low power with VIGV operation.

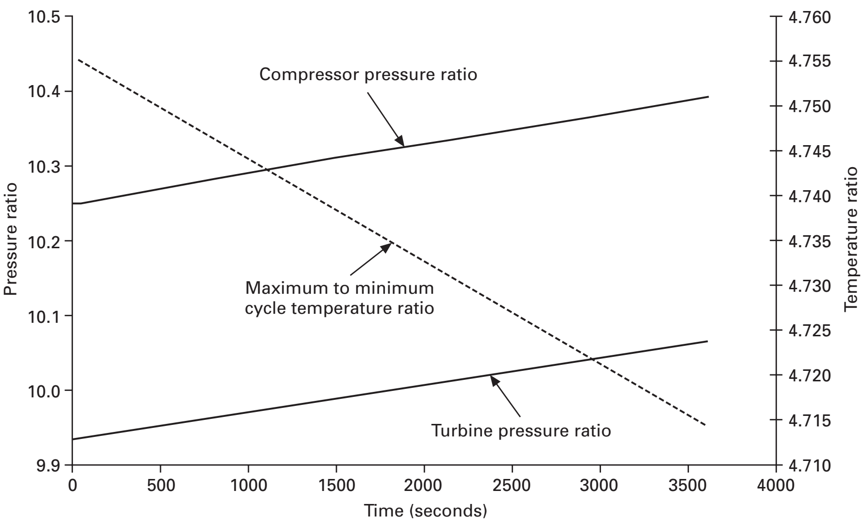

18.36 Trends in pressure and temperature ratios due to hot end damage when operating at low power with active VIGV operation.

18.5.2 Trends in power and efficiency

The increase in the compressor flow results in an increase in the compressor power absorbed. The turbine power output also increases to satisfy the work compatibility between the compressor and the turbine when operating at a fixed power demand from the generator. The compressor efficiency increases due to the opening of the VIGV, where the operating point on the compressor characteristic corresponds to a higher efficiency, as explained in Section 16.3.3. The decrease in the turbine efficiency is due to hot end damage (see Fig. 18.37).

Figure 18.38 shows the trends in the gas turbine and generator power outputs and thermal efficiency. The gas turbine and generator power outputs remain constant during this simulation as no engine operating limits are exceeded during hot end damage due to the low power demand from the gas turbine. The generator power output remains on the power set point of 35 MW. Although there is an increase in the compressor efficiency and pressure ratio, the loss in the turbine efficiency due to hot end damage results in a decrease in the thermal efficiency.

18.5.3 Trends in pressure and temperature

Since the compressor and turbine pressure ratios increase slightly, the trends in compressor discharge and turbine inlet pressure do not vary much, as seen

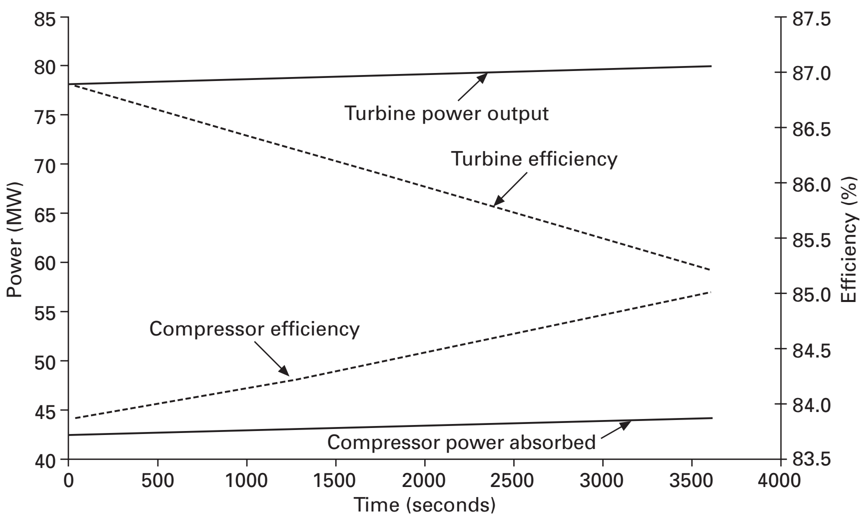

18.37 Trends in compressor and turbine power and efficiency due to the effect of hot end damage when operating at low power with VIGV operation.

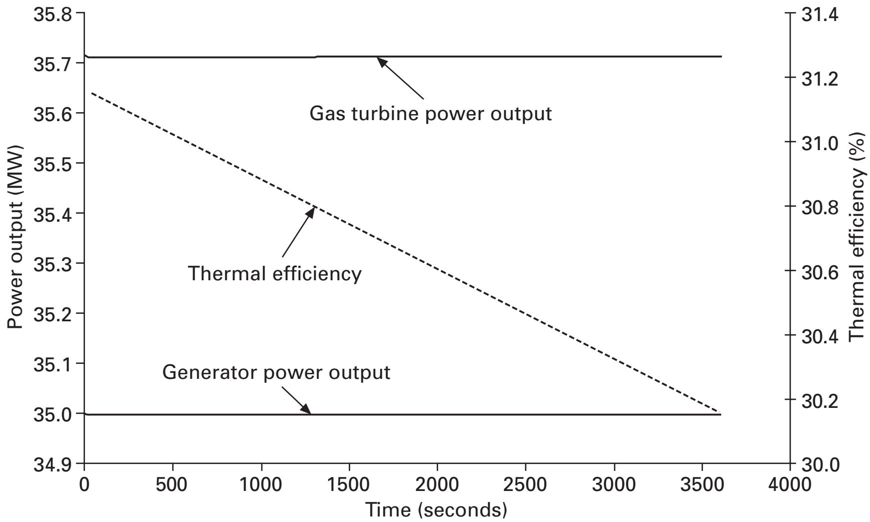

18.38 Trends in gas turbine and generator power outputs and thermal efficiency due to hot end damage when operating at low power with VIGV operation.

in Fig. 18.39. The small decrease in the maximum to minimum cycle temperature ratio, T_3/T_1, results in a small decrease in the turbine entry temperature, T_3, since the compressor inlet temperature, T_1, remains constant during this simulation. A small increase in the compressor pressure ratio and efficiency results in the compressor discharge temperature, T_2, remaining almost constant. The small decreases in turbine entry temperature and compressor discharge temperature results in a slight decrease in the turbine blade metal temperature. There is also a small reduction in the combustor primary zone temperature. These are shown as trends in Fig. 18.40.

18.5.4 Trends in flow

Since the compressor inlet temperature and pressure remain constant, the increase in the compressor non-dimensional flow due to the opening of the VIGV results in an increase in the compressor mass flow rate. This can be seen in Fig. 18.41, which shows the trends in flows due to hot end damage when operating at low powers.

The decrease in the gas turbine thermal efficiency results in an increase in fuel flow to maintain the power demand from the generator. To satisfy the increase in fuel flow the fuel valve also opens as shown in Fig. 18.41. From the trends in temperatures it has been seen that a slight decrease in the turbine entry temperature occurs while the compressor discharge temperature remains essentially constant. The air–fuel ratio therefore increases slightly as shown in Fig. 18.41.

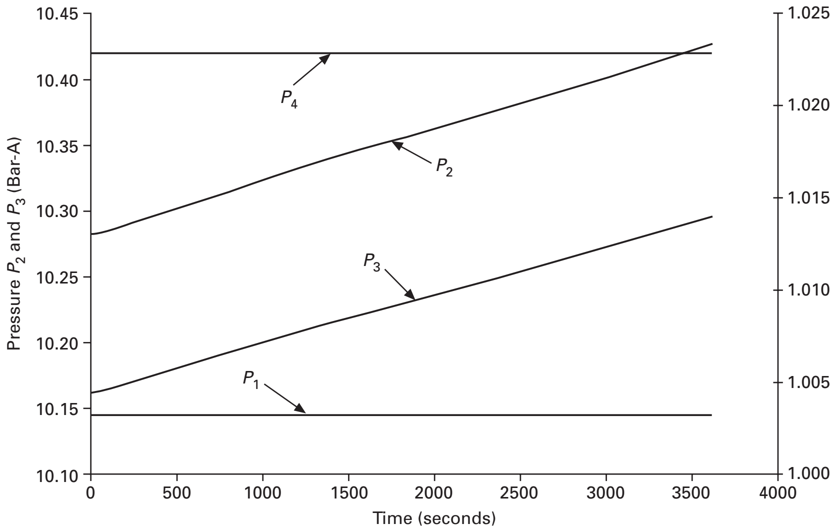

18.39 Trends in pressure due to hot end damage when operating at low power with VIGV operation.

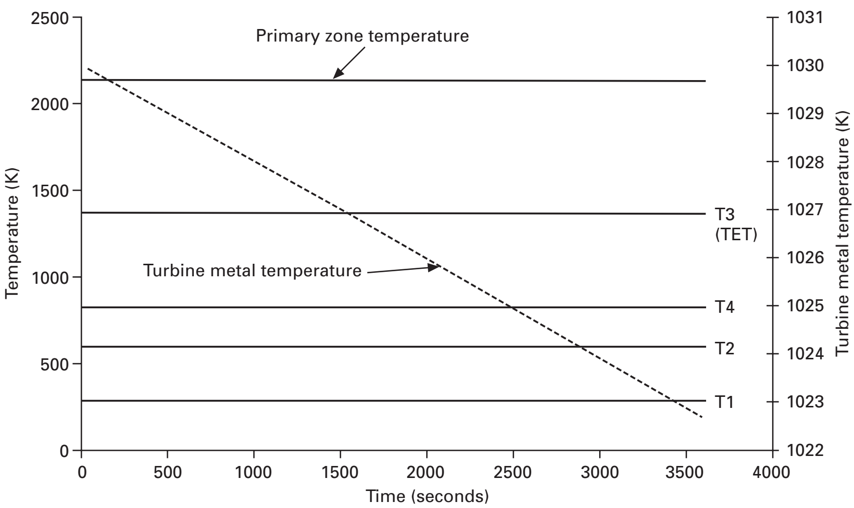

18.40 Trends in temperature due to hot end damage and operating at low power with VIGV operation.

18.5.5 Trends in VIGV position and speed

The increase in the VIGV position to maintain the EGT on its set point during hot end damage is shown as a trend in Fig. 18.42. The VIGV opens from about 72% to 92% in order to maintain the EGT on its set point. The

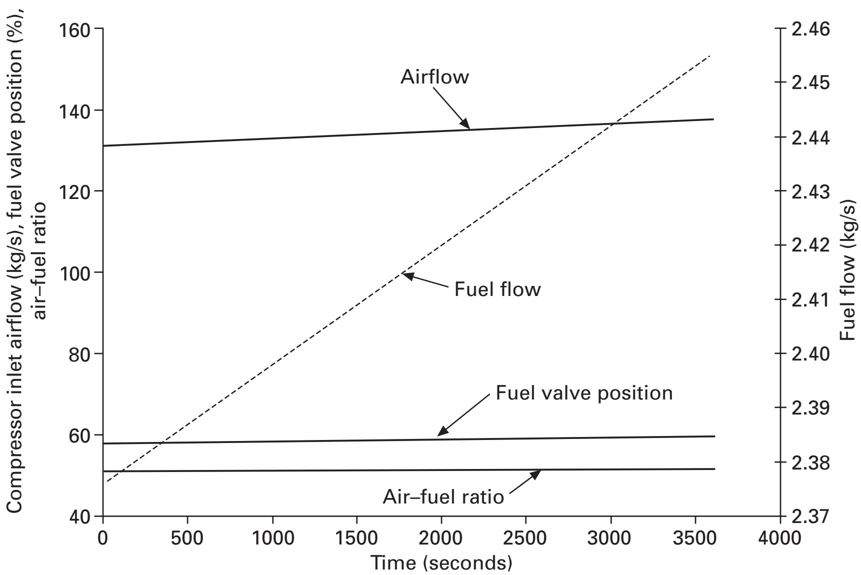

18.41 Trends in flow, fuel valve position and air–fuel ratio due to the effect of hot end damage when operating at low power with VIGV operation.

trend in the compressor non-dimensional speed shows no variation because the compressor speed and the inlet temperature remain constant. Since the turbine entry temperature is essentially constant and the gas turbine speed is constant, the turbine non-dimensional speed also essentially remains constant as shown in Fig. 18.42.

18.5.6 Trends in turbine creep life

Figure 18.43 shows the trend in the creep life usage due to hot end damage when operating at low power, and the VIGV operating to maintain the EGT on its limit. In Fig. 18.43 the noticeable decreasing turbine creep life usage is observed in real terms, which is primarily due to the decrease in the turbine metal temperature, although there is an increase in the stress in the turbine material due to the increased power output from the turbine, as seen in Fig. 18.37. This is indeed different to other cases that have been considered, where deterioration in gas turbine performance resulted in an increase in creep life usage in real terms and would generally result in increased life cycle costs due to the higher maintenance cost of the engine. It should be noted that, for a given turbine pressure ratio, the turbine entry temperature would decrease as the turbine efficiency decreases, while operating at a fixed EGT limit.

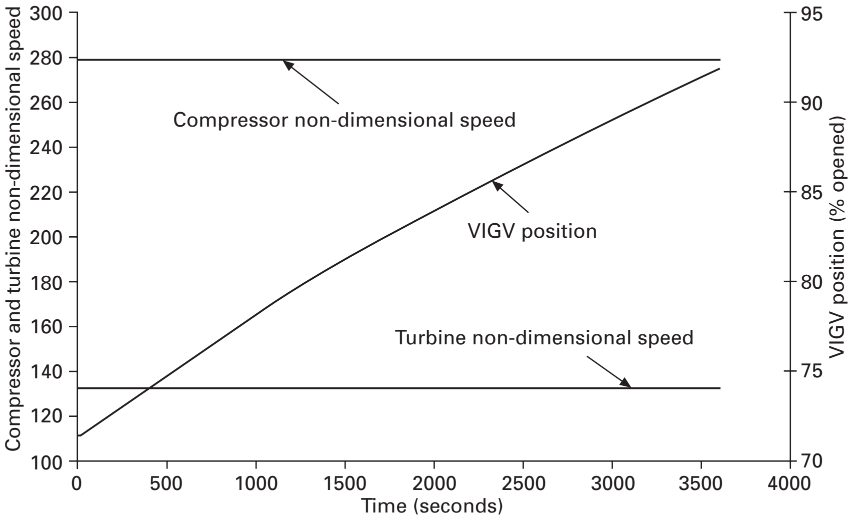

18.42 Trends in the VIGV and compressor and turbine non-dimensional speeds due to the effect of hot end damage.

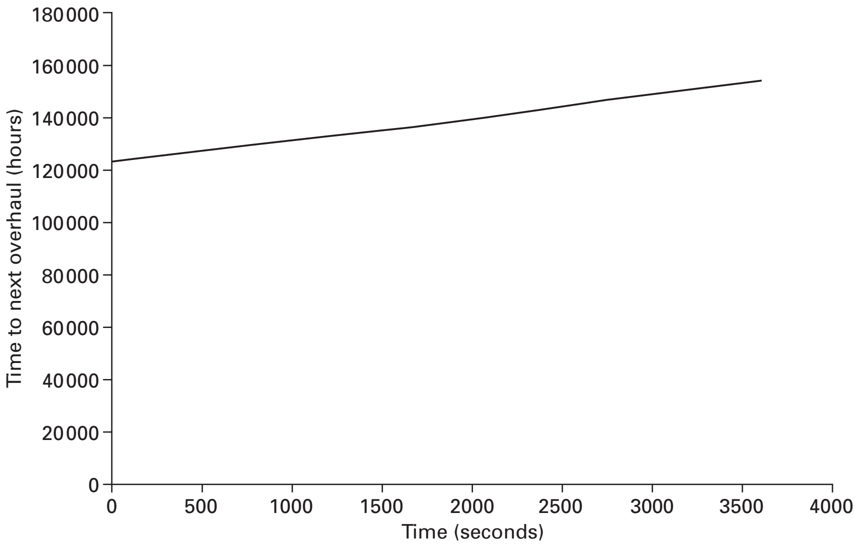

18.43 Trend in turbine creep life usage due to the effect of hot end damage when operating at low power with active VIGV operation.

18.5.7 Trends in gas turbine emissions

The small changes in combustion pressure and temperature due to hot end damage for this case result in very small changes in NO_x and CO emissions,

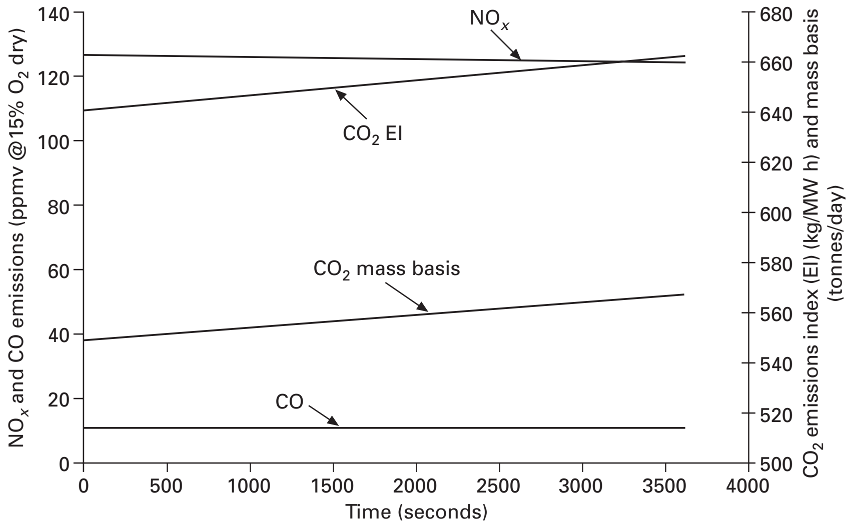

18.44 Trends in gas turbine emissions due to hot end damage when operating at low power with active VIGV operation.

as shown in Fig. 18.44. The decrease in the gas turbine thermal efficiency, however, results in an increase in the CO_2 emissions, on a mass and emission index basis.

19
Power augmentation

For a single-shaft gas turbine, the power output is limited by the EGT at high ambient temperatures and by the power limit at low ambient temperatures. This is necessary to achieve satisfactory turbine blade creep life by preventing the turbine over-heating and also to prevent operational problems such as compressor surge at low ambient temperatures. Unlike the two-shaft gas turbine discussed earlier, the single-shaft gas turbine usually operates at a constant speed so the radial or centrifugal stress will remain constant, although the bending stress will change due to the change in the power produced by the turbine. Thus, the performance-limiting parameters for a single-shaft gas turbine are generally EGT and power limit, unlike a two-shaft gas turbine operating with a free power turbine, where the speeds of the gas generator and the power turbine also limit the power output from the engine. The limiting values for the EGT and power of the single-shaft gas turbine (simulator), referred to as the base rating case, are as follows:

1. EGT limit 825 K
2. Power limit 45 MW.

The power output from the gas turbine at high ambient temperatures can be increased by raising the EGT limit by about 20 degrees. However, this will have an adverse impact on turbine blade creep life usage and the frequency of engine overhauls may increase, thus increasing the maintenance costs. Such augmentation of the power by increasing the EGT limit is often referred to as peak rating and is very similar to the case discussed for the two-shaft gas turbine.

At low ambient temperatures, the power output of the gas turbine is limited to reduce creep life usage, which can then be utilised at high ambient temperatures by increasing the EGT limit. In aero-gas turbines, this is referred to as flat rating, where the takeoff thrust can be increased on hot days, while the engine throttles are adjusted to provide only the required thrust on cold days (rating curves as discussed above in Chapter 11, Section 11.3.8). Limiting the power output at low ambient temperature also helps maintain adequate surge margin as discussed in Chapter 16. The power output from the gas turbine can be increased at low ambient temperatures by increasing the turbine non-dimensional flow capacity. This has the effect of maintaining an adequate compressor surge margin by reducing the compressor pressure ratio. It also lowers the turbine entry temperature for a given EGT thus minimising the effect on increased creep life usage at these increased power output conditions at low ambient temperatures. However, the performance of the gas turbine is reduced at high ambient temperatures when the EGT limits the power output. Thus, such modifications to the turbine section should only be considered if a substantial amount of operation occurs at lower limiting conditions. But such modifications will result in reduced turbine blade creep life usage at high ambient temperatures when the EGT limits the power output of the gas turbine and this is discussed later.

As with the case of the two-shaft gas turbine, the power output from a single-shaft gas turbine may be increased by water and steam injected directly into the combustor because of the increased flow rate through the turbine relative to the compressor. Alternatively, water may also be injected into the inlet system and the resultant evaporation produces a cooling effect (evaporative), thus increasing the power output from the gas turbine due to the reduction in compressor inlet temperature. Such power augmentation is often referred to as turbine inlet cooling (TIC). The impact of both direct water injection and turbine inlet cooling on power augmentation will be considered in this section.

Another means of augmenting the power output of a single-shaft gas turbine is to increase the air flow through the engine. This can be achieved by opening the VIGV and a useful increase in power output is possible by using such a technique.

The single-shaft gas turbine simulator will now be used to augment the power output from the gas turbine using each of these methods and their impact on performance, turbine blade life creep usage and emissions will be determined.

19.1 Peak rating

The simulator is run by setting the generator power demand at 60 MW (maximum capacity of the generator), thus ensuring that the engine is always on an operating limit such as the EGT. Peak rating is simulated by increasing the EGT limit by 20 degrees to 845 K. To consider the impact of peak rating at different ambient temperatures, the ambient temperature is changed from 35 degrees Celsius to –30 degrees Celsius in steps of 10 degrees. The increase in the EGT limit will result in an increase in the maximum to minimum cycle temperature ratio, T_3/T_1. To satisfy the flow compatibility between the compressor and turbine, there is also an increase in the compressor pressure ratio. The increases in these two performance parameters increase the power output and the thermal efficiency of the gas turbine, as shown in Fig. 19.1 and 19.2, respectively.

At high ambient temperature (30 degrees Celsius), the increase in power output is over 5%. Comparing the increase in power output with the case of

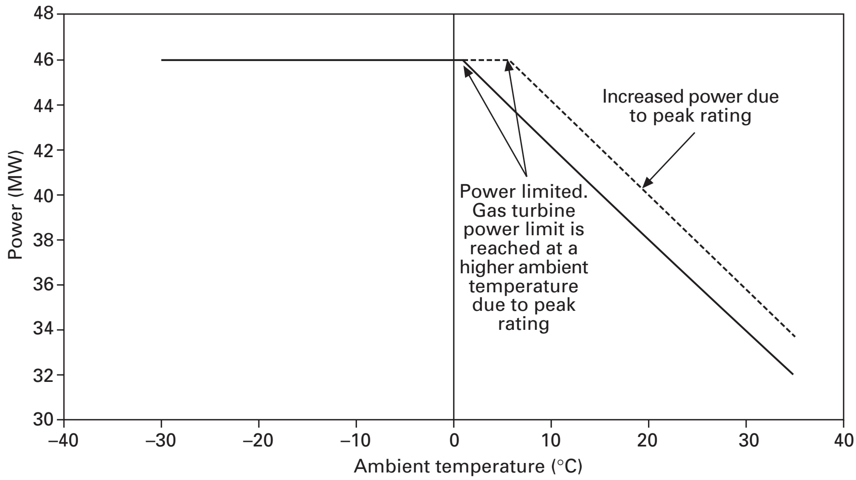

19.1 Increase in power outlet from gas turbine due to effect of peak rating.

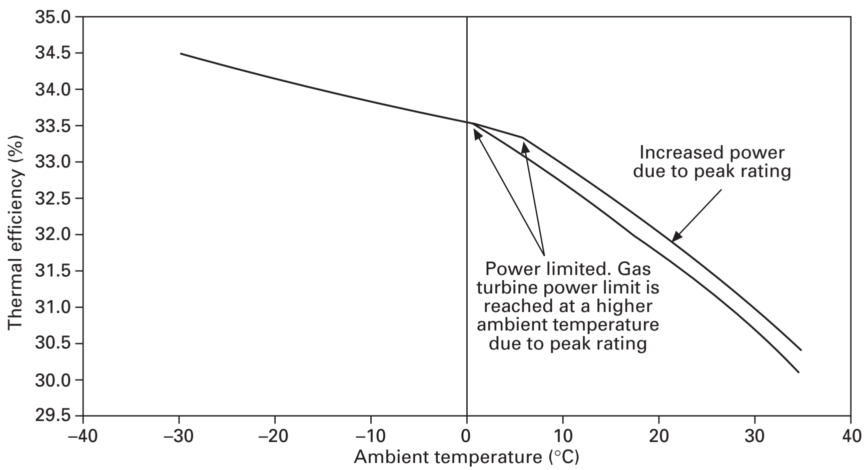

19.2 Increase in thermal efficiency from gas turbine due to effect of peak rating.

the two-shaft gas turbine, peak rating the two-shaft gas turbine is observed to give about a 7% increase in power output. In the case of the single-shaft gas turbine, for a given compressor inlet temperature, the compressor non-dimensional speed remains constant. Thus, the compressor mass flow rate and therefore the mass flow rate through the gas turbine remain constant, due to peak rating at a given ambient temperature. In the case of the two-shaft gas turbine, the gas generator speed increases with the increase in EGT, as the gas generator speed does not limit the power output from the gas turbine at high ambient temperatures. This results in an increase in the compressor non-dimensional speed and thus an increase in mass flow rate through the engine, hence the greater increase in power output from the two-shaft gas turbine due to peak rating. In general, and for the same increase in the EGT limit, peak rating a two-shaft gas turbine results in a greater increase in the percentage power output for this reason.

The increase in the thermal efficiency of the single-shaft gas turbine due to peak rating is shown in Fig. 19.2. At high ambient temperature, there is about a 1% increase in thermal efficiency and this is due to the increase in the compressor pressure ratio and T_3/T_1. A slightly higher increase in thermal efficiency is observed with the peak-rated two-shaft gas turbine. For a given increase in T_3/T_1, the increase in the gas generator speed results in a higher compressor pressure ratio due to the increase in the compressor non-dimensional speed. The higher compressor pressure ratio results in a better thermal efficiency due to peak rating of the two-shaft gas turbine operating with a free power turbine.

The higher EGT will result in an increase in the turbine entry temperature and thus an increase in the turbine blade metal temperature. The increase in turbine power will also increase the stress in the turbine blade material. Both these factors increase the turbine creep life usage, as shown in Fig. 19.3. The increase in creep life usage due to peak rating almost halves the time between turbine overhauls. Although there is a very useful increase in power output and thermal efficiency, peak rating is usually used sparingly to prevent high maintenance costs. It is normally used at high ambient temperatures, where the largest increase in power output occurs.

The higher turbine entry temperature and compressor pressure ratios result in an increase in the combustion pressure and temperature. These two factors increase the formation of NO_x while decreasing CO emissions, as shown in Fig. 19.4. The increase in the power output of the gas turbine is greater than the increase in the thermal efficiency, and therefore there will be increased CO_2 emissions on a mass basis. The better thermal efficiency decreases the CO_2 emissions index, thus peak rating decreases CO_2 emissions in real terms (i.e. peaking produces less CO_2 emissions per unit of power generated), as can be seen in Fig. 19.5.

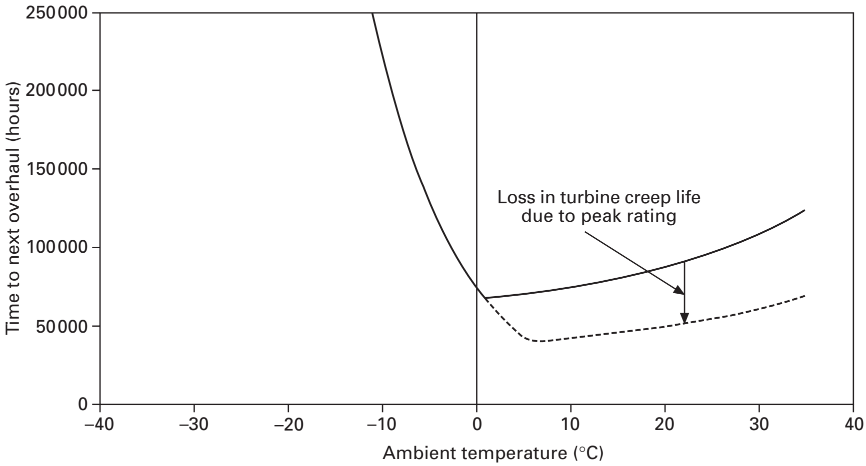

19.3 Increase in turbine creep life usage due to effect of peak rating.

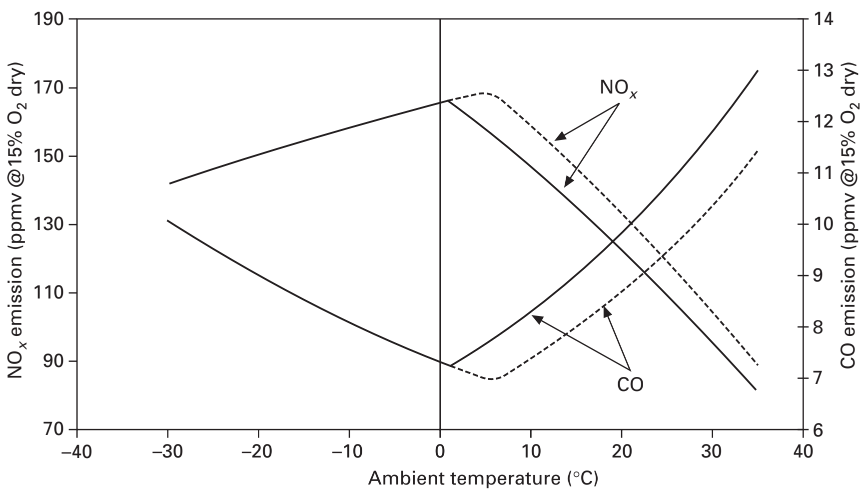

19.4 Change in NO_x and CO emissions due to effect of peak rating.

19.2 Power augmentation by increasing VIGV angle

Some manufacturers of single-shaft gas turbines offer a modification, where the VIGV angle may be increased by a small amount. Such modifications to the VIGV angle will increase the compressor flow rate and thus the power output from the gas turbine. However, this increase in power output is possible

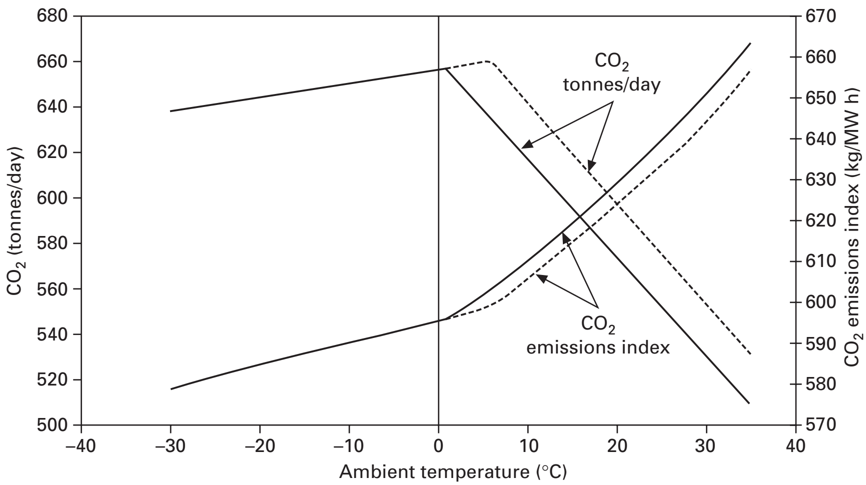

19.5 Change in CO_2 emissions due to effect of peak rating.

only when the engine power output is limited by the EGT, which normally occurs at high ambient temperatures. Opening of the VIGV angle could reduce the surge margin as shown in Fig. 16.21 (Chapter 16) and the maximum power limit of the gas turbine may have to be reduced, therefore decreasing the compressor pressure ratio to ensure a satisfactory compressor surge margin when operating at low ambient temperatures. Thus, at low ambient temperatures when the power output is limited, there may be a penalty paid in engine performance. Power augmentation by increasing the VIGV angle is simulated by increasing the compressor fouling fault index by 3%.

The increase in the compressor mass flow rate and thus the increase in the compressor non-dimensional flow due to the opening of the VIGV result in a higher compressor pressure ratio to satisfy the flow compatibility between the compressor and the turbine, as shown in Fig. 19.6. To maintain the compressor pressure ratio at or below the base rating case, and to ensure adequate compressor surge margin at low ambient temperatures, the maximum power limit is reduced to about 42MW, as can be seen in Fig. 19.7. There is a useful increase in the power output from the gas turbine of about 3.5% at high ambient temperatures, but at low ambient temperatures there is a substantial decrease in the power output of about 10%. It has been assumed that the maximum compressor pressure ratio is near or just below the base rating case at low ambient temperatures. However, if the opening of the VIGV erodes the surge margin significantly, the compressor pressure ratio must be decreased further at low ambient temperatures to ensure a satisfactory compressor surge margin. This will require a further reduction in the maximum power limit.

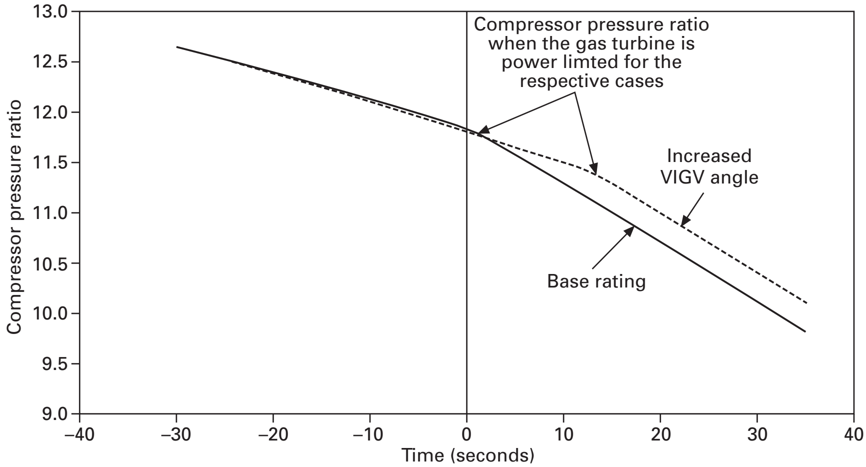

19.6 Change in compressor ratio due to effect of increasing the VIGV angle.

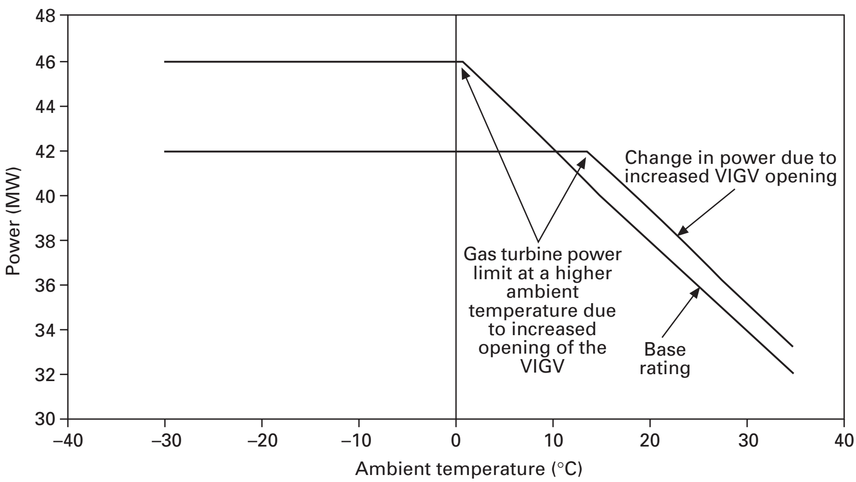

19.7 Change in gas turbine power output due to effect of increasing the VIGV angle.

The increase in the compressor pressure ratio at high ambient temperatures also results in an improvement in the gas turbine thermal efficiency due to the increase in the VIGV position. But, at low ambient temperatures, when the engine is operating at the maximum power limit, the turbine entry temperature decreases due to the reduced gas turbine maximum power limit. Thus there is a reduction in the maximum cycle temperature, T_3/T_1, relative to the base case, which results in a noticeable decrease in the thermal efficiency of the gas turbine at lower ambient temperatures, as shown in Fig. 19.8.

At high ambient temperatures, when the engine power output is EGT limited, the increase in power output from the gas turbine is due largely to the increase in the air flow rate through the engine, due to the increase in the VIGV angle. Thus, there is only a slight increase in the temperature entry temperature, and hence in the turbine blade metal temperature. However, the increase in turbine power results in an increase of the torque in the turbine blade material and this raises stresses in the turbine blade material. The increased turbine metal temperature and stress result in a small increase in the turbine creep life usage at higher ambient temperatures as shown in Fig. 19.9. At low ambient temperatures, the decrease in the gas turbine power output and reduced turbine entry temperature result in a substantial decrease in the turbine creep life usage. Thus there will be no need to increase the mean time between overhauls due to the increase in turbine creep life usage at high ambient temperature. In fact, it could be argued that the EGT limit should be increased to compensate for the significant decrease in creep life usage at low ambient temperatures. Such an increase in the EGT limit will augment the gas turbine power output and thermal efficiency further at high ambient temperatures, resulting in increased production and reduced fuel costs.

The increase in the VIGV angle results in an increase in compressor pressure ratio at high ambient temperature when the gas turbine power output is limited by the EGT. This results in an increase in the combustion pressure. The increase in the combustion pressure increases the NO_x emissions, while

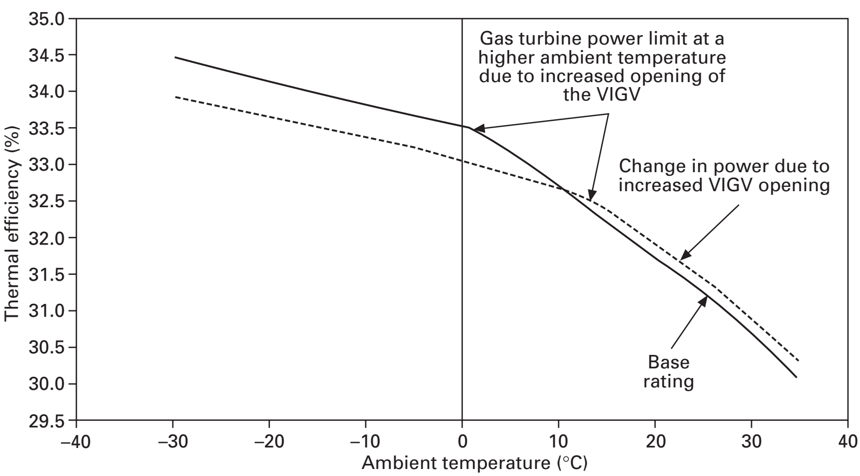

19.8 Change in gas turbine thermal efficiency due to effect of increasing the VIGV angle.

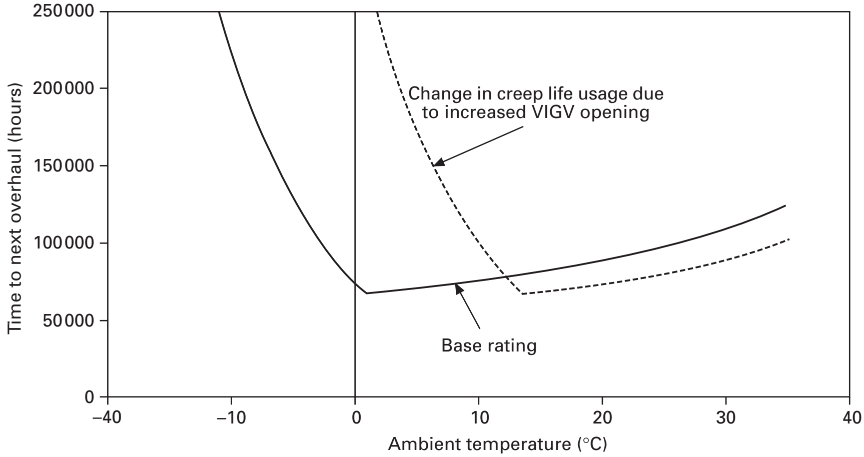

19.9 Change in turbine creep life usage due to effect of increasing the VIGV angle.

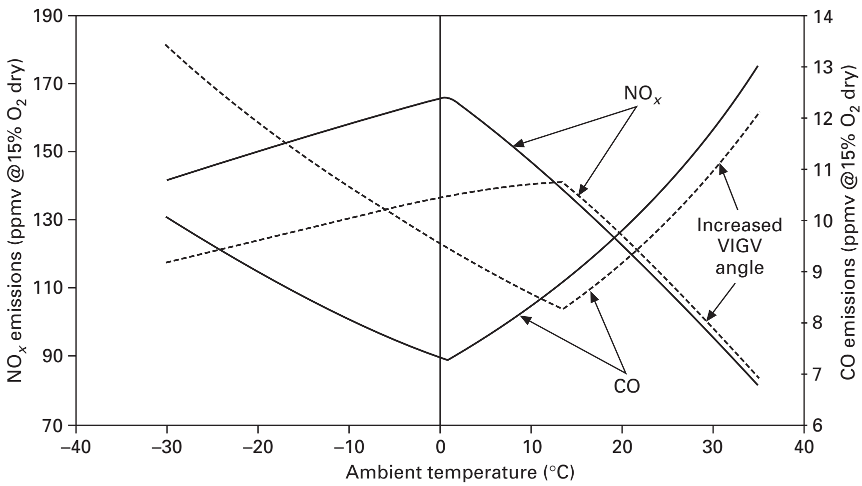

19.10 Change in NO_x and CO emissions due to effect of increasing the VIGV angle.

decreasing the CO emissions, as shown in Fig. 19.10. At low ambient temperatures, the decrease in the combustion temperature, due to the reduced maximum power limit, results in a decrease in NO_x emissions. However, there is a significant increase in CO emissions, as seen in Fig. 19.10.

Although there are increases in gas turbine power output and thermal efficiency at high ambient temperature, due to the increase in the VIGV angle, the increase in power output is greater than the increase in the thermal efficiency. This results in an increase in CO_2 on a mass flow basis. However, the increase in the thermal efficiency decreases the CO_2 emissions index, as can be seen in Fig. 19.11. Thus a decrease in CO_2 emissions is achieved in real terms due to the opening of the VIGV angle. At low ambient temperatures, the decrease in the maximum power limit of the gas turbine is greater than the decrease in the thermal efficiency. This results in a decrease in CO_2 emissions on a mass basis, but the decrease in the thermal efficiency results in an increase in the CO_2 emissions index, as shown in Fig. 19.11.

19.3 Power augmentation using water injection

The power output of a single-shaft gas turbine may also be augmented by the use of water injection. The water may be injected either at the inlet of the compressor or directly into the primary zone of the combustion system. As discussed earlier, power augmentation by injecting water into the compressor inlet occurs due to the suppression of the compressor inlet temperature, and the amount of compressor inlet temperature suppression depends on the humidity of the air at the inlet of the compressor (wetted media and inlet fogging).

The case of direct water injection into the combustion system will be considered where the increase in power output is a result of the increased mass flow rate through the turbine, relative to that through the compressor. The limit on the increase in power is normally governed by the increase in

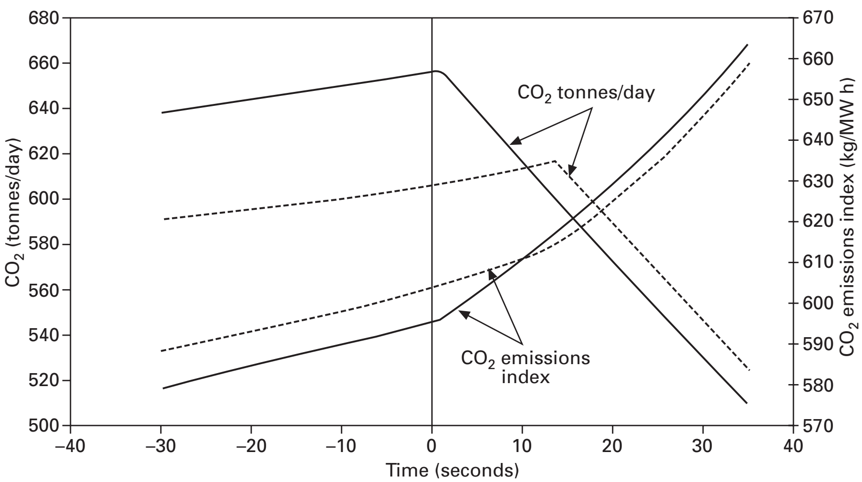

19.11 Change in CO_2 emissions due to effect of increasing the VIGV angle.

CO and UHC emissions due to the chilling of the flame in the primary zone. There is also an adverse effect on the turbine blade creep life usage, which must be taken into consideration.

Figure 19.12 shows the increase in gas turbine power output due to water injection where the water–fuel ratio is unity. At an ambient temperature of 30 degrees Celsius, there is about a 5% increase in gas turbine power output. This compares with about a 7% increase in power output for the two-shaft gas turbine. Unlike the case of the two-shaft gas turbine, the single-shaft gas turbine speed is constant and therefore the compressor flow essentially remains constant. In the case of the two-shaft gas turbine, there is an increase in the gas generator speed due to the increase in the power output from the gas generator turbine. This results in an increase in the compressor flow rate, contributing to the increased power output from the engine due to water injection. In the single-shaft gas turbine, the increase in power output due to water injection is due primarily to the increase in turbine power. With the decrease in ambient temperature, the gas turbine becomes power limited and, with water injection, the power limit is reached at a higher ambient temperature, as seen in Fig. 19.12.

As with the two-shaft gas turbine, there is a significant loss in gas turbine thermal efficiency due to water injection, as shown in Fig. 19.13. Additional fuel is needed to evaporate the water in the combustion chamber (latent heat) and heat the steam to the turbine entry temperature.

Injecting the water directly into the combustor results in an increase in compressor pressure ratio (Fig. 19.17) and in the turbine power output. The

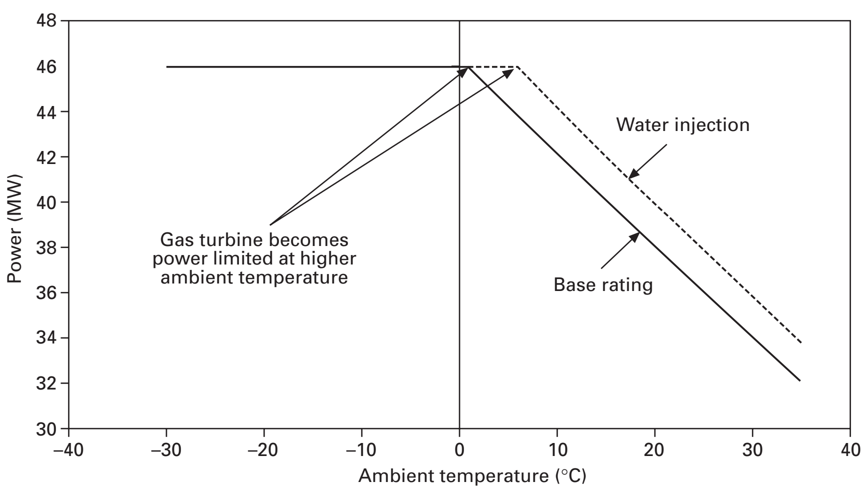

19.12 Increase in power output from the gas turbine due to effect of water injection.

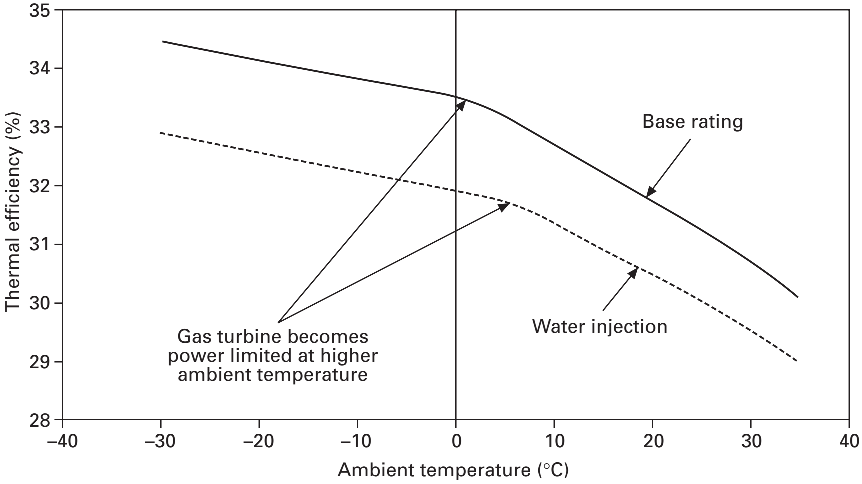

19.13 Change in gas turbine thermal efficiency due to water injection.

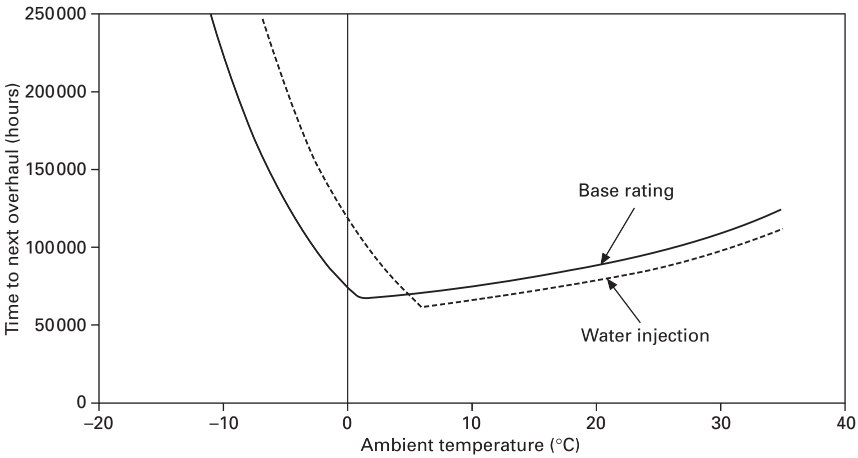

19.14 Change in turbine creep life usage due to water injection.

increased power output from the turbine also results in an increased stress due to the increased torque. There is also a small increase in the turbine entry temperature and therefore in the turbine blade temperature. These two factors have an adverse effect on turbine creep life usage at high ambient temperatures where the gas turbine power output is limited by the EGT. This can be seen in Fig. 19.14. At low ambient temperatures, however, the gas turbine is power limited and the increased flow rate through the turbine will result in a decrease in the turbine entry temperature relative to the base rating case. Thus the turbine creep life usage will decrease as can be seen in Fig. 19.14. Unfortunately, since the power is limiting at this ambient condition, water injection is not used unless NO_x suppression is required. Thus the decrease in creep life usage at low ambient temperature does not occur and water injection may result in an increase in turbine overhauls with increasing maintenance costs. It must also be noted that damage to the combustion system may arise due to water injection, as discussed in Chapter 6.

In spite of these drawbacks, water injection is an effective means of NO_x control and is quite widely used. Direct injection of water into the primary zone results in the suppression of the primary zone temperature where NO_x normally forms. Thus a significant decrease in NO_x emissions occurs due to the decrease in the primary zone temperature. However, the reduction in primary zone temperature also results in a substantial increase in the formation of CO and is a limiting factor on the amount of water injection. This can be seen in Fig. 19.15. The decrease in gas turbine thermal efficiency inevitably will increase the CO_2 emissions on a mass and emissions index basis, as shown in Fig. 19.16. Direct water injection into the combustor also increases the compressor pressure ratio, as shown in Fig. 19.17 and therefore the operating point moves towards the compressor surge line. This movement is only small and should not present any problems with respect to the transient performance of the gas turbine and may only be an issue at low ambient temperatures when the gas turbine is power limited.

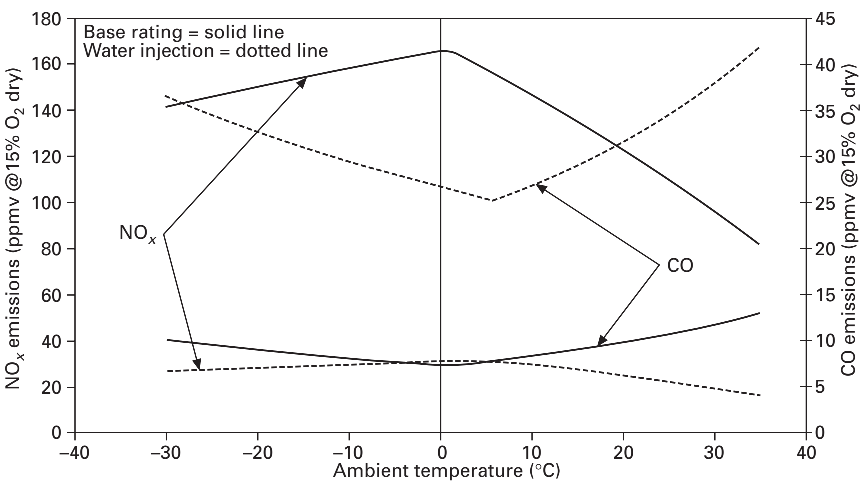

19.15 Change in NO_x and CO emissions due to water injection.

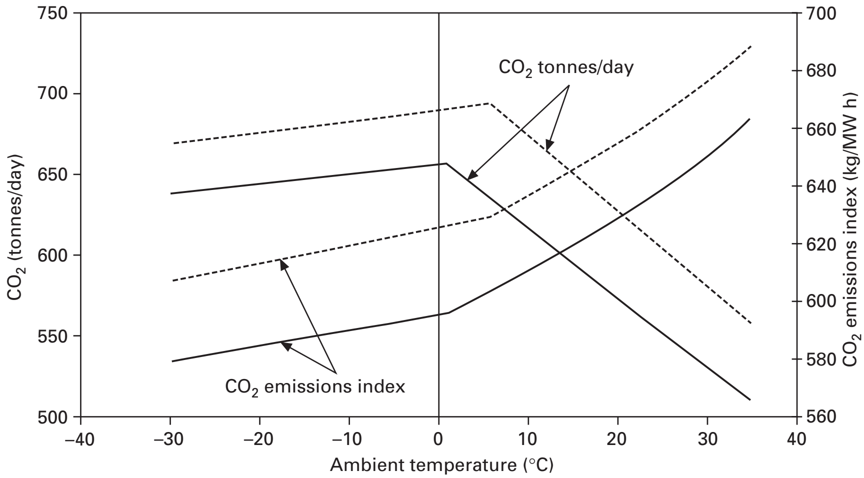

19.16 Increase in CO_2 due to water injection.

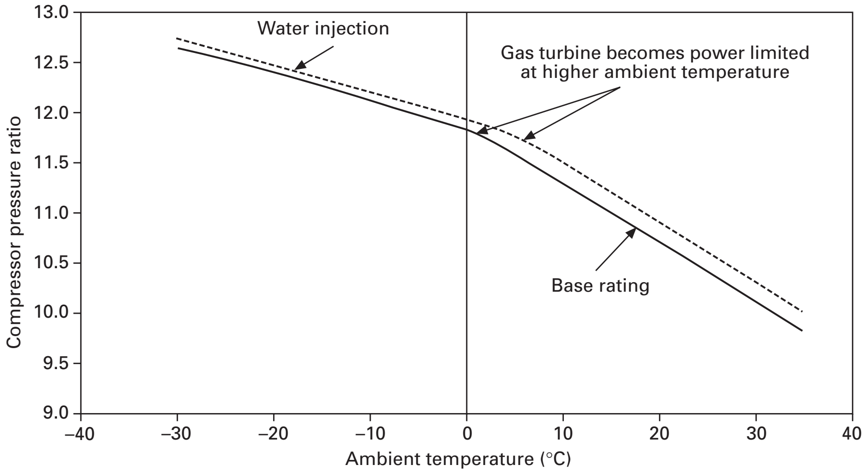

19.17 Increase in compressor pressure ratio due to water injection.

19.4 Power augmentation at low ambient temperatures

The power output of the gas turbine has been observed to become power limited at ambient temperatures below 2 degrees Celsius, and the EGT falls below the limiting value at lower ambient temperatures. Means to augment power at higher ambient temperature such as peak rating do not increase the power output of the gas turbine in the low ambient conditions. In fact, in Section 19.2 it was shown that the augmentation of power at high ambient temperature by increasing the VIGV angle may result in a decrease in power output from the gas turbine at lower ambient temperatures.

Increasing the gas turbine maximum power limit will indeed increase the power output from the gas turbine at low ambient temperatures. This will increase the turbine entry temperature and thus increase the turbine creep life usage requiring increased frequency of engine overhauls resulting in higher maintenance costs. The resultant increase in the compressor pressure ratio due to component matching then decreases the surge margin and increases the risk of compressor surge during transients, but this rise is usually very small. There will also be an increase in the power developed by the turbine and thus an increase in the power transmitted through the shaft to the load, seals and bearings. Thus, any power augmentation at low ambient temperature may need these components to be strengthened to ensure that no mechanical failure occurs due to the increased level of power that is transmitted. The modifications needed to achieve satisfactory aero-thermodynamic performance of the gas turbine due to power augmentation at low ambient temperatures will now be discussed.

It has been stated that increasing the maximum power limit will increase the EGT resulting in increased turbine creep life usage. If a substantial amount of engine operating occurs at low ambient temperatures, the gas turbine power limit can be increased but the EGT limit decreased. In this case the reduced creep life usage at high ambient temperature, when the engine power output is limited by the EGT, compensates for the increase turbine creep life usage at low ambient temperatures (flat rating in reverse). However, the power output of the gas turbine will be reduced at high ambient temperatures, but this will be of little consequence if the power demand from the generator is low under these operating conditions. Figure 19.18 shows the power output from the gas turbine when the EGT limit is reduced by 20 degrees, while the maximum power limit is raised to 47.5 MW. Thus the power output from the gas turbine has effectively been increased by about 6% without increasing the maintenance cost.

The increase in the turbine entry temperature and compressor pressure ratio due to the higher power limit of the gas turbine will also increase the thermal efficiency, thus reducing fuel costs and hence improving profit. The effects of increasing the power output at low ambient temperatures on thermal efficiency and compressor pressure ratio are shown in Figs 19.19 and 19.20, respectively.

The reduced power at high ambient temperature is about 5% (at an ambient temperature of 15 degrees Celsius) compared to the gain in power output from the gas turbine at low ambient temperature (6%). Reducing the EGT limit further, by 10 degrees, will almost halve the usage of turbine blade

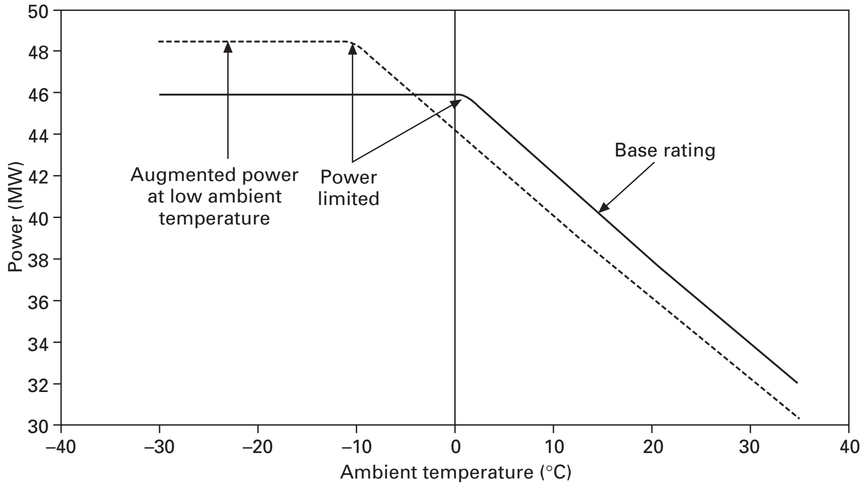

19.18 Variation of gas turbine power output due to increased power limit and reduced EGT limit.

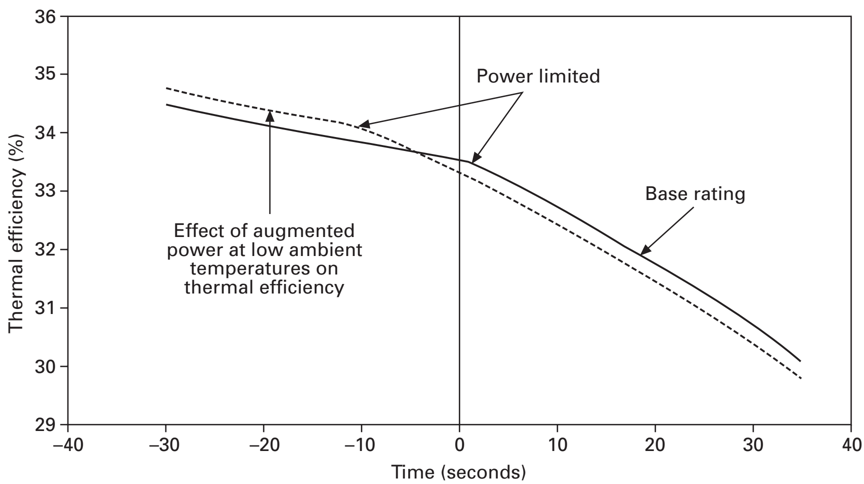

19.19 Variation of gas turbine thermal efficiency due to increased power limit and reduced EGT limit.

creep life at high ambient temperatures. Hence it could be argued that the EGT limit should be raised at high ambient temperature, whilst decreasing the maximum power limit to reduce the turbine blade creep life usage at low ambient temperatures. This would be more suitable if the power demand from the gas turbine is critical at high ambient temperatures (e.g. high air

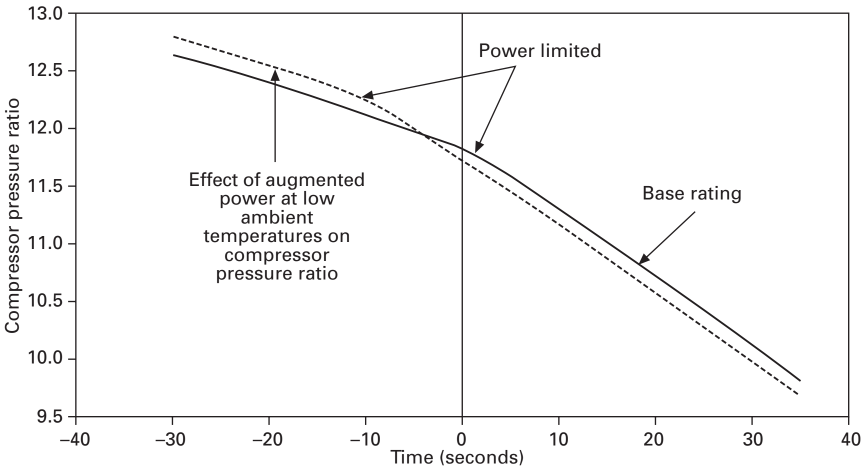

19.20 Variation of compressor pressure ratio due to increased power limit and reduced EGT limit.

conditioning loads in the summer). This is effectively peak rating the engine, but the reduced maximum power limit would prevent increased overhaul frequencies, thus preventing increased maintenance costs due to engine operation at peak rating conditions (normal flat rating).

Due to the increase in gas turbine power limit, it is observed that the compressor pressure ratio has increased. If the increase in the compressor pressure ratio is considered to be too high, the turbine capacity may be increased. This will decrease the compressor pressure ratio and also reduce the creep life usage due to the decrease in turbine entry temperature. However, the decrease in the compressor pressure ratio and turbine entry temperature will reduce the thermal efficiency.

The impact of the increased gas turbine power limit on turbine creep life usage is shown in Fig. 19.21. The increase in the turbine entry temperature at low ambient temperatures, due to the increase in the power limit, shows an increased usage of turbine blade creep life usage when the power output of the gas turbine limits its performance. At high ambient temperatures, the decrease in the turbine blade creep life usage is due to the reduction in the EGT limit.

The increases in compressor pressure ratio and combustion temperature due to the higher maximum power limit at low ambient temperatures, result in an increase in the emissions of NO_x, while decreasing the emissions of CO. At high ambient temperatures, when the engine power output is limited by the EGT, the decreases in the compressor pressure ratio and combustion temperature due to the reduction in EGT limit results in a decrease in NO_x emissions whilst increasing the CO emissions, as shown in Fig. 19.22.

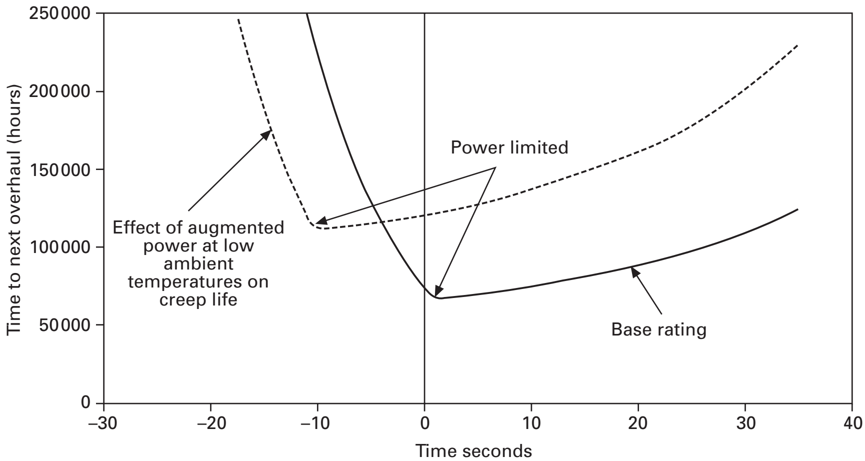

19.21 Variation of turbine creep life usage due to increased power limit and reduced EGT limit.

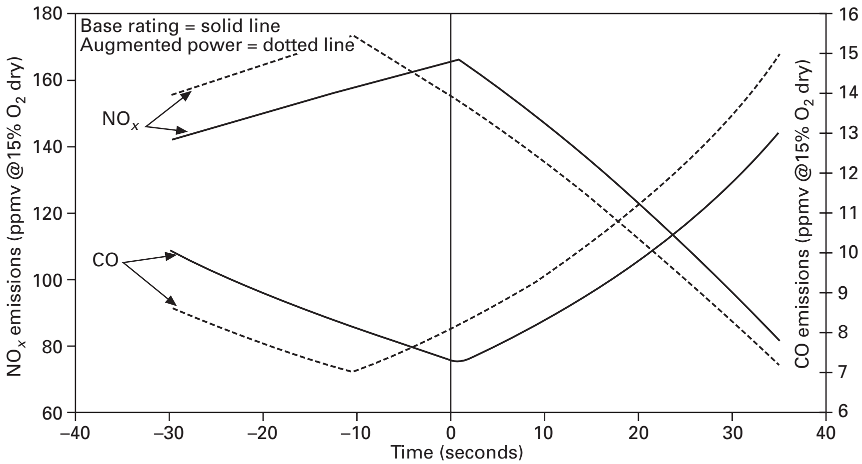

19.22 Variation of NO$_x$ and CO emissions due to increased power limit and reduced EGT limit.

The changes in the compressor ratio and turbine entry temperature result in an increase in the thermal efficiency at low ambient temperatures. At high ambient temperatures, the thermal efficiency decreases due to the decrease in the compressor ratio and turbine entry temperature, as the EGT limit is decreased. Thus it is observed that the CO_2 emissions index decreases at low ambient temperatures and increases at high ambient temperatures, as shown in Fig. 19.23. However, the CO_2 emissions on a mass basis are lower at high ambient temperatures, compared with the case at low ambient temperatures. This is due to the change in the gas turbine power output being greater than the change in the thermal efficiency.

When the VIGV is active in the normal operating power range, at low ambient temperatures, the increase in the gas turbine power limit will result in the opening of VIGV to maintain the EGT limit. However, the opening of the VIGV increases the compressor flow rate and thus the compressor pressure ratio in order to maintain the flow compatibility between the compressor and turbine. This will also increase the turbine entry temperature slightly and hence the turbine blade creep life usage. If the EGT limit is now decreased, this will result in a further opening of the VIGV, thus increasing the air flow rate through the engine further. This increase in the air flow rate compensates for the reduction in power output due to the lower EGT limit. The opening of the VIGV will improve the compressor efficiency, therefore reducing the turbine entry temperature further. Thus, the turbine blade creep life usage could remain unchanged due to the increase in the maximum power limit of the gas turbine when operating at low ambient temperatures with active VIGV in the normal operating power range. The decrease in EGT limit will, of course, decrease the power output at high ambient temperatures. Since there is no compromise in the turbine blade creep life usage when augmenting the gas turbine power output at low ambient temperatures, the EGT limit can be increased to its design (base) value at high ambient temperatures, thus incurring no penalty in turbine blade creep life usage due

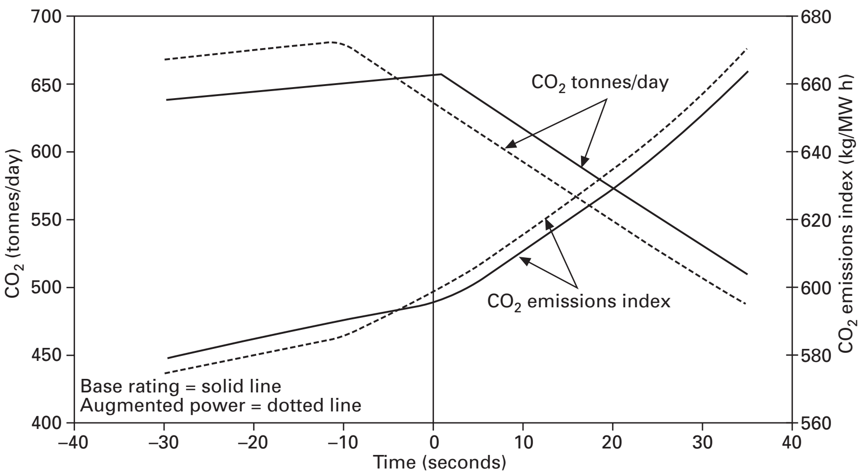

19.23 Variation of CO_2 emissions due to increased power limit and reduced EGT limit.

to power augmentation at low ambient temperatures. When the gas turbine is used in a combined cycle, the decrease in the EGT limit will have a detrimental effect on the performance of the steam plant and needs to be considered when augmenting the power output of the gas turbine by such means at low ambient temperatures.

An alternative is to increase the turbine capacity so that the compressor pressure ratio will decrease, thus resulting in a decrease in turbine entry temperature, in order to maintain turbine blade creep life. A significant increase in the turbine capacity may be necessary to achieve a sufficient decrease in the turbine entry temperature, but this could seriously penalise the gas turbine performance at high ambient temperatures, which may be unacceptable in terms of power output and thermal efficiency.

When the VIGV is active in the normal power range and used in conjunction with dry low emission (DLE) combustion systems, the decrease in the EGT limit, or increased turbine capacity to augment the power output from the gas turbine at low ambient temperatures, will result in a decrease in combustion temperature. Thus, there is a limit to how much the combustion temperature may decrease because there would be an increase in CO and UHC, which must be avoided. As an extreme case, the decrease in the combustion temperature could result in the weak extinction limit being exceeded, thus leading to engine trips.

The reader is left to use the simulator to illustrate the augmentation of the power output at low ambient temperatures using both these methods and producing the figures similar to those shown in Figs 19.18 to 19.23.

19.5 Turbine inlet cooling

In Section 19.3, power augmentation using direct water injection was discussed. An alternative means of water injection to augment the power output of gas turbines is to use it in turbine inlet cooling. In Chapter 14 Section 14.5, turbine inlet cooling applied to a two-shaft gas turbine operating with a free power turbine was discussed. Here, water can be evaporated in the inlet of the engine and the absorption of latent heat required for the evaporation process results in a decrease in the compressor inlet temperature. This results in an increase in power output and improved thermal efficiency of the gas turbine. Another means of turbine inlet cooling is the use of chillers (mechanical and absorption types), as also discussed in Section 14.5. These technologies are applicable equally to a single-shaft gas turbine and the benefits are similar to those discussed in Section 14.5; the figures produced in Section 14.5 can be determined for a single-shaft gas turbine. The reader is invited to reproduce these figures for the single-shaft gas turbine simulator.

The notable difference is that a single-shaft gas turbine normally operates at a constant speed, particularly in power generation, whereas in a two-shaft gas turbine the gas generator speed increases. At low compressor inlet temperatures (at about 13 degrees Celsius) the two-shaft gas turbine power output can become limited by the gas generator speed. Any further cooling will only result in a small increase in power output due to constant gas generator speed operation. Therefore, the cooler size has to be optimised for maximum gain in power output due to turbine inlet cooling.

In a single-shaft gas turbine, the maximum power limit is reached at a lower ambient temperature (at about 2 degrees Celsius). Thus a greater benefit from turbine inlet cooling would be achieved with the single-shaft gas turbine by cooling the turbine inlet air down to 10 degrees Celsius. Cooling the compressor inlet air to lower temperatures increases the risk of the formation of ice, particularly at high humidity, which occurs due to turbine inlet cooling. Such ice formation can break away and enter the compressor, which may damage the engine. Therefore, in practice, it is unlikely that we would consider turbine inlet cooling much lower than 10 degrees Celsius.

20 Simulation of engine control system performance

In Chapter 10 the principles of engine control and its function in preventing the engine from exceeding maximum limiting values, thereby protecting the engine from damage, were discussed. The principles of engine controls using the two-shaft gas turbine simulator were illustrated. Much of what was discussed using the two-shaft gas turbine simulator can be demonstrated with the single-shaft gas turbine simulator and similar conclusions drawn with respect to the performance of the fuel control system. However, it is the control of the VIGV in a single-shaft gas turbine that differs primarily from the two-shaft gas turbine. The problems associated with the control of the VIGV will therefore be demonstrated and the means to overcome these difficulties using the single-shaft gas turbine simulator, as discussed in Chapter 10, will be described.

20.1 VIGV control system simulation

One of the advantages of using a VIGV is that it reduces the starting power requirement due to the decreased mass flow rate through the compressor when the VIGV is closed. The VIGV is full opened during the normal operating range so that the mass flow rate through the engine is increased, so helping to achieve the designed power output of the gas turbine. This is accomplished by controlling the VIGV system independently of the fuel control system, where the VIGV modulates to maintain a certain value for the exhaust gas temperature (EGT). The limit or set point for the EGT may be at a value below the maximum/limiting value for the EGT needed to protect the engine. When the EGT is above the set point for VIGV control, the VIGV will be fully opened, enabling the engine to achieve its designed power output. When the EGT is below this set point, the VIGV will be fully closed, hence reducing starting power requirements.

The operation of the VIGV control system is illustrated by subjecting the single-shaft gas turbine simulator to a step change in power demand from the generator by increasing the power demand from 1 MW to 60 MW. The EGT set point for the VIGV control is 650 K and the maximum EGT limit is 825 K. The increase in power demand from the generator results in an increase in the EGT, which corresponds to T_4, as shown in Fig. 20.1, where it exceeds the VIGV set point after 23 seconds. Since the EGT exceeds the set point for VIGV control, the VIGV starts to open just after 23 seconds (Fig. 20.2) in order to maintain the EGT at 650 K (set point). The VIGV continues to open as the EGT increases to achieve the power demand by the generator and is fully opened after about 28 seconds. The continuous increase in EGT can be seen in Fig. 20.1, but the rate of increase decreases during the period when the VIGV is opening. In fact, the EGT falls slightly during the period when the VIGV is opening, before increasing to the maximum limiting value of 825 K. Figure 20.2 also shows the trend in the turbine non-dimensional speed, where a decrease in the turbine non-dimensional speed, $N/\sqrt{T_3}$, is observed, due to the increase in the turbine entry temperature, T_3, since the turbine speed, N, remains constant. The compressor non-dimensional speed, $N/\sqrt{T_1}$, remains constant since the ambient temperature, and hence T_1, do not change during this simulation.

The opening of the VIGV results in a change in the compressor characteristic, where the capacity of the compressor increases. This is shown in Fig. 20.3 where the operating points for when the VIGV is fully closed, fully opened and the period when the VIGV is opening are marked clearly on the compressor characteristic. Note that the compressor non-dimensional flow and hence flow capacity increase as the VIGV opens.

The increase in flow capacity results in an increase in the compressor flow rate, shown as a trend in Fig. 20.4. The increase in the compressor flow

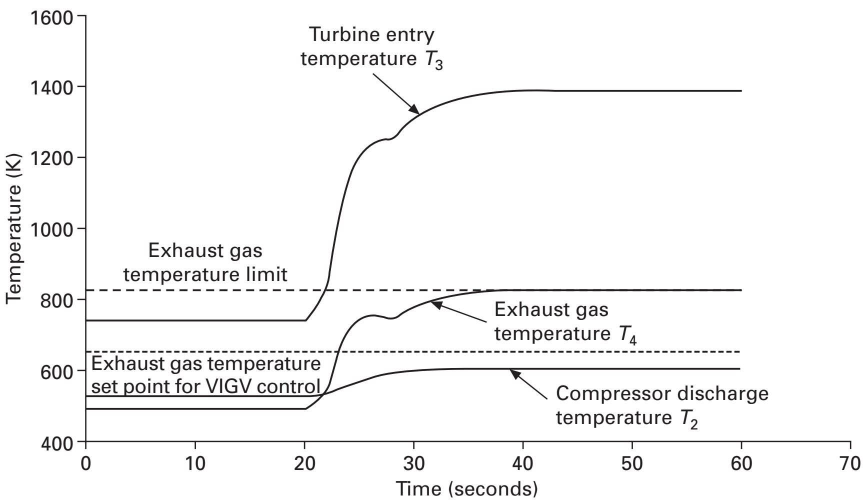

20.1 Trends in temperature due to a step change in power demand.

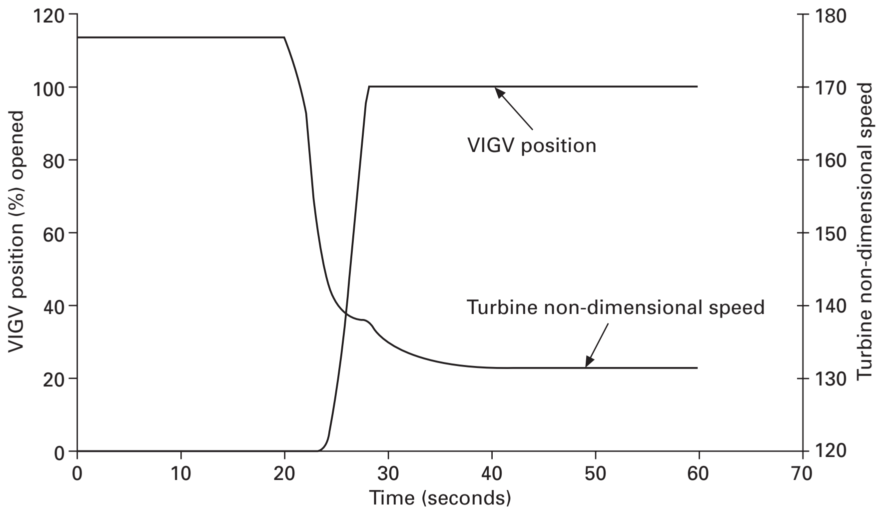

20.2 Trends in VIGV position and non-dimensional speed for a step change in power demand.

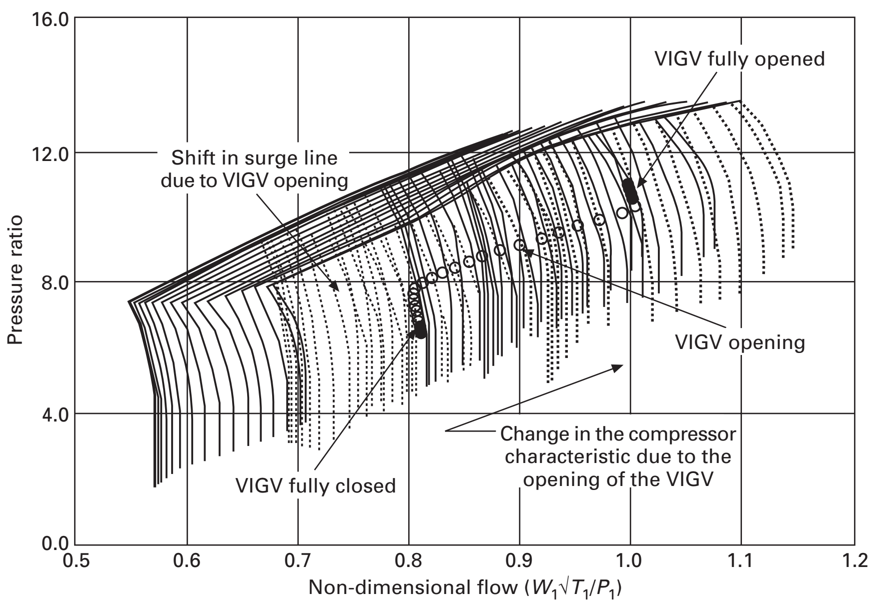

20.3 Change in compressor characteristic due to opening of VIGV resulting from increased power demand.

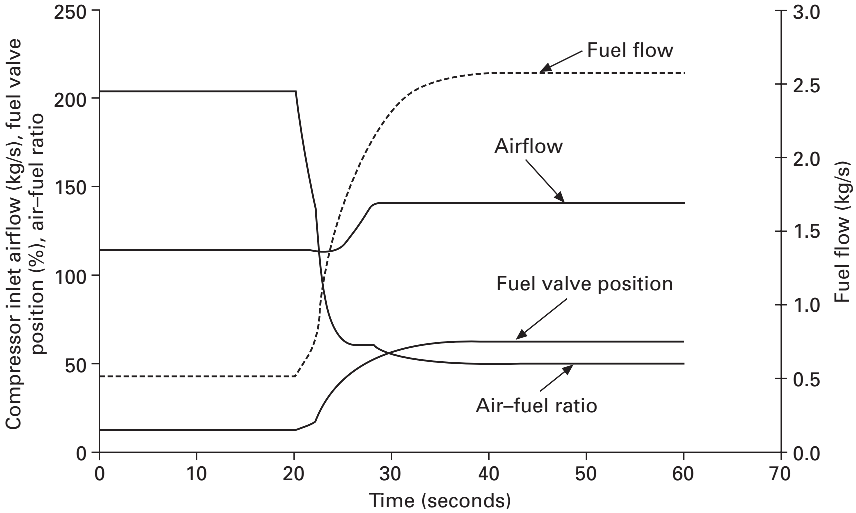

20.4 Increase in air flow through the compressor due to opening of the VIGV.

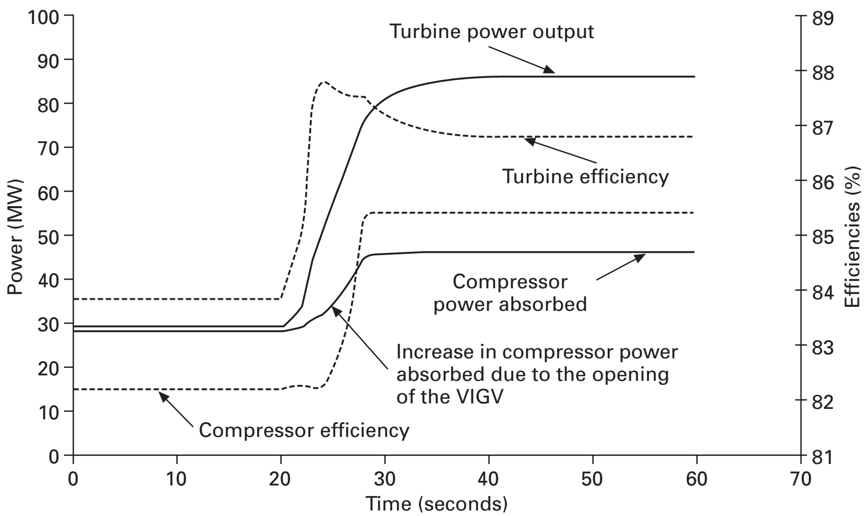

20.5 Increase in compressor power absorbed due to opening of the VIGV.

also results in an increase in the compressor power absorbed. This power increases substantially from about 28 MW to about 45 MW, as shown in Fig. 20.5 due to the opening of VIGV. The turbine produces the power required by the compressor during normal operation; however, during starting of the gas turbine, the turbine power output is very small and a significant amount

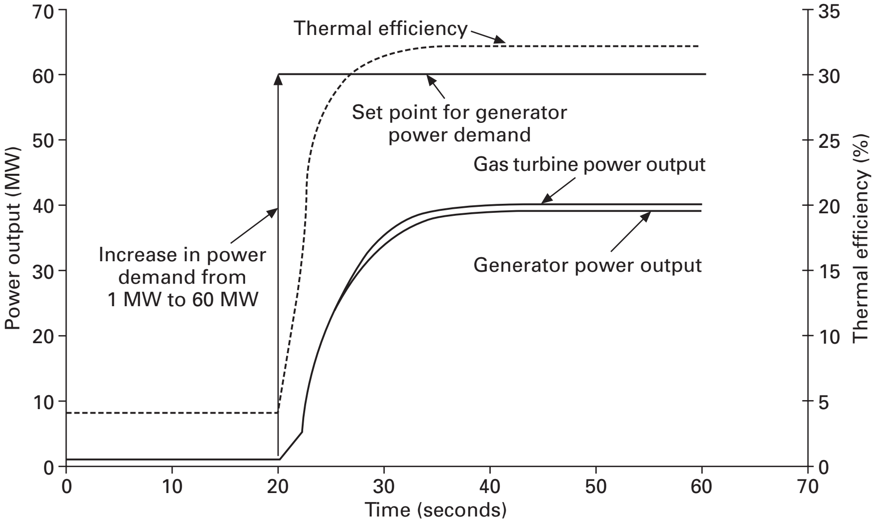

20.6 Change in power demand from generator and variation of gas turbine thermal efficiency due to increased power demand.

of starting power must be provided by an external source as discussed in Chapter 10. Thus, closing the VIGV during starting will result in a significant decrease in the starting power requirements. The increase in the gas turbine and generator power output is shown in Fig. 20.6. The figure also shows the trends in the gas turbine thermal efficiency and the set point for the power output. In this instance, the power is limited to about 40 MW by the EGT limit. In practice, this would trip the engine due to the shift in the generator frequency resulting from insufficient power available from the gas turbine. However, such trips are ignored so that the power capacity of the engine can be investigated in more detail.

20.2 VIGV control when the VIGV is active during the normal operating power range

In Section 20.1 the control of the VIGV was discussed when it is fully open during the normal operating power range. The performance of a single-shaft gas turbine has also been discussed when the VIGV is modulating at the normal power range of the gas turbine and maintaining the EGT on its maximum limit (i.e. the EGT set point for VIGV control corresponds to the maximum EGT limit). At first sight, it would appear that increasing the EGT limit for VIGV control to the limiting value required to protect the engine (i.e. increasing the EGT for VIGV control from 650 K to 825 K) would achieve the desired result. However, this presents some difficulties, as the engine may respond unexpectedly, as discussed in Chapter 10.

If the simulation carried out in Section 20.1 is repeated but with the EGT set point for VIGV control increased to the maximum value of 825 K, the power output from the gas turbine is significantly reduced while the engine is operating on the maximum EGT limit. The maximum power output of the gas turbine should be about 40 MW, but the power output in this instance is restricted to 28 MW and is well short of the required power from the gas turbine as shown in Fig. 20.7. As the power demand from the gas turbine is increased, the EGT increases. However, the EGT is below the VIGV operating set point and the VIGV remains closed. When the EGT exceeds the EGT limit for VIGV operation, the VIGV starts to open. Since the EGT set point for VIGV operation is the maximum permitted value, the low signal selection prevents the VIGV from opening fully, as it endeavours to protect the turbine from over-heating by preventing the EGT from exceeding the maximum value. Thus, the airflow through the compressor is severely restricted and hence the power output from the gas turbine also becomes severely limited. The restriction of flow through the compressor also results in a reduction in the maximum to minimum cycle temperature ratio, T_3/T_1. This is necessary to satisfy the flow compatibility between the compressor and turbine, thus reducing the specific work of the gas turbine. The reduction in specific work also contributes significantly to the loss in gas turbine power output due to insufficient opening of the VIGV.

This increase in EGT, T_4, can be seen in Fig. 20.8 and is due to the increase in power demand from the gas turbine. Note that the EGT reaches the limiting value while the VIGV has opened only marginally, as shown in

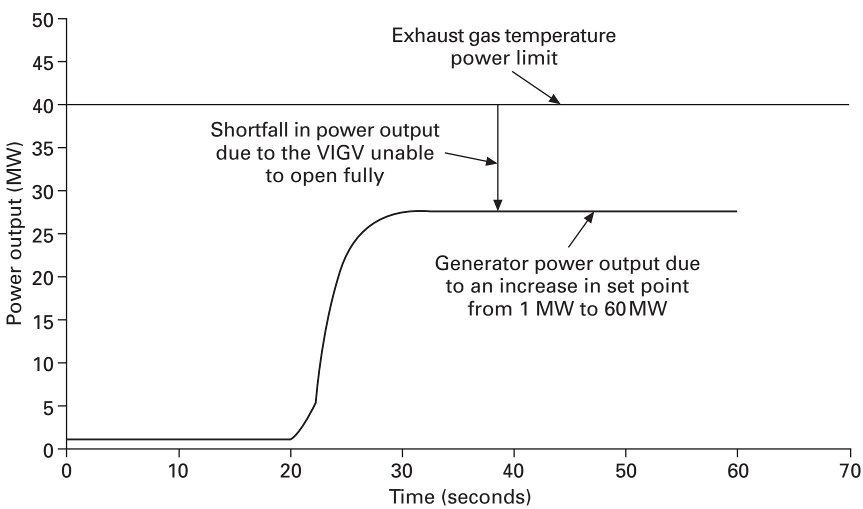

20.7 Severe reduction in power due to insufficient opening of the VIGV.

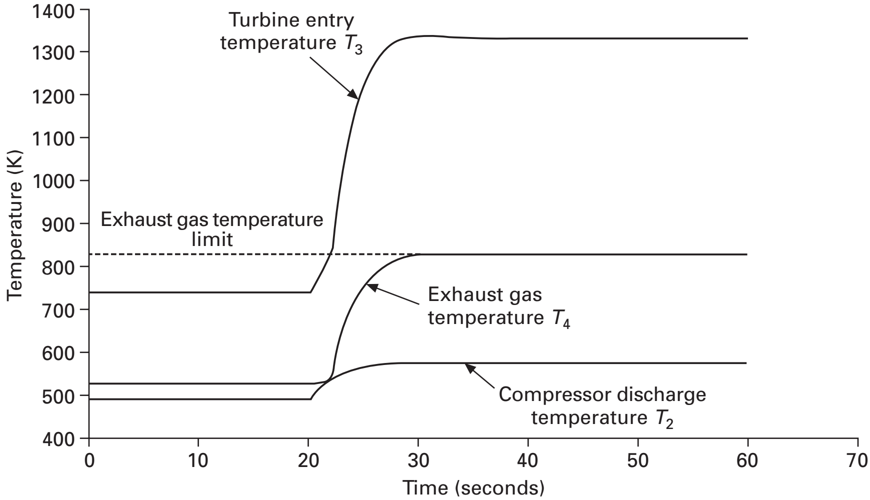

20.8 Increase in EGT due to increased power demand.

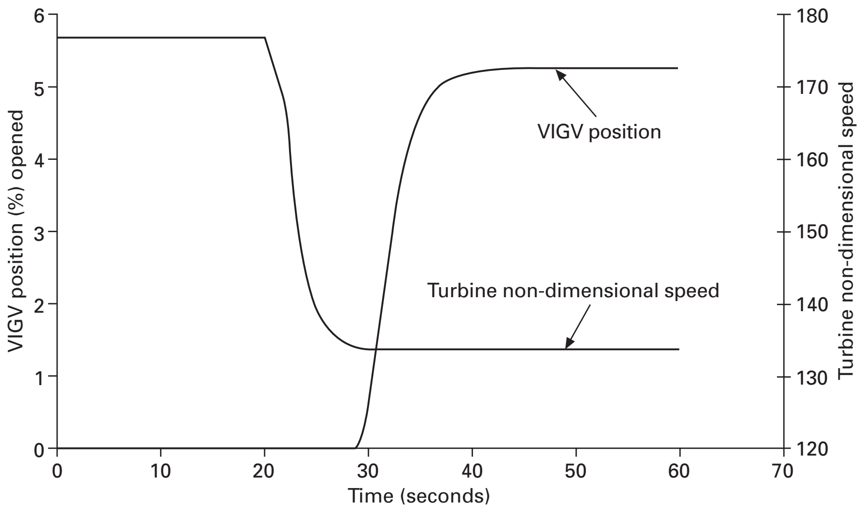

20.9 Insufficient opening of the VIGV due to the maximum EGT limit being reached.

Fig. 20.9. The change in the compressor characteristic is small due to this small opening of the VIGV (Fig. 20.10), resulting in little or no change in air-flow through the compressor, as shown in Fig. 20.11. It may be possible to reduce the response of the gas turbine by reducing the gain of the fuel control system or by increasing the gain of the VIGV control system, but this improves the situation only marginally and would result in an oscillatory response of the gas turbine and increase the likelihood of trips.

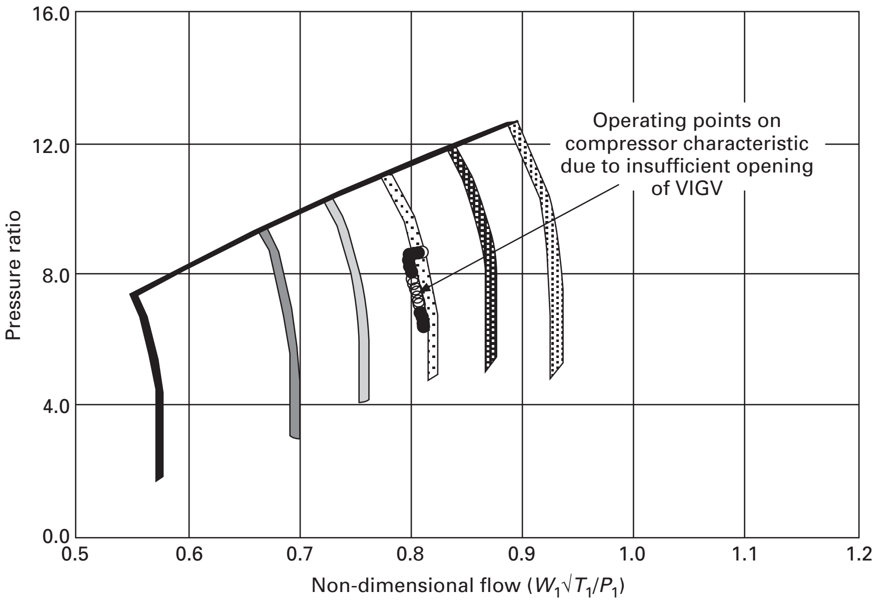

20.10 The small change in the compressor characteristic due to insufficient VIGV opening.

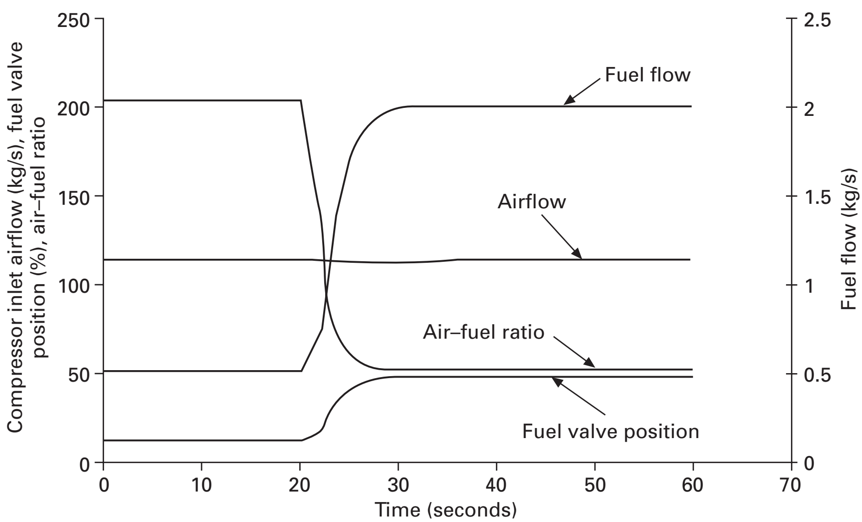

20.11 Little or no change in compressor flow resulting in the gas turbine power output becoming severely restricted.

20.2.1 Open and closed loop control system

It is clear that insufficient opening of the VIGV is the main cause of severe loss in the gas turbine power output, although the engine is on the EGT limit. The VIGV opening must be increased so that the mass flow rate through the compressor and thus the engine can increase. However, this would result in the engine behaving as discussed in Section 20.1, where the control system performance was considered when the VIGV is fully opened during the normal operating power range, when no problems in the VIGV action were experienced. This feature is exploited when the VIGV is opened, to say full, for a short period of time, thus decreasing the EGT. This allows the engine power to increase to the required set point or maximum engine operating power. When the VIGV action is implemented in this manner, it is referred to as an open loop control system, as there is no feedback mechanism to correct any errors after this period. Any error left by the open loop system can be rectified by switching to the closed loop control system.

The open and closed loop control systems are illustrated by repeating the earlier simulation but by activating the open loop response when the set point for the power output from the generator is increased. The VIGV is opened fully and linearly over a period of 2 seconds, which is its opening or stroke time. The VIGV is left fully opened for a period 15 seconds. On this occasion, the power demand is increased from 1 to 35 MW, as this will illustrate the opened and closed loop action more clearly. Increasing the power demand from the gas turbine results in the VIGV initially opening fully under open loop response, as shown in Fig. 20.12. During this period,

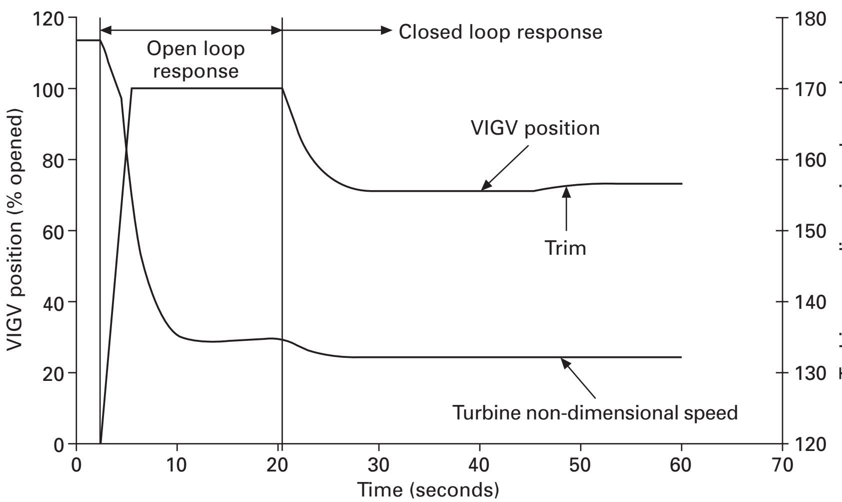

20.12 VIGV opening during open and closed loop response from VIGV control system.

the EGT increases, as shown in Fig. 20.13, but it does not reach the limit value as observed in the previous case. Thus the power demand from the gas turbine may be achieved as the VIGV remains fully opened for a sufficiently long period of time so that the EGT remains below its limiting value. Hence the fuel flow control system sees a sufficient error, thus allowing the power demand to be met. This is shown in Fig. 20.14.

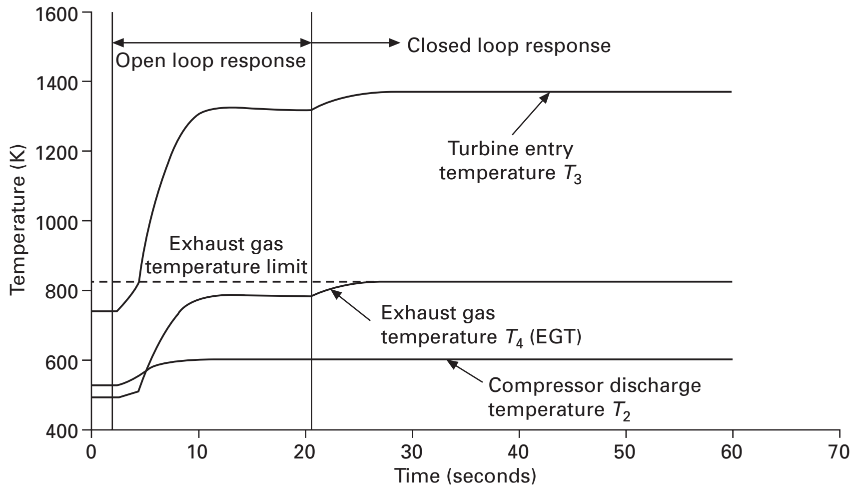

20.13 Change in temperature due to open and closed loop response of the VIGV control system.

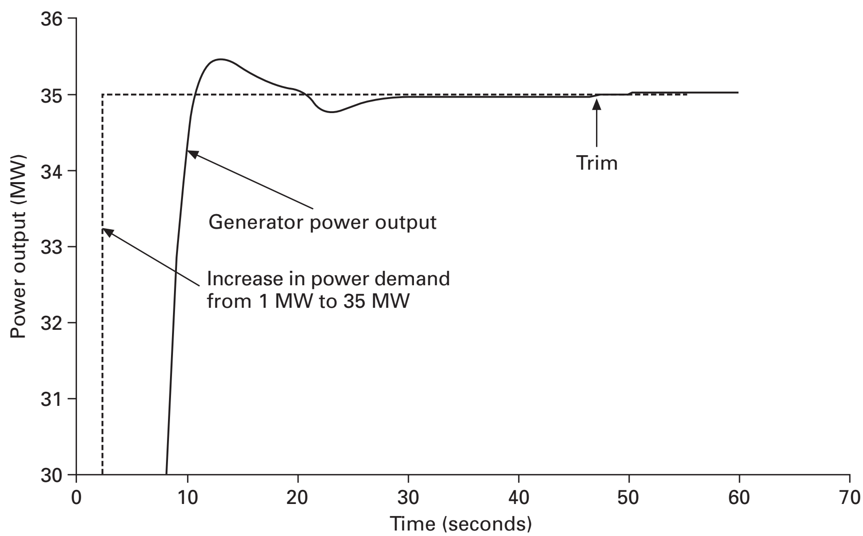

20.14 Increase in gas turbine power output due to the open and closed loop response of VIGV control system.

After 15 seconds of open loop response from the VIGV control system, the closed loop response takes over and results in the VIGV closing (Fig. 20.12) to maintain the EGT on the set point for the VIGV control system, which now corresponds to the maximum EGT limit. This results in the VIGV closing from 100% (open loop output) to about 70% (closed loop output) and the increase in the EGT during the closed loop response is shown in Fig. 20.13. Although this control strategy improves the response of the engine to power demand, as shown in Fig. 20.14, the open loop response may still leave an offset in the power output, resulting in the power output from the gas turbine being slightly lower than the power demand (Fig. 20.14). These small differences in outputs may be ironed out or trimmed by setting the EGT limit for VIGV operation to be slightly lower than the maximum EGT limit, thus enabling the required power demand to be met. The effect of trimming the VIGV movement on the gas turbine power output is shown in Figs 20.12 and 20.14, where the VIGV opens due to the slight decrease in the EGT set point and the power output reaches the generator power demand set point. The EGT limit for VIGV control is reduced by 2 degrees, from the 825 K to 823 K (for trimming). Such small temperature differences will have little impact on engine performance, but will provide a simple and effective means for overcoming control problems associated with variable guide vane systems under these conditions.

The effect of the VIGV opening on the compressor characteristic is shown in Figs 20.15 and 20.16. During the open loop response, the VIGV control system opens the VIGV fully and remains opened fully for a fixed period of time (15 seconds). The compressor characteristic changes from the fully closed position to the fully opened position of the VIGV and the change in the compressor characteristic (Fig. 20.15) is similar to that shown in Fig. 20.3 previously. However, the operating point on the characteristic differs from that shown in Fig. 20.3. The VIGV starts to open as soon as the set point in power demand from the gas turbine increases, whereas, in the case described in Fig. 20.3, the VIGV starts to open only when the EGT exceeds the set point (650 K) for VIGV control. Thus, there is a period of engine operation when the VIGV remains closed at low gas turbine power outputs, which is absent in the present case.

During the closed loop response, the VIGV sufficiently closes so that the EGT returns to the set point specified for VIGV control. This results in a decrease in compressor capacity by shifting the compressor speed lines to the left, as shown in Fig. 20.16. The operating points on the compressor characteristic are also shown during open and closed loop response of the VIGV control system. It is also observed that the compressor pressure ratio decreases during the closed loop response, as shown in Fig. 20.16.

This is due to the decrease in compressor flow capacity, resulting in a decrease in compressor pressure ratio to satisfy the flow compatibility between

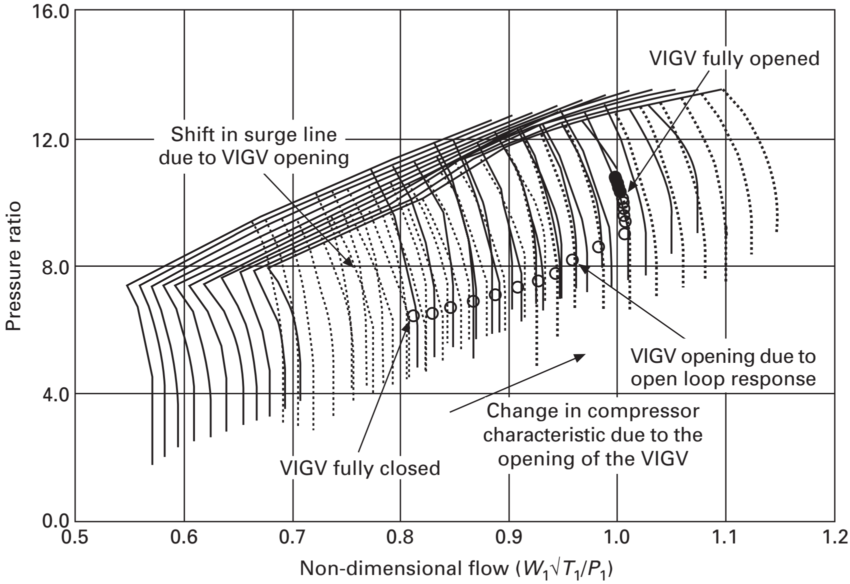

20.15 Change in compressor characteristic due to the open loop response of VIGV control system.

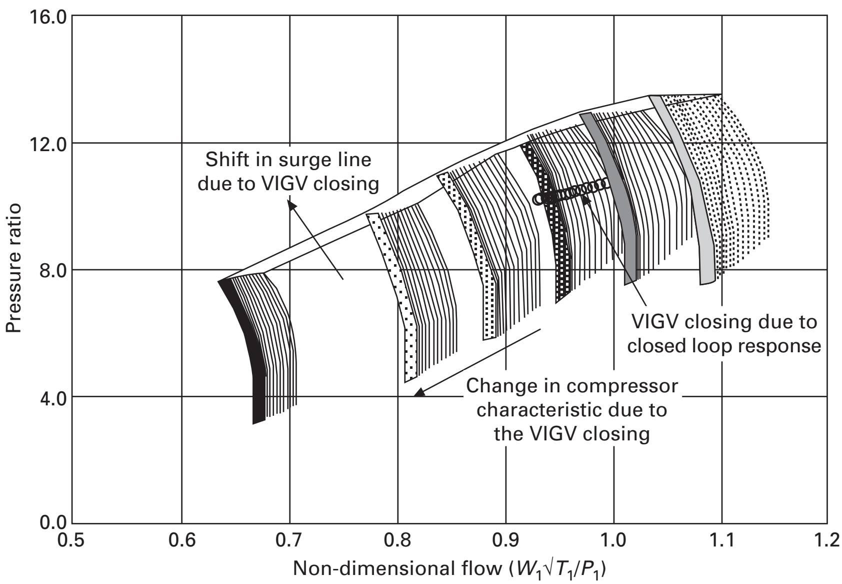

20.16 Change in compressor characteristic due to the closed loop response of VIGV control system.

the compressor and turbine. However, the maximum to minimum cycle temperature, T_3/T_1, is higher when the EGT set point for VIGV control is increased. The net effect on the gas turbine thermal efficiency is minimal, although a slight decrease in thermal efficiency occurs when operating with a higher EGT limit for VIGV control. It is only when a heat exchanger is incorporated or in combined cycle applications that a significant improvement in the thermal efficiency will occur at part loads due to the increased exhaust heat being available for recovery via the heat exchangers.

20.2.2 VIGV systems for dry low emission (DLE) combustor gas turbines

Apart from reducing starting power requirements of large gas turbines, VIGV systems are used widely in dry low emission combustion (DLE) engines. It was stated in Chapter 6 that gas turbine emissions such as NO_x and CO can be reduced significantly if the combustion temperature is kept within strict limits, which means the air–fuel ratio should remain approximately constant with the change in load. The application of VIGV to maintain a constant EGT with the decrease in engine power output does indeed maintain the turbine entry temperature and combustion temperature approximately constant. This is exploited in the manufacture of single-shaft gas turbines employing DLE combustion systems.

The suitability of the use of VIGV for DLE combustion gas turbines will now be demonstrated using the simulator. The power demand from the gas turbine is increased in steps of approximately 2.5 MW, so that the normal power range of the gas turbine is covered as shown in Fig. 20.17. The increase in the power demand results in the VIGV responding as described in Section 20.2.1 and as shown in Fig. 20.18. The open and closed loop responses of the VIGV control system is clearly shown for each step increase in the power demand from the generator. The corresponding trends in gas turbine temperatures are shown in Fig. 20.19. The simulator assumes a conventional (diffusion) combustion system, where the combustion temperature will be high and result in high NO_x emissions. In a DLE combustion system, these temperatures will be about 300 to 500 degrees lower, hence producing significantly lower NO_x emissions.

The EGT is observed to remain on its set point during the period of closed loop response from the VIGV control system. The turbine entry and combustion temperature also remain approximately constant. However, during the period of open loop response, the opening of the VIGV results in a decrease in the EGT below its set point, and the largest decrease occurs at low gas turbine power output. There is therefore a significant decrease in turbine entry and combustion temperatures. This will result in the air–fuel ratio increasing during the period of open loop response, whilst the air–fuel ratio remains

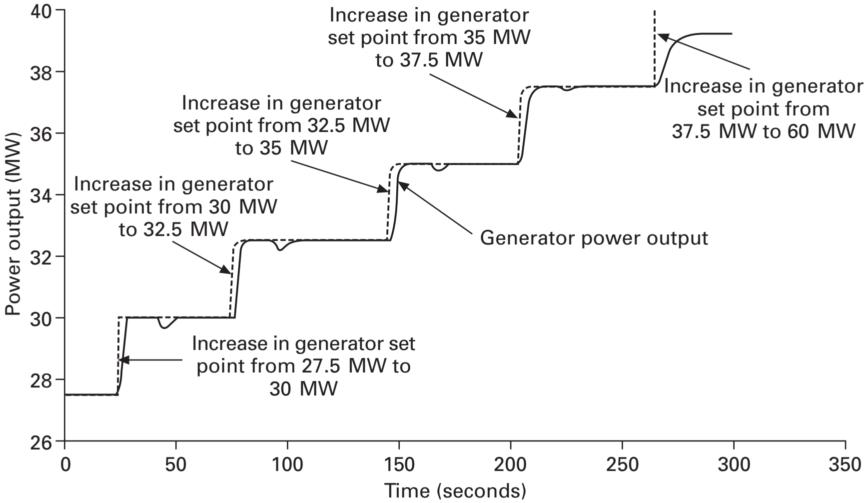

20.17 Change in gas turbine power output for a series of set increases in power demand from the generator.

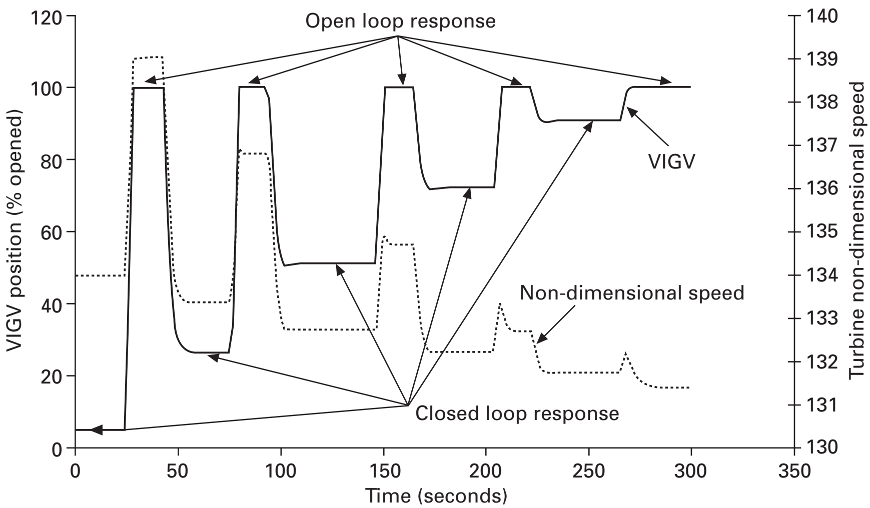

20.18 Open and closed loop response of the VIGV control system to a series of step increases in power demand from the gas turbine.

essentially constant during the period of closed loop response, as shown in Fig. 20.20. Such increases in air–fuel ratios can exceed the weak extinction limit for the DLE combustion system, resulting in the flaming out of combustion systems, particularly at low gas turbine power levels. The change in turbine creep life usage due to the open and closed loop response is shown in Fig. 20.21.

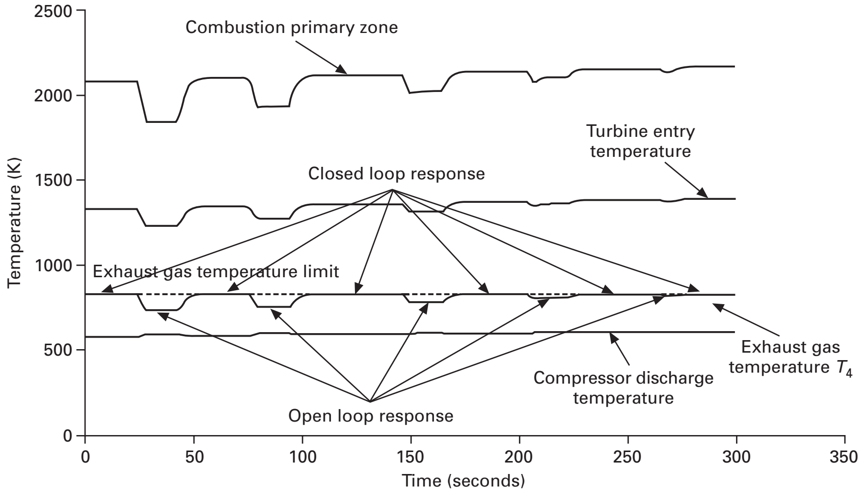

20.19 Gas turbine temperature changes due to a series of step increases in gas turbine power output.

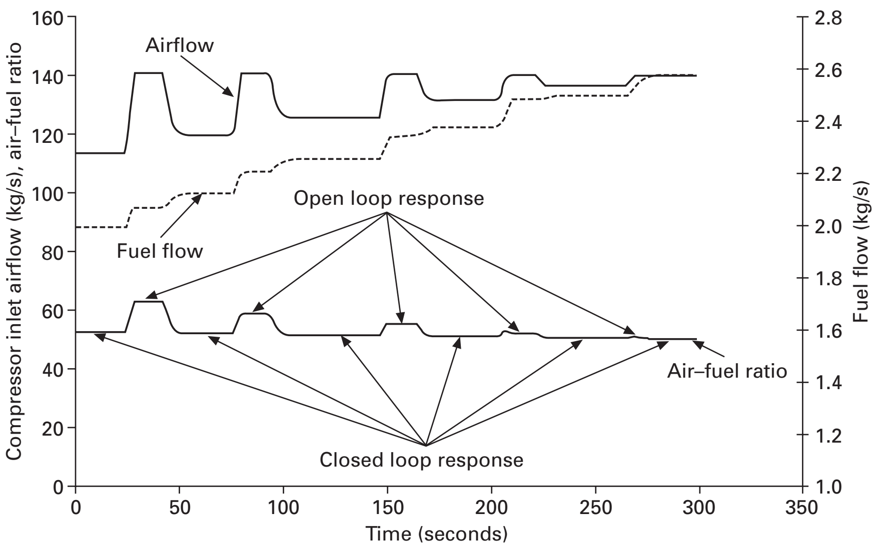

20.20 Change in air–fuel ratio and flow due to a series of step increases in power demand from the gas turbine.

An alternative engine control strategy is to modulate the VIGV in response to a change in power demand and modulate the fuel flow to maintain the EGT on its set point. Such a control strategy is described in Figure 10.11 (Chapter 10) and would eliminate the need for an open loop response or trimming from the control system. However, when the power demand falls

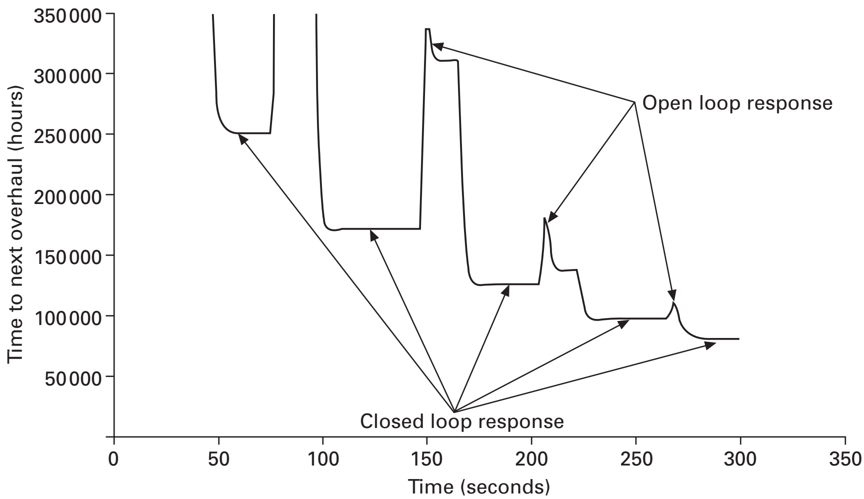

20.21 Increase in turbine creep life usage due to constant EGT operation at low power.

sufficiently the VIGV will remain closed, and the control strategy must shift to modulate the fuel flow to the change in power demand from the gas turbine at these power conditions. During this period of engine operation the air–fuel ratio cannot be maintained and the combustion system switches to a diffusion flame similar to that found in conventional combustion systems. Since this occurs at low power, typically below 65% of the design power output, the high NO_x emissions during this period of operation are normally of little consequence because the amount of operation at such low power is usually small. Generally, the control of DLE combustion gas turbines is much more complex. At the time of writing, these combustion systems are still being developed to overcome combustion instabilities, which occur quite frequently in production engines. The corresponding figures for the alternative control strategy are shown in Figs 20.22, 20.23, 20.24, 20.25 and 20.26, respectively. It can be seen that the absence of the open loop response gives a steady air–fuel ratio, as shown in Fig. 20.25.

20.2.3 Increasing the EGT limit to reduce CO at off-design conditions

The decrease in power results in a decrease in the compressor pressure ratio and thus a decrease in the turbine pressure ratio. If operation is at a constant EGT at lower power as discussed above, the turbine entry temperature and the combustion temperature decrease as the compressor pressure ratio decreases. The decreases in combustion temperature and pressure will increase

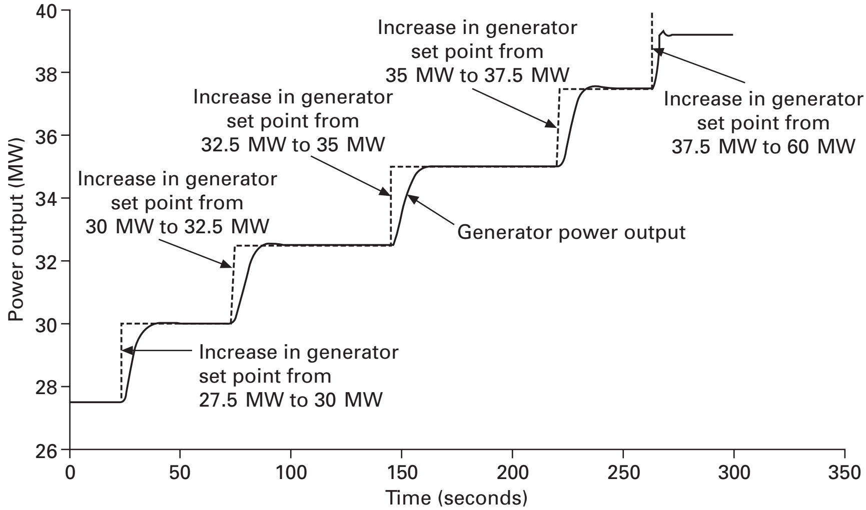

20.22 Change in gas turbine power output for a series of step increases in power demand from the generator using alternative control strategy.

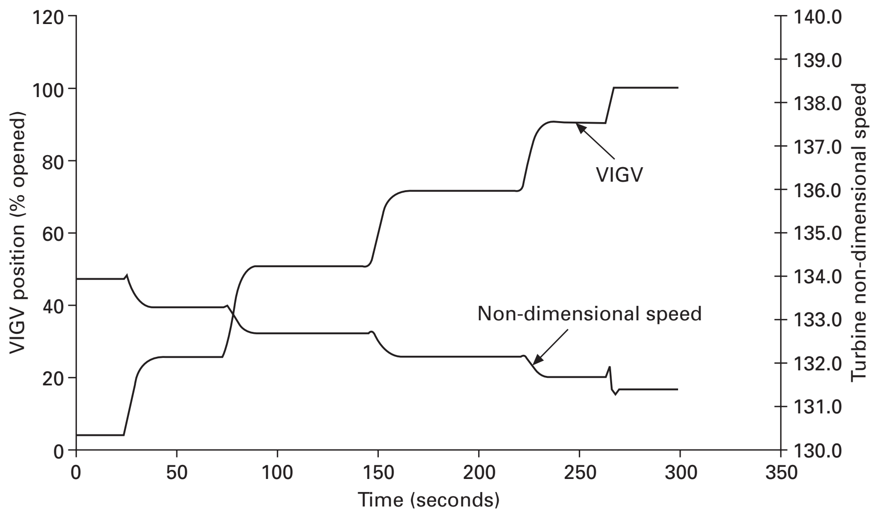

20.23 Response of the VIGV control system to a series of step increases in power demand from the gas turbine using alternative control strategy.

the CO and UHC emissions, particularly using DLE combustion. This problem is more acute in staged combustion employed in multi-shaft gas turbines operating with a free power turbine and using overboard bleeds, which adversely affect the gas turbine thermal efficiency. It was suggested earlier

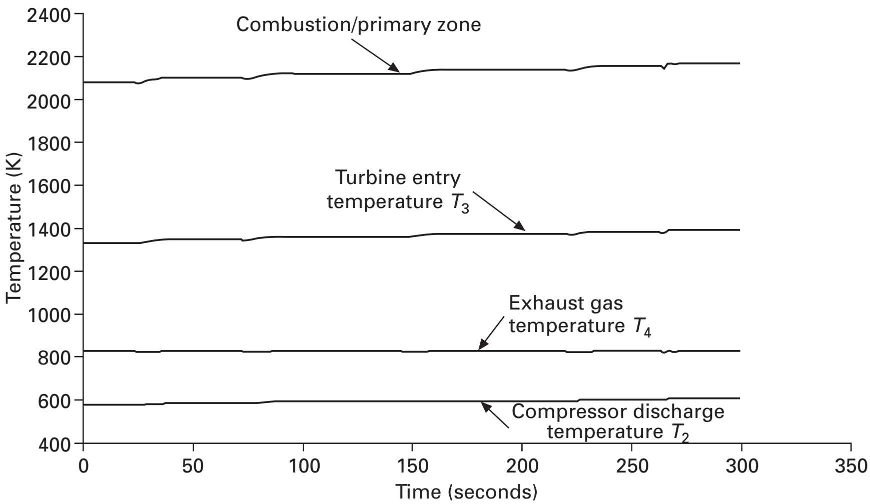

20.24 Gas turbine temperatures due to a series of step increases in gas turbine power output using alternative control strategy.

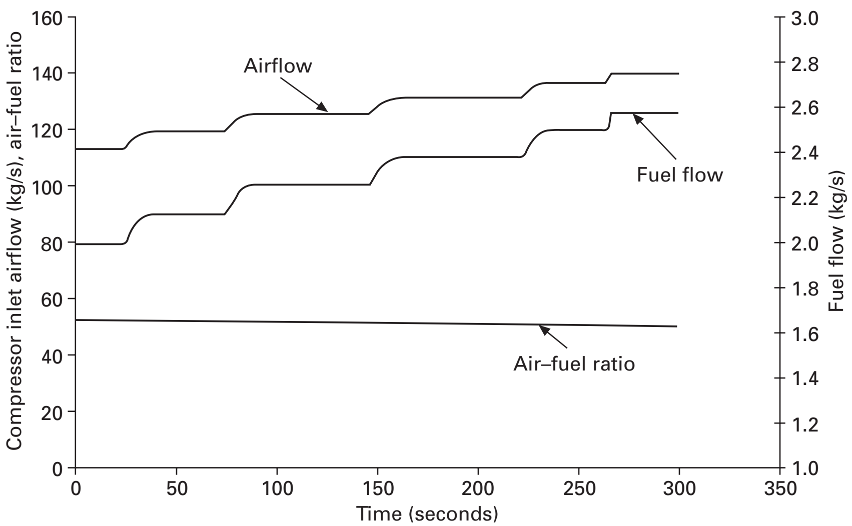

20.25 Change in air-to-fuel ratio due to a series of step increases in power demand from the gas turbine using alternative control strategy.

that the use of a variable geometry power turbine and higher EGT limit (Chapter 10) would indeed help maintain high combustion temperatures at lower power outputs and thus help eliminate such overboard bleeds and maintain low CO and UHC emissions.

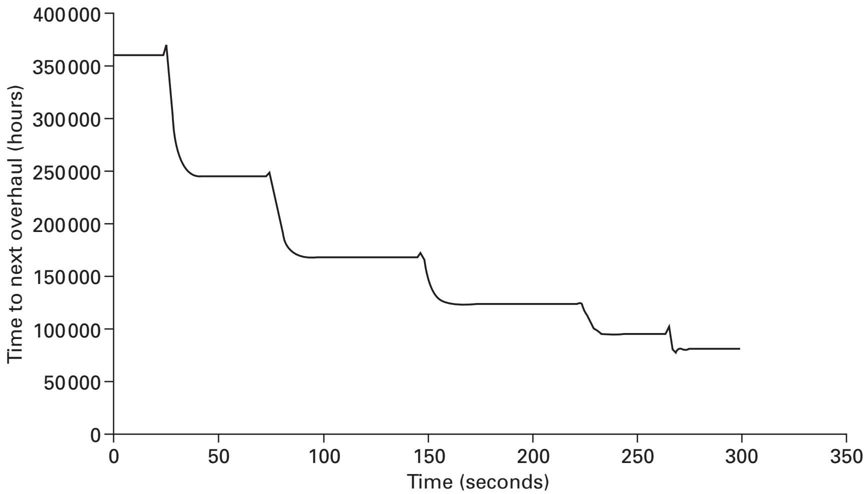

20.26 Increase in turbine creep life usage due to constant EGT operation at low power using alternative control strategy.

A similar strategy may be implemented for single-shaft gas turbines, where the EGT limit is increased at low power conditions to maintain high combustion temperatures, thus minimising CO and UHC emissions at these operating conditions. Increasing the EGT limit at reduced power outputs must take into account the increase in creep life usage due to the higher turbine metal temperature. From Fig. 20.26, it is observed that the turbine creep life usage decreases and this is because of the reduced turbine entry temperature and cooling air temperature due to the lower compressor pressure ratios at lower power. Thus the potential to increase the EGT limit at these powers exists, such that the turbine creep life usage remains constant with reducing power, hence minimising CO and UHC emissions at these operating conditions.

20.3 Optimisation of the EGT limit for a single-shaft gas turbine with ambient temperature

It has been assumed that the EGT limit remains constant with variation of the ambient temperature for both the single- and the two-shaft gas turbine simulators. This is a reasonable assumption for a two-shaft gas turbine, where the EGT is measured at the exit of the gas generator turbine rather than at the exit of the power turbine. Since the gas generator pressure ratio remains essentially constant due to the choked conditions in the power turbine, this forces the gas generator turbine to operate at an approximately fixed pressure ratio. Thus, the turbine entry temperature remains essentially constant as does the turbine creep life usage when the engine power output is limited by the EGT. With a single-shaft gas turbine, the EGT is usually measured at the exit of the turbine rather than at some intermediate point between the inlet and exit of the turbine. The increase in ambient temperature results in a decrease in the compressor pressure ratio and thus in the turbine pressure ratio. For a fixed EGT limit, this results in a decrease in the turbine entry temperature and hence a decrease in turbine creep life usage and therefore an increase in the time to next overhaul, as shown in Fig. 20.27.

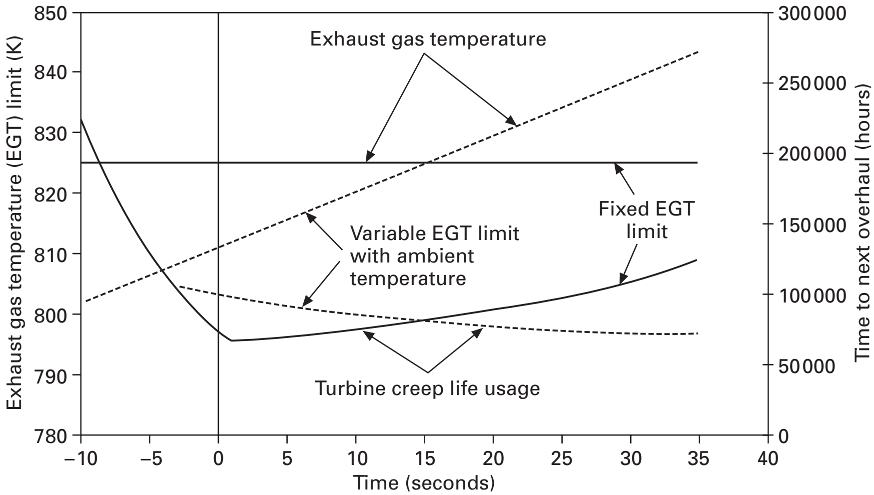

20.27 Effect of EGT limit on turbine creep life usage with ambient temperature.

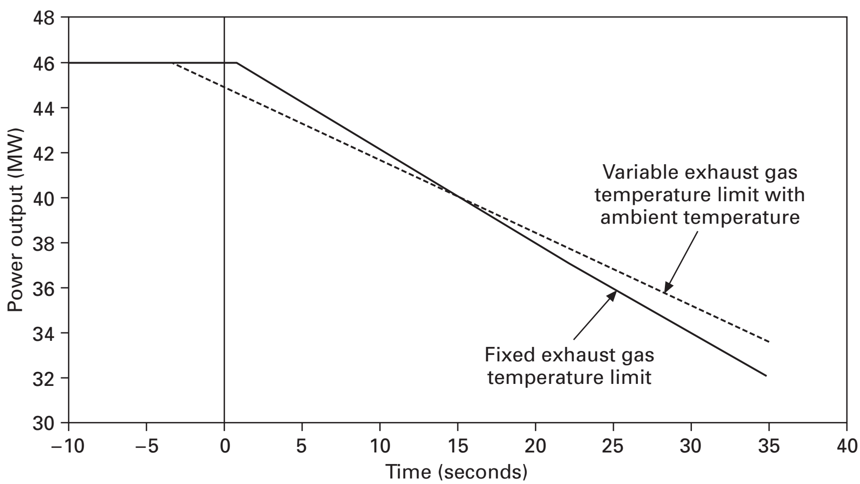

20.28 Change in gas turbine power output for a fixed and variable EGT limit with ambient temperature.

It is therefore possible to increase the EGT limit at higher ambient temperatures such that the turbine creep life usage remains approximately constant with the change in ambient temperature. The resultant increase in the EGT limit at high ambient temperatures will increase the power output of the gas turbine at these ambient temperatures, as shown in Fig. 20.28. At an ambient temperature of 30 degrees Celsius, the gas turbine power output increases by about 3%, compared with the case when the EGT limit remains constant with ambient temperature changes. There is also a useful increase in the thermal efficiency of the gas turbine due to the higher EGT limit.

21
Simulation exercises

Exercises using the single-shaft gas turbine simulator

The following exercises (1–46) use the single-shaft gas turbine simulator on the CD accompanying this book. The default values given in the simulator and the generator power demand set to 60 MW should be used unless other input values are specifically stated.

21.1 Effects of ambient temperature and pressure on engine performance

1. Determine the maximum generator power, gas turbine shaft power and thermal efficiency for the engine when operating at ISO conditions. What is the creep life usage of the turbine? ISO conditions refer to an ambient temperature of 15 degrees Celsius, pressure of 1.013 Bar, relative humidity of 60% and zero inlet and exhaust losses. What limits the power output from the gas turbine?

   Determine the emissions from the gas turbine and hence calculate the amount of NO_x, CO and CO_2 in tonnes/day.
2. The engine operating at site has the following conditions.
   - ambient temperature 15 degrees Celsius
   - ambient pressure 1.013 Bar
   - inlet and exhaust loss of 100 mm water gauge

   Determine the parameters in Exercise 1 above and calculate the percentage changes in the parameters when operating at site rated conditions. Explain the changes in the turbine life usage.
3. Determine the percentage changes in the parameters in Exercise 1 when

   (1) the ambient temperature is 30 degrees Celsius
   (2) the ambient temperature is zero degrees Celsius
   (3) the ambient temperature is –15 degrees Celsius

What limits the power output from the gas turbine when operating at these ambient temperatures? Repeat this exercise using the control system Option 2. Comment on the operation of the variable inlet guide vane (VIGV) at these ambient conditions.

4. When operating at site rated conditions as stipulated in Exercise 2, determine the parameters in Exercise 1 when the ambient pressure is 0.975 Bar and calculate the percentage change from the values determined in Exercise 1.
5. When the required power output from the generator is 37 MW and the ambient pressure and temperature, are 0.975 Bar and 15 degrees Celsius, respectively, determine the thermal efficiency of the gas turbine. If the ambient pressure increases to 1.03 Bar, explain why the thermal efficiency decreases and explain the changes in the turbine creep life usage and emissions.
6. Produce a graph describing the maximum gas turbine power output with ambient temperature, indicating which engine parameter restricts the capacity of the gas turbine at different ambient temperatures. Also, determine the ambient temperature when the engine power output is limited by exhaust gas temperature and maximum power limit. The variation in ambient temperature should be from 30 to –30 degrees Celsius in steps of 10 degrees.
7. Determine the maximum power output of the gas turbine when the relative humidity is 0.05% and 100%. The ambient temperature is 35 degrees Celsius. Repeat the simulation when the ambient temperature is –5 degrees Celsius and comment on the differences.
8. Increased filter loss and low ambient pressure reduces the compressor inlet pressure. When the engine is developing 37 MW of electrical power explain the difference in thermal efficiency when the compressor inlet pressure decreases due to a high filter loss and low ambient pressure.
9. Use the gas turbine to demonstrate the benefits of a closed cycle gas turbine.
10. If this engine operates as a closed cycle gas turbine using air as the working fluid with a system pressure of 5 Bar, estimate the maximum power output from the gas turbine. What is the thermal efficiency of the closed cycle gas turbine? Assume a compressor inlet temperature of 15 degrees Celsius.
11. A factory is being planned and it has been decided that the plant will generate its own electrical power of 32 MW, with the prospect of selling any surplus power to the grid. Two possible sites are suitable. The average ambient temperature and pressure of the first site is 30 degrees Celsius and 1.013 Bar, respectively. The second site is at a higher elevation and the average ambient temperature and pressure is 15 degrees Celsius and 0.975 Bar, respectively. Use the simulator to determine the

more suitable site based on engine performance. Assume an inlet and exhaust loss of 100 mm water gauge respectively.

21.2 Effects of component performance deterioration

12. Determine the loss in engine performance (loss in power output and thermal efficiency) due to moderate compressor fouling. Compressor fouling is simulated by reducing the compressor fouling and efficiency fault index to –3% and –1%, respectively. The engine is operating at site-rated conditions as described in Exercise 2.
 Also, determine the actual change in turbine creep life usage and emissions due to fouling.
13. Show the variation of the inlet non-dimensional flow with compressor non-dimensional speed due to compressor fouling. Assume the same compressor fault indices as used in the previous simulation (Exercise 12).
14. The gas turbine has been operating for 80,000 hours and is due for its major overhaul. The compressor and turbine efficiencies have each reduced by 1%. There is also some residual compressor fouling reducing the compressor capacity by 1.5%. Determine the loss in performance.
15. Simulate the effect of hot end damage on the turbine where the flow capacity of the turbine is increased by 3% and the efficiency of the turbine is reduced by 1%. Determine the loss in power output and thermal efficiency of the gas turbine. Explain why the turbine creep life usage decreased and determine the actual increase in turbine creep life usage due to this fault.
16. A piece of the transition duct has been dislodged and adhered to the turbine nozzle guide vane, resulting in a reduction in the flow capacity of the turbine by 4%. This damage also results in a loss in the turbine efficiency by 1%. Determine the loss in performance of the gas turbine when the ambient temperature is 30 and –15 degrees Celsius. What limits the power output from the gas turbine at each of these ambient temperatures?

21.3 Power augmentation

17. The engine is operating at site-rating conditions and the ambient pressure is 1.013 Bar. Determine the increase in maximum power output from the gas turbine at ambient temperature of 30, 0 and –15 degrees Celsius when the exhaust gas temperature limit is increased by 20 degrees Celsius. What is the impact on thermal efficiency, turbine creep life usage and emissions?
18. The engine is operating at site-rated conditions at an ambient pressure and temperature of 1.013 Bar and 30 degrees Celsius respectively. It is

necessary to increase the maximum power output of the gas turbine by 5%. Two methods of increasing the power output are considered:

(1) increase the exhaust gas temperature limit
(2) water injection.

Determine the increase in exhaust gas temperature limit and the water–fuel ratio required in each case to achieve the increased power output from the gas turbine. Comment on the advantages and disadvantages of each method.

19. The engine is operating at site rated conditions when the ambient pressure and temperature is 1.013 Bar and 30 degrees Celsius respectively. A generator power output of 37 MW is required. It is decided to use water injection to achieve the necessary power demand. Estimate the water–fuel ratio required and comment on the increase in turbine creep life usage.
20. It is thought that the loss in the turbine creep life determined in Exercise 19 is unacceptable. If we maintain the same water–fuel ratio, determine the generator output and exhaust gas temperature limit so that there is no change in turbine creep life usage.
21. The turbine is approaching its major overhaul. However, due to the unavailability of a replacement turbine it is decided to postpone the turbine overhaul. A generator power output of about 39.2 MW must be met. The manufacturer suggests that the turbine creep life usage should be halved. The user suggests water injection as a means to reduce the turbine creep life usage. Explain how this can be achieved and determine the water–fuel ratio necessary to halve the turbine creep life usage. What is the drawback using this method? The ambient pressure and temperature is 1.013 Bar and 15 degrees Celsius, respectively. Inlet and exhaust losses are 100 mm water gauge, respectively.
22. Determine the maximum generator power output when the ambient temperature is 35 degrees Celsius. Apply turbine inlet cooling using:

- wetted media
- fogging
- chillers

and determine the turbine inlet cooling (TIC), the percentage increase in power outputs (generator and gas turbine) and the increase in thermal efficiency using each of these cooling technologies. Comment on the change in gas turbine emissions. The coefficient of performance of chillers is 5. Also investigate the effect of vapour absorption chillers on generator output.

If the effectiveness of the wetted media is increased to 0.95, what is the turbine inlet cooling, increased power output and thermal efficiency for this case? Comment on the profit using each of the turbine inlet cooling technologies. What is the impact of emissions taxes on profit due to turbine inlet cooling?

23. Repeat Exercise 22 when the relative humidity is 20% and 90% and determine what parameter limits the power output of the gas turbine for each of these relative humidity cases.
24. It is thought that including a wetted media evaporative cooling stage before the chiller can improve increase turbine inlet cooling. Use the simulator to determine if this statement is true.
25. At low power, controlling the VIGV using Option 2 will partly close the VIGV. This results in a decrease in compressor efficiency. If turbine inlet cooling using chillers is applied, then the VIGV will close even further resulting in a greater loss in compressor efficiency. Determine if the decrease in compressor inlet temperature due to turbine inlet cooling is sufficient to improve the thermal efficiency in spite of the decrease in compressor efficiency, or if there is potential to optimise the turbine inlet cooling such that the thermal efficiency can be maximised.

21.4 Combined cycle and co-generation

26. The gas turbine simulator is a part of a combined cycle power plant. If the stack temperature is limited to 120 degrees Celsius and the steam plant thermal efficiency is 32%, estimate the maximum combined cycle thermal efficiency and power output. The ambient temperature and pressure are 15 degrees Celsius and 1.013 Bar at site conditions. Assume the mean specific heat at constant pressure for exhaust gases is 1.074 kJ/kgK.
27. Repeat Exercise 26 when the gas turbine compressor is moderately fouled. Determine the percentage change in the gas turbine and combined cycle power outputs and thermal efficiencies. Comment on these changes.
28. Repeat Exercises 26 and 27 when the generator power output is set at 32 MW. Compare the results with those obtained from Exercises 26, 27 and comment on the differences.
29. Repeat Exercise 28 using the engine control system Option 2.
30. The gas turbine is a part of a co-generation system where the exhaust heat is used to produce hot water to satisfy a process heat load. Determine the maximum generator power, maximum heat load, heat-to-power loading and the overall efficiency of the co-generation system.

    If the compressor is moderately fouled, determine these parameters for this case and comment on the differences.

    Assume the mean specific heat at constant pressure for exhaust gases is 1.074 kJ/kgK and the stack temperature is limited to 120 degrees Celsius. The ambient temperature and pressure are 15 degrees

Celsius and 1.013 Bar. Assume the inlet and exhaust losses are 100 mm water gauge respectively.

31. Repeat Exercise 30 using engine control system Option 2 when the generator output is set to 32 MW.
32. A co-generation system uses a gas turbine similar to that described by the simulator. An electrical power output and heat load of 32 MW and 135 MW are required. Determine the performance of the co-generation system and state if supplementary firing is required. Use the assumptions stated in Exercise 30. If the compressor is moderately fouled, what is the performance of the co-generation system compared with that of a cleaned compressor?

21.5 Engine control systems

33. Set the proportional band and the integral gain for the fuel control system to 1000% and 2 respectively. Load the generator output from 1 MW to 39.2 MW. Explain the response of the gas turbine.
34. Run the simulator for a generator output set point of 39 MW. A fuel control system fault occurs where the integral output becomes zero (see user guide on how to set the integral output to zero). Explain the resultant loss in power output. What would be the consequence of this fault to the electrical system? Determine the gas turbine power output when the proportional band is 75% and 200%.
35. Repeat Exercise 34 but simulate the control system fault for the VIGV control system. Explain the resultant trip of the gas turbine. Repeat this simulation using control system Option 2 and explain the response of the gas turbine.
36. Start the simulator and select (VIGV) control system Option 2. Set the power demand from the generator to 60 MW. After the engine reaches the EGT limit, switch off the integral wind up from the control settings for the VIGV system. After a lapse of 100 seconds, reduce the generator power demand to 30 MW. Explain the response of the gas turbine.
37. Repeat Exercise 36 but switch off the integral windup before loading the generator. Now set the generator power required to 35 MW. Explain why the required power output from the generator cannot be achieved. Describe the response of the gas turbine when the integral wind up is switched on.

21.6 Gas turbine emissions

38. A power plant consists of two gas turbines as described by the simulator. The total electrical power requirement is 39 MW. Determine the performance of the plant when operating one engine at 39 MW and

operating both engines at equal load of 19.5 MW. Comment on the effect on CO_2, NO_x and CO emissions for each case.

39. When operating at ISO conditions it is necessary to reduce the NO_x emissions to 25 ppmv. Direct water injection is used to suppress NO_x emissions. The power demand from the generator is set to 39.2 MW. Determine the water–fuel ratio and water flow rate. If the relative humidity is 20%, what is the water–fuel ratio and water flow rate to maintain the NO_x emissions at 25 ppmv? Comment on the difference.
40. Repeat Exercise 39 when the ambient temperature is 35 degrees Celsius. The generator power demand is 32.93 MW. Comment on the difference in water flow rate.
41. Produce a graph describing the NO_x emissions with ambient temperature and relative humidity. The range for ambient temperature is from +30 to –30 degrees Celsius in steps of 10 degrees and the range for relative humidity is from 10% to 100% in steps of 20%. The power demand from the generator is set to 60 MW. What will be the effect on NO_x emissions for this ambient temperature and relative humidity range when the power demand from the generator is set to 34 MW?
42. The gas turbine operates at three different ambient temperatures corresponding to 30, 15 and 0 degrees Celsius. The power demand from the generator is set to 32 MW. Determine the emissions of CO_2, NO_x and CO and comment on the changes in each of these emissions at the different ambient temperatures. The ambient pressure is 1.013 Bar with inlet and exhaust losses of 100 mm water gauge respectively.
43. Investigate the impact of the change in ambient pressure on engine emissions when operating at ambient pressures of 1.03, 1 and 0.97 Bar. Ignore inlet losses and assume an ambient temperature of 15 degrees Celsius. What is the effect of the change in inlet loss from 0 to 200 mm water gauge when operating at an ambient pressure of 1 Bar?
44. Determine the change in emissions when the gas turbine is operating on natural gas and diesel. The ambient temperature and pressure are 15 degrees Celsius and 1.013 Bar respectively. The inlet and exhaust losses are 100 mm of water gauge.
45. Simulate the effect of moderate compressor fouling on engine emissions when operating at a high power and limited by the exhaust gas temperature. Repeat the simulation at a power output of 37 MW. Comment on the changes in emissions. The ambient temperature is 15 degrees Celsius; pressure is 1.013 Bar. Assume an inlet and exhaust loss of 100 mm water gauge.
46. When the engine is operating at an ambient temperature of 30 degrees Celsius whilst the generator is producing 32 MW of electrical power output, it is necessary to reduce the NO_x by 40%. Determine the amount of water injection required to achieve the reduction in NO_x. Comment

on the changes in CO_2 and CO. What is the impact on turbine creep life usage? The ambient pressure is 1.013 Bar and the inlet and exhaust losses are 100 mm water gauge.

If a standby engine is available, what is the impact on emissions when operating both engines at 50% power output? Comment on whether operating two engines is better than operating one engine at 32 MW.

Exercises using the two-shaft gas turbine simulator

The following simulation exercises use the two-shaft gas turbine simulator provided on the CD accompanying this book. The default values given in the simulator and the generator power demand set to 25 MW should be used unless other input values are specifically stated.

21.7 Effects of ambient temperature, pressure and humidity on engine performance

47. Determine the maximum generator power, gas turbine shaft power, gas power output, thermal efficiency and the gas thermal efficiency for the engine when operating at ISO conditions. Hence, calculate the isentropic efficiency of the power turbine. What is the creep life usage of the gas generator and power turbine? ISO conditions refer to an ambient temperature of 15 degrees Celsius, ambient pressure of 1.013 Bar, relative humidity of 60% and zero inlet and exhaust losses. What limits the power output from the gas turbine?

    Determine the emissions (as an emissions index) from the gas turbine and hence calculate the amount of NO_x, CO and CO_2 in tonnes/year.
48. The engine operating at site has the following conditions:

    - ambient temperature 15 degrees Celsius
    - ambient pressure 1.013 Bar
    - inlet and exhaust loss of 100 mm water gauge
    - relative humidity of 60%.

    Determine the parameters in Exercise 47 and calculate the percent changes in the parameters when operating at site rated conditions. Explain the changes in power turbine life usage.
49. Determine the percent changes in the parameters in Exercise 47 when

    (1) the ambient temperature is 30 degrees Celsius
    (2) the ambient temperature is zero degrees Celsius
    (3) the ambient temperature is –15 degrees Celsius.

What limits the power output from the gas turbine when operating at these ambient temperatures?

50. When operating at site-rated conditions as stipulated in Exercise 48, determine the parameters in Exercise 47 when the ambient pressure is 0.975 Bar and calculate the percentage change from the values determined in Exercise 47.
51. When the required power output from the generator is 19 MW, the ambient pressure is 0.975 Bar and the temperature is 15 degrees Celsius. Determine the thermal efficiency of the gas turbine. If the ambient pressure increases to 1.03 Bar, explain why the thermal efficiency decreases. Also, explain changes in the turbine creep life usage and emissions.
52. Produce a graph describing the maximum gas turbine power output with ambient temperature, indicating what engine parameter restricts the capacity of the gas turbine at different ambient temperatures. Also, determine the ambient temperature when the engine power output is limited by exhaust gas temperature and gas generator speed limits. The variation in ambient temperature should be from 30 to –30 degrees Celsius in steps of 10 degrees.
53. Determine the maximum power output of the gas turbine when the relative humidity is 0.05% and 100%. The ambient temperature is 35 degrees Celsius. Repeat the simulation when the ambient temperature is zero degrees Celsius and comment on the differences.
54. Increased filter loss and low ambient pressure reduce the compressor inlet pressure. When the engine is developing 16 MW of electrical power, explain the difference in thermal efficiency when the compressor inlet pressure decreases due to a high filter loss and low ambient pressure.
55. Use the gas turbine to demonstrate the benefits of a closed cycle gas turbine.
56. If the engine operates as a closed-cycle gas turbine using air as the working fluid with a system pressure of 5 Bar, estimate the maximum power output from the gas turbine and the thermal efficiency. Assume a compressor inlet temperature of 15 degrees Celsius.
57. A factory is being planned and it has been decided that the plant shall generate its own electrical power of 16 MW with the prospect of selling any surplus power to the grid. Two possible sites are suitable. The average ambient temperature of the first site is 30 degrees Celsius and the pressure is 1.013 Bar. The second site is at a higher elevation and the average ambient temperature and pressure are 15 degrees Celsius and 0.975 Bar, respectively. Use the simulator to determine the most suitable site, based on engine performance. Assume an inlet and exhaust loss of 100 mm water gauge respectively.
58. The manufacturer of the engine claims the power output at ISO conditions

is 21.5 MW at an exhaust gas temperature limit (EGT) of 1,058K. An engine test is to be conducted to establish whether this power output from the gas turbine can be achieved. On the day of the test the ambient temperature and pressure are 15 degrees Celsius and 1.0 Bar respectively. The inlet and exhaust losses are 100 mm of water gauge. Use the simulator to conduct the engine test and demonstrate what the power capability of the engine is at ISO conditions (to an accuracy of about 2%).

Repeat the test when the ambient temperature is zero degrees Celsius.

21.8 Effects of component performance deterioration

59. Determine the loss in engine performance (loss in power output and thermal efficiency) due to moderate compressor fouling. Compressor fouling is simulated by reducing the compressor fouling and efficiency fault index to –3% and –1% respectively. The engine is operating at site rated conditions as described in Exercise 48.

    Also, determine the actual change in turbine creep life usage and emissions due to fouling.
60. Show the variation of the inlet non-dimensional flow with compressor non-dimensional speed due to compressor fouling. Assume the same compressor fault indices as used as in the previous simulation.
61. The gas turbine has been operating for 22,000 hours and is due for its major overhaul. The compressor and turbine efficiencies have each reduced by 1%. There is also some residual compressor fouling reducing the compressor capacity by 1.5%. Determine the loss in performance.
62. Simulate the effect of hot-end damage on the power turbine where the flow capacity of the power turbine is reduced by 3% and the efficiency of the power turbine is reduced by 1%. Determine the loss in power output and thermal efficiency of the gas turbine. Explain why the turbine (gas generator and power turbine) creep-life usage decreased and determine the actual changes in turbine creep-life usage due to this fault.
63. A piece of the transition duct has been dislodged and is adhering to the power turbine nozzle guide vane, resulting in a reduction in the flow capacity of the power turbine by 4%. This damage has also resulted in a loss in the power turbine efficiency of 1%. Determine the loss in performance of the gas turbine when the ambient temperature is 30 and –15 degrees Celsius. What limits the power output from the gas turbine at these ambient temperatures? Explain why there is an increase in power output due to this degradation at low ambient temperatures. Comment on the turbine creep life usage.
64. Repeat Exercises 62 and 63 by applying these degradations to the gas

generator turbine and compare the differences in performance of the engine.

65. An engine similar to that of the simulator is operating in the tropics where the ambient temperature is 30 degrees Celsius and the ambient pressure is 1.013 Bar. The engine persistently suffers from power turbine failure due to poor creep-life characteristics. It is suggested that the exhaust gas temperature should be reduced such that there is effectively a 75% increase in creep life of the power turbine. What changes or modification could be made to the power turbine so that no loss in power output would result when operating at the lower exhaust gas temperature limit?

    What is the consequence on engine performance due to this modification if this engine operates in temperate countries where the ambient temperature is zero degrees Celsius?

21.9 Power augmentation

66. The engine is operating at site rate conditions and the ambient pressure is 1.013 Bar. Determine the increase in maximum power output from the gas turbine when the ambient temperature is 30, 0 and –15 degrees Celsius when:

    (1) the exhaust gas temperature limit is increased by 20 degrees Celsius
    (2) the gas generator speed limit is increased by 5%.

    Discuss the impact on thermal efficiency, turbine creep life usage and emissions in each case.

67. The engine is operating at site rated conditions at an ambient pressure and temperature of 1.013 Bar and 30 degrees Celsius. It is necessary to increase the maximum power output of the gas turbine by 5%. Two methods of increasing the power output are considered:

    (1) increase the exhaust gas temperature limit
    (2) water injection.

    Determine the increase in exhaust gas temperature limit and the water–fuel ratio required to achieve the increased power output from the gas turbine for each case. Comment on the advantages and disadvantages of each method.

68. The engine is operating at site-rated conditions of 1.013 Bar and 30 degrees Celsius. A generator power output of 20.5 MW is required. It is decided to use water injection to achieve the necessary power demand. Estimate the water–fuel ratio required and comment on the increase in gas generator and power turbine creep life usage.

69. It is thought that the loss in the gas generator turbine creep life determined

in Exercise 68 is unacceptable. If we maintain the same water–fuel ratio, determine the generator output and exhaust gas temperature limit so that there is no change in gas generator creep life usage. Comment on the change in power turbine creep life usage.

70. The power turbine is approaching its major overhaul. However, due to the unavailability of a replacement engine, it is decided to postpone the overhaul. A generator power output of about 20.59 MW demand must be met. The manufacturer suggests that the power turbine creep-life usage should be halved. The user suggests water injection as a means to reduce the power turbine creep-life usage. Explain how this can be achieved and determine the water–fuel ratio necessary to halve the power turbine creep life usage. Comment on the change in gas generator creep-life usage. What is the drawback of using this method? The ambient pressure and temperature are 1.013 Bar and 15 degrees Celsius. Inlet and exhaust losses are 100 mm water gauge, respectively.
71. Determine the maximum generator power output, turbine inlet cooling, percentage increase in generator power output and thermal efficiency when applying turbine inlet cooling (the ambient temperature is 35 degrees Celsius) using:

   - wetted media
   - fogging
   - chillers (coefficient of performance (COP) = 5).

   Comment on the change in gas turbine emissions.

   If the effectiveness of the wetted media is increased to 0.95, what is the turbine inlet cooling, increased power output and thermal efficiency for this case? The increase in the effectiveness of the wetted media also results in an increased inlet loss of 50 mm water gauge.

   Comment on the profit using each of the turbine inlet cooling technologies. What is the impact of emissions taxes when using wetted media, fogging and chillers?
72. Determine the percentage increase in generator power output using wetted media, fogging and chillers (COP = 5) when the relative humidity is 20% and 90%. What parameter limits the power output of the gas turbine for each of these relative humidity cases? Ambient temperature is 35 degrees Celsius.
73. When using chillers for turbine inlet cooling, optimise the power turbine capacity for maximum power output based on EGT limit rather than GG speed limit. Comment on the turbine creep-life usage due to optimising the capacity of the power turbine. The ambient temperature is 35 degrees Celsius and the relative humidity is 20%.
74. If direct water injection into the combustor and turbine inlet cooling using chillers (COP = 5) are simultaneously employed to augment the

power output of the gas turbine, determine the generator power output when employing a water–fuel ratio of unity. What limits the maximum power output? Optimise the power turbine capacity for maximum power output based on EGT. The ambient temperature and relative humidity are 35 degrees Celsius and 60%, respectively.

What will be the optimised power turbine capacity if the relative humidity is 20%? Comment on the cooling load capacity for each case of relative humidity.

75. It is thought that including wetted media evaporative cooling before the chiller can increase turbine inlet cooling. Use the simulator to determine if this statement is true. The ambient temperature is 35 degrees Celsius.

21.10 Combined cycle and co-generation

76. The gas turbine simulator is a part of a combined-cycle power plant. If the stack temperature is limited to 120 degrees Celsius and the steam plant thermal efficiency is 32%, estimate the maximum combined-cycle thermal efficiency and power output. The ambient temperature and pressure are 15 degrees Celsius and 1.013 Bar at site conditions. Assume the mean specific heat at constant pressure for the exhaust gases is 1.074 kJ/kgK.
77. Repeat Exercise 76 when the gas turbine compressor is moderately fouled. Determine the percentage change in the gas turbine and combined cycle power outputs and thermal efficiencies. Comment on these changes.
78. Repeat Exercises 76 and 77 when the generator power output is set at 19 MW. Compare the results with those obtained from Exercises 76 and 77, and comment on the differences.
79. The gas turbine is a part of a co-generation system where the exhaust heat is used to produce hot water to satisfy a process heat load. Determine the maximum generator power, maximum heat load, heat-to-power loading and the overall efficiency of the co-generation system.

    If the compressor is moderately fouled, determine these parameters for this case and comment on the differences.

    Assume the mean specific heat at constant pressure for exhaust gases is 1.074 kJ/kgK and the stack temperature is limited to 120 degrees Celsius. The ambient temperature and pressure are 15 degrees Celsius and 1.013 Bar. Assume the inlet and exhaust losses are 100 mm water gauge respectively.
80. A co-generation system uses a gas turbine similar to that described by the simulator. An electrical power output and heat load of 19 MW and 35 MW are required. Determine the performance of the co-generation system and state if supplementary firing is required. Use the assumptions stated in Exercise 79.

If the compressor is moderately fouled, what is the performance of the co-generation system compared with that of a cleaned compressor?

21.11 Engine control systems

81. Set the proportional band and the integral gain to 400% and 1.2 respectively. Load the generator output from 1 MW to 20 MW. Explain the response of the gas turbine.
82. Run the simulator for a generator output set to 20 MW. A control system fault occurs where the integral output becomes zero (see the simulator user guide for instructions on how to set the integral output to zero). Explain the resultant loss in power output. What will be the consequence of this fault to the electrical system? What will the loss in power output be if the proportional band is 75% instead of 100%?
83. Start the simulator and introduce a variable stator vane (VSV) fault where the VSV has closed. This fault is simulated by setting the compressor fouling fault index to –10. Now load the gas turbine by setting the power demand from the generator to 20 MW. Explain why the generator power demand cannot be met and what limits the power output. Ambient pressure and temperature are 1.013 Bar and 15 degrees Celsius.
84. Due to combustion hot spots, the gas generator turbine nozzle guide vanes have eroded and this has effectively increased the capacity of the turbine by 10%. The damage to the gas generator turbine has also resulted in a turbine efficiency reduction of –8%. Simulate these faults and explain why the power demand cannot be met when no alarms have been raised by the control system. The power demand from the generator was set to 19 MW before the fault occurred.

    De-activate the 'Accel–Decel' lines and comment on the change in power output from the gas turbine. What limits the power output of the gas turbine in this case?
85. Repeat Exercise 83 but implement the turbine fault over a two second period. Explain why the engine trips.
86. The gas turbine undergoes a hot-end change on site. The replacement gas generator turbine has a smaller capacity than the original turbine. The reduction in the turbine capacity is 7.5%. During the acceptance test, the engine is loaded to generate a power output of 20 MW. Explain why the engine trips. Determine approximately the maximum generator power output above which the engine will trip.

21.12 Gas turbine emissions

87. A simple-cycle power plant consists of two gas turbines. The total power requirement is 20 MW. Determine the emissions of NO_x, CO

and CO_2 when both engines are operating at equal load and when running one engine. Comment on the performance of the gas turbine for each case.

88. When operating at ISO conditions it is necessary to reduce the NO_x emissions to 25 ppmv. Direct water injection is used to suppress NO_x emissions. The power demand from the generator is set to 20.5 MW. Determine the water–fuel ratio and water flow rate. If the relative humidity is 20%, what is the water–fuel ratio and water flow rate to maintain the NO_x emissions at 25 ppmv? Comment on the difference.
89. The gas turbine has to operate at three different ambient temperatures corresponding to 30, 15 and 0 degrees Celsius respectively. The power demand from the generator is set to 18 MW. Determine the emissions of CO_2, NO_x and CO and comment on the change in each of these emissions at the different ambient temperatures. The ambient pressure is 1.013 Bar with inlet and exhaust losses of 100 mm water gauge respectively.
90. Produce a graph describing the NO_x emissions with ambient temperature and relative humidity. The range for ambient temperature is from 30 to –30 degrees Celsius in steps of 10 degrees and the range for relative humidity is from 10% to 100% in steps of 10%. The power demand from the generator is set to 25 MW. What will be the effect on NO_x emissions for this ambient temperature and relative humidity range when the power demand from the generator is set to 18 MW?
91. Investigate the impact in the change in ambient pressure on engine emissions when operating at ambient pressures of 1.03, 1 and 0.97 Bar. Ignore inlet losses and assume an ambient temperature of 15 degrees Celsius. What is the effect of the change in inlet loss from 0 to 200 mm water gauge when operating at an ambient pressure of 1 Bar? Set the power demand from the generator to 25 MW.
92. Determine the change in emissions when the gas turbine is operating on natural gas and diesel respectively. The ambient temperature and pressure are 20 degrees Celsius and 1.013 Bar respectively. The inlet and exhaust losses are 100 mm of water gauge. The power demand from the generator is 25 MW. Comment on the change in gas generator speed.
93. Simulate the effect of moderate compressor fouling on engine emissions whilst operating at high power (generator power demand 25 MW) when limited by the exhaust gas temperature and when the generator power demand is 17 MW (low power demand). Comment on the changes in emissions. The ambient temperature and pressure are 15 degrees Celsius and 1.013 Bar. Assume an inlet and exhaust loss of 100 mm water gauge.

94. When the engine is operating at an ambient temperature of 30 degrees Celsius whilst the generator is producing 17 MW of electrical power output, it is necessary to reduce the NO_x by 40%. Determine the amount of water injection necessary to achieve the reduction in NO_x. Comment on the changes in CO_2 and CO. The ambient pressure is 1.013 Bar and the inlet and exhaust losses are 100 mm water gauge.

If a standby engine is available, discuss the impact on emissions when operating both engines at 50% power output. Comment whether operating two engines is better that operating one engine at 17 MW.

21.13 Answers to exercises

Single-shaft gas turbine simulator

A21.1 Effects of ambient temperature and pressure on engine performance

1. 40.408 MW, 41.232 MW, 32.673%, 72,955 hours. Exhaust gas temperature limits power output.
   NO_x, 2.718, CO, 0.104 and CO_2, 604.501 tonnes/day respectively.
2. 39.210 MW, 40.010 MW, 32.219%, 80,701 hours.
   NO_x, 2.626, CO, 0.106 and CO_2, 594.853 tonnes/day.
   –2.965%, –2.964%, –1.39%, 10.618, –3.385%, –1.923%, –1.596%.
3. At 30 degrees Celsius: 14.507%, –14.506%, –5.43%, –1.802%, –30.836%, 10.083%, 8.130%. Exhaust gas temperature limits power.
   At zero degrees Celsius: 8.969%, 8.971%, 2.271%, 35.933%, 27.535%, –6.196%, 8.282%. Exhaust gas temperature limited.
   At –15 degrees Celsius: 11.364%, 11.365%, 4.012%, >311.212%, 23.741%, 3.064%, 8.806%. Power limited.
   Control system option 2: At 30 degrees Celsius: –14.507%, –14.506%, –5.43%, –1.802%, –30.836%, 10.083%, –8.130%. Exhaust gas temperature limits power.
   At zero degrees Celsius: 8.969%, 8.971%, 2.271%, 35.933%, 27.535%, –6.196%, 8.282%. Exhaust gas temperature limited.
   At –15 degrees Celsius: 11.364%, 11.365%, 3.045%, 156.364%, 36.67%, –3.230%, 9.829%. Power limited.
4. 37.693 MW, 38.463 MW, 32.198%, 82,488 hours.
   NO_x, 2.475963, CO, 0.110736, CO_2, 572.22144 tonnes/day. –6.719%, –6.716%, –1.454%, 13.067%, –5.715%, 4.468%, –3.804%.
5. 32.1%.
7. At a relative humidity of 0.05%, 33.868 MW.
   At a relative humidity of 100%, 33.446 MW.
10. 97.405 MW and 32.212%.

A21.2 Effects of performance deterioration

12. Power loss –4.876%. Thermal efficiency loss –1.555%. Increase in creep life usage, 34.977%.
    NO_x, CO and CO_2 emissions change by 5.789%, –4.486%, 0.738% respectively.
14. Power loss –6.358%. Thermal efficiency loss –3.541%.
15. Power loss –4.179%. Thermal efficiency loss –3.101%. Turbine creep life increases by 15.356%.

16. At 30 degrees Celsius: power and thermal efficiency losses are –2.740%, –1.537%. Exhaust gas temperature limits the power output.

    At –15 degrees Celsius: power loss is zero and thermal efficiency loss –1.442%. Engine is power limited.

A21.3 Power augmentation

17. At 30 degrees Celsius: increase in power output is 5.007%. At zero degrees Celsius: increase in power output is 2.197%. At –15 degrees Celsius ambient temperature: there is a gain in power output and thermal efficiency due to the increase in exhaust gas temperature limit.
18. Exhaust gas temperature increases by 33.866 degrees Celsius. Water–fuel ratio is 0.9555.
19. 1.311.
20. 36.512 MW, 833.776K.
21. 1.492.
22. Maximum generator output 32.93 MW. Wetted media: Increase in generator output 5.366%. Increase in gas turbine power output 5.366%. Increase in thermal efficiency 1.654%. TIC 5.727 degrees Celsius. Fogging: Increase in generator output 6.301%. Increase in gas turbine power output 6.3%. Increase in thermal efficiency 1.924%. TIC 6.738 degrees Celsius. Chillers: Increase in generator output 11.585%. Increase in gas turbine power output 17.163%. Increase in thermal efficiency 5.416%. TIC 18.053 degrees Celsius. Wetted media effectiveness 0.95 case. Increase in generator output 5.998%. Increase in gas turbine power output 5.997%. Increase in thermal efficiency 1.838%, TIC 6.401 degrees Celsius.
23. Humidity 20% case. Maximum generator power 33.102. Wetted media: Increase in generator output 12.262%. Increase in gas turbine power output 12.259%. Increase in thermal efficiency 3.474%, TIC 15.547 degrees Celsius. Fogging: Increase in generator output 14.516%. Gas turbine power output 14.515%. Increase in thermal efficiency 4.063%, TIC 15.937 degrees Celsius. Chillers: Increase in generator output 21.138%. Increase in gas turbine power output 23.388%. Increase in thermal efficiency 6.702%. TIC 25 degrees Celsius. Wetted media effective 0.95 case. Increase in generator output 13.764%. Increase in gas turbine power output 13.763%. Increase in thermal efficiency 3.870%, TIC 15.141 degrees Celsius.

    Humidity 90%. Maximum power output 32.812 MW. Wetted media: Increase in generator output 1.201%. Increase in gas turbine power output 1.204%. Increase in thermal efficiency 0.367%. TIC 1.294 degrees Celsius. Fogging: Increase in generator output 1.417%. Increase in gas turbine power output 1.419%. Increase in thermal efficiency 0.437%, TIC 1.522 degrees Celsius. Chillers: Increase in generator output 3.517%. Increase in gas turbine thermal efficiency 9.116%. Increase in thermal efficiency 3.223%. TIC 9.304 degrees Celsius. Wetted media effective 0.95 case. Increase in generator output 1.347%. Increase in gas turbine power output 1.347%. Increase in thermal efficiency 0.414%, TIC 1.446 degrees Celsius.

A21.4 Combined cycle and co-generation

26. 49.246%, 61.143 MW.
27. Loss in gas turbine power output 4.876%. Loss in gas turbine thermal efficiency 1.588%. Combined cycle power loss, –4.109%. Combined cycle thermal efficiency loss –0.795%.
28. Repeating Exercise 26 with the generator power demand set at 32 MW, the thermal efficiency and power output is 47.833% and 50.182 MW respectively.

    Repeating Exercise 27, loss in gas turbine power output is 0. Loss in gas turbine thermal efficiency is –0.755%. Combined cycle power output gains by 0.706%. Combined cycle thermal efficiency decreases by 0.075%.
29. Using VIGV control system option 2: Repeating Exercise 26 when the generator power demand is 32 MW, the combined cycle thermal efficiency is 47.891% and the power output is 51.423 MW.

    Repeating Exercise 27, the loss in gas turbine power output is 0. Loss in gas turbine thermal efficiency is –0.802%. Power output of the combined cycle system increases by 0.404%. Thermal efficiency of the combined cycle system decreases by 0.402%.
30. 39.21 MW, 66.041 MW, 1.684, 84.772%. Fouled case, 37.298 MW, 64.286 MW, 1.724, 84.647%.
31. 32 MW, 58.652 MW, 1.833, 84.427%. Fouled case, 32 MW, 58.875 MW, 1.84, 84.408%.
32. Overall efficiency 90.205% without fouling and 90.345% when compressor is fouled. Supplementary firing is necessary. It has been assumed that no losses occur during supplementary firing.

A21.5 Engine control systems

34. 4.710 MW and 13.956 MW.
35. When the proportional band is 75% the power output is 31.481 MW and when the proportional band is 200% the power output is 29.293 MW. With VIGV control option 2, the power output is 30.950 MW when the proportional band is 75%. When the proportional band increases to 200% the power output is 29.267 MW.

A21.6 Gas turbine emissions

38. One engine operating: Thermal efficiency 32.192%, NO_x 134.078 ppmv at 15% O_2 dry, CO 9.131 ppmv at 15% O_2 dry, 592.168 tonnes/day.
    Two engines operating: Thermal efficiency 27.508%, NO_x 49.418 ppmv at 15% O_2 dry, CO 50.784 ppmv at 15% O_2 dry, 346.495 tonnes/day.
39. ISO: Water–fuel ratio 1.00583. Water flow rate 2.718 kg/s.
    At 20% relative humidity: Water–fuel ratio 1.0517. Water flow rate 2.844 kg/s.
40. At 60% relative humidity: Water–fuel ratio 0.7708. Water flow rate 1.834 kg/s. At 20% relative humidity: Water–fuel ratio 0.930699. Water flow rate 2.220 kg/s.
42. At 30 degrees Celsius: 513.527 tonnes/day, 89.871 ppmv at 15% O_2 dry, 12.999 ppmv at 15% O_2 dry. At 15 degrees Celsius: 502.622 tonnes/day, 96.558 ppmv at 15% O_2 dry, 15.25 ppmv at 15% O_2 dry. At 0 degrees Celsius: 494.634 tonnes/day, 93.834 ppmv at 15% O_2 dry, 18.208 ppmv at 15% O_2 dry.
44. Natural gas: NO_x 135.316 ppmv at 15% O_2 dry, 9.005 ppmv 15% O_2 dry, CO_2 594.853 tonnes/day. Diesel: NO_x 233.856 ppmv at 15% O_2 dry, CO 19.734 ppmv at 15% O_2 dry, CO_2 779.500 tonnes/day.
46. Water–fuel ratio 0.33068.

Two-shaft gas turbine simulator

In this section we quote emissions of NO_x and CO as an index.

A21.7 Effects of ambient temperature, pressure and humidity on engine performance

47. Generator output 21.011 MW. Gas turbine shaft power output 21.439 MW. Gas power 24.271 MW. Thermal efficiency 36.664%. Gas thermal efficiency 41.506%. Power turbine isentropic efficiency 88.335%. Gas turbine and power turbine creep life usage are 23,453 and 85,740 hours respectively. Exhaust gas temperature limits power output. NO_x, CO and CO_2 emissions 15.341 g/kg fuel, 0.435 g/kg fuel and 0.544 kg/kWh respectively. NO_x, CO and CO_2 emissions on a mass basis are 586.491, 16.644 and 102,239 tonnes/year respectively.
48. Generator output 20.59 MW. Gas turbine shaft power output 21.01 MW. Gas power 23.756 MW. Thermal efficiency 36.278%. Gas thermal efficiency 41.02%. Power turbine isentropic efficiency 88.44%. Gas turbine and power turbine creep life usage are 23,554 and 86,516 hours respectively. Exhaust gas temperature limits power output.

NO_x, CO and CO_2 emissions 15.266 g/kg fuel, 0.444 g/kg fuel and 0.550 kg/kWh respectively. NO_x, CO and CO_2 emissions on a mass basis are 578.029, 16.802 and 101,256 tonnes/year respectively.

Percentage changes: –2.004, –2.001, –2.119, –1.053, –1.169, 0.118, 0.432, 0.904, –0.486, 1.963, and 1.064.

49. At 30 degrees Celsius: –13.281, –13.278, –13.711, –4.464, –4.940, 0.5, –7.562, 5.929, –24.856, 21.53 and 4.673. EGT limited.

    At zero degrees Celsius: –0.362, –0.359, –0.533, 0.189, 0.015, 0.173, 158.59, 175.66, 5.156, 8.345 and –0.188. GG speed limits power.

    At –15 degrees Celsius: –0.62, –0.616, –0.99, 1.253, 0.876, 0.374, 883.971, >250, 2.231, 23.277 and –1.237. Quasi non-dimensional speed ($N1/\sqrt{T1}$) limits power.
50. 19.804 MW, 20.208 MW, 22.848%, 36.258%, 40.996%, 88.443%, 23,956 hours. 87,955 hours, 14.974 g/kg fuel, 0.479 g/kg fuel and 0.55 kg/kWh. Percentages: –5.745, –5.743, –5.860, –1.108, –1.230, 0.122, 2.145, 2.583, –2.393, 10.147 and 1.121.
51. 36.091%.
53. At 35 degrees Celsius: Relative humidity 0.05%, gas turbine power 17.42 MW. Relative humidity 100%, gas turbine power 17.834 MW.

    At zero degrees Celsius: Relative humidity 0.05%, gas turbine power 21.366 MW. Relative humidity 100%, 21.36 MW.
56. 105.05 MW, 36.278%.

A21.8 Effects of performance deterioration

59. Power output and thermal efficiency decrease by 3.979%, 1.442%. GG and PT creep life usage increase by 33.787% and 38.829% respectively. NO_x, CO and CO_2 emissions change by 4.148%, –4.766% and 1.011% respectively.
61. Power output and thermal efficiency loss 6.311% and 2.916% respectively.
62. Power output and thermal efficiency loss 4.531% and 1.158% respectively. GG and PT creep life usage increase by 13.666% and 42.542% respectively.
63. At 30 degrees Celsius: Power and thermal efficiency loss 10.94% and 3.409%. EGT limits the power output. At –15 degrees Celsius: Power and thermal efficiency increase by 7.605% and 0.738%. $N1/\sqrt{T1}$ limits the power output.
64. Repeating Exercise 62 by applying the damage to the GG turbine: power output and thermal efficiency decrease by 0.895% and 0.336%. GG turbine creep life usage increases by 10.754% while the power turbine creep life usage decreases by 0.391%. The actual increase in creep life for the GG and power turbine is 20.275% and 12.23 respectively.

Repeating Exercise 63 and applying the damage to the GG turbine: At 30 degrees Celsius: Power and thermal efficiency loss 0.32% and 0.151%. EGT limits the power output.

At –15 degrees Celsius: Power and thermal efficiency decrease by 0.572% and 0.14%. $N1/\sqrt{T1}$ limits the power output.

A21.9 Power augmentation

66. At 30 degrees Celsius: Increase in power due to an increase in EGT limit by 20 degrees Celsius is 6.54%. There is no increase in power output due to a 5% increase in GG speed limit. At zero degrees Celsius: There is no increase in power output due to a 20 degree increase in the EGT limit, but there is a 2.694% increase in power output due to a 5% increase in GG speed limit.

    At –15 degrees Celsius: There is no increase in power output due to an increase in EGT limit or GG speed due to the engine being controlled on $N1/\sqrt{T1}$.
67. 1. EGT increases to 1073.174K. 2. Water–fuel ratio is 0.75418.
68. 1.7332.
69. Generator output 19.9195 MW, EGT limit 1048.877K.
70. Water–fuel ratio 1.062255.
71. Wetted media: 18.434 MW, TIC = 5.727°C, 6.58%, 1.634%. Fogging: 18.62 MW, TIC = 6.738°C, 7.654%, 1.871%. Chillers: 19.578 MW, TIC = 18.823°C. 13.194%, 5.02% (gross), 0.311% (net - allowing for parasitic losses). Wetted media effectiveness = 0.95: 18.415 MW, TIC = 6.408°C, 6.467%, 1.485%.
72. Relative humidity 20%: Wetted media 14.813% EGT limiting power output. Fogging: 17.135% EGT limiting power output. Chillers: 19.672% gas generator speed limiting power output. Relative humidity 90%: Wetted media 1.646%, EGT limiting power output. Fogging: 1.941% EGT limiting power output. Chillers: 4.444% EGT limiting power output.
73. Power turbine capacity should be reduced by 0.67392%.
74. Net generator power output 20.079 MW. Gas generator speed limits the power output. Power turbine capacity should be reduced by 0.92145%. At 20% relative humidity, the power turbine capacity should be reduced by 2.0616%.

A21.10 Combined cycle and co-generation

76. 51.842%, 30.03 MW.
77. Simple/open cycle power and thermal efficiency loss: 3.979%, 1.44%. Combined cycle power and thermal efficiency loss: 3.257%, 0.694%.

78. Repeating Exercise 76: 27.784 MW, 51.429%. Repeating Exercise 77: Simple/open cycle power loss and thermal efficiency: 0%, 0.797%. Change in combined cycle power output and thermal efficiency: 0.5704%, –0.231%.
79. 20.59 MW, 28.196 MW, 1.369, 84.214%. Compressor fouled case: 19.77 MW, 27.752 MW, 1.404, 84.205%.
80. Overall efficiency 86%. Supplementary firing is required. Compressor fouled case: Overall efficiency 86.09%. Supplementary firing is required.

A21.11 Engine control systems

82. Power loss is –64.622%.
85. Repeat Exercise 84 but implement the turbine fault over a two second period. Explain why the engine trips.
86. Approximately 11MW.

A21.12 Gas turbine emissions

87. With two engines operating at 10 MW each: NO_x, CO and CO_2 emissions as indices are 7.275 g/kg fuel, 2.083 g/kg fuel and 0.646 kg/kWh respectively. One engine operating at 20 MW: NO_x, CO and CO_2 emissions as indices are 14.677 g/kg fuel, 0.478 g/kg fuel and 0.552 kg/kWh respectively.
88. At ISO: Water–fuel ratio 1.1283, water flow rate 1.433 kg/s. At 20% relative humidity: Water–fuel ratio 1.17165, water flow rate 1.489 kg/s.
89. At 30 degrees Celsius: NO_x, CO and CO_2 emissions are 11.379 g/kg fuel, 0.543 g/kg fuel and 0.571 kg/kWh respectively. At 15 degrees Celsius: NO_x, CO and CO_2 emissions are 13.005 g/kg fuel, 0.607 g/kg fuel and 0.562 kg/kWh respectively. At zero degrees Celsius: NO_x, CO and CO_2 emissions are 13.244 g/kg fuel, 0.692 g/kg fuel and 0.553 kg/kWh respectively.
92. When operating with natural gas: NO_x, CO and CO_2 emissions are 14.159 g/kg fuel, 0.467 g/kg fuel, 0.555 kg/kWh respectively. When operating with diesel: NO_x, CO and CO_2 emissions are 21.821 g/kg fuel, 0.941 g/kg fuel and 0.732 kg/kWh respectively.
94. Required water–fuel ratio 0.33242.

Appendix

Steady flow energy equation and stagnation properties

A1.1 Steady flow energy equation

A steady flow system is schematically represented in Fig. A1, where a fluid flows through the system at a steady rate while transferring work and heat with the surroundings.
The steady flow energy equation is given by:

$$Q - W = (h_1 - h_2) + \frac{1}{2}(v_1^2 - v_2^2) + g(z_1 - z_2) \qquad \text{[A1]}$$

where
Q is the specific heat transfer, kJ/kg

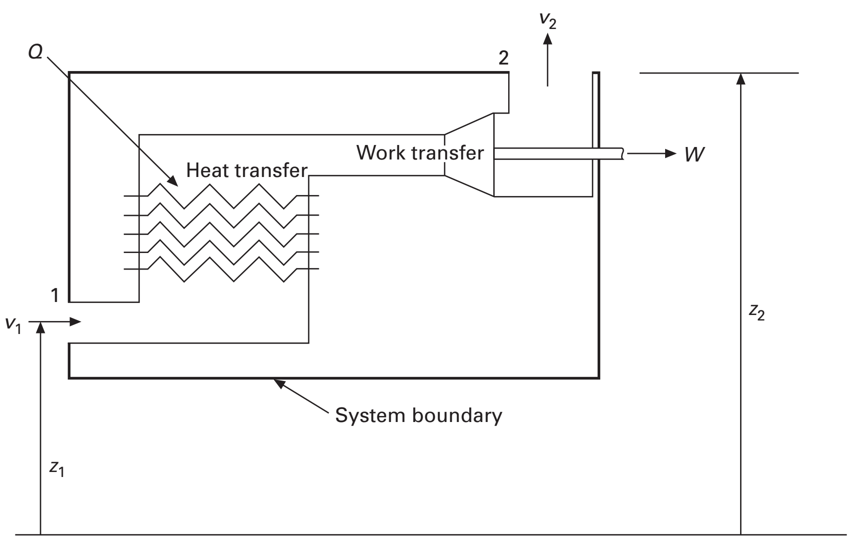

A1 Schematic representation of a steady flow system exchanging work and heat with the surroundings.

W is the specific work transfer, kJ/kg
$(h_1 - h_2)$ is the (specific) static enthalpy change, kJ/kg
$\frac{1}{2}(v_1^2 - v_2^2)$ is the kinetic energy change, kJ/kg
v_1 and v_2 are the fluid velocities at inlet and exit of the system as shown in Fig. A1,
$g(z_1 - z_2)$ is the potential energy change, where g is the gravitational constant (kJ/kg)

Stations 1 and 2 refer to the inlet and exit of the thermodynamic system. The term 'specific' refers to work and heat transfer, and to thermodynamic properties such as enthalpy for a unit of mass of the fluid.

The change in elevation, $z_1 - z_2$, is often small enough to be neglected, thus the steady flow energy equation reduces to:

$$Q - W = (h_1 - h_2) + \frac{1}{2}(v_1^2 - v_2^2) \qquad \text{[A2]}$$

For a perfect gas, $h = c_p \times Ts$, where c_p is the specific heat at constant pressure, Ts is the static temperature and h is the static specific enthalpy of the gas. Thus, for a perfect gas, the steady flow energy equation becomes:

$$Q - W = c_p(Ts_1 - Ts_2) + \frac{1}{2}(v_1^2 - v_2^2) \qquad \text{[A3]}$$

A1.2 Stagnation temperatures and pressures

In calculating the work and heat transfer in thermodynamic systems, the total work and heat transfer are often required. Therefore, the changes in kinetic energy which occur in thermodynamic processes such as compression, expansion and heat transfer need to be accounted for. The changes in kinetic energy can be accounted for by using the concept of stagnation or total values of the thermodynamic properties such as enthalpy.

The stagnation thermodynamic property of a fluid is the property of the fluid which is brought to rest, reversibly and adiabatically, without any work transfer. Therefore, the steady flow energy equation becomes:

$$H - h + \frac{1}{2}(0 - v^2) = 0$$

Therefore,

$$H = h + \frac{1}{2}v^2$$

where H is the specific stagnation or total enthalpy, h is the specific static enthalpy and v is the velocity.

When the fluid is a perfect gas, $H = c_p \times T$ and $h = c_p \times Ts$, where T and Ts are the stagnation (or total) temperature and static temperature, respectively. Thus,

$$T = Ts + \frac{1}{2}v^2/c_p \qquad [A4]$$

$^1/_2 v^2/c_p$ is referred to as the dynamic temperature. Thus, the total temperature is equal to the sum of the static temperature and the dynamic temperature. The steady flow Equation [A3] becomes:

$$Q - W = c_p(T_1 - T_2) \qquad [A5]$$

The total (specific) work done (i.e. work done per unit flow of fluid) during a compression process with no heat transfer (adiabatically) is given by:

$$W = -\,c_p(T_2 - T_1)$$

And for a heating process (i.e. no work transfer) the specific heat transfer:

$$Q = c_p(T_2 - T_1)$$

Thus, for a flow in a duct without heat and work transfer, the total temperature, T, remains constant.

By employing total or stagnation temperatures, there is no need to calculate the kinetic energy terms in the steady flow energy equation. Furthermore, it is easier to measure the total temperature of the flow rather than the static temperature.

The increase in temperature of a gas stream when it is brought to rest also results in an increase in pressure which is called the stagnation or total pressure. This increase in pressure or stagnation pressure can be calculated if it is assumed that the gas is brought to rest adiabatically and reversibly (i.e. isentropically). The total to static pressure ratio is given by:

$$\frac{P}{Ps} = \left(\frac{T}{Ts}\right)^{\frac{\gamma-1}{\gamma}} \qquad [A6]$$

where P is the total or stagnation pressure
Ps is the static pressure
and γ is the isentropic index, c_p/c_v.

Unlike the total temperature, which is constant for a stream flowing without heat and work transfer, the total pressure will only remain constant in the absence of friction. Further details on stagnation properties may be found in Rogers *et al.*[1]

A1.3 References

1. *Gas Turbine Theory*, 5th Edition. Rogers, C.F.G., Cohen, H. and Saravanamuttoo, H.I.H., Longman (2001).

Index

ABB/Alstom EV burner 162, 163
absorption refrigeration system 398
acceleration 217
/deceleration lines 267–70, 417–21
activation energy 137
adiabatic flame temperature 140, 141
aero-derivative combustors 147–9
aero-derived gas turbines 162, 239
aerodynamic coupling 187
air blast atomisers 150–1
air cooling techniques 130
air turbines 275
ambient pressure
single-shaft gas turbine 466–88
reduced power performance 472–9, 479–88
single-shaft gas turbine high power performance 467–72
two-shaft gas turbine 323–36
high-power performance 324–9
reduced power performance 329–36
ambient temperature 224–5, 415–17, 418
humidity and 398
inlet cooling and 397
single-shaft gas turbine 431–65, 563–5
configuration 431–2
high power performance 432–44, 454–62
humidity 463–5
power augmentation and 537–43
reduced power performance 444–54
two-shaft gas turbine 293–322
compressor fouling and 346–7
compressor running line 293–4
high-power performance 296–312
humidity 320–2
non-dimensional parameters 294–6
power augmentation and 383–8
reduced power performance 313–20
annular combustors 148–9
annulus geometry, compressor 113–15
atomisation, fuel injection and 149–52
atomiser, dual-orifice 150
axial compressors 98–9, 110, 250
characteristics 175
axial turbines 120–36
blade cooling 130–3
blading 120–2
characteristics 127–9
cooling technology 134–5
creep life 129–30
deviation and profile loss 125
metal temperature 133–4
stage load and flow coefficient 122–5
stage pressure ratio 125–7
axial velocity 101–2, 104, 124

Bakken correlation 311
Barber, John 1
base rating 376, 385, 524
blading
blade cooling 130–3
blade metal temperature 438–9
blade profile 242
blade velocity 102, 124–5
compressor 99–102
turbine 120–2
blow-off 209–10, 225, 285
valves 116, 211, 276
bluff bodies 144

boiler systems 94–5, 95
boundary layer 103–6, 114
  conditions 286–7
  growth 113, 122
  thickness 110

carbon capture 9
carbon dioxide (CO_2)
  calculation 172
  see also emissions
carbon monoxide (CO)
  correlations 171
  reduction 560–3
  see also emissions
Carnot efficiency 13–24 *passim*, 45, 83, 87, 91–2, 96
catalytic combustion 165–6
change flow 407
chemical reactions 96, 168
chillers 394–5, 397–401, 402
closed cycle gas turbines 6–7, 332, 474
closed loop control systems 262
clutches 234
co-generation systems 95–6
Combination of Gas turbine and Gas turbine (COGAG) 404
Combination of Gas turbine or Gas turbine (COGOG) 404
combined cycles 94–5
combustion 137–73
  air velocity 144
  aspects of achieving 140–6
  catalytic 165–6
  charts 39–40
  cooling 146–7
  in excess air 139–40
  fuel injection and atomisation 149–52
  hydrocarbon fuels 137–40
  lean premixed (LPM) 164–5
  pollutants 156–7, 157–8, 168–72
  pressure loss 154–6
  selective catalytic reduction (SCR) 158
  stability and heat release rate 152–4
  staged 160–2
  systems, regions and components 141
  temperature 39–40, 169
combustors 285
  dry low emission (DLE) 158–60, 166–8, 557–60
  rich-burn, quick-quench, lean-burn (RQL) 162–4
  types 147–9
  variable geometry 160
complex cycles 60–97
  co-generation 95–6
  combined 94–5
  Ericsson 89–93
  hybrid fuel cell-gas 96–7
  intercooled 60–72
  intercooled, reheat, regenerative (ICRHR) 85–9
  off-design performance 191–6
  reheat 72–85
  running lines 226–35
components 3, 300
  characteristics 174–7, 251, 255
  matching 174–7
compression process 25–6
  two-stage intercooled 61
compressor characteristic 109–10, 112, 228, 230, 233
  ambient pressure and 324–5, 329–30, 467, 468, 473, 480–2
  ambient temperature and 299–300, 313, 433–6, 446, 457–60
  compressor fouling and 338–9, 350, 490–2, 498–9
  efficiency 243–4
  flow 242–3
  fouling and 337
  hot end damage and 366, 509–10, 511, 516–18
  power demand and 547
  rotor tip rub and 369
  running line 268, 293–4, 387–8
  stator closure 118
  step change in power demand and 421–2
  variable inlet guide vanes (VIGVs) and 552, 556
compressor fouling 9, 242–6, 249
  single-shaft gas turbine
    high power 489–97
    reduced power 497–504, 504–8
  two-shaft gas turbine
    high power 337–49
    reduced power 349–57
  wash optimisation 258–61, 352–3
compressors 98–119

annulus geometry 113–15
axial 98–9, 110
blading 99–102
intercooled 61–2
off-design operation 115–18
rotating stall 110
running line 293–4
stage characteristics 283–4
stage load coefficient 103–6
stage pressure ratio 106–8
surge 110–16 *passim*, 262, 277, 294, 296, 376–7, 417–21 *passim*
work done factor 102–3
see also variable geometry compressors
configuration, engine 166–8, 431
conservation of mass, law of 278
constant pressure heat
addition 62, 75, 90, 92
rejection 62, 90, 92
continuity 278–9
continuous rating 376–7
maximum 380–3
control *see* engine control systems
convection cooling 131, 135
cooling technology 50–1, 134–5, 248
blade 130–3
combustion 146–7
convection cooling 131, 135
film cooling 132, 135, 146–7
impingement cooling 131
steam and mist 132–3
transpiration cooling 132, 146
turbine inlet 393–402, 543–4
creep life
ambient pressure and 326–8, 335–6, 470–1, 478–9, 486–8
ambient temperature and 308–10, 318–19, 440–1, 453, 460–2, 564
axial turbine 129–30
compressor fouling and 344–5, 354–5, 495–6, 503
hot end damage and 363–5, 514, 515, 521–3
rotor tip rub and 374
crude oil 405

Dalton's laws of partial pressures 36
de Haller number 101
deceleration lines 267–70, 417–21
deviation and profile loss 125
diagnostics 255–8
diesel 276, 405–7
Diesel and Gas Turbine Worldwide 65
differential equations 288
diffusers 142–3
dilution zone 145–6
'direct fired turbine' system 97
drag 102
dry bulb temperature 37, 394
dry low emission (DLE) systems 8–9, 158–60, 274, 486, 543
ambient temperature and 432, 455
combustors 557–60
engine configuration and 166–8
for industrial use 162
off-design operation and 213, 216
dual pressure boiler systems 94
dual-orifice atomiser 150

electric starter motor 275
electricity 96
element definition 283–6
Elling, Aegidius 1
emissions
ambient pressure and 328–9, 336, 471–2, 479–80, 487, 488
ambient temperature and 310–12, 318–20, 441–2, 443, 453–4, 462–3
compressor fouling and 345–6, 355–6, 496, 503–4
hot end damage and 365, 514–15, 516, 523
humidity and 320–2, 463–5, 465
power augmentation and 379–80, 382–3, 387, 390–2, 404–7
rotor tip rub and 374–5
variation with engine load 157
energy 96, 280–1
engine control systems 9, 262–77
acceleration/deceleration lines 267–70
PID loop 263–6, 409, 423
shutdown 276
signal selection 266–7
single-shaft gas turbine 545–65
EGT limit optimisation 563–5
variable inlet guide vanes (VIGVs) 545–9, 549–63

starting 275–6, 277
two-shaft gas turbine 409–28
acceleration/deceleration 417–21
engine trips 425–8
integral wind-up 421–5
proportional action 409–10
proportional/integral action 410–14
signal selection 414–17
variable geometry gas turbines 270–5
engines
configuration 166–8
limiting conditions 266
model 296
trip 426–7
enthalpy 37–9
entropy 14–15, 16, 37–9
environmental impact 7–9
Ericsson cycle 89–93
Euler method 288
evaporative cooling systems 393–4, 396, 398, 402
exhaust gas temperature (EGT) limit
and CO reduction 560–3
optimisation 563–5
exhaust system 286–7

fault indices 260
compressor fouling and 338, 489–90
hot end damage and 359, 509
performance deterioration and 251, 252–4, 255–8
trends in 255–6
turbine efficiency 368–9
film cooling 132, 135, 146–7
filtration 242, 286
firing temperatures *see* turbine entry temperature (TET)
flameout 267, 276, 277, 417, 421
flow
ambient pressure and 332–3, 471, 475–7, 486
ambient temperature and 300–3, 316, 317, 439, 449–51, 460
compatibility 230–1, 383
compressor fouling and 342, 353, 492–3, 501
hot end damage and 362–3, 513–14, 519–21
non-dimensional 109, 324–5
rotor tip rub and 371–2
stage load coefficent and 122–5
velocity 142–3
fogging 393–4, 397–8, 401
Fontana, Felice 8
forced vortex 144
free power turbines 254, 275
control 271, 273–5
dry low emission (DLE) systems and 167–8
off-design behaviour 217–20, 229–35
prediction 196–8
running line and 206–8
displacement 208–17
see also ambient temperature, two-shaft gas turbine
fuel
-air mixture 139, 152, 269, 276
change 404–7
costs 352, 385
injection and atomisation 149–52
residual 405
vaporisers 151–2

gas fuels 137, 152, 162
gas generator (GG)
function of 4, 5
hot end damage and 360–8
power transfer 234–5
speed 309–10, 328, 382, 402–3, 413–17
gas power and thermal efficiency 239–40
gas turbines
closed cycle 6–7, 332
components 3
engine controls 9
environmental impact 7–9
features of 2–3
history 1
layouts 3–6
performance deterioration 9
regenerative 42
simulators 10
single shaft 252
two-shaft 254
Gears method 288
General Electric 162
Greitzer B parameter 113

Hahn, Max 1
heat exchanger 67, 94, 235

constant pressure and 91–2
exit temperatures 193, 197
performance 40–2, 48–9
pressure losses 46–8
thermal efficiency 79, 84–5
heat release rate 154
specific fuel consumption (SFC) and 240
stability and 152–4
honeycomb seals 250
hot end damage 248–50, 358–68, 508–15, 515–23
hub-to-tip ratio 114
humidity 169, 178, 388, 398
calculation 395–6
performance effects 35–7, 58, 320–2, 463–5
relative 400–1, 433
specific 254, 310
hybrid fuel cell-gas system 96–7
hydraulic motors 275
hydrocarbon fuels 137–40
hydrocarbons *see* unburned hydrocarbons (UHC)

impingement cooling 131
industrial combustors 149
injection
fuel 149–52
water 388–93, 533–7
inlet cooling 393–402, 543–4
inlet flow 332
inlet guide vanes 167
instrumentation calibration 258
integral wind-up 264–5, 421–5
intercooled cycles 60–72
compressor optimisation 61–2
ideal regenerative 67–71
off-design behaviour 191–3, 193–5, 226–9
performance 76–7
practical 64–7
regenerative 71–2
specific work 62–4
thermal efficiency 62–4
intercooled, reheat, regenerative (ICRHR) cycles 85–9, 89
ideal 85–8
off-design performance 195–6, 196–8, 198–200
intermediate zone 145
irreversibilities 31–2, 71, 77–8, 89
isentropic compression 62, 75, 92
isentropic efficiency 26–7, 29–31, 109, 176, 459, 469
isentropic expansion 62, 75, 92
isentropic process 72
isothermal compression 89–91, 92, 394
isothermal expansion 89–91, 92

Jumo 004 turbine 147

kerosene 58, 137, 149, 276, 405

labyrinth seals 250, 251, 256
Larson-Miller (LM) parameter 129–30, 134, 413–14
lean mixtures 139, 153
lean, pre-mixed, pre-vaporised (LPP) combustion 165
lean premixed (LPM) combustion 164–5, 165
limit lines 267–9
linearly distributed model 281–2
liquid cooling systems 130
liquid fuels 137, 149, 151, 276, 405
liquid natural gas (LNG) evaporation systems 395
load changes 160
lumped model 281–2

Mach numbers 102, 106, 176–7, 282–3
matching
procedure 181–5
process 178–80
turbines 218, 221, 229, 232
matrix method 185–7
maximum continuous rating 380–3
mechanical coupling 187
methane 58, 405
methanol amine (MEA) 8
mist cooling 132–3
models
choice of 282–3, 296
linearly distributed/lumped 281–2
molten carbonate fuel cell (MCFC) 96
momentum 279–80
Modern Power Systems (publication) 51, 65, 133
multi-spooled engines 117, 276

multi-step method 288

naphtha 405
natural gas 137, 276, 404–7
Newton, Isaac 100, 279–80, 287
Newton-Raphson method 187, 254
nitrogen oxide (NO_x)
  correlations 169–71
  prediction 169–71
  suppression 157–8
  see also emissions
non-dimensional parameters 294–6, 349
nozzle guide vanes (NGV) 201, 358, 508
  axial turbines and 121, 127–9
  performance and 248, 250, 274
  variable 168, 213–17
nozzles, variable geometry propelling 233

off-design operation behaviour 202–40
  compressor 115–18
  gas power and thermal efficiency 239–40
  heat rate and specific fuel consumption (SFC) 240
  power turbine curves 237–9
  running line 221–3, 223–6, 226–35, 236–7
    displacement 208–17, 221–3
    steady-state 202–8
  single-shaft gas turbine 202–5, 208–17
  two-shaft gas turbine 206–8, 208–17, 223–6, 229–35
  three-shaft gas turbine 217–20, 221–3, 229–35
off-design performance 174–201
  complex cycle gas turbines 191–6
  component matching/characteristics 174–7
  matrix method 185–7
  single-shaft gas turbine 177–80
  two-shaft gas turbine 181–5, 188–9, 196–8
  three-shaft gas turbine 187–8, 190–1, 198–200
  variable geometry
    compressors 200–1
    turbines 201
online wash systems 245–6, 260–1
open/closed loop control 262, 553–7
operation *see* off-design operation behaviour
overboard bleeds 167–8, 216, 561
overspray 394

partial pressures (Dalton's laws) 36
pattern factor 145–6
peak rating 376, 377–80, 525–8
performance deterioration 9, 241–89
  causes 241
  diagnostics 255–8
  fault indices 251, 252–4, 255–8
  hot end damage 248–50
  quantifying 252–5
  root cause analysis (RCA) 258
  tip rubs/seal damage 250
  variable inlet guide vanes (VIGVs)/ variable stator vanes (VSVs) problems 246–8
  see also compressor fouling; off-design performance; transient performance; turbine damage
PID loop 263–6, 409, 423
  proportional (P) only 263
  proportional/integral (PI) 263–5
  proportional/integral/derivative (PID) 265–6, 272
pitch propeller 404
pollutants 149
  formation 156–7
  prediction 168–72
  suppression 157–8
  see also emissions
polytropic efficiency 27–31
power augmentation
  single-shaft gas turbine 524–44
    ambient temperature and 537–43
    peak rating 525–8
    turbine inlet cooling 543–4
    variable inlet guide vane (VIGV) angle increase 528–33
    water injection 533–7
  two-shaft gas turbine 376–408
    emissions 404–7
    low ambient temperature 383–8
    maximum continuous rating 380–3
    peak rating 377–80
    performance and 402–4, 404–7
    turbine inlet cooling 393–402

water injection 388–93
power transfer 234–5
power trends
ambient pressure 325–6, 331–2, 467–9, 474–5, 481–3
ambient temperature 302–6, 315–16, 433–6, 451–3, 457–60
compressor fouling and 341–2, 352–3, 494, 501–3
hot end damage and 362, 510–12, 518–19
integral wind-up and 424
reset wind-up and 425
rotor tip rub and 372–4
power turbines 4, 5
curves 237–9
predictor-corrector method 288
pressure 169
-volume/temperature-entropy diagram 16
Dalton's laws of partial 36
swirl atomisers 149–50
pressure loss
combustion and 154–6
heat exchanger 48–9
pressure ratio 109
ambient pressure and 330–1, 473–4, 480–1, 482
ambient temperature and 300, 314–15, 433–6, 444–6, 457
compressor fouling and 340, 353–4, 490–2, 498
hot end damage and 359–61, 509–10, 516–18
low 75–6
rotor tip rub and 370
pressure trends
ambient pressure and 326–7, 334–5, 469–70, 477–8, 483–4
ambient temperature and 307–8, 316–18, 436–9, 446, 460
compressor fouling and 340–1, 353–4, 492, 499–500
hot end damage and 359–61, 512–13, 519, 520
rotor tip rub and 370
see also ambient pressure
primary zone 143–5, 159
profile loss, deviation and 125
proportional (P) action 263, 409–10
proportional/integral (PI) action 263–5, 410–14
psychrometric chart 37
purging 276

radicals 137, 145, 156
Rayleigh flow 154
re-matching 490
reaction of the stage 99
reforming process 96
refrigeration systems 394–5
regenerative cycle 42
heat exchanger pressure losses 48–9
ideal reheat and 79–84
intercooled 67–71, 71–2
off-design performance and 193–5
performance 45–9
practical reheat- 84–5
see also intercooled, reheat, regenerative (ICRHR) cycles
reheat cycle 72–85
ideal regenerative and 79–84
optimisation 74
performance 76–7, 229–35
practical 77–9
regenerative- 84–5
specific work 74–6
thermal efficiency 74–6
see also intercooled, reheat, regenerative (ICRHR) cycles
revenue, lost 259–60
reversibility 25–6, 31–2
rich mixtures 139, 153
rich-burn, quick-quench, lean-burn (RQL) combustors 162–4
ring seals 250
Rizk and Mongia's correlation 311
root cause analysis (RCA) 258
rotating stall 110
rotor
choked 128
deflection 101, 123–4
tip rub 250, 368–75
Rung-Kutta-Felberg method 288
running line 223–6
complex cycle 226–35
data correction 236–7
displacement 208–17, 221–3, 249
compressor fouling and 347–9, 356–7, 497, 504, 507–8
hot end damage 366–8

rotor tip rub and 375
inlet cooling and 401
steady-state 202–8

seal 250, 251, 256
Second Law of Motion 279–80, 287
selective catalytic reduction (SCR) 158
shutdown 276
signal selection 266–7, 414–17
silicon carbide 84
silicon nitride 84
simple cycle gas turbines
irreversibility effect 31–2
performance 42–5
simulators 10
single-shaft gas turbines 252
control 272
dry low emission (DLE) systems and 167
elemental representation 286
layout 2, 3
off-design behaviour 202–5, 208–17, 226–9
prediction 177–80, 191–2, 193–5, 195–6
reheating 234
rotor system for 287
see also ambient pressure; ambient temperature; compressor fouling; engine control systems; power augmentation
single-step method 288
Smith's plot 124
solid oxide fuel cells (SOFC) 96
specific fuel consumption (SFC) 240
heat rate and 240
specific heat variation 32–7
humidity 35–7
specific humidity 254, 310
specific work
intercooled system 62–4
reheat cycles 74–6
speed
ambient pressure and 329–30, 485–6
ambient temperature and 298–9, 314, 417, 442–4, 449–50, 456–7
compressor fouling and 343–4, 350
compressor-turbine 287
hot end damage and 358–9, 360, 521, 522
rotor tip rub and 372, 373
see also under gas generator (GG)
spools 218, 221, 223
stability and heat release rate 152–4
stage characteristic 109
stage load coefficient 103–6, 114, 118
and flow 122–5
stage pressure ratio 106–8, 125–7
worked example 108, 126–7
stage stacking 109
staged combustion 160–2
stalling 113, 116, 376
starting 275–6, 277
stator outlet temperature (SOT) 50–1, 132
stators 118, 167, 225
steady flow energy equation 15–16
steady-state model 252
steady-state running line 202–8
steam 8
cooling 51, 132–3
turbines 94–5
Stirling cycles 91–3
stoichiometric fuel-air ratio 139
surge 110–16 *passim*, 262, 277, 294, 296, 376–7, 417–21 *passim*
swallowing capacity 387

tabular combustors 147
temperature
adiabatic flame 140, 141
metal, assessment 133–4
power output and 559, 562
wet bulb/dry bulb 395–7
see also ambient temperature
temperature ratio trends
ambient pressure and 473–4, 480–1, 482
ambient temperature and 433–6, 444–6, 457
compressor fouling and 490–2, 498–9
temperature trends
ambient pressure and 334, 477, 483–4
ambient temperature and 306–7, 316, 435–9, 455–6
compressor fouling and 343, 351–2, 492, 499–500
hot end damage and 361–2, 512–13, 519, 520
proportional/integral action 414, 415
rotor tip rub and 370–1

variable inlet guide vanes (VIGVs) and 546, 554
water injection and 428
temperature-entropy/pressure-volume diagram 16
tensile stress 129
thermal efficiency
ambient pressure and 325–6, 331–2, 467–9, 474–5, 481–3
ambient temperature and 302, 303–6, 315–16, 451–3, 457–60
compressor fouling and 341–2, 351–2, 494–5, 501–3
cooling technology and 134–5
gas power and 239–40
hot end damage and 362, 510–12, 518–19
humidity and 321, 465
intercooled system 62–4
pressure losses 48–9
reheat cycles 74–6
rotor tip rub and 372–4
thermal soaking 276
thermal storage system (TES) 395
thermodynamics 13–59
combustion charts 39–40
enthalpy 37–9
entropy 14–15, 16, 37–9
first law 13, 38
heat exchanger performance 40–2, 48–9
isentropic efficiency 26–7
polytropic efficiency 27–31
pressure losses 32, 48–9
pressure-volume/temperature-entropy diagram 16
principles of 13
processes 62, 68, 71, 75, 80, 90, 286
modified Ericsson cycle 92
regenerative cycle gas turbine 21–4, 45–9
reversibility 25–6, 31–2
second law 13–14, 15, 21, 38, 41
simple cycle gas turbine 16–21, 31–2, 42–5
specific heat variation 32–7
stator outlet temperature (SOT) 50–1
steady flow energy equation 15–16
turbine entry temperature (TET) 50–1
worked examples 51–9
three-shaft gas turbines
with free power turbine 5, 187–8
with ICRHR 198–200
off-design behaviour 217–20, 221–3
prediction 187–8, 190–1
three-term controller *see* PID loop
transient performance 277–88
boundary conditions 286–7
compressor-turbine speed 287
continuity 278–9
differential equations 288
element definition 283–6
energy 280–1
models
choice of 282–3
linearly distributed/lumped 281–2
momentum 279–80
see also performance deterioration
transition ducts 285
transpiration cooling 132, 146
trips, engine 425–8
tuboannular combustors 147–8
turbine characteristic 285–6
efficiency 176, 249
flow 175, 249
turbine damage 358–75
hot end damage 358–68, 508–15, 515–23
rotor tip rub 368–75
turbine entry temperature (TET) 50–1, 132, 166, 174, 276, 277
turbine thermal efficiency, maximum continuous rating and 381
two-shaft gas turbines 5–6, 254
with free power turbine 4, 181–5, 196–8, 206–8, 208–17
control of 273–5
with ICRHR 196–8
off-design behaviour 206–8, 208–17, 223–6
prediction 181–5, 188–9, 196–8
see also ambient pressure; ambient temperature; compressor fouling; engine control systems; power augmentation
two-stage intercooled compression process 61

unburned hydrocarbons (UHC) 7–9, 145, 149, 156–8, 161–8 *passim* correlation 171

valve flow coefficient (CG) 423
vaporisers 151–2
vapour absorption 394–5, 398–400
vapour compression 394–5, 400
variable geometry combustors 160
variable geometry compressors 117–18, 200–1
in free power turbine 271
in single-shaft gas turbine 272
variable geometry gas turbines 201, 270–5
two-shaft free power 168, 273–5
variable geometry propelling nozzle 233
variable inlet guide vanes (VIGVs)
/variable stator vanes (VSVs) problems 246–8
ambient pressure and 479–88
position trends 485–6
ambient temperature and 454–62
position trends 442–4, 449, 450, 456–7
angle increase 528–33
compressor fouling and 504–8
control system 545–9, 549–63
dry low emission (DLE) combustors 557–60
exhaust gas temperature (EGT) limit increase 560–3
open/closed loop 553–7
hot end damage and 515–23
position trends 521
running line displacement 210–13
variable nozzle guide vanes (NGV) 168, 213–17
variable stator vanes (VSVs)
/variable inlet guide vanes (VIGVs) problems 246–8
running line displacement 210–13
vectors
check 187–8, 189, 190–4, 196–9, 254–5
estimated 186–95, 197–8, 254–5
Vee gutter 144
velocity
axial 101–2, 104, 124
blade 102, 124–5
combustion air 144
flow 142–3
triangles 100–3, 113–14, 117, 121–5
whirl 102
von Ohain, Hans 1
vortex, forced 144
vortex-controlled diffuser (VCD) 142–3

wash
frequency factors 260
online systems 245–6, 260–1
optimisation 258–61, 352–3
procedures 246
waste heat recovery boiler (WHB) 94–5
water (H_2O) 405–7
condensation 398
cooling systems 51
gas shift reaction 8
water (H_2O) injection 388–93, 426, 428, 533–7
steam and 157–8, 525
wet bulb/dry bulb temperature 37, 394, 395–7
wet compression 394
wetted media 397, 397–8, 401
evaporative cooling 393–4, 396
fogging 393–4
whirl velocity 102
Whittle, Frank 1
Whittle W2B turbine 147
wind-up, integral 421–5
work done factor 102–3, 122

Zeolite 158